frontiers | Research Topics

Microbial diversity and resources in tidal flats

Edited by
Xue-Wei Xu, Feng-Yan Bai
and Gaëtan Burgaud

Published in
Frontiers in Marine Science
Frontiers in Microbiology

ISSN 1664-8714
ISBN 978-2-8325-5012-0
DOI 10.3389/978-2-8325-5012-0

About Frontiers

Frontiers is more than just an open access publisher of scholarly articles: it is a pioneering approach to the world of academia, radically improving the way scholarly research is managed. The grand vision of Frontiers is a world where all people have an equal opportunity to seek, share and generate knowledge. Frontiers provides immediate and permanent online open access to all its publications, but this alone is not enough to realize our grand goals.

Frontiers journal series

The Frontiers journal series is a multi-tier and interdisciplinary set of open-access, online journals, promising a paradigm shift from the current review, selection and dissemination processes in academic publishing. All Frontiers journals are driven by researchers for researchers; therefore, they constitute a service to the scholarly community. At the same time, the *Frontiers journal series* operates on a revolutionary invention, the tiered publishing system, initially addressing specific communities of scholars, and gradually climbing up to broader public understanding, thus serving the interests of the lay society, too.

Dedication to quality

Each Frontiers article is a landmark of the highest quality, thanks to genuinely collaborative interactions between authors and review editors, who include some of the world's best academicians. Research must be certified by peers before entering a stream of knowledge that may eventually reach the public - and shape society; therefore, Frontiers only applies the most rigorous and unbiased reviews. Frontiers revolutionizes research publishing by freely delivering the most outstanding research, evaluated with no bias from both the academic and social point of view. By applying the most advanced information technologies, Frontiers is catapulting scholarly publishing into a new generation.

What are Frontiers Research Topics?

Frontiers Research Topics are very popular trademarks of the *Frontiers journals series*: they are collections of at least ten articles, all centered on a particular subject. With their unique mix of varied contributions from Original Research to Review Articles, Frontiers Research Topics unify the most influential researchers, the latest key findings and historical advances in a hot research area.

Find out more on how to host your own Frontiers Research Topic or contribute to one as an author by contacting the Frontiers editorial office: frontiersin.org/about/contact

Microbial diversity and resources in tidal flats

Topic editors

Xue-Wei Xu – National Deep Sea Center (NDSC), China

Feng-Yan Bai – Institute of Microbiology, Chinese Academy of Sciences (CAS), China

Gaëtan Burgaud – Université de Bretagne Occidentale, France

Citation

Xu, X.-W., Bai, F.-Y., Burgaud, G., eds. (2024). *Microbial diversity and resources in tidal flats*. Lausanne: Frontiers Media SA. doi: 10.3389/978-2-8325-5012-0

Table of contents

frontiers | Frontiers in Marine Science

TYPE Original Research
PUBLISHED 23 December 2022
DOI 10.3389/fmars.2022.1028967

OPEN ACCESS

EDITED BY
Martin W. Hahn,
University of Innsbruck, Austria

REVIEWED BY
Huahua Jian,
Shanghai Jiao Tong University, China
Heng-Lin Cui,
Jiangsu University, China

*CORRESPONDENCE
Zong-Jun Du
duzongjun@sdu.edu.cn

SPECIALTY SECTION
This article was submitted to Aquatic Microbiology, a section of the journal Frontiers in Marine Science

RECEIVED 26 August 2022
ACCEPTED 07 December 2022
PUBLISHED 23 December 2022

CITATION
Gong Y, Ma L, Du Z-Z, Zheng W-S, Lu D-C and Du Z-J (2022) *Spiribacter halobius* sp. nov., a novel halophilic Gammaproteobacterium with a relatively large genome. *Front. Mar. Sci.* 9:1028967. doi: 10.3389/fmars.2022.1028967

Spiribacter halobius sp. nov., a novel halophilic Gammaproteobacterium with a relatively large genome

Ya Gong[1,2], Lu Ma[1], Zhao-Zhong Du[1], Wei-Shuang Zheng[3], De-Chen Lu[1] and Zong-Jun Du[1,2]*

[1]Marine College, Shandong University, Weihai, Shandong, China, [2]State Key Laboratory of Microbial Technology, Shandong University, Qingdao, Shandong, China, [3]Peking University-The Hong Kong University of Science and Technology (PKU-HKUST) Shenzhen-Hong Kong Institution, Marine Institute for Bioresources and Environment, Shenzhen, Guangdong, China

Spiribacter is the most abundant bacterial genus in the intermediate-salinity zones of hypersaline environments. However, *Spiribacter* strains are extremely difficult to isolate in pure culture. Therefore, the characteristics, genome features, and adaption mechanisms that allow *Spiribacter* strains to thrive in highly saline conditions are largely unknown. Here, we show that *Spiribacter* is predominant in brines from marine solar salterns and sulfate-type salt lakes with intermediate to saturated salinities. Using a high-salt medium, we isolated a novel strain, *Spiribacter halobius* E85^T, which possesses a relatively large and distinct genome. The genome of strain E85^T has a length of 4.17 Mbp, twice that of other *Spiribacter* species genomes and the largest described genome within the family *Ectothiorhodospiraceae*. Comparative genomic analyses indicate that approximately 50% of E85^T genes are strain-specific, endowing functional differences in its metabolic capabilities, biosynthesis of compatible solutes, and transport and pumping of solutes into the cell from the environment. Hundreds of insertion sequences result in many pseudogenes and frequent gene fragment rearrangements in the E85^T genome. Dozens of genomic islands, which show a significant preference for replication, recombination and repair, and cell motility and may have been gained from other bacterial species, are scattered in the genome. This study provides important insights into the general genetic basis for the abundance of *Spiribacter* in hypersaline environments and the strain-specific genome evolutionary strategies of strain E85^T.

KEYWORDS

marine bacteria, *Spiribacter*, insertion sequences, genomic islands, hypersaline environments

Introduction

Hypersaline environments, such as saline lakes and solar salterns, are distributed worldwide (Saccò et al., 2021; Shu and Huang, 2021). The unique environments of hypersaline lakes are considered representations of the conditions on Mars and the early Earth, providing an opportunity to study the presence of life in these distinct habitats (Pontefract et al., 2017; Belilla et al., 2019). The microbial community structure and the potential underlying ecological and evolutionary processes in these extreme hypersaline environments have been extensively studied using cultivation-independent methods (Narasingarao et al., 2012; Fernández et al., 2014). The square haloarchaeon *Haloquadratum walsbyi* and the halophilic bacterium *Salinibacter ruber* predominate crystallizer ponds with the highest salinities, while surprisingly high prokaryotic diversity and abundance are observed in intermediate-salinity conditions (Ventosa et al., 2015). However, these relatively abundant halophilic microbes are commonly slow growing and extremely difficult to isolate in pure culture (Bolhuis et al., 2004; Ghai et al., 2011). Homologous recombination and horizontal gene transfer are prevalent among halophilic bacteria and archaea, enabling adaptation to extreme and sometimes highly fluctuating environmental conditions. High recombination frequencies have been observed between populations of *Halobacterium* sp. AUS1 (Papke et al., 2004) and between different species in the genus *Haloferax* (Naor et al., 2012), indicating that halophilic archaea prefer genetic exchange and recombination. In prokaryotic genomes, horizontal gene transfer is the main source of gene gain and has been observed between *S. ruber* and haloarchaea. However, the genomes of many taxa have not yet been sequenced, and the genome evolution of halophilic bacteria remains to be uncovered.

The assembly of metagenomic data from intermediate-salinity marine solar saltern ponds revealed that the most abundant bacteria was a novel genus, *Spiribacter*, which belongs to the family *Ectothiorhodospiraceae* and the class *Gammaproteobacteria* (Fernández et al., 2014; León et al., 2014). The first cultured species of this genus, *Spiribacter salinus*, was documented in 2013 (León et al., 2013), and two streamlined genomes were reported in 2013 (López-Pérez et al., 2013). To date, the genus *Spiribacter* comprises four species with validly published names: *S. salinus*, *S. curvatus*, *S. roseus*, and *S. vilamensis*, which are halophilic bacteria isolated from salterns (León et al., 2014; León et al., 2015; León et al., 2016; León et al., 2020). The novel taxon '*S. halalkaliphilus*', which is most similar to the type strain *S. salinus*, was recently obtained from soda-saline lakes in Inner Mongolia, China (Xue et al., 2021). The relatively restricted metabolic versatility and osmoregulatory mechanisms of *Spiribacter* have been investigated based on the genomes of *S. salinus*, *S. curvatus*, and '*S. halalkaliphilus*' (López-Pérez et al., 2013; León et al., 2018; Xue et al., 2021). These genomes are approximately 2 Mbp in length, representing the smallest genomes within *Ectothiorhodospiraceae* and among all halophilic bacteria. Elucidation of the genomic and phenotypic repertoire of the genus *Spiribacter* has been limited by the lack of pure cultured strains.

Yuncheng Salt Lake is located in China's Shanxi province and contains sulfate. Wendeng Solar Saltern, in China's Shandong province, is a multi-pond saltern that originated from seawater. In a recent study, we sequenced samples from five Wendeng Solar Saltern ponds and analyzed the prokaryotic community composition, including the *Spiribacter* genus, the abundance of which was found to be positively related to the salinity of the water samples (Song et al., 2022). In the present study, we conducted amplicon sequencing variant (ASV) analyses of brine and sediment samples with different salinities from Yuncheng Salt Lake and Wendeng Solar Saltern. A novel *Spiribacter* strain (E85^T) was isolated, and its taxonomic status was investigated based on phenotypic, chemotaxonomic, and genotypic data. Comparative genomics analyses of all *Spiribacter* genomes were performed to identify the potential metabolic capabilities, high-salinity adaptation mechanisms, and expansion pathways of the relatively large and distinct genome of strain E85^T.

Results and discussion

Spiribacter was highly abundant in solar salterns and salt lakes

Considering the high abundance of the genus *Spiribacter* in different saline environments (López-Pérez et al., 2013; Zhao et al., 2020), we performed ASV sequencing analyses of brines and sediments to gain insights into the microbial community composition of marine solar salterns and sulfate-type salt lakes. In a previous study, samples from five Wendeng Solar Saltern ponds were sequenced and operational taxonomic units were clustered with a cut-off value of 97%, and the results showed that the abundance of *Spiribacter* exhibited a positive relationship with salinity in the water samples (Song et al., 2022). The sequence data and physicochemical parameters of hypersaline Wendeng Solar Saltern samples were used and compared in this study, but the 16S rRNA gene sequence data (accession numbers PRJNA559148 and PRJNA799174 in the Sequence Read Archive) were re-analyzed *via* ASV analyses with a threshold of 100% similarity. In this study, we also collected brine and sediment samples from six Yuncheng Salt Lake ponds in Yuncheng, China (Data S1). The physicochemical properties of the Yuncheng Salt Lake and Wendeng Solar Saltern brines were distinct. The salinities of Yuncheng Salt Lake ponds ranged from 170‰ to 340‰, with pH values of 7.84–8.53, and the salinities of Wendeng Solar Saltern ponds ranged from 45‰ to 265‰, with pH values of 7.53–8.02. The sulfate and chloride concentrations of Yuncheng Salt Lake ponds ranged from 47.13

to 136.37 g/L and from 24.22 to 23.91 g/L, respectively, and the chloride concentrations of the Wendeng Solar Saltern ponds ranged from 22.59 to 118.71 g/L.

Microbial genomic DNA from all brine and sediment samples of Yuncheng Salt Lake ponds was extracted, the V4–V5 region of the bacterial 16S rRNA gene sequence was amplified and sequenced, and the raw data were deposited in the Sequence Read Archive under accession numbers PRJNA825478 and PRJNA825481. With a threshold of 100% similarity, ASVs from all Yuncheng Salt Lake and Wendeng Solar Saltern samples were defined and assigned (Data S2). More than 50% of ASVs in most brine and sediment samples were not assigned to any previously described genus (Figure 1), suggesting that more pure culture, classification, and function studies of microbes in saline environments are needed.

The community compositions of brine and sediment samples differed. Some brine samples, such as W265 from Wendeng Solar Saltern (265‰ salinity) and W340 from Yuncheng Salt Lake (340‰ salinity), were enriched in the archaea genera *Halorubrum*, *Halobellus*, and *Halohasta*. Additionally, the genus *Spiribacter* was abundant in all brine samples from both Yuncheng Salt Lake and Wendeng Solar Saltern, despite the vastly different physicochemical parameters of the two sets of samples. The relative abundance of *Spiribacter* exceeded 10% in brine samples W175 and W265 from Wendeng Solar Saltern and all Yuncheng Salt Lake brine samples. The W340 sample had the highest relative abundance of *Spiribacter*, accounting for 43.60%. At the ASV level, there were some highly abundant *Spiribacter* ASVs; ASV_3 and ASV_5 accounted for approximately 20%. By contrast, the relative abundance of *Spiribacter* was below 2% in all sediment samples. These results showed that *Spiribacter* was predominant in the brines of marine solar salterns and sulfate-type salt lakes with intermediate and saturation salinities ranging from 125‰ to 340‰. The data confirmed that *Spiribacter* species are very abundant in brines, but not saline sediments, of soda-saline lakes (Zhao et al., 2020). Thus, *Spiribacter* was abundant in different hypersaline environments.

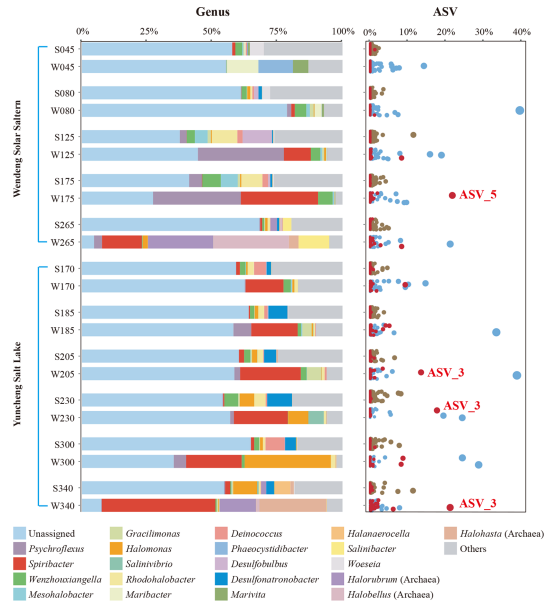

FIGURE 1
The prokaryotic community composition of two different saline environments along a gradient of increasing salinity at the genus and ASV levels. The top 22 most abundant genus taxa (including unassigned and others) and all ASVs are shown. In the sample names, the prefixes "S" and "W" represent sediment and water samples, respectively, and the numbers represent the salinity (‰). ASVs of the genus *Spiribacter* are shown in red, and the two representative ASVs are labeled.

Isolation, identification, and characteristics of a novel *Spiribacter* species

Given the high abundance of this genus in high-salt conditions, we intended to isolate *Spiribacter* species to investigate the novel metabolic pathways and potential osmotic regulatory mechanisms enabling them to function at high salinity. Considering the halotolerance of *Spiribacter*, the brine and sediment samples of Yuncheng Salt Lake and Wendeng Solar Saltern were 10-fold serially diluted and plated on marine agar 2216 supplemented with 10% (*w*/*v*) NaCl. All cultured colonies were picked, and several pure colonies were identified as *Spiribacter*. Among them, strain E85^T was identified as a novel species that grew faster than other *Spiribacter* strains and was thus chosen for further study.

The optimal growth of strain E85^T occurred at 37–40°C (range 20–50°C), pH 7.5–8.0 (range 7.0–9.0), and 3–6% NaCl (range 0.5–16%, *w*/*v*). Distinctively, *S. salinus* LMG 27464^T could tolerate 10–25% NaCl and showed optimal growth at 15% (León et al., 2014). E85^T cells were Gram stain-negative, straight to curved rods measuring 0.2–0.3 μm × 1.2–4.5 μm in size and possessing a single polar flagellum (Figure S1). Unlike other *Spiribacter* strains, E85^T grew under anaerobic conditions and could reduce nitrate to nitrite. Strain E85^T was susceptible to ampicillin (10 μg), clindamycin (2 μg), chloromycetin (30 μg), streptomycin (10 μg), and norfloxacin (30 μg), but resistant to penicillin (10 μg), tetracycline (30 μg), neomycin (30 μg), cefotaxime sodium (30 μg), gentamycin (30 μg), sulfamethoxydiazine (10 μg), vancomycin (30 μg), and kanamycin (30 μg). In the Biolog Gen III test, strain E85^T was resistant to troleandomycin, rifamycin SV, minocycline, lincomycin, and vancomycin.

The predominant respiratory quinone of strain E85^T was ubiquinone-8, consistent with previous *Spiribacter* genus descriptions. Similarly, the major fatty acids of strain E85^T were $C_{18:1}\omega7c$ (36.8%) and $C_{16:0}$ (19.2%, Table S1), but the details of the fatty acids were different; for example, strain E85^T had four unique

fatty acids, summed feature 2, iso-$C_{15:0}$, anteiso-$C_{15:0}$, and $C_{13:1}$. The polar lipids of strain E85^T were one phosphatidylcholine, one phosphatidylglycerol, one phosphatidylethanolamine, one diphosphatidylglycerol, one phosphoaminoglycolipid, and three phospholipids (Figure S2). *S. salinus* LMG 27464^T and strain E85^T shared four polar lipids, whereas the former exclusively contained a phosphoglycolipid and the latter harbored a phosphatidylcholine and a diphosphatidylglycerol. More differential morphological, physiological, and biochemical characteristics of strain E85^T and closely related species are provided in the species description and summarized in Table S2.

Phylogenetic placement of strain E85^T

An almost complete 16S rRNA gene sequence (1461 bp) was cloned from strain E85^T and deposited in GenBank under the accession number KY407792.1. A sequence similarity calculation using the EzBioCloud database revealed that the closest relatives of strain E85^T were *S. salinus* LMG 27464^T (97.3%), *S. curvatus* CECT 8396^T (96.3%), *S. roseus* CECT 9117^T (96.2%), '*S. halalkaliphilus*' IM2438^T (96.2%), and *S. vilamensis* SV525^T (96.0%). The phylogenetic tree constructed based on the 16S rRNA gene sequences of all cultured *Spiribacter* strains and the type strains of the related genera of the family *Ectothiorhodospiraceae* showed that strain E85^T formed a separate clade within the genus *Spiribacter* (Figure S3). Additionally, the phylogenomic tree of 14 *Spiribacter* genomes, 11 genomes from pure culture strains, three metagenome-assembled genomes, and genomes from the type strains of related genera based on 120 ubiquitous bacterial single-copy genes also support the conclusion that strain E85^T represents a novel lineage within the *Spiribacter* genus (Figure 2).

Furthermore, phylogenomic analyses of strain E85^T, four validly published *Spiribacter* species, and the recently isolated strain '*S. halalkaliphilus*' IM2438^T were performed (Table S3). The average nucleotide identity value between the genomes of strain E85^T and *S. roseus* CECT 9117^T was 74.5%, followed by *S. vilamensis* SV525^T (73.9%), '*S. halalkaliphilus*' IM2438^T (73.5%), *S. curvatus* CECT 8396^T (73.4%), and *S. salinus* LMG 27464^T (73.2%). The digital DNA-DNA hybridization value between the genomes of strain E85^T and *S. vilamensis* SV525^T was highest at 20.1%, followed by *S. roseus* CECT 9117^T (19.4%), *S. curvatus* CECT 8396^T (19.3%), *S. salinus* LMG 27464^T (19.2%), and '*S. halalkaliphilus*' IM2438^T (19.1%). These values were far below the species threshold values of 95–96% for average nucleotide identity (Goris et al., 2007) and 70% for digital DNA-DNA hybridization (Auch et al., 2010). In addition, the average amino-acid identity values between genomes of strain E85^T and other *Spiribacter* species ranged from 68.8% to 70.8%. This also suggested that strain E85^T might be a novel species according to the genera boundary of 45–65% and the species boundary of 65–95% (Konstantinidis et al., 2017). Therefore, based on these phylogenetic and phylogenomic analyses, we propose that strain E85^T is a novel species of the genus *Spiribacter*.

Strain E85^T possesses a relatively large and distinct genome

The draft genome of strain E85^T (GenBank accession number QFFI00000000.1) was assembled, with a total

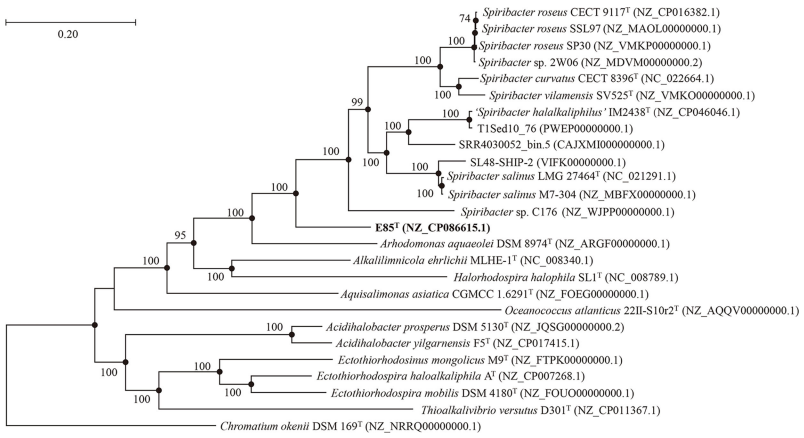

FIGURE 2
Phylogenetic tree generated from the alignment of 120 conserved proteins from 26 genomes of related strains, showing the taxonomic position of strain E85^T among members of the genus *Spiribacter*. The numbers on the nodes represent bootstrap values (IQTree) based on 1,000 replications; bootstrap values higher than 70% are marked on the branches. Filled circles indicate nodes overlapping on trees reconstructed using the FastTree and IQTree algorithms. The genome sequence GenBank accession numbers are given in parentheses. The genome of *Chromatium okenii* DSM 169^T (NRRQ00000000.1) is used as an outgroup. Bar: 0.20 substitutions per nucleotide position.

sequence length of 4,155,782 bp, 90 scaffolds, 150× genome coverage, and a scaffold N50 value of 118,172 bp. The National Center for Biotechnology Information (NCBI) Prokaryotic Genome Annotation Pipeline was used to annotate 3,863 genes. Among them, 3,755 protein-coding genes and 52 RNA genes were identified. Furthermore, the complete genome of strain E85^T was defined by assembling the next-generation sequencing data. A circular 4,172,350 bp sequence was obtained and deposited in the GenBank database under accession number NZ_CP086615.1 (Figure 3A). The complete genome of strain E85^T contained 3,874 genes, with 3,821 coding sequences (CDSs), 3,771 protein-coding genes, three rRNAs, 46 tRNAs, four ncRNAs, and 50 pseudogenes. The similarity between the draft genome and the complete genome of strain E85^T was compared based on the whole-genome alignment, and the results indicated that the gene sequences were highly similar; however, the gene arrangements differed due to the different contigs (Figure S4A). The complete genome of strain E85^T was used for the genomic analyses of this study.

The genome of strain E85^T was distinctly larger than other *Spiribacter* genomes, 14 pure culture strain genomes (from 1.74 Mb for *S. salinus* LMG 27464^T to 2.24 Mb for *Spiribacter* sp. C176) and three metagenome-assembled genomes, including SL48-SHIP-2 (4.02 Mb, Figure 3B). The E85^T genome is the largest described within the family *Ectothiorhodospiraceae* (the detailed information of genomes included in this research is

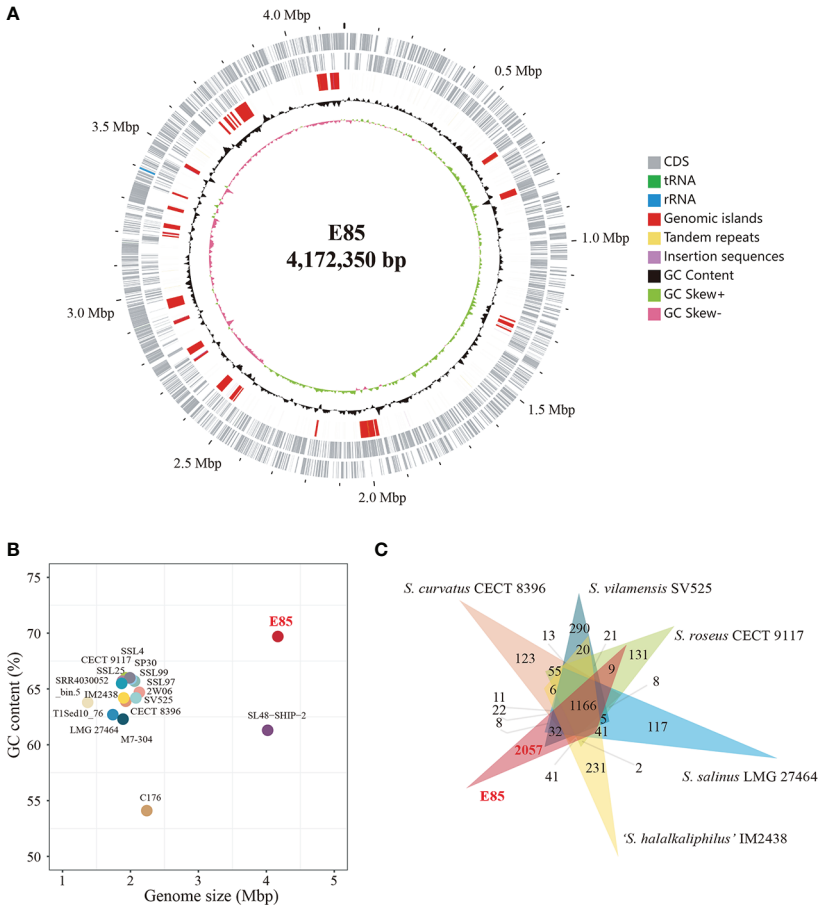

FIGURE 3
Genome features of strain E85 and closely related species. **(A)** Genome map of Strain E85. Ordered from outer ring to inner ring: 1) forward CDS, tRNA, and rRNA; 2) reverse CDS, tRNA, and rRNA; 3) genomic islands, tandem repeats, and insertion sequences; 4) GC content; 5) GC skew. **(B)** Genome size and GC content of all *Spiribacter* genomes: 14 genomes from pure culture strains (strain E85, *S. roseus* CECT 9117, *S. roseus* SSL97, *S. roseus* SP30, *Spiribacter* sp. 2W06, *S. curvatus* CECT 8396, *S. vilamensis* SV525, '*S. halalkaliphilus*' IM2438, *S. salinus* LMG 27464, *Spiribacter* sp. C176, *S. roseus* SSL4, *S. roseus* SSL25, *S. roseus* M7-304, and *Spiribacter* sp. SSL99) and three metagenome-assembled genomes (SL48-SHIP-2, T1Sed10_76, and SRR4030052_bin.5). **(C)** Distribution of homologous genes in the genomes of strain E85 and five other published *Spiribacter* species: 1,166 core gene clusters were represented in all genomes. Strain E85, '*S. halalkaliphilus*' IM2438, *S. salinus* LMG 27464, *S. roseus* CECT 9117, *S. vilamensis* SV525, and *S. curvatus* CECT 8396 contained 2,057, 231, 117, 131, and 290 species-specific gene clusters, respectively. The clustering results were used to generate a Venn diagram (Data S3).

shown in Table S4). Additionally, the DNA G+C content of strain E85^T was 69.7%, which corresponds to that obtained using HPLC (70.2 mol%) and is the highest among the *Spiribacter* genomes. The annotated gene numbers and CDS numbers of strain E85^T were almost double those of other *Spiribacter* genomes (Table 1). Moreover, 288 tandem repeats, generally non-coding DNA, were found in the genome of strain E85^T.

Further, the homologous genes of strain E85^T, '*S. halalkaliphilus*' IM2438^T, *S. salinus* LMG 27464^T, *S. curvatus* CECT 8396^T, *S. roseus* CECT 9117^T, and *S. vilamensis* SV525^T were clustered using the GeneFamily Method and Pan-Genome Analysis Web Server (Chen et al., 2018) with an e-value of 1e-10, coverage of 0.5, and identity of 0.5. A total of 4,961 homologous gene clusters were identified, and 1,166 gene clusters were shared by the six genomes (Figure 3C, Data S3). Strikingly, strain E85^T harbored 2,057 unique gene clusters, corresponding to 2,173 genes and accounting for approximately 56.09% of the total gene number of strain E85^T. These substantial differences between the genomes were also reflected in the progressiveMauve algorithm results based on the whole-genome alignment. The homologous gene regions were matched, whereas several gene regions of strain E85^T were not shared with other strains (Figure S4B). Thus, the genome of strain E85^T was relatively distinct.

Potential metabolic capabilities and high-salinity adaptation mechanisms

Bioinformatics analyses revealed that 3,197 CDSs were devoted to a clear Clusters of Orthologous Genes (COG) functional category, accounting for 83.67% of the total CDSs in the strain E85^T genome (Table S5). Meanwhile, the predicted results showed that, on average, 93.31% of the total CDSs in the genomes of the other five *Spiribacter* species were assigned to a functional category, with the functions of COG-J (translation, ribosomal structure, and biogenesis) and COG-M (cell wall/membrane/envelope biogenesis) as the top terms (Figure 4A). However, CDSs with the functions of COG-K (transcription), COG-L (replication, recombination, and repair), COG-T (signal transduction mechanisms), COG-E (amino acid transport and metabolism), COG-C (energy production and conversion), COG-P (inorganic ion transport and metabolism), COG-G (carbohydrate transport and metabolism), COG-I (lipid transport and metabolism), and COG-Q (secondary metabolite biosynthesis, transport, and catabolism) were abundant in the genome of strain E85^T, suggesting that they may play a role in survival strategies. These functions enriched in strain E85^T were consistent with the previous finding that larger genomes

TABLE 1 General genome features of strain E85^T and other *Spiribacter* species.

Feature	E85^T	*Spiribacter curvatus* **CECT 8396^T**	*'Spiribacter halalkaliphilus'* **IM2438^T**	*Spiribacter roseus* **CECT 9117^T**	*Spiribacter salinus* **LMG 27464^T**	*Spiribacter vilamensis* **SV525^T**
Accession number	NZ_CP086615.1	NC_022664.1	NZ_CP046046.1	NC_CP016382.1	NC_021291.1	NZ_VMKO00000000.1
Assembly status	Complete	Complete	Complete	Complete	Complete	Contig
Genome size (bp)	4,172,350	1,926,631	1,900,931	1,930,413	1,739,487	2,076,385
G+C content (%)	69.7	63.9	64.2	66	62.7	64.2
Number of genes	3874	1921	1900	1918	1744	2057
Number of CDSs	3821	1868	1848	1866	1692	2005
complete rRNAs	3	3	3	3	3	3
tRNAs	46	45	45	45	45	45
ncRNAs	4	5	4	4	4	4
Pseudogenes (total)	51	23	20	6	9	20
Tandem repeats	288	42	64	54	25	33
Unique gene clusters	1867	107	231	113	122	303
Mobile genetic elements						
Insertion Sequence	181	4	59	46	1	29
Genomic islands	29	4	7	9	3	9
Interspersed nuclear elements	18	12	11	13	14	13
Prophage	4	5	4	1	5	2
CRISPR	1	0	0	0	0	1

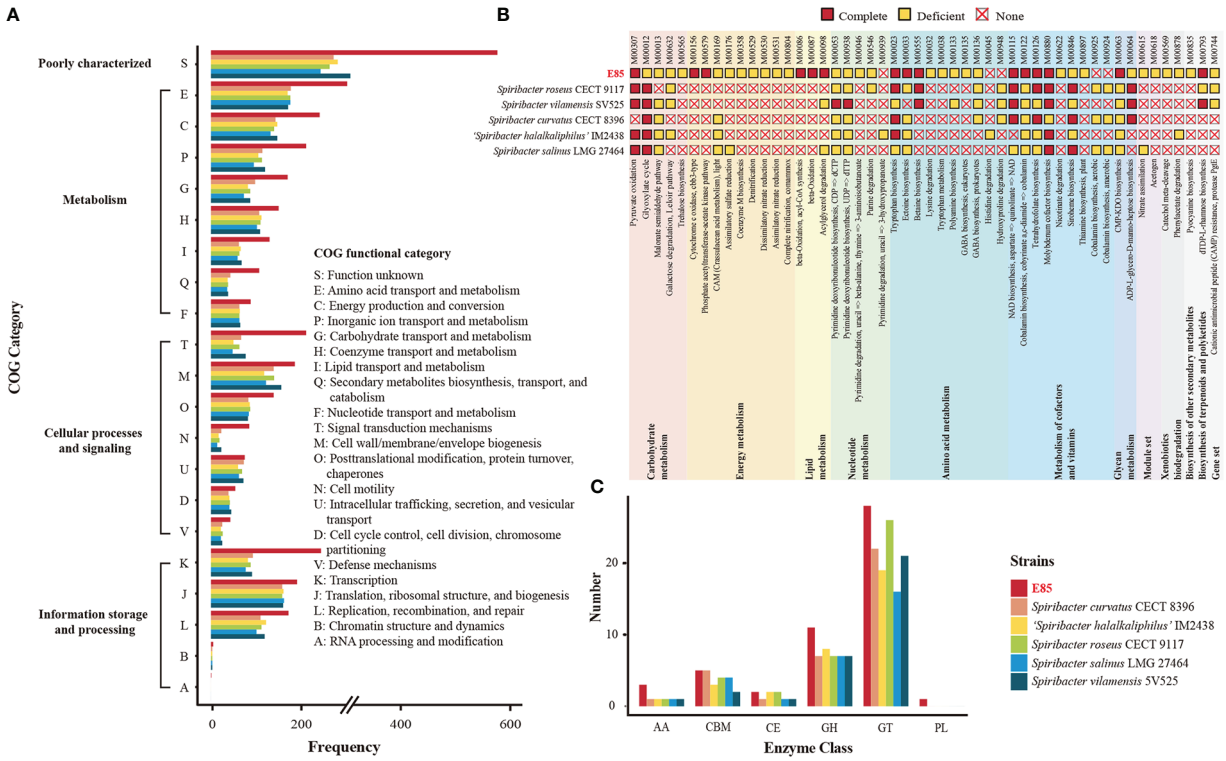

FIGURE 4
Comparison of potential function between the six *Spiribacter* genomes. **(A)** Functional distribution based on the COG classifications. The COG features are divided into four broad categories: information storage and processing, cellular processes and signaling, metabolism, and poorly characterized. **(B)** Inferred metabolism of six *Spiribacter* strains based on the KEGG database. Modules were manually categorized as complete, deficient (one block missing, two blocks missing, and incomplete), and none. **(C)** Quantification of carbohydrate-active enzyme genes in *Spiribacter* genomes. GH, glycoside hydrolases; GT, glycosyl transferases; PL, polysaccharide lyases; CE, carbohydrate esterases; CBM, carbohydrate-binding modules; AA, auxiliary activities; Annotation details are provided in Table S5.

preferentially accumulate genes related to secondary metabolism and energy conversion (Konstantinidis and Tiedje, 2004).

To determine the possible ecological benefits possessed within the large genome of strain E85^T, the KEGG database was used to identify metabolic pathways. The KEGG annotation results revealed that 50 pathway modules differed between the genomes of strain E85^T and the other five *Spiribacter* species (Figure 4B). Among them, several pathways were only complete in the genome of strain E85^T. For example, strain E85^T had two complete energy metabolism pathways, M00156 (cytochrome *c* oxidase, *cbb*$_3$-type) and M00579 (phosphate acetyltransferase-acetate kinase pathway), whereas other *Spiribacter* strains lacked these pathways. The *cbb*$_3$ cytochrome *c* oxidases contain four-subunit integral membrane complexes and use *c*-type cytochromes as electron donors with high oxygen affinity, functioning in O_2 reduction, proton pumping across the inner membrane, and the initiation of other metabolic pathways required for growth under microaerobic conditions (Durand et al., 2018). The bacterial enzymes acetate kinase and phosphotransacetylase form key pathways for synthesis of the central metabolic intermediate acetyl coenzyme A from acetate or ATP from excess acetyl coenzyme A, playing an important role in physiology and metabolism (Ingram-Smith et al., 2006). These two complete energy metabolism pathways might be beneficial for the growth of strain E85^T, which grew faster than the other *Spiribacter* strains. The colony diameter of strain E85^T reached 0.5–1.5 mm after 3 days of incubation at 37°C, while *S. salinus* LMG 27464^T, *S. curvatus* CECT 8396^T, and *S. roseus* CECT 9117^T reached colony diameters of 0.5–1.5 mm, 0.2–0.5 mm, and 0.5–1.0 mm, respectively, after 10 days of incubation at 37°C (León et al., 2014; León et al., 2015; León et al., 2016). The colony diameter of *S. vilamensis* SV525^T was pinpoint (< 0.5 mm) after 5 days of incubation at 30°C, and that of '*S. halalkaliphilus*' IM2438^T was 1.0–2.0 mm after 3–5 days of incubation at 37°C (León et al., 2014; León et al., 2015; León et al., 2016; León et al., 2020; Xue et al., 2021).

Considering the halotolerance of *Spiribacter* strains, the biosynthesis of compatible solutes and transport pumping solutes into the cell from the environment were investigated. Water-soluble organic molecules, including sugars, alcohols, and

amino acid derivatives, are typically compatible solutes with the amino acids ectoine, glycine betaine, and proline, which are widespread in prokaryotes (Gunde-Cimerman et al., 2018). The genome analyses showed that strain E85^T harbored three complete amino acid metabolism pathways, M00555 (betaine biosynthesis, choline → betaine), M00033 (ectoine biosynthesis, aspartate → ectoine), and M00015 (proline biosynthesis, glutamate → proline), to synthesize these compatible solutes. Among the other five *Spiribacter* species, all strains possessed the complete proline biosynthesis pathway, and *S. roseus* CECT 9117^T and *S. vilamensis* SV525^T had the complete betaine biosynthesis pathway. In addition, the compatible solute transporters, betaine/carnitine transporter, choline/glycine/proline betaine transport protein, and glycine betaine/proline transport system (glycine betaine/proline transport system ATP-binding protein [EC:7.6.2.9]; glycine betaine/proline transport system permease protein; glycine betaine/proline transport system substrate-binding protein), were identified in the *Spiribacter* genomes, functioning in the uptake of compatible solutes (Table S5). All six *Spiribacter* strains harbored betaine/carnitine transporter and the glycine betaine/proline transport system, but strain E85^T lacked choline/glycine/proline betaine transport protein. Therefore, the adaptation strategies of *Spiribacter* to high-salt environments might differ between species. Strain E85^T produces diverse compatible solutes, whereas other *Spiribacter* species might depend on an enhanced uptake capacity for compatible solute accumulation in cells. The ability of *S. salinus* LMG 27464^T and '*S. halalkaliphilus*' IM2438^T to import and synthesize compatible solutes has been documented (López-Pérez et al., 2013; León et al., 2018; Xue et al., 2021). *S. salinus* LMG 27464^T produces ectoine and trehalose and possesses several uptake systems, and some marker genes for ectoine, glycine betaine, and trehalose were annotated in the genome of '*S. halalkaliphilus*' IM2438^T, indicating that these compatible solutes might not be synthesized *de novo* for these metabolism pathways in these strains.

Other unique pathway modules of strain E85^T were lipid metabolism M00086 (beta-oxidation, acyl-CoA synthesis), M00087 (beta-oxidation), and M00098 (acylglycerol degradation); metabolism of cofactors and vitamins M00122 (cobalamin biosynthesis); and glycan metabolism M00063 (CMP-KDO biosynthesis). These pathways might be beneficial to the growth of strain E85^T in saline environments. The pathway modules of strain E85^T and related strains identified by KEGG are listed in Table S5. Many pathway modules involving carbohydrate metabolism (glycolysis, citrate cycle, pentose phosphate pathway, PRPP biosynthesis, and the Entner–Doudoroff pathway), energy metabolism (NADH: quinone oxidoreductase, succinate dehydrogenase, cytochrome bc_1 complex respiratory unit, cytochrome *c* oxidase, and F-type ATPase), and amino acid biosynthesis were shared by all *Spiribacter* strains. To analyze the potential ability of *Spiribacter* strains to degrade and metabolize complex carbohydrates, carbohydrate-active enzymes were identified by dbCAN2 annotation. The results showed that strain E85^T contained more glycoside hydrolases than other *Spiribacter* strains, which contained more glycosyltransferases (Figure 4C). Glycoside hydrolases usually catalyze glycosidic bond breakage, which suggests that strain E85^T may utilize organic compounds as carbon and energy sources.

The strain E85^T genome contains many insertion sequences and DNA fragment rearrangements

Mobile genetic elements were analyzed to explore the genetic basis for the apparent differences in gene contents and metabolic capabilities between strain E85^T and other *Spiribacter* strains. Mobile genetic elements are DNA sequences, such as transposons, integrons, and genomic islands, that can mediate horizontal gene transfer between bacterial strains and species, facilitating genome expansion, rapid evolution, and environmental adaptation (Frost et al., 2005). Compared with other *Spiribacter* genomes, the genome of strain E85^T was enriched in insertion sequences (181, Table 1, Figure 3A). Insertion sequences are small transposable elements widespread in bacterial genomes, representing a dynamic evolutionary force. In bacterial genomes, copy number increases and subsequent insertion sequence losses can have functional consequences such as gene inactivation, pseudogene formation, mediation of intervening sequence deletion between two copies of the insertion sequence, and genome rearrangements (Siguier et al., 2014). The strain E85^T genome contained 51 pseudogenes (Table 1), and the *S. curvatus* CECT 8396^T, *S. vilamensis* SV525^T, '*S. halalkaliphilus*' IM2438^T, *S. salinus* LMG 27464^T, and *S. roseus* CECT 9117^T genomes contained 21, 18, 15, 9, and 7 pseudogenes, respectively. To determine whether gene fragment rearrangement occurred in strain E85^T, synteny between the genomes of strain E85^T and the other five *Spiribacter* strains was analyzed. Obvious genome synteny existed between *S. salinus* LMG 27464^T, '*S. halalkaliphilus*' IM2438^T, and *S. curvatus* CECT 8396^T, but no genome synteny was observed between strain E85^T and the other five *Spiribacter* strains (Figure 5). Although there was genome synteny between *S. vilamensis* SV525^T and *S. salinus* LMG 27464^T, '*S. halalkaliphilus*' IM2438^T, *S. curvatus* CECT 8396^T, and *S. roseus* CECT 9117^T, the rearrangement of a large DNA fragment containing approximately half of the genome was found in *S. vilamensis* SV525^T. A small DNA fragment, approximately one-sixth of the genome, was also rearranged in the genome of *S. roseus* CECT 9117^T. These results indicate that genome mutation caused by gene fragment rearrangement frequently occurs in *Spiribacter*, especially in strain E85^T.

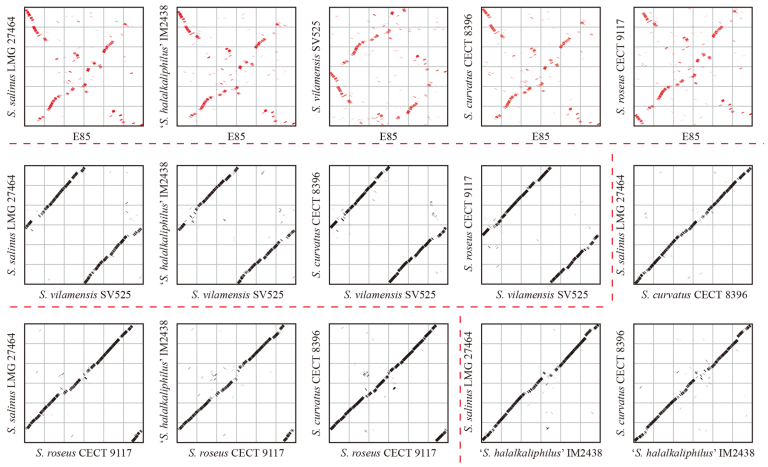

FIGURE 5
Genome synteny analyses of six *Spiribacter* species genomes. Significant synteny between genomes is represented by a clear line on the graph, whereas no synteny is represented by scattered points. Obvious synteny is observed between the genomes of *S. salinus* LMG 27464, '*S. halalkaliphilus*' IM2438, and *S. curvatus* CECT 8396, but no synteny is observed between strain E85 and the other five *Spiribacter* strains (marked in red).

The genome of strain E85^T was enriched in genomic islands, which might be from different sources

Genomic islands (GIs) are, in essence, discrete DNA segments that differ between closely related bacterial strains to which some past or present mobility is attributable. Horizontal gene transfer facilitated by GIs is widely recognized to play a crucial role in the evolution of bacterial species (Juhas et al., 2009). In these six *Spiribacter* genomes, GIs were recognized using IslandViewer 4 (Bertelli et al., 2017). The results showed that 29 GIs were scattered in the genome of strain E85^T, and relatively few GIs were present in other *Spiribacter* genomes (Table 1). Other than strain E85^T, *S. roseus* CECT 9117^T and *S. vilamensis* SV525^T harbored the highest number of GIs (nine each). *S. salinus* LMG 27464^T contained the fewest GIs (three), which might be a consequence of having the smallest genome among the species examined (López-Pérez et al., 2013). Therefore, the genome of strain E85^T was enriched in GIs.

To determine the potential function of GIs in strain E85^T, the gene features and functional differences were analyzed. The 29 GIs were distributed throughout the genome, with sequence lengths ranging from 4,684 to 48,684 bp (Data S4). Among them, eight large GIs were longer than 20 Kbp, and 13 small GIs were shorter than 10 Kbp. The total length of all 29 GIs was 484,275 bp, accounting for 11.61% of the strain E85^T genome length. The GIs harbored 481 genes, representing 12.42% of the total number of genes. According to the COG functional annotation, 313 CDSs were classified into COG functional categories, accounting for 65.07% of the total CDSs in the 29 GIs, far less than the proportion of functional CDSs (83.67%) in the genome of strain E85^T. Based on the COG categories, the functional preferences of CDSs encoded by GIs and the complete genome were analyzed (Figure 6A). The proportions of CDSs encoded by the genome of strain E85^T in COG-J (translation, ribosomal structure, and biogenesis), COG-C (energy production and conversion), COG-E (amino acid transport and metabolism), COG-F (nucleotide transport and metabolism), COG-H (coenzyme transport and metabolism), and COG-P (inorganic ion transport and metabolism) were 5.97, 7.54, 9.45, 2.75, 4.69, and 6.60%, respectively, more than twice that in the GIs. However, the GIs were enriched in COG-L (replication, recombination, and repair) and COG-N (cell motility) functional CDSs, accounting for 16.61 and 14.80% of total COG functional CDSs in the 29 GIs, respectively. These two proportions were very different from those in the genome of strain E85^T, which corresponded to 5.38 and 2.66%, respectively. These results indicate that core cell functions, such as the translation process, energy metabolism, and transport and metabolism of amino acids, nucleic acids, coenzymes, and inorganic ions, were concentrated in the genome of strain E85^T, while the CDSs encoded by the 29 GIs were related to replication, recombination and repair, and cell motility functions. More importantly, the GIs encoded plenty of transposases, integrases, and phage-related proteins, reflecting the potential for horizontal gene transfer and recombination. In addition, the GIs were genomic regions with GC skew, and the GC content of GIs was often low (Figure 2A), suggesting that the GIs might have been gained from the genomes of other strains or bacterial species.

We searched for homologs of the strain E85^T GIs and discovered that several homologous genes were gained from the genomes of

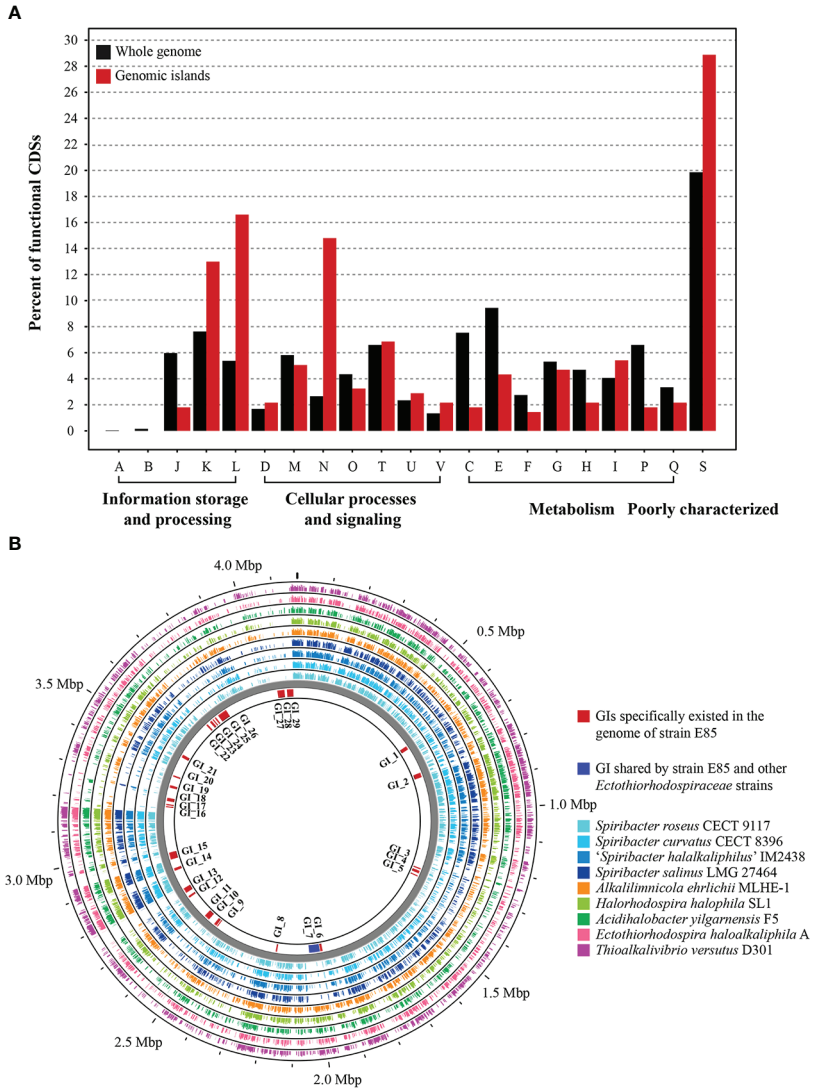

FIGURE 6
Genomic islands in the genome of strain E85. **(A)** Functional differences between the genomic islands and the whole genome of strain E85. The percentages of CDSs belonging to each COG are presented, and the function of each COG is shown in Figure 4. Compared with the functional CDSs in the whole genome of strain E85, the genomic islands harbor more than twice the proportions of COG-L and COG-N CDSs. **(B)** Whole-genome comparison of strain E85 and the complete genomes of *Spiribacter* and related genera within the *Ectothiorhodospiraceae* family. Genomic islands are shown inside the backbone and scattered in the genome of strain E85. Circular plots were generated using the BLASTn Proksee tools. Genomes are ordered from the inner ring to the outer ring: 1) *S. roseus* CECT 9117; 2) *S. curvatus* CECT 8396; 3) '*S. halalkaliphilus*' IM2438; 4) *S. salinus* LMG 27464; 5) *Alkalilimnicola ehrlichii* MLHE-1; 6) *Halorhodospira halophila* SL1; 7) *Acidihalobacter yilgarnensis* F5; 8) *Ectothiorhodospira haloalkaliphila* A; 9) *Thioalkalivibrio versutus* D301. The BLASTn results of each CDS in the genomic islands of strain E85 are displayed in Data S4.

other *Spiribacter* species and other taxa within the *Ectothiorhodospiraceae* family. Therefore, the genome of strain E85^T was compared with the complete genomes of *Spiribacter* and related genera within the family *Ectothiorhodospiraceae* to confirm the sources of these GIs. The BLASTn results indicated that most GIs were unique to the genome of strain E85^T, but the flagellar gene cluster GI_7 was shared by other *Ectothiorhodospiraceae* strains, suggesting that this GI might have been lost in other *Spiribacter* strains with smaller genomes (Figure 6B, Data S4). This result is consistent with the cell micrograph of strain E85^T, which showed a single polar flagellum that was not observed in other *Spiribacter* strains. The functions of the E85^T strain-specific GIs were diverse and included phage-related GI_1, GI_6, GI_13, and GI_15, terpene biosynthetic gene cluster GI_2, NRPS-like biosynthetic gene clusters GI_4 and GI_5, and antitoxin/toxin GI_16, GI_17, and GI_18. These GIs might have been gained through other sources. Transposases

existed in GI_3, GI_4, GI_7, GI_12, GI_14, GI_15, GI_17, GI_18, GI_21, GI_26, GI_28, and GI_29, and integrases were found in GI_1, GI_2, GI_6, GI_8, GI_11, and GI_26, which might be involved in gene shuffling. The nucleic acid of a temperate phage integrated into the host genome is called a prophage (Freifelder and Meselson, 1970). The prediction results identified four prophages in the genome of strain E85^T in the gene regions of 1,879,172–1,885,707, 2,751,299–2,767,792, 2,780,026–2,791,106, and 2,931,958–2,968,527 bp. The strain-specific phage-related GI_13 and GI_15 were prophages in the regions of 2,751,299–2,767,792 and 2,780,026–2,791,106 bp, respectively. The homologous proteins of these strain-specific GIs were searched using BLASTp in the standard NCBI nr database, and five proteins in GI_2 were similar to proteins from *Halomonas rituensis*, with approximately 50% amino acid sequence similarity (Figure S5). In GI_22, three neighboring genes, *LMH63_RS17140*, *LMH63_RS17145*, and *LMH63_RS17150*, corresponding to the proteins WP_109680169.1, WP_109680170.1, and WP_146205287.1, respectively, showed the highest amino acid sequence similarity with proteins WP_199257896.1 (65.98%), WP_199257897.1 (48.61%), and WP_199257898.1 (44.96%) encoded by three neighboring genes from the α-proteobacteria *Paracoccus binzhouensis*. In GI_29, similar results were gained. However, the sources of this strain-specific GI could not be determined due to low amino acid sequence similarity, indicating that additional detailed studies are needed to identify the source.

Description of *Spiribacter halobius* sp. nov.

Spiribacter halobius (ha.lo′bi.us. Gr. n. *halos*, salt; Gr. n. *bios*, life; M. L. masc. adj. *halobius*, living on salt).

The cells are Gram stain-negative, facultatively anaerobic, motile, straight to curved rods approximately 0.2–0.3 μm in width and 1.2–4.5 μm in length. The colonies are circular, smooth, convex, entire, cream-white, and 0.5–1.5 mm in diameter after incubation at 37°C for 3 days. Growth occurs at 20–50°C (optimum 37–40°C), pH 7.0–9.0 (optimum 7.5–8.0), and 0.5–16% (*w/v*) NaCl (optimum 3–6%). Nitrate can be reduced to nitrite. The cells cannot produce indole or H_2S. Gelatin is weakly hydrolyzed. Starch; Tween 20, 40, 60, and 80; alginate; agar; and cellulose are not hydrolyzed. The cells are positive for citrate utilization and negative for the Voges–Proskauer reaction. Myoinositol, glycerol, glucuronamide, L-lactic acid, D-malic acid, L-malic acid, β-hydroxy-D, and L-butyric acid are oxidized. Acids are produced from mannose, D-fructose, inositol, 2-keto-potassium gluconate, and 5-keto-potassium gluconate. The cells are positive for oxidase, catalase, alkaline phosphatase, esterase lipase (C8), leucine arylamidase, valine arylamidase, naphthol-AS-BI-phosphohydrolase, α-glucosidase arginine, dihydrolase, and urease; negative for esterase (C4), lipase (C14), cystine arylamidase, trypsin, α-chymotrypsin, acid phosphatase, α-galactosidase, β-galactosidase, β-glucuronidase, β-glucosidase, N-acetyl-glucosaminidase, α-mannosidase, o-nitrophenyl-beta-D-galactopyranoside, lysine decarboxylase, ornithine decarboxylase, and tryptophan deaminase. The major respiratory quinone is ubiquinone-8. The predominant cellular fatty acids are $C_{18:1}\omega7c$ and $C_{16:0}$. The polar lipids are one hosphatidylcholine, one phosphatidylglycerol, one phosphatidylethanolamine, one diphosphatidylglycerol, one phosphoaminoglycolipid, and three phospholipids.

The type strain is E85^T (= KCTC 52699^T = MCCC 1H00230^T) isolated from sediment collected from a marine solar saltern in Weihai, China. The DNA G+C content is 69.7% (data from genome sequence).

Materials and methods

Sampling, DNA extraction, and sequencing

Samples were collected in June 2019 from six Yuncheng Salt Lake ponds with salinities of 170, 185, 205, 230, 300, and 340‰ (Figure S6). Brine and sediment samples were collected in triplicate from each pond. After collection, samples were kept at 4°C during transport to the laboratory and −80°C after treatment. Brine samples were filtered through 0.22-μm polycarbonate membrane filters (Millipore, MA, USA). A FastDNA Spin Kit for soil (MP Biomedical, France) was used to extract DNA from all samples following the manufacturer's protocol. The V4–V5 region of the bacterial 16S rRNA gene was amplified using the specific barcoded primer set 515F (5′ barcode-GTGCCAGCMGCCGCGG-3′) and 907R (5′-CCGTCAATTCMTTTRAGTTT-3′). Sequencing libraries were generated following Illumina's genomic DNA library preparation procedure using an Illumina MiSeq PE300 platform at Shanghai Majorbio Bio-pharm Technology Co., Ltd. (Shanghai, China). The raw reads were deposited into the NCBI Sequence Read Archive database (Bioproject Numbers: PRJNA825478 and PRJNA825481).

Sequence analyses

The pipeline of VSEARCH v2.15.2 (Rognes et al., 2016) was used for quality filtering and dereplicating sequences. The unique sequences among the remaining reads were used to define ASVs using the UNOISE3 pipeline (Edgar and Flyvbjerg, 2015) in USEARCH (version 10.0.240, http://drive5.com/usearch/) with a threshold of 100% similarity. VSEARCH was used to analyze the phylogenetic affiliation of each 16S rRNA gene sequence against the Ribosomal Database Project (v18) 16S rRNA database (Cole et al., 2013) with a confidence threshold of 60%. Chloroplast and mitochondrial sequences were removed in downstream analyses. The data statistics of

each sample are listed in Table S6. The rarefication curves of each group based on the richness and Shannon index (Figure S7) indicated that the sequencing depth was sufficient to cover most of the prokaryotic sequences in the sample, which could be used for subsequent analyses.

Measurement of physicochemical factors

The water salinity and pH values of each pond were measured *in situ*. The sediment samples were weighed in a Petri dish and then dried for 6 h at 105°C. The sediment weights before and after drying were used to calculate the moisture content. The pH was measured through extracts by combining the dried sediment samples and water in a 1:2.5 ratio. Dried sediment samples (5 g) were mixed with 25 mL of water in a 50-mL centrifuge tube. The mixture was shaken for 3 min to obtain a 5:1 water–sediment extract. The water–sediment extracts and water samples from the salt lakes were filtered through 0.22-μm polyether sulfone membranes (Millipore, MA, USA). The solution ion concentrations of sediment samples and other ions (Cl^-, Br^-, SO_4^{2-}, Na^+, NH_4^+, K^+, Mg^{2+}, and Ca^{2+}) in brine and sediment samples were measured using an ICS-1100 (Thermo, Sunnyvale, CA, USA). The dissolved organic and inorganic carbon were measured using an ISO TOC CUBE-ISOPRIME 100 (Elementar, German) and a Delta V Advantage (Thermo, Sunnyvale, CA, USA), respectively. The total nitrogen and total phosphorus contents were determined using an alkaline potassium persulphate digestion-UV spectrophotometric method (Baird et al., 2017).

Bacterial isolation and cultivation

Strain E85^T was isolated from sediment of Wendeng Solar Saltern using the standard dilution plating technique on marine agar 2216 (MA; Becton Dickinson) supplemented with 10% (*w*/*v*) NaCl. The effects of different NaCl concentrations (0, 0.5, 1, 2, 4, 6, 8, 10, 12, 14, 16, 18, and 20%, *w*/*v*) on growth were assessed using a medium composed of yeast extract (0.1%), peptone (0.5%), and agar (1.8%) and prepared with artificial seawater (0.32% $MgSO_4$, 0.23% $MgCl_2$, 0.12% $CaCl_2$, 0.07% KCl, and 0.02% $NaHCO_3$, *w*/*v*). Strain E85^T was cultured on modified MA plates (MA 2216 supplemented with 3% NaCl), and modified marine broth (MB 2216 supplemented with 3% NaCl) was used as the liquid medium. Cell cultures were maintained at −80°C in sterile modified MB supplemented with 20% (*v*/*v*) glycerol. The type strains *S. salinus* LMG 27464^T from the Belgian Coordinated Collections of Microorganisms and *S. curvatus* CECT 8396^T and *S. roseus* CECT 9117^T from the Spanish Type Culture Collection were used as related type strains for comparative purposes in this study.

Phenotypic, physiological, and biochemical characteristics

The influence of temperature on the growth of visible colonies on modified MA plates was tested at 15, 20, 25, 28, 30, 33, 37, 42, 45, 50, and 55°C for approximately 7 days. To test the effects of pH on growth, the pH of modified MB was adjusted by adding buffer solutions: MES (pH 5.5 and 6.0), PIPES (pH 6.5 and 7.0), HEPES (pH 7.5 and 8.0), tricine (pH 8.5), and CAPSO (pH 9.0 and 9.5). After incubation at 37°C for 3 days, the OD_{600} values of the cultures were measured, and the morphological and physiological features of E85^T on modified MA plates or in modified MB were examined. All tests were independently conducted twice with three replicates. Cell size and morphology were observed using a transmission electron microscope (JEM-1200EX, JEOL). Motility was examined according to the hanging-drop method using a light microscope (E600, Nikon), and gliding motility was determined according to the method of (Bowman, 2000). Gram staining was performed as described by (Smibert and Krieg, 1994).

Anaerobic growth was determined by placing inoculated plates containing modified MA with or without 0.1% (*w*/*v*) KNO_3 in an anaerobic jar. Modified MB supplemented with 0.1% (*v*/*v*) nitrate in test tubes was used to assess nitrate reduction. The inoculated test tubes were placed in aerobic and anaerobic conditions for cultivation. Uninoculated test tubes served as controls. Catalase activity was detected by the production of bubbles after the addition of a drop of 3% (*v*/*v*) H_2O_2, and oxidase activity was determined using a bioMérieux oxidase reagent kit. Starch, cellulose, lipid, and alginate hydrolysis were tested on modified MA plates supplemented with 0.2% (*w*/*v*) soluble starch, 0.5% (*w*/*v*) CM-cellulose, 1% (*v*/*v*) Tweens (20, 40, 60, and 80), and 2% (*w*/*v*) sodium alginate, respectively (Smibert and Krieg, 1994). Tests for other physiological and biochemical characteristics were determined with API 20E and API ZYM (bioMérieux), and the ability to oxidize different compounds was tested using Biolog GEN III. Acid production from carbohydrates was tested using an API 50CHB fermentation kit (bioMérieux). All API and Biolog tests were conducted according to the manufacturers' instructions, replacing the suspension with sterilized 6% (*w*/*v*) NaCl solution. The results were recorded every 12 h after incubation at 37°C for up to 7 days. All API and Biolog tests were also performed in duplicate on the related type strains *S. salinus* LMG 27464^T, *S. curvatus* CECT 8396^T, and *S. roseus* CECT 9117^T. Antibiotic sensitivity was assessed as described by the Clinical and Laboratory Standards Institute (CLSI, 2022). Briefly, a cell suspension (McFarland standard 0.5) was swabbed over the surface of modified MA plates to create a uniform lawn, and antibiotic discs were aseptically placed onto the agar surface. Inoculated plates were incubated at 37°C for up to 7 days.

Chemotaxonomic characterization

To determine the respiratory quinone, cellular fatty acid composition, and polar lipid profile, cultures shaken at 37°C for 3 days were harvested and freeze-dried. Polar lipids analysis was performed by the Identification Service of DSMZ (Braunschweig, Germany). Respiratory quinone was extracted, purified, and analyzed by HPLC (Kroppenstedt, 1982). Fatty acids were extracted, methylated, and analyzed according to the standard protocol of MIDI (Sherlock Microbial Identification System, version 6.1; (Sasser, 1990).

16S rRNA gene sequence analyses

The 16S rRNA gene of strain E85^T was amplified by PCR using the universal primers 27F and 1492R as previously described (Liu et al., 2014). The PCR products were purified, ligated to the pMD18-T vector (Takara), and cloned according to the manufacturer's instructions. Sequencing was performed by Life Biotechnology (Shanghai). The 16S rRNA gene sequence for strain E85^T was submitted to the NCBI GenBank database. Gene similarities were calculated using the EzBioCloud Database (Yoon et al., 2017a). 16S rRNA gene sequence alignment was performed using the CLUSTAL_X program (Thompson et al., 1997), and positions with insertions or deletions were excluded during calculations. Phylogenetic trees were constructed using the neighbor-joining (Saitou and Nei, 1987), maximum-parsimony (Fitch, 1971), and maximum-likelihood (Felsenstein, 1981) methods with MEGA X (Kumar et al., 2018). The reliability of relationships was ensured by performing bootstrap analyses based on 1,000 replications.

Genome sequencing, assembly, and annotation

Genomic DNA of strain E85^T was obtained using a genomic DNA extraction kit (Takara), and the DNA G+C content was determined by HPLC (Mesbah et al., 1989). The genome was sequenced by the Shanghai Personal Biotechnology Co., China, using the Illumina HiSeq platform and Pacbio platform. The Illumina raw sequencing data were assembled using SOAPdenovo (Li et al., 2008), and the PacBio genomes were assembled using SMRT Link (v5.0.1). The phylogenetic relationships based on amino acid sequences were analyzed *via* GTDB-Tk, and the phylogenetic trees were reconstructed using FastTree with JTT+CAT parameters and IQTree with the LG+F +I+G4 model and 1,000 bootstrap replicates based on the 26 genomes. The average nucleotide identity was calculated using the EzGenome web service (Yoon et al., 2017b). The Genome-to-Genome Distance Calculator (GGDC 2.0, http://ggdc.dsmz.de, (Meier-Kolthoff et al., 2013) was used to calculate digital DNA-DNA hybridization. The average amino-acid identity values were calculated based on BLAST algorithm (Konstantinidis and Tiedje, 2005).

All genomes were annotated using NCBI Prokaryote Genome Automatic Annotation Pipeline (Tatusova et al., 2016). For potential function analysis, the draft genome was annotated using KofamKOALA (https://www.genome.jp/tools/kofamkoala/; (Aramaki et al., 2020), eggNOG (http://eggnog-mapper.embl.de/; (Huerta-Cepas et al., 2019), and dbCAN2 meta server (http://bcb.unl.edu/dbCAN2; (Zhang et al., 2018). Potential prophage sequences in the genome were identified and categorized as intact, incomplete, or questionable using the PHASTER website (http://phaster.ca/; (Arndt et al., 2016). CRISPRCasFinder was used to predict CRISPR in the genomes (https://crispr.i2bc.paris-saclay.fr/Server/; (Grissa et al., 2007). Insertion sequences located within the genome were identified using the ISfinder website (https://wwwis.biotoul.fr/; (Siguier et al., 2006). Interspersed repetitive sequences and tandem repetitive sequences were identified using the RepeatMasker Web Server (http://www.repeatmasker.org/cgi-bin/WEBRepeatMasker/) and Tandem Repeats Finder (https://tandem.bu.edu/trf/trf.html; (Benson, 1999), respectively. Genomic islands were identified using IslandViewer 4 (https://www.pathogenomics.sfu.ca/islandviewer; (Bertelli et al., 2017). Ortholog clusters were identified using the pan-genomes analysis pipeline (http://pgaweb.vlcc.cn; (Zhao et al., 2012). The genome map was generated using Proksee (https://proksee.ca; (Grant and Stothard, 2008), and the Venn diagram was created using the jvenn platform (http://jvenn.toulouse.inra.fr; (Bardou et al., 2014).

Data availability statement

The data presented in the study are deposited in the GenBank and Sequence Read Archive. The accession number for the 16S rRNA gene sequence of strain E85T is KY407792.1. The accession number of draft genome and complete genome are QFFI00000000.1 and NZ_CP086615.1, respectively. The accession number of 16S rRNA gene sequence raw data from all brine and sediment samples of Yuncheng Salt Lake are PRJNA825478 and PRJNA825481.

Author contributions

D-CL isolated the strain E85^T. YG, LM, Z-ZD, and W-SZ performed material preparation, experimental operation, data collection, and analyses. YG and LM wrote the manuscript. YG and Z-JD performed project guidance and critical revision of manuscript. All authors contributed to the article and approved the submitted version.

Funding

This work was supported by Science & Technology Fundamental Resources Investigation Program (Grant No. 2019FY100700) and the National Natural Science Foundation of China (Grant No. 32070002, 31900091).

Conflict of interest

The authors declare that the research was conducted in the absence of any commercial or financial relationships that could be construed as a potential conflict of interest.

Publisher's note

All claims expressed in this article are solely those of the authors and do not necessarily represent those of their affiliated organizations, or those of the publisher, the editors and the reviewers. Any product that may be evaluated in this article, or claim that may be made by its manufacturer, is not guaranteed or endorsed by the publisher.

Supplementary material

The Supplementary Material for this article can be found online at: https://www.frontiersin.org/articles/10.3389/fmars.2022.1028967/full#supplementary-material

References

Aramaki, T., Blanc-Mathieu, R., Endo, H., Ohkubo, K., Kanehisa, M., Goto, S., et al. (2020). KofamKOALA: KEGG ortholog assignment based on profile HMM and adaptive score threshold. *Bioinf. (Oxford England)* 36 (7), 2251–2252. doi: 10.1093/bioinformatics/btz859

Arndt, D., Grant, J. R., Marcu, A., Sajed, T., Pon, A., Liang, Y., et al. (2016). PHASTER: a better, faster version of the PHAST phage search tool. *Nucleic Acids Res.* 44 (W1), W16–W21. doi: 10.1093/nar/gkw387

Auch, A. F., von Jan, M., Klenk, H.-P., and Göker, M. (2010). Digital DNA-DNA hybridization for microbial species delineation by means of genome-to-genome sequence comparison. *Stand. genomic Sci.* 2 (1), 117–134. doi: 10.4056/sigs.531120

Baird, R. B., Eaton, A. D., and Rice, E. W. (2017). *Standard methods for the examination of water and wastewater. 23rd ed* (Washington DC: American Water Works Association).

Bardou, P., Mariette, J., Escudié, F., Djemiel, C., and Klopp, C. (2014). Jvenn: an interactive Venn diagram viewer. *BMC Bioinf.* 15 (1), 293. doi: 10.1186/1471-2105-15-293

Belilla, J., Moreira, D., Jardillier, L., Reboul, G., Benzerara, K., Lopez-Garcia, J. M., et al. (2019). Hyperdiverse archaea near life limits at the polyextreme geothermal dallol area. *Nat. Ecol. Evol.* 3 (11), 1552–1561. doi: 10.1038/s41559-019-1005-0

Benson, G. (1999). Tandem repeats finder: a program to analyze DNA sequences. *Nucleic Acids Res.* 27 (2), 573–580. doi: 10.1093/nar/27.2.573

Bertelli, C., Laird, M. R., Williams, K. P., Lau, B. Y., Hoad, G., Winsor, G. L., et al. (2017). IslandViewer 4: expanded prediction of genomic islands for larger-scale datasets. *Nucleic Acids Res.* 45 (W1), W30–W35. doi: 10.1093/nar/gkx343

Bolhuis, H., Poele, E. M., and Rodriguez-Valera, F. (2004). Isolation and cultivation of walsby's square archaeon. *Environ. Microbiol.* 6 (12), 1287–1291. doi: 10.1111/j.1462-2920.2004.00692.x

Bowman, J. P. (2000). Description of cellulophaga algicola sp. nov., isolated from the surfaces of Antarctic algae, and reclassification of *Cytophaga uliginosa* (ZoBell and upham 1944) reichenbach 1989 as *Cellulophaga uliginosa* comb. nov. *Int. J. Syst. evol. Microbiol.* 50 Pt 5, 1861–1868. doi: 10.1099/00207713-50-5-1861

Chen, X., Zhang, Y., Zhang, Z., Zhao, Y., Sun, C., Yang, M., et al. (2018). PGAweb: A web server for bacterial pan-genome analysis. *Front. Microbiol.* 9. doi: 10.3389/fmicb.2018.01910

CLSI (2022). *Performance standards for antimicrobial susceptibility testing, 32nd ed.* Malvern, PA: Clinical and Laboratory Standards Institute.

Cole, J. R., Wang, Q., Fish, J. A., Chai, B., McGarrell, D. M., Sun, Y., et al. (2013). Ribosomal database project: data and tools for high throughput rRNA analysis. *Nucleic Acids Res.* 42 (D1), D633–D642. doi: 10.1093/nar/gkt1244

Durand, A., Bourbon, M.-L., Steunou, A.-S., Khalfaoui-Hassani, B., Legrand, C., Guitton, A., et al. (2018). Biogenesis of the bacterial cytochrome oxidase: Active subcomplexes support a sequential assembly model. *J. Biol. Chem.* 293 (3), 808–818. doi: 10.1074/jbc.M117.805184

Edgar, R. C., and Flyvbjerg, H. (2015). Error filtering, pair assembly and error correction for next-generation sequencing reads. *Bioinf. (Oxford England)* 31 (21), 3476–3482. doi: 10.1093/bioinformatics/btv401

Felsenstein, J. (1981). Evolutionary trees from DNA sequences: a maximum likelihood approach. *J. Mol. Evol.* 17 (6), 368–376. doi: 10.1007/BF01734359

Fernández, A. B., Ghai, R., Martin-Cuadrado, A.-B., Sánchez-Porro, C., Rodriguez-Valera, F., and Ventosa, A. (2014). Prokaryotic taxonomic and metabolic diversity of an intermediate salinity hypersaline habitat assessed by metagenomics. *FEMS Microbiol. Ecol.* 88 (3), 623–635. doi: 10.1111/1574-6941.12329

Fitch, W. M. (1971). Toward defining the course of evolution: minimum change for a specific tree topology. *Syst. Biol.* 20 (4), 406–416. doi: 10.1093/sysbio/20.4.406

Freifelder, D., and Meselson, M. (1970). Topological relationship of prophage λ to the bacterial chromosome in lysogenic cells. *Proc. Natl. Acad. Sci. United States America* 65 (1), 200–205. doi: 10.1073/pnas.65.1.200

Frost, L. S., Leplae, R., Summers, A. O., and Toussaint, A. (2005). Mobile genetic elements: the agents of open source evolution. *Nat. Rev. Microbiol.* 3 (9), 722–732. doi: 10.1038/nrmicro1235

Ghai, R., Pašić, L., Fernández, A. B., Martin-Cuadrado, A.-B., Mizuno, C. M., McMahon, K. D., et al. (2011). New abundant microbial groups in aquatic hypersaline environments. *Sci. Rep.* 1, 135. doi: 10.1038/srep00135

Goris, J., Konstantinidis, K. T., Klappenbach, J. A., Coenye, T., Vandamme, P., and Tiedje, J. M. (2007). DNA-DNA Hybridization values and their relationship to whole-genome sequence similarities. *Int. J. Syst. Evol. Microbiol.* 57 (Pt 1), 81–91. doi: 10.1099/ijs.0.64483-0

Grant, J. R., and Stothard, P. (2008). The CGView server: a comparative genomics tool for circular genomes. *Nucleic Acids Res.* 36 (Web Server issue), W181–W184. doi: 10.1093/nar/gkn179

Grissa, I., Vergnaud, G., and Pourcel, C. (2007). CRISPRFinder: a web tool to identify clustered regularly interspaced short palindromic repeats. *Nucleic Acids Res.* 35 (Web Server issue), W52–W57. doi: 10.1093/nar/gkm360

Gunde-Cimerman, N., Plemenitaš, A., and Oren, A. (2018). Strategies of adaptation of microorganisms of the three domains of life to high salt concentrations. *FEMS Microbiol. Rev.* 42 (3), 353–375. doi: 10.1093/femsre/fuy009

Huerta-Cepas, J., Szklarczyk, D., Heller, D., Hernández-Plaza, A., Forslund, S. K., Cook, H., et al. (2019). eggNOG 5.0: a hierarchical, functionally and phylogenetically annotated orthology resource based on 5090 organisms and 2502 viruses. *Nucleic Acids Res.* 47 (D1), D309–D314. doi: 10.1093/nar/gky1085

Ingram-Smith, C., Martin, S. R., and Smith, K. S. (2006). Acetate kinase: not just a bacterial enzyme. *Trends Microbiol.* 14 (6), 249–253. doi: 10.1016/j.tim.2006.04.001

Juhas, M., van der Meer, J. R., Gaillard, M., Harding, R. M., Hood, D. W., and Crook, D. W. (2009). Genomic islands: tools of bacterial horizontal gene transfer and evolution. *FEMS Microbiol. Rev.* 33 (2), 376–393. doi: 10.1111/j.1574-6976.2008.00136.x

Konstantinidis, K. T., Rosselló-Móra, R., and Amann, R. (2017). Uncultivated microbes in need of their own taxonomy. *ISME J.* 11 (11), 2399–2406. doi: 10.1038/ismej.2017.113

Konstantinidis, K. T., and Tiedje, J. M. (2004). Trends between gene content and genome size in prokaryotic species with larger genomes. *Proc. Natl. Acad. Sci. U S A* 101 (9), 3160–3165. doi: 10.1073/pnas.0308653100

Konstantinidis, K. T., and Tiedje, J. M. (2005). Towards a genome-based taxonomy for prokaryotes. *J. Bacteriol.* 187 (18), 6258–6264. doi: 10.1128/JB.187.18.6258-6264.2005

Kroppenstedt, R. M. (1982). Separation of bacterial menaquinones by HPLC using reverse phase (RP18) and a silver loaded ion exchanger as stationary phases. *J. Liquid Chromatogr.* 5 (12), 2359–2367. doi: 10.1080/01483918208067640

Kumar, S., Stecher, G., Li, M., Knyaz, C., and Tamura, K. (2018). MEGA X: Molecular evolutionary genetics analysis across computing platforms. *Mol. Biol. Evol.* 35 (6), 1547–1549. doi: 10.1093/molbev/msy096

León, M. J., Fernández, A. B., Ghai, R., Sánchez-Porro, C., Rodriguez-Valera, F., and Ventosa, A. (2014). From metagenomics to pure culture: isolation and characterization of the moderately halophilic bacterium *Spiribacter salinus* gen. nov., sp. nov. *Appl. Environ. Microbiol.* 80 (13), 3850–3857. doi: 10.1128/AEM.00430-14

León, M. J., Galisteo, C., Ventosa, A., and Sánchez-Porro, C. (2020). *Spiribacter aquaticus* Leon et al. 2017 is a later heterotypic synonym of *Spiribacter roseus* Leon et al. 2016. Reclassification of *Halopeptonella vilamensis* Menes et al. 2016 as *Spiribacter vilamensis* comb. nov. *Int. J. Syst. evol. Microbiol.* 70 (4), 2873–2878. doi: 10.1099/ijsem.0.004113

León, M. J., Ghai, R., Fernandez, A. B., Sanchez-Porro, C., Rodriguez-Valera, F., and Ventosa, A. (2013). Draft genome of *Spiribacter salinus* M19-40, an abundant gammaproteobacterium in aquatic hypersaline environments. *Genome Announc.* 1 (1),e00179-12. doi: 10.1128/genomeA.00179-12

León, M. J., Hoffmann, T., Sanchez-Porro, C., Heider, J., Ventosa, A., and Bremer, E. (2018). Compatible solute synthesis and import by the moderate halophile *Spiribacter salinus*: Physiology and genomics. –. *Front. Microbiol.* 9. doi: 10.3389/fmicb.2018.00108

León, M. J., Rodriguez-Olmos, Á., Sánchez-Porro, C., López-Pérez, M., Rodríguez-Valera, F., Soliveri, J., et al. (2015). *Spiribacter curvatus* sp. nov., a moderately halophilic bacterium isolated from a saltern. *Int. J. Syst. Evol. Microbiol.* 65 (12), 4638–4643. doi: 10.1099/ijsem.0.000621

León, M. J., Vera-Gargallo, B., Sánchez-Porro, C., and Ventosa, A. (2016). *Spiribacter roseus* sp. nov., a moderately halophilic species of the genus *Spiribacter* from salterns. *Int. J. Syst. evol. Microbiol.* 66 (10), 4218–4224. doi: 10.1099/ijsem.0.001338

Li, R., Li, Y., Kristiansen, K., and Wang, J. (2008). SOAP: short oligonucleotide alignment program. *Bioinformatics* 24 (5), 713–714. doi: 10.1093/bioinformatics/btn025

Liu, Q.-Q., Li, X.-L., Rooney, A. P., Du, Z.-J., and Chen, G.-J. (2014). *Tangfeifania diversioriginum* gen. nov., sp. nov., a representative of the family *Draconibacteriaceae*. *Int. J. Syst. evol. Microbiol.* 64 (Pt 10), 3473–3477. doi: 10.1099/ijs.0.066902-0

López-Pérez, M., Ghai, R., Leon, M. J., Rodríguez-Olmos, Á., Copa-Patiño, J. L., Soliveri, J., et al. (2013). Genomes of "*Spiribacter*", a streamlined, successful halophilic bacterium. *BMC Genomics* 14, 787. doi: 10.1186/1471-2164-14-787

Meier-Kolthoff, J. P., Auch, A. F., Klenk, H.-P., and Göker, M. (2013). Genome sequence-based species delimitation with confidence intervals and improved distance functions. *BMC Bioinf.* 14, 60. doi: 10.1186/1471-2105-14-60

Mesbah, M., Premachandran, U., and Whitman, W. B. (1989). Precise measurement of the g+ c content of deoxyribonucleic acid by high-performance liquid chromatography. *Int. J. Syst. Evol. Microbiol.* 39 (2), 159–167. doi: 10.1099/00207713-39-2-159

Naor, A., Lapierre, P., Mevarech, M., Papke, R. T., and Gophna, U. (2012). Low species barriers in halophilic archaea and the formation of recombinant hybrids. *Curr. Biol.* 22 (15), 1444–1448. doi: 10.1016/j.cub.2012.05.056

Narasingarao, P., Podell, S., Ugalde, J. A., Brochier-Armanet, C., Emerson, J. B., Brocks, J. J., et al. (2012). *De novo* metagenomic assembly reveals abundant novel major lineage of archaea in hypersaline microbial communities. *ISME J.* 6 (1), 81–93. doi: 10.1038/ismej.2011.78

Papke, R. T., Koenig, J. E., Rodríguez-Valera, F., and Doolittle, W. F. (2004). Frequent recombination in a saltern population of *Halorubrum*. *Science* 306 (5703), 1928–1929. doi: 10.1126/science.1103289

Pontefract, A., Zhu, T. F., Walker, V. K., Hepburn, H., Lui, C., Zuber, M. T., et al. (2017). Microbial diversity in a hypersaline sulfate lake: A terrestrial analog of ancient mars. *Front. Microbiol.* 8. doi: 10.3389/fmicb.2017.01819

Rognes, T., Flouri, T., Nichols, B., Quince, C., and Mahé, F. (2016). VSEARCH: A versatile open source tool for metagenomics. *PeerJ* 4, e2584. doi: 10.7717/peerj.2584

Saccò, M., White, N. E., Harrod, C., Salazar, G., Aguilar, P., Cubillos, C. F., et al. (2021). Salt to conserve: a review on the ecology and preservation of hypersaline ecosystems. *Biol. Rev. Camb. Philos. Soc.* 96 (6), 2828–2850. doi: 10.1111/brv.12780

Saitou, N., and Nei, M. (1987). The neighbor-joining method: a new method for reconstructing phylogenetic trees. *Mol. Biol. Evol.* 4 (4), 406–425. doi: 10.1093/oxfordjournals.molbev.a040454

Sasser, M. (1990). Identification of bacteria by gas chromatography of cellular fatty acids. *USFCC Newsl* 20, 1–6.

Shu, W.-S., and Huang, L.-N. (2021). Microbial diversity in extreme environments. *Nat. Rev. Microbiol.* 20 (4), 219–235. doi: 10.1038/s41579-021-00648-y

Siguier, P., Gourbeyre, E., and Chandler, M. (2014). Bacterial insertion sequences: their genomic impact and diversity. *FEMS Microbiol. Rev.* 38 (5), 865–891. doi: 10.1111/1574-6976.12067

Siguier, P., Perochon, J., Lestrade, L., Mahillon, J., and Chandler, M. (2006). ISfinder: the reference centre for bacterial insertion sequences. *Nucleic Acids Res.* 34 (Database issue), D32–D36. doi: 10.1093/nar/gkj014

Smibert, R. M., and Krieg, N. R. (1994). *Phenotypic characterization* (Washington DC: Society for Microbiology).

Song, T., Liang, Q., Du, Z., Wang, X., Chen, G., Du, Z., et al. (2022). Salinity gradient controls microbial community structure and assembly in coastal solar salterns. *Genes* 13 (2), 385. doi: 10.3390/genes13020385

Tatusova, T., DiCuccio, M., Badretdin, A., Chetvernin, V., Nawrocki, E. P., Zaslavsky, L., et al. (2016). NCBI prokaryotic genome annotation pipeline. *Nucleic Acids Res.* 44 (14), 6614–6624. doi: 10.1093/nar/gkw569

Thompson, J. D., Gibson, T. J., Plewniak, F., Jeanmougin, F., and Higgins, D. G. (1997). The CLUSTAL_X windows interface: flexible strategies for multiple sequence alignment aided by quality analysis tools. *Nucleic Acids Res.* 25 (24), 4876–4882. doi: 10.1093/nar/25.24.4876

Ventosa, A., de la Haba, R. R., Sánchez-Porro, C., and Papke, R. T. (2015). Microbial diversity of hypersaline environments: a metagenomic approach. *Curr. Opin. Microbiol.* 25, 80–87. doi: 10.1016/j.mib.2015.05.002

Xue, Q., Zhao, D., Zhang, S., Zhou, H., Zuo, Z., Zhou, J., et al. (2021). Highly integrated adaptive mechanisms in *Spiribacter halalkaliphilus*, a bacterium abundant in Chinese soda-saline lakes. *Environ. Microbiol.* 23 (11), 6463–6482. doi: 10.1111/1462-2920.15794

Yoon, S.-H., Ha, S.-M., Kwon, S., Lim, J., Kim, Y., Seo, H., et al. (2017a). Introducing EzBioCloud: a taxonomically united database of 16S rRNA gene sequences and whole-genome assemblies. *Int. J. Syst. evol. Microbiol.* 67 (5), 1613–1617. doi: 10.1099/ijsem.0.001755

Yoon, S. H., Ha, S. M., Lim, J., Kwon, S., and Chun, J. (2017b). A large-scale evaluation of algorithms to calculate average nucleotide identity. *Antonie Van Leeuwenhoek* 110 (10), 1281–1286. doi: 10.1007/s10482-017-0844-4

Zhang, H., Yohe, T., Huang, L., Entwistle, S., Wu, P., Yang, Z., et al. (2018). dbCAN2: A meta server for automated carbohydrate-active enzyme annotation. *Nucleic Acids Res.* 46 (W1), W95–W101. doi: 10.1093/nar/gky418

Zhao, Y., Wu, J., Yang, J., Sun, S., Xiao, J., and Yu, J. (2012). PGAP: Pan-genomes analysis pipeline. *Bioinf. (Oxford England)* 28 (3), 416–418. doi: 10.1093/bioinformatics/btr655

Zhao, D., Zhang, S., Xue, Q., Chen, J., Zhou, J., Cheng, F., et al. (2020). Abundant taxa and favorable pathways in the microbiome of soda-saline lakes in inner mongolia. *Front. Microbiol.* 11. doi: 10.3389/fmicb.2020.01740

frontiers | Frontiers in Marine Science

TYPE Original Research
PUBLISHED 17 January 2023
DOI 10.3389/fmars.2023.1105929

OPEN ACCESS

EDITED BY
Xue-Wei Xu,
Ministry of Natural Resources, China

REVIEWED BY
Satya P. Singh,
Saurashtra University, India
Rafael Montalvo,
University of Puerto Rico at Mayagüez, Puerto Rico

*CORRESPONDENCE
Heng-Lin Cui
cuihenglin@ujs.edu.cn

†These authors have contributed equally to this work

SPECIALTY SECTION
This article was submitted to Aquatic Microbiology, a section of the journal Frontiers in Marine Science

RECEIVED 23 November 2022
ACCEPTED 02 January 2023
PUBLISHED 17 January 2023

CITATION
Sun Y-P, Wang B-B, Wu Z-P, Zheng X-W, Hou J and Cui H-L (2023) *Halorarius litoreus* gen. nov., sp. nov., *Halorarius halobius* sp. nov., *Haloglomus halophilum* sp. nov., *Haloglomus salinum* sp. nov., and *Natronomonas marina* sp. nov., extremely halophilic archaea isolated from tidal flat and marine solar salt.
Front. Mar. Sci. 10:1105929.
doi: 10.3389/fmars.2023.1105929

Halorarius litoreus gen. nov., sp. nov., *Halorarius halobius* sp. nov., *Haloglomus halophilum* sp. nov., *Haloglomus salinum* sp. nov., and *Natronomonas marina* sp. nov., extremely halophilic archaea isolated from tidal flat and marine solar salt

Ya-Ping Sun†, Bei-Bei Wang†, Zhang-Ping Wu, Xi-Wen Zheng, Jing Hou and Heng-Lin Cui*

School of Food and Biological Engineering, Jiangsu University, Zhenjiang, China

Five novel halophilic archaeal strains, named BND22^T, ZY10^T, ZY41^T, ZY58^T, and ZY43^T, were isolated from the coastal saline sediment of the intertidal zone located in Qingdao and the natural sea salt produced from Huanghua marine solar saltern, PRChina. These five strains demonstrated the typical morphology and growth characteristics of haloarchaea. The comparison of 16S rRNA gene revealed that strain BDN22^T was associated with *Salinirubellus salinus* ZS-35-S2^T (95.2% similarity), strain ZY10^T was related to *Halosegnis rubeus* F17-44^T (95.1% similarity), both strains ZY41^T and ZY58^T were closely related to *Haloglomus irregulare* F16-60^T (98.1% and 98.2% similarities, respectively), and strain ZY43^T was close to *Natronomonas salina* YPL13^T (98.0% similarity). In addition to the 16S rRNA gene, the *rpoB'* gene is undoubtedly another important molecular marker for the identification of halophilic archaea, and concatenated-conserved-protein phylogeny was widely used in archaeal classification in recent years. Phylogenetic and phylogenomic analyses based on *rpoB'* genes and 122 concatenated archaeal protein genes showed that these haloarchaea construct three different clades and gathered together with the current members of *Haloarculaceae*. Strains BND22^T and ZY10^T formed two distinct clades separated from *Salinirubellus salinus* ZS-35-S2^T and *Halosegnis* members, strains ZY41^T and ZY58^T clustered with *Haloglomus irregulare* F16-60^T, and strain ZY43^T gathered with the current members of *Natronomonas*. The ANI, DDH, and AAI values of these five strains against phylogenetic neighbours were no more than 91%, 45%, and 92%, respectively, far below the cut-off values for species delineation, supporting their placements in new taxa. Based on the phenotypic, chemotaxonomic, phylogenetic, and phylogenomic properties, these five strains represent five novel taxa of the family *Haloarculaceae*, *Halorarius litoreus* gen. nov., sp. nov. (type strain BND22^T = CGMCC 1.18780^T = JCM 34966^T), *Halorarius halobius* sp. nov. (type strain ZY10^T = CGMCC 1.17475^T = JCM 34319^T), *Haloglomus halophilum* sp. nov. (type strain ZY41^T = CGMCC 1.17030^T = JCM

34161^T), *Haloglomus salinum* sp. nov. (type strain ZY58^T = CGMCC 1.17216^T = JCM 34163^T), and *Natronomonas marina* sp. nov. (type strain ZY43^T = CGMCC 1.17202^T = JCM 34162^T). This is the first report of description of a novel haloarchaeon isolated from a marine intertidal zone.

KEYWORDS

Halorarius, Haloglomus, Hatronomonas, halophilic archaea, tidal flat, marine solar salt

Introduction

Halophilic archaea of class *Halobacteria*, belonging to phylum *Euryarchaeota* of domain *Archaea*, flourish in different hypersaline habitats, including salt lakes, marine solar salterns, salted brown algae, and coarse sea salt (Cui and Dyall-Smith, 2021; Han and Cui, 2020; Wang et al., 2022). Currently, there are 73 genera and 318 species with validly published names assigned in the class *Halobacteria* (List of Prokaryotic names with Standing in Nomenclature, https://lpsn.dsmz.de/class/halobacteria). None of these *Halobacteria* members was isolated from the marine intertidal zone. In the previous surveys on the halophilic archaeal diversity of coastal beaches located in Shandong and coarse sea salt produced from the coastal solar saltern of Hebei, five novel halophilic archaeal strains were isolated and purified. Strains BND22^T and ZY10^T were related to each other, then to *Salinirubellus salinus* ZS-35-S2^T and *Halosegnis* members, strains ZY41^T and ZY58^T were close to *Haloglomus irregulare* F16-60^T, and strain ZY43^T was found to be a member of genus *Natronomonas*, according to 16S rRNA gene comparison.

The genera *Haloglomus*, *Halosegnis*, *Natronomonas*, and *Salinirubellus* are four phylogenetically-related groups within the order *Halobacteriales*. The genus *Haloglomus* was established by Durán-Viseras in 2020, and only contained one species *Haloglomus irregulare* F16-60^T which was cultivated from the brine of Isla Cristina saltern, Huelva, Spain (Durán-Viseras et al., 2020a). And based on the strains *Halosegnis longus* F12-1^T and *Halosegnis rubeus* F17-44^T, the genus *Halosegnis* was described in 2021 (Durán-Viseras et al., 2021). As one of the oldest and most famous halophilic archaeal genera, *Natronomonas* was established in 1997 and at present comprises six species: *Natronomonas pharaonis* (Kamekura et al., 1997), *Natronomonas moolapensis* (Burns et al., 2010), *Natronomonas gomsonensis* (Kim et al., 2013), *Natronomonas salsuginis* (Durán-Viseras et al., 2020b), *Natronomonas halophila* and *Natronomonas salina* (Yin et al., 2020). The genus *Salinirubellus* related to the above three genera was proposed based on a strain isolated from the sediment sample of a marine solar saltern in Zhejiang, PRChina (Hou et al., 2018). Most of these halophilic archaea cannot hydrolyze starch, gelatin, casein, and Tween 80, but can utilize simple sugars for aerobic growth. The polar lipid profiles of them were diverse, the members of *Halosegnis*, *Haloglomus*, and *Natronomonas* contained phosphatidylglycerol sulphate (PGS) but that of *Salinirubellus* did not, and *Halosegnis* members contained S-TGD-1 (sulfated galactosyl mannosyl glucosyl diether) in addition to S-DGD-1 (sulfated mannosyl glucosyl diether), the common glycolipid of these four genera. In this study, two novel species of a new genus, and three novel species of the genera *Haloglomus* and *Natronomonas* within the family *Haloarculaceae* are proposed to accommodate strains BND22^T, ZY10^T, ZY41^T, ZY58^T, and ZY43^T, respectively.

Materials and methods

Cultivation and isolation of pure haloarchaeal cultures

Strain BND22^T was cultivated from the coastal saline soil sample of the intertidal zone located in Qingdao, PRChina (36°12′36″ N, 120° 22′10″ E; elevation, 0 m) in 2019. The pH, salt concentration, and organic matter content of the saline soil were 7.9, 5.3 g/kg, and 1.3 g/kg, respectively. Strains ZY10^T, ZY41^T, ZY58^T, and ZY43^T were isolated from the natural sea salt produced from Huanghua marine solar saltern in Hebei, PRChina, in 2018. These samples were diluted with liquid NHM, spread on NHM agar plates, and incubated aerobically at 37°C for 30 days (Sun et al., 2022). Single colonies with a shade of red were selected and streaked on fresh NHM agar slants, and the pure colonies were formed after three-time repeated. For further use, the purified strains were preserved in liquid NHM with 15% (w/v) glycerol at -20°C. *Halobacterium salinarum* CGMCC 1.2367, *Haloglomus irregulare* JCM 33318^T, *Halosegnis longus* JCM 33319^T, *Natronomonas gomsonensis* KCTC 4088^T, *Natronomonas halophila* C90^T, *Natronomonas salina* YPL13^T, and *Salinirubellus salinus* ZS-35-S2^T were used as reference strains and routinely grown aerobically in NHM liquid medium.

Phylogenetic analysis

The genomic DNA of strains BND22^T, ZY10^T, ZY41^T, ZY58^T, and ZY43^T was prepared using a DNA extraction kit for bacteria (Jiangsu Cowin Biotech Co., Ltd.). The PCR amplification of the 16S rRNA genes and the *rpoB′* (RNA polymerase subunit B′) genes were carried out by two pairs of primers, 20F (5'-ATTCCGGTTGATCCTGCCGG-3') and 1452R (5'-AGGAGGTGATCCAGCCGCAG-3'), and HrpoB2 1420F and HrpoA 153R, respectively (Cui et al., 2009; Minegishi et al., 2010). The sequencing of purified PCR amplicons was performed by SinoGenoMax (Beijing). The 16S rRNA and *rpoB′* genes of related species of the *Haloarculaceae* were downloaded from the NCBI database. Phylogenetic trees were constructed with MEGA 6 (Tamura et al., 2013) based on three different algorithms, ML

(maximum-likelihood) (Felsenstein, 1981), MP (maximum-parsimony) (Fitch, 1971) and NJ (neighbor-joining) (Saitou and Nei, 1987). The calculation of pairwise sequence similarities of 16S rRNA and *rpoB′* gene between strains BND22^T, ZY10^T, ZY41^T, ZY58^T, ZY43^T, and related species was performed by using the online pairwise sequence alignment tool of EzBioCloud (Yoon et al., 2017).

Genome assembly, annotation, and comparative genomics

The PacBio Sequel platform was used to sequence the complete genomes of these five strains. CheckM was exploited for the evaluation of the quality of assembled genome sequences (Parks et al., 2015). The 122 conserved archaeal protein marker genes were extracted from the genomes of the isolated five strains and related halophilic archaea for phylogenomic analyses according to the protocol of GTDB (Parks et al., 2018). The sequences of these core orthologous genes were aligned using GTDB-Tk and trimmed by trimAL version 1.4.1 (Capella-Gutiérrez et al., 2009; Chaumeil et al., 2019). The ML phylogenomic tree was constructed based on a standard model by IQ-TREE (Nguyen et al., 2015), and *Natronobacterium gregoryi* SP2^T was selected as the outgroup.

The annotation of these genomes was performed by means of RAST Annotation Sever (Aziz et al., 2008). The metabolic pathways were figured out based on the KEGG database (Kanehisa et al., 2004). To explore the industrial applications of these halophilic archaea, the biotechnological potential of functional genes was identified following the methodology described previously (Sun et al., 2022). The online OrthoVenn was used to compare orthologous clusters (OCs) of related species and generate the Venn diagrams (Xu et al., 2019).

The whole genomic indexes, ANI (average nucleotide identity), DDH (DNA–DNA hybridization), and AAI (average amino acid identity) among strains BND22^T, ZY10^T, ZY41^T, ZY58^T, ZY43^T, and the related members were estimated by using JSpeciesWS online ANI calculator (https://jspecies.ribohost.com/jspeciesws/) (Richter et al., 2016), Genome-to-Genome Distance Calculator 3.0 (formula 2) (http://ggdc.dsmz.de/ggdc.php) (Meier-Kolthoff et al., 2013), and AAI calculator (http://enve-omics.ce.gatech.edu/aai/) (Luo et al., 2014), respectively.

Phenotypic characterization

For microscopical examination, these five isolates were grown in liquid NHM for 7–10 days. The cells of these haloarchaea were observed under a phase-contrast microscope (Eclipse Ci-L, Nikon). Gram staining was performed according to an improved technique developed by Dussault (Dussault, 1955). The pigmentation of the colonies was examined on NHM agar plates after aerobic incubation for 10–15 days at 37°C. The ranges of NaCl and $MgCl_2$ concentrations, temperature, and pH for growth were determined following the methodology described previously (Sun et al., 2022). The remaining phenotypic features of the five isolates and related members were based on the minimal criteria for the description of halophilic archaeal new taxa (Oren et al., 1997). Each test was carried out in triplicates.

Chemotaxonomic characterization

Polar lipids of strains BND22^T, ZY10^T, ZY41^T, ZY58^T, and ZY43^T were extracted with chloroform and methanol mixture, then precipitated by ten volumes of cold acetone after concentration. The polar lipid profiles of isolated halophilic archaea were analyzed by one-dimensional and two-dimensional thin-layer chromatography (TLC) (Cui et al., 2010). The phosphate stain reagent was prepared to detect phospholipids (Vaskovsky and Kostetsk, 1968). Glycolipids and phospholipids were shown with sulfuric acid-ethanol (1:2, v/v) followed by heating at 150 °C for 3 min. The polar lipids of these halophilic archaea were characterized by MALDI-TOF/MS (Xin et al., 2022).

Results and discussion

Phylogenetic analyses

Strains BND22^T, ZY10^T, ZY41^T, ZY58^T, and ZY43^T all had a single copy of the 16S rRNA gene (1,467 bp, 1,467 bp, 1,472 bp, 1,472 bp, and 1,466 bp, respectively). These sequences are identical to the same genes in their genomes. Based on the 16S rRNA gene similarity, the closest relatives of strains BND22^T, ZY10^T, ZY41^T, ZY58^T, and ZY43^T were *Salinirubellus salinus* ZS-35-S2^T (95.2%), *Halosegnis rubeus* F17-44^T (95.1%), *Haloglomus irregulare* F16-60^T (98.1%), *Haloglomus irregulare* F16-60^T (98.2%), *Natronomonas salina* YPL13^T (98.0%), respectively (Table S1). Except for 99.6% gene similarity between strains ZY41^T and ZY58^T, those among strains BND22^T, ZY10^T, and ZY43^T were 92.9–96.8%, less than 98.65%, the suggested threshold for separating different archaeal or bacterial species (Kim et al., 2014). The 16S rRNA gene phylogeny indicated that strains BND22^T and ZY10^T formed two distinct clades separated from *Salinirubellus salinus* ZS-35-S2^T and *Halosegnis* members, strains ZY41^T and ZY58^T clustered with *Haloglomus irregulare* F16-60^T, and strain ZY43^T gathered with the current members of *Natronomonas* (Figure 1A).

The full length of the *rpoB′* genes from strains BND22^T, ZY10^T, ZY41^T, ZY58^T, and ZY43^T were 1,827 bp. The gene similarities among these five strains were 84.9–95.2%, and they shared 81.1–91.7% sequence similarities with related members of the family *Haloarculaceae* (Table S2). Strains BND22^T, ZY10^T, ZY41^T, ZY58^T, and ZY43^T shared maximum sequence similarities with *Sala cibi* CBA1133^T (88.3%), *Halosegnis longus* F12-1^T (89.4%), *Haloglomus irregulare* F16-60^T (91.4%), *Haloglomus irregulare* F16-60^T (91.6%), *Natronomonas salina* YPL13^T (91.7%), respectively. The *rpoB'* gene phylogeny revealed that strains BND22^T and ZY10^T clustered together and separated from the genus *Halosegnis*, strains ZY41^T and ZY58^T formed a monophyletic branch closely clustered with *Haloglomus irregulare* F16-60^T, strain ZY43^T was a close relative of *Natronomonas salina* YPL13^T within *Natronomonas* (Figure 1B).

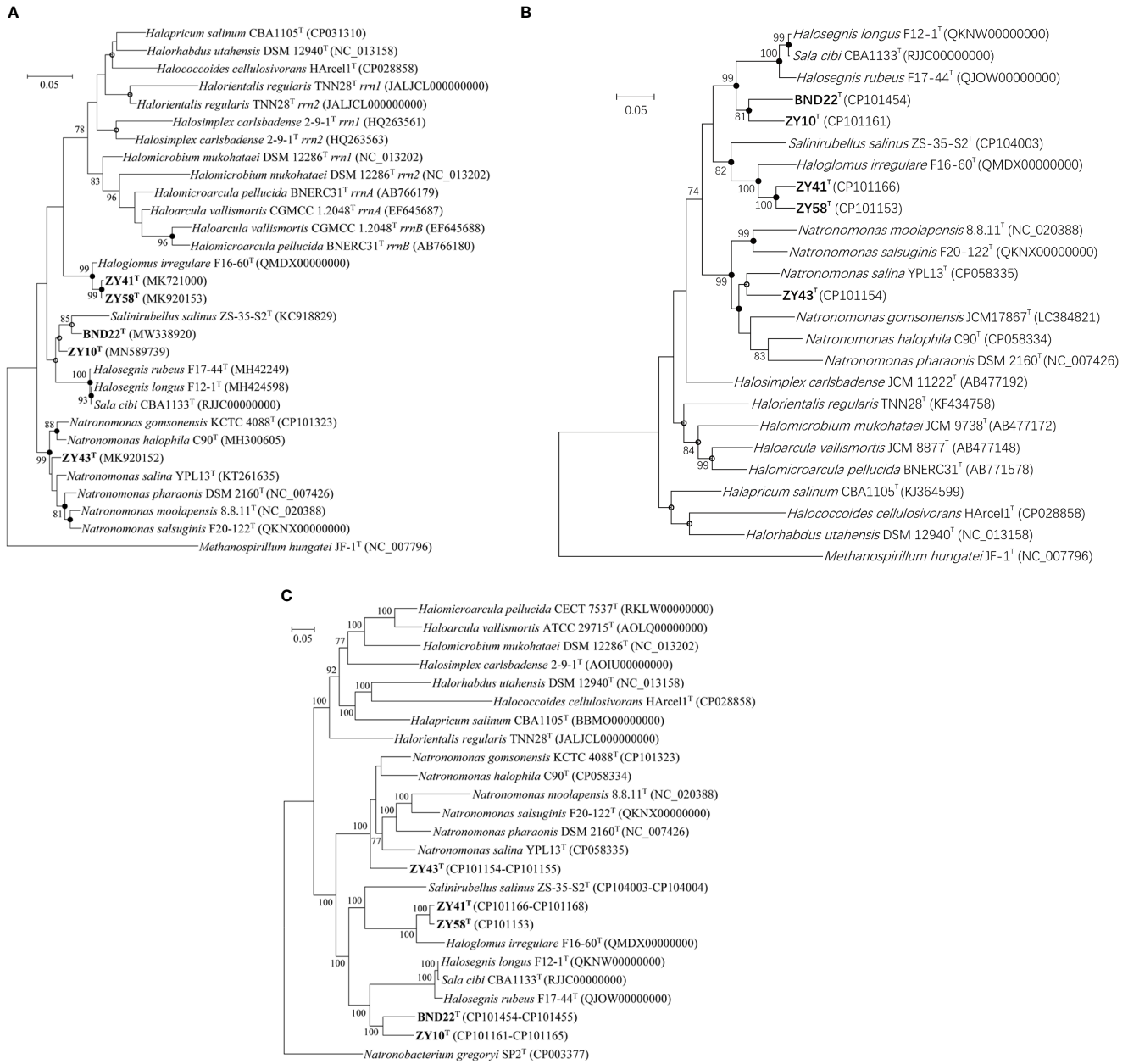

FIGURE 1
ML phylogenetic tree reconstructions based on 16S rRNA gene sequence **(A)**, *rpoB'* gene sequence **(B)** and 122 conserved archaeal protein marker genes **(C)**, showing the relationship among strains BND22^T, ZY10^T, ZY41^T, ZY58^T, ZY43^T and related species within *Haloarculaceae*. The numbers at the nodes represent bootstrap values of 1,000 replicates and support ≥ 70% bootstrap. Filled circles highlight branches that were supported by the neighbour-joining, maximum-likelihood and maximum-parsimony algorithms. Empty circles highlight branches that were supported by the maximum-likelihood and maximum-parsimony algorithms or the maximum-likelihood and neighbour-joining algorithms. The bar represents expected substitutions per nucleotide position.

Genomic features and biotechnological potential

The complete genomes of strains BND22^T, ZY10^T, ZY41^T, ZY58^T, and ZY43^T were *de novo* assembled in a total of 2, 5, 3, 1, and 2 contigs, respectively. The complete genome size of new strains ranged from 4.0 to 4.4 Mb, within those of the current *Haloarculaceae* members (2.6–5.1 Mb). These five strains had one ribosomal RNA operon in their genomes and had different numbers (47, 47, 45, 43, and 48, respectively) of tRNA genes. The DNA G+C content of strains BND22^T, ZY10^T, ZY41^T, ZY58^T, and ZY43^T are 66.6%, 66.8%, 67.9%, 68.5%, and 66.9%, respectively (Table S3). These values are higher than those of *Halosegnis* members (64.7–66.0 mol%) and *Haloglomus* (68.0 mol%), within the range of the genus *Natronomonas* (63.2–67.4 mol%), and less than that of *Salinirubellus salinus* ZS-35-S2^T (69.0 mol%). Other genomic features were detailed in Table S3.

The ML phylogenomic tree based on 122 concatenated archaeal protein genes indicated that strain BND22^T gathered with ZY10^T and distinctly separated from *Halosegnis* and *Sala*, strains ZY41^T and ZY58^T formed a tight clade with *Haloglomus irregulare* F16-60^T, and

strain ZY43^T tightly clustered with the current *Natronomonas* members (Figure 1C).

The ANI, AAI, and DDH values among these five strains and *Haloarculaceae* members were 70–91%, 56–92%, and 18–45% (Tables S4-S6), significantly below the cut-off values, 95–96% (ANI), 95% (AAI), and 70% (DDH), for species delineation (Goris et al., 2007; Richter and Rosselló-Móra, 2009; Luo et al., 2014). This suggested that strains BND22^T, ZY10^T, ZY41^T, ZY58^T, and ZY43^T represent five different species. The AAI values were proved to be useful for genera demarcation and a cut-off value (≤ 76%) was proposed to differentiate genera within the family *Natrialbaceae* (de la Haba et al., 2021); but the value was inappropriate to be used in grouping the current *Haloarculaceae* members. If the cut-off value was used to separate the genera within the family *Haloarculaceae*, the current six *Natronomonas* species should represent six different genera (Table S6). A cut-off value of < 69% is appropriate to distinguish genera within *Haloarculaceae* according to the AAI values and evolutionary relationships among the current members of this family. Thus, strains BND22^T and ZY10^T represent two novel species of a new genus, strains ZY41^T and ZY58^T two novel different species of *Haloglomus*, and strain ZY43^T a new species of *Natronomonas* based on the AAI cut-off (< 69%).

It must be noted that the ANI, AAI, and DDH values between *Halosegnis longus* F12-1^T and *Sala cibi* CBA1133^T described recently are 99%, 94%, and 98%, much more than the threshold values of the species boundary. This close relatedness was supported by the 16S rRNA, *rpoB'*, and 122 conserved archaeal protein marker genes -based phylogenies between *Halosegnis longus* F12-1^T and *Sala cibi* CBA1133^T (Figure 1). According to these results *Sala cibi* (Song et al., 2022) should be proposed as a later heterotypic synonym of *Halosegnis longus* (Durán-Viseras et al., 2021).

The subsystem category distribution of novel isolates was annotated by the RAST server (Figure S1). The amino acids and derivatives, and carbohydrates and protein metabolism were the richest RAST subsystems of these five isolates, indicating their possibility to metabolize diverse proteins and carbohydrates. Based on the KEGG database, strains BND22^T and ZY58^T, ZY41^T and ZY43^T contained the genes involved in both glycolysis and pyruvate oxidation pathways, respectively, corresponding to their capability to utilize glucose and pyruvate for growth. In contrast, the genes related to fructose utilization, casein, starch, or Tween 80 hydrolysis were not found in all these strains, which was confirmed by the results of phenotypic tests. Additionally, none of the four key enzymes involved in complete denitrification, NarG (nitrate reductase), NirK (copper-containing nitrite reductase), Nor (nitric oxide reductase), and Nos (nitrous-oxide reductase), was found in the genomes of these five strains, this confirmed by their inability to produce nitrogen growing with nitrate anaerobically.

Total of 3,788 orthologous clusters, 566 core clusters, 3,077 accessory clusters, and 145 unique clusters were found in the genomes of strains BND22^T, ZY10^T, *Salinirubellus salinus* ZS-35-S2^T, *Halosegnis longus* F12-1^T, and *Halosegnis rubeus* F17-44^T. The isolates BND22^T and ZY10^T contained 62 and 61 unique clusters, while the related members only contained 9, 9, and 4 unique clusters, respectively (Figure S2A). Strains ZY41^T, ZY58^T, and *Haloglomus irregulare* F16-60^T had 3,850 OCs, including 2,427 core OCs, 1,320 accessory OCs and 103 unique clusters, and contained 22, 13, and 68 unique clusters, respectively (Figure S2B). Strain ZY43^T, *Natronomonas moolapensis* 8.8.11^T, *Natronomonas pharaonis* DSM 2160^T, *Natronomonas salina* YPL13^T and *Natronomonas salsuginis* F20-122^T had 3,472 clusters, including 1,427 core OCs, 1,851 accessory OCs and 194 unique clusters. These strains contained 63, 24, 16, 70, and 21 unique clusters, respectively (Figure S2C). The patterns of shared and unique OCs differentiated these novel strains from their relatives.

Many previous studies reported that haloarchaea could produce valuable products of biotechnological aspects, such as haloenzymes, bacteriorhodopsin, biodegradable polyhydroxyalkanoates (PHAs), and carotenoids (Han et al., 2010; Amoozegar et al., 2017; Ashwini et al., 2017; Serrano et al., 2022). Strains ZY10^T, ZY41^T, ZY58^T, and ZY43^T possessed bacteriorhodopsin protein genes, indicating their capacity for light-mediated ATP synthesis. Strain BND22^T contained the gene cluster encoding for PHA synthesis regulatory protein (PhaR), PHA granule binding protein (PhaP), and type IIIA PHA synthase (PhaE and PhaC subunits), and strain ZY41^T contained the gene cluster encoding for acetoacetyl CoA reductase (PhaB), PhaC, PhaE and PhaR (Figure S3), indicating the probable synthesis of PHAs by the new isolates. Additionally, the genes encoded the enzymes involved in the production of β-carotene, phytoene synthase (CrtB), phytoene desaturase (CrtI), and lycopene cyclase (CrtY), were detected in strains ZY41^T and ZY58^T (Serrano et al., 2022). Moreover, one β-carotene monooxygenase (Brp) was detected in the vicinity of the *crtY* gene, suggesting the possibility of strain ZY41^T to produce retinal from β-carotene (Figure S4). These results indicate that these novel halophilic archaeal strains have much potential in biotechnological applications.

Phenotypic characteristics

Cells of strains BND22^T, ZY10^T, ZY41^T, ZY58^T, and ZY43^T were motile and Gram-stain-negative. Except for strains BND22^T and ZY58^T were pleomorphic, while other strains were coccoid (Figure S5). The colonies of all strains were red and their cells lysed in distilled water. The growth of strains BND22^T, ZY10^T, ZY41^T, ZY58^T, and ZY43^T occurred in NHM with NaCl concentrations of 1.7–4.8 M, 3.1–5.1 M, 2.1–4.8 M, 2.6–4.3 M, and 2.1–4.8 M, respectively; the five strains grew best at 3.1–4.8 M NaCl. The optimum magnesium concentration varied between 0.05 and 0.7 M, even if magnesium was not necessary for their growth. The growth temperature ranges for these five strains were 20–55 °C, 30–50 °C, 25–60 °C, 25–55 °C, and 30–60 °C, respectively, with optima between 35 and 40°C. These five strains are mainly neutrophilic with pH optima at 6.5–7.5. These strains could not grow with arginine or DMSO anaerobically. Reduction of nitrate to nitrite was found in strains BND22^T, ZY10^T, ZY41^T, and ZY43^T but not in strain ZY58^T. Indole and H_2S were not produced by these strains, and none of the casein, gelatin, starch, or Tween 80 was found to be hydrolyzed. Of the 19 antibiotics tested, only bacitracin (0.04 IU per disc), nitrofurantoin (300 μg), novobiocin (30 μg per disc), nystatin (100 μg), rifampin (5 μg), and trimethoprim (5) could inhibit growth. The remained antibiotics, ampicillin (10 μg), chloramphenicol (30 μg), ciprofloxacin (5 μg), erythromycin (15 μg), gentamicin (10 μg), kanamycin (30 μg), nalidixic acid (30 μg), neomycin (30 μg), norfloxacin (10 μg), penicillin G (10 IU), streptomycin (10 μg), tetracycline (30 μg), or vancomycin (30 μg), were not found to be effective. The distinct phenotypic

characteristics differentiating isolates BND22^T and ZY10^T from the related species of the family *Haloarculaceae* (*Salinirubellus salinus* ZS-35-S2^T, *Halosegnis longus* JCM 33317^T, *Halosegnis rubeus* JCM 33319^T, and *Haloglomus irregulare* JCM 33318^T) were optimum NaCl, utilization of specific carbon sources, and presence of PGS. Strains ZY41^T and ZY58^T could be differentiated from *Haloglomus irregulare* JCM 33318^T based on cell motility, gelatin hydrolysis and presence of PGS. The difference between strain ZY43^T and the current members of the *Natronomonas* included H_2S formation, cell morphology, catalase, and oxidase activity (Tables 1, 2) (Kamekura et al., 1997; Burns et al., 2010; Kim et al., 2013; Durán-Viseras et al., 2020a; Durán-Viseras et al., 2020b; Yin et al., 2020; Durán-Viseras et al., 2021).

Chemotaxonomic characteristics

The common phospholipids, phosphatidylglycerol (PG) and phosphatidylglycerol phosphate methyl ester (PGP-Me), were detected in strains BND22^T, ZY10^T, ZY41^T, and ZY58^T. It was remarkable that the absence of phosphatidylglycerol sulfate (PGS) in these four strains compared with the *Halosegnis* and *Haloglomus* members. The phospholipid profile of strain ZY43^T was PG, PGP-Me, and PGS, similar to that of the *Natronomonas* members (Figure S6). Diverse glycolipids were detected in these five strains, three glycolipids (GL1, GL-PL1, and GL-PL2) in strain BND22^T, two glycolipids (GL1, GL2) in strain ZY10^T, one glycolipid (GL1) in strains ZY41^T and ZY58^T, and two different glycolipids (GL01, GL02) in strain ZY43^T. The TLC mobilities of GL1, GL2 (GL-PL1), and GL02 were similar to those of sulfated mannosyl glucosyl diether (S-DGD-1), mannosyl glucosyl diether (DGD-1), and sulfated galactosyl mannosyl glucosyl diether (S-TGD-1), respectively, based on one-dimensional TLC (Figure S6).

The MALDI-TOF/MS patterns of the polar lipids of strains BND22^T, ZY10^T, ZY41^T, ZY58^T, and ZY43^T were obtained based on the mode of negative ion (Figure S7). The signals at m/z 731.6, 805.7, 875.7, 885.6, 899.6, 955.7, and 969.6 represented PA, PG, PG ($C_{20}C_{25}$), PGS, PGP-Me, PGS ($C_{20}C_{25}$), and PGP-Me ($C_{20}C_{25}$), respectively. Except for strains ZY41^T and ZY58^T, the ion of m/z 991.7 appearing in others represented DGD-1. Strains BND22^T, ZY10^T, ZY41^T, and ZY58^T showed S-DGD-1 signals at m/z 1055.7, 1071.7, and 1125.7. The ion at m/z 1217.7 detected in strain ZY43^T corresponded to S-TGD-1. In addition, several glycosyl-cardiolipins, DGD-PA, S-DGD-PA, and S-DGD-PA (+Na) were detected and judged by the signals of m/z 1690.4, 1770.3, and 1792.3, respectively (Lobasso et al., 2015). These results were mostly in accordance with those detected by TLC.

Taxonomic conclusions

The polyphasic and genome-based classification indicated that strains BND22^T (= CGMCC 1.18780^T = JCM 34966^T) and ZY10^T (= CGMCC 1.17475^T = JCM 34319^T), represent two different new species of a novel genus within *Haloarculaceae*, *Halorarius litoreus* gen. nov., sp. nov. *Halorarius halobius* sp. nov.; strains ZY41^T (= CGMCC 1.17030^T = JCM 34161^T) and ZY58^T (= CGMCC 1.17216^T = JCM 34163^T) represent two different new species of *Haloglomus*, *Haloglomus halophilum* sp. nov. and *Haloglomus salinum* sp. nov.; and strain ZY43^T (= CGMCC 1.17202^T = JCM 34162^T) represents a novel species of *Natronomonas*, *Natronomonas marina* sp. nov.

TABLE 1 Differential characteristics of strains BND22^T, ZY10^T, ZY41^T, ZY58^T and their closely related species within the family *Haloarculaceae*.

Characteristics	1	2	3	4	5	6	7	8
Cell morphology	pleomorphic	coccoid	coccoid	pleomorphic	pleomorphic	rod	rod	pleomorphic
Motility	+	+	+	+	+	–	–	–
NaCl growth range (M)	1.7–4.8	3.1–5.1	2.1–4.8	2.6–4.3	1.4–4.8	2.6–4.3	2.6–5.1	3.4–6.0
Optimum growth NaCl (M)	3.4	4.8	3.1	3.1	2.1	4.3	4.3	5.1
Temperature growth range (°C)	20–55	30–50	25–60	25–55	25–50	25–45	30–50	30–45
Optimum growth temperature (°C)	35	37	40	37	37	37	37	37
pH range for growth	6.5–8.0	7.0–8.5	6.0–8.5	5.5–8.0	5.0–9.5	6.0–8.5	6.5–8.5	6.5–9.0
Optimum growth pH	7.5	7.5	7.5	7.0	7.5	7.5	7.5	7.5
Gelatin hydrolysis	–	–	–	–	–	–	–	+
Reduction of nitrate to nitrite	+	+	+	–	+	–	–	+
Oxidase	–	+	–	–	–	–	–	–
Utilization as sole carbon source:								
Fructose	–	–	–	–	–	+	–	–
Glycerol	–	+	+	–	+	–	+	–
Presence of PGS	–	–	–	–	–	+	+	+

Taxa: 1, strain BND22^T; 2, strain ZY10^T; 3, strain ZY41^T; 4, strain ZY58^T; 5, *Salinirubellus salinus* ZS-35-S2^T; 6, *Halosegnis longus* JCM 33317^T; 7, *Halosegnis rubeus* JCM 33319^T; 8, *Haloglomus irregulare* JCM 33318^T. +, Positive; –, negative.

TABLE 2 Differential characteristics of strain ZY43^T and *Natronomonas* species.

Characteristics	1	2	3	4	5	6	7
Cell morphology	coccoid	pleomorphic	pleomorphic	rod	pleomorphic	coccoid	coccoid
NaCl range (M) for growth	2.1–4.8	0.9–4.8	0.9–4.8	2.1–5.1	2.4–6.2	3.1–5.1	1.7–5.1
Optimum growth NaCl (M)	3.1	4.3	3.4	3.5	3.1–3.4	4.1	4.3
Temperature range (°C) for growth	30–60	30–60	25–50	20–55	25–45	20-45	25–50
Optimum growth temperature (°C)	40	40	37	45	45	40	37
pH range for growth	5.5–9.0	6.5–9.5	5.0–8.0	8.0–11.0	5.5–8.5	5.5–8.0	6.0–9.5
Optimum growth pH	6.5	8.0	6.5	8.5–9.0	7.0–7.5	7.0	8.0
Gelatin hydrolysis	–	–	–	+	–	–	–
Reduction of nitrate to nitrite	+	+	+	–	+	–	+
Catalase	+	–	–	+	–	+	–
Oxidase	–	–	+	+	–	+	–
Utilization as sole carbon source:							
Fructose	–	–	–	–	–	+	–
Glycerol	+	–	–	+	+	+	–
L-lysine	+	–	–	+	–	–	+
Pyruvate	+	+	+	+	+	+	–
H_2S formation	–	–	–	+	–	–	–

Taxa: 1, ZY43^T; 2, *Natronomonas halophila* C90^T; 3, *Natronomonas salina* YPL13^T; 4, *Natronomonas pharaonis* CGMCC 1.1965^T; 5, *Natronomonas moolapensis* JCM 14361^T; 6, *Natronomonas gomsonensis* KCTC 4088^T; 7, *Natronomonas salsuginis* JCM 33320^T. +, Positive; –, negative.

We propose *Sala cibi* Song et al., 2022 as a later heterotypic synonym of *Halosegnis longus* (Durán-Viseras et al., 2021). (type strain F12-1^T = CECT 9685^T = JCM 33317^T; another reference strain of this species, CBA1133 = KACC 22148 = JCM 34265).

Description of *Halorarius* gen. nov.

Halorarius (Hal.o.ra'ri.us. Gr. masc. n. *hals halos*, salt; L. masc. adj. *orarius*, belonging to the seashore; N.L. masc. n. *Halorarius* salt microorganism isolated from the seashore).

Cells are Gram-stain-negative, motile, pleomorphic and coccoid under optimal growth conditions. Cells are found to be lysed in distilled water. Colonies on NHM agar plate are red, moist and round. Growth was found at 20–55°C, 1.7–5.1 M NaCl, 0–1.0 M $MgCl_2$ and pH 6.5–8.5. The activity of catalase was positive while that of oxidase was negative. Some sugars can be utilized for growth and with the production of acids. The cultures contain PA, PG, PGP-Me, S-DGD-1, and DGD-1. The type species is *Halorarius litoreus*. Recommended three-letter abbreviation: *Hor*.

Description of *Halorarius litoreus* sp. nov.

Halorarius litoreus (li.to're.us. L. masc. adj. *litoreus*, of or belonging to the seashore).

The cells of type strain are pleomorphic (1.0–1.2×1.0–3.0 μm), motile, and Gram-negative. Colonies are red and circular, about 5 mm in diameter following incubation for 14 days at 37°C. The type strain could grow in NHM with NaCl concentrations of 1.7–4.8 M and grew best at 3.4 M NaCl. The optimum magnesium concentration was 0.03 M, even if magnesium was not necessary for growth. The growth temperature range for the type strain was 20–55 °C, with optimum at 35°C. The type strain is neutrophilic with pH optima at 7.5. The type strain can grow anaerobically with nitrate but not with arginine or DMSO. Reduction of nitrate to nitrite was found but gas was not produced. Diverse substrates, $_D$-glucose, sucrose, $_D$-mannitol, $_D$-sorbitol, acetate, succinate, $_L$-aspartate, $_L$-glutamate, $_L$-lysine and $_L$-ornithine, can be utilized for growth, while $_D$-fructose, $_D$-galactose, lactose, maltose, $_D$-mannose, $_D$-ribose, $_L$-sorbose, $_D$-xylose, glycerol, citrate, fumarate, $_{DL}$-lactate, $_L$-malate, pyruvate, $_L$-arginine, glycine or $_L$-alanine do not support growth. The catalase test is positive while the oxidase is negative. Indole and H_2S formation are not detected. None of casein, gelatin, starch or Tween 80 was found to be hydrolyzed. The type strain contains PA, PG, PGP-Me, DGD-1 (DGD-PA), and S-DGD-1 (S-DGD-PA).

The type strain, BND22^T (= CGMCC 1.18780^T = JCM 34966^T), was isolated from the coastal saline soil sample of the intertidal zone located in Qingdao, PRChina. The DNA G+C content of the type strain is 66.6% (genome). The GenBank/EMBL/DDBJ accession numbers for the 16S rRNA gene and genome of strain BND22^T are MW338920 and CP101454–CP101455, respectively.

Description of *Halorarius halobius* sp. nov.

Halorarius halobius (ha.lo'bi.us. Gr. masc. n. *hals*, halos, salt; Gr. masc. n. *bios*, life; N.L. masc. adj. *halobius*, growing in salt).

The cells of type strain are coccoid (0.5–2.0 μm), motile, and Gram-negative. Colonies are red and circular, about 0.5 mm in diameter following incubation for 14 days at 37°C. The type strain could grow in NHM with NaCl concentrations of 3.1–5.1 M and grew best at 4.8 M NaCl. The optimum magnesium concentration was 0.5 M, even if magnesium was not necessary for growth. The growth temperature range for the type strain was 30–50 °C, with optimum at 37°C. The type strain is neutrophilic with pH optima at 7.5. The type strain can grow anaerobically with nitrate but not with arginine or DMSO. Reduction of nitrate to nitrite was found but gas was not produced. Diverse substrates, $_{D}$-mannose, sucrose, glycerol, $_{D}$-mannitol, $_{D}$-sorbitol, fumarate, $_{DL}$-lactate, $_{L}$-malate, pyruvate, succinate, glycine, $_{L}$-aspartate, $_{L}$-glutamate and $_{L}$-lysine, can be utilized for growth, while $_{D}$-fructose, $_{D}$-galactose, $_{D}$-glucose, lactose, maltose, $_{D}$-ribose, $_{L}$-sorbose, $_{D}$-xylose, acetate, citrate, $_{L}$-arginine, $_{L}$-alanine or $_{L}$-ornithine do not support growth. Positive for catalase and oxidase activity. Indole and H_2S formation are not detected. None of casein, gelatin, starch or Tween 80 was found to be hydrolyzed. The type strain contains PG, PGP-Me, DGD-1 and S-DGD-1.

The type strain, ZY10^T (= CGMCC 1.17475^T = JCM 34319^T), was isolated from the natural sea salt produced from Huanghua marine solar saltern in Hebei, PRChina. The DNA G+C content of the type strain is 66.8% (genome). The GenBank/EMBL/DDBJ accession numbers for the 16S rRNA gene and whole genome of strain ZY10^T are MN589739 and CP101161–CP101165, respectively.

Description of *Haloglomus halophilum* sp. nov.

Haloglomus halophilum (ha.lo'phi.lum. Gr. masc. n. *hals, halos* salt; Gr. masc. adj. *philos* loving; N.L. neut. adj. *halophilum* salt-loving, concerning the requirement for salt).

The cells of type strain are coccoid (0.5–2.0 μm), motile, and Gram-negative. Colonies are red and circular, about 0.5 mm in diameter following incubation for 14 days at 37°C. The type strain could grow in NHM with NaCl concentrations of 2.1–4.8 M and grew best at 3.1 M NaCl. The optimum magnesium concentration was 0.7 M, even if magnesium was not necessary for growth. The growth temperature range for the type strain was 25–60 °C, with optimum at 40°C. The type strain is neutrophilic with pH optima at 7.5. The type strain cannot grow anaerobically with arginine, DMSO, or nitrate. Reduction of nitrate to nitrite was found but gas was not produced. Diverse substrates, glycerol, $_{D}$-mannitol, $_{D}$-sorbitol, acetate, $_{DL}$-lactate, pyruvate, succinate, $_{L}$-ornithine and $_{L}$-lysine, can be utilized for growth, while $_{D}$-fructose, $_{D}$-galactose, $_{D}$-glucose, lactose, maltose, $_{D}$-mannose, $_{D}$-ribose, $_{L}$-sorbose, sucrose, $_{D}$-xylose, citrate, fumarate, $_{L}$-alanine, $_{L}$-arginine, $_{L}$-aspartate, $_{L}$-glutamate, glycine, or $_{L}$-malate do not support growth. Catalase positive and oxidase negative. Indole and H_2S are not produced. None of casein, gelatin, starch or Tween 80 was found to be hydrolyzed. The type strain contains PG, PGP-Me, and S-DGD-1.

The type strain, ZY41^T (= CGMCC 1.17030^T = JCM 34161^T), was isolated from the natural sea salt produced from Huanghua marine solar saltern in Hebei, PRChina. The DNA G+C content of the type strain is 67.9% (genome). The GenBank/EMBL/DDBJ accession numbers for the 16S rRNA gene and whole genome of strain ZY41^T are MK721000 and CP101166–CP101168, respectively.

Description of *Haloglomus salinum* sp. nov.

Haloglomus salinum (sa.li'num. N.L. neut. adj. *salinum* belonging to salt works)

The cells of type strain are pleomorphic (0.8–1.0×1.0–2.0 μm), motile, and Gram-negative. Colonies are red and circular, about 0.5 mm in diameter following incubation for 14 days at 37°C. The type strain could grow in NHM with NaCl concentrations of 2.6–4.3 M and grew best at 3.1 M NaCl. The optimum magnesium concentration was 0.03 M, even if magnesium was not necessary for growth. The growth temperature range for the type strain was 25–55 °C, with optimum at 37°C. The type strain is neutrophilic with pH optima at 7.0. The type strain cannot grow anaerobically with arginine, DMSO, or nitrate. Reduction of nitrate to nitrite was not found and gas was not produced. Diverse substrates, $_{D}$-galactose, $_{D}$-glucose, $_{D}$-mannose, sucrose, acetate, pyruvate, $_{DL}$-lactate, can be utilized for growth, while $_{D}$-fructose, lactose, maltose, $_{D}$-ribose, $_{L}$-sorbose, $_{D}$-xylose, glycerol, $_{D}$-mannitol, $_{D}$-sorbitol, citrate, fumarate, $_{L}$-malate, succinate, $_{L}$-aspartate, $_{L}$-alanine, $_{L}$-arginine, $_{L}$-glutamate, glycine, $_{L}$-lysine, or $_{L}$-ornithine do not support growth. Catalase positive and oxidase negative. Indole and H_2S production are not detected. None of casein, gelatin, starch or Tween 80 was found to be hydrolyzed. The type strain contains PG, PGP-Me, and S-DGD-1.

The type strain, ZY58^T (= CGMCC 1.17216^T = JCM 34163^T), was isolated from the natural sea salt produced from Huanghua marine solar saltern in Hebei, PRChina. The DNA G+C content of the type strain is 68.5% (genome). The GenBank/EMBL/DDBJ accession numbers for the 16S rRNA gene and whole genome of strain ZY58^T are MK920153 and CP101153, respectively.

Description of *Natronomonas marina* sp. nov.

Natronomonas marina (ma.ri'na. L. fem. adj. *marina* of the marine).

The cells of type strain are coccoid (0.5–2.0 μm), motile, and Gram-negative. Colonies are red and circular, about 0.5 mm in diameter following incubation for 14 days at 37°C. The type strain could grow in NHM with NaCl concentrations of 2.1–4.8 M and grew best at 3.1 M NaCl. The optimum magnesium concentration was 0.05 M, even if magnesium was not necessary for growth. The growth temperature range for the type strain was 30–60 °C, with optimum at 40°C. The type strain is neutrophilic with pH optima at 6.5. The type strain cannot grow anaerobically with arginine, DMSO, or nitrate. Reduction of nitrate to nitrite was found but gas was not produced. Diverse substrates, glycerol, $_{D}$-sorbitol, acetate, $_{DL}$-lactate, pyruvate, succinate, $_{L}$-aspartate, $_{L}$-alanine, $_{L}$-lysine, and $_{L}$-ornithine can be utilized for growth, while $_{D}$-fructose, $_{D}$-galactose, $_{D}$-glucose, lactose, maltose, $_{D}$-mannose, $_{D}$-ribose, $_{L}$-sorbose, sucrose, $_{D}$-xylose, $_{D}$-mannitol, acetate, citrate, fumarate, $_{L}$-arginine, $_{L}$-glutamate glycine or $_{L}$-malate do not support growth. The catalase test is positive while the oxidase is

negative. Indole and H_2S production are not detected. None of casein, gelatin, starch or Tween 80 was found to be hydrolyzed. The type strain contains PG, PGP-Me, PGS, DGD-1, and S-TGD-1.

The type strain, ZY43^T (= CGMCC 1.17202^T = JCM 34162^T), was isolated from the natural sea salt produced from Huanghua marine solar saltern in Hebei, PRChina. The DNA G+C content of the type strain is 66.9% (genome). The GenBank/EMBL/DDBJ accession numbers for the 16S rRNA gene and whole genome of strain ZY43^T are MK920152 and CP101154–CP101155, respectively.

Data availability statement

The sequence data of the study are deposited in the NCBI database with accession numbers MW338920, MN589739, MK721000, MK920153, MK920152, CP101454-CP101455, CP101161-CP101165, CP101166-CP101168, CP101153, and CP101154-CP101155.

Author contributions

Y-PS, B-BW, Z-PW, X-WZ performed the experiments and Y-PS drafted the manuscript. JH and H-LC designed and supervised the study. JH and H-LC revised the manuscript. All authors contributed to the article and approved the submitted version.

Funding

This work was financially supported by Science & Technology Fundamental Resources Investigation Program (Grant No. 2019FY100700; No. 2021FY100900), and the National Natural Science Foundation of China (No. 32070003).

Acknowledgments

We are grateful to Prof. Aharon Oren (The Hebrew University of Jerusalem) for his generous and meaningful comments.

Conflict of interest

The authors declare that the research was conducted in the absence of any commercial or financial relationships that could be construed as a potential conflict of interest.

Publisher's note

All claims expressed in this article are solely those of the authors and do not necessarily represent those of their affiliated organizations, or those of the publisher, the editors and the reviewers. Any product that may be evaluated in this article, or claim that may be made by its manufacturer, is not guaranteed or endorsed by the publisher.

Supplementary material

The Supplementary Material for this article can be found online at: https://www.frontiersin.org/articles/10.3389/fmars.2023.1105929/full#supplementary-material

References

Amoozegar, M. A., Siroosi, M., Atashgahi, S., Smidt, H., and Ventosa, A. (2017). Systematics of haloarchaea and biotechnological potential of their hydrolytic enzymes. *Microbiology* 163, 623–645. doi: 10.1099/mic.0.000463

Ashwini, R., Vijayanand, S., and Hemapriya, J. (2017). Photonic potential of haloarchaeal pigment bacteriorhodopsin for future electronics: A review. *Curr. Microbiol.* 74, 996–1002. doi: 10.1007/s00284-017-1271-5

Aziz, R. K., Bartels, D., Best, A. A., DeJongh, M., Disz, T., Edwards, R. A., et al. (2008). The RAST server: rapid annotations using subsystems technology. *BMC Genomics* 9, 75. doi: 10.1186/1471-2164-9-75

Burns, D. G., Janssen, P. H., Itoh, T., Minegishi, H., Usami, R., Kamekura, M., et al. (2010). *Natronomonas moolapensis* sp. nov., non-alkaliphilic isolates recovered from a solar saltern crystallizer pond, and emended description of the genus *Natronomonas*. *Int. J. Syst. Evol. Microbiol.* 60, 1173–1176. doi: 10.1099/ijs.0.010132-0

Capella-Gutiérrez, S., Silla-Martínez, J. M., and Gabaldón, T. (2009). trimAl: a tool for automated alignment trimming in large-scale phylogenetic analyses. *Bioinformatics* 25, 1972–1973. doi: 10.1093/bioinformatics/btp348

Chaumeil, P. A., Mussig, A. J., Hugenholtz, P., and Parks, D. H. (2019). GTDB-tk: a toolkit to classify genomes with the genome taxonomy database. *Bioinformatics* 36, 1925–1927. doi: 10.1093/bioinformatics/btz848

Cui, H. L., and Dyall-Smith, M. L. (2021). Cultivation of halophilic archaea (class *Halobacteria*) from thalassohaline and athalassohaline environments. *Mar. Life Sci. Technol.* 3, 243–251. doi: 10.1007/s42995-020-00087-3

Cui, H. L., Gao, X., Yang, X., and Xu, X. W. (2010). *Halorussus rarus* gen. nov., sp. nov., a new member of the family *Halobacteriaceae* isolated from a marine solar saltern. *Extremophiles* 14, 493–499. doi: 10.1007/s00792-010-0329-0

Cui, H. L., Zhou, P. J., Oren, A., and Liu, S. J. (2009). Intraspecific polymorphism of 16S rRNA genes in two halophilic archaeal genera, *Haloarcula* and *Halomicrobium*. *Extremophiles* 13, 31–37. doi: 10.1007/s00792-008-0194-2

de la Haba, R. R., Minegishi, H., Kamekura, M., Shimane, Y., and Ventosa, A. (2021). Phylogenomics of haloarchaea: The controversy of the genera *Natrinema-Haloterrigena*. *Front. Microbiol.* 12. doi: 10.3389/fmicb.2021.740909

Durán-Viseras, A., Andrei, A.Ş., Vera-Gargallo, B., Ghai, R., Sánchez-Porro, C., and Ventosa, A. (2021). Culturomics-based genomics sheds light on the ecology of the new haloarchaeal genus *Halosegnis*. *Environ. Microbiology* 23, 3418–3434. doi: 10.1111/1462-2920.15082

Durán-Viseras, A., Sánchez-Porro, C., and Ventosa, A. (2020a). *Haloglomus irregulare* gen. nov., sp. nov., a new halophilic archaeon isolated from a marine saltern. *Microorganisms* 8, 206. doi: 10.3390/microorganisms8020206

Durán-Viseras, A., Sánchez-Porro, C., and Ventosa, A. (2020b). *Natronomonas salsuginis* sp. nov., a new inhabitant of a marine solar saltern. *Microorganisms* 8, 605. doi: 10.3390/microorganisms8040605

Dussault, H. P. (1955). An improved technique for staining red halophilic bacteria. *J. Bacteriol.* 70, 484–485. doi: 10.1128/jb.70.4.484-485.1955

Felsenstein, J. (1981). Evolutionary trees from DNA sequences: A maximum likelihood approach. *J. Mol. Evol.* 17, 368–376. doi: 10.1007/BF01734359

Fitch, W. M. (1971). Toward defining the course of evolution: Minimum change for a specific tree topology. *Syst. Biol.* 20, 406–416. doi: 10.2307/2412116

Goris, J., Konstantinidis, K. T., Klappenbach, J. A., Coenye, T., Vandamme, P., and Tiedje, J. M. (2007). DNA-DNA Hybridization values and their relationship to whole-genome sequence similarities. *Int. J. Syst. Evol. Microbiol.* 57, 81–91. doi: 10.1099/ijs.0.64483-0

Han, D., and Cui, H. L. (2020). *Halostella pelagica* sp. nov. and *Halostella litorea* sp. nov., isolated from salted brown alga *Laminaria*. *Int. J. Syst. Evol. Microbiol.* 70, 1969–1976. doi: 10.1099/ijsem.0.004003

Han, J., Hou, J., Liu, H., Cai, S., Feng, B., Zhou, J., et al. (2010). Wide distribution among halophilic archaea of a novel polyhydroxyalkanoate synthase subtype with

homology to bacterial type III synthases. *Appl. Environ. Microbiol.* 76, 7811–7819. doi: 10.1128/AEM.01117-10

Hou, J., Zhao., Y. J., Zhu, L., and Cui, H. L. (2018). *Salinirubellus salinus* gen. nov., sp. nov., isolated from a marine solar saltern. *Int. J. Syst. Evol. Microbiol.* 68, 1874–1878. doi: 10.1099/ijsem.0.002757

Kamekura, M., Dyall-Smith, M. L., Upasani, V., Ventosa, A., and Kates, M. (1997). Diversity of alkaliphilic halobacteria: Proposals for transfer of *Natronobacterium vacuolatum*, *Natronobacterium magadii*, and *Natronobacterium pharaonis* to *Halorubrum*, *Natrialba*, and *Natronomonas* gen. nov., respectively, as *Halorubrum vacuolatum* comb. nov., *Natrialba magadii* comb. nov., and *Natronomonas pharaonis* comb. nov., respectively. *Int. J. Syst. Bacteriol.* 47, 853–857. doi: 10.1099/00207713-47-3-853

Kanehisa, M., Goto, S., Kawashima, S., Okuno, Y., and Hattori, M. (2004). The KEGG resource for deciphering the genome. *Nucleic Acids Res.* 32, D277–D280. doi: 10.1093/nar/gkh063

Kim, T. Y., Kim, S. J., Park, S. J., Kim, J. G., Cha, I. T., Jung, M. Y., et al. (2013). *Natronomonas gomsonensis* sp. nov., isolated from a solar saltern. *Antonie van Leeuwenhoek* 104, 627–635. doi: 10.1007/s10482-013-9970-9

Kim, M., Oh, H. S., Park, S. C., and Chun, J. (2014). Towards a taxonomic coherence between average nucleotide identity and 16S rRNA gene sequence similarity for species demarcation of prokaryotes. *Int. J. Syst. Evol. Microbiol.* 64, 346–351. doi: 10.1099/ijs.0.059774-0

Lobasso, S., Pérez-Davó, A., Vitale, R., Sánchez, M. M., and Corcelli, A. (2015). Deciphering archaeal glycolipids of an extremely halophilic archaeon of the genus *Halobellus* by MALDI-TOF/MS. *Chem. Phys. Lipids* 186, 1–8. doi: 10.1016/j.chemphyslip.2014.11.002

Luo, C., Rodriguez-R, L. M., and Konstantinidis, K. T. (2014). MyTaxa: An advanced taxonomic classifier for genomic and metagenomic sequences. *Nucleic Acids Res.* 42, e73. doi: 10.1093/nar/gku169

Meier-Kolthoff, J. P., Auch, A. F., Klenk, H. P., and Göker, M. (2013). Genome sequence-based species delimitation with confidence intervals and improved distance functions. *BMC Bioinf.* 14, 60. doi: 10.1186/1471-2105-14-60

Minegishi, H., Kamekura, M., Itoh, T., Echigo, A., Usami, R., and Hashimoto, T. (2010). Further refinement of the phylogeny of the *Halobacteriaceae* based on the full-length RNA polymerase subunit b′ (*rpoB′*) gene. *Int. J. Syst. Evol. Microbiol.* 60, 2398–2408. doi: 10.1099/ijs.0.017160-0

Nguyen, L. T., Schmidt, H. A., von Haeseler, A., and Minh, B. Q. (2015). IQ-TREE: A fast and effective stochastic algorithm for estimating maximum-likelihood phylogenies. *Mol. Biol. Evol.* 32, 268–274. doi: 10.1093/molbev/msu300

Oren, A., Ventosa, A., and Grant, W. D. (1997). Proposed minimal standards for description of new taxa in the order *Halobacteriales*. *Int. J. Syst. Evol. Microbiol.* 47, 233–238. doi: 10.1099/00207713-47-1-233

Parks, D. H., Chuvochina, M., Waite, D. W., Rinke, C., Skarshewski, A., Chaumeil, P. A., et al. (2018). A standardized bacterial taxonomy based on genome phylogeny substantially revises the tree of life. *Nat. Biotechnology* 36, 996–1004. doi: 10.1038/nbt.4229

Parks, D. H., Imelfort, M., Skennerton, C. T., Hugenholtz, P., and Tyson, G. W. (2015). CheckM: assessing the quality of microbial genomes recovered from isolates, single cells, and metagenomes. *Genome Res.* 25, 1043–1055. doi: 10.1101/gr.186072.114

Richter, M., and Rosselló-Móra, R. (2009). Shifting the genomic gold standard for the prokaryotic species definition. *Proc. Natl. Acad. Sci. U.S.A.* 106, 19126–19131. doi: 10.1073/pnas.0906412106

Richter, M., Rosselló-Móra, R., Glöckner, F. O., and Peplies, J. (2016). JSpeciesWS: a web server for prokaryotic species circumscription based on pairwise genome comparison. *Bioinformatics* 32, 929–931. doi: 10.1093/bioinformatics/btv681

Saitou, N., and Nei, M. (1987). The neighbor-joining method: A new method for reconstructing phylogenetic trees. *Mol. Biol. Evol.* 4, 406–425. doi: 10.1093/oxfordjournals.molbev.a040454

Serrano, S., Mendo, S., and Caetano, T. (2022). Haloarchaea have a high genomic diversity for the biosynthesis of carotenoids of biotechnological interest. *Res. Microbiology* 173, 103919. doi: 10.1016/j.resmic.2021.103919

Song, H. S., Kim, J., Kim, Y. B., Lee, S. H., Whon, T. W., and Roh, S. W. (2022). Sala cibi gen. nov., sp. nov., an extremely halophilic archaeon isolated from solar salt. *J. Microbiol.* 60, 899–904. doi: 10.1007/s12275-022-2137-5

Sun, Y. P., Wang, B. B., Zheng, X. W., Wu, Z. P., Hou, J., and Cui, H. L. (2022). Description of *Halosolutus amylolyticus* gen. nov., sp. nov., *Halosolutus halophilus* sp. nov. and *Halosolutus gelatinilyticus* sp. nov., and genome-based taxonomy of genera *Natribaculum* and *Halovarius*. *Int. J. Syst. Evol. Microbiol.* 72, 5598. doi: 10.1099/ijsem.0.005598

Tamura, K., Stecher, G., Peterson, D., Filipski, A., and Kumar, S. (2013). MEGA6: molecular evolutionary genetics analysis version 6.0. *Mol. Biol. Evol.* 30, 2725–2729. doi: 10.1093/molbev/mst197

Vaskovsky, V. E., and Kostetsk, E. Y. (1968). Modified spray for the detection of phospholipids on thin-layer chromatograms. *J. Lipid Res.* 9, 396. doi: 10.1016/S0022-2275(20)43111-6

Wang, B. B., Sun, Y. P., Wu, Z. P., Zheng, X. W., Hou, J., and Cui, H. L. (2022). *Halorientalis salina* sp. nov., *Halorientalis marina* sp. nov., *Halorientalis litorea* sp. nov.: Three extremely halophilic archaea isolated from a salt lake and coarse sea salt. *Extremophiles* 26, 26. doi: 10.1007/s00792-022-01275-y

Xin, Y. J., Bao, C. X., Li, S. Y., Hu, X. Y., Zhu, L., Wei, W., et al. (2022). Genome-based taxonomy of genera *Halomicrobium* and *Halosiccatus*, and description of *Halomicrobium salinisoli* sp. nov. *Syst. Appl. Microbiol.* 45, 126308. doi: 10.1016/j.syapm.2022.126308

Xu, L., Dong, Z., Fang, L., Luo, Y., Wei, Z., Guo, H., et al. (2019). OrthoVenn2: A web server for whole-genome comparison and annotation of orthologous clusters across multiple species. *Nucleic Acids Res.* 47, W52–W58. doi: 10.1093/nar/gkz333

Yin, X. M., Yang, X. Y., Hou, J., Zhu, L., and Cui, H. L. (2020). *Natronomonas halophila* sp. nov. and *Natronomonas salina* sp. nov., two novel halophilic archaea. *Int. J. Syst. Evol. Microbiol.* 70, 5686–5692. doi: 10.1099/ijsem.0.004463

Yoon, S. H., Ha, S. M., Kwon, S., Lim, J., Kim, Y., Seo, H., et al. (2017). Introducing EzBioCloud: A taxonomically united database of 16S rRNA and whole genome assemblies. *Int. J. Syst. Evol. Microbiol.* 67, 1613–1617. doi: 10.1099/ijsem.0.001755

frontiers | Frontiers in Marine Science

TYPE Original Research
PUBLISHED 12 April 2023
DOI 10.3389/fmars.2023.1144912

OPEN ACCESS

EDITED BY
Xue-Wei Xu,
Ministry of Natural Resources, China

REVIEWED BY
Rosa León-Zayas,
Willamette University, United States
Heng-Lin Cui,
Jiangsu University, China

*CORRESPONDENCE
Zong-Jun Du
duzongjun@sdu.edu.cn
Meng-Qi Ye
yemengqi@126.com

†These authors have contributed equally to this work and share first authorship

SPECIALTY SECTION
This article was submitted to Aquatic Microbiology, a section of the journal Frontiers in Marine Science

RECEIVED 15 January 2023
ACCEPTED 29 March 2023
PUBLISHED 12 April 2023

CITATION
Tan X-Y, Liu X-J, Li Z, Yu F, Yang H, Du Z-J and Ye M-Q (2023) *Thiomicrorhabdus marina* sp.nov., an obligate chemolithoautotroph isolated from tidal zone sediment, and genome insight into the genus *Thiomicrorhabdus*. *Front. Mar. Sci.* 10:1144912. doi: 10.3389/fmars.2023.1144912

Thiomicrorhabdus marina sp.nov., an obligate chemolithoautotroph isolated from tidal zone sediment, and genome insight into the genus *Thiomicrorhabdus*

Xin-Yun Tan[1†], Xin-Jiang Liu[1†], Zhao Li[2], Fan Yu[1], Hui Yang[1], Zong-Jun Du[1,3*] and Meng-Qi Ye[1,3,4*]

[1]Marine College, Shandong University, Weihai, Shandong, China, [2]College of Bioengineering and Biotechnology, Tianshui Normal University, Tianshui, Gansu, China, [3]Weihai Research Institute of Industrial Technology, Shandong University, Weihai, Shandong, China, [4]Shenzhen Research Institute of Shandong University, Shenzhen, Guangdong, China

The contribution of microbes to the marine sulfur cycle has received considerable attention in recent years. In this study, a new Gram-stain-negative, aerobic sulfur-oxidizing bacterium, designated strain 6S2-11^T, was isolated from tidal zone sediment of the coast of Weihai, China. Strain 6S2-11^T was an obligate chemolithoautotroph utilizing thiosulfate as the energy source. Physiological and biochemical experiments, phylogenetic analysis, and comparative genomic analysis were done with strain 6S2-11^T. According to genomic analysis, strain 6S2-11^T owned a complete thiosulfate oxidation pathway and an untypical nitrogen metabolism pathway. Its relatively small genome also has multiple environmental adaptation mechanisms. The DNA G +C content of strain 6S2-11^T was 44.1%. Strain 6S2-11^T was observed to grow at 20-37°C (optimum, 35°C), pH 6.0-9.5 (optimum, pH 7.5), and 0.5-5% (w/v) NaCl (optimum, 2.5%). The major cellular fatty acids (>10%) of strain 6S2-11^T were Summed Feature 8 ($C_{18:1}\omega7c/C_{18:1}\omega6c$), $C_{16:0}$ and Summed Feature 3 ($C_{16:1}\omega7c/C_{16:1}\omega6c$). The comparison of 16S rRNA gene sequences indicated that strain 6S2-11^T was most closely to *Thiomicrorhabdus xiamenensis* G2^T (96.8%). Based on the results of phylogenetic analysis, the strain 6S2-11^T is a novel specie of the genus *Thiomicrorhabdus*, for which name *Thiomicrorhabdus marina* sp.nov. is proposed with the type strain 6S2-11^T (=MCCC 1H00523^T=KCTC 82994^T).

KEYWORDS

***Thiomicrorhabdus*, comparative genomic analysis, obligate chemolithoautotroph, carbon, nitrogen and sulfur metabolism, environmental adaptation**

Abbreviations: KCTC, Korean Collection for Type Cultures; MCCC, Marine Culture Collection of China; DDH, Digital DNA–DNA hybridization; ANI, Average nucleotide identity; TLC, Thin-layer chromatography; MEGA, Molecular evolutionary genetics analysis.

Introduction

The genus *Thiomicrorhabdus* now has 11 species, four of which were reclassified from the genus *Thiomicrospira* in 2017 (Boden et al., 2017). Members of the genus *Thiomicrorhabdus* are capable of inorganic autotrophic growth using thiosulfates, sulfides, and monosulfides (Boden et al., 2017). They are all obligately chemolithoautotrophic sulfur-oxidizing bacteria (SOB) (Brinkhoff et al., 1999a; Boden et al., 2017). All members of genus *Thiomicrorhabdus* have been found in diverse environments, from deep-sea hydrothermal vents where SOB dominates to continental shelf sediments and intertidal mud flats (Brinkhoff et al., 1999a; Brinkhoff et al., 1999b; Liu et al., 2020). In this study, the strain 6S2-11^T was isolated from coastal sediments.

A critical step in the biogeochemical sulfur cycle is the sulfur redox reactions. (Jørgensen, 1990; Jørgensen and Bak, 1991). About 11.3 teramoles of sulfate are reduced to hydrogen sulfide in seafloor sediments each year, which in turn is oxidized by biotic or abiotic means (Bowles et al., 2014). One study showed that sulfate-reducing bacteria (SRB) drive the remineralization of up to 29% of seafloor organic matter globally, reducing it to form hydrogen sulfide and other sulfides, which are then oxidized by SOB (Bowles et al., 2014). Therefore, the role of SOB and SRB in biogeochemical sulfur cycling is significant.

In addition to playing an important role in the global biogeochemical sulfur cycle, microorganisms are also extensively involved in the nitrogen cycle, including nitrification, denitrification, assimilatory nitrate reduction (ANR), and dissimilatory nitrate reduction to ammonia (DNRA), etc (Hutchins and Capone, 2022). In the context of human activities that have increased the flux of reactive nitrogen (Nr, mainly nitrate) from land to aquatic ecosystems and the eutrophication of many lakes and coastal waters, many studies are exploring the contribution of microbial activities in these aquatic ecosystems to nitrate reduction (Galloway et al., 2004, 2008).

Therefore, this study focused on the metabolic pathways of sulfur and nitrogen in a novel strain 6S2-11^T isolated from coastal sediments, which can help to understand the microbiome-mediated sulfur and nitrogen transformation pathways in coastal sediments.

Experimental procedure

Bacteria isolation and cultivation

The strain 6S2-11^T was isolated from tidal zone sediment of the coast of Weihai, China (36°58′37″ N, 122°2′37″ E). After sample enrichment, 100 μL of samples with dilution gradients of 10^{-3} and 10^{-4} were spread on SOB medium (Peptone 5 g/L, yeast powder 1 g/L, sodium pyruvate 0.3 g/L, NH_4Cl 0.26 g/L, $Na_2S_2O_3$ 4.96 g/L) and incubated at 30°C. The isolated strain 6S2-11^T was cultured on SOB medium at 30°C, stored in a sterile mixture of 1% (w/v) saline and 15% glycerol at -80°C. The type strain *Thiomicrorhabdus xiamenensis* G2^T and. *Thiomicrorhabdus sediminis* G1^T were used as reference strains which are also cultivated on SOB medium at 30°C.

Gene extraction and analysis

Gene sequence acquisition

The 16S rRNA gene sequence of strain 6S2-11^T was obtained by PCR with universal primers 27F and 1492R (Lane, 1991). The sequence was ligated to the pMD18-T vector (Takara) and cloned to obtain a complete 16S rRNA gene sequence. The genome was extracted using a DNA kit (Takara) and then sequenced on the Hiseq X Ten platform (Illumina Inc., San Diego, USA) at Beijing Novogene Bioinformatics Technology, using the pair-end 350-bp sequencing protocol. All sequenced reads were assembled by SOAPdenovo software v2.04. The 16S rRNA gene sequences and whole genome sequences of other strains were downloaded from the NCBI database.

Genetic analysis

The obtained 16S rRNA gene sequences were compared in the EzBioCloud database (https://www.ezbiocloud.net/) and the NCBI database (https://www.ncbi.nlm.nih.gov/) for preliminary confirmation of taxonomic status. The ANI values (https://www.ezbiocloud.net/tools/ani) (Yoon et al., 2017) and DDH values (https://ggdc.dsmz.de/ggdc.php) (Meier-Kolthoff et al., 2013) betwee the strain 6S2-11^T and other *Thiomicrorhabdus* strains were calculated based on genome sequences to confirm their taxonomic status further. Phylogenetic trees were built using neighbor-joining (NJ), maximum-likelihood (ML), and maximum-parsimony (MP) algorithms in MEGA version 7.0 with the bootstrap value being set to 1000 (Kumar et al., 2016). The genome phylogenetic trees were built using IQ-Tree (Nguyen et al., 2015). The genome was annotated using the KEGG database to study the metabolic pathways of the strains (Kanehisa et al., 2016). The antiSMASH database (https://antismash.secondarymetabolites.org/#!/start) was used to predict the secondary metabolites of the strain (Blin et al., 2021). Prediction of antibiotic resistance of strains was performed using the CARD database (https://card.mcmaster.ca/) (Alcock et al., 2020). The analysis of metabolic pathways and insight into environmental adaptation mechanisms are based on the classification results of KEGG annotations. Strains for genome analysis were all *Thiomicrorhabdus* strains for which the genomes were available from NCBI. Details of the strains and their genome sequence accession numbers are shown in Table 1.

Physiology, biochemical and chemotaxonomic analyses

The experiments to investigate the morphological and physiological characteristics of the strains were performed using the microorganisms that had been cultured on SOB medium for three days. Among them, the size and morphology of the cells were observed by light microscopy (E600; Nikon) and transmission electron microscope (JEM-1200, JEOL). Gram-staining experiments were performed by the method described by Smibert (Smibert, 1994). The motility experiments were then performed on

SOB medium with 0.3% agar, and the results were obtained by direct observation. The temperature range for growth and the optimum growth temperature were tested at different temperatures of 0, 4, 10, 15, 20, 25, 28, 30, 33, 35, 37, 40, and 43°C. The suitable salinity range and optimum salinity for growth were tested in SOB medium with different NaCl concentrations (0, 0.5, 1, 1.5, 2, 2.5, 3, 4, 5, 6, 7, 8, 9, 10%, w/v) and the aged seawater was replaced with artificial seawater ($MgSO_4$ 1.62g/L, $MgCl_2$ 4.83 g/L, $CaCl_2$ 1.15 g/L, KCl 0.72 g/L). The appropriate pH range for growth was tested by adjusting pH to 5.5-9.5 at the interval of 0.5 with appropriate amounts of HCl or NaOH as well as the different buffers before sterilization (including MES-pH 5.5 and 6.0, PIPES-pH 6.5 and 7.0, HEPES-pH 7.5 and 8.0, Tricine-pH 8.5, CAPSO-9.0 and 9.5). The OD_{600} values were determined in the stationary phase of the strain growth curve. Three experimental groups and one control group were set up for SOX validation experiments with strains 6S2-11^T, G1^{T}and G2^T. To exclude interference, the medium was prepared using artificial seawater without sulfate ($MgCl_2$ 4.83 g/L, $CaCl_2$ 1.15 g/L, KCl 0.72 g/L, NaCl 30 g/L). After 5 days of incubation, 200 μL of culture solution was taken in a ninety-six-well plate, 50 μL of ferric chloride and barium chloride were added respectively to observe whether precipitation was produced (Zhu et al., 2021). The nitrate utilization validation experiment was designed with three parallel experimental groups (2 g/L potassium nitrate and 2% bacterial inoculum) and three parallel control groups (2 g/L potassium nitrate and 2% sterilized medium). In addition, blank groups (without potassium nitrate, 2% bacterial inoculum or 2% sterilized medium) was set up separately. These were all performed in liquid medium. After 0h, 12h, 24h and 36h of incubation respectively, 5mL of liquid medium was taken as samples for detection. After centrifugation, filtration, and dilution (with pure water in a 1:50 ratio), the absorbance of the samples was measured at 220 nm using a UV spectrophotometer. Catalase activity was tested by direct observation of bubble production in a 3% hydrogen peroxide solution. The strains were tested for hydrolytic activity against agar, sodium alginate, cellulose, starch, DNA, casein, and Tween 20, 40, 60, and 80 according to the method of Smibert (Smibert, 1994). The antibiotic susceptibility of strains was tested using the disc diffusion method described by Du (Du et al., 2014), and strain susceptibility was described according to the guidelines of the Clinical and Laboratory Standards Institute (CLSI). Other physiological and biochemical characteristics of the strains were determined using API 20E and Biolog GENIII, referring to their instructions for specific steps (except for salinity, which was adjusted to 3%).

Polar lipids were extracted using a chloroform/methanol system according to the method described by Komagata and Suzuki (Komagata and Suzuki, 1988) and measured by two-dimensional thin-layer assay chromatography (TLC) (Minnikin et al., 1984). Fatty acids were extracted according to the standard protocol of MIDI (Sherlock Microbial Identification System, version 6.1). Analysis was performed with a gas chromatograph. Cellular fatty acids were identified using the TSBA40 database of the Microbial Identification System to determine fatty acid names and percentages (Sasser, 1990).

Results and discussion

Phylogenetic analysis and genome comparison

The almost complete 16S rRNA gene sequence of strain 6S2-11^T was amplified (MW712743) and the genomic sequence of the strain were extracted (NZ_JAGETV010000010). The preliminary identification of the 16S rRNA gene sequence was performed by the EzBioCloud database. The 16S rRNA gene sequence of *Thiomicrorhabdus xiamenensis* G2^T was found to be the closest to that of strain 6S2-11^T with 96.81% similarity. To further confirm the relationship between strain 6S2-11^T and related taxa, their ANI and DDH values were calculated (Table 1). The results showed that the ANI values were all less than the classification threshold for ANI (95-96%) (Goris et al., 2007). The DDH values are also below the species identification boundary for DDH (70%) (Meier-Kolthoff et al., 2013). Phylogenetic trees were built using NJ, ML, and MP methods for 16S rRNA genes (Figure 1) and IQ-Tree for genomes (Figure 2). The results all indicated that strain 6S2-11^T belongs to the genus *Thiomicrorhabdus*. The genome of the strain 6S2-11^T was annotated by NCBI PGAP and compared with the genomic data of several other strains of the genus *Thiomicrorhabdus*, *Thiomicrospira*, *Hydrogenovibrio*, and *Thiosulfativibrio* (Figure 2).

Genomic features of different species of strains were collected and compared in Table 1. Strain 6S2-11^T contained 2637 genes, including 2573 protein-coding genes, and 52 RNAs genes (6 rRNA genes, 43 tRNA genes, and 3 ncRNA). The G+C content was 44.1%. The strain 6S2-11^T has 6 rRNA genes, and in comparison to other strains (except the strain HH3^T) it has the least amount. This may indicate that strain 6S2-11^T is not outstanding in its ability to respond to complex environmental resources compared with other strains in this genus. It has been shown that the number of rRNA genes correlates with the rate of bacterial response to resource availability(Klappenbach et al., 2000). The bacteria exposed to nutrient-complex media that rapidly form colonies contain an average of 5.5 small-subunit rRNA genes (Klappenbach et al., 2000). Thus, the number of rRNA genes in the strains of genus *Thiomicrorhabdus* may help improve their ability to respond to complex environmental resource.

Metabolic pathway analysis

The genomes of nine strains of the genus *Thiomicrorhabdus*, including strain 6S2-11^T, were annotated (These nine strains are all the strains of genus *Thiomicrorhabdus* for which the genomes were vailable from NCBI). The pathway types and gene count of strain 6S2-11^T (Supplementary Figure 1) and the metabolic modules integrity of *Thiomicrorhabdus* strains (Figure 3) were obtained from the annotation. Metabolic module integrity was obtained from the annotation results by calculating the proportion of pathways that the strain has to the total pathways required for this module to proceed. All pathways required for the

TABLE 1 Genomic characteristics of all strains and ANI/DDH values between strains of genus *Thiomicrorhabdus* and strain 6S2-11^T.

	Size(bp)	GC%	gene	Protein-coding	rRNA	tRNA	ncRNA	ANI/DDH (%)
Hydrogenovibrio kuenenii DSM 12350^T (JAGP01000001.1)	2,452,457	42	2,278	2,216	9	43	3	–
Hydrogenovibrio marinus MH-110^T (AP020335.1)	2,491,293	44	2,354	2,290	9	43	3	–
Thiomicrospira halophila DSM 15072^T (KB913033.1)	2,356,686	55	2,225	2,199	9	45	3	–
Hydrogenovibrio thermophilus JR-2 (CP035033.1)	2,612,894	51	2,454	2,386	9	44	3	–
Hydrogenovibrio crunogenus SP-41 (CP032096.1)	2,453,259	43	2,334	2,266	9	43	4	–
Thioalkalimicrobium cyclicum ALM1^T (CP002776.1)	1,932,455	47	1,724	1,668	6	41	3	–
Thioalkalimicrobium aerophilum AL3^T (CP007030.1)	2,158,359	46	2,103	2,041	6	41	3	–
Thiomicrospira microaerophila ASL8-2^T (JYNN01000001.1)	3,102,228	46	2,844	2,736	10	39	4	–
Thiomicrorhabdus aquaedulcis HaS4^T (AP018722.1)	2,440,205	45	2,302	2,160	9	44	3	69.81/20
Thiomicrorhabdus sediminis G1^T (CP040602.1)	2,373,486	45	2,164	2,087	9	45	3	71.79/21.5
Thiomicrorhabdus heinhorstiae HH1^T (JACBGI020000001.1)	2,611,196	48	2,499	2,423	7	44	4	71.92/20.9
Thiomicrorhabdus indica 13-15A^T (CP033040.1)	2,829,883	42	2,490	2,413	9	51	3	72.81/22.5
6S2-11^T (NZ_JAGETV010000010.1)	**2,831,073**	**44**	**2,637**	**2,573**	**6**	**43**	**3**	-
Thiomicrorhabdus xiamenensis G2^T (CP054020.1)	2,594,948	48	2,394	2,314	9	50	3	73.75/20.5
Thiomicrorhabdus cannonii HH3^T (NR_181717.1)	2,493,962	52	2,384	2,312	4	43	3	76.8/13.2
Thiomicrorhabdus chilensis DSM 12352^T (NZ_AXZC00000000.1)	2,440,706	48	2,261	2,199	6	43	3	76.69/13.3
Thiomicrorhabdus arctica DSM 13458^T (NZ_ARLF00000000.1)	2,552,678	42	2,303	2,237	7	45	3	76.25/13.1
Thiosulfativibrio zosterae AkT22^T (AP021888.1)	2,645,427	43	2,415	2,346	9	43	3	–

ANI/DDH values between strains of other genus and strain 6S2-11^T were unnecessarily calculated and are indicated by -. Strain 6S2-11T is bolded to indicate.

corresponding metabolic module to proceed are obtained from KEGG.

Nitrogen metabolism

Of all the strains analyzed, strain 6S2-11^T, DSM 13458^T, HaS4^T, G1^{T}and HH1^T have pathway modules related to nitrogen metabolism. These strains have half of DNRA (M00530, NirBD, nitrite reductase, EC 1.7.1.15) and ANR (M00531, NasA, assimilatory nitrate reductase, EC 1.7.99.-), without Nitrogen fixation, Denitrification, and Nitrification.

The integrity of both DNRA and ANR metabolic modules is only 50%, but this does not mean that the strains are incapable of nitrogen metabolism. In a previous study, it was found that nirBD-encoded nitrite reductase can not only catalyze fermentation-mode-dependent DNRA but also regulate ANR (Luque-Almagro et al., 2011). Nitrite reductase (NirBD) and assimilatory nitrate reductase (NasA) can work together to enable ANR to proceed properly (Hu et al., 2022). In the microbial nitrogen cycle, ANR is a form of anabolic metabolism in which nitrate is first reduced to nitrite by NasA, then nitrite is converted to ammonia (Reitzer, 2003). Ammonia is synthesized into glutamate by glutamine synthetase (glnA, EC 6.3.1.2) and glutamate synthase (gltBD, EC 1.4.1.13) (These two enzymes were also annotated in the genome of strain 6S2-11^T) (Reitzer, 2003). Eventually, the nitrogen in nitrate is

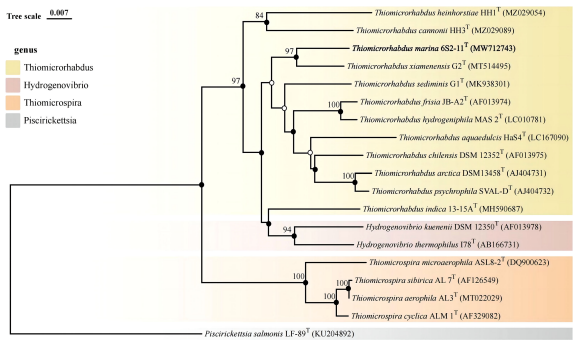

FIGURE 1
Phylogenetic tree of 16S rDNA based on NJ algorithm. Bootstrap values are shown on the branch nodes (only bootstrap values higher than 70% are marked on the branches). Solid circles represent consistent results with ML and MP algorithms.

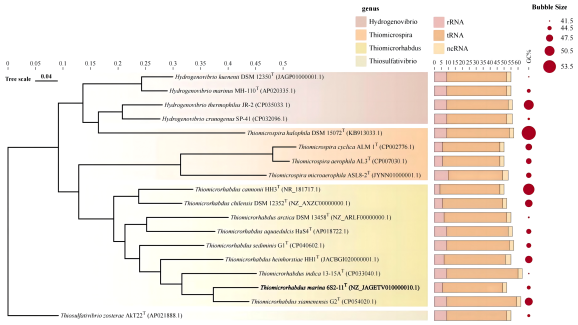

FIGURE 2
Genome phylogenetic tree. Stacked bar charts represent the number of different RNAs. Circle plots indicate GC content.

incorporated into the organism (Reitzer, 2003). DNRA is a catabolic pathway that does not incorporate nitrogen into the organism (Sparacino-Watkins et al., 2014). Instead, after reduction to obtain nitrite, the end product ammonia obtained by NirBD is secreted from the cells (Reitzer, 2003; Sparacino-Watkins et al., 2014). We also realized that this ANR process works only if the strain has a system capable of transporting nitrate to the cytoplasm. Through genomic analysis, we found the existence of nasF (nitrate/nitrite transport system substrate-binding protein), nasE (nitrate/nitrite transport system permease protein), and nasD (nitrate/nitrite transport system ATP-binding protein), which form an ATP dependent nitrate transport system. Due to the combination of proteins, ANR allows these strains to assimilate nitrate and use NirBD to remove nitrogen pollutants from aquatic ecosystems under low ammonium conditions (Jack and Joop, 2000). The reactive nitrogen transformation pathway *via* ANR sometimes occurs at more than the DNRA and denitrification (Hu et al., 2022).

To verify whether the strain is nitrate-reducing, we used API 20E and UV spectrophotometric method to detect. The results of 20E showed that the strain was negative for nitrate reduction (Supplementary Table 1). This may be because the experiment was conducted to determine whether the strains had nitrate-reducing ability by the nitrite content in the environment. But the ANR process mentioned above always occurs in the cytoplasm and no nitrite is released into the environment and detected. The result of UV spectrophotometric detection at 220 nm was shown in the Supplementary Figure 2. The measured data were subjected to one-way ANOVA test using SPSS software, and it was concluded that the nitrate content in the environmental samples with the strain 6S2-11^T growth was significantly reduced in 0-12 hours ($p< 0.01$). While the change of nitrate content in 12-36 hours was not significant. The difference in nitrate concentration between the experimental and control groups at 0 h was not significant. Compared to the control group (without bacteria), the differences in nitrate content during 36 hours were at highly significant levels. Therefore, the utilization of nitrate by strain 6S2-11^T can be observed using UV spectrophotometry.

The confirmation that strain 6S2-11^T has such a nitrogen metabolism pathway on the one hand corroborates previous findings that chemoautotrophic sulfur-oxidizing bacterium is the dominant nitrogen-assimilating bacteria in hydrothermal vent (Jiang et al., 2015). On the other hand, it further illustrates the importance of understanding its nitrogen metabolism for understanding the nitrogen cycle in its habitat.

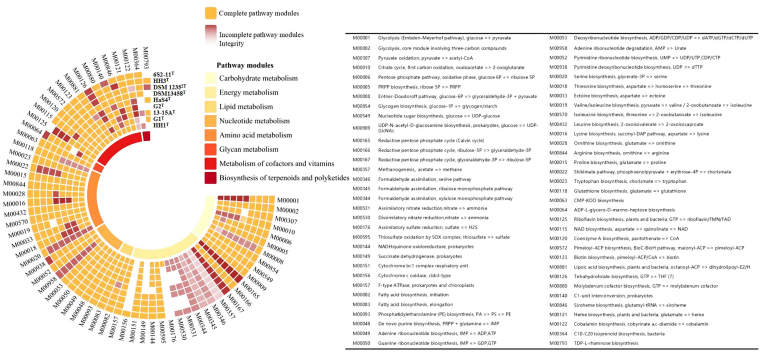

FIGURE 3
The metabolic modules integrity of *Thiomicrorhabdus* strains. The orange color blocks represent intact metabolic modules, and the red-brown color blocks represent incomplete metabolic modules. The integrity of incomplete metabolic modules is indicated by color shades. The lowest integrity is 0 for white.

Sulfur metabolism

All nine strains of the genus *Thiomicrorhabdus* have the complete thiosulfate oxidation pathway-SOX system (M00595), and HH1^T also has the complete assimilatory sulfate reduction pathway (M00176). However, no strain was found to have the Dissimilatory sulfate reduction pathway. The sulfur metabolic pathway diagram of strain 6S2-11^T was compiled from the annotated results (Figure 4).

To validate the results obtained from genome annotation, we designed experiments to verify whether strain 6S2-11^T can oxidize thiosulfate to sulfate *via* SOX. It was found that after incubation, there were significant precipitates in the bacterial suspension of all three strains with barium chloride and no precipitates in the bacterial suspension of all three strains with iron chloride compared to the bacterial suspension of day 0 (Supplementary Table 2). This indicates that after incubation, all three strains produced SO_4^{2+} that could be precipitated by Ba^{2+}. It was verified that these three strains do have the ability to oxidize thiosulfate to sulfate. In combination with the genomic analysis, only the SOX system was annotated in all pathways of sulfur metabolism to produce sulfate. Also, the annotated SOX system was complete. Therefore, it is presumed that these strains possess the complete SOX system.

In strain 6S2-11^T, besides annotating the complete SOX system, it also annotates thiosulfate sulfurtransferase (EC 2.8.1.1), sulfite reductase (NADPH) (EC 1.8.1.2), sulfide-cytochrome -c reductase (FCC, EC 1.8.2.3), sulfide: quinone oxidoreductase (SQR, EC 1.8.5.4), 3'(2'), 5'-bisphosphate nucleotidase (EC 3.1.3.7), and sulfur dioxygenase (EC 1.13.11.18). Among them, FCC is a periplasmic enzyme, together with thiosulfate sulfurtransferase (EC 2.8.1.1) and sulfite reductase (NADPH) (EC 1.8.1.2), mediating the reduction of thiosulfate to monosulfide (Nguyen et al., 2022). Meanwhile, sulfide: quinone oxidoreductase (EC 1.8.5.4) acts as a membrane-bound enzyme to mediate the formation of the inorganic polysulfide H_2S_n from H_2S, which in turn spontaneously forms S_8 in the cytoplasm and aggregates into spheres (Wang et al., 2022). S_8 is the major component of elemental sulfur (Wang et al., 2022). Therefore, it can be assumed that strain 6S2-11^T has two different pathways for the formation of elemental sulfur. However, the importance of these two elemental sulfur production pathways varies for different species. For example, in *Allochromatium vinosum*, mutational inactivation of FCC did not affect its sulfide oxidation, whereas in the genus *Thioalkalivibrio*, FCC plays a crucial role in sulfide oxidatio (Griesbeck et al., 2000). Both FCC and SQR were present in strain 6S2-11^T, and the effect of FCC and SQR on their specific sulfide oxidation still needs further investigation.In general, these sulfur metabolic processes are not only a metabolic and detoxification mechanism for Chemoenergetic autotrophic bacteria but also an essential microbial involvement in the biogeochemical sulfur cycle.

Carbon metabolism

In the analysis of the pathway modules, both strains 6S2-11^T and HH1^T have an intact ED pathway (M00008), while the remaining four strains have a low ED pathway integrity (Figure 3). Compared to the intact EMP, the ED pathway is expected to require much fewer enzymatic proteins to achieve the same rate of glucose conversion as the EMP (Flamholz et al., 2013). It reflects a trade-off between energy (ATP) production and the amount of enzymatic protein required, which is a metabolic strategy of the strain to adapt to its environment (Flamholz et al., 2013). Furthermore, all nine strains were annotated to have an almost complete Calvin cycle, indicating that all nine strains of the genus *Thiomicrorhabdus* are likely to be able to obtain energy through carbon fixation *via* the CBB cycle, which is also the main mode of carbon fixation by autotrophic Gammaproteobacteria (Hügler and Sievert, 2011).

Other metabolic modules

Strains 6S2-11^T, HaS4^T, G1^T, and HH1^T all have complete ectoine synthesis pathways, while the integrity of the ectoine synthesis pathway in G2^T and 13-15A^T is also high. It is also the

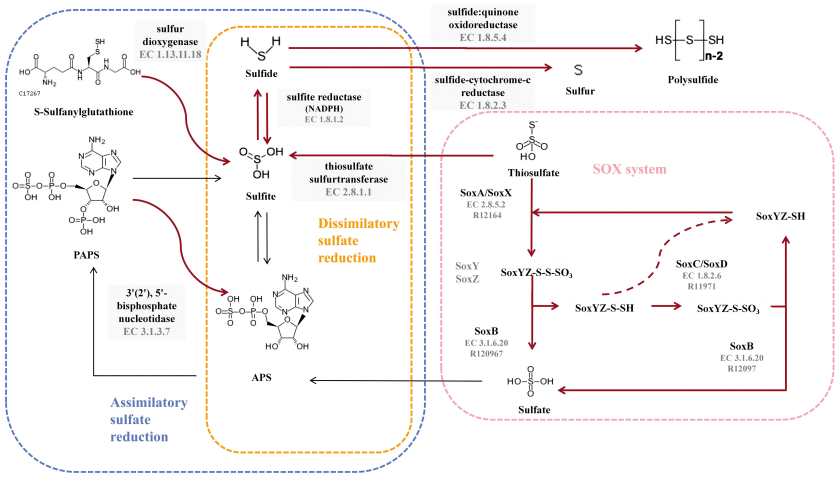

FIGURE 4
Diagram of the sulfur metabolic pathway. The pink blocks indicate SOX pathway-related enzymes, and the gray blocks indicate enzymes owned by strain 6S2-11^T that are not related to SOX but are related to sulfur metabolism. The red bolded arrows indicate pathways available to strain 6S2-11^T.

case that four strains 6S2-11^T, HaS4^T, G1^T, and HH1^T have complete siroheme synthesis pathways. Siroheme is a heme-like prosthetic group in microorganisms and some plants, which is involved in the assimilation of nitrate as a cofactor for nitrite reductase (Murphy et al., 1974; Dietl et al., 2018).

Environmental adaptation mechanisms

The role of secondary metabolites in adverse environments

Nine strains of the genus *Thiomicrorhabdus* were annotated using the antiSMASH database to predict secondary metabolites. The results obtained revealed that all strains produce ectoine and TypeIII polyketides synthase (T3PKS). In addition, G1^T, 13-15A^T, DSM 12352^T, DSM 13458^T and HH3^T produce RiPP-like (other unspecified ribosomally synthesised and post-translationally modified peptide product); DSM 13458^T and HH3^T produce arylpolyene; HH1^T produce N-acetylglutaminylglutamine amide (NAGGN) (Figure 5).

Ectoine is a compatible solute that can be found in a wide range of different salt-loving and salt-tolerant microorganisms (Reed, 1990). It protects the organism from hyperosmotic stress by regulating the intracellular concentration of low molecular weight solutes (Reed, 1990; Roesser and Müller, 2001). It can prevent cell leakage, irreversible plasmolysis, and dehydration. It also has the ability to generate swelling pressure within the range required for growth, all of which are survival strategies for a bacterial adaptation to the environment (Reed, 1990; Roesser and Müller, 2001). Other recent studies have revealed that ectoine production is related to the mechanism of thermal adaptation of bacteria (Salvador et al., 2018).Ectoine can be seen as a heterocyclic amino acid (Galinski et al., 1985). Moreover, HH1^T can produce NAGGN, which is also a compatible solute that protects the cell by regulating the concentration of small molecular weight solutes. However, the mechanism of its biosynthesis is not clear (Csonka and Hanson, 1991). The phenomenon that different cells select different solutes is mainly due to different growth conditions (Ventosa et al., 1998). In general, the secondary metabolites of all nine strains of the genus *Thiomicrorhabdus* are functioning mostly to adapt to a hyperosmotic environment or high-temperature environment. It suggests that their survival strategies are not only the production of secondary metabolites that help them survive in extreme environments. They also choose to ensure their survival by reducing unnecessary energy expenditure in metabolic processes.

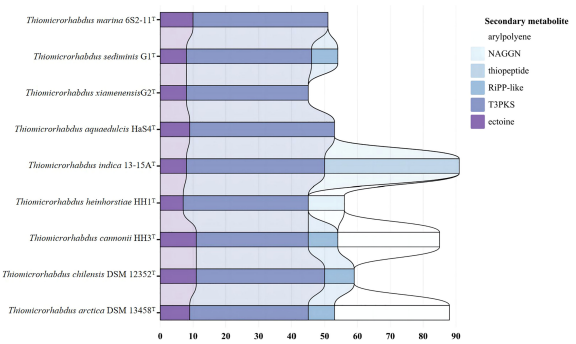

FIGURE 5
Predicted secondary metabolite results for nine strains annotated by antismash database.

Heavy metal resistance and environmental adaptation mechanisms

Combined with the above analysis in this study, it can be found that nine strains of the genus *Thiomicrorhabdus*, including strain 6S2-11^T, have multiple mechanisms of adaptation to the environment. For example, more rRNA genes, ED pathway, and production of secondary metabolites Ectoine and NAGGN. It can also be seen in Supplementary Figure 1 that there are some genes of the environmental adaptation pathway present in the genome of strain 6S2-11^T.Therefore, the genes related to environmental adaptation were predicted and analyzed by KEGG. The czc-A protein, czc-B protein, and czc-C protein of the CzcCBA-mediated heavy metal efflux system were predicted in several strains of the genus *Thiomicrorhabdus* (Supplementary Table 3) (Nies, 2003). CzcCBA mainly mediates resistance to Co^{2+}, Zn^{2+}, and Cd^{2+} (Mergeay et al., 1985). This resistance is based on the reduced cellular accumulation of the three cations due to proton-driven cation efflux (Nies and Silver, 1989; Nies, 1995).

Analysis and validation of antibiotic resistance

The antibiotic resistance of nine strains of the genus *Thiomicrorhabdus*, including strain 6S2-11^T, was predicted using the CARD database to analyze their potential antibiotic resistance properties. The results are displayed in Figure 6. And the results of the antibiotic resistance properties of strain 6S2-11^T using drug-sensitive paper are shown in Supplementary Table 4.

Thiomicrorhabdus strains behaved similarly in gene count of different antibiotics resistance. In the CARD database, antibiotics resistance is annotated by both rigorous and loose algorithms. All the *Thiomicrorhabdus* strains (except DSM 13458$^{T)}$ annotated with tetracycline antibiotic and fluoroquinolone antibiotic resistance by rigorous algorithm, and the gene count was significantly greater than the other antibiotics resistant genes. In addition, strain 6S2-11^T was also annotated with glycopeptide antibiotics, disinfecting agents, and antiseptics resistant genes by rigorous algorithm. The experimental results supported part of the analysis, strain 6S2-11^T was indeed highly resistant to tetracycline, Polymyxin B, and Vancomycin (Polymyxin B and Vancomycin are both glycopeptide antibiotics). 30μg of tetracycline, 30μg of vancomycin, and 300μg of Polymyxin B all did not affect strain 6S2-11^T. The results also showed that strain 6S2-11^T was highly resistant to lincomycin. 2μg of lincomycin did not affect its growth. However, all nine strains in the biographical analysis were not significantly resistant to lincomycin, strain 6S2-11^T had the lowest number of genes (2).

These antibiotic resistances possessed by strain 6S2-11^T may be related to the composition of the microbial community in its habitat

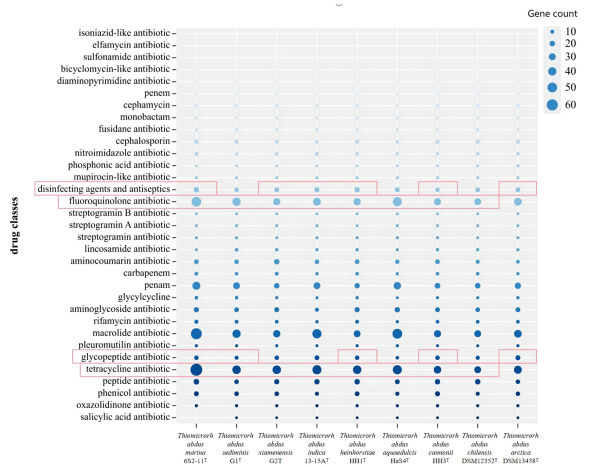

FIGURE 6
The gene count of different antibiotics resistance genes annotated for *Thiomicrorhabdus* strains. Red highlighting indicates that it has genes that are annotated by a rigorous algorithm.

as a way of adapting to unfavorable environments. It fights for survival by resisting the antibiotics released by microorganisms in its habitat.

Physiological and biochemical characteristics

Strain 6S2-11^T is an oval-shape, aerobic, Gram-negative bacterium with a single polar flagellum that grows at 20-37°C (optimum, 35°C), pH 6.0-9.5 (optimum, pH 7.5-8.0), and 0.5-5% (w/v) NaCl (optimum, 2.5%) (Supplementary Figure 3). It was positive for oxidase activity and peroxidase activity and was unable to hydrolyze agar, sodium alginate, CM-cellulose, starch, Tween20, Tween40, Tween60, Tween80, DNA, and casein. In addition, the carbon sources that both strain 6S2-11^T and reference strains G1^T and G2^T could oxidize D-Galacturonic Acid, D-Fucose, D-Glucuronic Acid, Glucuronamide, L-Fucose, D-Fructose-6-PO_4, L-Rhamnose (Supplementary Table 5). And in API 20E, both strain 6S2-11^T and reference strain G1^T and G2^T were positive for TDA and GEL only (Supplementary Table 1).

Chemotaxonomic analyses

The dominant fatty acids (>10%) of strain 6S2-11^T were Summed Feature 8 ($C_{18:1}\omega7c/C_{18:1}\omega6c$) (46.58%), $C_{16:0}$ (21.69%), Summed Feature 3 ($C_{16:1}\omega7c/C_{16:1}\omega6c$) (14.57%). The fatty acid composition of strain 6S2-11^T and the reference strains G1^T, G2^T are shown in Supplementary Table 6.

The major polar lipids of strain 6S2-11^T were phosphatidylglycerol (PG), phosphatidylethanolamine (PE), aminophospholipids (APL) and three unidentifiied lipids (L) (Supplementary Figure 4).

Description of *Thiomicrorhabdus marina* sp. nov.

Thiomicrorhabdus marina (ma.ri'na. L. fem. adj. *marina*, of the sea, marine)

Cells of *Thiomicrorhabdus marina* are oval-shaped with a single polar flagellum. It is an aerobic, Gram-negative bacterium that grows at 20-37°C (optimum, 35°C), pH 6.0-9.5 (optimum, pH 7.5-8.0), and 0.5-5% (w/v) NaCl (optimum, 2.5%). It was positive for oxidase activity and peroxidase activity and was unable to hydrolyze agar, sodium alginate, CM-cellulose, starch, Tween20, Tween40, Tween60, Tween80, DNA, and casein. The dominant fatty acids (>10%) of *Thiomicrorhabdus marina* were Summed Feature 8 ($C_{18:1}\omega7c/C_{18:1}\omega6c$), $C_{16:0}$, Summed Feature 3 ($C_{16:1}\omega7c/C_{16:1}\omega6c$).

The type strain, 6S2-11^T (=MCCC 1H00523^T=KCTC 82994^T), was isolated from marine sediment from the coast of Weihai, China (36°58′37″ N, 122°2′37″ E). The Genebank accession number for the 16S rRNA gene sequence of strain 6S2-11^T was MW712743 and the draft genome has been deposited in GenBank under the accession number NZ_JAGETV010000010.

Data availability statement

The datasets presented in this study can be found in online repositories. The names of the repository/repositories and accession number(s) can be found in the article/Supplementary Material.

Author contributions

X-JL isolated the strain strains 6S2-11T. X-YT, X-JL, FY, HY performed material preparation, experimental operation, data collection and analysis. X-JL and X-YT finished the experiment and manuscript. ZL performed genomic analysis. Z-JD and M-QY offered experiment guidance and critical revision of manuscripts. All authors contributed to the article and approved the submitted version.

Funding

This work was funded by National Science and Technology Fundamental Resources Investigation Program of China (2019FY100700), National Natural Science Foundation of China (32200003), Natural Science Foundation of Shandong Province (ZR2022QC106), Guangdong Basic and Applied Basic Research Foundation (2022A1515110773), Youth Science and Technology Fund Program of Gansu Province (20JR10RA803), Science and Technology Support Program of Qinzhou District Tianshui City (2021-JHGLG-4062) and Innovation Fund of Tianshui Normal University (CXJ2020-01).

Conflict of interest

The authors declare that the research was conducted in the absence of any commercial or financial relationships that could be construed as a potential conflict of interest.

Publisher's note

All claims expressed in this article are solely those of the authors and do not necessarily represent those of their affiliated organizations, or those of the publisher, the editors and the reviewers. Any product that may be evaluated in this article, or claim that may be made by its manufacturer, is not guaranteed or endorsed by the publisher.

Supplementary material

The Supplementary Material for this article can be found online at: https://www.frontiersin.org/articles/10.3389/fmars.2023.1144912/full#supplementary-material

References

Alcock, B. P., Raphenya, A. R., Lau, T. T. Y., Tsang, K. K., Bouchard, M., Edalatmand, A., et al. (2020). CARD 2020: antibiotic resistome surveillance with the comprehensive antibiotic resistance database. *Nucleic Acids Res.* 48, D517–D525. doi: 10.1093/nar/gkz935

Blin, K., Shaw, S., Kloosterman, A. M., Charlop-Powers, Z., van Wezel, G. P., Medema, M. H., et al. (2021). antiSMASH 6.0: improving cluster detection and comparison capabilities. *Nucleic Acids Res.* 49, W29–W35. doi: 10.1093/nar/gkab335

Boden, R., Scott, K. M., Williams, J., Russel, S., Antonen, K., Rae, A. W., et al. (2017). An evaluation of thiomicrospira, hydrogenovibrio and thioalkalimicrobium: reclassification of four species of thiomicrospira to each thiomicrorhabdus gen. nov. and hydrogenovibrio, and reclassification of all four species of thioalkalimicrobium to thiomi. *Int. J. Syst. Evol. Microbiol.* 67, 1140–1151. doi: 10.1099/ijsem.0.001855

Bowles, M. W., Mogollón, J. M., Kasten, S., Zabel, M., and Hinrichs, K.-U. (2014). Global rates of marine sulfate reduction and implications for sub-sea-floor metabolic activities. *Science* 344, 889–891. doi: 10.1126/science.1249213

Brinkhoff, T., Muyzer, G., Wirsen, C. O., and Kuever, J. (1999a). Thiomicrospira chilensis sp. nov., a mesophilic obligately chemolithoautotrophic sulfuroxidizing bacterium isolated from a thioploca mat. *Int. J. Syst. Bacteriol.* 49 (Pt 2), 875–879. doi: 10.1099/00207713-49-2-875

Brinkhoff, T., Muyzer, G., Wirsen, C. O., and Kuever, J. (1999b). Thiomicrospira kuenenii sp. nov. and thiomicrospira frisia sp. nov., two mesophilic obligately chemolithoautotrophic sulfur-oxidizing bacteria isolated from an intertidal mud flat. *Int. J. Syst. Evol. Microbiol.* 49, 385–392. doi: 10.1099/00207713-49-2-385

Csonka, L. N., and Hanson, A. D. (1991). Prokaryotic osmoregulation: genetics and physiology. *Annu. Rev. Microbiol.* 45, 569–606. doi: 10.1146/annurev.mi.45.100191.003033

Dietl, A.-M., Binder, U., Shadkchan, Y., Osherov, N., and Haas, H. (2018). Siroheme is essential for assimilation of nitrate and sulfate as well as detoxification of nitric oxide but dispensable for murine virulence of aspergillus fumigatus. *Front. Microbiol.* 9. doi: 10.3389/fmicb.2018.02615

Du, Z.-J., Wang, Y., Dunlap, C., Rooney, A. P., and Chen, G.-J. (2014). Draconibacterium orientale gen. nov., sp. nov., isolated from two distinct marine environments, and proposal of draconibacteriaceae fam. nov. *Int. J. Syst. Evol. Microbiol.* 64, 1690–1696. doi: 10.1099/ijs.0.056812-0

Flamholz, A., Noor, E., Bar-Even, A., Liebermeister, W., and Milo, R. (2013). Glycolytic strategy as a tradeoff between energy yield and protein cost. *Proc. Natl. Acad. Sci. U. S. A.* 110, 10039–10044. doi: 10.1073/pnas.1215283110

Galinski, E. A., Pfeiffer, H. P., and Trüper, H. G. (1985). doi: 10.1111/j.1432-1033.1985.tb08903.x

Galloway, J. N., Dentener, F. J., Capone, D. G., Boyer, E. W., Howarth, R. W., Seitzinger, S. P., et al. (2004). Nitrogen cycles: past, present, and future. *Biogeochemistry* 70, 153–226. doi: 10.1007/s10533-004-0370-0

Galloway, J. N., Townsend, A. R., Erisman, J. W., Bekunda, M., Cai, Z., and Freney, J. R. (2008). Transformation of the nitrogen cycle: recent trends, questions, and potential solutions. *Science* 320, 889–892. doi: 10.1126/science.1136674

Goris, J., Konstantinidis, K. T., Klappenbach, J. A., Coenye, T., Vandamme, P., and Tiedje, J. M. (2007). DNA–DNA Hybridization values and their relationship to whole-genome sequence similarities. *Int. J. Syst. Evol. Microbiol.* 57, 81–91. doi: 10.1099/ijs.0.64483-0

Griesbeck, C., Hauska, G., and Schütz, M. (2000). Biological sulfide oxidation: Sulfide-quinone reductase (SQR), the primary reaction. *Recent Res. Dev. Microbiol.* 4, 179–203.

Hu, R., Liu, S., Huang, W., Nan, Q., Strong, P. J., Saleem, M., et al. (2022). Evidence for assimilatory nitrate reduction as a previously overlooked pathway of reactive nitrogen transformation in estuarine suspended particulate matter. *Environ. Sci. Technol.* 56, 14852–14866. doi: 10.1021/acs.est.2c04390

Hügler, M., and Sievert, S. M. (2011). Beyond the Calvin cycle: autotrophic carbon fixation in the ocean. *Ann. Rev. Mar. Sci.* 3, 261–289. doi: 10.1146/annurev-marine-120709-142712

Hutchins, D. A., and Capone, D. G. (2022). The marine nitrogen cycle: new developments and global change. *Nat. Rev. Microbiol.* 20, 401–414. doi: 10.1038/s41579-022-00687-z

Jørgensen, B. B. (1990). A thiosulfate shunt in the sulfur cycle of marine sediments. *Science* 249, 152–154. doi: 10.1126/science.249.4965.152

Jørgensen, B. B., and Bak, F. (1991). Pathways and microbiology of thiosulfate transformations and sulfate reduction in a marine sediment (kattegat, denmark). *Appl. Environ. Microbiol.* 57, 847–856. doi: 10.1128/aem.57.3.847-856.1991

Jack, J. M., and Joop, N. (2000). Nitrogen uptake by heterotrophic bacteria and phytoplankton in the nitrate-rich Thames estuary. *Mar. Ecol. Prog. Ser.* 203, 13–21. doi: 10.3354/meps203013

Jiang, X., Dang, H., and Jiao, N. (2015). Ubiquity and diversity of heterotrophic bacterial nasA genes in diverse marine environments. *PloS One* 10, e0117473. doi: 10.1371/journal.pone.0117473

Kanehisa, M., Sato, Y., Kawashima, M., Furumichi, M., and Tanabe, M. (2016). KEGG as a reference resource for gene and protein annotation. *Nucleic Acids Res.* 44, D457–D462. doi: 10.1093/nar/gkv1070

Klappenbach, J. A., Dunbar, J. M., and Schmidt, T. M. (2000). rRNA operon copy number reflects ecological strategies of bacteria. *Appl. Environ. Microbiol.* 66, 1328–1333. doi: 10.1128/AEM.66.4.1328-1333.2000

Komagata, K., and Suzuki, K.-I. (1988). "4 lipid and cell-wall analysis in bacterial systematics," in *Methods in microbiology* (Elsevier) 19, 161–207. doi: 10.1016/S0580-9517(08)70410-0

Kumar, S., Stecher, G., and Tamura, K. (2016). MEGA7: molecular evolutionary genetics analysis version 7.0 for bigger datasets. *Mol. Biol. Evol.* 33, 1870–1874. doi: 10.1093/molbev/msw054

Lane, D. J. (1991). 16S/23S sequencing. *Nucl. Acid Techniques Bacterial Syst.* 116–147.

Liu, X., Jiang, L., Hu, Q., Lyu, J., and Shao, Z. (2020). Thiomicrorhabdus indica sp. nov., an obligately chemolithoautotrophic, sulfur-oxidizing bacterium isolated from a deep-sea hydrothermal vent environment. *Int. J. Syst. Evol. Microbiol.* 70, 234–239. doi: 10.1099/ijsem.0.003744

Luque-Almagro, V. M., Gates, A. J., Moreno-Vivián, C., Ferguson, S. J., Richardson, D. J., and Roldán, M. D. (2011). Bacterial nitrate assimilation: gene distribution and regulation. *Biochem. Soc Trans.* 39, 1838–1843. doi: 10.1042/BST20110688

Meier-Kolthoff, J. P., Auch, A. F., Klenk, H.-P., and Göker, M. (2013). Genome sequence-based species delimitation with confidence intervals and improved distance functions. *BMC Bioinf.* 14, 1–14. doi: 10.1186/1471-2105-14-60

Mergeay, M., Nies, D., Schlegel, H. G., Gerits, J., Charles, P., and Van Gijsegem, F. (1985). Alcaligenes eutrophus CH34 is a facultative chemolithotroph with plasmid-bound resistance to heavy metals. *J. Bacteriol.* 162, 328–334. doi: 10.1128/jb.162.1.328-334.1985

Minnikin, D. E., O'donnell, A. G., Goodfellow, M., Alderson, G., Athalye, M., Schaal, A., et al. (1984). An integrated procedure for the extraction of bacterial isoprenoid quinones and polar lipids. *J. Microbiol. Methods* 2, 233–241. doi: 10.1016/0167-7012(84)90018-6

Murphy, M. J., Siegel, L. M., Tove, S. R., and Kamin, H. (1974). Siroheme: a new prosthetic group participating in six-electron reduction reactions catalyzed by both sulfite and nitrite reductases. *Proc. Natl. Acad. Sci. U. S. A.* 71, 612–616. doi: 10.1073/pnas.71.3.612

Nguyen, P. M., Do, P. T., Pham, Y. B., Doan, T. O., Nguyen, X. C., Lee, W. K., et al. (2022). Roles, mechanism of action, and potential applications of sulfur-oxidizing

bacteria for environmental bioremediation. *Sci. Total Environ.* 852, 158203. doi: 10.1016/j.scitotenv.2022.158203

Nguyen, L.-T., Schmidt, H. A., Von Haeseler, A., and Minh, B. Q. (2015). IQ-TREE: a fast and effective stochastic algorithm for estimating maximum-likelihood phylogenies. *Mol. Biol. Evol.* 32, 268–274. doi: 10.1093/molbev/msu300

Nies, D. H. (1995). The cobalt, zinc, and cadmium efflux system CzcABC from alcaligenes eutrophus functions as a cation-proton antiporter in escherichia coli. *J. Bacteriol.* 177, 2707–2712. doi: 10.1128/jb.177.10.2707-2712.1995

Nies, D. H. (2003). Efflux-mediated heavy metal resistance in prokaryotes. *FEMS Microbiol. Rev.* 27, 313–339. doi: 10.1016/S0168-6445(03)00048-2

Nies, D. H., and Silver, S. (1989). Plasmid-determined inducible efflux is responsible for resistance to cadmium, zinc, and cobalt in alcaligenes eutrophus. *J. Bacteriol.* 171, 896–900. doi: 10.1128/jb.171.2.896-900.1989

Reed, R. H. (1990). Microbial water stress physiology: principles and perspectives. *Trends Biotechnol.* 8, 365.

Reitzer, L. (2003). Nitrogen assimilation and global regulation in escherichia coli. *Annu. Rev. Microbiol.* 57, 155–176. doi: 10.1146/annurev.micro.57.030502.090820

Roesser, M., and Müller, V. (2001). Osmoadaptation in bacteria and archaea: common principles and differences. *Environ. Microbiol.* 3, 743–754. doi: 10.1046/j.1462-2920.2001.00252.x

Salvador, M., Argandoña, M., Naranjo, E., Piubeli, F., Nieto, J. J., Csonka, L. N., et al. (2018). Quantitative RNA-seq analysis unveils osmotic and thermal adaptation mechanisms relevant for ectoine production in chromohalobacter salexigens. *Front. Microbiol.* 9. doi: 10.3389/fmicb.2018.01845

Sasser, M. (1990). Identification of bacteria by gas chromatography of cellular fatty acids. *Usfcc Newsl.* 20, 1–7.

Smibert, R. M. (1994). Phenotypic characterization. *Methods Gen. Mol. Bacteriol.*, 607–654.

Sparacino-Watkins, C., Stolz, J. F., and Basu, P. (2014). Nitrate and periplasmic nitrate reductases. *Chem. Soc Rev.* 43, 676–706. doi: 10.1039/c3cs60249d

Ventosa, A., Nieto, J. J., and Oren, A. (1998). Biology of moderately halophilic aerobic bacteria. *Microbiol. Mol. Biol. Rev.* 62, 504–544. doi: 10.1128/MMBR.62.2.504-544.1998

Wang, T., Ran, M., Li, X., Liu, Y., Xin, Y., Liu, H., et al. (2022). The pathway of sulfide oxidation to octasulfur globules in the cytoplasm of aerobic bacteria. *Appl. Environ. Microbiol.* 88, e0194121. doi: 10.1128/AEM.01941-21

Yoon, S.-H., Ha, S.-M., Kwon, S., Lim, J., Kim, Y., Seo, H., et al. (2017). Introducing EzBioCloud: a taxonomically united database of 16S rRNA gene sequences and whole-genome assemblies. *Int. J. Syst. Evol. Microbiol.* 67, 1613–1617. doi: 10.1099/ijsem.0.001755

Zhu, K.-L., Wang, X.-Q., Zhang, T.-S., Shang, D.-D., and Du, Z.-J. (2021). Salibaculum halophilum gen. nov., sp. nov. and salibaculum griseiflavum sp. nov., in the family rhodobacteraceae. *Int. J. Syst. Evol. Microbiol.* 71, 4808. doi: 10.1099/ijsem.0.004808

frontiers | Frontiers in Marine Science

TYPE Original Research
PUBLISHED 19 May 2023
DOI 10.3389/fmars.2023.1166287

OPEN ACCESS

EDITED BY
Xue-Wei Xu,
Ministry of Natural Resources, China

REVIEWED BY
Ravi Raghavbhai Sonani,
University of Virginia, United States
Bin Wei,
Zhejiang University of Technology, China

*CORRESPONDENCE
Heng-Lin Cui
cuihenglin@ujs.edu.cn

RECEIVED 15 February 2023
ACCEPTED 09 May 2023
PUBLISHED 19 May 2023

CITATION
Han D, Hou J and Cui H-L (2023) An extracellular protease containing a novel C-terminal extension produced by a marine-originated haloarchaeon. *Front. Mar. Sci.* 10:1166287. doi: 10.3389/fmars.2023.1166287

An extracellular protease containing a novel C-terminal extension produced by a marine-originated haloarchaeon

Dong Han[1,2], Jing Hou[1] and Heng-Lin Cui[1]*

[1]School of Food and Biological Engineering, Jiangsu University, Zhenjiang, China, [2]School of Grain Science and Technology, Jiangsu University of Science and Technology, Zhenjiang, China

Marine microorganisms have long been acknowledged as a significant reservoir of enzymes required for industrial use. In this study, a novel extracellular protease *Hsl*HlyB derived from marine-originated haloarchaeon *Halostella pelagica* DL-M4^T was identified. *Hsl*HlyB contained polycystic kidney disease (PKD) domain and pre-peptidase C-terminal (PPC) domain at the C-terminus. Truncation and replacement of the C-terminal extension (CTE) of *Hsl*HlyB demonstrated the importance of the CTE in maintaining the protease activity secreted by haloarchaeon. *Hsl*HlyB and *Hsl*HlyBΔCTE were expressed in *Escherichia coli* BL21(DE3), and purified by high-affinity column refolding and gel filtration chromatography. The molecular masses of *Hsl*HlyB and *Hsl*HlyBΔCTE were 42 kDa and 20 kDa, respectively. The optimum catalytic reaction conditions were 50°C, pH 8.5, NaCl 3.5 M and 50°C, pH 7.5, NaCl 3 M, respectively. They showed good stability and hydrolysis capabilities towards a wide range of protein substrates. *Hsl*HlyBΔCTE showed higher catalytic reaction rate and better thermal stability than the wild type against azocasein and tetrapeptide substrate. The hydrolysates of soybean protein hydrolyzed by *Hsl*HlyBΔCTE had smaller average molecular masses and shorter average peptide chain lengths than those by *Hsl*HlyB. These results indicated the diversity of halolysins from marine-originated haloarchaea to harness organic nitrogen in the marine environment and provided promising candidates for application in various industries.

KEYWORDS

halolysin, C-terminal extension, haloarchaeon, tidal flat, marine solar salt

Introduction

It is widely recognized that marine is a reservoir of biological resources, harboring diverse microorganisms and functional enzymes. Intertidal zones with variable salinity, temperature and nutrient are kinds of important marine ecosystems including a variety of habitats, such as rocky shores, sandy beaches, soft sediments, salt marshes and mangroves

(Kon et al., 2020). Haloarchaea are the most salt-requiring and salt-resistant microorganisms partly thriving in marine salt inhabitants, such as marine solar salterns, marine lagoons and costal sediment (Lee, 2013; Cui and Dyall Smith, 2021; Sun et al., 2023). The haloarchaea that inhabit this zone have adapted to extremely harsh environments and evolved the ability to produce enzymes that function optimally in high salt concentrations, even in extreme pH and temperatures (Amoozegar et al., 2017). It is increasingly interesting to look for specific enzymes with high thermal stability, high tolerance with wide range of salinities produced by haloarchaea to meet the needs of industrial applications.

Halolysin is a kind of proteases that are secreted extracellularly by haloarchaea and exert endo-protease activity. Halolysins reported so far all belong to serine proteases with molecular masses range of 21-130 kDa (Studdert et al., 1997; Elsztein et al., 2001; Studdert et al., 2001; Elbanna et al., 2015). Halolysin plays important ecological roles in organic nitrogen degradation in saline environments and provides its host with antagonistic and defensive activities against other haloarchaea for competitive advantage (Chen et al., 2021). Halolysins were considered as excellent candidates in industries such as food production (Chaveesuk et al., 1994; Yongsawatdigul et al., 2007; Akolkar et al., 2010), cleaning agent (Jaouadi et al., 2008), peptide synthesis (Ryu et al., 1994; Ruiz et al., 2010), detergent (Akolkar et al., 2008) and waste management (Lefebvre and Moletta, 2006).

A number of halolysins have been already reported with known coding genes, including halolysins 172P1 from *Natrialba asiatica* 172P1 (Kamekura et al., 1992), R4 from *Haloferax mediterranei* R4 (Kamekura et al., 1996), SptA and SptC from *Natrinema* sp. J7 (Zhang et al., 2014; Du et al., 2015), Nep from *Natrialba magadii* (De Castro et al., 2008), HlyA from *Halococcus salifodinae* (Hou et al., 2020), Hly_{Hap} from *Haladaptatus* sp. DYF46 (Hou et al., 2022). For protein domain organization, those halolysin precursors are usually made up of a Tat (twin-arginine translocation) signal peptide, an N-terminal propeptide, an S8/S53 family catalytic domain and a C-terminal extension (CTE). The CTE of halolysins are usually prepeptidase C-terminal (PPC) domain, except a combined polycystic kidney disease (PKD) domain and chitin-binding domain (ChBD) was reported in the CTE of SptC (Du et al., 2015). In recent years a marine halolysin Hly_{Hap} without CTE was discovered to prefer a low salinity in contrast to most halolysins (Hou et al., 2022). CTE domains have been shown to have a significant impact on the structure and function of a protease (Gao et al., 2010), especially those secreted by the marine bacteria (Huang et al., 2017). The halolysins thus far reported are much less diverse than those of proteases from bacteria, especially halolysins of marine origin that possess ecological significance and deserve to be explored more deeply.

Strain DL-M4^T with ability of hydrolysis of gelatin and casein is the type strain of *Halostella pelagica* and was isolated from the salted seaweed produced in Dalian, Liaoning Province, China (Han and Cui, 2020). Strain DL-M4^T may originate from marine solar salt or *Laminaria* farmed in tidal zone. In this study, the potential extracellular protease genes from *Hsl. pelagica* DL-M4^T were identified, and the recombinant halolysins with different CTE domains were expressed in the heterologous host, *Haloferax volcanii* H1424, in order to explore the effect of different CTE on *Hsl*HlyB activity. Furthermore, *Hsl*HlyB and *Hsl*HlyBΔCTE were purified and characterized to explore the diversity of the catalytic properties of halolysins and the effect of CTE on enzymatic properties. At last, the potential application of *Hsl*HlyB and *Hsl*HlyBΔCTE in hydrolysis of soybean protein under high-salt concentration were evaluated. This study would enrich our knowledge of the diversity of marine halolysins and provide a promising halophilic protease.

Materials and methods

Strains and growth conditions

Hsl. pelagica DL-M4^T (=CGMCC 1.13603^T = JCM 32954^T, GenBank accession numbers: 16S rRNA gene MH062945, genome CP040678-CP040681) with the hydrolysis ability towards casein and gelatin was isolated from the salted brown alga *Laminaria* in the previous study (Han and Cui, 2020). Other halolysin producing strains of *Hfx. mediterranei* ATCC 33500^T, *Nab. magadii* CGMCC 1.1966^T and *Hcc. salifodinae* DSM 8989^T were also used in this study. They were grown under aerobic conditions at 37°C in neutral haloarchaeal medium (NHM) (Cui et al., 2011). *Hfx. volcanii* H1424 used as the haloarchaeal host for expression was cultured in Hv-YPC medium (Stroud et al., 2012). *Escherichia coli* DH5α and BL21 (DE3) were used as host strains for cloning and protein expression, respectively. Luria-Bertani medium was used to cultivate the above *E. coli* strains at 37°C, if necessary, 100 μg mL^{-1} of ampicillin or 50 μg mL^{-1} of kanamycin was added.

In silico analysis of halolysin genes

The hmm model of Peptidase_S8 domain (Pfam accession: PF00082) was used to search for model-compatible proteins in *Hsl. pelagica* DL-M4^T via the Hmmsearch of Hmmer software (Finn et al., 2011). The protein sequence of Nep from *Nab. magadii* (accession no. AAV66536) was also used to find halolysin genes in the genome of *Hsl. pelagica* DL-M4^T by BlastP tool (Altschul et al., 1997). The resulting potential halolysins were also confirmed against Swiss-Prot databases. The theoretical molecular mass and isoelectric point were predicted using Prot Param (https://web.expasy.org/protparam/). Signal peptide prediction was performed using SignalP 5.0 (Armenteros et al., 2019). Protein domain prediction was performed using InterProScan (Quevillon et al., 2005). The C-terminal domain structure was modelled by SWISS-MODEL Workspace (https://swissmodel.expasy.org/). The structure of *Hsl*HlyB was predicted by AlphaFold2 (Jumper et al., 2021).

Vector construction

Three potential halolysin genes and *Hsl*HlyB without CTE or PKD domain encoding genes were amplified by PCR using *Hsl.*

pelagica DL-M4^T genomic DNA as the template. The encoding genes for chimeras of *Hsl*HlyB with different CTE domains were obtained using the overlapping extension PCR method as described previously (Hou et al., 2020) using *Hsl. pelagica* DL-M4^T, *Hfx. mediterranei* ATCC 33500^T, *Nab. magadii* CGMCC 1.1966 and *Hcc. salifodinae* DSM 8989^T genomic DNA as the template. The PCR amplification was performed using the KOD-plus-neo DNA polymerase (Toyobo), and primer pairs shown in Table S1. The products were digested with a pUCm-T vector using *Eco*RI, *Bam*HI/*Sph*I or *Nco*I, *Xho*I as the restriction enzyme sites (the restriction endonucleases used for corresponding genes shown in Table S1). The purified amplicons of potential halolysin genes and encoding genes of *Hsl*HlyB variants were cloned into the haloarchaeal shuttle vector pTA under the strong promoter P.*phaR* (Liu et al., 2015) for expression in *Hfx. volcanii*. The purified amplicons of *HslHlyB* and *HslHlyBΔCTE* were cloned into the vector pET28a under *Lac* promoter for expression in *E. coli* BL21 (DE3). The colony PCR and Sanger sequencing were used to verify the inserts in the constructed plasmids.

Expression and purification of halolysins

There were two kinds of expressing hosts used in this study. For expressing *Hsl*HlyA, *Hsl*HlyB, *Hsl*HlyC and *Hsl*HlyB variants, the expression plasmid was transformed into *Hfx. volcanii* H1424. Cell cultures were grown in Hv-YPC medium at 37°C until the stationary phase. Culture supernatant (12,000 g, 10 min, 4°C) was used as the crude enzyme to assay the extracellular protease activity. To obtain purified enzymes, the *Hsl*HlyB and *Hsl*HlyBΔCTE precursors were expressed in *E. coli* BL21 (DE3) and *in vitro* refolded as previously described (Hou et al., 2021; Hou et al., 2022). For *in vitro* refolding, the recombinant cells were firstly resuspended in lysis buffer (8 M urea, 10 mM $CaCl_2$, 50 mM Tris-HCl, 2 mM β-mercaptoethanol, pH 8.0). After sonicating and centrifuging, the supernatant containing denatured precursors was loaded onto the 2 mL Ni-column, then washed with lysis buffer containing 40 mM imidazole. The Ni-column bound precursors were incubated in refolding buffer (4 M NaCl, 10 mM $CaCl_2$, 50 mM Tris-HCl, pH 8.0) for 24 h at 37°C to fully refold. After washing with the refolding buffer containing 20 mM imidazole, the target proteins were eluted using the refolding buffer containing 100 mM imidazole. The refolded halolysins were further purified by molecular sieves using the Superdex 200 10/300 GL column (GE healthcare).

Functional screening of potential halolysins and *Hsl*HlyB mutants for hydrolytic activities

The Hv-YPC agar plates added with 0.5% (w/v) skim milk or gelatin were used to evaluate the protein hydrolysis capacity of the recombinant haloarchaeal cells (inoculation amount: 5 μL). The plates were incubated at 37°C for 14 days for activity verification. Frazier's reagent (g/L: $HgCl_2$, 150 g; concentrated HCl, 200 mL) was used to detect the hydrolysis of gelatin.

Enzyme activity assay

Enzyme activity towards azocasein (Sigma-Aldrich, USA) and N-Succinyl-Ala-Ala-Pro-Phe p-nitroanilide (Suc-AAPF-pNA, Sigma-Aldrich, USA) was determined as previously described (Hou et al., 2021). For determination of azocaseinolytic activity, 250 μL of crude enzyme was reacted with an equal volume of 0.5% azocasein (buffer: 2 M NaCl, 50 mM Tris-HCl, pH 8.0) at 37°C for 1 h. The reaction was terminated by the addition of 500 μL of 10% TCA, left at room temperature for 15 min and then centrifuged at 10,000 g for 10 min. 300 μL of supernatant was added to an equal volume of 1 M NaOH, and then centrifuged to remove the precipitate. The absorbance of the supernatant at 440 nm (A_{440}) was recorded. In the control experiments, solutions of the enzyme and substrate were incubated separately. Under specific reaction conditions the amount of enzyme required to increase OD_{440} by 0.01 was defined as 1 unit of enzyme activity. When purified enzyme was used for azocaseinolytic activity assay, 10 μg of enzyme was used in each reaction. For the enzyme activity towards Suc-AAPF-pNA, 300 μL of crude enzyme was mixed with 300 μL of Suc-AAPF-pNA (0.4 mM) in the buffer of 2 M NaCl, 50 mM Tris HCl (pH 8.0). The initial hydrolysis rate of the tetrapeptide substrate was measured at 410 nm using a DU800 Nucleic Acid Protein Analyzer with the temperature controlled at 37°C. One unit of protease activity (U) was defined as the amount of enzyme required to produce 1 μmol pNa (extinction coefficient of 8,480 $M^{-1}cm^{-1}$) per minute under certain conditions. Protein concentration was measured by Bradford assay (Beyotime Institute of Biotechnology, China) (Bradford, 1976).

Effect of temperature, pH and salinity on protease activities

To determine the optimal reaction temperature, protease activities were measured at temperatures of 20°C, 30°C, 35°C, 40°C, 45°C, 50°C, 55°C, 60°C and 65°C, respectively, in 2 M NaCl, 50 mM Tris-HCl (pH 8.0). Thermal stability was determined by pre-incubation of the enzyme at 30°C, 40°C, 50°C and 60°C for 0 min, 20 min, 40 min and 60 min, respectively. Then the protease activity was measured at optimum temperature.

The optimal pH was determined by assaying protease activities at the optimum temperature and 2 M NaCl in different buffers of 50 mM K_2HPO_4/KH_2PO_4 buffer at pH 6.0, pH 6.5, pH 7.0 and pH 7.5; 50 mM Tris-HCl buffer at pH 7.5, pH 8.0, pH 8.5 and pH 9.0; 50 mM CHES-NaOH buffer at pH 9.0, pH 10.0 and pH 10.5. pH stability was determined by pre-incubation of the enzyme at room temperature at pH 6.0 (50 mM K_2HPO_4/KH_2PO_4 buffer), pH 8.0 (50 mM Tris-HCl buffer) and pH 10.0 (50 mM CHES-NaOH buffer) for 0 min, 20 min, 40 min and 60 min, respectively. Then the protease activity was measured at the optimum temperature.

The optimal NaCl concentration was determined by assaying at NaCl concentrations of 0.4 M, 0.5 M, 1.0 M, 1.5 M, 2.0 M, 2.5 M, 3.0 M, 3.5 M and 4.0 M, respectively, at the optimum pH and temperature. Salinity stability was determined by pre-incubation of the enzyme at room temperature with 0 M, 2 M and 4 M NaCl for 0 min, 20 min, 40 min and 60 min, respectively. Then the protease activity was measured at the optimum reaction condition.

Effect of different compounds on protease activities

The protease activities were measured with additives of 5 mM of metal ions or 5% (v/v) of organic solvents or 10% (v/v) of detergents. The protease inhibitors included 4 mM phenylmethylsulfonyl fluoride (PMSF), 10 mM pepsin inhibitor (Pepstatin A), 1 mM p-chloromercuribenzoate (PCMB), 10 mM dithiothreitol (DTT) and 5 mM ethylene diamine tetraacetic acid (EDTA). The protease activities were measured at their respective optimal conditions (3.5 M NaCl, 50°C, pH 8.5 for *Hsl*HlyB and 3 M NaCl, 50°C, pH 7.5 for *Hsl*HlyBΔCTE).

Hydrolysis of different protein substrates

The enzyme activity (in terms of tyrosine produced) was determined by reacting with azocasein, casein, gelatin, bovine serum protein, bovine hemoglobin, egg albumin, fish collagen or skim milk at a final concentration of 5 g/L under their respective optimal conditions (3.5 M NaCl, 50°C, pH 8.5 for *Hsl*HlyB and 3 M NaCl, 50°C, pH 7.5 for *Hsl*HlyBΔCTE).

Determination of K_m and V_{max}

The kinetic parameters of the purified halolysins were determined against 0.01-9.44 mM azocasein or 0.01-2 mM Suc-AAPF-pNA. The reaction with 0.8 μg protease was performed at the optimal conditions. The K_m and V_{max} values were calculated from the Michaelis-Menten equation by nonlinear regression (GraphPad Prism 7).

Sodium dodecyl sulphate-polyacrylamide gel electrophoresis analysis

Tris-glycine SDS-PAGE was performed according to the method of King and Laemmli (King and Laemmli, 1971). To prevent the self-degradation of halolysin during the sample pretreatment, TCA-acetone precipitation was used to denature halolysin, referring to Hou's method (Hou et al., 2021). After that, 20-40 μL of loading buffer containing 8 M urea was added to the protein precipitate with DTT at a final concentration of 100 mM, and the supernatant was used for SDS-PAGE analysis.

Protein sequencing and molecular mass determination

After tris-glycine SDS-PAGE analysis, the protein bands were in-gel digested as described by Shevchenko (Shevchenko et al., 1996), and the tryptic peptides were sequenced using Matrix-Assisted Laser Desorption Ionization Time of Flight/Time of Flight Mass Spectrometry (MALDI-TOF/TOF MS) (AB Sciex 5800, USA). The molecular mass of the mature halolysin was determined by gel filtration chromatography as previously described (Hou et al., 2021).

Mass spectrometry analysis of the soybean protein isolate hydrolysates

Soybean protein isolate (Sinopharm) was washed three times with sterile distilled water to remove soluble peptides. The reaction with 0.1 mg/mL enzyme and 5% (m/v) soybean protein isolate was carried out under optimum reaction conditions (3.5 M NaCl, 50°C, pH 8.5 for *Hsl*HlyB and 3 M NaCl, 50°C, pH 7.5 for *Hsl*HlyBΔCTE) for 24 h. The enzyme was inactivated in boiling water bath for 10 min. The protein hydrolysate solution was filtered, then desalted by a C18 column and identified by LC-MS (Agilent 1260/6460 LC/Triple Quadrupole MS).

Results and discussion

Identification of potential halolysin genes from *Hsl. pelagica* DL-M4^T

Hmmer is a sensitive search tool for searching homologs protein by using hidden Markov models. The Pfam hmm model of Peptidase_S8 domain was used to search for potential halolysin genes. Nep, a most intensively-studied halolysin from *Nab. magadii* (De Castro et al., 2008), was also used to search for potential halolysin by BlastP tool. Three potential halolysins *Hsl*HlyA, *Hsl*HlyB and *Hsl*HlyC were found, with 24.5-56.0% identities to Nep (Table S2). Their amino acid sequences were compared against the SwissProt database. The most similar protein for *Hsl*HlyA was found to be SubE, the Bacillus subtilis protease, from *Bacillus licheniformis*, with 37.8% amino acid identity; the most similar proteins for *Hsl*HlyB and *Hsl*HlyC were halolysin from *Hfx. mediterranei* R4, with amino acid identities of 57.4% and 23.9%, respectively. The theoretical molecular masses of *Hsl*HlyA (383 aa), *Hsl*HlyB (613 aa) and *Hsl*HlyC (488 aa) were 39.5, 63.0 and 51.2 kDa and pI values of 4.20, 4.06 and 4.30, respectively. All of them contained Tat signal peptide and S8/S53 peptidase catalytic domain with aspartate-histidine-serine catalytic active sites. *Hsl*HlyA and *Hsl*HlyC did not contain any CTE while *Hsl*HlyB was found to contain two domains, PKD domain and PPC domain, at the C-terminus. SWISS-MODEL homology modeling was used to predict the secondary structure of PKD and PPC domains of *Hsl*HlyB, and found that they both have seven β-sheets (Figure S1). The structure

of *Hsl*HlyB was determined with molecular replacement using a model obtained from Alphafold2 (the predicted local distance difference test score is 87.4). The 3D structure shows that *Hsl*HlyB consists of 4 domains, with 2 independent β-sandwich structures at the C-terminus (Figure S1). Some proteases distributed in different families contain CTEs, such as PKD domain, PPC domain and ChBD domain (Huang et al., 2017). These domains are different in amino acid sequences and also structures (Huang et al., 2019). But they are all rich in β-sheets (Huang et al., 2017). There are several studies on CTE function of bacterial proteases (Wang et al., 2010; He et al., 2012), but few studies on CTE of haloarchaeal proteases (Xu et al., 2011; Marem et al., 2018).

The potential halolysin genes were expressed in the non-extracellular protease-producing *Hfx. volcanii* H1424, a halophilic archaeal host, to investigate whether the encoded protein was active. Only the recombinant strain expressing *Hsl*HlyB showed significant hydrolysis zones on milk and gelatin plates, those expressing *Hsl*HlyA or *Hsl*HlyC could not hydrolyze milk or gelatin (Figures 1A, B). Meanwhile, the extracellular supernatant of the recombinant strain with *Hsl*HlyB had the ability to hydrolyze azocasein and Suc-AAPF-pNA, that of *Hsl*HlyA could weekly hydrolyze Suc-AAPF-pNA but not azocasein, and that of *Hsl*HlyC could not hydrolyze azocasein or Suc-AAPF-pNA (Figure 1C). According to these results, *Hsl*HlyB has low sequence similarity to other reported proteases (with the highest identity of 57.4% in SwissProt database) and ability to hydrolyze milk, gelatin, azocasein and tetra-peptide substrate. To our knowledge, no halolysin from the genus *Halostella* has been characterized. Additionally, this is the first reported halolysin with PKD and PPC domains at the C-terminus.

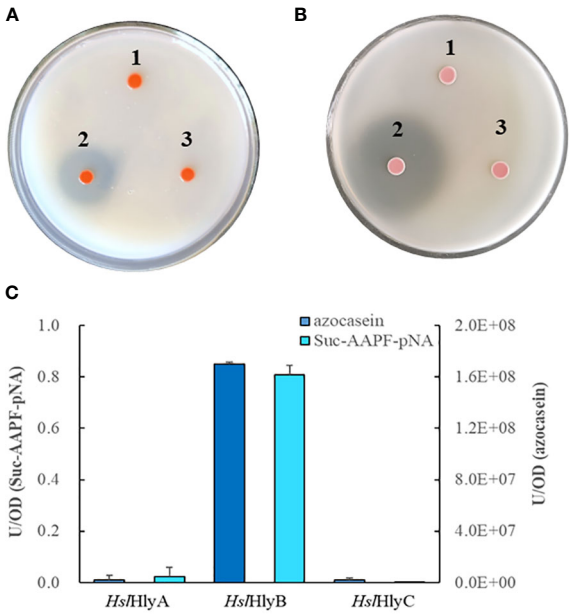

FIGURE 1
Protein hydrolysis by recombinant *Hfx. volcanii* cells. Hydrolysis of skim milk **(A)** and gelatin **(B)** on YPC agar plates, azocasein and Suc-AAPF-pNA hydrolytic activity **(C)** of cell-free culture supernatants of recombinant *Hfx. volcanii*. 1, *Hsl*HlyA; 2, *Hsl*HlyB; 3, *Hsl*HlyC.

Effect of CTEs on *Hsl*HlyB activity

CTE is prevalent in halolysins. It has important effects on enzyme activity and enzyme secretion. The novel C-terminal domains of *Hsl*HlyB consist of a PKD domain and a PPC domain. To investigate the effect of CTEs on enzymatic activity, *Hsl*HlyBΔPKD and *Hsl*HlyBΔCTE were constructed, with deletion of *Hsl*HlyB PKD domain and the whole CTE domain. In contrast to the strain expressing wild-type *Hsl*HlyB, the recombinant strains showed reductions in hydrolysis circle size on milk plates and also decreased activities against azocasein and Suc-AAPF-pNA (Figures 2B, C). The extracellular supernatant activity of the recombinant strain with *Hsl*HlyBΔPKD towards azocasein and Suc-AAPF-pNA decreased by 54.5% and 56.5%, respectively. The extracellular supernatant activity of the strain expressing *Hsl*HlyBΔCTE showed undetectable protease activity.

The CTE domain is self-stabilizing and can fold independently. Our previous study found that CTE domain can be functionally interchangeable among halolysins (Hou et al., 2020). To investigate the effect of CTE on *Hsl*HlyB activity, three chimeras, *Hsl*HlyB-HlyAC, *Hsl*HlyB-R4C and *Hsl*HlyB-NepC, namely, *Hsl*HlyB catalytic domain with the CTE of HlyA from *Hcc. salifodinae* (119 aa), R4 from *Hfx. mediterranei* (114 aa) and Nep from *Nab. magadii* (131 aa) (Kamekura et al., 1996; De Castro et al., 2008; Hou et al., 2020) (Figure 2A) were heterologously expressed in *Hfx. volcanii* H1424. The extracellular proteolytic activities were determined. The strains expressing *Hsl*HlyB-NepC cannot hydrolyze milk and had no activity towards azocasein and Suc-AAPF-pNA (Figures 2B, C). The strains expressing *Hsl*HlyB-HlyAC can hydrolyze milk. The hydrolysis zone of *Hsl*HlyB-R4C expressing strains is larger than those of *Hsl*HlyB-HlyAC expressing strains, while both are smaller than that of wildtype *Hsl*HlyB expressing strains (Figure 2B). The activity of the culture supernatant of cells expressing *Hsl*HlyB-HlyAC towards azocasein and Suc-AAPF-pNA decreased by 89.5% and 87.9%, respectively, and that of *Hsl*HlyB-R4C decreased by 93.9% and 89.6%, respectively (Figure 2C). The extracellular activities of recombinant strains expressing *Hsl*HlyB-HlyAC and *Hsl*HlyB-R4C towards tetrapeptide, a small molecule substrate, decreased less than that of azocasein, indicating that the CTE may affect the hydrolysis ability towards different substrates. The CTE of halolysins R4 from *Hfx. mediterranei*, HlyA from *Hcc. salifodinae*, Nep from *Nab. magadii* significantly reduced or abolished the extracellular enzyme activity of *Hsl*HlyB after substitution. The decreased extracellular enzyme activity is possibly because heterologous CTEs affect the correct folding of the *Hsl*HlyB catalytic domain. The effect of CTEs on halolysin activity remains to be investigated in depth.

Purification and refolding of *Hsl*HlyB and *Hsl*HlyBΔCTE

*Hsl*HlyB and *Hsl*HlyBΔCTE with 6×His tag at the C-terminus were expressed in *E. coli* BL21 (DE3). Both intracellular lysate and culture supernatant of *E. coli* were without protease activity after induced expression. The protease precursors were obtained by affinity chromatography and confirmed by MALDI-TOF/TOF MS

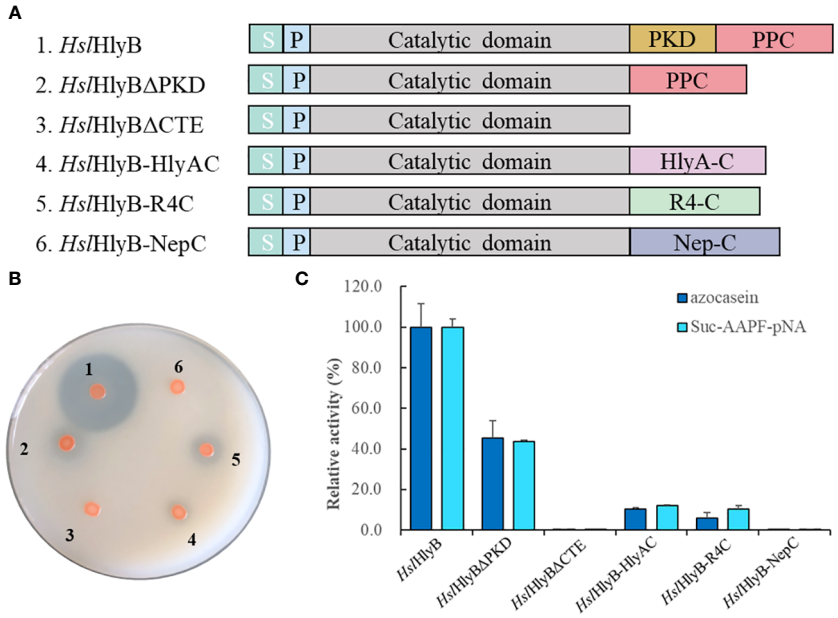

FIGURE 2
Effect of CTE on *Hsl*HlyB activity. **(A)** Domain arrangement of *Hsl*HlyB and the chimeras. S: signal peptide, P: propeptide, PKD: polycystic kidney disease domain, PPC: prepeptidase C-terminal domain, HlyA-C:C-terminal extension of HlyA, R4-C: C-terminal extension of R4, Nep-C: C-terminal extension of Nep. **(B)** Hydrolysis of skim milk by recombinant *Hfx. volcanii* cells on YPC agar plates. **(C)** Azocasein and Suc-AAPF-pNA hydrolytic activity of cell-free culture supernatants of recombinant *Hfx. volcanii*. 1, *Hsl*HlyB; 2, *Hsl*HlyBΔPKD; 3, *Hsl*HlyBΔCTE; 4, *Hsl*HlyB-HlyAC; 5, *Hsl*HlyB-R4C; 6, *Hsl*HlyB-NepC.

(Figure 3). The molecular mass of the protease precursor estimated from the *Hsl*HlyB protein sequence was 63 kDa, while the apparent molecular masses from SDS-PAGE were 108 kDa and 96 kDa. The presence of two bands of *Hsl*HlyB precursor was due to the excision of N-terminal sequences (Figure 3C). As for *Hsl*HlyBΔCTE, a single band with an apparent molecular mass of about 68 kDa was obtained. The phenomenon that the apparent molecular mass is much larger than the predicted molecular mass is common in the SDS-PAGE analysis of halophilic proteins (Alves et al., 2004; Karan et al., 2013; Gao et al., 2017), which is caused by the decrease of protein migration rate with the high content of acidic amino acids in halophilic proteins.

On-column refolding was performed to allow the mature enzymes to be obtained by self-processing with its C-terminus bound to Ni-agarose. The refolding product of *Hsl*HlyB revealed two bands on SDS-PAGE gel, and that of *Hsl*HlyBΔCTE revealed a major band (Figures 3A, B). The *Hsl*HlyB refolding product consisted of mature enzyme, and also CTE fraction from autodegradation (Figure 3C). The refolding product of *Hsl*HlyBΔCTE corresponded to the catalytic domain identified by MALDI-TOF/TOF MS (Figure 3C). The refolding products were further purified by Superdex 200 GL column (Figures S2A, B). The purified products each revealed a major band on SDS-PAGE gel (Figures S2C, D). Combined with the molecular sieve profiles of protein standards with known molecular mass, the molecular mass of *Hsl*HlyB and *Hsl*HlyBΔCTE were estimated to be 42 kDa and 20 kDa, respectively. Halolysins, like most subtilases, are autocatalyzed into mature enzymes by *cis*- and *trans*-processing (Ruiz et al., 2012; Du et al., 2015). The purified precursors could autocatalyze to mature enzymes in high salt environments. Both CTE truncates and wild-type proteases were able to mature *in vitro*. However, when *Hsl*HlyBΔCTE was expressed in *Hfx. volcanii*, the recombinant strains showed no extracellular protease activity, similarly to the removal of the CTE from halolysin R4 and SptA (Kamekura et al., 1996; Xu et al., 2011). The immunoblot analysis of CTE truncates of SptA showed that no pro- or mature forms were secreted into the extracellular matrix (Xu et al., 2011). In contrast, the studies on Nep from *Nab. magadii* revealed that the absence of CTE did not affect the secretion and maturation of the enzyme in the halophilic archaeon (Marem et al., 2018). These results indicated that CTEs may have different effects on the structure of other domains *in vivo*, thus affecting maturation or secretion for different halolysins. In the case of *Hsl*HlyB in this study, as a subtilisin family enzyme with two β-sandwich domains at the C-terminus, its domain distribution is identical to that of fervidolysin (from *Fervidobacterium pennivorans*) with a sequence identity of 37.69%. The crystal structure of fervidolysin (PDB accession no. 1R6V) suggests that its CTE can create an open hydrophobic pocket that contributes to the fixation of the N-terminal elongated chain of the N-terminal pre-peptide domain (Kim et al., 2004). The study of the metalloprotease PrtV (from *Vibrio cholerae*) showed that the PKD domain with calcium ions controls the flexibility of the protein domain linker (Edwin et al., 2013). The CTE of *Hsl*HlyB probably affects the domain linker of the pre-peptide and plays a regulatory role in proper folding, thus affecting the secretion and autocatalytic maturation of the enzyme *in vivo*. CTE has also been reported to be involved in maintaining the stability of the catalytic domain. The halolysin SptA from *Natrinema* sp. J7 without CTE

10.3389/fmars.2023.1166287

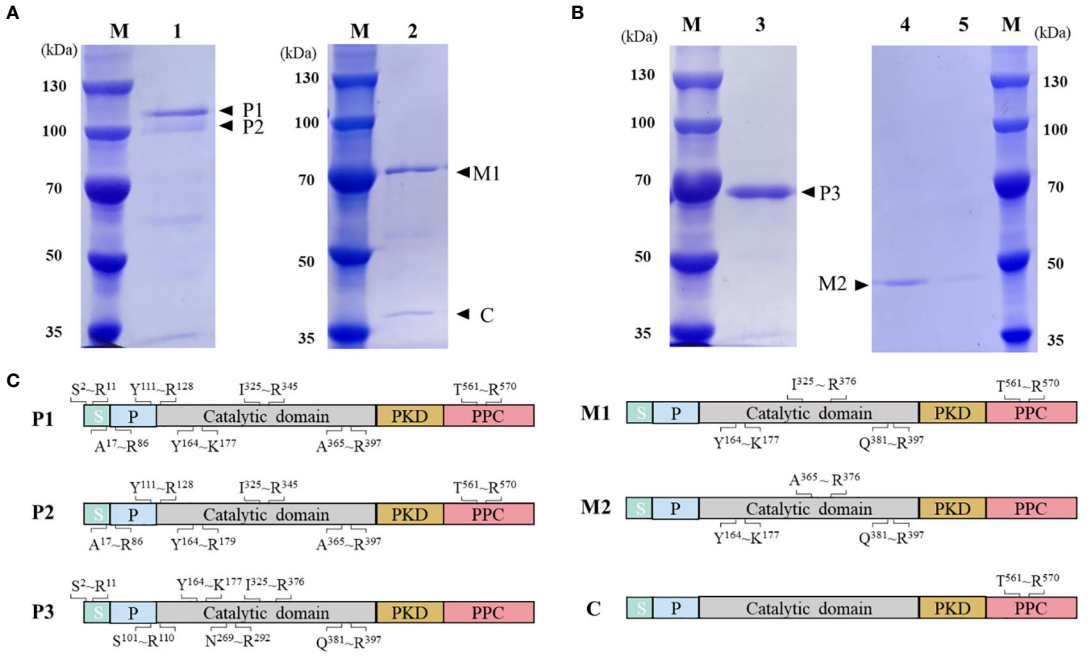

FIGURE 3
Purification and on-column refolding of *Hsl*HlyB and *Hsl*HlyBΔCTE. **(A)** SDS-PAGE analysis of *Hsl*HlyB precursor and mature *Hsl*HlyB. **(B)** SDS-PAGE analysis of *Hsl*HlyBΔCTE precursor and mature *Hsl*HlyBΔCTE. **(C)** MALDI-TOF/TOF MS analysis of protein bands in SDS-PAGE analysis. Sequenced tryptic peptides are marked. P1 and P2: *Hsl*HlyB precursor, P3, *Hsl*HlyBΔCTE precursor; C, the cleaved C-terminal fragments; M1, mature *Hsl*HlyB; M2, mature *Hsl*HlyBΔCTE; M, marker; lane 1, recombinant *Hsl*HlyB precursor purified under denaturing conditions; lane 2, refolded product of *Hsl*HlyB precursor; lane 3, recombinant *Hsl*HlyBΔCTE precursor purified under denaturing conditions; lane 4-5, refolded product of *Hsl*HlyBΔCTE precursor; S, signal peptide; P, propeptide; PKD, polycystic kidney disease domain; PPC, prepeptidase C-terminal domain.

would be more prone to enzyme autolysis (Xu et al., 2011). However, the catalytic domain of *Hsl*HlyB remained stable *in vitro* in the absence of the entire CTE. The structure of halolysins would help dissect the underlying mechanisms.

Effect of temperature, pH and NaCl concentration on *Hsl*HlyB and *Hsl*HlyBΔCTE activity

The optimum reaction temperature for *Hsl*HlyB and *Hsl*HlyBΔCTE was 50°C. They were able to maintain more than 79% and 88% of the maximum enzyme activity at 40-60°C, respectively (Figures 4A, B). The thermal stability of the enzymes was studied based on the residual enzyme activities of the proteases after incubation at different temperatures (Figures 4C, D). The activity of *Hsl*HlyB decreased with increasing incubation time at 60°C, but it could still maintain about 80% of the original enzyme activity after incubation for 60 min. *Hsl*HlyB maintained about 91% of the original enzyme activity after incubation at 50°C for 60 min, and the activity of *Hsl*HlyB did not change significantly after incubation at 30-40°C. Notably, the activity of *Hsl*HlyBΔCTE remained essentially the same after incubation at 30-60°C for 0-60 min. The residual activity of Nep from *Nab. magadii* was >30% of original activity after incubation at 60° C for 2 h (Giménez et al., 2000), that of Hly_{Hap} from *Haladaptatus* sp. DYF46 was 33.9% after incubation at 60°C for 1 h (Hou et al., 2022), and that of Hly from *Hgn. rubrum* RO2-11 was <20% after incubation at 60°C for 1 h (Gao et al., 2017). Both *Hsl*HlyB and *Hsl*HlyBΔCTE have good thermal stability, and *Hsl*HlyBΔCTE shows better thermal stability than wild type enzyme.

The activities of *Hsl*HlyB and *Hsl*HlyBΔCTE in Tris-HCl buffer (pH 7.5-9.0) showed different trends, with *Hsl*HlyB activity increasing and then decreasing, and *Hsl*HlyBΔCTE activity decreasing within pH rise. Their optimal pH was 8.5 and 7.5, respectively (Figures 5A, B). *Hsl*HlyB displayed >83% of the maximal activity within pH 7.5-9.0, and *Hsl*HlyBΔCTE displayed >74% of the maximal activity within pH 7.5-8.5. The activities of *Hsl*HlyB and *Hsl*HlyBΔCTE did not significantly change from 0-60 min when the proteases were incubated at different pH (Figures 5C, D), indicating their good pH stability.

The activities of *Hsl*HlyB and *Hsl*HlyBΔCTE increased with increasing NaCl concentrations at NaCl < 3 M. They maintained more than 93% of the highest catalytic activity in 3-4 M NaCl. Their optimum NaCl concentrations were 3.5 M and 3 M (Figures 6A, B). The salinity stability of *Hsl*HlyB and *Hsl*HlyBΔCTE was similar (Figures 6C, D). The enzyme activity decreased slightly (<10%) after 60 min incubation at NaCl concentrations of 2-4 M. The activity decreased rapidly after 0-60 min of incubation with a NaCl concentration of 0.8 M. The inactivation rate of *Hsl*HlyBΔCTE was faster than that of *Hsl*HlyB. *Hsl*HlyB and *Hsl*HlyBΔCTE were stable at NaCl concentrations >2 M and inactivated at low salt environments. Most halolysin activities increase and then decrease with increasing salt concentration, and the optimal salt concentration for the catalytic reaction is around 2-3 M

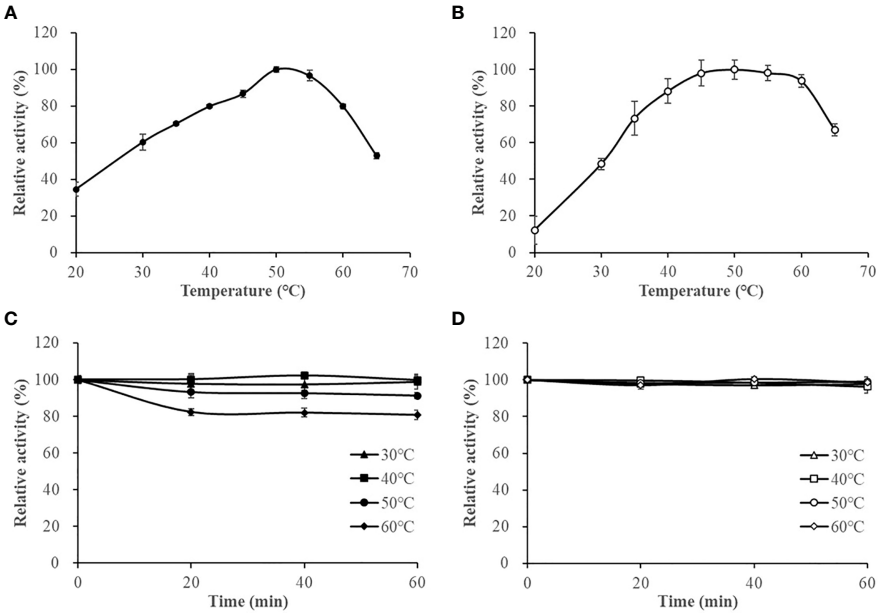

FIGURE 4
The effect of temperature on *Hsl*HlyB **(A)** and *Hsl*HlyBΔCTE activity **(B)**, and the thermal stability of *Hsl*HlyB **(C)** and *Hsl*HlyBΔCTE **(D)**. In **(A, B)**, relative activities were calculated with the maximal activity defined as 100%. In **(C, D)**, the initial enzyme activity was set as 100%, upon which the relative activities of enzymes after incubation at different temperatures for 20, 40 or 60 min were calculated. Mean ± SD of three biological replicates.

(Kamekura et al., 1996; Giménez et al., 2000; Shi et al., 2006; Vidyasagar et al., 2006; Elbanna et al., 2015; Dammak et al., 2016; Hou et al., 2021). In this study, the catalytic activities of *Hsl*HlyB and *Hsl*HlyBΔCTE increased and then remained stable with increasing salt concentration. They reached the highest activity at >3 M salt concentration, thus were more suitable for catalysis in high salt environment.

Effect of metal ions, solvents, surfactants and inhibitors on *Hsl*HlyB and *Hsl*HlyBΔCTE activity

Metal ions are often used as enzyme cofactors. Different metal ions were reported to have different effects on halolysin activity. For *Hsl*HlyB, Fe^{3+}, K^{+}, Mg^{2+} and Mn^{2+} had almost no effect on the

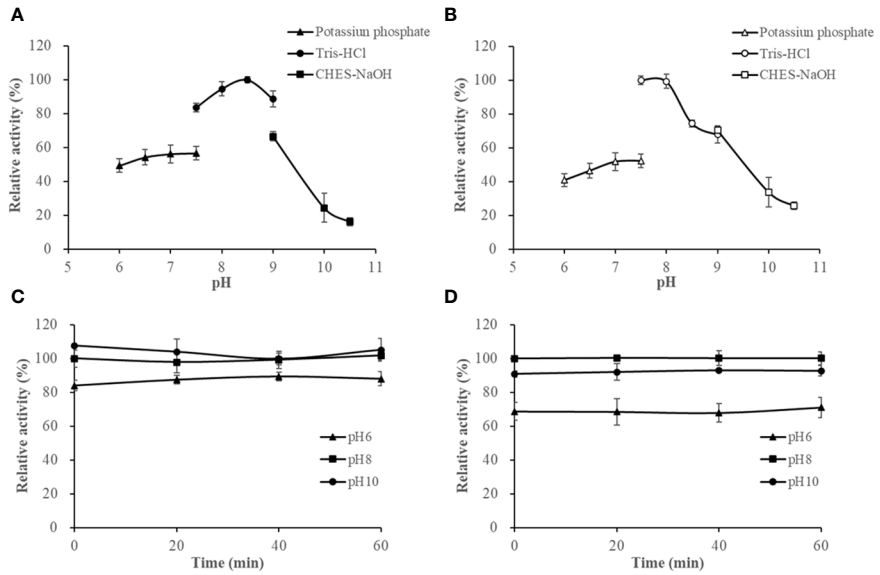

FIGURE 5
The effect of pH on *Hsl*HlyB **(A)** and *Hsl*HlyBΔCTE activity **(B)**, and the pH stability of *Hsl*HlyB **(C)** and *Hsl*HlyBΔCTE **(D)**. In **(A, B)**, relative activities were calculated with the maximal activity defined as 100%. In **(C, D)**, the initial enzyme activity at pH 8.0 was set as 100%, upon which the relative activities of enzymes after incubation at different pH for 20, 40 or 60 min were calculated. Mean ± SD of three biological replicates.

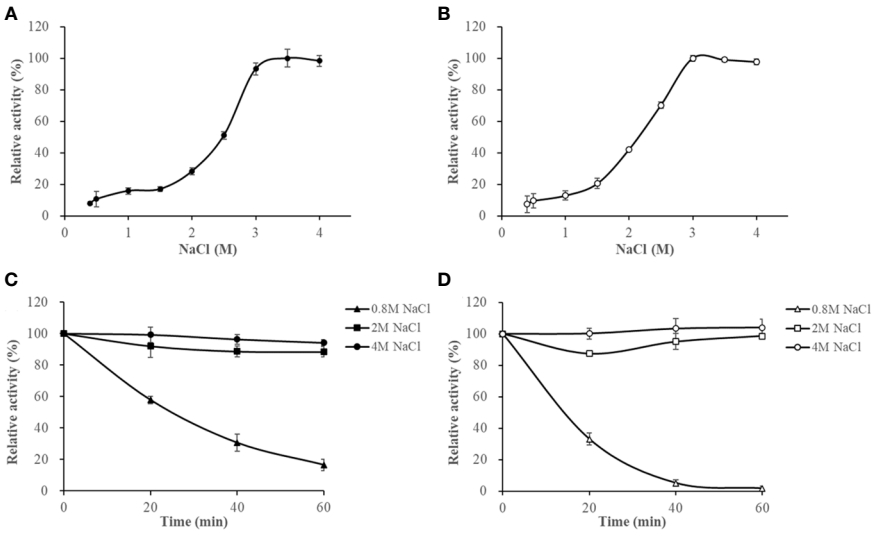

FIGURE 6
The effect of NaCl on *Hsl*HlyB **(A)** and *Hsl*HlyBΔCTE activity **(B)**, and the salinity stability of *Hsl*HlyB **(C)** and *Hsl*HlyBΔCTE **(D)**. In **(A, B)**, relative activities were calculated with the maximal activity defined as 100%. In **(C, D)**, the initial enzyme activity was set as 100%, upon which the relative activities of enzymes after incubation at different salinities for 20, 40 or 60 min were calculated. Mean ± SD of three biological replicates.

enzyme activity, Ca^{2+} and Sr^{2+} slightly promoted the enzyme activity, and Cu^{2+} and Zn^{2+} inhibited 55.1% and 29.6% of the enzyme activity (Figure 7A). For *Hsl*HlyBΔCTE, K^{+}, Ca^{2+}, Mg^{2+}, Sr^{2+} slightly promoted the enzyme activity, Fe^{3+}, Cu^{2+}, Mn^{2+} and Zn^{2+} inhibited 25.2%, 44.4%, 56.5% and 22.4% of the enzyme activity (Figure 7A). Cu^{2+} and Zn^{2+} significantly inhibited both *Hsl*HlyB and *Hsl*HlyBΔCTE activities. Fe^{3+} and Mn^{2+} had a much higher inhibitory effect on the activity of *Hsl*HlyBΔCTE than *Hsl*HlyB. The CTE domain of *Hsl*HlyB affects the tolerance of halolysin to some metal ions.

Different solvents and surfactants decreased the activity of *Hsl*HlyB and *Hsl*HlyBΔCTE to different degrees (Table 1; Figure 7B). The solvents in which the *Hsl*HlyB activity remained above 80% were glycerol, dimethyl sulfoxide (DMSO), and polyethylene glycol (PEG) 600. Isopropyl alcohol and SDS had a significant inhibitory effect on *Hsl*HlyB activity (<50%). The solvents in which *Hsl*HlyBΔCTE activity maintained more than 80% were methanol, glycerol, acetone, DMSO, dimethylformamide (DMF), Tween 20, Tween 80 and PEG 600. Isopropanol, SDS and TritonX-100 had a significant inhibitory effect on *Hsl*HlyBΔCTE activity (<50%). *Hsl*HlyBΔCTE had a better tolerance to organic solvents than wild type enzyme.

The effect of protease inhibitors on *Hsl*HlyB and *Hsl*HlyBΔCTE activity was essentially the same (Figure 7B). 4 mM PMSF completely inhibited the activity of both enzymes, EDTA reduced their activity by 93.0% and 94.3% respectively, Pepstatin A reduced their activity by 4.3%, DTT reduced their activity by 60.3% and 59.1% respectively, and PCMB increased their enzymatic activity by 14.1% and 9.2%. This suggested that *Hsl*HlyB and *Hsl*HlyBΔCTE may be metal ion-dependent serine proteases and that disulfide bonds are important for their activity.

Determination of K_m, V_{max} and proteolytic activity

The data obtained were well described by the Michaelis-Menten equation using azocasein and Suc-AAPF-pNA as reaction substrates (Figure 8). The K_m and V_{max} of *Hsl*HlyB and *Hsl*HlyBΔCTE were 0.07 mM, 2814 U/min/mg and 0.16 mM, 4485 U/min/mg against azocasein, 0.36 mM, 8.4×10^{9} μmol/min/mg and 0.27 mM, 2.1×10^{10} μmol/min/mg against Suc-AAPF-pNA. *Hsl*HlyBΔCTE showed higher maximum reaction rates for both substrates, 1.6-fold and 2.5-fold of the wild type, respectively. *Hsl*HlyBΔCTE had a higher K_m value for azocasein and a lower K_m value for Suc-AAPF-pNA than wild type. The above results indicated that *Hsl*HlyBΔCTE had better catalytic effect on small molecule substrates, as shown by higher maximum reaction rate and higher substrate affinity. As for azocasein, *Hsl*HlyBΔCTE had higher maximum reaction rate but lower substrate affinity than wild-type. Similar phenomenon on the hydrolysis of small peptide substrates by *Hsl*HlyB and *Hsl*HlyBΔCTE has been reported for Nep from *Nab. magadii* (De Castro et al., 2008). CTE are involved in protein-protein interactions. PKD domain does not show any proteolysis activity, but can adsorb and swell insoluble proteins (Chen et al., 2007). The PPC domain also plays a key role in binding to the substrate (Xu et al., 2011; He et al., 2012). In the present study, CTE of *Hsl*HlyB also affected the affinity of the enzyme against the protein substrate.

*Hsl*HlyB and *Hsl*HlyBΔCTE can hydrolyze casein, bovine hemoglobin, azocasein, skim milk, gelatin, egg albumin and bovine serum albumin, with the highest catalytic activity towards casein (Figure 7C). Their wide substrate spectra make them good candidates for industrial applications.

10.3389/fmars.2023.1166287

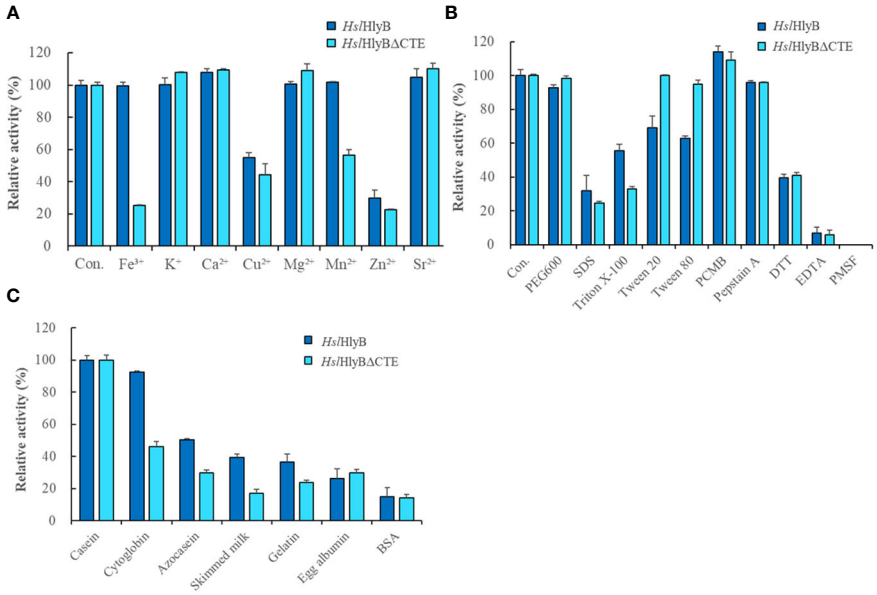

FIGURE 7
The effect of metal ions **(A)**, detergents, and inhibitors **(B)** on *Hsl*HlyB and *Hsl*HlyBΔCTE activity, and proteolytic activity against different substrates of *Hsl*HlyB and *Hsl*HlyBΔCTE **(C)**. Con.: control. In **(A, B)**, the enzyme assay was carried out with different metal ions at the concentration of 5 mM, with 10% detergents, 1 mM PCMB, 10 mM Pepstatin A, 10 mM DTT, 5 mM EDTA, 4 mM PMSF. In **(C)**, the protein substrate concentration of 5 g/L was used and the enzyme activity was measured by the amount of tyrosine produced. Mean ± SD of three biological replicates.

Hydrolysis of soybean protein isolate by *Hsl*HlyB and *Hsl*HlyBΔCTE

High-salt fermentation of soybeans is a common production process for soy sauce. The hydrolysis of soybean protein contributes the flavor and raw material utilization of soy sauce. To expand the application of halolysin in high-salt foods, the peptides from hydrolyzed soybean isolate protein by *Hsl*HlyB and *Hsl*HlyBΔCTE were identified. 128 peptides with an average molecular mass of 1928.87 Da and an average peptide chain length of 16.2 amino acids were identified from soybean protein isolate hydrolysate by *Hsl*HlyB (Table S3). 205 peptides with an average molecular mass of 1894.01 Da and an average peptide chain length of 15.6 amino acids were identified from soybean protein isolate hydrolysate by *Hsl*HlyBΔCTE (Table S3). The average molecular mass of the peptide profile after hydrolysis by *Hsl*HlyBΔCTE was smaller, and the average length of the peptide chains was shorter. Soybean protein isolate hydrolysates by both enzymes showed the highest peptide content in the range of 11-20 amino acids. The amino acid number distribution of peptides generated by *Hsl*HlyB was more uniform. The cleavage sites of *Hsl*HlyB and *Hsl*HlyBΔCTE were counted based on the peptides identified from the soybean protein isolate hydrolysates (Tables S4, 5). Similar to most serine proteases, *Hsl*HlyB and *Hsl*HlyBΔCTE do not have specific cleavage sites, but they seem to prefer to cleave proteins with acidic amino acids at the P1' position and proline at the P2 position. Halolysins exert endo-

TABLE 1 Effect of solvents on *Hsl*HlyB and *Hsl*HlyBΔCTE activity.

Solvents	log $P_{o/w}$ [a]	*Hsl*HlyB Relative activity (%) [b]	*Hsl*HlyBΔCTE Relative activity (%) [b]
Glycerol	-1.76	94.8 ± 5.3	94.2 ± 2.9
DMSO	-1.35	81.0 ± 2.3	98.2 ± 0.7
DMF	-1.0	70.6 ± 1.5	81.2 ± 0.3
Methanol	-0.82	75.0 ± 5.0	83.3 ± 0.9
Acetonitrile	-0.34	69.6 ± 2.2	75.9 ± 1.3
Ethanol	-0.31	56.8 ± 1.0	50.5 ± 0.7
Acetone	-0.24	72.1 ± 1.1	87.4 ± 1.7
Isopropanol	0.05	41.6 ± 3.2	40.8 ± 0.9

[a]log $P_{o/w}$ represents a quantitative measure of solvent polarity.
[b]The activity assayed in the absence of organic solvents was defined as the control activity of 100%. The organic solvent is added to the reaction system at 5% (v/v). Mean ± SD of three biological replicates.

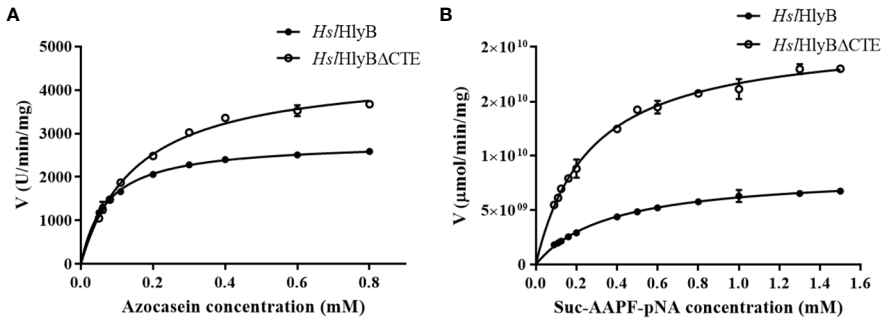

FIGURE 8
Michaelis-Menten graph of *Hsl*HlyB and *Hsl*HlyBΔCTE against azocasein **(A)** and Suc-AAPF-pNA **(B)**. Mean ± SD of three biological replicates.

protease activity that hydrolyze protein into peptides. *Hsl*HlyB and *Hsl*HlyBΔCTE can hydrolyze a wide range of protein substrates, such as soybean protein, which is mainly hydrolyzed to peptides of 11-20 amino acids. The variety of soybean protein hydrolysates were important compounds for soy sauce flavor. There are also several reports on halolysins for accelerating fish sauce fermentation in high-salt or low-salt conditions (Akolkar et al., 2010; Gao et al., 2017; Hou et al., 2020). Halolysins thus revealed potential application in food industry.

Conclusion

In summary, the gene *hslhlyB* encodes a novel halolysin with PKD and PPC domains at the C-terminus in *Hsl. pelagica* DL-M4^T. *Hsl*HlyB and *Hsl*HlyBΔCTE, like most halolysins, were highly salt tolerant. They show relatively good tolerance to organic solvents and good thermal stability. The absence of CTE of *Hsl*HlyB resulted in the increased activity and thermal stability of the protease while maintaining similar catalytic properties. The CTE affected maturation or secretion of *Hsl*HlyB *in vivo*, while it had no effect on maturation *in vitro*. Based on the biochemical characterization of halolysin from *Hsl. pelagica* DL-M4^T, *Hsl*HlyB and in particular the CTE deletion mutant, are promising salt-tolerant protease candidates for high-salt food processing applications, such as protein hydrolysis in soy sauce.

Data availability statement

The datasets presented in this study can be found in online repositories. The names of the repository/repositories and accession number(s) can be found in the article/Supplementary Material.

Author contributions

DH: conducted experiments, analyzed data and wrote the manuscript, acquired funding. JH: conceived and designed research, wrote and reviewed the manuscript. H-LC: supervised experiments, reviewed and edited the manuscript, acquired funding. All authors contributed to the article and approved the submitted version.

Funding

This work was financially supported by the National Science and Technology Fundamental Resources Investigation Program of China (No. 2019FY100700), the National Natural Science Foundation of China (No. 32070003, No. 32200012 and No. 31770005), the Natural Science Research of Jiangsu Higher Education Institutions of China (22KJB180016), and the start-up fund from Jiangsu University of Science and Technology.

Conflict of interest

The authors declare that the research was conducted in the absence of any commercial or financial relationships that could be construed as a potential conflict of interest.

Publisher's note

Supplementary material

The Supplementary Material for this article can be found online at: https://www.frontiersin.org/articles/10.3389/fmars.2023.1166287/full#supplementary-material

References

Akolkar, A. V., Deshpande, G. M., Raval, K. N., Durai, D., Nerurkar, A. S., and Desai, A. J. (2008). Organic solvent tolerance of *Halobacterium* sp. SP1 (1) and its extracellular protease. *J. Basic Microb.* 48, 421–425. doi: 10.1002/jobm.200800012

Akolkar, A. V., Durai, D., and Desai, A. J. (2010). *Halobacterium* sp. SP1 (1) as a starter culture for accelerating fish sauce fermentation. *J. Appl. Microbiol.* 109, 44–53. doi: 10.1111/j.1365-2672.2009.04626.x

Altschul, S. F., Madden, T. L., Schäffer, A. A., Zhang, J., Zhang, Z., Miller, W., et al. (1997). Gapped BLAST and PSI-BLAST: a new generation of protein database search programs. *Nucleic Acids Res.* 25, 3389–3402. doi: 10.1093/nar/25.17.3389

Alves, V. S., Pimenta, D. C., Sattlegger, E., and Castilho, B. A. (2004). Biophysical and functional characterization of Gir2, a highly acidic protein of *Saccharomyces cerevisiae*. *Biochem. Biophys. Res. Commun.* 314, 229–234. doi: 10.1016/j.bbrc.2003.12.086

Amoozegar, M. A., Siroosi, M., Atashgahi, S., Smidt, H., and Ventosa, A. (2017). Systematics of haloarchaea and biotechnological potential of their hydrolytic enzymes. *Microbiology* 163, 623–645. doi: 10.1099/mic.0.000463

Armenteros, J. J. A., Tsirigos, K. D., Sønderby, C. K., Petersen, T. N., Winther, O., Brunak, S., et al. (2019). SignalP 5.0 improves signal peptide predictions using deep neural networks. *Nat. Biotechnol.* 37, 420. doi: 10.1038/s41587-019-0036-z

Bradford, M. M. (1976). A rapid and sensitive method for the quantitation of microgram quantities of protein utilizing the principle of protein-dye binding. *Anal. Boichem.* 72, 248–254. doi: 10.1016/0003-2697(76)90527-3

Chaveesuk, R., Smith, J. P., and Simpson, B. K. (1994). Production of fish sauce and acceleration of sauce fermentation using proteolytic enzymes. *J. Aquat. Food. Prod. T.* 2, 59–77. doi: 10.1300/J030v02n03_05

Chen, S. X., Sun, S. Q., Wang, R., Feng, H. L., and Xiang, H. (2021). *Haloferax mediterranei* halolysin R4 confers antagonistic and defensive capabilities. *Appl. Environ. Microb.* 87, e02889–e02820. doi: 10.1128/AEM.02889-20

Chen, X. L., Xie, B. B., Lu, J. T., He, H. L., and Zhang, Y. (2007). A novel type of subtilase from the psychrotolerant bacterium *Pseudoalteromonas* sp. SM9913: catalytic and structural properties of deseasin MCP-01. *Microbiology* 153, 2116–2125. doi: 10.1099/mic.0.2007/006056-0

Cui, H. L., and Dyall Smith, M. L. (2021). Cultivation of halophilic archaea (class *Halobacteria*) from thalassohaline and athalassohaline environments. *Mar. Life. Sci. Tech.* 3, 243–251. doi: 10.1007/s42995-020-00087-3

Cui, H. L., Yang, X., and Mou, Y. Z. (2011). *Salinarchaeum laminariae* gen. nov., sp. nov.: a new member of the family *Halobacteriaceae* isolated from salted brown alga *Laminaria*. *Extremophiles* 15, 625–631. doi: 10.1007/s00792-011-0393-0

Dammak, D. F., Smaoui, S. M., Ghanmi, F., Boujelben, I., and Maalej, S. (2016). Characterization of halo-alkaline and thermostable protease from *Halorubrum ezzemoulense* strain ETR14 isolated from sfax solar saltern in Tunisia. *J. Basic Microb.* 56, 337–346. doi: 10.1002/jobm.201500475

De Castro, R. E., Ruiz, D. M., Giménez, M. I., Silveyra, M. X., Paggi, R. A., and Maupin-Furlow, J. A. (2008). Gene cloning and heterologous synthesis of a haloalkaliphilic extracellular protease of *Natrialba magadii* (Nep). *Extremophiles* 12, 677. doi: 10.1007/s00792-008-0174-6

Du, X., Li, M. R., Tang, W., Zhang, Y. X., Zhang, L., Wang, J., et al. (2015). Secretion of tat-dependent halolysin SptA capable of autocatalytic activation and its relation to haloarchaeal growth. *Mol. Microbiol.* 96, 548–565. doi: 10.1111/mmi.12955

Edwin, A., Rompikuntal, P., Bjorn, E., Stier, G., Wai, S. N., and Sauer-Eriksson, A. E. (2013). Calcium binding by the PKD1 domain regulates interdomain flexibility in *Vibrio cholerae* metalloprotease PrtV. *FEBS Open Bio.* 3, 263–270. doi: 10.1016/j.fob.2013.06.003

Elbanna, K., Ibrahim, I. M., and Revol Junelles, A. M. (2015). Purification and characterization of halo-alkali-thermophilic protease from *Halobacterium* sp. strain HP25 isolated from raw salt, lake qarun, fayoum, Egypt. *Extremophiles* 19, 763–774. doi: 10.1007/s00792-015-0752-3

Elsztein, C., Herrera Seitz, M. K., Sanchez, J. J., and De Castro, R. E. (2001). Autoproteolytic activation of the haloalkaliphilic archaeon *Natronococcus occultus* extracellular serine protease. *J. Basic Microb.* 41, 319–327. doi: 10.1002/1521-4028(200112)41:6<319::AID-JOBM319>3.0.CO;2-8

Finn, R. D., Clements, J., and Eddy, S. R. (2011). HMMER web server: interactive sequence similarity searching. *Nucleic Acids Res.* 39, W29–W37. doi: 10.1093/nar/gkr367

Gao, R. C., Shi, T., Liu, X. D., Zhao, M. Q., Cui, H. L., and Yuan, L. (2017). Purification and characterisation of a salt-stable protease from the halophilic archaeon *Halogranum rubrum*. *J. Sci. Food Agr.* 97, 1412–1419. doi: 10.1002/jsfa.7879

Gao, X., Wang, J., Yu, D. Q., Bian, F., Xie, B. B., Chen, X. L., et al. (2010). Structural basis for the autoprocessing of zinc metalloproteases in the thermolysin family. *Proc. Natl. Acad. Sci. U.S.A.* 107, 17569–17574. doi: 10.1073/pnas.1005681107

Giménez, M. I., Studdert, C. A., Sánchez, J. J., and De Castro, R. E. (2000). Extracellular protease of *Natrialba magadii*: purification and biochemical characterization. *Extremophiles* 4, 181–188. doi: 10.1007/s007920070033

Han, D., and Cui, H. L. (2020). *Halostella pelagica* sp. nov. and *Halostella litorea* sp. nov., isolated from salted brown alga *Laminaria*. *Int. J. Syst. Evol. Micr.* 70, 1969–1976. doi: 10.1099/ijsem.0.004003

He, H. L., Guo, J., Chen, X. L., Xie, B. B., Zhang, X. Y., Yu, Y., et al. (2012). Structural and functional characterization of mature forms of metalloprotease E495 from arctic sea-ice bacterium *Pseudoalteromonas* sp. SM495. *PloS One* 7, e35442. doi: 10.1371/journal.pone.0035442

Hou, J., Han, D., Zhou, Y., Li, Y., and Cui, H. L. (2020). Identification and characterization of the gene encoding an extracellular protease from haloarchaeon *Halococcus salifodinae*. *Microbiol. Res.* 236, 126468. doi: 10.1016/j.micres.2020.126468

Hou, J., Li, S. Y., Zhao, Y. J., and Cui, H. L. (2022). A novel halolysin without c-terminal extension from an extremely halophilic archaeon. *Appl. Microbiol. Biot.* 106, 3009–3019. doi: 10.1007/s00253-022-11903-4

Hou, J., Yin, X. M., Li, Y., Han, D., Lü, B., Zhang, J. Y., et al. (2021). Biochemical characterization of a low salt-adapted extracellular protease from the extremely halophilic archaeon *Halococcus salifodinae*. *Int. J. Biol. Macromol.* 176, 253–259. doi: 10.1016/j.ijbiomac.2021.02.081

Huang, J. F., Wu, R. B., Liu, D., Liao, B. Q., Lei, M., Wang, M., et al. (2019). Mechanistic insight into the binding and swelling functions of prepeptidase c-terminal (PPC) domains from various bacterial proteases. *Appl. Environ. Microb.* 85, e00611–e00619. doi: 10.1128/AEM.00611-19

Huang, J., Wu, C., Liu, D., Yang, X., Wu, R., Zhang, J., et al. (2017). C-terminal domains of bacterial proteases: structure, function and the biotechnological applications. *J. Appl. Microbiol.* 122, 12–22. doi: 10.1111/jam.13317

Jaouadi, B., Ellouz-Chaabouni, S., Rhimi, M., and Bejar, S. (2008). Biochemical and molecular characterization of a detergent-stable serine alkaline protease from *Bacillus pumilus* CBS with high catalytic efficiency. *Biochimie* 90, 1291–1305. doi: 10.1016/j.biochi.2008.03.004

Jumper, J., Evans, R., Pritzel, A., Green, T., Figurnov, M., Ronneberger, O., et al. (2021). Highly accurate protein structure prediction with AlphaFold. *Nature* 596, 583–589. doi: 10.1038/s41586-021-03819-2

Kamekura, M., Seno, Y., and Dyall Smith, M. (1996). Halolysin R4, a serine proteinase from the halophilic archaeon *Haloferax mediterranei*: gene cloning, expression and structural studies. *Biochim. Biophys. Acta-Protein Struct. Mol. Enzymol.* 1294, 159–167. doi: 10.1016/0167-4838(96)00016-7

Kamekura, M., Seno, Y., Holmes, M. L., and Smith, M. L. D. (1992). Molecular cloning and sequencing of the gene for a halophilic alkaline serine protease (halolysin) from an unidentified halophilic archaea strain (172P1) and expression of the gene in *Haloferax volcanii*. *J. Bacteriol.* 174, 736–742. doi: 10.1128/jb.174.3.736-742.1992

Karan, R., Capes, M. D., DasSarma, P., and DasSarma, S. (2013). Cloning, overexpression, purification, and characterization of a polyextremophilic β-galactosidase from the Antarctic haloarchaeon *Halorubrum lacusprofundi*. *BMC Biotechnol.* 13, 3. doi: 10.1186/1472-6750-13-3

Kim, J. S., Kluskens, L. D., de Vos, W. M., Huber, R., and van der Oost, J. (2004). Crystal structure of fervidolysin from *Fervidobacterium pennivorans*, a keratinolytic enzyme related to subtilisin. *J. Mol. Biol.* 335, 787–797. doi: 10.1016/j.jmb.2003.11.006

King, J., and Laemmli, U. K. (1971). Polypeptides of the tail fibres of bacteriophage T4. *J. Mol. Biol.* 62, 465–477. doi: 10.1016/0022-2836(71)90148-3

Kon, K., Shimanaga, M., and Horinouchi, M. (2020). "Marine ecology: Intertidal/Littoral zone," in *Japanese Marine life*. Eds. K. Inaba and J. Hall-Spencer (Singapore: Springer), 241–254. doi: 10.1007/978-981-15-1326-8_20

Lee, H. S. (2013). Diversity of halophilic archaea in fermented foods and human intestines and their application. *J. Microb. Biotechn.* 23, 1645–1653. doi: 10.4014/jmb.1308.08015

Lefebvre, O., and Moletta, R. (2006). Treatment of organic pollution in industrial saline wastewater: a literature review. *Water Res.* 40, 3671–3682. doi: 10.1016/j.watres.2006.08.027

Liu, G. M., Hou, J., Cai, S. F., Zhao, D. H., Cai, L., Han, J., et al. (2015). A patatin-like protein associated with the polyhydroxyalkanoate (PHA) granules of *Haloferax mediterranei* acts as an efficient depolymerase in the degradation of native PHA. *Appl. Environ. Microb.* 81, 3029–3038. doi: 10.1128/AEM.04269-14

Marem, A., Okamoto, D. N., Oliveira, L. C., Ruiz, D. M., Paggi, R. A., Kondo, M. Y., et al. (2018). Functional roles of c-terminal extension (CTE) of salt-dependent peptidase activity of the *Natrialba magadii* extracellular protease (NEP). *Int. J. Biol. Macromol.* 113, 1134–1141. doi: 10.1016/j.ijbiomac.2018.03.026

Quevillon, E., Silventoinen, V., Pillai, S., Harte, N., Mulder, N., Apweiler, R., et al. (2005). InterProScan: protein domains identifier. *Nucleic Acids Res.* 33, W116–W120. doi: 10.1093/nar/gki442

Ruiz, D. M., Iannuci, N. B., Cascone, O., and De Castro, R. E. (2010). Peptide synthesis catalysed by a haloalkaliphilic serine protease from the archaeon *Natrialba magadii* (Nep). *Lett. Appl. Microbiol.* 51, 691–696. doi: 10.1111/j.1472-765X.2010.02955.x

Ruiz, D. M., Paggi, R. A., Giménez, M. I., and De Castro, R. E. (2012). Autocatalytic maturation of the tat-dependent halophilic subtilase nep produced by the archaeon *Natrialba magadii*. *J. Bacteriol.* 194, 3700–3707. doi: 10.1128/JB.06792-11

Ryu, K., Kim, J., and Dordick, J. S. (1994). Catalytic properties and potential of an extracellular protease from an extreme halophile. *Enzyme Microb. Tech.* 16, 266–275. doi: 10.1016/0141-0229(94)90165-1

Shevchenko, A., Wilm, M., Vorm, O., and Mann, M. (1996). Mass spectrometric sequencing of proteins from silver-stained polyacrylamide gels. *Anal. Chem.* 68, 850–858. doi: 10.1021/ac950914h

Shi, W. L., Tang, X. F., Huang, Y. P., Gan, F., Tang, B., and Shen, P. (2006). An extracellular halophilic protease SptA from a halophilic archaeon *Natrinema* sp. J7: gene cloning, expression and characterization. *Extremophiles* 10, 599–606. doi: 10.1007/s00792-006-0003-8

Stroud, A., Liddell, S., and Allers, T. (2012). Genetic and biochemical identification of a novel single-stranded DNA-binding complex in *Haloferax volcanii*. *Front. Microbiol.* 3. doi: 10.3389/fmicb.2012.00224

Studdert, C. A., De Castro, R. E., Seitz, K. H., and Sánchez, J. J. (1997). Detection and preliminary characterization of extracellular proteolytic activities of the haloalkaliphilic archaeon *Natronococcus occultus*. *Arch. Microbiol.* 168, 532–535. doi: 10.1007/s002030050532

Studdert, C. A., Herrera Seitz, M. K., Plasencia Gil, M. I., Sanchez, J. J., and De Castro, R. E. (2001). Purification and biochemical characterization of the haloalkaliphilic archaeon *Natronococcus occultus* extracellular serine protease. *J. Basic Microb.* 41, 375–383. doi: 10.1002/1521-4028(200112)41:6<375::AID-JOBM375>3.0.CO;2-0

Sun, Y. P., Wang, B. B., Wu, Z. P., Zheng, X. W., Hou, J., and Cui, H. L. (2023). *Halorarius litoreus* gen. nov., sp. nov., *Halorarius halobius* sp. nov., *Haloglomus halophilum* sp. nov., *Haloglomus salinum* sp. nov., and *Natronomonas marina* sp. nov., extremely halophilic archaea isolated from tidal flat and marine solar salt. *Front. Mar. Sci.* 10. doi: 10.3389/fmars.2023.1105929

Vidyasagar, M., Prakash, S., Litchfield, C., and Sreeramulu, K. (2006). Purification and characterization of a thermostable, haloalkaliphilic extracellular serine protease from the extreme halophilic archaeon *Halogeometricum borinquense* strain TSS101. *Archaea* 2, 51–57. doi: 10.1155/2006/430763

Wang, Y. K., Zhao, G. Y., Li, Y., Chen, X. L., Xie, B. B., Su, H. N., et al. (2010). Mechanistic insight into the function of the c-terminal PKD domain of the collagenolytic serine protease deseasin MCP-01 from deep sea *Pseudoalteromonas* sp. SM9913: binding of the PKD domain to collagen results in collagen swelling but does not unwind the collagen triple helix. *J. Biol. Chem.* 285, 14285–14291. doi: 10.1074/jbc.M109.087023

Xu, Z. S., Du, X., Li, T.-T., Gan, F., Tang, B., and Tang, X. F. (2011). Functional insight into the c-terminal extension of halolysin SptA from haloarchaeon *Natrinema* sp. J7. *PloS One* 6, e23562. doi: 10.1371/journal.pone.0023562

Yongsawatdigul, J., Rodtong, S., and Raksakulthai, N. (2007). Acceleration of Thai fish sauce fermentation using proteinases and bacterial starter cultures. *J. Food Sci.* 72, M382–M390. doi: 10.1111/j.1750-3841.2007.00532.x

Zhang, Y. X., Wang, M. X., Du, X., Tang, W., Zhang, L., Li, M. R., et al. (2014). Chitin accelerates activation of a novel haloarchaeal serine protease that deproteinizes chitin-containing biomass. *Appl. Environ. Microb.* 80, 5698–5708. doi: 10.1128/AEM.01196-14

frontiers | Frontiers in Microbiology

TYPE Original Research
PUBLISHED 19 May 2023
DOI 10.3389/fmicb.2023.1164937

OPEN ACCESS

EDITED BY
Xue-Wei Xu,
Ministry of Natural Resources, China

REVIEWED BY
Xuwang Zhang,
Dalian University of Technology, China
Mingyang Zhou,
Qilu University of Technology, China
Huijuan Li,
Shandong University of Science and Technology, China
Jun-Hui Cheng,
Qingdao University, China

*CORRESPONDENCE
Jie Yang
✉ phdyang1314@163.com

RECEIVED 13 February 2023
ACCEPTED 24 April 2023
PUBLISHED 19 May 2023

CITATION
Liu Z, Liu G, Guo X, Li Y, Ji N, Xu X, Sun Q and Yang J (2023) Diversity of the protease-producing bacteria and their extracellular protease in the coastal mudflat of Jiaozhou Bay, China: in response to clam naturally growing and aquaculture. *Front. Microbiol.* 14:1164937. doi: 10.3389/fmicb.2023.1164937

Diversity of the protease-producing bacteria and their extracellular protease in the coastal mudflat of Jiaozhou Bay, China: in response to clam naturally growing and aquaculture

Zhiyun Liu[1], Guangchao Liu[2], Xuzhen Guo[1], Yang Li[1,3], Na Ji[1,3], Xingfeng Xu[1,3], Qingjie Sun[1,3] and Jie Yang[1,3]*

[1]College of Food Science and Engineering, Qingdao Agricultural University, Qingdao, China, [2]College of Life Science, Qingdao Agricultural University, Qingdao, China, [3]Qingdao Special Food Research Institute, Qingdao, China

The booming mudflat aquaculture poses an accumulation of organic matter and a certain environmental threat. Protease-producing bacteria are key players in regulating the nitrogen content in ecosystems. However, knowledge of the diversity of protease-producing bacteria in coastal mudflats is limited. This study investigated the bacterial diversity in the coastal mudflat, especially protease-producing bacteria and their extracellular proteases, by using culture-independent methods and culture-dependent methods. The clam aquaculture area exhibited a higher concentration of carbon, nitrogen, and phosphorus when compared with the non-clam area, and a lower richness and diversity of bacterial community when compared with the clam naturally growing area. The major classes in the coastal mud samples were Bacteroidia, Gammaproteobacteria, and Alphaproteobacteria. *The Bacillus*-like bacterial community was the dominant cultivated protease-producing group, accounting for 52.94% in the non-clam area, 30.77% in the clam naturally growing area, and 50% in the clam aquaculture area, respectively. Additionally, serine protease and metalloprotease were the principal extracellular protease of the isolated coastal bacteria. These findings shed light on the understanding of the microbes involved in organic nitrogen degradation in coastal mudflats and lays a foundation for the development of novel protease-producing bacterial agents for coastal mudflat purification.

KEYWORDS

bacterial community, protease-producing bacteria, diversity, clam naturally growing area, clam aquaculture area, coastal mudflats

Introduction

The coastal mudflat is a complex and dynamic ecological system, which is deeply influenced by the geological, physicochemical, and biological factors of marine and terrestrial land. Previous studies have reported that the spatiotemporal dynamics of bacterial abundance, diversity, and activity in tidal flat sediments were significantly affected by the

biogeochemical heterogeneity of salinity, pH, carbon, nitrogen, sulfur, and phosphorus (Taylor et al., 2014; Soares et al., 2018; Zhang G. et al., 2021; Niu et al., 2022; Zhang et al., 2022). The seasonality and sediment depth also affected the bacterial communities in the mudflat (Böer et al., 2009; Gobet et al., 2012). Moreover, bacteria were found to be deeply involved in carbon fixation and carbon-containing compound degradation, as well as nitrogen cycling processes including nitrogen fixation, ammonium oxidation, and nitrite and nitrous oxide reduction in the coastal mudflats (Hou et al., 2013; Zhou et al., 2018; Li et al., 2021; Li Q. et al., 2022).

Coastal mudflats are of great significance in regulating regional climate and sustaining ecological balance. In recent years, mudflat planting, mudflat aquaculture, and eco-tourism are flourishing in coastal areas, which have promoted economic growth, but also posed serious environmental threats (Long et al., 2016). With the expansion of human activities, the contents of organic carbon and nitrogen in coastal mudflats were significantly increased, resulting in a large amount of organic matter entering the sea and the atmosphere (Hu et al., 2019; Li T. et al., 2022). The nitrogen cycle is a main component of global biochemical cycles, and the nitrogen budget plays an important role in keeping ecological balance (Zhang X. et al., 2020; Hutchins and Capone, 2022). Current studies of bacterial functions in the nitrogen cycle mainly focused on nitrogen fixation, anaerobic ammonia oxidation, nitrification, and denitrification (Zhou et al., 2018; Li et al., 2021; Li Q. et al., 2022).

Protease is an important participant in the degradation of organic nitrogen, and protease-producing bacteria have been reported as the main microflora that regulate the nitrogen content in ecosystems (Zhou et al., 2013; Zhang et al., 2015; Tornkvist et al., 2019; Zhang Y. Z. et al., 2020). Related studies based on culture-dependent methods have been conducted in a tropical aquaculture environment (Wei et al., 2021), in the coastal sediments and soils of Antarctica (Zhou et al., 2013; Liu et al., 2021), the sediments of the Bohai Sea, Yellow Sea, and South China Sea (Zhou et al., 2009; Zhang et al., 2019), and the sediments of Jiaozhou Bay (Zhang et al., 2015), showing the diversity of protease-producing bacteria and their extracellular protease in various environments. In addition, a variety of microorganisms with enzyme-producing capacities have been isolated from coastal mudflats (Das, 2012; Suthindhiran et al., 2013; Gaonkar and Furtado, 2020). To the best of our knowledge, reports on the diversity of protease-producing bacteria in coastal mudflats are relatively rare. We speculated that an abundant and diverse protease-producing bacteria community existed in the coastal mudflats, especially in mudflat aquaculture with a high content of organic nitrogen. Therefore, it is necessary to study the diversity of protease-producing bacteria in coastal mudflats that are heavily influenced by anthropogenic activity.

Jiaozhou Bay is a representative semi-enclosed bay of China's Yellow Sea. Under the influence of dense and long-time human activities, the ecological factors of Jiaozhou Bay have changed significantly (Zhang L. et al., 2021; Lin et al., 2022). Eutrophication and high organic nitrogen content occurred in the coastal sediments of the bay due to terrestrial inputs (Liu et al., 2010; Li H. et al., 2019; Zhang L. et al., 2021), all of which make it an ideal area for studying the organic nitrogen biodegradation in the coastal mudflats. In this study, mud samples were collected from three stations in the coastal mudflat of Jiaozhou Bay, including the non-clam area, the clam naturally growing area, and the clam aquaculture area. The variation of bacterial taxonomy composition of different loci was investigated by culture-independent methods. In addition, protease-producing bacteria were isolated from these samples by culture-dependent methods, and the diversity of both the bacteria and the extracellular proteases as well as their distribution in different stations were further analyzed. Our research provides experimental evidence to elucidate the ecological role of microorganisms in organic nitrogen degradation by decomposing protein in coastal mudflats and lays a foundation for the development of measures to protect the coastal mudflat.

Materials and methods

Sampling and geochemical characteristics detection

Mud samples were collected from the coastal mudflat of Jiaozhou Bay, including three stations: the non-clam area (sample D1-3, hereafter collectively referred to as sample D), the clam naturally growing area (sample F1-3, hereafter collectively referred to as sample F), and the clam aquaculture area (sample H1-3, hereafter collectively referred to as sample H) on 18 March 2021. The geographic location of sampling sites is shown in Supplementary Figures S1–S4. The surface mud of each station was removed, and then, a deeper mud sample (5–10 cm) was collected aseptically using stainless-steel sterile shovels. Three replicates of all samples were taken from each station. The collected mud samples were stored in airtight sterile plastic bags at 4°C for subsequent geochemical characteristics detection and microbiological analysis. The salinity of the mud samples was measured using a soil salt meter PNT3000 (STEPS, Germany). The pH, total carbon content (TC), total nitrogen content (TN), and total phosphorus content (TP) of each sample were measured according to NY/T 1121.2-2006, NY/T1121.6-2006, NY/T1121.24-2012, and NY/T88-1988, respectively. The paired sample *t*-test was applied to evaluate the statistical significance between different variables of this study. The level of significance was set to a p-value of <0.05.

DNA extraction, Illumina sequencing, and analysis

The total genomic DNA of the mud samples was extracted with OMEGA-soil DNA Kit (Omega Bio-Tek, USA). The V3–V4 regions of bacterial 16S rRNA gene were amplified using TransStart FastPfu Polymerase (TransGen Biotech, China), with Barcoded sequencing primers 338F (5′-ACTCCTACGGGAGGCAGCA-3′) and 806R (5′-GGACTACHVGGGTWTCTAAT-3′). The generated PCR mixtures were then sequenced on an Illumina Miseq PE300 sequencing platform (Shanghai Majorbio, China). The obtained large short-read libraries were merged and trimmed, and the standard quality control was performed with Usearch 8.0.161 by the sequencing company. The remaining reads of the three samples were then pooled, dereplicated, and finally assigned to

each OTU using a 97% identity. OTU clustering and taxonomy assignment were processed by mapping the reads of each sample to representative OTU sequences using a Perl script, followed by comparing with a 16S rRNA gene database (RDP Release 11.1 http://rdp.cme.msu.edu/) at an 80% confidence threshold. The data were analyzed on the online Majorbio Cloud Platform (www.majorbio.com) developed by Shanghai Majorbio Bio-pharm Technology Co. Ltd. (Ren et al., 2022). Statistical analysis of alpha diversity was conducted via *t*-test at a significance level of 5% ($p < 0.05$).

Screening of protease-producing bacteria

Synthetic sea salt was purchased from Qingdao Sea-Salt Aquarium Technology Co. Ltd. and then dissolved at a concentration of 3% to make artificial seawater. The screening solid medium was prepared by adding 1% casein, 2% gelatin, 0.2% yeast extract, and 1.5% agar into artificial seawater with a final pH of 8.0. Protease-producing bacteria were screened using the dilution-plate method according to previous studies, with minor modifications (Zhang et al., 2015; Liu et al., 2021). In brief, approximately 1 g of mud sample was diluted serially 10 times to 10^{-6} using artificial seawater. Aliquots of 100 μl of each diluted sample were spread on the screening plates for subsequent incubation at 20°C until visible hydrolytic zones were formed. Colonies of different morphology with hydrolytic zone were further repeatedly streaked on the same medium at least three times to obtain a pure strain.

16S rRNA gene amplification, sequencing, and phylogenetic analysis

The *16S rRNA* gene of culturable bacteria was amplified by colony PCR technique using a Colony PCR kit (Mei5 Biotechnology, China) with the universal primers 27F (5′-AGAGTTTGATCCTGGCTCAG-3′) and 1492R (5′-GGTTACCTTGTTACGACTTC-3′), and then, the PCR products were sequenced by Shanghai Tsingke Biotechnology Co. Ltd., China. Isolates with at least two different nucleotides in their 16S rRNA gene sequences were identified as different strains. Phylogenetic trees were constructed using MEGA 11 with the neighbor-joining method. The GenBank accession numbers of 16S rRNA gene sequences in this study were OQ625902, OQ625903, OQ625905–OQ625912, OQ625916, OQ625917, OQ625921, OQ625938, OQ625939, OQ625941, OQ625993–OQ625996, OQ626000–OQ626019, OQ626205-OQ626214, OQ626220, OQ626221, OQ626228, OQ629890, OQ629902, OQ629992–OQ629994, OQ642131, OQ651245, and OQ690495. The strains' corresponding accession numbers are shown in Supplementary Table 1.

Protein substrate specificity test

The protease hydrolysis ability of the pure strains toward different substrates, including milk powder, casein, and gelatin, was detected using the method of Zhou et al. (2009), with minor modifications. Protein substrate solid media were prepared by mixing each protein substrate (1.0% milk powder, 0.5% casein, or 0.5% gelatin) with 0.2% yeast extract, 1.5% agar, and artificial seawater and adjusting the final pH to 8.0. The bacterial strains were streaked on the substrate plates and then incubated at 20°C for 4 days. The specific value of the diameter of the formed hydrolytic zone divided by the diameter of the colony, and the H/C ratio was measured and calculated.

Protease inhibitor assay

The bacterial strain was cultured in a liquid screening medium at 20°C and 200 rpm for 4 days. The supernatant of the bacterial culture was collected after centrifugation at 12,000 rpm at 4°C for 10 min and then used for subsequent protease inhibitor assay. The inhibitors contained phenylmethylsulfonyl fluoride (PMSF, Sigma) at a concentration of 1.0 mM, 1,10-phenanthroline (OP, Sigma) at a concentration of 1.0 mM, E64 (Merck) at a concentration of 0.1 mM, and pepstatin A (PA, Merck) at a concentration of 0.1 mM. The supernatant was properly diluted with 50 mM Tris-HCl (pH 8.0), followed by incubating with each inhibitor at 4°C for 60 min, and then, the residue protease activity was measured by the digestion of casein as formerly described (Chen et al., 2003). In brief, 100 μl of diluted solution and 100 μl of 2% casein in 50 mM Tris-HCl (pH 8.0) were mixed and incubated at 25°C for 20 min. To stop the reaction, 200 μl of 0.4 M TCA was added to the reaction mixture. After centrifugation at 12,000 rpm and 4°C for 5 min, the supernatant was collected and every 100 μl of supernatant was incubated with 500 μl of 0.4 M Na_2CO_3 and 100 μl of Folin–Ciocalteu's phenol reagent at 40°C for 10 min, and then, the absorbance was measured at 660 nm. One unit of protease activity was defined as the amount of enzyme that released 1 μg of tyrosine per milliliter of reaction mixture per minute. A sample without the addition of an inhibitor was set as the negative control. The difference between the relative residue activity of each sample and the negative control was taken as the inhibition ratio (%).

Results

Geochemical characteristics of the mud samples

The mud samples were collected from three stations in a coastal mudflat of Jiaozhou Bay, including the non-clam area (sample D), the clam naturally growing area (sample F), and the clam aquaculture area (sample H). The results of the geochemical analysis are shown in Table 1. All mud samples exhibited slightly alkaline pH (8.21–8.74). The salinity ranged from 4.75 to 6.25 g/kg, with the highest observed in sample H and the lowest in sample D. The contents of TC, TN, and TP in the samples ranged from 9.64–22.42 g/kg (TC), 0.52–0.79 g/kg (TN), and 0.31–0.62 g/kg (TP), respectively. The highest values were found in sample H (TC and TP) and sample F (TN), while the lowest were found in sample D (TC, TN, and TP). The carbon content, nitrogen content, and phosphorus content in the clam naturally growing

TABLE 1 Characteristics of the mud sampling stations in the coastal mudflat of Jiaozhou Bay[1].

Station	Sample	Location (E, N)	Temperature (°C)	pH	Salinity (g/kg)	TC (g/kg)	TN (g/kg)	TP (g/kg)
Non-clam area	D	120°15'60", 36°10'55"	15.8	8.51 ± 0.11[a]	4.75 ± 0.18[a]	9.64 ± 0.04[a]	0.52 ± 0.01[a]	0.31 ± 0.02[a]
Clam naturally growing area	F	120°16'1", 36°10'56"	15.8	8.74 ± 0.08[b]	5.85 ± 0.20[c]	16.39 ± 0.53[c]	0.79 ± 0.11[b]	0.42 ± 0.03[b]
Clam aquaculture area	H	120°16'22", 36°11'6"	15.8	8.21 ± 0.15[b]	6.25 ± 0.31[c]	22.4 ± 0.08[c]	0.76 ± 0.04[c]	0.62 ± 0.10[b]

[1] *T*-test was applied to evaluate the statistical differences between the studied variables compared to their corresponding variable of the non-clam area. Different letters in the same column are significantly different at a *p*-value of <0.05 (ab) and at a *p*-value of <0.01 (ac) between the non-clam area and the other stations.

area and the clam aquaculture area were significantly higher than the corresponding values in the non-clam area, indicating that the artificial culture and growth of clams may be relevant to eutrophication in a tidal area.

Bacterial taxonomy composition analysis

The microbial community of the mud samples was investigated by using culture-independent methods based on Illumina high-throughput sequencing. A total of 113,717 effective sequence reads were obtained, and the sequencing coverage rate exceeded 97%. A total of 5,135 OTUs were assigned, which were arranged from high to low as sample F (2,090), sample D (1,574), and sample H (1,471). The alpha diversity indexes are shown in Table 2. The estimators Ace and Chao reveal the richness of the bacterial community. Sample F showed higher Ace and Chao values than samples D and H, indicating higher bacterial richness in sample F. The estimators Shannon and Simpson express the diversity of the microbial community, with a positive correlation between Shannon and a negative correlation between Simpson. Sample F, again, exhibited the highest Shannon value and the lowest Simpson value, implying that the microbial diversity of Sample F was the highest of all the samples analyzed. The richness and diversity of the bacterial community in the clam naturally growing area were significantly higher than that of the clam aquaculture area and the non-clam area. However, the results of statistical analysis indicated that there are no statistically significant differences in microbial richness and diversity between the clam aquaculture area and the non-clam area.

In total, 52 phyla, 136 classes, 304 orders, 468 families, and 833 genera were identified in the three mud samples. Figure 1 shows the top phyla and classes of the mud samples. It seems that the bacterial diversity of sample F was the highest and that of H was the lowest (Figure 1), which was consistent with the above alpha diversity estimators. The phylum with more than 5% was considered the dominant phylum. Proteobacteria (44.47%) and Bacteroidota (27.26%) were definitively dominant in sample D, with a sum of 71.73% (Figure 1A), while in sample F, the major phyla were Proteobacteria (22.76%), Desulfobacterota (17.92%), Bacteroidota (13.44%), Chloroflexi (10.14%), and Acidobacteriota (7.45%), with a sum of 71.71% (Figure 1A). The dominant phyla constituted 89.76% of the bacterial community in sample H, which were Proteobacteria (29.13%), Bacteroidota (23.40%), Firmicutes (21.03%), Desulfobacterota (9.93%), and Campilobacterota (6.27%) (Figure 1A). On class level, Bacteroidia, Gammaproteobacteria, and Alphaproteobacteria were dominant in the mud samples, contributing to a sum of 70.92, 36.40, and 52.35% of the bacterial community in samples D, F, and H, respectively. It is noted that *Bacilli* with an abundance of 11.38% and *Clostridia* with an abundance of 9.34% were two major classes in sample H but were barely found in sample D and sample F (Figure 1B). On the genus level, *Woeseia* and *Loktanella* were the major bacterial genera in the non-clam area, *Woeseia* was dominant in the clam naturally growing area, and *Trichococcus*, *Lutibacter*, and *Psychrobacter* were dominant in the clam aquaculture area (Supplementary Figure 5).

Diversity of cultivable protease-producing bacteria

Protease is a key factor involved in nitrogen recycling (Zaman et al., 1999; Kamimura and Hayano, 2000). To further study the microbe-associated organic nitrogen degradation in coastal mudflats, we examined the cultivable protease-producing bacterial communities in mud samples by using culture-dependent methods. Moreover, culture-dependent methods have been commonly used for the discovery of novel species and bacterial products, which may further develop as protease-producing microbial agents for depollution of the environment. In general, the cultivability of the microbial community in the coastal area ranges from 0.1 to 0.01% (Al-Mailem et al., 2014; Rajeev et al., 2019). A number of colonies appeared on the screening plates of the 10^{-1}-10^{-4} diluted mud samples after cultivation. The bacterial abundance reached 10^4 cells/g mud in the non-clam area (sample D) and the clam aquaculture area (sample H) and 10^5 cells/g mud in the clam naturally growing area (sample F). Clear hydrolytic zones were found around approximately 60% of the colonies on the screening plates. These results indicated that a large quantity of protease-producing bacteria inhabited the studied coastal muds.

The pure strain of the above colonies was obtained by repeated streaking cultivation. The nearly full-length *16S rRNA* genes of the isolates were amplified and sequenced, and isolates with

10.3389/fmicb.2023.1164937

TABLE 2 Alpha diversity estimators of the bacterial community in the mud samples[1].

Station	Sample	Coverage (%)	OTUs	Bacterial richness index		Bacterial diversity index	
				Ace	Chao	Shannon	Simpsonx 10^{-3}
Clam naturally growing area	F	97.74	2,055 ± 50[a]	2,509 ± 37[a]	2,469 ± 42[a]	6.28 ± 0.005[a]	5.72 ± 0.32[a]
Clam aquaculture area	H	97.95	1,493 ± 31[c]	2,087 ± 73[b]	2,005 ± 61[b]	5.47 ± 0.25[b]	19.15 ± 0.30[b]
Non-clam area	D	97.97	1,545 ± 41[c]	2,018 ± 74[b]	1,991 ± 104[b]	5.73 ± 0.01[c]	8.68 ± 0.36[b]

[1]Statistical analysis was made by *t*-test. Different lower cases in the same column represent significance at a *p*-value of <0.05 (ab) and at a *p*-value of <0.01 (ac) between the clam naturally growing area and the other studied stations.

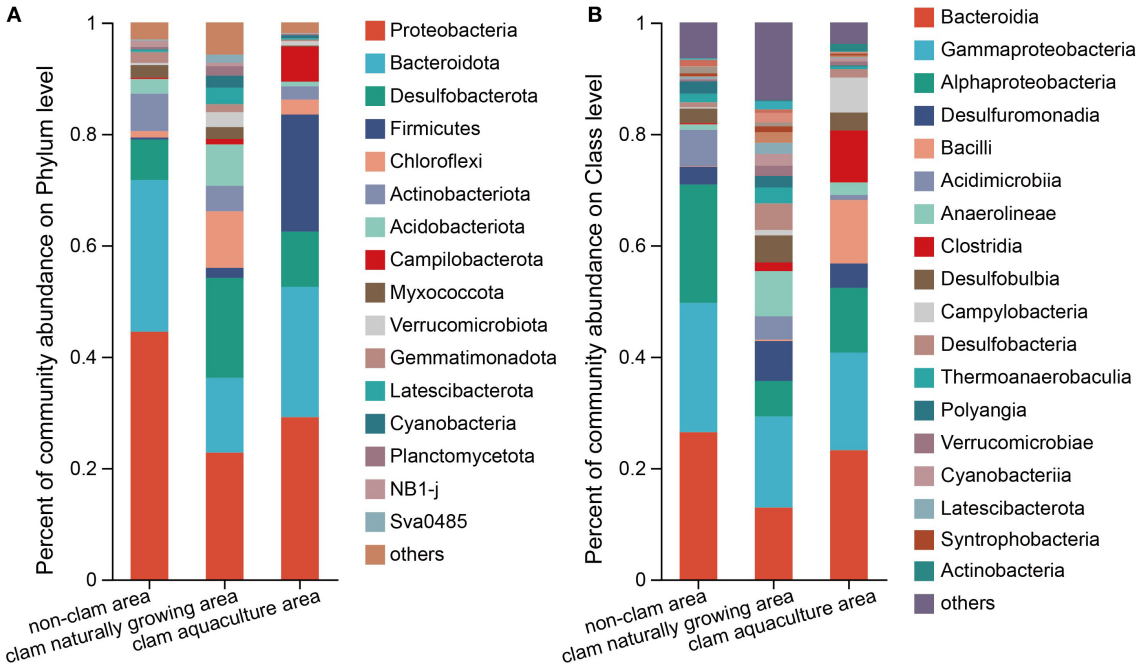

FIGURE 1
Composition of the bacterial community of the mud samples on phylum level **(A)** and class level **(B)**. The mud samples were taken from the non-clam area (sample D), the clam naturally growing area (sample F), and the clam aquaculture area (sample H). The microbial community was investigated by culture-independent methods. The column stands for different mud samples, and the row represents the relative percentage of each bacterial type, which is depicted by different colors.

two or more different nucleotides in their *16S rRNA* gene were considered as different strains. Finally, a total of 61 different protein hydrolyzing bacterial strains were isolated; 17 strains from sample D, 26 strains from sample F, and 18 strains from sample H (Supplementary Table 2). The 61 strains were classified into three phyla, four classes, nine families, and 18 genera (Figure 2). On the phylum and class level of the culturable fraction, the phyla Firmicutes and Proteobacteria and the classes Bacilli and Gammaproteobacteria were the largest groups in the three studied areas (Figure 2A). On the family level of the culturable fraction, Bacillaceae was the major family in all the studied areas and the dominance of Pseudoalteromonadaceae exists only in the clam naturally growing area (Figure 2B). The family Bacillaceae contains *Bacillus*-like species, including the five genera *Bacillus*, *Alkalihalobacillus*, *Rossellomorea*, *Halobacillus*, and *Cytobacillus*, with an abundance of 52.94% in sample D, 30.77% in sample F, and 50% in sample H, implying a dominance of *Bacillus*-like bacteria in the analyzed culturable fraction from coastal mudflats (Figures 2B, C). *Pseudoalteromonas* dominated in sample F (34.62%), meanwhile only a minor genus dominated in sample D (5.88%) and sample H (5.6%) (Figure 2C). In addition, the isolated protease-producing bacteria of sample F affiliated with 13 genera were apparently more diverse than that of sample D with seven genera and sample H with eight genera (Figure 2C), which was consistent with the findings of bacterial diversity by the above culture-independent methods.

In addition, neighbor-joining phylogenetic trees of the protease-producing strains with different genera based on *16S rRNA* gene sequences were constructed (Figure 3). The relationship between the strains isolated from the non-clam area, the clam naturally growing area, and the clam aquaculture area is shown in Figures 3A–C, respectively. *Alkalihalobacillus* strain H1-7 illustrated a distant relationship with other recognized species and may

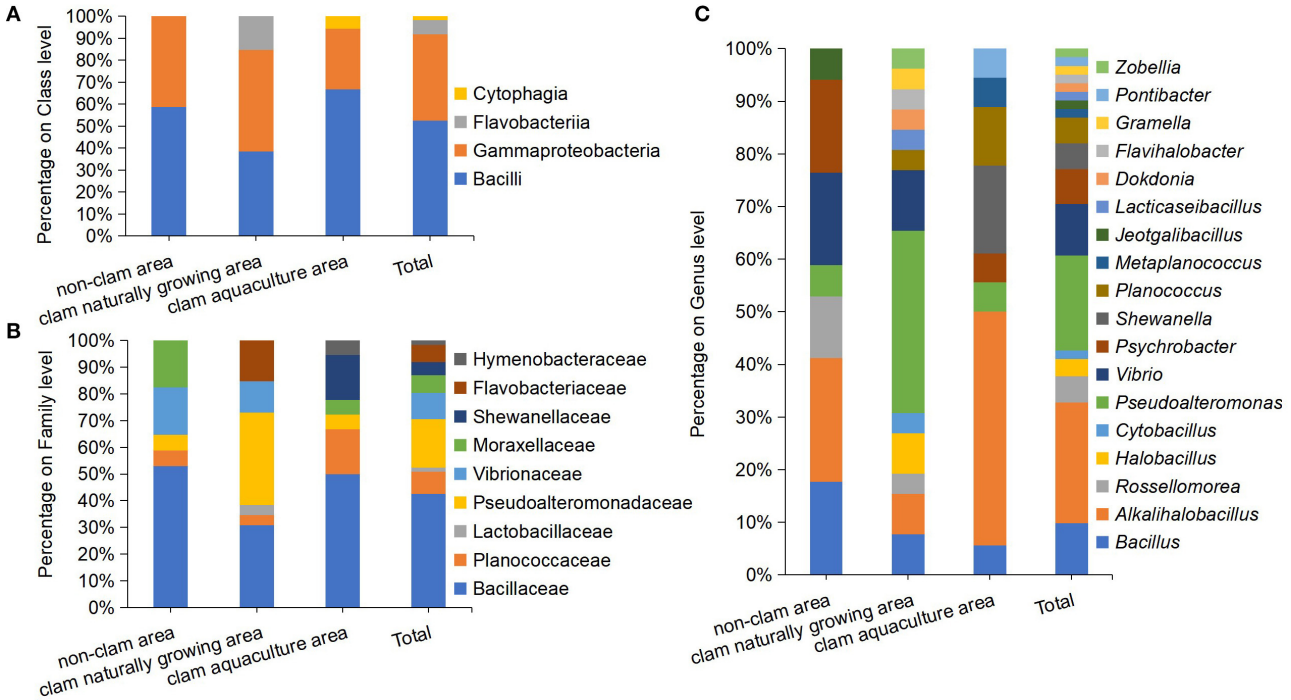

FIGURE 2
Diversity and distribution of culturable protease-producing bacteria of mud samples on class level **(A)**, family level **(B)**, and genus level **(C)**. The mud samples were taken from the non-clam area (sample D), the clam naturally growing area (sample F), and the clam aquaculture area (sample H), and the microbial community was investigated by culture-dependent methods. Each color represents the percentage of the taxon in the total isolates.

represent a new taxonomic unit worthy of further research and investigation.

Diversity analysis of bacterial extracellular proteases

Furthermore, the diversity of the bacterial extracellular protease was investigated by protein substrate specificity testing and protease inhibitor assay. Among the total 61 isolated strains, the extracellular proteases from 59, 55, and 55 strains could hydrolyze milk powder, casein, and gelatin, respectively, forming clear hydrolytic zones (Supplementary Table 2). The difference in the H/C ratios of the bacterial strains reflected their variation in substrate specificity. There was a certain variety in the activity of extracellular protease toward different protein substrates. The extracellular proteases secreted from *Alkalihalobacillus* strains F4-9 and H1-7, *Bacillus* strains D1-8, F1-2, and F2-3, *Halobacillus* strain F1-13, *Jeotgalibacillus* strain D2-1, and *Psychrobacter* strains H1-5 had high hydrolytic activity toward milk powder, with H/C ratios higher than five. The proteases from the *Alkalihalobacillus* strain D1-12, *Bacillus* strains D1-8 and F1-2, and *Planococcus* strain H1-3 showed high hydrolytic activity toward casein. The proteases from the *Bacillus* strain D2-9, *Halobacillus* strain F1-13, and *Psychrobacter* strains D2-13, D1-1, and H1-5 exhibited high hydrolytic activity toward gelatin.

In addition, the diversity of bacterial extracellular proteases was further investigated by detecting the inhibition ratios of PMSF (serine protease inhibitor), OP (metalloprotease inhibitor), Pepstatin A (aspartic protease inhibitor), and E64 (cysteine protease inhibitor). The 61 strains were cultivated in the liquid screening medium, and only 20 strains affiliated with the genera *Alkalihalobacillus*, *Bacillus*, *Planococcus*, *Rossellomorea*, *Halobacillus*, *Jeotgalibacillus*, *Psychrobacter*, *Pseudoalteromonas*, and *Shewanella* were able to produce enough extracellular proteases for protease inhibitor assay (Table 3). The extracellular protease activities of all 20 strains were inhibited by PMSF at the degree of 8.77–68.97%, indicating that all the coastal mudflat strains produced serine proteases. OP inhibited the protease activities of 16 strains by more than 10%, indicating that a majority of the isolated strains produced extracellular metalloproteases. In particular, an inhibition ratio as high as 84.97% was observed in the *Alkalihalobacillus* strain F1-12, suggesting that the *Alkalihalobacillus* strain F1-12 mainly produced extracellular metalloproteases. In contrast, Pepstatin A inhibited extracellular protease activity by 20% or less, indicating that these strains secrete very little aspartic or cysteine proteases. Moreover, E64 exhibited little inhibitory effect on the extracellular protease activities, with the exception of the *Alkalihalobacillus* strain F1-12, *Bacillus* strains D1-8 and D1-9, and *Halobacillus* strain F1-13, demonstrating that only a minority of the strains produced extracellular cysteine protease.

Discussion

Investigating microbial diversity and functionality is of crucial importance in demonstrating "who's there and what do they do." The culture-dependent method is the traditional way to explore

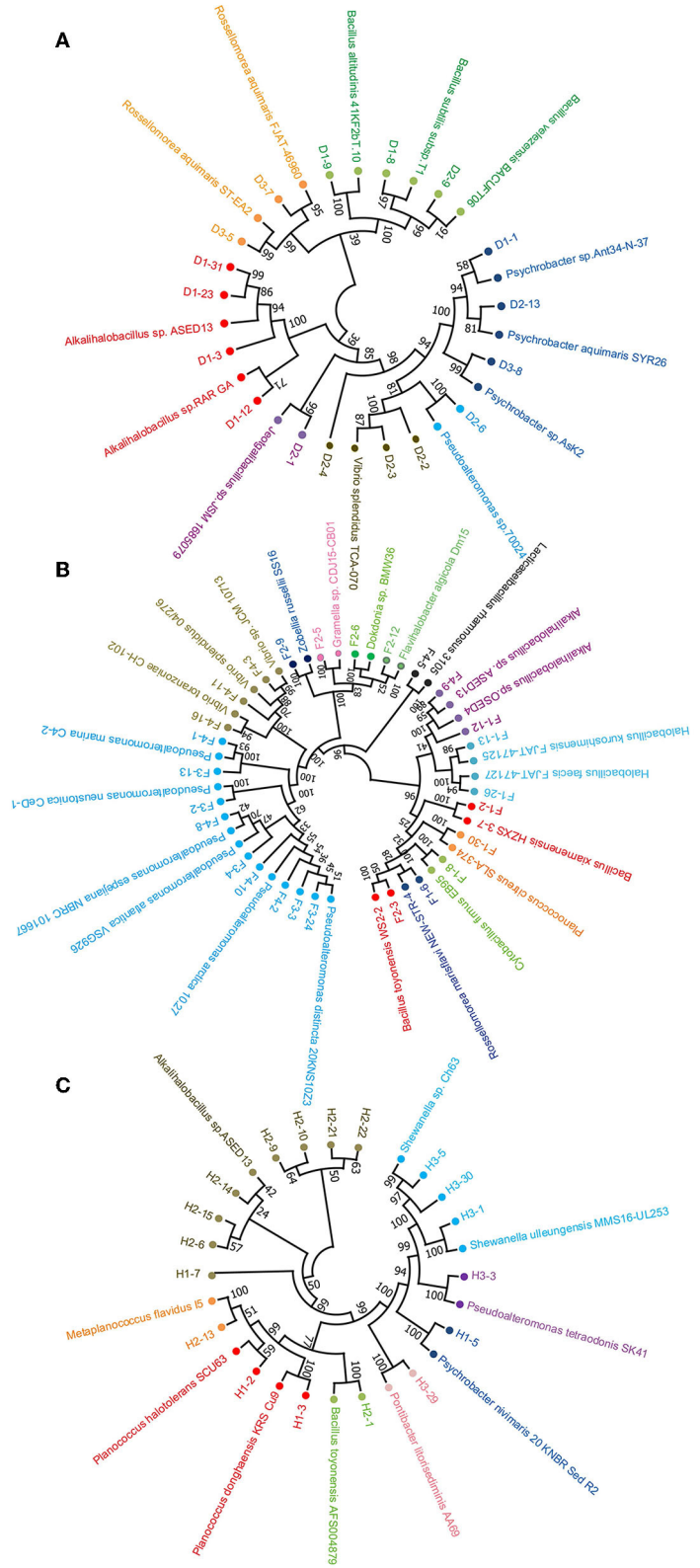

FIGURE 3
Neighbor-joining phylogenetic tree based on 16S rRNA sequencing of protease-producing bacteria isolated from three stations of coastal mudflat in Jiaozhou Bay using MEGA 11. The stations were the non-clam area **(A)**, the clam naturally growing area **(B)**, and the clam aquaculture area **(C)**. Strains affiliated with different genera are shown in different colors.

TABLE 3 Inhibition ratios of inhibitors on bacterial extracellular proteases.

Phyla	Genera	Strains	Inhibition ratio (%)[a]			
			PMSF (1.0 mM)	OP (1.0 mM)	Pepstatin A (0.1 mM)	E64 (0.1 mM)
Firmicutes	Alkalihalobacillus	D1-3	28.83	52.28	11.66	6.1
		F1-12	36.58	84.97	10.87	25.59
		H1-7	24.31	29.13	13.72	4.93
		H2-9	8.77	28.02	—	—
	Bacillus	D1-8	38.56	56.64	2.59	21.82
		D1-9	53.12	19.51	18.94	22.03
		D2-9	48.08	4.24	—	—
		F2-3	18.01	57.52	20.06	11.66
	Planococcus	F1-30	37.17	41.78	4.53	1.67
		H1-3	53.21	18.68	—	—
		H1-2	61.22	33.83	—	—
	Metaplanococcus	H2-13	10.26	28.16	—	—
	Rossellomorea	D3-7	21.66	10.3	—	—
		D3-5	29.33	11.88	—	—
	Halobacillus	F1-26	52.25	4.2	—	—
		F1-13	41.18	66.2	15.92	27.24
	Jeotgalibacillus	D2-1	68.97	—	—	—
Proteobacteria	*Psychrobacter*	D1-1	27.6	32.65	14.98	2.18
	Pseudoalteromonas	F4-2	51.61	5.01	—	4.7
	Shewanella	H3-5	44.28	28.31	—	—

[a]Inhibition ratio refers to the difference between the relative residue activity of each sample after incubation with and without an inhibitor.

and discover novel bacterial strains and products (Chen et al., 2003; Zhang et al., 2015). In recent years, the microbial diversity of environmental samples has been commonly investigated by culture-independent methods based on the rapid development of Illumina sequencing (Li Q. et al., 2022; Zhang et al., 2022). In this study, culture-dependent methods and culture-independent methods were interrelated for a better understanding of the bacterial diversity in the coastal mudflat, especially the protease-producing bacteria and their extracellular proteases.

The coastal mudflats are the transition zone of marine and terrestrial land, serving as an indispensable member of the global biogeochemical system. Excessive anthropogenic nitrogen input is a key factor influencing the coastal ecosystem (Li K. et al., 2019). Nitrogen loading caused eutrophication of the tidal flat environment, leading to hypoxia, red tides, and sediment loss (Cui et al., 2013; Cheng et al., 2020). In addition to inorganic nitrogen, environmental organic matters contain nitrogen mostly as protein. The organic feed and fertilizers applied in farming and aquaculture, animal feces and carcasses, as well as plant debris, contained a large amount of protein, an excess of which is an organic pollutant in coastal areas (Hodge et al., 2000; Davies et al., 2022). Soil enzymatic activity, especially soil hydrolase enzymes including protease, serves as a biological indicator to examine soil health (Maliang et al., 2020; Farooq et al., 2021). Microbes that inhabit coastal sediments play an important part in coastal biochemical cycling (Jiao et al., 2018). The protease-producing bacteria participated in the protection of coastal mudflats by secreting protease and degrading the protein in coastal mud.

It has been reported that nitrogen and phosphorus were released from an aquaculture farm and introduced pollution and eutrophication to the surrounding environments (Kawasaki et al., 2016). Consistently, in our study, the total concentrations of carbon, nitrogen, and phosphorus in the clam aquaculture area were 22.4 g/kg, 0.76 g/kg, and 0.62 g/kg, respectively, all of which were significantly higher than the corresponding values in the non-clam area of 9.64 g/kg (TC), 0.52 g/kg (TN), and 0.31 g/kg (TP). Recent studies have reported that 57% of nitrogen and 76% of phosphorus in aquatic feed were lost to the aquaculture water environment (Kong et al., 2020), and that the total nitrogen concentrations in the contaminated seawater of fishing harbors were two times higher than those of uncontaminated samples (Cheffi et al., 2022). All the related studies demonstrated that the fast-growing aquaculture industry had a great influence on the biogeochemistry factors of the surrounding areas.

We found that Proteobacteria was the most abundant phylum (44.47%) of the non-clam area in the coastal mudflat of Jiaozhou Bay, and the dominant class Gammaproteobacteria constituted 23.23% of the bacterial community. The dominance of Proteobacteria in the microbiota of various coastal environments has been reported in previous studies. Proteobacteria was found

to be the most abundant phylum in two Atlantic coastal areas of France and Portugal, representing 89.3 and 82.3% of the total microbiota, respectively (Leite et al., 2017), as well as in the surrounding seawater of cultivation farms along coastal areas of the Yellow Sea (35.25%) (Ahmed et al., 2021), and in three Kerkennian fishing harbors (51.02–66.7%) (Cheffi et al., 2022). The bacterial community of Jiaozhou Bay sediments was also investigated, and the results showed that Proteobacteria was the most dominant phylum (61.3%), among which Gammaproteobacteria constituted the most abundant class (32.8%) (Liu et al., 2014). In addition, Proteobacteria and Gammaproteobacteria predominantly existed in the clam naturally growing area and the clam aquaculture area, with the composition of Proteobacteria accounting for 22.76 and 29.13%, as well as Gammaproteobacteria accounting for 16.37 and 17.51%. This was consistent with previous reports on the prevalence of Proteobacteria in the microbiota of marine invertebrates, such as oysters and hydroid (Fernández et al., 2013; Guo et al., 2017). On the other hand, we investigated the cultivable protease-producing bacteria in the studied areas and found an abundant bacterial community in the phylum Proteobacteria, especially in the class Gammaproteobacteria, which was affiliated with four genera *Pseudoalteromonas*, *Vibrio*, *Psychrobacter*, and *Shewanella*. *Proteobacteria* accounted for 41.18% in the non-clam area, 46.15% in the clam naturally growing area, and 27.78% in the clam aquaculture area of the total culturable protease-producing bacteria, which was consistent with the findings of the culture-independent approaches.

Members of Firmicutes were found as a minor phylum in the sediments of Jiaozhou Bay (Liu et al., 2014), which was consistent with our findings that Firmicutes only account for 0.37% of the microbial biomass in the non-clam area. However, the amount of Firmicutes increased to 1.85% in the clam naturally growing area and even to 21.03% in the clam aquaculture area. These findings are in line with the reports of Zhao et al. (2022), who observed Firmicutes as the most abundant phylum of the core bacterial communities in clams, with a composition of 26.2%. The prevalence of Firmicutes has also been shown in the microbiota of several marine invertebrates and aquatic environments of different geographic locations, such as the marine ark shell in the Japan Sea (Romanenko et al., 2009), the Easter oyster in the coastal Bay of USA (King et al., 2012), and the sponge in the Western Mediterranean Sea (Bauvais et al., 2015).

On the genus level, we found that *Woeseia*, *Loktanella, Trichococcus*, *Lutibacter,* and *Psychrobacter* were dominant genera in the studied mudflat areas. *Woeseia* genus was considered a core member of the microbial community in the marine ecosystem, which is characterized by the ability to assimilate inorganic carbon (Dyksma et al., 2016). *Woeseia* strains have been frequently isolated from coastal sediments and coastal seawaters (Du et al., 2016; Xu et al., 2022). *Loktanella* was reported to be a dominant genus in the coastal microbial community (Cardoso et al., 2019), and large numbers of *Loktanella* strains have been isolated from tidal flat sediments (Park et al., 2013, 2014; Tanaka et al., 2014). *Trichococcus* strains were characterized by their psychrotolerant ability, which was commonly isolated from environments at low temperatures such as cold spring (Zakharyuk et al., 2021). *Lutibacter* was reported to be predominant in shallow water marine sediment (Kerfahi et al., 2014), and some strains have been isolated from tidal flat sediments (Choi and Cho, 2006). However, except for a *Trichococcus pasteurii* strain that was isolated from freshwater crawfish and has been reported to produce alkaline proteases to degrade the myofibrillar protein (Qiu et al., 2022), no other studies report on the protease-producing ability of these four genera. What is different is the *Psychrobacter* genus. *Psychrobacter* strains were also known for psychrophilic characteristics, and some strains have been reported to produce cold-active protease (Amato and Christner, 2009; Perfumo et al., 2020). In this study, the *Psychrobacter* genus was found to be the third in abundance in sample H and the 35th in sample D based on the results of culture-independent methods. Correspondingly, as a result of culture-dependent methods, *Psychrobacter* was found to be a predominant genus of the analyzed culturable fraction in coastal mudflats, with an abundance of 17.65% in sample D, 5.6% in sample H, and 6.56% in total.

Bacillus genus, as a member of the phylum Firmicutes, has been frequently reported because of their bioremediation potentials of organic and inorganic compounds, which are also essential in the clam aquaculture area (Hsieh et al., 2020; Kumar et al., 2022; Liu et al., 2023). Zhang et al. (2015) isolated sixty-six protease-producing bacteria from Jiaozhou Bay sediments. Of all these cultivable protease-producing bacteria, *Bacillus* was found to be a major group (25.8%) (Zhang et al., 2015). Correspondingly, in our study, *Bacillus*-like bacterial communities in the class Bacilli and family Bacillaceae that were affiliated with five genera, including *Bacillus*, *Alkalihalobacillus*, *Rossellomorea*, *Halobacillus,* and *Cytobacillus*, accounted for 52.94% in the non-clam area, 30.77% in the clam naturally growing area, and 50% in the clam aquaculture area. Analogously, *Bacillus*-like species were also found as one of the dominant groups in other marine habits, e.g., sediments of mangrove wetlands in Hainan, China (Liu et al., 2017), the coast of South India (Sinimol et al., 2016), and the continental slope of eastern Arabian Sea (Farha et al., 2019). In addition, members of the genus *Bacillus* and related genera were widespread in terrestrial environments and exhibited rapid growth in high protein media (Manktelow et al., 2020), which may also cause the high composition of *Bacillus*-like species isolated from the studied areas, originating from surrounding terrestrial habits.

Additionally, according to the inhibitor assay on protease, we found that serine protease and metalloprotease were secreted by the isolated bacteria of the studied area as the principal types of proteases, generally similar to previous studies on sediments of the Antarctic Sea, sediments of the South China Sea, soils of the Antarctica South Shetland Islands, and sediments of Jiaozhou Bay (Zhou et al., 2009; Hou et al., 2013; Zhang et al., 2015; Liu et al., 2021). Relatively few strains isolated from Jiaozhou Bay sediments were found to secrete cysteine proteases (Zhang et al., 2015), and a minority of bacterial strains isolated from the soils of the Antarctica South Shetland Islands were reported to secrete aspartic and/or cysteine proteases (Liu et al., 2021). In this study, we also found that a small quantity of aspartic protease and cysteine protease was produced by a few strains isolated from the non-clam area and the clam naturally growing area. These bacterial extracellular protease findings may shed light on the understanding of organic nitrogen degradation in coastal mudflat areas and the

development of microbial protease agents to prevent pollution and eutrophication.

Conclusion

In summary, this study analyzed the bacterial taxonomy composition of different clam-growing areas in the coastal mudflats of Jiaozhou Bay, especially protease-producing bacteria and their extracellular protease. The results showed that the diversity of the bacterial community and the protease-producing bacteria of the clam naturally growing area was higher than that of the non-clam area and the clam aquaculture area. *Bacillus*-like species, including the genera *Bacillus*, *Alkalihalobacillus*, *Rossellomorea*, *Halobacillus*, and *Cytobacillus*, were the dominant cultivated protease-producing groups in the Jiaozhou Bay coastal mudflats, and serine proteases and metalloproteases were the principal types of proteases produced by the bacteria. These findings contribute to a better understanding of the function of protease-producing bacteria in organic nitrogen degradation in coastal mudflat areas and the development of bacterial protease agents to improve the coastal aquaculture quality.

Data availability statement

The datasets presented in this study can be found in online repositories. The names of the repository/repositories and accession number(s) can be found in the article/Supplementary material.

Author contributions

JY designed the research and wrote the manuscript. ZL and XG conducted the research. GL collected samples, carried out bioinformatic analyzes, and revised the manuscript. YL, NJ, XX, and QS contributed ideas to the study. All authors contributed to the article and approved the submitted version.

Funding

This study was supported by the National Natural Science Foundation of China (Grant No. 32000004), the Research Fund of Qingdao Special Food Research Institute (Grant No. 6602422203), the Qingdao Agricultural University Research Fund for High-level Professionals (Grant No. 1120088), and the Breeding Plan of Shandong Provincial Qingchuang Research Team-Innovation Team of Functional Plant Protein-Based Food (2021).

Conflict of interest

The authors declare that the research was conducted in the absence of any commercial or financial relationships that could be construed as a potential conflict of interest.

Publisher's note

All claims expressed in this article are solely those of the authors and do not necessarily represent those of their affiliated organizations, or those of the publisher, the editors and the reviewers. Any product that may be evaluated in this article, or claim that may be made by its manufacturer, is not guaranteed or endorsed by the publisher.

Supplementary material

The Supplementary Material for this article can be found online at: https://www.frontiersin.org/articles/10.3389/fmicb.2023.1164937/full#supplementary-material

References

Ahmed, A., Khurshid, A., Tang, X., Wang, J., Khan, T. U., Mao, Y., et al. (2021). Structural and Functional Impacts of Microbiota on *Pyropia yezoensis* and Surrounding Seawater in Cultivation Farms along Coastal Areas of the Yellow Sea. *Microorganisms*. 9, 1291. doi: 10.3390/microorganisms9061291

Al-Mailem, D., Eliyas, M., Khanafer, M., and Radwan, S. (2014). Culture-dependent and culture-independent analysis of hydrocarbonoclastic microorganisms indigenous to hypersaline environments in Kuwait. *Microb. Ecol.* 67, 857–865. doi: 10.1007/s00248-014-0386-5

Amato, P., and Christner, B. C. (2009). Energy metabolism response to low-temperature and frozen conditions in *Psychrobacter cryohalolentis*. *Appl. Environ. Microbiol.* 75, 711–718. doi: 10.1128/AEM.02193-08

Bauvais, C., Zirah, S., Piette, L., Chaspoul, F., Domart-Coulon, I., Chapon, V., et al. (2015). Sponging up metals: bacteria associated with the marine sponge *Spongia officinalis*. *Marine Environ. Res.* 104, 20–30. doi: 10.1016/j.marenvres.2014.12.005

Böer, S. I., Hedtkamp, S. I. C., van Beusekom, J. E. E., Fuhrman, J. A., Boetius, A., and Ramette, A. (2009). Time- and sediment depth-related variations in bacterial diversity and community structure in subtidal sands. *ISME J.* 3, 780–791. doi: 10.1038/ismej.2009.29

Cardoso, D. C., Cretoiu, M. S., Stal, L. J., and Bolhuis, H. (2019). Seasonal development of a coastal microbial mat. *Scient. Rep.* 9, 490. doi: 10.1038/s41598-019-45490-8

Cheffi, M., Belmabrouk, S., Karray, F., Hentati, D., Bru-Adan, V., and Godon, J.-J. (2022). Study of microbial communities and environmental parameters of seawater collected from three Tunisian fishing harbors in Kerkennah Islands: Statistical analysis of the temporal and spatial dynamics. *Marine Pollut. Bull.* 185, 114350. doi: 10.1016/j.marpolbul.2022.114350

Chen, X.-L., Zhang, Y.-Z., Gao, P.-J., and Luan, X.-W. (2003). Two different proteases produced by a deep-sea psychrotrophic bacterial strain, *Pseudoaltermonas* sp. SM9913. *Marine Biol.* 143, 989–993. doi: 10.1007/s00227-003-1128-2

Cheng, F. Y., Van Meter, K. J., Byrnes, D. K., and Basu, N. B. (2020). Maximizing US nitrate removal through wetland protection and restoration. *Nature.* 588, 625–630. doi: 10.1038/s41586-020-03042-5

Choi, D. H., and Cho, B. C. (2006). *Lutibacter litoralis* gen. nov., sp. nov., a marine bacterium of the family *Flavobacteriaceae* isolated from tidal flat sediment. *Int. J. Syst. Evol. Microbiol.* 56, 771–776. doi: 10.1099/ijs.0.64146-0

Cui, S., Shi, Y., Groffman, P. M., Schlesinger, W. H., and Zhu, Y. G. (2013). Centennial-scale analysis of the creation and fate of reactive nitrogen in China (1910–2010). *Proc. Nat. Acad. Sci. USA.* 110, 2052–2057. doi: 10.1073/pnas.12216 38110

Das, n. (2012). Bacterial isolates of marine coast as commercial producer of protease. *OnLine J. Biol. Sci.* 12, 96–107. doi: 10.3844/ojbsci.2012.96.107

Davies, B., Coulter, J. A., and Pagliari, P. H. (2022). Soil enzyme activity behavior after urea nitrogen application. *Plants*. 11, 2247. doi: 10.3390/plants11172247

Du, Z. J., Wang, Z. J., Zhao, J. X., and Chen, G. J. (2016). Woeseia oceani gen. nov., sp. nov., a chemoheterotrophic member of the order Chromatiales, and proposal of Woeseiaceae fam. nov. *Int. J. Syst. Evol. Microbiol.* 66, 107–112. doi: 10.1099/ijsem.0.000683

Dyksma, S., Bischof, K., Fuchs, B. M., Hoffmann, K., and Mumann, M.arc. (2016). Ubiquitous *Gammaproteobacteria* dominate dark carbon fixation in coastal sediments. *ISME J.* 10, 1939–1953. doi: 10.1038/ismej.2015.257

Farha, A. K., Tr, T., Purushothaman, A., Salam, J. A., and Hatha, A. M. (2019). Phylogenetic diversity and biotechnological potentials of marine bacteria from continental slope of eastern Arabian Sea. *J. Genetic Eng. Biotechnol.* 16, 253–258. doi: 10.1016/j.jgeb.2018.06.002

Farooq, T., Kumar, U., Mo, J., Shakoor, A., Wang, J., Rashid, M., et al. (2021). Intercropping of peanut-tea enhances soil enzymatic activity and soil nutrient status at different soil profiles in subtropical southern China. *Plants (Basel, Switzerland)*. 10, 881. doi: 10.3390/plants10050881

Fernández, T. N., Mazón-Suástegui, J. M., Vázquez-Juárez, R., Ascencio-Valle, F., and Romero, J. (2013). Changes in the composition and diversity of the bacterial microbiota associated with oysters (*Crassostrea corteziensis*, *Crassostrea gigas* and *Crassostrea sikamea*) during commercial production. *FEMS Microbiol. Ecol.* 88, 69–83. doi: 10.1111/1574-6941.12270

Gaonkar, S. K., and Furtado, I. J. (2020). Characterization of Extracellular Protease from the *Haloarcheon Halococcus* sp. Strain GUGFAWS-3 (MF425611). *Current Microbiol.* 77, 1024–1034. doi: 10.1007/s00284-020-01896-6

Gobet, A., Böer, S. I., Huse, S. M., van Beusekom, J. E. E., Quince, C., Sogin, M. L., et al. (2012). Diversity and dynamics of rare and of resident bacterial populations in coastal sands. *ISME J.* 6, 542–553. doi: 10.1038/ismej.2011.132

Guo, H., Rischer, M., Sperfeld, M., Weigel, C., Menzel, K. D., Clardy, J., et al. (2017). Natural products and morphogenic activity of γ-*Proteobacteria* associated with the marine hydroid polyp *Hydractinia echinata*. *Bioorg. Med. Chem.* 25, 6088–6097. doi: 10.1016/j.bmc.2017.06.053

Hodge, A., Stewart, J., Robinson, D., Griffiths, B. S., and Fitter, A. H. (2000). Plant N capture and microfaunal dynamics from decomposing grass and earthworm residues in soil. *Soil. Biol. Biochem.* 32, 1763–1772. doi: 10.1016/S0038-0717(00)00095-X

Hou, L., Zheng, Y., Liu, M., Gong, J., Zhang, X., Yin, G., et al. (2013). Anaerobic ammonium oxidation (anammox) bacterial diversity, abundance, and activity in marsh sediments of the Yangtze Estuary. *J. Geophys. Res.* 118, 1237–1246 doi: 10.1002/jgrg.20108

Hsieh, H.-Y., Lin, C.-H., Hsu, S.-Y., and Stewart, G. C. (2020). A *Bacillus* spore-based display system for bioremediation of atrazine. *Appl. Environ. Microbiol.* 86, e01230–e01220. doi: 10.1128/AEM.01230-20

Hu, W., Zhang, W., Zhang, L., Tong, C., Sun, Z., Chen, Y., et al. (2019). Nitrogen along the hydrological gradient of marsh sediments in a subtropical estuary: pools, processes, and fluxes. *Int. J. Environ. Res. Public Health*. 16, 2043. doi: 10.3390/ijerph16112043

Hutchins, D. A., and Capone, D. G. (2022). The marine nitrogen cycle: new developments and global change. *Nat. Rev. Microbiol.* 20, 401–414. doi: 10.1038/s41579-022-00687-z

Jiao, S., Chen, W., Wang, J., Du, N., Li, Q., Wei, G., et al. (2018). Soil microbiomes with distinct assemblies through vertical soil profiles drive the cycling of multiple nutrients in reforested ecosystems. *Microbiome.* 6, 146. doi: 10.1186/s40168-018-0526-0

Kamimura, Y., and Hayano, K. (2000). Properties of protease extracted from tea-field soil. *Biol. Fertil. Soils.* 30, 351–355. doi: 10.1007/s003740050015

Kawasaki, N., Kushairi, M. R. M., Nagao, N., Yusoff, F., and Imai, A., Kohzu, A., et al. (2016). Release of Nitrogen and Phosphorus from Aquaculture Farms to Selangor River, Malaysia. *Int. J. Environ. Sci. Develop.* 7, 113–116. doi: 10.7763/IJESD.2016.V7.751

Kerfahi, D., Hall-Spencer, J. M., Tripathi, B. M., Milazzo, M., Lee, J., Adams, J., et al. (2014). Shallow water marine sediment bacterial community shifts along a natural CO_2 gradient in the mediterranean sea off Vulcano, Italy. *Microbial. Ecol.* 67, 819–828. doi: 10.1007/s00248-014-0368-7

King, G. M., Judd, C., Kuske, C. R., and Smith, C. (2012). Analysis of stomach and gut microbiomes of the eastern oyster (*Crassostrea virginica*) from coastal Louisiana, USA. *PLoS ONE*. 7, e51475. doi: 10.1371/journal.pone.0051475

Kong, W., Huang, S., Yang, Z., Shi, F., Feng, Y., Khatoon, Z., et al. (2020). Fish feed quality is a key factor in impacting aquaculture water environment: evidence from incubator experiments. *Scient. Rep.* 10, 187. doi: 10.1038/s41598-019-57063-w

Kumar, R., Singh, A., Maurya, A., Yadav, P., Yadav, A., Chowdhary, P., et al. (2022). Effective bioremediation of pulp and paper mill wastewater using *Bacillus cereus* as a possible kraft lignin-degrading bacterium. *Bioresour. Technol.* 352, 127076. doi: 10.1016/j.biortech.2022.127076

Leite, L., Jude-Lemeilleur, F., Raymond, N., Henriques, I., Garabetian, F., and Alves, A. (2017). Phylogenetic diversity and functional characterization of the Manila clam microbiota: a culture-based approach. *Environ. Sci. Pollut. Res.* 24, 21721–21732. doi: 10.1007/s11356-017-9838-z

Li, H., Chi, Z., Li, J., Wu, H., and Yan, B. (2019). Bacterial community structure and function in soils from tidal freshwater wetlands in a Chinese delta: Potential impacts of salinity and nutrient. *Sci. Total Environ.* 696, 134029.1–134029.9. doi: 10.1016/j.scitotenv.2019.134029

Li, K., Liu, C., Ma, Y., and Wang, X. (2019). Land-based dissolved organic nitrogen dynamics and bioavailability in Jiaozhou Bay, China. *Estuarine, Coastal Shelf Sci.* 220, 13–24. doi: 10.1016/j.ecss.2019.02.045

Li, Q., Zhang, Y., Hu, J., and Dai, Q. (2022). Response of bacterial communities and nitrogen-cycling genes in newly reclaimed mudflat paddy soils to nitrogen fertilizer gradients. *Environ. Sci. Pollut. Res.* 29, 71113–71123. doi: 10.1007/s11356-022-20770-5

Li, T., Zhang, G., Wang, S., Mao, C., Tang, Z., Rao, W., et al. (2022). The isotopic composition of organic carbon, nitrogen and provenance of organic matter in surface sediment from the Jiangsu tidal flat, southwestern Yellow Sea. *Marine Pollut. Bull.* 182, 114010. doi: 10.1016/j.marpolbul.2022.114010

Li, Y., Wang, Y., Shen, C., Xu, L., Yi, S., Zhao, Y., et al. (2021). Structural and predicted functional diversities of bacterial microbiome in response to sewage sludge amendment in coastal mudflat soil. *Biology*. 10, 1302. doi: 10.3390/biology10121302

Lin, J., Zhang, L., Zhang, M., Zhang, H., Guo, C., Feng, S., et al. (2022). Distribution, sources, and ecological risk of organophosphate esters in the urbanized Jiaozhou Bay, East China. *Environ. Sci. Pollut. Res.* 29, 70167–70178. doi: 10.1007/s11356-022-20367-y

Liu, C., Ma, S., Wang, X., Ou, Y., and Du, H. (2023). Biodegradation of organic compounds in the coal gangue by *Bacillus sp.* into humic acid. *Biodegradation*. 34, 125–138. doi: 10.1007/s10532-022-10007-0

Liu, J., Liu, W., Xing, S., Zhang, X., He, H., Chen, J., et al. (2021). Diversity of protease-producing bacteria in the soils of the South Shetland Islands, Antarctica. *Antonie van Leeuwenhoek* 114, 457–464. doi: 10.1007/s10482-021-01533-7

Liu, M., Cui, Y., Chen, Y., Lin, X., Huang, H., Bao, S., et al. (2017). Diversity of *Bacillus*-like bacterial community in the sediments of the Bamenwan mangrove wetland in Hainan, China. *Can. J. Microbiol.* 63, 238–245. doi: 10.1139/cjm-2016-0449

Liu, S. M., Zhu, B. D., Zhang, J., Wu, Y., Liu, G. S., Deng, B., et al. (2010). Environmental change in Jiaozhou Bay recorded by nutrient components in sediments. *Marine Pollut. Bull.* 60, 1591–1599. doi: 10.1016/j.marpolbul.2010.04.003

Liu, X., Hu, H.-W., Liu, Y.-R., Xiao, K.-Q., Cheng, F.-S., Li, J., et al. (2014). Bacterial composition and spatiotemporal variation in sediments of Jiaozhou Bay, China. *J. Soils Sed.* 15, 732–744. doi: 10.1007/s11368-014-1045-7

Long, X. H., Liu, L. P., Shao, T. Y., Shao, H. B., and Liu, Z. P. (2016). Developing and sustainably utilize the coastal mudflat areas in China. *Sci. Total Environ.* 569–570, 1077–1086. doi: 10.1016/j.scitotenv.2016.06.170

Maliang, H., Tang, L., Lin, H., Chen, A., and Ma., J (2020). Influence of high-dose continuous applications of pyroligneous acids on soil health assessed based on pH, moisture content and three hydrolases. *Environ. Sci. Pollut. Res.* 27, 15426–15439. doi: 10.1007/s11356-020-08075-x

Manktelow, C. J., White, H., Crickmore, N., and Raymond, B. (2020). Divergence in environmental adaptation between terrestrial clades of the *Bacillus cereus* group. *FEMS Microbiol. Ecol.* 97, 228. doi: 10.1093/femsec/fiaa228

Niu, Y., Zheng, Y., Hou, L., Gao, D., Chen, F., Pei, C., et al. (2022). Microbial dynamics and activity of denitrifying anaerobic methane oxidizers in China's estuarine and coastal wetlands. *Sci. Total Environ.* 806, 150425. doi: 10.1016/j.scitotenv.2021.150425

Park, S., Jung, Y. T., and Yoon, J. H. (2013). Loktanella sediminilitoris sp. nov., isolated from tidal flat sediment. *Int. J. System. Evolut. Microbiol.* 63, 4118–4123. doi: 10.1099/ijs.0.049841-0

Park, S.ooyeon., Jung, Yong-Taek., Won, Sung-Min., Park, Ja-Min., and Yoon, Jung-Hoon. (2014). *Loktanella aestuariicola* sp. nov., an alphaproteobacterium isolated from a tidal flat. *Antonie van Leeuwenhoek.* 106, 707–714. doi: 10.1007/s10482-014-0240-2

Perfumo, A., Freiherr von Sass, G. J., Nordmann, E. L., Budisa, N., and Wagner, D. (2020). Discovery and characterization of a new cold-active protease from an extremophilic bacterium via comparative genome analysis and in vitro expression. *Front. Microbiol.* 11, 881. doi: 10.3389/fmicb.2020.00881

Qiu, L., Zhao, Y., Ma, H., Tian, X., Bai, C., Liao, T., et al. (2022). The quality and bacterial community changes in freshwater crawfish stored at 4°C in vacuum packaging. *Molecules.* 27, 8618. doi: 10.3390/molecules27238618

Rajeev, M., Sushmitha, T. J., Toleti, S. R., and Pandian, S. K. (2019). Culture dependent and independent analysis and appraisal of early stage biofilm-forming bacterial community composition in the Southern coastal seawater of India. *Sci. Total Environ.* 666, 308–320. doi: 10.1016/j.scitotenv.2019.02.171

Ren, Y., Yu, G., Shi, C., Liu, L., Guo, Q., Han, C., et al. (2022). Majorbio Cloud: A one-stop, comprehensive bioinformatic platform for multiomics analyses. *iMeta*. 1, e12. doi: 10.1002/imt2.12

Romanenko, L. A., Uchino, M., Kalinovskaya, N. I., and Mikhailov, V. V. (2009). Isolation, phylogenetic analysis and screening of marine mollusc-associated bacteria

for antimicrobial, hemolytic and surface activities. *Microbiol. Res.* 163, 633–644. doi: 10.1016/j.micres.2006.10.001

Sinimol, S., Sarika, A. R., and Jayakumaran Nair, A. (2016). Diversity and antagonistic potential of marine microbes collected from south-west coast of India. *3 Biotech.* 6, 7. doi: 10.1007/s13205-015-0318-1

Soares, A. R. A., Kritzberg, E. S., Custelcean, I., and Berggren, M. (2018). Bacterioplankton responses to increased organic carbon and nutrient loading in a boreal estuary—separate and interactive effects on growth and respiration. *Microbial. Ecol.*76, 144–155. doi: 10.1007/s00248-017-1115-7

Suthindhiran, K., Jayasri, M. A., Dipali, D., and Prasar, A. (2013). Screening and characterization of protease producing actinomycetes from marine saltern. *J. Basic Microbiol.* 54, 1098–1109. doi: 10.1002/jobm.201300563

Tanaka, N., Romanenko, L. A., Kurilenko, V. V., Svetashev, V. I., Kalinovskaya, N. I., Mikhailov, V. V., et al. (2014). *Loktanella maritima* sp. nov. isolated from shallow marine sediments. *Int. J. Syst. Evol. Microbiol.* 64, 2370–2375. doi: 10.1099/ijs.0.061747-0

Taylor, J. D., Ellis, R., Milazzo, M., Hall-Spencer, J. M., and Cunliffe, M. (2014). Intertidal epilithic bacteria diversity changes along a naturally occurring carbon dioxide and pH gradient. *FEMS Microbiol. Ecol.* 89, 670–678. doi: 10.1111/1574-6941.12368

Tornkvist, A., Liu, C., and Moschou, P. N. (2019). Proteolysis and nitrogen: emerging insights. *J. Exper. Botany*. 70, 2009–2019 doi: 10.1093/jxb/erz024

Wei, Y., Bu, J., Long, H., Zhang, X., Cai, X., and Huang, A. (2021). Community structure of protease-producing bacteria cultivated from aquaculture systems: potential impact of a tropical environment. *Front. Microbiol.* 12, 638129. doi: 10.3389/fmicb.2021.638129

Xu, N., Wang, W., Xu, K., Xu, Y., Ji, D., Chen, C., et al. (2022). Cultivation of different seaweed species and seasonal changes cause divergence of the microbial community in coastal seawaters. *Front. Microbiol.* 13, 988743. doi: 10.3389/fmicb.2022.988743

Zakharyuk, A., Valyshev, A., Plotnikov, A., Kopitsyn, D., Suzina, N., Shcherbakova., et al. (2021). Trichococcus shcherbakoviae subsp. psychrophilus subsp. nov., a psychrotolerant facultative anaerobe isolated from a cold spring. *Int. J. Syst. Evol. Microbiol.* 71, 5068. doi: 10.1099/ijsem.0.005068

Zaman, M., Di, H. J., Cameron, K. C., and Frampton, C. M. (1999). Gross nitrogen mineralization and nitrification rates and their relationships to enzyme activities and the soil microbial biomass in soils treated with dairy shed effluent and ammonium fertilizer at different water potentials. *Biol. Fertil. Soils.* 29, 178–186. doi: 10.1007/s003740050542

Zhang, G., Bai, J., Tebbe, C. C., Zhao, Q., Jia, J., Wang, W., et al. (2021). Salinity controls soil microbial community structure and function in coastal estuarine wetlands. *Environ. Microbiol.* 23, 1020–1037. doi: 10.1111/1462-2920.15281

Zhang, J., Chen, M., Huang, J., Guo, X., Zhang, Y., Liu, D., et al. (2019). Diversity of the microbial community and cultivable protease-producing bacteria in the sediments of the Bohai Sea, Yellow Sea and South China Sea. *PLoS ONE.* 14, e0215328. doi: 10.1371/journal.pone.0215328

Zhang, L., Xiong, L., Li, J., and Huang, X. (2021). Long-term changes of nutrients and biocenoses indicating the anthropogenic influences on ecosystem in Jiaozhou Bay and Daya Bay, China. *Marine Pollut Bull.* 168, 112406. doi: 10.1016/j.marpolbul.2021.112406

Zhang, X., Ward, B. B., and Sigman, D. M. (2020). Global nitrogen cycle: critical enzymes, organisms, and processes for nitrogen budgets and dynamics. *Chem. Rev.* 120, 5308–5351. doi: 10.1021/acs.chemrev.9b00613

Zhang, X. Y., Han, X. X., Chen, X. L., Dang, H. Y., Xie, B. B., Qin, Q. L., et al. (2015). Diversity of cultivable protease-producing bacteria in sediments of Jiaozhou Bay, China. *Front. Microbiol.* 6, 1021. doi: 10.3389/fmicb.2015.01021

Zhang, Y. Z., Zhang, W. X., and Chen, X. L. (2020). Mechanisms for induction of microbial extracellular proteases in response to exterior proteins. *Appl. Environ. Microbiol.* 86, e01036–e01020. doi: 10.1128/AEM.01036-20

Zhang, Z., Han, P., Zheng, Y., Jiao, S., Dong, H., Liang, X., et al. (2022). Spatiotemporal Dynamics of Bacterial Taxonomic and Functional Profiles in Estuarine Intertidal Soils of China Coastal Zone. *Microb. Ecol.* 85, 383–399. doi: 10.21203/rs.3.rs-1155844/v1

Zhao, Z., Mao, Z., Xing, P., Tao, Y., and Wu, Q. (2022). Intrahabitat differences in bacterial communities associated with *Corbicula fluminea* in the large shallow eutrophic Lake Taihu. *Appl. Environ. Microbiol.* 88, e02328–e02321. doi: 10.1128/aem.02328-21

Zhou, M. Y., Chen, X. L., Zhao, H. L., Dang, H. Y., Luan, X. W., Zhang, X. Y., et al. (2009). Diversity of both the cultivable protease-producing bacteria and their extracellular proteases in the sediments of the South China sea. *Microb. Ecol.* 58, 582–590. doi: 10.1007/s00248-009-9506-z

Zhou, M. Y., Wang, G. L., Li, D., Zhao, D. L., Qin, Q. L., Chen, X. L., et al. (2013). Diversity of both the cultivable protease-producing bacteria and bacterial extracellular proteases in the coastal sediments of King George Island, Antarctica. *PLoS ONE.* 8, e79668. doi: 10.1371/journal.pone.0079668

Zhou, X., Li, B., Guo, Z., Wang, Z., Luo, J., and Lu, C. (2018). Niche separation of ammonia oxidizers in mudflat and agricultural soils along the Yangtze River, China. *Front. Microbiol.* 9, 3122. doi: 10.3389/fmicb.2018.03122

frontiers | Frontiers in Marine Science

TYPE Original Research
PUBLISHED 23 May 2023
DOI 10.3389/fmars.2023.1186809

OPEN ACCESS

EDITED BY
Xue-Wei Xu,
Ministry of Natural Resources, China

REVIEWED BY
Heng-Lin Cui,
Jiangsu University, China
Guohong Liu,
Fujian Academy of Agricultural Sciences, China

*CORRESPONDENCE
Song-Gun Kim
sgkim@kribb.re.kr

RECEIVED 15 March 2023
ACCEPTED 09 May 2023
PUBLISHED 23 May 2023

CITATION
Muhammad N, Avila F, Lee Y-J, Han HL, Kim K-H and Kim S-G (2023) *Chondrinema litorale* gen. nov., sp. nov., of the phylum *Bacteroidota*, carrying multiple megaplasmids isolated from a tidal flat in the West Sea, Korea.
Front. Mar. Sci. 10:1186809.
doi: 10.3389/fmars.2023.1186809

Chondrinema litorale gen. nov., sp. nov., of the phylum *Bacteroidota*, carrying multiple megaplasmids isolated from a tidal flat in the West Sea, Korea

Neak Muhammad[1,2], Forbes Avila[1,2], Yong-Jae Lee[1], Ho Le Han[3], Kyoung-Ho Kim[4] and Song-Gun Kim[1,2]*

[1]Biological Resource Center/Korean Collection for Type Cultures (KCTC), Korea Research Institute of Bioscience and Biotechnology, Jeongeup, Republic of Korea, [2]Department of Environmental Biotechnology, KRIBB School of Biotechnology, University of Science and Technology (UST), Daejeon, Republic of Korea, [3]The University of Danang, University of Science and Technology, Danang, Vietnam, [4]Department of Microbiology, Pukyong National University, Busan, Republic of Korea

A Gram-stain-negative, long rod, oxidase and catalase-positive strain WSW3-B12^T was isolated from red algae on tidal flats in the West Sea, Korea. Phylogenetic analysis based on the 16S rRNA gene sequence revealed that the strain WSW3-B12^T had the highest sequence similarity, 92.7%, to *Flexithrix dorotheae* DSM 6795^T, followed by *Rapidithrix thailandica* TISTR 1750^T at 90.8% in the family *Flammeovirgaceae* of the phylum *Bacteroidota*. The whole genome sequence determined using both the Nanopore and Illumina platforms revealed that the complete genome consists of 29 contigs, among which contig 1 was a circular chromosome, while the remaining 28 contigs were plasmids. The size of the genome was 10.1 Mbp and the G+C content was 34.1%. The average nucleotide identity (ANI), digital DNA–DNA hybridization (dDDH), average amino acid identity (AAI), and percentage of conserved proteins (POCP), phylogenomic-related indexes between the strain WSW3-B12^T and the closest strain *Flexithrix dorotheae* DSM 6795^T, were 76.6%, 19.9%, 57.2%, and 55.6%, respectively, which were all lower than the threshold values to support the creation of a novel genus. A comprehensive genome analysis revealed that the strain WSW3-B12^T harbored many of the key genes involved in central metabolism in the main chromosome and also carried important genes for the production of vitamins, quinone, and antimicrobial resistance on the plasmids. The strain also carried genes that are involved in the metabolism of heavy metals such as arsenic, cobalt, copper, and iron on both the chromosome and plasmids. Furthermore, the genome of the strain was highly enriched with carbohydrate-active enzymes (CAZymes), carrying a total of 241 CAZymes. Moreover, a complete CRISPR/Cas system was detected on plasmid 20. The major fatty acids of the strain were iso-$C_{15:0}$ and $C_{16:1}$ ω5. The polar lipids contained phosphatidylethanolamine, four unidentified lipids, and four glycolipids. The respiratory quinone was menaquinone 7. Based on the phenotypic,

chemotaxonomic, and genomic analyses, the strain WSW3-B12^T could be assigned to a novel species and novel genus within the family *Flammeovirgaceae*, for which the name *Chondrinema litorale* gen. nov., sp. nov. (type strain WSW3-B12^T = KCTC 82707^T = GDMCC 1.3198^T) is proposed.

KEYWORDS

red algae, microbial diversity, polyphasic taxonomy, comparative genomics, carbohydrate-active enzymes

1 Introduction

The sea covers around 70% of the surface of our planet, and tidal flats connect the sea and land. Tidal flats are located between marine ecosystems and land environments, providing a habitat for aquatic organisms and an ideal place for isolating unique microbial taxa (Wilms et al., 2006). They are exposed to certain environmental events, such as flooding, habitat destruction, climate changes, and pollution (Duarte et al., 2008), which result in the formation of unique microbial communities (Lv et al., 2016). Microbes in tidal flats play critical roles in regulating ecological processes and biogeochemical cycles (Beam et al., 2020). They are a key player in nutrient cycling by converting organic matter into inorganic forms, which enhance the nutrient supply in marine environments (Lee et al., 2021). Furthermore, these microbes also decompose pollutants flowing into the tidal flats (Cheng et al., 2017; Lee et al., 2019; Kim et al., 2022). The productivity of tidal flat ecosystems is largely due to these microbes. However, the precise relationship between their diversity and functioning is little understood.

The microbes in the tidal flats interact with invertebrates, animals, plants, and seaweed. Seaweed or sea macroalgae, which perform primary production using sunlight and nutrients from the environment, refer to thousands of species of macroscopic, multicellular marine algae. Macroalgae include red, brown, and green algae, which are essential components of the marine food chain (Lobban and Harrison, 1994). Furthermore, macroalgae are biological reservoirs of abundant marine bacteria (Singh and Reddy, 2015; Juhmani et al., 2020). These microbes produce bioactive compounds that can be used to combat drug resistance and cancer (Menaa et al., 2020; Kizhakkekalam and Chakraborty, 2021). A large number of novel bacterial strains have been isolated from marine algae (Karthick and Mohanraju, 2018; Asharaf et al., 2022; Muhammad et al., 2022a).

The phylum *Bacteroidota* (a heterotypic synonym of *Bacteroidetes*) was first established by Leadbetter in 1974 (Leadbetter, 1974), subsequently amended by Reichenbach in 1992 (Reichenbach, 1992), and again revised by Ludwig (Ludwig et al., 2010). The phylum was initially described as a monophyletic branch of three genera, *Cytophaga, Flavobacterium*, and *Bacteroides* (CFB) (Paster et al., 1994). But it was expanded to include six classes and six orders (https://lpsn.dsmz.de/phylum/bacteroidota). The class *Cytophagia* is currently represented by the sole order *Cytophagales* (https://lpsn.dsmz.de/order/cytophagales) comprising 20 families, among which *Flammeovirgaceae* (https://lpsn.dsmz.de/family/flammeovirgaceae) is the second largest family, comprising nine validly published genera and three genera unassigned to the family. The nine validly published genera are *Flammeovirga, Flexithrix, Imperialibacter, Limibacter, Perexilibacter, Rapidithrix, Sediminitox, Tunicatimonas*, and *Xanthovirga*.

Members of the family *Flammeovirgaceae* are heterotrophic, Gram-stain-negative, non-flagellated, non-spore-forming, rod-shaped cells, and share menaquinone 7 (MK-7) as the major respiratory quinone (Yoon et al., 2011). They are widely distributed in various environments, particularly in marine aquatic systems (Yoon et al., 2012; Wang et al., 2013; Goldberg et al., 2020). Members of the family *Flammeovirgaceae* and other members of the phylum *Bacteroidota* are relatively enriched in a large number of glycoside hydrolases (GHs), glycosyl transferases, peptidases, and adhesion proteins that degrade organic biomacromolecules (Fernández-Gómez et al., 2013). They contain a large number of genes encoding carbohydrate-active enzymes, which potentially participate in polysaccharide degradation (Mckee et al., 2021). There are a number of reported strains of the phylum *Bacteroidota* that can degrade various types of complex polysaccharides (Hehemann et al., 2012; Mann et al., 2013).

During a study on the microbial diversity of the tidal flats in the West Sea, Korea, a number of novel bacterial strains were isolated (Muhammad et al., 2022a; Muhammad et al., 2022b). Strain WSW3-B12^T isolated from the red algae of the genus *Chondrus* was characterized by polyphasic taxonomy and genome analysis. Based on the polyphasic taxonomic analysis, it is proposed that the isolate represents a novel species and a novel genus of the family *Flammeovirgaceae* in the phylum *Bacteroidota*. A comparative genomic analysis of the strain WSW3-B12^T and its close strains highlighted the uniqueness in terms of multiple plasmids and the presence of various functional genes for possible application. Genome mining emphasized the presence of abundant genes for heavy metal metabolism, for CAZymes of polysaccharide degradation, and for CRISPR candidates that are expected to have potential biotechnological applications. Furthermore, the degradation of polysaccharides (starch, inulin, and cellulose) and the presence of heavy metal metabolism genes (arsenic, cobalt, and

copper) highlighted the contribution of strain in the carbon cycle (Fernández-Gómez et al., 2013) and its important role in the remediation of heavy metals (Chen et al., 2018; Dell'Anno et al., 2021) in the tidal flat ecosystem.

2 Materials and methods

2.1 Isolation and cultivation

A red alga belonging to the genus *Chondrus* was collected in the West Sea, Byeonsan, Republic of Korea (35° 40′ 53.76″ N 126° 31′ 51.96″ E) in late autumn, 2020. The red alga genus *Chondrus* is abundant across the east and west coasts of the Republic of Korea. The genus can be found on rocks from the middle intertidal zone into the subtidal zone (Lee et al., 2013; Kristyanto et al., 2022). One gram of the alga was cut into small pieces and then placed at the center of agar plates, which was composed of 60% seawater and 1.5% agar. The primary plates were incubated at 15 °C for five days and then routinely observed under a stereoscopic microscope. The colonies from the primary plate were picked up and transferred to marine agar 2216 (MA; BD) at 30°C which is also called Zobell media, a standard plate medium for the cultivation of marine bacteria (ZoBell, 1941). The pure cultures of the novel strain were preserved in 20% glycerol at -80°C. The cultures were deposited in the Korean Collection for Type Cultures (KCTC) and the Guangdong Microbial Culture Collection Center (GDMCC), under the culture depositing numbers KCTC 82707^T and GDMCC 1.3198^T.

2.2 16S rRNA phylogeny

The genomic DNA of the strain WSW3-B12^T was extracted from cells grown in MA at 30°C, by a NucleoSpin Microbial DNA kit (Macherey-nagel, Germany) following the manufacturer's instructions. The 16S rRNA gene was amplified with bacterial universal primers and sequenced with Sanger's sequencing method (Biofact, South Korea) (Pheng et al., 2020). Pairwise sequence similarity values of the 16S rRNA gene sequence (1454 bp) were obtained through the EzBioCloud server (http://www.ezbiocloud.net) (Yoon et al., 2017a). All sequences of the related strains retrieved from EzBioCloud were aligned and edited with the BioEdit software (version 7.2.5). Phylogenetic trees were constructed by using neighbor-joining (NJ) (Saitou and Nei, 1987), maximum-likelihood algorithms (ML) (Felsenstein, 1981), and the maximum parsimony (MP) method (Felsenstein, 1981) in the Molecular Evolutionary Genetics Analysis (MEGA X) program (Kumar et al., 2018). For the ML tree, Kimura's two-parameter model was used for the calculation of the evolutionary distance. For the construction of NJ and MP phylogenetic trees Tajima-Nei model and subtree-pruning-regrafting (SRF) model were used. The bootstrap resampling method of 1000 replicates was applied to evaluate the phylogenetic tree. Bootstrap values >70% are presented in nodes of each branch.

2.3 Morphological, physiological, and biochemical analyses

Gram-staining was performed with the BBL^{TM} Gram-staining kit (BD, USA) according to the manufacturer's instructions. Cells of the strain WSW3-B12^T were incubated for 48 h on MA at 30 °C and examined for morphology through a scanning electron microscope (Regulus 8100, Hitachi) (Jeon et al., 2022). The motility was tested by the hanging drop method (Bowman, 2000). The optimal temperature for growth was determined in MA, for seven days at 4, 10, 15, 20, 25, 30, 37, and 45 °C. The salt tolerance was determined for a novel and reference strains by making a media having the same composition as MA except with the supplementation of salt from 0 to 0.5, and 1.0-8.0% (w/v) (Muhammad et al., 2022a). Growth at pH 5 to 10 (at intervals of 0.5 unit) was determined in MA adjusted with various buffers, at a concentration of 20 mM: acetate for pH 5.0–5.5, phosphate for pH 6.0–8.0, Tris for pH 8.5–9.0, and carbonate for pH 9.5–10.0 (Muhammad et al., 2022b). Catalase activity was tested by the production of oxygen bubbles when 3% (v/v) H_2O_2 was added to fresh cells (Ueno et al., 2021). The oxidase reaction was carried out using 1% (w/v) tetramethyl-*p*-phenylenediamine.

The degradation of polysaccharides was studied in basal media made of 60% (v/v) seawater, 0.1% (w/v) peptone, 0.6% (w/v) gellan gum as a solidifying agent, and 0.1% (w/v) of each test polysaccharide (cellulose, chitin, κ-carrageenan, inulin, sodium alginate, starch, and xylan) (Gao et al., 2017). The degradation of polysaccharides was further determined by using basal broth, which contained 0.2% of the above sugar molecules. Each sugar broth was inoculated with a 48 hours' old culture and incubated at 30 °C in the shaker. The supernatant of the culture was harvested at 0, 2, and 4 days and then reacted with 3,5-dinitrosalicylic acid (DNS) to detect reduced sugar production (Gao et al., 2017; Deshavath et al., 2020). The hydrolysis of Tweens 20, 40, 80, and casein was determined by the method of Cowan & Steel (Phillips, 1993; Amrina et al., 2021). DNase activity was checked by using DNase agar (BD).

The enzymatic activities and carbon source utilization were determined by using API ZYM, API 20E, API 50CH (bioMérieux), and GEN III Microplates (Biolog), following the manufacturer's instructions, except that the inoculum suspensions were adjusted to a final concentration of 2% (w/v) NaCl (Jeong et al., 2020). To test for growth under an anaerobic condition, the strain WSW3-B12^T was cultivated on MA plates and incubated in an anaerobic jar at 30°C for seven days, following the manufacturer's instructions (BD GasPak Systems). Susceptibility to antibiotics was tested on MA plates using various antibiotic discs (μg/disc): chloramphenicol (30), erythromycin (15), kanamycin (30), novobiocin (30), neomycin (30), penicillin (10 IU), tetracycline (30), and vancomycin (30) (Jorgensen and Turnidge, 2015).

2.4 Chemotaxonomic analysis

For the fatty acid analysis, cells of the strain WSW3-B12^T and the reference strains *Flexithrix dorotheae* KCTC 82993^T,

Rapidithrix thailandica KCTC 82795^T, and *Sediminitomix flava* KCTC 12970^T were collected from MA agar at the same physiological age. The standard MIDI protocol (version 6.2) was used to extract the fatty acids from the cell (Sasser, 1990). The extracted fatty acid methyl esters were then injected into a gas chromatograph and were analyzed by the Sherlock Microbial Identification System (TSBA; library version 6.0). For respiratory quinones, the compounds were extracted from bacterial biomass using the protocol of Komagata and Suzuki (Komagata and Suzuki, 1988). First, 100 mg of freeze-dried cells was treated with chloroform-methanol (2:1, v/v), and then crude compounds were separated by thin-layer chromatography (TLC, 20cm×20cm, silica gel 60 F254 plate, Merck) using petroleum benzene/diethyl ether (9:1, v/v) as the developing solvent. The quinone band was collected from a TLC plate and dissolved in acetone. Finally, the compound was purified and identified by reverse-phase high-performance liquid chromatography with a UV detector at 270 nm. Polar lipids were extracted from the freeze-dried cells by chloroform/methanol followed by two-dimensional TLC, as described by Minnikin et al. (Komagata and Suzuki, 1988). The two-dimensional TLC (10 cm×10 cm, silica gel 60 F254 plate, Merck) plates were run using chloroform-methanol-water (65:25:4, v/v/v) and chloroform-methanol-acetic acid-water (80:12:15:4, v/v/v/v) as the solvent systems for the first and second dimensions, respectively. Finally, the TLC plates were sprayed with 0.2% ninhydrin for the amino group-containing lipids, α-naphthol for sugar-containing lipids, molybdenum blue for phosphorus-containing lipids, 0.5% phosphomolybdic acid reagent for total lipids, and Dragendorff's solution for quaternary nitrogen-containing lipids.

2.5 Genome sequencing and analysis

The total genomic DNA of the strain WSW3-B12^T was extracted from two-day old culture on MA. The quality and quantity of the DNA samples were measured with a spectrophotometer (Nanodrop 2000/2000c), and the size and length were monitored by electrophoresis using 1% (w/v) agarose gel. The whole genome sequencing was performed by a combination of Illumina Novaseq 6000 and Oxford Nanopore Technologies (ONT) (at HME, Republic of Korea). For Illumina sequencing, the short-length DNA was used to build up a library while for the ONT high-molecular-weight DNA was used to prepare the library using a ligation sequencing kit (SQK-LSK109; ONT) following the manufacturer's protocol (version RPB_9059_v1_revC_08Mar2018). Sequencing was performed as multiplex runs on a MinION with MinKnow v1.15.1 using FLO-MIN106 R9.4 flow cells. Illumina reads were trimmed and filtered from raw reads using Trimmomatic (Bolger et al., 2014) and Filtlong v0.20 (https://github.com/rrwick/Filtlong) filtering tools. For Nanopore reads, the raw Fast5 files were demultiplexed with Guppy to retain the barcoded reads. Porechop v0.2.4 (https://github.com/rrwick/Porechop) was used to remove the barcode and adapters. The filtered Illumina and Nanopore reads were assembled using four different programs: Spades, CANU (Koren et al., 2017) Unicycler, and Flye (Lin et al., 2016). The quality initial genomes bins were then evaluated using CheckM (Parks et al., 2015).

2.6 Genome annotation and phylogeny

First, the genomes were annotated by NCBI Prokaryotic Genomes Automatic AnnotationPipeline (PGAAP) and Prokka version 1.14.6 (Seemann, 2014). The genome of the strain WSW3-B12^T contained 29 contigs. Each contig was predicted for plasmids and then blasted to find the most similar plasmids and their closest host using the PLSDB server v. 2021_06_23_v2 (Schmartz et al., 2022).

To determine the taxonomic position of the strain WSW3-B12^T the average nucleotide identity (ANI) and digital DNA-DNA hybridization (dDDH) were calculated using the ANI calculator tool in Kostas Lab Service (http://enve-omics.ce.gatech.edu/ani/) and the Genome to Genome Distance Calculator version 3.0 of DSMZ (https://ggdc.dsmz.de/ggdc.php#) (Meier-Kolthoff et al., 2013). For genus confirmation, amino acid identity (AAI) and percentage of conserved proteins (POCP) values were further calculated using Kostas Lab Service (http://enve-omics.ce.gatech.edu/aai/) and the BLASTP program (https://github.com/hoelzer/pocp), respectively (Qin et al., 2014). The whole-genome-based phylogenetic tree was built based on the alignment of 400 marker genes with FastTree using PhyloPhlAn version 3.0 (Asnicar et al., 2020). A nonmetric multidimensional scaling (nMDS) plot was made using a matrix of functional genes found in the COGs (Clusters of Orthologous Groups) database (Galperin et al., 2021), which was used to find the clustering of the strain WSW3-B12^T and the existing strains.

2.7 Genome functional analysis

The functional genes within each genome were annotated using the KEGG database and then translated into pathways using KEGG Decoder (Graham et al., 2018) and KEGG-Expander (https://github.com/bjtully/BioData/tree/master/KEGGDecoder). The prediction and classification of the orthologous groups associated with the protein coding genes were annotated using the COGs database (Galperin et al., 2021). The genomes were further annotated for functional genes using the rapid annotations based on subsystem technology (RAST) database (https://rast.nmpdr.org/rast.cgi). Carbohydrate active enzymes were annotated using the dbCAN2 meta server (Zhang et al., 2018). Biosynthesis gene clusters (BGCs) and metabolic gene clusters (MGCs) possessed by each genome were identified using antiSMASH 6.01 (Blin et al., 2019). The antimicrobial resistance (AMR) genes were predicted using the comprehensive antibiotic resistance database (CARD) database (Konaté et al., 2019; Alcock et al., 2022). The CRISPRCasFinder server (Couvin et al., 2018) and CRISPRcasIdentifier (https://github.com/BackofenLab/CRISPRcasIdentifier) were used to predict the CRISPR-Cas system (Padilha et al., 2020). Finally,

the cas enzyme's sequences were blasted using UniProt for confirmation (The UniProt Consortium, 2023). Phage sequences were identified by the PHAST (phage search tool) (Arndt et al., 2016).

3 Results and discussion

3.1 Isolation and identification

The strain WSW3-B12^T was isolated from the red alga genus *Chondrus* collected from tidal flats at the West Sea, Byeonsan, Republic of Korea. The strain grew well on MA and produced regular pin-pointed, light brown colonies after 48 hours' incubation. The diameters of the colonies ranged from 325-420 µm. Cells of the strain WSW3-B12^T were Gram-stain-negative, non motile and rod-shaped with a length of 5-7 µm and width of 0.46-0.54 µm (Figure S1).

3.2 16S rRNA gene analyses

The analysis of 16S rRNA gene sequences from the EzBioCloud server (http://www.ezbiocloud.net) revealed that the strain WSW3-B12^T was phylogenetically affiliated with the family *Flammeovirgaceae*, and the closest relatives were *Flexithrix dorotheae* DSM 6795^T (92.7%) and *Rapidithrix thailandica* TISTR 1750^T (90.8%). Furthermore, the phylogenetic trees based on 16S rRNA gene sequences showed clustering of the strain WSW3-B12^T with *Rapidithrix thailandica* TISTR 1750^T and *Flexithrix dorotheae* DSM 6795^T, (Figure 1). The closest strains *Flexithrix dorotheae* DSM 6795^T, *Rapidithrix thailandica* TISTR 1750^T, and *Sediminitomix flava* DSM 28229^T were isolated from marine silt, algae, and sediment, respectively (Hosoya and Yokota, 2007; Khan et al., 2007; Srisukchayakul et al., 2007). The strains *Flexithrix dorotheae* KCTC 82993^T, *Rapidithrix thailandica* KCTC 82795^T, and *Sediminitomix flava* KCTC 12970^T were used as reference strains. Finally, the 16S rRNA gene sequences of the strain WSW3-B12^T were submitted to the NCBI database under the accession number OP823709.

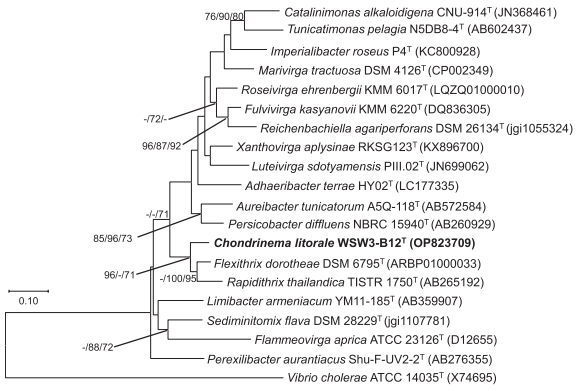

FIGURE 1
Maximum likelihood tree based on 16S rRNA gene sequences showing the phylogenetic relationship of the strain WSW3-B12^T and closely related genus of family *Flammeovirgaceae* and order *Cytophagales*. Bootstrap values (>70%) in the order of ML/NJ/MP are shown at the branch points based on 1000 replications. *Vibrio cholerae* ATCC 14035^T *were* used as outgroups. Bar 0.10 substitutions per nucleotide position.

3.3 Physiological and biochemical characteristics

The strain WSW3-B12^T was Gram-stain-negative, oxidase and catalase positive, strictly aerobic and long rod-shaped bacteria. Growth occurred in a temperature range of 15–30°C (optimum, 25–30°C), a pH range of 5.5–9.0 (optimum, 6.5–8.5), and a NaCl range of 1.0–7.0% (optimum, 2.0–5.0%) (w/v). The strain degraded cellulose, inulin, and starch but not chitin, κ-carrageenan, sodium alginate, and xylan. Cells were positive for the hydrolysis of Tweens 20, 40, and 80 but negative for the hydrolysis of casein and DNase. The strain was sensitive to chloramphenicol, novobiocin, tetracycline, and vancomycin, but resistant to erythromycin, kanamycin, neomycin, and penicillin. In the API ZYM test, activities of acid phosphatase, alkaline phosphatase, N-acetyl-β-glucosaminidase, cystine arylamidase, α-chymotrypsin, esterase (C4), esterase lipase (C8), α-galactosidase, β-galactosidase, α-glucosidase, β-glucosidase, leucine arylamidase, naphthol-AS-BI-phosphohydrolase, trypsin, and valine arylamidase were present while activities of α-fucosidase, β-glucuronidase, lipase (C14), and α-mannosidase were absent. The strain was only positive for gelatinase in API 20E. In the API 50CH strip, acid is produced from L-arabinose, amidon (starch), arbutin, N- acetylglucosamine, D-cellobiose, gentibiose, D-galactose, glucose, D-lactose, methyl-αD-glucopyranoside, methyl-αD-mannopyranoside, D-maltose, D-melibiose, D-mannose, D-melezitose, D-raffinose, L-rhamnose, D-sucrose, D-trehalose, D-turanose, and D-xylose. In a GEN III MicroPlate (Biolog) test, cells utilize dextrin, L-fucose, D-glucose-6-phosphate, D-glucuronic acid, β-methyl-D-glucoside, L-malic acid, sucrose, D-trehalose, D-turanose, and quinic acid. Details of physiological and biochemical characteristics that differentiate the strain WSW3-B12^T from its closest relatives in the family *Flammeovirgaceae* are listed in (Table 1).

3.4 Chemotaxonomic analysis

The major fatty acids (>5.0%) of the strain WSW3-B12^T were iso-$C_{15:0}$ (24.9%), $C_{16:1}$ ω5c (23.8%), $C_{17:1}$ ω6c (9.4%), and iso-$C_{16:0}$ (7.9%). Meanwhile, iso-$C_{17:0}$ 3-OH (3.5%), summed feature 3 ($C_{16:1}$ *ω7c* and/or $C_{16:1}$ *ω6c*) (3.5%), $C_{15:0}$ 3-OH (3.2%), $C_{16.0}$ (2.8%), $C_{18:1}$ ω9c (2.3%), $C_{12:0}$ (2.0%), $C_{16:0}$ 3-OH (1.5%), and $C_{14:0}$ (1.4%) were the minor fatty acids (Table 2). The novel strain and all three reference strains showed a higher percentage of $C_{16:1}$ ω5c (15.3-41.0%) and iso-$C_{15:0}$ (8.5-24.9%) components of fatty acids. The strain WSW3-B12^T had a higher percentage of iso-$C_{16:0}$ (7.9%) and a lower percentage of $C_{16.0}$ (2.8%) as compared to the reference strains. Interestingly, among the four strains, only the strain WSW3-B12^T had $C_{17:1}$ ω6c (9.4%) component of fatty acid. The respiratory

10.3389/fmars.2023.1186809

TABLE 1 Differential characteristics of the strain WSW3-B12^T and phylogenetically closely related type species of the genus belongs to *Flammeovirgaceae*.

Characteristic	1	2	3	4
Temperature (°C)	15-30	17-40	25-30	10-37
pH optimum	5.5-9.0	6.5-8.0	5-10	6.0-9.0
NaCl (%, w/v)	1.0-7.0	0.5-5.0	0.5-7.0	0.5-5.0
Hydrolysis of Tween 40	+	+	–	+
Hydrolysis of Tween 80	+	+	–	+
Enzyme activity (API ZYM)				
N-Acetyl-β-glucosaminidase	+	–	–	–
α-Fucosidase	–	+	–	–
α-Galactosidase	+	+	–	–
β-Galactosidase	+	+	–	–
α-Glucosidase	+	–	–	–
β-Glucosidase	+	–	–	–
API 50CH				
Amygdalin	+	w	–	–
Amidon (starch)	+	w	–	+
Arbutin	+	–	–	–
N-Acetylglucosamine	+	–	+	–
D-Cellobiose	+	+	–	+
L-Fucose	–	–	+	–
D-Fructose	–	+	+	–
Glycogen	–	–	w	+
Glycerol	–	–	+	–
D-Galactose	+	+	+	–
Gentibiose	+	–	–	+
D-lactose	+	+	+	–
D-Mannose	+	+	+	–
Methyl-αD-glucopyranoside	+	+	–	–
Methyl-αD-mannopyranoside	+	+	–	–
D-Melezitose	+	–	–	–
D-Maltose	+	+	+	–
D-Melibiose	+	–	+	–
L-Rhamnose	+	+	–	–
D-Rafinose	+	–	–	–
D-Sucrose	+	+	–	–
D-Trehalose	+	+	+	–
D-Turanose	+	–	–	–
D-Xylose	+	+	+	–
GEN III MicroPlate assay (Biolog):				

(Continued)

TABLE 1 Continued

Characteristic	1	2	3	4
Acetic acid	–	+	+	–
L-Aspartic acid	–	+	+	–
Aztreonam	–	+	+	–
N-Acetyl-β-D-mannosamine	–	+	+	+
N-Acetyl-neuraminic acid	–	+	+	–
D-Cellobiose	–	–	–	+
Dextrin	+	+	+	–
D-Glucuronic acid	+	+	+	–
D-Glucose-6-PO4	+	–	–	–
Glycerol	–	–	+	–
Gelatin	–	–	+	–
L-Glutamic acid	–	+	+	–
α-D-Lactose	+	–	–	–
β-Methyl-D-glucoside	+	+	+	–
D-Mannose	–	–	+	+
L-Malic acid	+	–	–	–
Nalidixic acid	+	–	–	–
Quinic acid	+	–	–	–
Sucrose	+	–	+	–
1% Sodium Lactate	–	–	+	–
D-Serine	–	–	+	–
L-Serine	–	+	+	–
Tetrazolium violet	–	–	+	–
Tetrazolium blue	–	–	+	–

Strain: 1, WSW3-B12^T; 2, *Flexithrix dorotheae* KCTC 82993^T; 3, *Rapidithrix thailandica* KCTC 82795^T; 4, *Sediminitomix flava* KCTC 12970^T All strains were positive for the hydrolysis of starch and Tween 20 and for the activities of oxidase and catalase. All the data are from this study except for the temperature and pH determination of the reference strains are from the literature (Hosoya and Yokota, 2007; Khan et al., 2007; Srisukchayakul et al., 2007). +, Positive; –, negative; w, weak.

quinones of the strain WSW3-B12^T was menaquinone 7 (MK-7) which was also founded in the reference strains. The polar lipids of the strain WSW3-B12^T contained phosphatidylethanolamine, one unidentified aminophospholipid, four unidentified glycolipids, and three unidentified lipids (Figure S2).

3.5 Genomic general features

The combined Nanopore and Illumina sequencing platforms were used to determine the complete genomes of the strains WSW3-B12^T. The CheckM analysis showed that the strain had 99.4% completeness and only 1.45% contamination, which indicated the high quality and reliability of the genomes. The complete genome of the strain WSW3-B12^T comprises 29 contigs, among which contig 1 was a circular chromosome length of 4.938441 bp while the remaining 28 contigs were plasmids, out of which six were mobile plasmids and the rest were non-mobilizable plasmids. Some genomes of the family *Flammeovirgaceae*, the phylum *Bacteroidota* are relatively large (Feng et al., 2021a): the genomes of *Flammeovirga yaeyamensis* NBRC 100898 (Feng et al., 2021b), *Flammeovirga* sp. SJP92 (Dong et al., 2017), *Flexithrix dorotheae* DSM 6795^T, and *Flammeovirga aprica* JL-4^T are 7.4, 8.4, 9.5, and 9.3 Mbp, respectively. The details of each plasmid are summarized in Table S1. Interestingly, limited numbers of bacteria have been discovered to have multiple plasmids (Cazares et al., 2020, Feng et al., 2021b). Some marine members of the phylum *Bacteroidota* carry a single large plasmid (Zhong et al., 2001; Saw et al., 2012). We hypothesize that the strain WSW3-B12^T received plasmids from other bacteria in the environment, which explains the presence of the high number of plasmids and the mobile genetic elements in the genome of the strain WSW3-B12^T.

Genome annotation by PGAAP pipeline in the NCBI identified a total of 8199 genes, nine ribosomal RNA genes (5S, 3; 16S, 3; 23S, 3), and a total of 51 transfer RNA genes. The G+C content of the strain WSW3-B12^T was 34.1%, while for the reference strains *Flexithrix*

TABLE 2 Cellular fatty acid compositions (%) of the strain WSW3-B12^T and phylogenetically closely related type species of genus belonging to *Flammeovirgaceae*.

Fatty acid (%)	1	2	3	4
Saturated				
$C_{10:0}$	–	–	1.2	–
$C_{12:0}$	2.0	–	–	–
$C_{14:0}$	1.4	1.2	2.2	5.1
$C_{16:0}$	2.8	8.5	12.5	8.0
$C_{18:0}$	–	1.5	3.9	–
Unsaturated:				
$C_{16:1}\omega5c$	23.8	41.0	36.2	15.3
$C_{18:1}\omega9c$	2.3	–	6.4	–
$C_{17:1}\omega6c$	9.4	–	–	–
Branched:				
iso-$C_{11:\ 0}$	–	–	1.7	–
iso-$C_{15:0}$	24.9	12.8	8.5	22.4
iso-$C_{15:1}$ G	–	–	–	2.3
anteiso-$C_{15:\ 0}$	–	1.4	–	1.3
iso-$C_{16:0}$	7.9	–	2.3	1.7
iso-$C_{17:0}$	–	–	2.5	–
Hydroxy:				
iso-$C_{15:0}$ 3-OH	–	4.33	3.0	1.9
$C_{15:0}$ 3-OH	3.2	–	–	1.3
$C_{16:0}$ 3-OH	1.5	3.6	2.7	17.2
iso-$C_{16:0}$ 3-OH	–	–	–	1.1
iso-$C_{17:0}$ 3-OH	3.5	10.2	8.4	2.3
Summed features:*				
2	–	–	–	1.7
3	3.5	10.3	2.1	13.0
4	2.7	2.6	5.7	–
9	–	–	–	2.7

Summed features 2, ($C_{14:0}$ 3-OH/$C_{16:0}$ iso I); Summed features 3, ($C_{16:0}$ ω7c/$C_{16:10}$ ω6c); Summed features 4, ($C_{17:\ 0}$ iso I/anteiso B); summed feature 9, ($C_{16:0}$ 10-methyl and/or iso-$C_{17:0}$ x9c) Strain: 1, WSW3-B12^T; 2, *Flexithrix dorotheae* KCTC 82993^T; 3, *Rapidithrix thailandica* KCTC 82795^T; 4, *Sediminitomix flava* KCTC 12970^T All data are from this study. Numbers indicate the percentages of the fatty acids. -, not detected (<1%).

dorotheae DSM 6795^T and *Sediminitomix flava* DSM 28229^T the content was 36.4 and 35.6%, respectively. The genomic features of the strain WSW3-B12^T and the existing strains are presented in (Table 3). The genome of the strain WSW3-B12^T was submitted to the NCBI with the GenBank accession number GCA_026250525.

3.6 Whole-genome-based phylogeny

To further confirm the taxonomic position of the strain WSW3-B12^T, the ANI and dDDH were calculated among the novel strain and type species of four genus of *Flammeovirgaceae Flexithrix dorotheae* DSM 6795^T, *Sediminitomix flava* DSM 28229^T, *Flammeovirga aprica* JL-4^T, and *Xanthovirga aplysinae* RKSG123^T. The ANI and dDDH between the strain WSW3-B12^T and *Flexithrix dorotheae* DSM 6795^T, *Sediminitomix flava* DSM 28229^T, *Flammeovirga aprica* JL-4^T, and *Xanthovirga aplysinae* RKSG123^T were ranged from 72.3-76.6 and 19.2-26.1%, respectively. The values of ANI and dDDH were below the standard cut-off values for speciation, which are ANI (95-96%) (Yoon et al., 2017b) and dDDH (70%) (Auch et al., 2010). The AAI and POCP values between the strain WSW3-B12^T and *Flexithrix*

TABLE 3 Genome features of the strain WSW3-B12^T and its closest related members in the family *Flammeovirgaceae.*

	1	2	3	4
Accession no.	GCA_026250525	NZ_ARBP00000000	NZ_QGDO01000001	NZ_JABANE010000001
Approximate genome size (Mbp)	10.1	9.5	6.6	9.3
G+C content (%)	34.1	36.4	35.6	35.2
Completeness	99.4	99.4	99.0	98.8
Contamination	1.45	0.6	2.98	3.21
Total number of genes	8199	7205	5059	7020
rRNAs (5S, 16S, 23S)	3,3,3	2,2,2	7,3,2	1,4,6
tRNAs	51	44	107	75
Pseudo Genes	69	51	11	153

Strain: 1, WSW3-B12^T; 2, *Flexithrix dorotheae* DSM 6795 ^{T}; 3, *Sediminitomix flava* DSM 28229 ^{T}; 4, *Flammeovirga aprica* JL-4 ^{T}.

dorotheae DSM 6795^T, *Sediminitomix flava* DSM 28229^T, *Flammeovirga aprica* JL-4^T, and *Xanthovirga aplysinae* RKSG123 ^{T} were ranged from 46.79-57.2 and 28.3-55.6%, respectively. The AAI cut-off value applied for the delineation of genus has a wide range of 60–80% (Park et al., 2022). A POCP value of 50% can be used for genus delineation, with a 55% value as the genus boundary (Qin et al., 2014; Barco et al., 2020). Thus, the strain WSW3-B12^T could represent a novel genus because genome-relatedness values are significantly lower than the species and genus boundaries. The phylogenomic tree showed that the strain WSW3-B12^T formed a clade with the closest strains, *Flexithrix dorotheae* DSM 6795^T and *Sediminitomix flava* DSM 28229^T, which also belongs to *Flammeovirgaceae* (Figure 2). The nonmetric multidimensional scaling (nMDS) plots further presented the same cluster between the strains WSW3-B12^T and *Flexithrix dorotheae* DSM 6795^T (Figure S3).

3.7 Genome functional analysis

3.7.1 Metabolic pathways analysis

First, a comparison of the distribution of genes in the KEGG module pathways for the strain WSW3-B12^T and existing stains is presented in a heatmap (Figure 3). The figure shows that the central metabolic pathways that are typically involved in aerobic respiration, sugar metabolism, amino acid synthesis, etc. appeared to be similar among these strains. The strain WSW3-B12^T contains genes that are involved in the biosynthesis of vitamins such as cobalamin, thiamin, and retinal. Furthermore, the KEGG pathways showed that the strain harbors genes for various enzymes, among which the genes for oligogalacturonide lyase (OGL) were only found in the genome of WSW3-B12^T. Interestingly, *OGL* genes exists on plasmid 3 instead of the main chromosome. This makes strain WSW3-B12^T unique compared to other *Flammeovirgaceae* genera that do not have the OGL genes. The *OGL* genes may give the strain WSW3-B12^T evolutionary advantages compared to other microorganisms. The *OGL* genes catalyzed the eliminative removal of unsaturated terminal residues from oligosaccharides of D-galacturonate, which is a key constituent of pectin in plant biomass (Linhardt et al., 1987; Abbott and Boraston, 2008; Abbott et al., 2010). The *OGL* genes is present in a group of pectinolytic bacteria, such as *Erwinia* species, that are involved in the

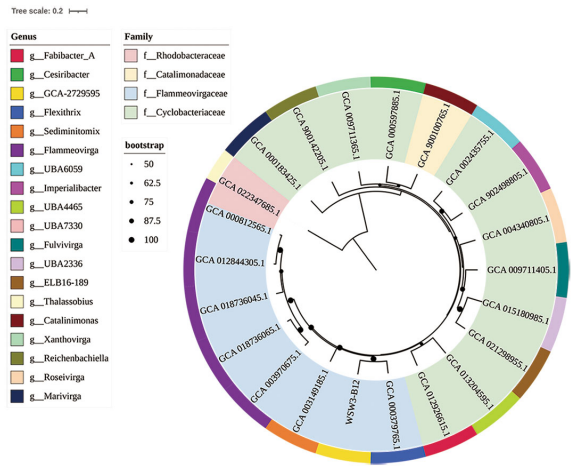

FIGURE 2
A whole-genome-based phylogenetic tree based on 400 marker genes using PhyloPhlAn version 3.0 shows the position of the strain WSW3-B12^T among the members of the families *Flammeovirgaceae, Catalimonadaceae*, and *Cyclobacteriaceae* in the order *Cytophagales.* The strain *Thalassobius* sp. Cn5-15 (GCA_022347685) of family *Rhodobacteraceae* was used as an outgroup. Strains: WSW3-B12^T, *Flexithrix dorotheae* DSM 6795^T (GCA_000379765), *Marinigracilibium pacificum* KN852 (GCA_012926615), *Flammeovirgaceae* sp. bin.302 (GCA_013204595), *Flammeovirgaceae* sp. CoA8N_M18 (GCA_021298955), *Flammeovirgaceae* sp. H1_BAC1 (GCA_015180985), *Fulvivirga kasyanovii* JCM 16186 ^{T} (GCA_009711405), *Roseivirga ehrenbergii* DSM 102268 ^{T} (GCA_004340805), *Imperialibacter* sp. EC-SDR9 ^{T} (GCA_902498805), *Flammeovirgaceae* sp. UBA6059 (GCA_002435755), *Catalinimonas alkaloidigena* DSM2516^T (GCA_900100765), *Flammeovirgaceae* sp. 311 (GCA_000597885), *Xanthovirga aplysinae* RKSG123^T (GCA_009711365), *Reichenbachiella agariperforans* DSM 26134^T (GCA_900142205), *Marivirga tractuosa* DSM 4126^T (GCA_000183425), *Thalassobius* sp. Cn5-15 (GCA_022347685), *Flammeovirga* sp. OC4 (GCA_000812565), *Flammeovirga aprica* JL-4^T (GCA_012844305), *Flammeovirga yaeyamensis* (GCA_018736045), *Flammeovirga kamogawensis* (GCA_018736065), *F pectinis* (GCA_003970675), *Sediminitomix flava* DSM 28229^T GCA_003970675.

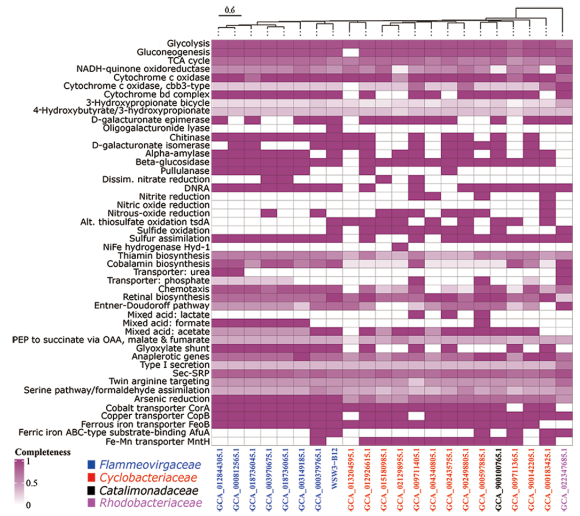

FIGURE 3
Heatmap of discriminated metabolic pathways within the genome of the strain WSW3-B12^T and 21 representative genomes of the existing members of the *Flammeovirgaceae, Catalimonadaceae*, and *Cyclobacteriaceae* in the order *Cytophagales* as used in Figure 2. The cell indicates the completeness of each pathway referring to annotations using KEGG. The heatmap of metabolic pathways was created using the same strains as in Figure 2 for a comparative study.

degradation of pectin, resulting in characteristic plant cell necrosis and tissue maceration (Collmer and Bateman, 1981).

Second, the COG analysis showed that the major genes were those involved in general function prediction, followed by signal transduction mechanisms, while the minor genes were those involved in cytoskeleton formation (Figure 4). The COG analysis further showed that genes for signal transduction were higher in the strain WSW3-B12^T compared to existing strains. Microbes use

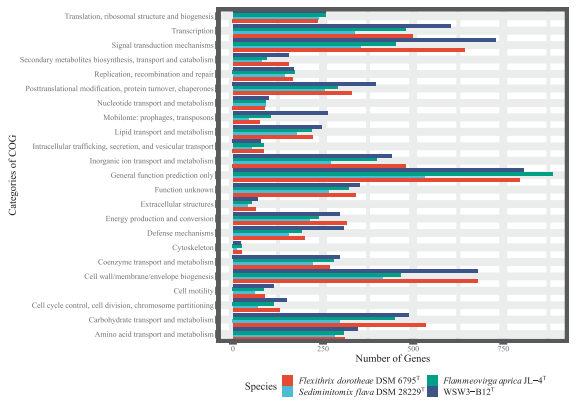

FIGURE 4
Clusters of Orthologous Group (COG), functional classification of proteins in the genome of the WSW3-B12^T and three existing strains of *Flammeovirgaceae*.

multiple signal transduction systems to respond to environmental changes and mediate diverse physiological processes and intercellular communication, including antibiotic resistance, virulence, symbiotic bacteria-host interactions, and biofilm assemblage (Wang et al., 2021). In the RAST system, a total of 8525 protein-encoding genes were predicted and assigned to 275 subsystems. In the subsystem category, the highest number of genes were assigned to the metabolism of amino acids and derivatives (303) and carbohydrates (251), followed by cofactors, vitamins, prosthetic groups, and pigment metabolism (171). Although the distribution of genes between novel strains and the closest strains was similar. The numbers of genes involved in regulation/cell signaling and cell wall/capsule synthesis were higher in the strain WSW3-B12^T than in the other strains (Table S2). Bacteria use these regulatory and cell signaling pathways for intercellular communication and diverse biological processes including biofilm formation (Wang et al., 2021). Furthermore, the higher number of cell wall and capsule synthesis pathways further helps the strain WSW3-B12^T in unfavorable conditions as well as in interaction of the strain with algae where the strain is isolated from.

The genes for polysaccharide degradation were identified using dbCAN meta servers, which detected a number of CAZyme gene clusters (CGCs) in the genome of the strain WSW3-B12^T and the existing strains. The strain WSW3-B12^T carried a total of 241 CAZymes. The distribution of CAZyme gene clusters (CGCs) between the novel and existing strains is summarized in (Table S3). The percentage of CAZyme genes out of the total genes and the ratio of the number of glycoside hydrolases (GHs) per Mbp genome were calculated. The strain WSW3-B12^T carried 2.94% CAZym and 13.86 GHs per Mbp of genome (Table S4). GHs and PLs that are expected to participate in degradation of polysaccharide were searched from the dbCAN meta server and compared in terms of the *in vitro* activities of the strain WSW3-B12^T (Table S5). The strain degraded cellulose, inulin, and starch. The strain carried four GH3 and five GH5 for cellulose degradation, one GH32 for inulin degradation, and eight GH13 for starch degradation. These GHs may participate in the degradation of the test polysaccharides. The strain did not carry any genes for the degradation of agar and alginate while it carried two genes for the degradation of κ-carrageenan.

3.7.2 Metabolism of heavy metals

The KEGG pathways showed that the strain WSW3-B12^T and the existing strain of *Flammeovirgaceae* had complete pathways for arsenic reduction (Figure 3) and also carried transporter genes such as *Cor*A, *CopA*, *FeoB*, and *AfuA* for cobalt, copper, ferrous, and ferric iron, respectively. The *CorA* proteins are generally associated with the transport of magnesium ions, but some members of the *CorA* family can also transport other ions such as cobalt (Co) and nickel (Ni) (Zhang et al., 2009). The strain WSW3-B12^T carried *CorA* in both chromosome and plasmid 11. *CopA* is one of the most well-known microbial metal transporters. The monomer of *CopA* binds to two Cu^{2+} ions and subsequently transfers them to the periplasm using the Cu chaperone (CusF) and ATP energy (Li et al., 2022). For the transportation of ferrous and ferric iron, the strain carries the FeoB protein, a cytoplasmic membrane transporter

protein, and *AfuA*, an ABC-type transporter protein. The ABC transporters help the microbes in membrane translocation of HMs ions (Hantke, 2003; Lau et al., 2016). Interestingly, *FeoB* genes exist on both chromosome and plasmid 6. Plasmid 6 even has two *FeoB* genes, compared to only one on the chromosome (Figure S5).

More HMs metabolism genes were discovered on the chromosome and in the plasmids as a result of the Prokka annotation. Many iron and copper metabolic genes were distributed in both the chromosome and the plasmids proportionally. Meanwhile, most of the arsenic and cobalt metabolic genes come from the plasmids. Thus, the plasmid has an interesting relationship with heavy metal metabolism. Details of these genes are listed in (Table S6).

3.7.3 Prediction of biosynthetic gene clusters and antibiotic resistance genes

The strain possessed six types of putative BGCs (terpene, type I polyketide synthases, type III polyketide synthases, betalactone, acyl amino acid, and lanthipeptide class I). Compared to the novel strain, only two BGCs in *Flexithrix dorotheae* DSM 6795^T, three BGCs in *Sediminitomix flava* DSM 28229^T, and five BGCs in *Flammeovirga aprica* JL-4^T were detected. (Table S7). Among the BGCs, the polyketide synthases are a family of multi-domain enzymes that produce polyketides, a large class of antimicrobial secondary metabolites (Hochmuth and Piel, 2009), while lanthipeptide class I are ribosomally synthesized antimicrobial compounds that are also called lantibiotics. Lanthipeptide can be used as an alternative to antibiotics in the food industry and veterinary medicine, and against multi-drug resistant strains methicillin-resistant Staphylococcus aureus.(MRSA) and vancomycin-resistant enterococcus (VRE) (Barbosa et al., 2015).

Based on CARD database prediction, there are a total of four antibiotic resistance genes, one on the chromosome and three on the plasmids (plasmid 3, 5, and 9). The chromosome contains a glycopeptide antibiotic resistance gene cluster and the plasmids contain fluoroquinolone and tetracycline antibiotic resistance.

3.7.4 CRISPR-Cas system and prophage analysis

CRISPR-Cas system consists of CRISPR array (spacers and repeats) and Cas system (collection of Cas enzymes). First, the CRISPRCasFinder was used to detect the CRISPR array. CRISPRcasIdentifier was then used to identify CRISPR related enzymes in the genome. The sequences were then blasted using UniProt for confirmation (Table S8). The CRISPRCasFinder server detected seven CRISPR arrays candidates in the genome of the strain WSW3-B12^T. However, only one CRISPR array, located in plasmid 20, that are long enough to be consider CRISPR array. The CRISPRcasIndetifier and Uniprot also only detects Cas enzymes in the plasmid 20 upstream of the CRISPR array. There were eight Cas enzymes, Cas1 to 7 and an unknown Cas enzyme (Figure S4). Thus, the CRISPR/Cas system could be classified as an incomplete Class I type I-B that is missing the Cas8 enzyme (Makarova et al., 2020). Based on this analysis we confirmed that the strain WSW3-B12^T have the CRISPR-Cas system in the plasmid 20.

When we compared the genome of the strain WSW3-B12^T with that of other reference strains, only the genome of *Sediminitomix flava* DSM 28229^T contained two CRISPR arrays. The other reference strains did not have a CRISPR array. When we searched similar sequences from Uniprot, the highest sequence identity of Cas3, 5, 6, and 7 of the strain WSW3-B12^T were found from the Cas genes of *Sediminitomix flava* DSM 28229^T (Table S8). *Sediminitomix flava* DSM 28229^T contains only Cas 3, 5, 6, and 7 on its chromosome. Thus, it also has an incomplete Class I type I-B CRISPR/Cas system. It is very likely that the Cas enzymes (3, 5, 6, and 7) of strains WSW3-B12^T and *Sediminitomix flava* DSM 28229^T came from the same lineage. Based on their isolation sites, this is also probable because strain WSW3-B12^T was isolated from the West Sea, Korea and *Sediminitomix flava* DSM 28229^T was isolated from Okinawa, Japan: both locations are connected by a sea current.

The PHAST search tool identified two prophage regions, one of which is incomplete and the other is questionable. The high number of CRISPRs candidates per strain described as the prokaryotic defense mechanism against external attacks and the presence of bacteriophages in their genomes suggest that the strain is also prone to phage infections. The CRISPR-based technologies are also useful for either sequence-specific killing of pathogenic bacteria or for the removal of accessory genes (antimicrobial resistance, virulence, etc.) (Palacios Araya et al., 2021).

3.7.5 Plasmid functional analysis

The function of the chromosome and each plasmid were analyzed using the KEGG database. Based on this analysis we classified the pathways into three categories based on their locations: found exclusively in the chromosome (Figure S5A); found both in the chromosome and plasmids (Figure S5B); and found exclusively in the plasmids (Figure S5C). The existence of plasmids in addition to the chromosome could help the strain WSW3-B12^T to have more robust and highly expressed metabolic pathways. The addition of plasmids may increase the competitive edge of the strain WSW3-B12^T in terms of nutrition, growth, and defense in the marine environments. For example, the chromosome of the strain WSW3-B12^T lacked cysteine pathways but plasmids 3 and 11 carried genes for the cysteine pathway that may supplement cysteine metabolism (Figure S5C).

3.8 Description of *Chondrinema* gen. nov.

Chondrinema (Chon.dri.ne'ma. N.L. masc. n. Chondrus, a genus of red algae; Gr. neut. n. nema, a thread; N.L. neut. n. Chondrinema, a thread associated with the algal genus Chondrus).

This genus falls within the phylum *Bacteroidota*, class *Cytophagia*, and order *Cytophagales*. Cells are Gram-stain negative, oxidase and catalase-positive, and aerobic. The major fatty acids of the strain are iso-$C_{15:0}$ and $C_{16:1}$ ω5. The major respiratory quinone and polar lipid are menaquinone 7 (MK-7) and phosphatidylethanolamine.

3.9 Description of *Chondrinema litorale* sp. nov.

Chondrinema litorale (li. to. ra'le. L. neut. adj. *litorale*, of or belonging to the seashore)

Cells grow well on MA and produce light brown colonies with a diameter in a range from 325-420 μm. Cells of the strain are rod-shaped with a length 5-7 μm and width 0.46-0.54 μm.

Growth occurs at 15-30°C (optimum, 20-30°C), at pH 5.5-9.0 (optimum, pH 6.5-8.0), and with 1-7.0% NaCl (w/v) (optimum, 2-5%). The cell can degrade cellulose, inulin, and starch. Cells are positive for the hydrolysis of Tweens 20, 40, and 80. They are also positive for the activities of acid phosphatase, alkaline phosphatase, N-acetyl-β-glucosaminidase, cystine arylamidase, α-chymotrypsin, esterase (C4), esterase lipase (C8), α-galactosidase, β-galactosidase, α-glucosidase, β-glucosidase, leucine arylamidase, naphthol-AS-BI-phosphohydrolase, trypsin, and valine arylamidase. The cell can produce acid from L-arabinose, amidon (starch), arbutin, N-acetylglucosamine, D-cellobiose, gentibiose, D-galactose, glucose, D-lactose, methyl-αD-glucopyranoside, methyl-αD-mannopyranoside, D-maltose, D-melibiose, D-mannose, D-melezitose, D-raffinose, L-rhamnose, D-sucrose, D-trehalose, D-turanose, and D-xylose.

The type strain WSW3-B12^T (= KCTC 82707^T = GDMCC 1.3198^T) was isolated from a red algae genus (*Chondrus*). The size of the genome is 10.1 Mbp and the G+C content is 34.1%. The genome contains one circular chromosome and 28 plasmids.

Repositories: The GenBank/EMBL/DDBJ accession number for the 16S rRNA gene sequence of strain WSW3-B12^T is OP823709 and that for the whole genome sequence is GCA_026250525.

Data availability statement

The datasets presented in this study can be found in online repositories. The names of the repository/repositories and accession number(s) can be found below: GenBank, OP823709.1 and GCA_026250525.1.

Author contributions

NM and S-GK designed the study. NM performed the isolation and the morphological, physiological, and biochemical characterization. FA and Y-JL performed bioinformatic analyses with help from K-HK and HLH. NM, FA and S-GK wrote the manuscript. All authors contributed to the article and approved the submitted version.

Funding

The Korea Research Institute of Bioscience and Biotechnology (KRIBB) Research Initiative Program (KGM5232322) and a National Research Foundation of Korea (NRF) grant funded by the Korean government (MSIT) (No. NRF-2021M3H9A1030164) supported this research.

Acknowledgments

The authors thank Prof. Aharon Oren from the Hebrew University of Jerusalem for his help on the nomenclature of the novel strain.

Conflict of interest

The authors declare that the research was conducted in the absence of any commercial or financial relationships that could be construed as a potential conflict of interest.

Publisher's note

Supplementary material

The Supplementary Material for this article can be found online at: https://www.frontiersin.org/articles/10.3389/fmars.2023.1186809/full#supplementary-material

References

Abbott, D. W., and Boraston, A. B. (2008). Structural biology of pectin degradation by *Enterobacteriaceae*. *Microbiol. Mol. Biol. Rev.* 72, 301–316. doi: 10.1128/mmbr.00038-07

Abbott, D. W., Gilbert, H. J., and Boraston, A. B. (2010). The active site of oligogalacturonate lyase provides unique insights into cytoplasmic oligogalacturonate beta-elimination. *J. Biol. Chem.* 285, 39029–39038. doi: 10.1074/jbc.M110.153981

Alcock, B. P., Huynh, W., Chalil, R., Smith, K. W., Raphenya, A. R., Wlodarski, M. A., et al. (2022). CARD 2023: expanded curation, support for machine learning, and resistome prediction at the comprehensive antibiotic resistance database. *Nucleic Acids Res.* 6:51, D690–D699. doi: 10.1093/nar/gkac920

Amrina, R. A., Furusawa, G., and Lau, N.-S. (2021). *Saccharobesus litoralis* gen. nov., sp. nov., a novel alginate-degrading bacterium isolated from the surface of intertidal algal turf. *Int. J. Syst. Evol. Microbiol.* 71, 5087. doi: 10.1099/ijsem.0.005087

Arndt, D., Grant, J. R., Marcu, A., Sajed, T., Pon, A., Liang, Y., et al. (2016). PHASTER: a better, faster version of the PHAST phage search tool. *Nucleic Acids Res.* 44, W16–W21. doi: 10.1093/nar/gkw387

Asharaf, S., Chakraborty, K., and Chakraborty, R. D. (2022). Seaweed-associated heterotrophic bacteria: are they future novel sources of antimicrobial agents against drug-resistant pathogens? *Arch. Microbiol.* 204, 232. doi: 10.1007/s00203-022-02835-8

Asnicar, F., Thomas, A. M., Beghini, F., Mengoni, C., Manara, S., Manghi, P., et al. (2020). Precise phylogenetic analysis of microbial isolates and genomes from metagenomes using PhyloPhlAn 3.0. *Nat. Commun.* 11, 2500. doi: 10.1038/s41467-020-16366-7

Auch, A. F., Von Jan, M., Klenk, H. P., and Göker, M. (2010). Digital DNA-DNA hybridization for microbial species delineation by means of genome-to-genome sequence comparison. *Stand Genomic Sci.* 2, 117–134. doi: 10.4056/sigs.531120

Barbosa, J., Caetano, T., and Mendo, S. (2015). Class I and class II lanthipeptides produced by *Bacillus* spp. *J. Nat. Prod.* 78, 2850–2866. doi: 10.1021/np500424y

Barco, R. A., Garrity, G. M., Scott, J. J., Amend, J. P., Nealson, K. H., and Emerson, D. (2020). A genus definition for bacteria and archaea based on a standard genome relatedness index. *mBio.* 11, e02475–e02419. doi: 10.1128/mBio.02475-19

Beam, J. P., George, S., Record, N. R., Countway, P. D., Johnston, D. T., Girguis, P. R., et al. (2020). Mud, microbes, and macrofauna: seasonal dynamics of the iron biogeochemical cycle in an intertidal mudflat. *Front. Mar. Sci.* 7. doi: 10.3389/fmars.2020.562617

Blin, K., Shaw, S., Steinke, K., Villebro, R., Ziemert, N., Lee, S. Y., et al. (2019). antiSMASH 5.0: updates to the secondary metabolite genome mining pipeline. *Nucleic Acids Res.* 47, W81–W87. doi: 10.1093/nar/gkz310

Bolger, A. M., Lohse, M., and Usadel, B. (2014). *Trimmomatic*: a flexible trimmer for illumina sequence data. *Bioinformatics.* 30, 2114–2120. doi: 10.1093/bioinformatics/btu170

Bowman, J. P. (2000). Description of cellulophaga algicola sp. nov., isolated from the surfaces of Antarctic algae, and reclassification of *Cytophaga uliginosa* (ZoBell and upham 1944) reichenbach 1989 as *Cellulophaga uliginosa* comb. nov. *Int. J. Syst. Evol. Microbiol.* 50, 1861–1868. doi: 10.1099/00207713-50-5-1861

Cazares, A., Moore, M. P., Hall, J. P. J., Wright, L. L., Grimes, M., Emond-Rhéault, J. G., et al. (2020). A megaplasmid family driving dissemination of multidrug resistance in *Pseudomonas*. *Nat. Commun.* 11, 1370. doi: 10.1038/s41467-020-15081-7

Chen, Y., Jiang, Y., Huang, H., Mou, L., Ru, J., Zhao, J., et al. (2018). Long-term and high-concentration heavy-metal contamination strongly influences the microbiome and functional genes in yellow river sediments. *Sci. Total Environ.* 637, 1400–1412. doi: 10.1016/j.scitotenv.2018.05.109

Cheng, H., Wu, Y. H., Huo, Y. Y., Zhou, P., Liu, Q., Wang, C. S., et al. (2017). Complete genome sequence of *Altererythrobacter dongtanensis* KCTC 22672^{T}, isolated from a tidal flat. *Mar. Genomics* 34, 11–14. doi: 10.1016/j.margen.2017.02.003

Collmer, A., and Bateman, D. F. (1981). Impaired induction and self-catabolite repression of extracellular pectate lyase in *Erwinia chrysanthemi* mutants deficient in oligogalacturonide lyase. *Proc. Natl. Acad. Sci. U S A.* 78, 3920–3924. doi: 10.1073/pnas.78.6.3920

Couvin, D., Bernheim, A., Toffano-Nioche, C., Touchon, M., Michalik, J., Néron, B., et al. (2018). CRISPRCasFinder, an update of CRISRFinder, includes a portable version, enhanced performance and integrates search for cas proteins. *Nucleic Acids Res.* 46, W246–W251. doi: 10.1093/nar/gky425

Dell'Anno, F., Rastelli, E., Tangherlini, M., Corinaldesi, C., Sansone, C., Brunet, C., et al. (2021). Highly contaminated marine sediments can host rare bacterial taxa potentially useful for bioremediation. *Front. Microbiolo* 12. doi: 10.3389/fmicb.2021.584850

Deshavath, N. N., Mukherjee, G., Goud, V. V., Veeranki, V. D., and Sastri, C. V. (2020). Pitfalls in the 3, 5-dinitrosalicylic acid (DNS) assay for the reducing sugars: interference of furfural and 5-hydroxymethylfurfural. *Int. J. Biol. Macromol.* 156, 180–185. doi: 10.1016/j.ijbiomac.2020.04.045

Dong, Q., Ruan, L., and Shi, H. (2017). Genome sequence of a high agarase-producing strain *Flammeovirga* sp. SJP92. *Stand Genom Sci.* 12, 1–6. doi: 10.1186/s40793-017-0221-y

Duarte, C. M., Dennison, W. C., Orth, R. J., and Carruthers, T. J. (2008). The charisma of coastal ecosystems: addressing the imbalance. *Estuaries coasts.* 31, 233–238. doi: 10.1007/s12237-008-9038-7

Felsenstein, J. (1981). Evolutionary trees from DNA sequences: a maximum likelihood approach. *J. Mol. Evol.* 17, 368–376. doi: 10.1007/bf01734359

Feng, Y., Wang, Y., Zhu, B., Gao, G. F., Guo, Y., and Hu, Y. (2021a). Metagenome-assembled genomes and gene catalog from the chicken gut microbiome aid in deciphering antibiotic resistomes. *Commun. Biol.* 4, 1305. doi: 10.1038/s42003-021-02827-2

Feng, Z., Zhang, Z., Liu, Y., Gu, J., Cheng, Y., Hu, W., et al. (2021b). The second chromosome promotes the adaptation of the genus *Flammeovirga* to complex environments. *Microbiol. Spectr.* 9, e0098021. doi: 10.1128/Spectrum.00980-21

Fernández-Gómez, B., Richter, M., Schüler, M., Pinhassi, J., Acinas, S. G., González, J. M., et al. (2013). Ecology of marine *Bacteroidetes*: a comparative genomics approach. *ISME J.* 7, 1026–1037. doi: 10.1038/ismej.2012.169

Galperin, M. Y., Wolf, Y. I., Makarova, K. S., Vera Alvarez, R., Landsman, D., and Koonin, E. V. (2021). COG database update: focus on microbial diversity, model organisms, and widespread pathogens. *Nucleic Acids Res.* 49, D274–D281. doi: 10.1093/nar/gkaa1018

Gao, B., Jin, M., Li, L., Qu, W., and Zeng, R. (2017). Genome sequencing reveals the complex polysaccharide-degrading ability of novel deep-sea bacterium *Flammeovirga pacifica* WPAGA1. *Front. Microbiol.* 8. doi: 10.3389/fmicb.2017.00600

Goldberg, S. R., Correa, H., Haltli, B. A., and Kerr, R. G. (2020). *Fulvivirga aurantia* sp. nov. and *Xanthovirga aplysinae* gen. nov., sp. nov., marine bacteria isolated from the sponge *Aplysina fistularis*, and emended description of the genus *Fulvivirga*. *Int. J. Syst. Evol. Microbiol.* 70, 2766–2781. doi: 10.1099/ijsem.0.004108

Graham, E. D., Heidelberg, J. F., and Tully, B. J. (2018). Potential for primary productivity in a globally-distributed bacterial phototroph. *ISME J.* 12, 1861–1866. doi: 10.1038/s41396-018-0091-3

Hantke, K. (2003). Is the bacterial ferrous iron transporter FeoB a living fossil? *Trends Microbiol.* 11, 192–195. doi: 10.1016/s0966-842x(03)00100-8

Hehemann, J. H., Correc, G., Thomas, F., Bernard, T., Barbeyron, T., Jam, M., et al. (2012). Biochemical and structural characterization of the complex agarolytic enzyme system from the marine bacterium *Zobellia galactanivorans*. *J. Biol. Chem.* 287, 30571–30584. doi: 10.1074/jbc.M112.377184

Hochmuth, T., and Piel, J. (2009). Polyketide synthases of bacterial symbionts in sponges–evolution-based applications in natural products research. *Phytochemistry.* 70, 1841–1849. doi: 10.1016/j.phytochem.2009.04.010

Hosoya, S., and Yokota, A. (2007). Reclassification of *Flexibacter aggregans* (Lewin 1969) leadbetter 1974 as a later heterotypic synonym of *Flexithrix dorotheae* lewin 1970. *Int. J. Syst. Evol. Microbiol.* 57, 1086–1088. doi: 10.1099/ijs.0.64798-0

Jeon, D., Jiang, L., Peng, Y., Seo, J., Li, Z., Park, S. H., et al. (2022). *Sphingomonas cannabina* sp. nov., isolated from cannabis sativa l. 'Cheungsam'. *Int. J. Syst. Evol. Microbiol.* 72, 005566. doi: 10.1099/ijsem.0.005566

Jeong, Y. S., Kang, W., Sung, H., Lee, J. Y., Yun, J. H., Shin, N. R., et al. (2020). *Flammeovirga pectinis* sp. nov., isolated from the gut of the Korean scallop, *Patinopecten yessoensis*. *Int. J. Syst. Evol. Microbiol.* 70, 499–504. doi: 10.1099/ijsem.0.003783

Jorgensen, J. H., and Turnidge, J. D. (2015). "Susceptibility test methods: dilution and disk diffusion methods," in *Manual of clinical microbiology*. Eds. J. H.Jorgensen, K. C. Carroll, G. Funke, M. A. Pfaller, M. L. Landry, S. S. Richter and D. W. Warnock (New York: NY: Wiley), 1253–1273.

Juhmani, A. S., Vezzi, A., Wahsha, M., Buosi, A., Pascale, F., Schiavon, R., et al. (2020). Diversity and dynamics of seaweed associated microbial communities inhabiting the lagoon of venice. *Microorganisms.* 8, 1657. doi: 10.3390/microorganisms8111657

Karthick, P., and Mohanraju, R. (2018). Antimicrobial potential of epiphytic bacteria associated with seaweeds of little andaman, India. *Front. Microbiol.* 9. doi: 10.3389/fmicb.2018.00611

Khan, S. T., Nakagawa, Y., and Harayama, S. (2007). *Sediminitomix flava* gen. nov., sp. nov., of the phylum *Bacteroidetes*, isolated from marine sediment. *Int. J. Syst. Evol. Microbiol.* 57, 1689–1693. doi: 10.1099/ijs.0.64854-0

Kim, J., Cha, I. T., Lee, K. E., Son, Y. K., Yu, J., and Seol, D. (2022). Characteristics and adaptability of *Flavobacterium panici* BSSL-CR3 in tidal flat revealed by comparative genomic and enzymatic analysis. *Arch. Microbiol.* 205, 22. doi: 10.1007/s00203-022-03359-x

Kizhakkekalam, V. K., and Chakraborty, K. (2021). Seaweed-associated heterotrophic bacteria: new paradigm of prospective anti-infective and anticancer agents. *Arch. Microbiol.* 203, 1241–1250. doi: 10.1007/s00203-020-02106-4

Komagata, K., and Suzuki, K. (1988). Lipid and cell-wall analysis in bacterial systematics. *Methods Microbiol.* 19, 161–207. doi: 10.1016/S0580-9517(08)70410-0

Konaté, M. M., Plata, G., Park, J., Usmanova, D. R., Wang, H., and Vitkup, D. (2019). Molecular function limits divergent protein evolution on planetary timescales. *Elife.* 8, e39705. doi: 10.7554/eLife.39705

Koren, S., Walenz, B. P., Berlin, K., Miller, J. R., Bergman, N. H., and Phillippy, A. M. (2017). Canu: scalable and accurate long-read assembly via adaptive k-mer weighting and repeat separation. *Genome Res.* 27, 722–736. doi: 10.1101/gr.215087.116

Kristyanto, S., Kim, K. R., Jung, J., Kim, H. M., Kim, K., and Jeon, C. O. (2022). *Tenacibaculum aquimarinum* sp. nov., isolated from a marine alga and seawater. *Int. J. Syst. Evol. Microbiol.* 72, 005477. doi: 10.1099/ijsem.0.005477

Kumar, S., Stecher, G., Li, M., Knyaz, C., and Tamura, K. (2018). MEGA X: molecular evolutionary genetics analysis across computing platforms. *Mol. Biol. Evol.* 35, 1547–1549. doi: 10.1093/molbev/msy096

Lau, C. K., Krewulak, K. D., and Vogel, H. J. (2016). Bacterial ferrous iron transport: the feo system. *FEMS Microbiol. Rev.* 40, 273–298. doi: 10.1093/femsre/fuv049

Leadbetter, E. (1974). *Order II. cytophagales nomen novum. bergey's manual of determinative bacteriology. 8th ed* Vol. 99 (Baltimore: The Williams & Wilkins Co.).

Lee, H., Heo, Y. M., Kwon, S. L., Yoo, Y., Kim, D., Lee, J., et al. (2021). Environmental drivers affecting the bacterial community of intertidal sediments in the yellow Sea. *Sci. Total Environ.* 755, 142726. doi: 10.1016/j.scitotenv.2020.142726

Lee, H., Lee, D. W., Kwon, S. L., Heo, Y. M., Jang, S., Kwon, B. O., et al. (2019). Importance of functional diversity in assessing the recovery of the microbial community after the hebei spirit oil spill in Korea. *Environ. Int.* 128, 89–94. doi: 10.1016/j.envint.2019.04.039

Lee, S. J., Park, M., Ogandaga M, C. A., Park, S. K., Kim, H., Kim, Y., et al. (2013). A study on the growth and disease of *Chondrus ocellatus* in Korea. *J. fish Pathol.* 26, 265–274. doi: 10.7847/jfp.2013.26.3.265

Li, W., Wang, L., Li, X., Zheng, X., Cohen, M. F., and Liu, Y. X. (2022). Sequence-based functional metagenomics reveals novel natural diversity of functioning *CopA* in

environmental microbiomes. *Genom Proteom Bioinf.* S1672-0229, 00101–00112. doi: 10.1016/j.gpb.2022.08.006

Lin, Y., Yuan, J., Kolmogorov, M., Shen, M. W., Chaisson, M., and Pevzner, P. A. (2016). Assembly of long error-prone reads using de bruijn graphs. *Proc. Natl. Acad. Sci. U S A.* 113, E8396–e8405. doi: 10.1073/pnas.1604560113

Linhardt, R., Galliher, P., and Cooney, C. (1987). Polysaccharide lyases. *Appl. Biochem. Biotechnol.* 12, 135–176.

Lobban, C. S., and Harrison, P. J. (1994). *Seaweed ecology and physiology* (New York: Cambridge University Press). doi: 10.1007/BF02798420

Ludwig, W., Euzéby, J., and Whitman, W. B. (2010). "Road map of the phyla bacteroidetes, spirochaetes, tenericutes (Mollicutes), acidobacteria, fibrobacteres, fusobacteria, dictyoglomi, gemmatimonadetes, lentisphaerae, verrucomicrobia, chlamydiae, and planctomycetes," in *Bergey's manual® of systematic bacteriology* (New York: Springer), 1–19.

Lv, X., Ma, B., Yu, J., Chang, S. X., Xu, J., Li, Y., et al. (2016). Bacterial community structure and function shift along a successional series of tidal flats in the yellow river delta. *Sci. Rep.* 6, 36550. doi: 10.1038/srep36550

Makarova, K. S., Wolf, Y. I., Iranzo, J., Shmakov, S. A., Alkhnbashi, O. S., Brouns, S. J. J., et al. (2020). Evolutionary classification of CRISPR–cas systems: a burst of class 2 and derived variants. *Nat. Rev. Microbiol.* 18, 67–83. doi: 10.1038/s41579-019-0299-x

Mann, A. J., Hahnke, R. L., Huang, S., Werner, J., Xing, P., Barbeyron, T., et al. (2013). The genome of the alga-associated marine *flavobacterium Formosa agariphila* KMM 3901T reveals a broad potential for degradation of algal polysaccharides. *Appl. Environ. Microbiol.* 79, 6813–6822. doi: 10.1128/aem.01937-13

Mckee, L. S., La Rosa, S. L., Westereng, B., Eijsink, V. G., Pope, P. B., and Larsbrink, J. (2021). Polysaccharide degradation by the *Bacteroidetes*: mechanisms and nomenclature. *Environ. Microbiol. Rep.* 13, 559–581. doi: 10.1111/1758-2229.12980

Meier-Kolthoff, J. P., Auch, A. F., Klenk, H. P., and Göker, M. (2013). Genome sequence-based species delimitation with confidence intervals and improved distance functions. *BMC Bioinf.* 14, 60. doi: 10.1186/1471-2105-14-60

Menaa, F., Wijesinghe, P., Thiripuranathar, G., Uzair, B., Iqbal, H., Khan, B. A., et al. (2020). Ecological and industrial implications of dynamic seaweed-associated microbiota interactions. *Mar. Drugs* 18, 641. doi: 10.3390/md18120641

Muhammad, N., Le Han, H., Lee, Y. J., Ko, J., Nguyen, T. T. H., and Kim, S. G. (2022a). Flavobacterium litorale sp. nov., isolated from red alga. *Int. J. Syst. Evol. Microbiol.* 72, 005458. doi: 10.1099/ijsem.0.005458

Muhammad, N., Nguyen, T. T. H., Lee, Y. J., Ko, J., Avila, F., and Kim, S. G. (2022b). Vibrio ostreae sp. nov., a novel gut bacterium isolated from a yellow sea oyster. *Int. J. Syst. Evol. Microbiol.* 72, 005586. doi: 10.1099/ijsem.0.005586

Padilha, V. A., Alkhnbashi, O. S., Shah, S. A., De Carvalho, A., and Backofen, R. (2020). CRISPRcasIdentifier: machine learning for accurate identification and classification of CRISPR-cas systems. *Gigascience.* 9, giaa062. doi: 10.1093/gigascience/giaa062

Palacios Araya, D., Palmer, K. L., and Duerkop, B. A. (2021). CRISPR-based antimicrobials to obstruct antibiotic-resistant and pathogenic bacteria. *PloS Pathog.* 17, e1009672. doi: 10.1371/journal.ppat.1009672

Park, M. J., Kim, Y. J., Park, M., Yu, J., Namirimu, T., Roh, Y. R., et al. (2022). Establishment of genome based criteria for cclassification of the family *Desulfovibrionaceae* and proposal of two novel genera, *Alkalidesulfovibrio* gen. nov. and *Salidesulfovibrio* gen. nov. *Front. Microbiol.* 13. doi: 10.3389/fmicb.2022.738205

Parks, D. H., Imelfort, M., Skennerton, C. T., Hugenholtz, P., and Tyson, G. W. (2015). CheckM: assessing the quality of microbial genomes recovered from isolates, single cells, and metagenomes. *Genome Res.* 25, 1043–1055. doi: 10.1101/gr.186072.114

Paster, B. J., Dewhirst, F. E., Olsen, I., and Fraser, G. J. (1994). Phylogeny of *Bacteroides*, prevotella, and *Porphyromonas* spp. and related bacteria. *J. Bacteriol.* 176, 725–732. doi: 10.1128/jb.176.3.725-732.1994

Pheng, S., Han, H. L., Park, D. S., Chung, C. H., and Kim, S. G. (2020). *Lactococcus kimchii* sp. nov., a new lactic acid bacterium isolated from kimchi. *Int. J. Syst. Evol. Microbiol.* 70, 505–510. doi: 10.1099/ijsem.0.003782

Phillips, I. (1993). Cowan and steel's manual for the identification of medical bacteria. *J. Clin. Pathol.* 46, 975. doi: 10.1017/CBO9780511527104

Qin, Q. L., Xie, B. B., Zhang, X. Y., Chen, X. L., Zhou, B. C., Zhou, J., et al. (2014). A proposed genus boundary for the prokaryotes based on genomic insights. *J. Bacteriol.* 196, 2210–2215. doi: 10.1128/jb.01688-14

Reichenbach, H. (1992). "The order cytophagales," in *The prokaryotes: a handbook on the biology of bacteria: ecophysiology, isolation, identification, applications*. Eds. A. Balows, H. G. Trüper, M. Dworkin, K. H. Schleifer and W. Harder (New York: Springer), 3631–3675.

Saitou, N., and Nei, M. (1987). The neighbor-joining method: a new method for reconstructing phylogenetic trees. *Mol. Biol. Evol.* 4, 406–425. doi: 10.1093/oxfordjournals.molbev.a040454

Sasser, M. (1990). "Identification of bacteria by gas chromatography of cellular fatty acids," in *MIDI technical note 101* (Newark: DE: MIDI Inc).

Saw, J. H. W., Yuryev, A., Kanbe, M., Hou, S., Young, A. G., Aizawa, S., et al. (2012). Complete genome sequencing and analysis of *Saprospira grandis* str. lewin, a predatory marine bacterium. *Stand Genom Sci.* 6, 84–93. doi: 10.4056/sigs.2445005

Schmartz, G. P., Hartung, A., Hirsch, P., Kern, F., Fehlmann, T., Müller, R., et al. (2022). PLSDB: advancing a comprehensive database of bacterial plasmids. *Nucleic Acids Res.* 50, D273–D278. doi: 10.1093/nar/gkab1111

Seemann, T. (2014). Prokka: rapid prokaryotic genome annotation. *Bioinformatics.* 30, 2068–2069. doi: 10.1093/bioinformatics/btu153

Singh, R. P., and Reddy, C. R. (2015). Seaweed-microbial interactions: key functions of seaweed-associated bacteria. *FEMS Microbiol. Ecol.* 88, 213–230. doi: 10.1111/1574-6941.12297

Srisukchayakul, P., Suwanachart, C., Sangnoi, Y., Kanjana-Opas, A., Hosoya, S., Yokota, A., et al. (2007). *Rapidithrix thailandica* gen. nov., sp. nov., a marine gliding bacterium isolated from samples collected from the andaman sea, along the southern coastline of Thailand. *Int. J. Syst. Evol. Microbiol.* 57, 2275–2279. doi: 10.1099/ijs.0.65087-0

The UniProt Consortium (2023). UniProt: the universal protein knowledgebase in 2023. *Nucleic Acids Res.* 51, D523–D531. doi: 10.1093/nar/gkac1052

Ueno, A., Tamazawa, S., Tamamura, S., Murakami, T., Kiyama, T., Inomata, H., et al. (2021). *Desulfovibrio subterraneus* sp. nov., a mesophilic sulfate-reducing deltaproteobacterium isolated from a deep siliceous mudstone formation. *Int. J. Syst. Evol. Microbiol.* 71, 004683. doi: 10.1099/ijsem.0.004683

Wang, H., Li, J., Zheng, T., Hill, R. T., and Hu, X. (2013). *Imperialibacter roseus* gen. nov., sp. nov., a novel bacterium of the family *Flammeovirgaceae* isolated from permian groundwater. *Int. J. Syst. Evol. Microbiol.* 63, 4136–4140. doi: 10.1099/ijs.0.052662-0

Wang, R., Zhang, W., Ding, W., Liang, Z., Long, L., Wong, W. C., et al. (2021). Profiling signal transduction in global marine biofilms. *Front. Microbiol.* 12. doi: 10.3389/fmicb.2021.768926

Wilms, R., Sass, H., Köpke, B., Köster, J., Cypionka, H., and Engelen, B. (2006). Specific bacterial, archaeal, and eukaryotic communities in tidal-flat sediments along a vertical profile of several meters. *Appl. Environ. Microbiol.* 72, 2756–2764. doi: 10.1128/aem.72.4.2756-2764.2006

Yoon, J., Adachi, K., Park, S., Kasai, H., and Yokota, A. (2011). *Aureibacter tunicatorum* gen. nov., sp. nov., a marine bacterium isolated from a coral reef sea squirt, and description of *Flammeovirgaceae* fam. nov. *Int. J. Syst. Evol. Microbiol.* 61, 2342–2347. doi: 10.1099/ijs.0.027573-0

Yoon, S. H., Ha, S. M., Kwon, S., Lim, J., Kim, Y., Seo, H., et al. (2017a). Introducing EzBioCloud: a taxonomically united database of 16S rRNA gene sequences and whole-genome assemblies. *Int. J. Syst. Evol. Microbiol.* 67, 1613–1617. doi: 10.1099/ijsem.0.001755

Yoon, S. H., Ha, S. M., Lim, J., Kwon, S., and Chun, J. (2017b). A large-scale evaluation of algorithms to calculate average nucleotide identity. *Antonie Van Leeuwenhoek.* 110, 1281–1286. doi: 10.1007/s10482-017-0844-4

Yoon, J., Oku, N., Park, S., Katsuta, A., and Kasai, H. (2012). *Tunicatimonas pelagia* gen. nov., sp. nov., a novel representative of the family *Flammeovirgaceae* isolated from a sea anemone by the differential growth screening method. *Antonie Van Leeuwenhoek.* 101, 133–140. doi: 10.1007/s10482-011-9626-6

Zhang, Y., Rodionov, D. A., Gelfand, M. S., and Gladyshev, V. N. (2009). Comparative genomic analyses of nickel, cobalt and vitamin B12 utilization. *BMC Genomics* 10, 78. doi: 10.1186/1471-2164-10-78

Zhang, H., Yohe, T., Huang, L., Entwistle, S., Wu, P., Yang, Z., et al. (2018). dbCAN2: a meta server for automated carbohydrate-active enzyme annotation. *Nucleic Acids Res.* 46, W95–W101. doi: 10.1093/nar/gky418

Zhong, Z., Toukdarian, A., Helinski, D., Knauf., V., Sykes, S., Wilkinson, J. E., et al. (2001). Sequence analysis of a 101-kilobase plasmid required for agar degradation by a *Microscilla* isolate. *Appl. Environ. Microbiol.* 67, 5771–5779. doi: 10.1186/1471-2164-10-78

ZoBell, C. E. (1941). Studies on marine bacteria, I: the cultural requirements of heterotrophic aerobes. *J. Mar. Res.* 4, 42–75.

frontiers | Frontiers in Marine Science

TYPE Original Research
PUBLISHED 30 June 2023
DOI 10.3389/fmars.2023.1213051

OPEN ACCESS

EDITED BY
Xue-Wei Xu,
Ministry of Natural Resources, China

REVIEWED BY
Heng-Lin Cui,
Jiangsu University, China
Guohong Liu,
Fujian Academy of Agricultural Sciences, China

*CORRESPONDENCE
Da-Shuai Mu
dashuai.mu@sdu.edu.cn

RECEIVED 27 April 2023
ACCEPTED 14 June 2023
PUBLISHED 30 June 2023

CITATION
Yu W-X, Liang Q-Y, Du Z-J and Mu D-S (2023) Characterization of *Plebeiobacterium marinum* gen. nov., sp. nov. and *Plebeiobacterium sediminum* sp. nov., revealing the potential nitrogen fixation capacity of the order *Marinilabiliales*.
Front. Mar. Sci. 10:1213051.
doi: 10.3389/fmars.2023.1213051

Characterization of *Plebeiobacterium marinum* gen. nov., sp. nov. and *Plebeiobacterium sediminum* sp. nov., revealing the potential nitrogen fixation capacity of the order *Marinilabiliales*

Wen-Xing Yu[1], Qi-Yun Liang[1], Zong-Jun Du[1,2,3] and Da-Shuai Mu[1,2,3]*

[1]Marine College, Shandong University, Weihai, China, [2]State Key Laboratory of Microbial Technology, Shandong University, Qingdao, China, [3]Weihai Research Institute of Industrial Technology of Shandong University, Weihai, China

Biological nitrogen fixation plays a crucial role in the marine nitrogen cycle, impacting global marine productivity and related carbon fluxes. The strains were analyzed by gene annotation, growth conditions and phylogenetic analysis of 16S rRNA gene sequences.These two strains were isolated from the coastal sediment at Xiaoshi Island in Weihai, China. The strains were analyzed by gene annotation, growth conditions and phylogenetic analysis of 16S rRNA gene sequences. It was revealed that strains D04^T and AAT^T contain a set of *nif* gene clusters responsible for nitrogen fixation. Cell are yellow-colored, Gram-stain-negative, facultatively anaerobic, and rod-shaped bacteria. The optimal growth conditions for strain D04^T were found to be at 33 °C, pH 7.0, and in 2% (w/v) NaCl, while strain AAT^T prefers growth conditions at 33 °C, pH 6.5, and in 3% (w/v) NaCl. The highest similarity of strains D04^T and AAT^T was to *Saccharicrinis fermentans* NBRC 15936^T, with a similarity of 94.1% and 94.8%, respectively. The 16S rRNA gene sequence similarity between the two strains was 96.6%. These novel strains were found to represent new taxa of the *Marinilabiliaceae* family, and we propose the names *Plebeiobacterium marinum* gen. nov., sp. nov. and *Plebeiobacterium sediminum* sp. nov. with type strains D04^T (MCCC 1H00493^T = KCTC 92026^T) and AAT^T (MCCC 1H00485^T = KCTC 92028^T), respectively. In this study, nitrogen fixation genes were predicted for 53 strains from the whole order *Marinilabiliales* and it was found that nitrogen fixation gene clusters were present in 26 strains. These gene clusters were found in every family in the order, highlighting that the presence of nitrogen-fixing gene clusters in the order is common. Nitrogen-fixing bacteria in sediments play an important role in various biogeochemical cycles. Thus, understanding the oceanic nitrogen cycle can provide insights into the energy flow of marine systems.

KEYWORDS

***Plebeiobacterium*, analysis of genome, metabolic pathways, nitrogen fixation, polyphasic taxonomy**

1 Introduction

Nitrogen is an essential element for all living organisms. Molecular nitrogen (N_2) comprises 78% of the Earth's atmosphere and is also abundant in the ocean water column. However, N_2 is highly stable and cannot be easily converted into a form that most organisms can utilize. The process of converting N_2 into bioavailable NH_3 is known as biological nitrogen fixation. (Weisburg et al., 1991; Chakraborty et al., 2021). In natural ecosystems, the supply of nitrogen to organisms plays a critical role in regulating primary productivity (Isobe and Ohte, 2014). It has been proved that microorganisms can mediate many N cycle processes, and microbial communities significantly contribute to N cycle processes (Isobe and Ohte, 2014). Biological nitrogen fixation is a critical aspect of the marine nitrogen cycle and plays a significant role in regulating global marine productivity and carbon flux (Sohm et al., 2011; Halm et al., 2012). It was long believed that the majority of nitrogen fixation in the ocean was carried out by cyanobacteria in surface waters. However, recent research has shown that nitrogen fixation also occurs in deeper waters, coastal regions, and even marine sediments, indicating that it is a widespread and significant phenomenon (Chakraborty et al., 2021; Luo et al., 2021). Similar to nitrogen-fixing microorganisms in terrestrial environments, a wide range of prokaryotes are capable of fixing nitrogen in the ocean. Recent studies have shown that nitrogen fixation can occur in marine sediments around seaweed communities, where heterotrophic sulfate-reducing bacteria play a significant role. These bacteria can fix nitrogen and provide bioavailable nitrogen directly to the seaweed, promoting its growth and productivity (Lehnen et al., 2016; Mohr et al., 2021). Nitrogen-fixing bacteria have been found to play a crucial role in nitrogen cycling in deep-sea sediments, with several groups identified, including *Acidobacteria*, *Firmicutes*, *Nitrospirae*, *Gammaproteobacteria*, and *Deltaproteobacteria*. These groups of bacteria are characterized by their ability to use a range of electron acceptors, including oxygen, nitrate, iron, sulfur, sulfate, and organic compounds, which allow them to couple nitrogen fixation with multiple biogeochemical cycles. This enables them to make important contributions to other elemental cycles, such as those of carbon, sulfur, and iron in deep-sea sediments (Kapili et al., 2020). Heterotrophic nitrogen-fixing bacteria have been found to be present in marine sediments, including aerobic, microaerobic, facultative, and specific anaerobic bacteria. The presence of these bacteria, such as *Azotobacter*, *Clostridium*, *Enterobacter*, *Desulfobacter*, *Desulfovibrio*, and *Klebsiella*, is critical for nitrogen cycling in marine ecosystems (Herbert, 1999).

Nitrogen plays a central role in marine biogeochemistry as a limiting element in biological production (Kuypers et al., 2018). Biological nitrogen fixation is the main process controlling the nitrogen supply of marine organisms (Zehr, 2011). Microbes use nitrogenase to catalyze biological nitrogen fixation, and nitrogenase is highly conserved during evolution. Nitrogen-fixing bacteria are divided into five clusters by constructing a gene phylogenetic tree (Zehr et al., 2003; Raymond et al., 2004). Three clusters (I, II, and III) contain genes encoding nitrogenase, while clusters IV and V are mainly homologous genes of nitrogenase genes and do not participate in nitrogen fixation (Gaby and Buckley, 2011). Cluster IV and V genes have various functions, including some genes involved in the biosynthesis of photopigments and some electron transfer reactions. (Gaby and Buckley, 2011). Most known *nifH* sequences belong to cluster I. Cluster I is composed entirely of *nifH* genes from the bacteria's regular FeMo nitrogen-fixing enzyme (*nifH*). The cluster contains genes from all *Cyanobacteria*, most *Proteobacteria*, and certain *Firmicutes* and *Actinobacteria*. Cluster II contains sequences of certain methanogenic *archaea* that belong mainly to alternative FeV (*vnfH*) and FeFe (*anfH*) nitrogen-fixing enzymes, with relatively few sequences. Cluster III consists mainly of sequences of anaerobic bacteria and archaea, including spirochetes, methanogens, acetogens, sulfate-reducing bacteria, green sulfur bacteria, and clostridia (Gaby and Buckley, 2011). These genes include the key gene *nifH*, encoding the dinitrogenase reductase; *nifD* and *nifK*, encoding the MoFe dinitrogenase; as well as *nifE*, *nifN*, and *nifB*, encoding the FeMo cofactor biosynthesis machinery. The *nifN* and *nifB* genes were fused into a single gene (*nifN*-B) and two genes encoding PII-like nitrogen regulatory proteins (Sayavedra et al., 2021). *nifA* is an essential transcriptional activator for *nif* genes (Sarkar and Reinhold-Hurek, 2014). *nifO* seems to be necessary for nitrogen fixation in the presence of nitrate (Gutierrez et al., 1997).

Nitrogen fixation enzymes are mainly composed of two metalloproteins, including diazotrope in the catalytic part and diazoreductase in the electron transport part. Molybdenum-dependent nitrogen fixation enzymes are mainly composed of *nifH* (diazoreductase subunit), *nifD*, and *nifK* (diazotrope subunit) (López-Torrejón et al., 2016). The *nifD* and *nifK* genes encode the α- and β-subunits of diazoxide synthase, respectively, forming an $\alpha_2\beta_2$-tetramer, the *nifE* and *nifN* genes encode another $\alpha_2\beta_2$-tetramer necessary for metal cofactors, and *nifB* plays a major role in the biosynthesis of Fe and S donors for metal cofactors. The above six *nif* genes are used to define *nif* (*nif*HDKENB) (Pi et al., 2022).

Previous studies have primarily focused on nitrogen-fixing bacteria within the *Proteobacteria* phylum, with little attention paid to the potential role of *Bacteroidetes*. However, recent research has shown that several families of *Bacteroidetes* have the potential for nitrogen fixation. Gene sequencing analysis has predicted that *Bacteroidetes* families such as *Marinilabiliaceae* (*Geofilum*, *Saccharicrinis*, and *Alkiflexus*), *Porphyromonadaceae* (*Paludibacter* and *Dysgonomonas*), and *Bacteroidaceae* have nitrogen fixation potential (Inoue et al., 2015). Additionally, another study has also identified members of the *Prolixibactaceae* family, including *Maribellus*, *Mangrovibacterium*, and *Draconibacillus*, as *Bacteroidetes* with the potential for nitrogen fixation (Huang et al., 2020). *Marinilabiliaceae*, *Prolixibacteraceae*, and *Marinifilaceae* were transferred from the *Bacteroides* order to

Abbreviations: DSM, German Collection of Microorganisms and Cell Cultures GmbH; MCCC, Marine Culture Collection of China; KCTC, Korean Collection for Type Cultures; dDDH, digital DNA-DNA hybridization; AAI, average amino acid identity; MIDI, Microbial Identification System; TLC, thin-layer chromatography; MEGA, Molecular Evolutionary Genetics Analysis; HPLC, High Performance Liquid Chromatography.

Marinilabiliales. (Wu et al., 2016). The current study of nitrogen-fixing enzymes is performed through the *nifH* gene (Zehr et al., 2003). This study annotates the obtained genome and analyzes the nitrogen fixation–related gene clusters of this order. The results of this study help to fill the gap in our knowledge of the nitrogen-fixing potential of this microbial group, and provide a theoretical basis for further research on nitrogen-fixing microbial communities in marine sediments.

As of the time of writing, the family *Marinilabiliaceae* is composed of twelve genera with a validly published and correct name[1]. These genera include *Alkaliflexus*, *Alkalitalea*, *Anaerophaga*, *Breznakibacter*, *Carboxylicivirga*, *Geofilum*, *Labilibacter*, *Mangroviflexus*, *Marinilabilia*, *Natronoflexus*, *Saccharicrinis*, and *Thermophagus*. The family encompasses a total of twenty-two species. Apart from the strains *Alkaliflexus imshenetskii* (Zhilina et al., 2004), *Alkalitalea saponilacus* (Zhao and Chen, 2012), and *Natronoflexus pectinivorans* (Sorokin et al., 2011), isolated from lakes and *Anaerophaga thermohalophila* (Denger et al., 2002) isolated from oil, others come from marine environments. Bacterial cells of the family *Marinilabiliaceae* are facultatively anaerobic and Gram-stain-negative, with menaquinone-7 (MK-7) as the major respiratory quinone. In this study, two yellow-colored, Gram-stain-negative, facultatively aerobic, and rod-shaped bacterium; strains D04^T and AAT^T, were proposed as representing novel species belonging to the family *Marinilabiliaceae*.

2 Materials and methods

2.1 Sample collection, bacterial isolation, and preservation

A marine sediment sample was collected off the coast of Xiaoshi Island, Weihai, PR China (122°00′58′′ E, 37°31′36′′ N) and subjected to an enrichment culture technique as described by Mu (Mu et al., 2018). The sample was collected at a depth of approximately 10 cm and was kept cold and in the dark during transportation to the laboratory. Incubation was performed at 25°C for 8 months using a 350 ml sealed glass bottle. The bottle was shaken twice a day and kept sealed during the incubation. The sediment sample was serially diluted to 10^{-3} in sterilized seawater and 0.1 ml aliquots of each dilution were spread on to the surface of modified marine agar (MA) 2216. The modified MA medium used for the characterization of strains contained the following components (g L^{-1}, pH 7.0): 5.0 tryptone, 1.0 yeast extract, 1.5 pyruvic acid sodium, and 2 ml vitamin mixture. The vitamin mixture contained the following components (mg L^{-1}): 5.0 thiamine, 5.0 riboflavin, 5.0 nicotinic acid, 5.0 D-Ca-pantothenate, 10.0 pyridoxine-HCl, 2.0 biotin, 2.0 folic acid, 0.1 cobalamin, 5.0 lipoic acid and 5.0 p-aminobenzoic acid. After incubation for 7 days at 33°C, colonies of the two strains were selected from the plate and re-streaked to obtain pure cultures. These strains were then cultivated on modified MA 2216 at 33°C for further physiological, biochemical, and chemical analyses. Pure cultures of the strains were preserved at −80°C in a sterile 1% (w/v) saline solution supplemented with 15% (v/v) glycerol.

2.2 Morphological, physiological, and biochemical analyses

The morphological and physiological features of strains D04^T and AAT^T were tested with cells grown on the modified MA at optimum growth conditions for 5 days. The experiment was repeated three times. Cell morphology and size were examined by light microscopy (E600; Nikon), transmission electron microscopy (JEM-1200, JEOL) and scanning electron microscopy (model Nova NanoSEM450; FEI). Gram reactions were carried out as described previously (CLSI, 2021). Gliding motility was examined in modified marine broth 2216 (MB; BD) supplemented with 0.3% agar as described previously (Bernardet et al., 2002). The growth temperature range was tested on the modified MA at various temperatures (4, 20, 25, 28, 30, 33, 37, 40, 45, and 50°C). To test for the pH range suitable for growth, bacterial strains were grown in modified marine broth 2216 with different buffers at a concentration of 20 mM. MES buffer was used for pH 5.5 and 6.0, PIPES buffer for pH 6.5 and 7.0, HEPES buffer for pH 7.5 and 8.0, Tricine buffer for pH 8.5, and CAPSO buffer for pH 9.0 and 9.5. For investigating growth at different NaCl concentrations, a medium containing 1 g/L^{-1} yeast extract, 5 g/L^{-1} peptone, and 20 g/L^{-1} agar prepared with artificial seawater [0.22% $MgCl_2$, 0.15% $CaCl_2$, 0.32% $MgSO_4$, 0.02% $NaHCO_3$, and 0.07% KCl, with 3% NaCl (w/v)] was used. The bacterial strains were grown in this medium at NaCl concentrations ranging from 0% to 9% in increments of 0.5%.

The susceptibility of the bacterial strains D04^T and AAT^T to various antibiotics was tested using the disc diffusion method, as previously described (Du et al., 2014). A cell suspension of 0.5 McFarland standard was swabbed over the modified marine agar to create a uniform lawn before the aseptic placement of antibiotic discs onto the surface. After incubation for 5 days, the plates were examined for a clear zone of growth inhibition around the antibiotic discs. A total of 20 different antibiotic discs (with varying concentrations measured in micrograms per disc) were used to test the susceptibility of the bacterial strains D04^T and AAT^T: lincomycin (2), streptomycin (10), erythromycin (15), clarithromycin (15), kanamycin (30), ampicillin (10), rifampin (5), tetracycline (30), penicillin (10), chloramphenicol (30), cefotaxime sodium (30), gentamycin (10), ofloxacin (5), norfloxacin (30), neomycin (30), carbenicillin (100), ceftriaxone (30) tobramycin (10), vancomycin (30), and polymyxin B (300). CLSI standards were strictly followed for cultivation and inhibition zone diameter reading (Gcrhardt et al., 1994).

Bacterial growth was monitored at 600 nm using a spectrophotometer. Catalase and oxidase activity were tested by pouring 3% H_2O_2 solution onto the cells and by using an oxidase test reagent (bioMérieux), respectively. Anaerobic growth was tested for 15 days at 30°C on the modified MA with or without 0.1% (w/v) $NaNO_3$ in an anaerobic bag (hopebio). Hydrolyses of

1 https://lpsn.dsmz.de/family/Marinifilaceae

agar, starch, alginate, casein, CM-cellulose, DNA, and lipase (Tweens 20, 40, 60, and 80) were examined according to the method of CLSI (2021). API 20E and API 50CH tests (bioMérieux) were carried out according to the manufacturer's instructions (except for salinity, which was adjusted to 3%). Enzyme activities were examined using the API ZYM test (bioMérieux). Oxidization of different compounds was tested in Biolog GEN III microplates according to the manufacturer's instructions. All the API and Biolog tests were performed with three biological replicates each time and with two reference strains.

2.3 16S rRNA gene sequence analysis

The 16S rRNA gene sequences were amplified using PCR with the primer pair 27F (5'-AGAGTTTGATCMTGGCTCAG-3') and 1492R (5'-TACGGYTACCTTGTTACGACTT-3') (Jordan et al., 2007; Du et al., 2014). Purified PCR products were ligated into the pMD18-T vector (Takara) and cloned by following the manufacturer's instructions. Sequencing was performed by BGI Co. Ltd (Qingdao, PR China). The nearly complete 16S rRNA gene sequences of strains D04^T and AAT^T were obtained and compared with those available from the EzBioCloud[2] (Yoon et al., 2017a) database for further phylogenetic analysis. Phylogenetic trees were constructed using MEGA version 11 employing the neighbor-joining (Saitou and Nei, 1987), maximum-likelihood (Felsenstein, 1981), and maximum-parsimony methods (Kumar, 1996). Bootstrap analyses were performed based on 1,000 replicates to estimate the confidence of branches in the generated phylogenetic trees (Felsenstein, 1985).

2.4 Genome sequencing analysis

Genomic DNA of strains D04^T and AAT^T was extracted and purified using a bacteria genomic DNA kit (Takara). The draft genome sequences of strains D04^T and AAT^T were sequenced by Majorbio (MajorBio Co., Shanghai, China) using an Illumina MiSeq (Illumina, USA). The final genome was assembled with SOPA *de novo* version 2.04 (Luo et al., 2012). The resulting genomes were annotated using RAST (rapid annotation using subsystem technology online server)[3] (Aziz et al., 2008). The molecular functions of genes and proteins are associated with ortholog groups and stored in the KEGG orthology (KO) database (Kanehisa et al., 2016). The genes involved in metabolic pathways and ortholog groups of proteins were analyzed using the[4] and dbCAN2 meta servers[5] (Zhang et al., 2018). The presence of gene clusters encoding secondary metabolites was predicted using antiSMASH 6.1.1[6] (Blin et al., 2021). The DNA G+C content was calculated based on the whole genome sequence. The AAI calculator estimates the average amino acid identity using both best hits (one-way AAI) and reciprocal best hits (two-way AAI) between two genomic datasets of proteins[7]. Average nucleotide identity (ANI) values were calculated using the ChunLab's online ANI Calculator[8] (Lee et al., 2016). The genome-to-genome distance calculator (GGDC 3.0)[9] (Meier-Kolthoff et al., 2013) was used to calculate the digital DNA-DNA hybridization (dDDH).

2.5 Chemotaxonomic analyses

The reference strain *Saccharicrinis fermentans* DSM 9555^T was obtained from the German Collection of Microorganisms and Cell Cultures GmbH and *Labilibacter aurantiacus* HQYD1^T was obtained from our laboratory. Both strains were cultured on modified MA at 33°C and studied in parallel with strains D04^T and AAT^T for physiological and chemotaxonomic comparisons. Cellular fatty acids and polar lipids were identified from a freeze-dried sample (40 mg and 50 mg) of cells grown to the exponential growth phase under optimal culture conditions on the modified MA. Cellular fatty acid methyl esters (FAMEs) were obtained from cells by saponification, methylation, and extraction following the MIDI protocol (Sasser, 1990). Cellular FAMEs were separated using gas chromatography and were identified and quantified using the Sherlock Microbial Identification System (version 6.1, MIDI 6890 with database TSBA6). Polar lipids were separated via two-dimensional silica gel TLC. Total lipid material was detected using molybdatophosphoric acid and the functional groups were determined using spray reagents specific for each group according to Fang et al. (2017). All polar lipid images were further analyzed as described by Minnikin et al. (1984). For respiratory quinone analyses, respiratory quinones were extracted from 200 mg of freeze-dried cell material using the two-stage method described by Minnikin et al. (1984). A silica-gel TLC plate (Merck Kieselgel 60 F254) was used to analyze the quinone type and the content of each quinone type was subsequently analyzed by HPLC according to the process described previously (Kroppenstedt, 1982).

3 Results and discussion

3.1 Morphology, physiology, and biochemical characteristics

The newly discovered strains D04^T and AAT^T of bacteria belonging to the *Marinilabiliaceae* family were facultative

2 https://www.ezbiocloud.net/pa

3 https://rast.nmpdr.org/

4 https://www.genome.jp/tools/kofamkoala/

5 http://bcb.unl.edu/dbCAN2

6 https://antismash.secondarymetabolites.org/

7 http://enve-omics.ce.gatech.edu/aai/

8 https://www.ezbiocloud.net/tools/ani

9 http://ggdc.dsmz.de

anaerobes, Gram-negative, rod-shaped, oxidase-positive, and catalase-negative. Strain D04^T had a width of 0.3 µm and a length of 3.4–4.1 µm, while strain AAT^T had a width of 0.4–0.5 µm and a length of 0.6–1.4 µm (Supplementary Figure 1). Strain D04^T also demonstrated gliding motility, while strain AAT^T did not. Both strains grew as yellow-colored, smooth, and circular colonies on modified MA medium at 33°C. They were oxidase-positive, catalase-negative, and reduced nitrate to nitrite. The growth temperature range of the bacterial strains studied was between 20°C and 40°C and they were unable to grow at temperatures of 4°C and 45°C. Strains D04^T and AAT^T showed optimal growth at a temperature of 33°C. The pH range for growth of strain D04^T was 6.5–7.5, with optimal growth occurring at pH 7.0. Strain AAT^T was able to grow at pH values ranging from 6.0–7.5, with optimal growth occurring at a pH of 6.5. In terms of salt tolerance, strain D04^T was able to grow at NaCl concentrations ranging from 0% to 8.0% w/v, with an optimum NaCl concentration of 2.0%. Strain AAT^T was able to grow at NaCl concentrations ranging from 0.5% to 8.0% w/v, with an optimum NaCl concentration of 3.0%. The addition of a vitamin mixture to the medium increased their growth. The strains were positive for the hydrolysis of starch but negative for casein, CM-cellulose, alginate, and Tweens 20, 40, 60, and 80. Strain AAT^T was positive for DNA, while strain D04^T was negative. Both strains were resistant to antibiotics such as tobramycin, vancomycin, tetracycline, norfloxacin, neomycin, gentamycin, ofloxacin, streptomycin, kanamycin, and polymyxinB. However, strain D04^T was susceptible to erythromycin, ampicillin, penicillin, chloramphenicol, rifampin, and lincomycin, while strain AAT^T was between resistant and sensitive to cefotaxime sodium and carbenicillin.

Strains D04^T and AAT^T share similar morphological and biochemical characteristics with the other two species in the *Marinilabiliaceae* family, including being rod-shaped, Gram-stain-negative, and facultatively aerobic. They also showed positive results for various enzyme activities such as alkaline phosphatase, esterase (C4), esterase lipase (C8), acid phosphatase, and naphthol-AS-BI-phosphohydrolase, as well as for tryptophan deaminase, Voges–Proskauer reaction, and arabinose. However, there were some differential phenotypic characteristics between strains D04^T and AAT^T and the two reference strains, as shown in Table 1.

3.2 Comparison and phylogenetic analysis of the 16S rRNA gene sequences

The nearly complete 16S rRNA gene sequences of strains D04^T (1480 bp) and AAT^T (1525 bp) were obtained. Sequence comparisons showed that strains D04^T and AAT^T had the highest 16S rRNA gene sequence similarity with the type strain of *Saccharicrinis fermentans* DSM 9555^T (94.1% and 94.9%, respectively), followed by *Saccharicrinis marinus* Y11^T (93.3% and 94.5%, respectively). The 16S rRNA gene sequences of strains D04^T and AAT^T were similar to those of *Labilibacter aurantiacus* HQYD1^T type strains (93.3% and 93.4%, respectively). The similarity of the 16S rRNA gene sequence between the two strains was 96.6%. The neighbor-joining, maximum-likelihood, and maximum-parsimony phylogenetic trees formed an independent sub-cluster supported by very high bootstrap values (Figure 1). In the phylogenetic tree, strains D04^T and AAT^T are closely related to the members of the genera *Saccharicrinis* and *Labilibacter*. By using 16S rRNA gene sequence similarity and phylogenetic trees, *Saccharicrinis fermentans* DSM 9555^T and *Labilibacter aurantiacus* HQYD1^T were selected as reference strains.

3.3 Genomic features

3.3.1 Basic characteristics

The obtained draft genome of D04^T is comprised of 187 scaffolds (N50 = 106,391 bp) and is 5,621,283 bp in length. The obtained draft genome of AAT^T is comprised of 428 scaffolds (N50 = 74,668 bp) and is 6,588,154 bp in length. The G+C content of strains D04^T and AAT^T were 36.6% and 33.4%. The annotated genome of strain D04^T contained a total of 4,522 genes, with 4,456 protein-coding genes, 3 rRNAs, and 63 tRNAs. The annotated genome of strain AAT^T contained a total of 5,207 genes, with 5,130 protein-coding genes, 7 rRNAs, and 70 tRNAs. The range of the AAI values of strains D04^T and AAT^T in the family *Marinilabiliaceae* genus are 62–72% and 61–71%, respectively, which were below the threshold value (74%) for genus delineation (Nicholson et al., 2020). The AAI value of strains D04^T and AAT^T is 77%, which was higher than the threshold value (74%) for genus delineation (Supplementary Figure 2A). The ANI value of strains D04^T and AAT^T is less than 74%, which is below the threshold (95%) for new species identification (Supplementary Figure 2B) (Yoon et al., 2017b). The dDDH value of strains D04^T and AAT^T is less than 22%, which is below the threshold (70%) for new species identification (Goris et al., 2007). The phylogenomic maximum-likelihood tree based on 120 core genes showed that strains D04^T and AAT^T formed distinct lineages within the family *Marinilabiliaceae* (Supplementary Figure 3).

3.3.2 Carbohydrate-active enzymes and analysis of *SusC* and *SusD* genes

The carbohydrate-active enzyme (CAZy) database builds and breaks down complex carbohydrates and glycoconjugates, covering the following classes of enzyme activities: glycoside hydrolases (GHs), carbohydrate esterases (CEs), glycosyltransferases (GTs), polysaccharide lyases (PLs), auxiliary activities (AA), and carbohydrate-binding modules (CBMs) (Cantarel et al., 2009). Four strains of the family *Marinilabiliaceae* have been analyzed using the CAZyme database. The strains D04^T, AAT^T, *Labilibacter aurantiacus* HQYD1^T, and *Saccharicrinis fermentans* DSM 9555^T contain 336, 341, 252, and 272 carbohydrate-active enzymes, respectively. Among these carbohydrate-active enzymes, glycoside hydrolases (GHs) are the most abundant CAZymes (more than 70% of the identified enzymes were assigned to the GH family). The strains D04^T, AAT^T, *Labilibacter aurantiacus* HQYD1^T, and *Saccharicrinis fermentans* DSM 9555^T all lack the AA gene

10.3389/fmars.2023.1213051

TABLE 1 Differential characteristics between the new strains and reference strains.

Characteristic	1	2	3	4
Colony color	Yellow	Yellow	Orange [a]*	Orange [b]*
Temperature (°C) (optimum temperature)	20–40 (33)	20–40 (33)	19–37 (30–32) [a]*	4–37 (28) [b]*
NaCl (%) (optimum NaCl%)	0–8.0 (2.0)	0.5–8.0 (3.0)	1.0–6.0 (2.5) [a]*	1.0–5.0 (2.0-3.0) [b]*
pH (optimum pH)	6.5–7.5 (7.0)	6.0–7.6 (6.5)	7.0–9.0 (8.0) [a]*	6.0–8.5 (7.0–7.5) [b]*
Nitrate reduction	+	+	–[a]*	–[b]*
Enzyme activity (API ZYM):				
leucine arylamidase	–	+	–	–
cystine arylamidase	–	+	–	–
trypsin	–	+	–	+
β-galactosidase	+	+	+	–
α-glucosidase	–	+	–	–
β-glucosidase	+	+	–	–
N-acetyl-β-glucosaminidase	–	+	–	–
Utilization of (API 20E)				
arginine dihydrolase	–	–	+	+
ornithine decarboxylase	–	–	–	+
urease	–	–	–	+
gelatinase	–	–	+	+
glucose	–	–	+	+
mannitol	–	–	+	–
inositol	–	–	+	–
sorbitol	–	–	+	–
sucrose	–	–	+	–
melibiose	–	–	+	+
amygdalin	–	–	+	–
Acid production from (API 50CH)				
mannose	–	–	+	–
erythritol	–	+	–	–
L-arabinose	+	+	+	–
L-xylose	–	–	+	–
D-adonitol	+	–	–	–
methyl-β-D-xylopyranoside	+	–	+	–
D-fructose	+	+	–	+
D-mannose	+	+	+	–
L-rhamnose	+	+	–	–
dulcitol	+	–	+	–
inositol	+	–	–	–
methyl-α-D-mannopyranoside	–	–	+	–
N-acetylglucosamine	–	+	+	+

(Continued)

TABLE 1 Continued

Characteristic	1	2	3	4
Colony color	Yellow	Yellow	Orange [a]*	Orange [b]*
amygdalin	–	+	+	+
D-trehalose	–	–	+	+
inulin	+	+	–	–
D-raffinose	+	+	–	+
xylitol	+	+	–	–
D-tagatose	+	–	+	–
D-fucose	–	+	+	–
L-fucose	+	+	+	–
D-arabitol	+	–	–	–
L-arabitol	+	+	–	–

Strains: 1, D04^T; 2, AAT^T; 3, Saccharicrinis fermentans DSM 9555^T; and 4, Labilibacter aurantiacus HQYD1^T. All data are from this study unless indicated otherwise. All strains are positive for alkali phosphatase, esterase (C4), esterase lipase (C8), acid phosphatase, and naphthol-AS-BI-phosphohydrolase, but negative for lipase (C14), valine arylamidase, a-chymotrypsin, α-galactosidase, β-glucuronidase, α-mannosidase and β-fucosidase. All strains are also positive for the utilization of tryptophan deaminase, Voges–Proskauer reaction, and arabinose, but negative for lysine decarboxylase, citrate utilization, H_2S production, indole production, rhamnol, and o-nitrophenyl-β-D-galactopyranoside. All strains produced acid from D-arabinose, D-ribose, D-xylose, D-galactose, D-glucose, arbulin, aesculin ferric citrate, salicin, D-cellobiose, D-maltose, D-lactose, D-melibiose, D-saccharose, starch, glycogen, D-gentiobiose, D-turanose, D-lyxose, potassium 2-keto-gluconate, and potassium 5-keto-gluconate, but not from L-sorbose, D-mannitol, D-sorbitol, methyl-α-D-glucopyranoside, D-melezitose and potassium gluconate. +, Positive; –, negative. *Data taken from: [a] (Yang et al., 2014); [b] (Lu et al., 2017).

(Supplementary Figure 4A). The first starch utilization system (Sus) was reported in human gut bacterium *Bacteroides*. The Sus operon is proposed to be essential for glycan degradation. *SusC* (*SusC* represents the actual TonB-dependent transporter) and *SusD* (*SusD* is an associated substrate binding outer membrane lipoprotein) are indispensable (Zheng et al., 2021). Prediction of *SusC* and *SusD* genes in strains D04^T and AAT^T was performed using RAST. The strain D04^T contains 19 *SusC* protein genes and 9 *SusD* protein genes. The strain AAT^T contains 14 *SusC* protein genes and 6 *SusD* protein genes (Supplementary Table 1).

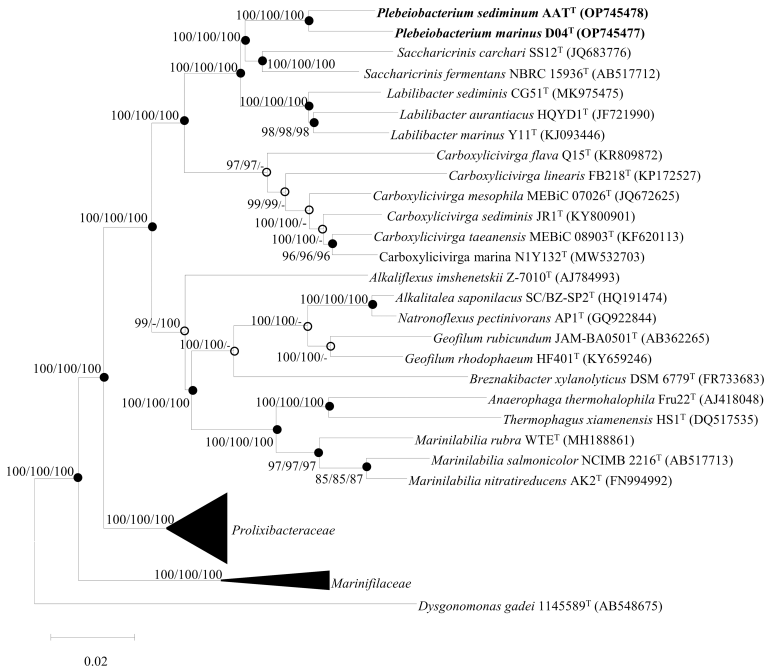

FIGURE 1
Neighbor-joining phylogenetic tree based on the 16S rRNA gene sequences showing the phylogenetic position of strains D04^T and AAT^T among members of the order *Marinilabiliales*. Numbers on nodes represent bootstrap values (NJ, ML, and MP) based on 1,000 replications. The sequence of *Dysgonomonas gadei* 1145589^T (AB548675) was used as an outgroup. Bar, 0.02 substitutions per nucleotide position.

3.3.3 Prediction of secondary metabolites

Based on secondary metabolite analysis predicted by antiSMASH, the strains D04^T, AAT^T, *Labilibacter aurantiacus* HQYD1^T, and *Saccharicrinis fermentans* DSM 9555^T shared gene cluster encoding for RRE-containing (RRE-element containing cluster), NRPS-like (NRPS-like fragment), and terpene cyclase (terpene). Compared with other strains, the two new strains possess more biosynthetic clusters, among which, strains D04^T and AAT^T possess arylpolyene (aryl polyene cluster) and resorcinol (resorcinol cluster) biosynthetic gene clusters. The *Labilibacter aurantiacus* HQYD1^T strain clusters include lanthipeptide-class-IV (class IV lanthipeptide clusters such as venezuelin), NRPS (non-ribosomal peptide synthetase cluster), and T1PKS (type I PKS (polyketide synthase)) biosynthetic clusters (Supplementary Figure 4B).

3.3.4 Analysis of metabolic pathways

Metabolic pathways were analyzed using the KEGG Orthology (KO) database service. All four strains possessed many complete metabolic pathways, including carbon metabolism, energy metabolism, lipid metabolism, nucleic acid metabolism, amino acid metabolism, metabolism of cofactors and vitamins, and biosynthesis of terpenoids and polyketides. The strain D04^T possessed the least complete pathways. The strain AAT^T possessed the most complete pathways. All strains showed a complete PE biosynthesis pathway (M00093), which was consistent with the polar lipid detected in the four strains. It is noteworthy that these strains have complete nitrogen fixation pathways (M00175) (Supplementary Figure 4C).

3.3.5 Analysis of nitrogen fixation

The *Marinilabiliaceae*, *Prolixibacteraceae*, and *Marinifilaceae* of *Bacteroidetes* was classified as a new order named *Marinilabiliales* (Wu et al., 2016). At the time of writing, 63 species of *Marinilabiliales* can be found on LPSN[1], of which 12 have no genomic data (Figure 2). Recently, a study was conducted to predict the presence of nitrogen fixation genes in five different strains of the family *Prolixibacteraceae* (Huang et al., 2020). The nitrogen fixation genes of 53 strains of the order *Marinilabiliales* were annotated using the genome. Of the 53 strains, 26 were found to contain nitrogen fixation gene clusters. These gene clusters were detected in all three families within the order. The proportion of nitrogen-fixing gene clusters in *Marinilabiliaceae*, *Prolixibacteraceae*, and *Marinifilaceae* genomes was 57%, 50%, and 25%, respectively (Figure 2). *Marinilabiliales* are mainly found in microbial mats, animal intestines and feces, and various sediments. The

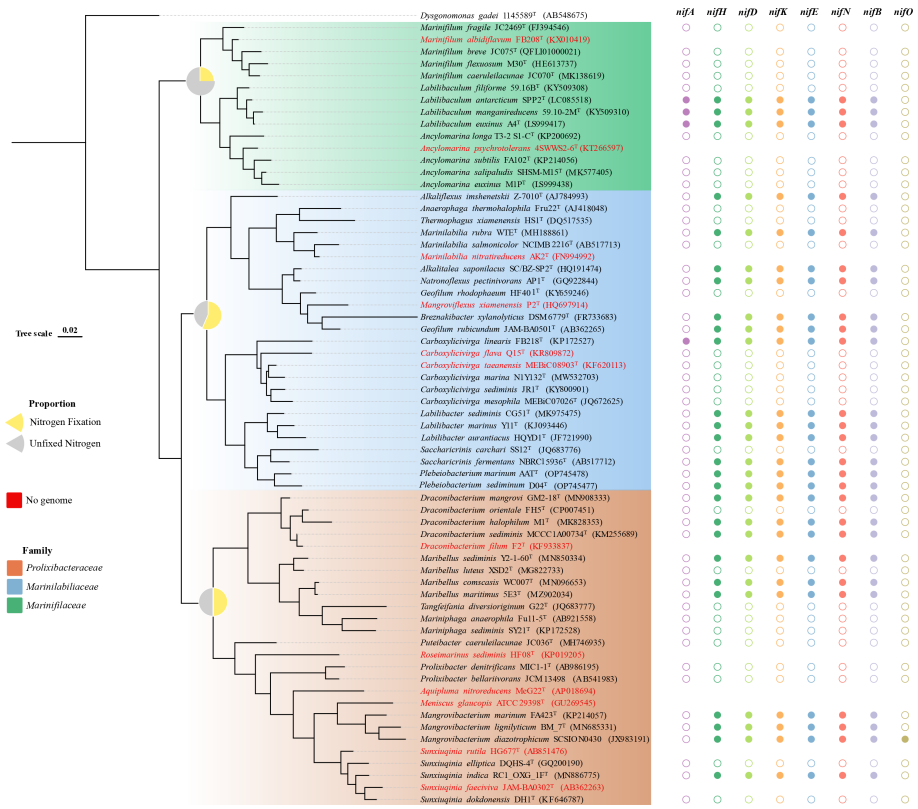

FIGURE 2
Distribution of the nitrogenase gene cluster among *Marinilabiliacea* bacteria. The tree was constructed using the maximum-likelihood method employing the 16S rRNA gene sequences. The tree was rooted with *Dysgonomonas gadei* 1145589^T. Different colored shapes (solid: gene cluster exists, hollow: gene cluster absence) represent the presence of genes *nifH*, *nifD*, *nifK*, *nifE*, *nifN*, *nifB*, *nifA*, and *nifO*. Pie charts on the nodes show the proportion of nitrogen fixation and nitrogen fixation gene clusters missing in the three families. *Marinifilaceae*, *Marinilabiliaceae*, and *Prolixibacteraceae* are colored in the corresponding leaves of the tree (see figure legend). In the phylogenetic tree, no genome is found when the species name is in red.

Marinilabiliaceae family has more strains with nitrogen fixation potential. This family mainly exists in the deep anoxic zone of the microbial mat, where cyanobacteria are degraded and nourish the surrounding microorganisms as organic matter. Nitrogen-fixing flora provide the cyanobacteria with fixed nitrogen and other factors necessary for growth, forming a reciprocal nitrogen fixation alliance. This alliance is important for the cycling of nitrogen in marine environments and contributes to the productivity and sustainability of marine ecosystems (Steppe et al., 1996; Ben Hania et al., 2017). Nitrogen-fixing enzymes are inactivated when exposed to oxygen. However, the nitrogen-fixing enzyme activity increases significantly when the oxygen concentration in the sediment environment is close to 5% (Smercina et al., 2019) (Supplementary Figure 5). It has been hypothesized that the retention of nitrogen-fixing gene clusters in taxon is related to environmental distribution (Harwood, 2020). The absence of nitrogen fixation-related gene clusters in the genomes of some members of the *Marinilabiliales* order suggests that the not all *Marinilabiliales* members contained *nif* gene clusters. Particularly in the family *Marinifilaceae*, the nitrogen-fixing gene cluster only exists in the genus *Labilibaculum*. Analysis of the results showed that the conserved features of *nif* gene clusters in some lineages of the order *Marinilabiliales* were lost (Figures 2, 3). *Marinilabiliales* strains all have a complete set of nitrogen fixation gene clusters, including *nifH*, *nifD*, *nifK*, *nifE*, *nifN*, and *nifB*. It is hypothesized that this taxon has nitrogen fixation potential, providing a basis for studying nitrogen fixation by nitrogen-fixing organisms in ecosystems (Figure 3; Supplementary Table 2). The phylogenetic tree based on the *nifH* gene is not similar to that based on the 16S rRNA gene; however, the phylogenetic relationship of *nifH* genes in the novel isolate and reference strains are closely related, similar to that in the phylogenetic tree using the 16S rRNA gene (Figures 4A, B). Nitrogen-fixing bacteria living in the sediment surrounding seagrass play a crucial role in providing bioavailable nitrogen directly to the plant and promoting its growth. This bacterial process helps to maintain the productivity and sustainability of seagrass ecosystems. Similarly, nitrogen-fixing bacteria in deep-sea sediments can use a range of terminal electron acceptors, including oxygen, nitrate, iron, sulfur, sulfate, and organic compounds, to fix nitrogen. The potential coupling of deep-sea diazo nutrition with a variety of biogeochemical cycles can have significant implications for global nutrient cycling. The bacterial strains used in this study were isolated from intertidal sediment, providing a foundation for future research on the ecological functions of microbial communities in intertidal sediments.

3.4 Chemotaxonomic characteristics

The major fatty acids (>10%) of D04^T and AAT^T were iso-$C_{15:0}$ and anteiso-$C_{15:0}$, which was similar with the profiles of the two reference strains, although there were differences in the proportions of some fatty acids. Strain AAT^T also possesses major fatty acids, including iso-$C_{15:0}$ 3-OH and iso-$C_{17:0}$ 3-OH. Fatty acids (>0.5%) were listed in detail in Table 2. The polar lipid profile of strain D04^T consisted of phosphatidylethanolamine (PE), three glycolipid (GL1-3) and one unknown polar lipid. The polar lipid profile of strain

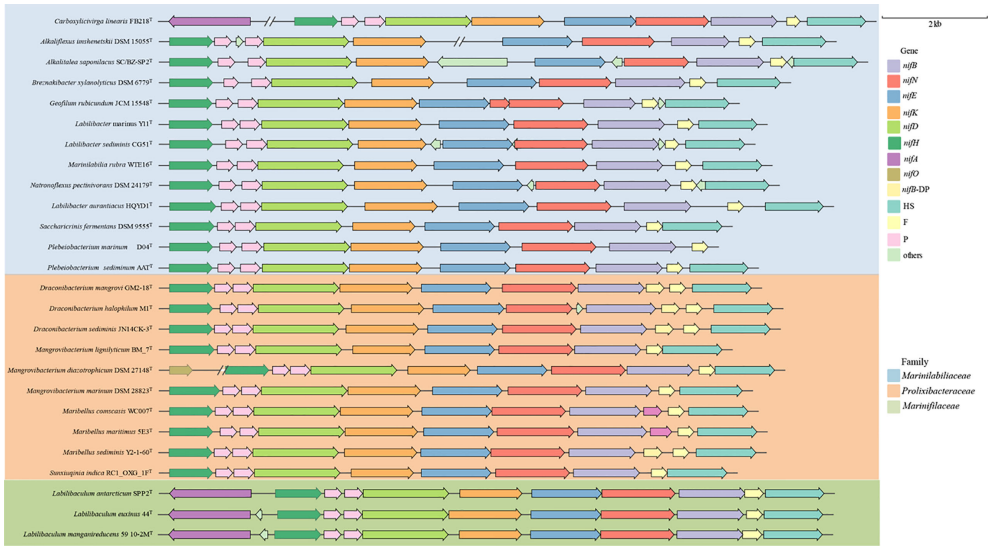

FIGURE 3
Comparative analysis of the *nif* gene cluster among the genomes of the order *Marinilabiliales*. Arrows with different colors represent the presence of corresponding *nif* genes (see figure legend) and the direction of the arrows represents the direction of the gene clusters. The gene numbers indicated by HS and F are homocitrate synthase and ferredoxin (2Fe-2S), respectively. The genes indicated by P are nitrogen regulatory protein P-II. The genes indicated by *nifB*-DP are *nifB*-domain protein. Families colored blue indicate the *Marinilabiliacea* family, orange indicate *Prolixibacteraceae*, and green indicate *Marinifilaceae*.

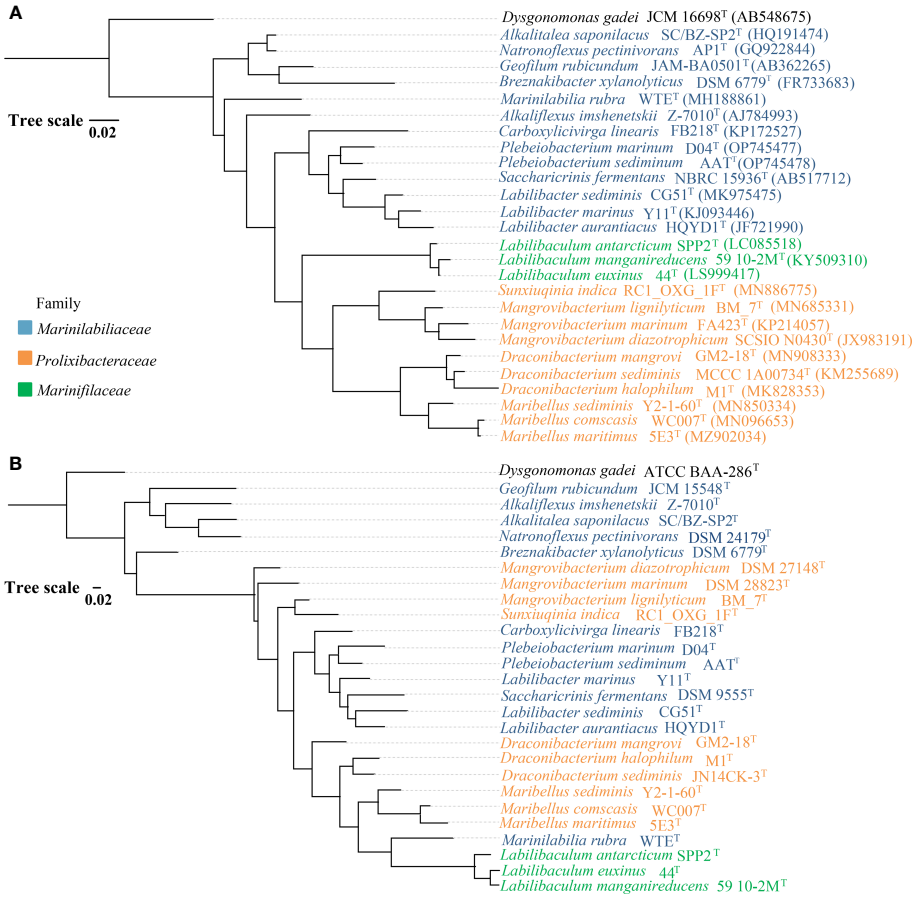

FIGURE 4
Phylogenetic relationships of the *Marinilabiliales* species based on 16S rRNA gene sequences **(A)** and the *nifH* nucleotide sequence **(B)**. The tree was constructed using the maximum-likelihood method and rooted with *Dysgonomonas gadei*. Bar, 0.02. Blue, orange, and green indicate *Marinilabiliacea*, *Prolixibacteraceae*, and *Marinifilaceae*, respectively.

AAT^T consisted of phosphatidylethanolamine (PE), one glycolipid (GL), one aminophosphoglycolipid and one phosphoglycolipid. The presence of phosphatidylethanolamine (PE) was conserved in all strains. Further detailed polar lipid images with different specific strains are given in Supplementary Figure 6. For respiratory quinone analyses, the results indicated that the major respiratory quinone of strains $D04^T$ and AAT^T were identified to be MK-7, which matched other members in the family *Marinilabiliaceae*.

4 Description of *Plebeiobacterium* gen. nov.

Plebeiobacterium (Ple.beio.bacterium' adj. *Plebeio*, Common, ordinary. n. *bakterion* a small rod. N.L. fem. n. *Plebeiobacterium*, Common rod-shaped bacteria)

Cells are Gram-stain-negative, motile, facultatively anaerobic and straight rods. The major cellular fatty acids are dominant cellular fatty acids were identified as iso-$C_{15:0}$ and anteiso-$C_{15:0}$. MK-7 is the major menaquinone. The major polar lipid is phosphatidylethanolamine. The type species is *Plebeiobacterium marinum*.

4.1 Description of *Plebeiobacterium marinum* sp. nov.

Plebeiobacterium marinum (ma.ri'num. L. fem. marinum, from the sea).

Cells are facultatively anaerobic, Gram-stain-negative, and rod-shaped, roughly 0.3 µm wide and 3.4–4.1 µm long. Gliding motility was not observed. Cells were observed to be yellow colored, flat, smooth, and with circular colonies at 33°C on the modified MA grown after 5 days. Strain was oxidase positive, catalase negative, and nitrate reduced to nitrite. Growth occurs at 20–40°C (optimum 33°C), pH 6.5–7.5 (optimum pH 7.0), and with 0–8% NaCl (optimum 2% w/v). The strain was positive for the hydrolysis of starch but negative for casein, DNA, CM-cellulose, alginate, and Tweens 20, 40, 60, and 80. The major fatty acids are iso-$C_{15:0}$ and anteiso-$C_{15:0}$. The predominant respiratory quinone is MK-7. The polar lipid profile consisted of a phosphatidylethanolamine, three glycolipids (GL1-3), and one unknown polar lipid. Cells are positive for alkali phosphatase, esterase (C4), esterase lipase (C8), acid phosphatase, naphthol-AS-BI-phosphohydrolase, β-galactosidase, and β-glucosidase. Cells are also positive for the utilization of tryptophan

10.3389/fmars.2023.1213051

TABLE 2 Major cellular fatty acids comparison of strains D04^T and AAT^T and relative type strains of the family *Marinilabiliaceae*.

Fatty acid	1	2	3	4
Saturated				
$C_{12:0}$	0.8	1.4	2.2	TR
$C_{13:0}$	0.5	TR	ND	ND
$C_{14:0}$	1.3	1.5	0.6	6.6
$C_{16:0}$	ND	5.9	1.1	5.3
$C_{18:0}$	TR	0.8	ND	TR
Branched saturated				
iso-$C_{13:0}$	5.0	8.8	1.3	0.6
iso-$C_{14:0}$	TR	0.9	1.7	1.3
iso-$C_{15:0}$	**37.5**	**24.4**	**34.4**	**34.1**
iso-$C_{16:0}$	1.0	1.1	0.5	1.2
iso-$C_{15:1}$ F	ND	ND	2.2	0.9
anteiso-$C_{15:0}$	**16.5**	**15.5**	**16.9**	**17.2**
Unsaturated				
$C_{15:1}$ *ω6c*	ND	1.1	ND	TR
$C_{18:1}$ *ω9c*	0.9	0.7	TR	0.6
Hydroxy				
iso-$C_{13:0}$ 3-OH	ND	ND	0.5	4.1
iso-$C_{15:0}$ 3-OH	9.4	**11.8**	6.8	ND
iso-$C_{16:0}$ 3-OH	1.0	0.6	1.2	ND
iso-$C_{17:0}$ 3-OH	7.9	**10.3**	7.4	ND
$C_{15:0}$ 2-OH	0.5	1.3	1.5	ND
$C_{15:0}$ 3-OH	2.4	3.5	ND	ND
$C_{16:0}$ 3-OH	1.7	1.5	0.5	ND
$C_{17:0}$ 2-OH	0.5	1.5	0.9	ND
Summed features*				
1	TR	ND	1.2	TR
3	TR	TR	0.8	3.5
4	ND	ND	1.3	TR
9	ND	TR	3.4	2.0

*Summed features are fatty acids that cannot be reliably resolved from another fatty acid using the chosen chromatographic conditions. The MIDI system groups these fatty acids together as one feature with a single percentage of the total. Summed feature1, $C_{15:1}$ and/or iso-$C_{13:0}$ 3-OH; Summed feature3, $C_{16:1}$ ω6c and/or $C_{16:1}$ ω7c; Summed feature4, iso-$C_{17:1}$ I and/or anteiso-$C_{17:1}$ B; Summed feature9, iso-$C_{17:1}$ ω9c and/or $C_{16:1}$ 10-methyl.

Strains: 1, D04^T; 2, AAT^T; 3, Saccharicrinis fermentans DSM 9555^T; and 4, Labilibacter aurantiacus HQYD1^T. All data are from this study unless indicated otherwise. Fatty acids that represented >10.0% are indicated in bold type. Fatty acids that represented <1.0% in all columns were omitted.TR, traces (<1.0%); ND, Not detected

deaminase, Voges–Proskauer reaction, and arabinose. Acid is produced from D-arabinose, D-ribose, D-xylose, D-galactose, D-glucose, arbulin, aesculin ferric citrate, salicin, D-cellobiose, D-maltose, D-lactose, D-melibiose, D-saccharose, starch, glycogen, D-gentiobiose, D-turanose, D-lyxose, potassium 2-keto-gluconate, potassium 5-keto-gluconate, L-arabinose, D-adonitol, methyl-β-D-xylopyranoside, D-fructose, D-mannose, L-rhamnose, dulcitol, inositol, inulin, D-raffinose, xylitol, D-tagatose, L-fucose, D-arabitol, and L-arabitol. In carbon source oxidation tests, positive results are obtained for dextrin, D-maltose, D-trehalose, D-cellobiose, gentiobiose, sucrose, D-turanose, stachyose, D-raffinose, α-D-lactose, D-melibiose, D-salicin, N-acetyl-β-D-mannosamine, N-acetyl-D-galactosamine, α-D-glucose, D-mannose, D-fructose, D-galactose, 3-methyl glucose, L-fucose, myo-inositol, D-glucose-6-PO_4, D-fructose-6-PO_4, gelatin, L-alanine, L-histidine, L-pyroglutamic acid, pectin, D-glucuronic acid, glucuronamide, α-keto-glutaric acid, L-malic acid, α-keto-butyric acid, propionic

acid, acetoacetic acid, and acetic acid. The genomic DNA G+C content of the type strain is 36.8%.

The type strain D04^T (MCCC 1H00493^T = KCTC 92026^T) was isolated from coastal sediment collected from Xiaoshi Island, Weihai, China. Strain D04^T was stored in our own laboratory repository,[10] with code SDUM258008. The GenBank accession number for the 16S rRNA gene and the draft genome sequence of D04^T are OP745477 and JAPDPI000000000, respectively.

4.2 Description of *Plebeiobacterium sediminum* sp. nov.

Plebeiobacterium sediminum (*se.di.minum*. L. gen. pl. n. sediminum of sediments, pertaining to source of isolation).

Cells are facultatively anaerobic, Gram-stain-negative, and rod-shaped, roughly 0.4–0.5 µm wide and 0.6–1.4 µm long. Gliding motility was observed. Cells were observed to be yellow colored, flat, smooth, and with circular colonies at 33°C on the modified MA grown after 5 days. Strain was oxidase positive, catalase negative, and nitrate reduced to nitrite. Growth occurs at 20–40°C (optimum 33°C), pH 6.0–7.5 (optimum pH 6.5), and with 0.5–8% NaCl (optimum 3% w/v). The strain was positive for the hydrolysis of starch, DNA, but negative for casein, CM-cellulose, alginate, and Tweens 20, 40, 60, and 80. The major fatty acids are iso-$C_{15:0}$, anteiso-$C_{15:0}$, iso-$C_{15:0}$ 3-OH, and iso-$C_{17:0}$ 3-OH. The predominant respiratory quinone is MK-7. The polar lipid profile consisted of phosphatidylethanolamine, one glycolipid (GL), one aminophosphoglycolipid, and one phosphoglycolipid. Cells are positive for alkali phosphatase, esterase (C4), esterase lipase (C8), acid phosphatase, naphthol-AS-BI-phosphohydrolase, β-galactosidase, leucine arylamidase, cystine arylamidase, trypsin, N-acetyl-β-glucosaminidase, α-glucosidase, and β-glucosidase. Cells are also positive for the utilization of tryptophan deaminase, Voges–Proskauer reaction, and arabinose. Acid is produced from D-arabinose, D-ribose, D-xylose, D-galactose, D-glucose, arbulin, aesculin ferric citrate, salicin, D-cellobiose, D-maltose, D-lactose, D-melibiose, D-saccharose, starch, glycogen, D-gentiobiose, D-turanose, D-lyxose, potassium 2-keto-gluconate, potassium 5-keto-gluconate, erythritol, L-arabinose, D-fructose, D-mannose, L-rhamnose, N-acetylglucosamine, amygdalin, inulin, D-raffinose, xylitol, D-fucose, L-fucose, and L-arabitol. In carbon source oxidation tests, positive results are obtained for dextrin, D-maltose, D-trehalose, D-cellobiose, gentiobiose, sucrose, D-turanose, stachyose, D-raffinose, α-D-lactose, D-melibiose, β-methyl-D-glucoside, D-salicin, α-D-glucose, D-mannose, D-fructose, D-galactose, L-rhamnose, D-glucose-6-PO_4, glycyl-L-proline, pectin, D-galacturonic acid, L-galactonic acid lactone, D-glucuronic acid, glucuronamide, methyl pyruvate, α-keto-butyric acid, and acetic acid. The genomic DNA G+C content is 33.4%.

The type strain AAT^T (MCCC1H00485^T = KCTC92028^T) was isolated from coastal sediment collected from Xiaoshi Island, Weihai, China. Strain AAT^T was stored in our own laboratory repository,[10] with code SDUM258009. The GenBank accession number for the 16S rRNA gene and the draft genome sequence of AAT^T are OP745478 and JAPDPJ000000000, respectively.

10 http://sdum.wh.sdu.edu.cn/

Data availability statement

The datasets presented in this study can be found in online repositories. The names of the repository/repositories and accession number(s) can be found below: the accession numbers for the 16S rRNA gene sequence of strains D04^T and AAT^T are OP745477 and OP745478, respectively (Genbank); the accession number for the whole genome shotgun project of strains D04^T and AAT^T are JAPDPI000000000 and JAPDPJ000000000, respectively (GenBank).

Author contributions

W-XY and Q-YL isolated the strains D04^T and AAT^T. W-XY performed experimental operation, collected data, analysis and wrote the manuscript. Z-JD and D-SM offered experiment guidance and critical revision of the article. All authors contributed to the article and approved the submitted version.

Funding

This work was supported by the Science and Technology Fundamental Resources Investigation Program (Grant Nos. 2019FY100700 and 2022FY101100) and the National Natural Science Foundation of China (41876166).

Acknowledgments

The scanning electron microscopy was supported by the Physical-Chemical Materials Analytical and Testing Center of Shandong University at Weihai. A scanning electron microscope (Nova NanoSEM 450, FEI) was used to observe the cell size and morphology.

Conflict of interest

The authors declare that the research was conducted in the absence of any commercial or financial relationships that could be construed as a potential conflict of interest.

Publisher's note

Supplementary material

The Supplementary Material for this article can be found online at: https://www.frontiersin.org/articles/10.3389/fmars.2023.1213051/full#supplementary-material

References

Aziz, R. K., Bartels, D., Best, A. A., DeJongh, M., Disz, T., Edwards, R. A., et al. (2008). The RAST server: rapid annotations using subsystems technology. *BMC Genomics* 9, 75. doi: 10.1186/1471-2164-9-75

Ben Hania, W., Joseph, M., Bunk, B., Spröer, C., Klenk, H. P., Fardeau, M. L., et al. (2017). Characterization of the first cultured representative of a bacteroidetes clade specialized on the scavenging of cyanobacteria. *Environ. Microbiol.* 19 (3), 1134–1148. doi: 10.1111/1462-2920.13639

Bernardet, J. F., Nakagawa, Y., Holmes, B.Subcommittee On The Taxonomy Of, F and Cytophaga-Like Bacteria Of The International Committee On Systematics Of, P (2002). Proposed minimal standards for describing new taxa of the family flavobacteriaceae and emended description of the family. *Int. J. Syst. Evol. Microbiol.* 52 (Pt 3), 1049–1070. doi: 10.1099/00207713-52-3-1049

Blin, K., Shaw, S., Kloosterman, A. M., Charlop-Powers, Z., van Wezel, G. P., Medema, M. H., et al. (2021). antiSMASH 6.0: improving cluster detection and comparison capabilities. *Nucleic Acids Res.* 49 (W1), W29–w35. doi: 10.1093/nar/gkab335

Cantarel, B. L., Coutinho, P. M., Rancurel, C., Bernard, T., Lombard, V., and Henrissat, B. (2009). The carbohydrate-active EnZymes database (CAZy): an expert resource for glycogenomics. *Nucleic Acids Res.* 37 (Database issue), D233–D238. doi: 10.1093/nar/gkn663

Chakraborty, S., Andersen, K. H., Visser, A. W., Inomura, K., Follows, M. J., and Riemann, L. (2021). Quantifying nitrogen fixation by heterotrophic bacteria in sinking marine particles. *Nat. Commun.* 12 (1), 4085. doi: 10.1038/s41467-021-23875-6

CLSI. (2021). *Performance standards for antimicrobial susceptibility testing, M100, 31st ed.* (Wayne, PA: Clinical and Laboratory Standards Institute).

Denger, K., Warthmann, R., Ludwig, W., and Schink, B. (2002). Anaerophaga thermohalophila gen. nov., sp. nov., a moderately thermohalophilic, strictly anaerobic fermentative bacterium. *Int. J. Syst. Evol. Microbiol.* 52 (Pt 1), 173–178. doi: 10.1099/00207713-52-1-173

Du, Z. J., Wang, Y., Dunlap, C., Rooney, A. P., and Chen, G. J. (2014). Draconibacterium orientale gen. nov., sp. nov., isolated from two distinct marine environments, and proposal of draconibacteriaceae fam. nov. *Int. J. Syst. Evol. Microbiol.* 64 (Pt 5), 1690–1696. doi: 10.1099/ijs.0.056812-0

Fang, D. B., Han, J. R., Liu, Y., and Du, Z. J. (2017). Seonamhaeicola marinus sp. nov., isolated from marine algae. *Int. J. Syst. Evol. Microbiol.* 67 (11), 4857–4861. doi: 10.1099/ijsem.0.002396

Felsenstein, J. (1981). Evolutionary trees from DNA sequences: a maximum likelihood approach. *J. Mol. Evol.* 17 (6), 368–376. doi: 10.1007/bf01734359

Felsenstein, J. (1985). Confidence limits on phylogenies: an approach using the bootsrap. *Evolution* 39 (4), 783–791. doi: 10.1111/j.1558-5646.1985.tb00420.x

Gaby, J. C., and Buckley, D. H. (2011). A global census of nitrogenase diversity. *Environ. Microbiol.* 13 (7), 1790–1799. doi: 10.1111/j.1462-2920.2011.02488.x

Gcrhardt, P., Murray, R. G. E., Wood, W. A., and Krieg, N. R. (1994). *Methods for general and molecular bacteriology*. (Washington, DC: American Society for Microbiology). 607 p.

Goris, J., Konstantinidis, K. T., Klappenbach, J. A., Coenye, T., Vandamme, P., and Tiedje, J. M. (2007). DNA-DNA Hybridization values and their relationship to whole-genome sequence similarities. *Int. J. Syst. Evol. Microbiol.* 57 (Pt 1), 81–91. doi: 10.1099/ijs.0.64483-0

Gutierrez, J. C., Santero, E., and Tortolero, M. (1997). Ammonium repression of the nitrite-nitrate (nasAB) assimilatory operon of azotobacter vinelandii is enhanced in mutants expressing the nifO gene at high levels. *Mol. Gen. Genet.* 255 (2), 172–179. doi: 10.1007/s004380050486

Halm, H., Lam, P., Ferdelman, T. G., Lavik, G., Dittmar, T., LaRoche, J., et al. (2012). Heterotrophic organisms dominate nitrogen fixation in the south pacific gyre. *Isme J.* 6 (6), 1238–1249. doi: 10.1038/ismej.2011.182

Harwood, C. S. (2020). Iron-only and vanadium nitrogenases: fail-safe enzymes or something more? *Annu. Rev. Microbiol.* 74, 247–266. doi: 10.1146/annurev-micro-022620-014338

Herbert, R. A. (1999). Nitrogen cycling in coastal marine ecosystems. *FEMS Microbiol. Rev.* 23 (5), 563–590. doi: 10.1111/j.1574-6976.1999.tb00414.x

Huang, Z., Hu, Y., Lai, Q., and Guo, Y. (2020). Description of maribellus sediminis sp. nov., a marine nitrogen-fixing bacterium isolated from sediment of cordgrass and mangrove. *Syst. Appl. Microbiol.* 43 (4), 126099. doi: 10.1016/j.syapm.2020.126099

Inoue, J., Oshima, K., Suda, W., Sakamoto, M., Iino, T., Noda, S., et al. (2015). Distribution and evolution of nitrogen fixation genes in the phylum bacteroidetes. *Microbes Environ.* 30 (1), 44–50. doi: 10.1264/jsme2.ME14142

Isobe, K., and Ohte, N. (2014). Ecological perspectives on microbes involved in n-cycling. *Microbes Environ.* 29 (1), 4–16. doi: 10.1264/jsme2.me13159

Jordan, E. M., Thompson, F. L., Zhang, X. H., Li, Y., Vancanneyt, M., Kroppenstedt, R. M., et al. (2007). Sneathiella chinensis gen. nov., sp. nov., a novel marine alphaproteobacterium isolated from coastal sediment in qingdao, China. *Int. J. Syst. Evol. Microbiol.* 57 (Pt 1), 114–121. doi: 10.1099/ijs.0.64478-0

Kanehisa, M., Sato, Y., Kawashima, M., Furumichi, M., and Tanabe, M. (2016). KEGG as a reference resource for gene and protein annotation. *Nucleic Acids Res.* 44 (D1), D457–D462. doi: 10.1093/nar/gkv1070

Kapili, B. J., Barnett, S. E., Buckley, D. H., and Dekas, A. E. (2020). Evidence for phylogenetically and catabolically diverse active diazotrophs in deep-sea sediment. *Isme J.* 14 (4), 971–983. doi: 10.1038/s41396-019-0584-8

Kroppenstedt, R. M. (1982). Separation of bacterial menaquinones by HPLC using reverse phase (RP18) and a silver loaded ion exchanger as stationary phases. *J. Liquid Chromatogr. \& Related Technol.* 5 (12), 2359–2367. doi: 10.1080/01483918208067640

Kumar, S. (1996). A stepwise algorithm for finding minimum evolution trees. *Mol. Biol. Evol.* 13 (4), 584–593. doi: 10.1093/oxfordjournals.molbev.a025618

Kuypers, M. M. M., Marchant, H. K., and Kartal, B. (2018). The microbial nitrogen-cycling network. *Nat. Rev. Microbiol.* 16 (5), 263–276. doi: 10.1038/nrmicro.2018.9

Lee, I., Ouk Kim, Y., Park, S. C., and Chun, J. (2016). OrthoANI: an improved algorithm and software for calculating average nucleotide identity. *Int. J. Syst. Evol. Microbiol.* 66 (2), 1100–1103. doi: 10.1099/ijsem.0.000760

Lehnen, N., Marchant, H. K., Schwedt, A., Milucka, J., Lott, C., Weber, M., et al. (2016). High rates of microbial dinitrogen fixation and sulfate reduction associated with the Mediterranean seagrass posidonia oceanica. *Syst. Appl. Microbiol.* 39 (7), 476–483. doi: 10.1016/j.syapm.2016.08.004

López-Torrejón, G., Jiménez-Vicente, E., Buesa, J. M., Hernandez, J. A., Verma, H. K., and Rubio, L. M. (2016). Expression of a functional oxygen-labile nitrogenase component in the mitochondrial matrix of aerobically grown yeast. *Nat. Commun.* 7, 11426. doi: 10.1038/ncomms11426

Lu, D.-C., Zhao, J.-X., Wang, F.-Q., Xie, Z.-H., and Du, Z.-J. (2017). Labilibacter aurantiacus gen. nov., sp. nov., isolated from sea squirt (Styela clava) and reclassification of saccharicrinis marinus as labilibacter marinus comb. nov. *Int. J. System. Evolution. Microbiol.* 67 (2), 441–446. doi: 10.1099/ijsem.0.001649

Luo, R., Liu, B., Xie, Y., Li, Z., Huang, W., Yuan, J., et al. (2012). SOAPdenovo2: an empirically improved memory-efficient short-read *de novo* assembler. *Gigascience* 1 (1), 18. doi: 10.1186/2047-217x-1-18

Luo, Z., Zhong, Q., Han, X., Hu, R., Liu, X., Xu, W., et al. (2021). Depth-dependent variability of biological nitrogen fixation and diazotrophic communities in mangrove sediments. *Microbiome* 9 (1), 212. doi: 10.1186/s40168-021-01164-0

Meier-Kolthoff, J. P., Auch, A. F., Klenk, H.-P., and Göker, M. (2013). Genome sequence-based species delimitation with confidence intervals and improved distance functions. *BMC Bioinf.* 14, 60. doi: 10.1186/1471-2105-14-60

Minnikin, D. E., O'Donnell, A. G., Goodfellow, M., Alderson, G., Athalye, M., Schaal, A., et al. (1984). An integrated procedure for the extraction of bacterial isoprenoid quinones and polar lipids. *Microbiol. Methods* 2 (5), 233–241. doi: 10.1016/0167-7012(84)90018-6

Mohr, W., Lehnen, N., Ahmerkamp, S., Marchant, H. K., Graf, J. S., Tschitschko, B., et al. (2021). Terrestrial-type nitrogen-fixing symbiosis between seagrass and a marine bacterium. *Nature* 600 (7887), 105–109. doi: 10.1038/s41586-021-04063-4

Mu, D. S., Liang, Q. Y., Wang, X. M., Lu, D. C., Shi, M. J., Chen, G. J., et al. (2018). Metatranscriptomic and comparative genomic insights into resuscitation mechanisms during enrichment culturing. *Microbiome* 6 (1), 230. doi: 10.1186/s40168-018-0613-2

Nicholson, A. C., Gulvik, C. A., Whitney, A. M., Humrighouse, B. W., Bell, M. E., Holmes, B., et al. (2020). Division of the genus chryseobacterium: observation of discontinuities in amino acid identity values, a possible consequence of major extinction events, guides transfer of nine species to the genus epilithonimonas, eleven species to the genus kaistella, and three species to the genus halpernia gen. nov., with description of kaistella daneshvariae sp. nov. and epilithonimonas vandammei sp. nov. derived from clinical specimens. *Int. J. Syst. Evol. Microbiol.* 70 (8), 4432–4450. doi: 10.1099/ijsem.0.003935

Pi, H. W., Lin, J. J., Chen, C. A., Wang, P. H., Chiang, Y. R., Huang, C. C., et al. (2022). Origin and evolution of nitrogen fixation in prokaryotes. *Mol. Biol. Evol.* 39 (9), msac181. doi: 10.1093/molbev/msac181

Raymond, J., Siefert, J. L., Staples, C. R., and Blankenship, R. E. (2004). The natural history of nitrogen fixation. *Mol. Biol. Evol.* 21 (3), 541–554. doi: 10.1093/molbev/msh047

Saitou, N., and Nei, M. (1987). The neighbor-joining method: a new method for reconstructing phylogenetic trees. *Mol. Biol. Evol.* 4 (4), 406–425. doi: 10.1093/oxfordjournals.molbev.a040454

Sarkar, A., and Reinhold-Hurek, B. (2014). Transcriptional profiling of nitrogen fixation and the role of NifA in the diazotrophic endophyte azoarcus sp. strain BH72. *PloS One* 9 (2), e86527. doi: 10.1371/journal.pone.0086527

Sayavedra, L., Li, T., Bueno Batista, M., Seah, B. K. B., Booth, C., Zhai, Q., et al. (2021). Desulfovibrio diazotrophicus sp. nov., a sulfate-reducing bacterium from the human gut capable of nitrogen fixation. *Environ. Microbiol.* 23 (6), 3164–3181. doi: 10.1111/1462-2920.15538

Smercina, D. N., Evans, S. E., Friesen, M. L., and Tiemann, L. K. (2019). To fix or not to fix: controls on free-living nitrogen fixation in the rhizosphere. *Appl. Environ. Microbiol.* 85 (6), e02546–e02518. doi: 10.1128/aem.02546-18

Sohm, J. A., Webb, E. A., and Capone, D. G. (2011). Emerging patterns of marine nitrogen fixation. *Nat. Rev. Microbiol.* 9 (7), 499–508. doi: 10.1038/nrmicro2594

Sorokin, D. Y., Panteleeva, A. N., Tourova, T. P., Kaparullina, E. N., and Muyzer, G. (2011). Natronoflexus pectinivorans gen. nov. sp. nov., an obligately anaerobic and alkaliphilic fermentative member of bacteroidetes from soda lakes. *Extremophiles* 15 (6), 691–696. doi: 10.1007/s00792-011-0399-7

Steppe, T. F., Olson, J. B., Paerl, H. W., Litaker, R. W., and Belnap, J. (1996). Consortial N2 fixation: a strategy for meeting nitrogen requirements of marine and terrestrial cyanobacterial mats. *FEMS Microbiol. Ecol.* 21 (3), 149–156. doi: 10.1111/j.1574-6941.1996.tb00342.x

Weisburg, W. G., Barns, S. M., Pelletier, D. A., and Lane, D. J. (1991). 16S ribosomal DNA amplification for phylogenetic study. *J. Bacteriol.* 173 (2), 697–703. doi: 10.1128/jb.173.2.697-703.1991

Wu, W. J., Zhao, J. X., Chen, G. J., and Du, Z. J. (2016). Description of ancylomarina subtilis gen. nov., sp. nov., isolated from coastal sediment, proposal of marinilabiliales ord. nov. and transfer of marinilabiliaceae, prolixibacteraceae and marinifilaceae to the order marinilabiliales. *Int. J. Syst. Evol. Microbiol.* 66 (10), 4243–4249. doi: 10.1099/ijsem.0.001342

Yang, S.-H., Seo, H.-S., Woo, J.-H., Oh, H.-M., Jang, H., Lee, J.-H., et al. (2014). Carboxylicivirga gen. nov. in the family marinilabiliaceae with two novel species, carboxylicivirga mesophila sp. nov. and carboxylicivirga taeanensis sp. nov., and reclassification of cytophaga fermentans as saccharicrinis fermentans gen. nov., comb. nov. *Int. J. System. Evolution. Microbiol.* 64 (Pt_4), 1351–1358. doi: 10.1099/ijs.0.053462-0

Yoon, S. H., Ha, S. M., Kwon, S., Lim, J., Kim, Y., Seo, H., et al. (2017a). Introducing EzBioCloud: a taxonomically united database of 16S rRNA gene sequences and whole-genome assemblies. *Int. J. Syst. Evol. Microbiol.* 67 (5), 1613–1617. doi: 10.1099/ijsem.0.001755

Yoon, S. H., Ha, S. M., Lim, J., Kwon, S., and Chun, J. (2017b). A large-scale evaluation of algorithms to calculate average nucleotide identity. *Antonie Van Leeuwenhoek* 110 (10), 1281–1286. doi: 10.1007/s10482-017-0844-4

Zehr, J. P. (2011). Nitrogen fixation by marine cyanobacteria. *Trends Microbiol.* 19 (4), 162–173. doi: 10.1016/j.tim.2010.12.004

Zehr, J. P., Jenkins, B. D., Short, S. M., and Steward, G. F. (2003). Nitrogenase gene diversity and microbial community structure: a cross-system comparison. *Environ. Microbiol.* 5 (7), 539–554. doi: 10.1046/j.1462-2920.2003.00451.x

Zhang, H., Yohe, T., Huang, L., Entwistle, S., Wu, P., Yang, Z., et al. (2018). dbCAN2: a meta server for automated carbohydrate-active enzyme annotation. *Nucleic Acids Res.* 46 (W1), W95–w101. doi: 10.1093/nar/gky418

Zhao, B., and Chen, S. (2012). Alkalitalea saponilacus gen. nov., sp. nov., an obligately anaerobic, alkaliphilic, xylanolytic bacterium from a meromictic soda lake. *Int. J. Syst. Evol. Microbiol.* 62 (Pt 11), 2618–2623. doi: 10.1099/ijs.0.038315-0

Zheng, R., Cai, R., Liu, R., Liu, G., and Sun, C. (2021). Maribellus comscasis sp. nov., a novel deep-sea bacteroidetes bacterium, possessing a prominent capability of degrading cellulose. *Environ. Microbiol.* 23 (8), 4561–4575. doi: 10.1111/1462-2920.15650

Zhilina, T. N., Appel, R., Probian, C., Brossa, E. L., Harder, J., Widdel, F., et al. (2004). Alkaliflexus imshenetskii gen. nov. sp. nov., a new alkaliphilic gliding carbohydrate-fermenting bacterium with propionate formation from a soda lake. *Arch. Microbiol.* 182 (2-3), 244–253. doi: 10.1007/s00203-004-0722-0

frontiers | Frontiers in Marine Science

TYPE Original Research
PUBLISHED 20 July 2023
DOI 10.3389/fmars.2023.1222157

OPEN ACCESS

EDITED BY
Danny Ionescu,
Leibniz-Institute of Freshwater Ecology and Inland Fisheries (IGB), Germany

REVIEWED BY
Jiwen Liu,
Ocean University of China, China
Wei Li,
Shantou University, China

*CORRESPONDENCE
Xue-Wei Xu
xuxw@sio.org.cn
Cong Sun
michael_sc@sina.com

RECEIVED 13 May 2023
ACCEPTED 03 July 2023
PUBLISHED 20 July 2023

CITATION
Ma K-J, Ye Y-L, Fu Y-H, Fu G-Y, Sun C and Xu X-W (2023) Genomic and phylotypic properties of three novel marine *Bacteroidota* from bare tidal flats reveal insights into their potential of polysaccharide metabolism.
Front. Mar. Sci. 10:1222157.
doi: 10.3389/fmars.2023.1222157

Genomic and phylotypic properties of three novel marine *Bacteroidota* from bare tidal flats reveal insights into their potential of polysaccharide metabolism

Kuo-Jian Ma[1,2], Yong-Lian Ye[1], Yun-Han Fu[1,2], Ge-Yi Fu[1], Cong Sun[3,4]* and Xue-Wei Xu[1,2]*

[1]Key Laboratory of Marine Ecosystem Dynamics, Ministry of Natural Resources and Second Institute of Oceanography, Ministry of Natural Resources, Hangzhou, China, [2]Ocean College, Zhejiang University, Zhoushan, China, [3]College of Life Sciences and Medicine, Zhejiang Sci-Tech University, Hangzhou, China, [4]Center of Marine Microbial Resource, Zhejiang Sci-Tech University Shaoxing Academy of Biomedicine Co., Ltd., Shaoxing, China

Special geographical location and abundant organic matter profiles in tidal flats have resulted in great microbial diversity, in which *Bacteroidota* strains are considered as one of the primary degraders of polysaccharides, playing a crucial role in the carbon cycle. In this study, we collected sediment or sand samples from 34 bare tidal flats in China and investigated the profile of culturable bacteria, selected three *Bacteroidota* for polyphasic taxonomic analysis and revealed their polysaccharide metabolic potential. Totally, we isolated 352 pure cultured bacteria and they mainly distributed in *Bacteroidota*, *Pseudomonadota*, *Bacillota*, and *Actinomycetota*. It is shown that the bare tidal flats contained a large number of potential novel species, mainly distributed in *Flavobacteriales* and *Cytophagales* within *Bacteroidota*. Three *Bacteroidota* strains, M17^T, M82^T, and M415^T, isolated from mudflat were selected for polyphasic taxonomic analysis. The 16S rRNA gene sequence similarity between strain M17^T and *Mangrovivirga cuniculi* KCTC 72349^T was 99.28%, and less than 90.09% with other species; strain M82^T shared the highest 16S rRNA gene sequence similarity of 97.85% with *Pontibacter litorisediminis* KCTC 52252^T, and less than 97.43% with other species; strain M415T had higher 16S rRNA gene sequence similarities with type species of genera *Eudoraea* (92.62-93.68%), *Zeaxanthinibacter* (92.02-92.91%), and *Muriicola* (92.21-92.83%). Phylogenetic analysis based on 16S rRNA gene sequences and single-copy orthologous clusters showed that strains M17^T and M82^T represent novel species within the genus *Mangrovivirga* and *Pontibacter*, respectively, and strain M415^T represents a novel species of a novel genus within the family *Flavobacteriaceae*. The potential in polysaccharide metabolism of all these three strains was analyzed by genomes. The analysis revealed that glycoside hydrolases and glycosyltransferases account for more than 70% of the total CAZymes.

Additionally, the numbers of polysaccharide utilization loci (PULs) and annotated CAZymes in *Cytophagales* spp. M17^T and M82^T were found to be higher than those in *Flavobacteriales* sp. M415^T. Highly specialized saccharolytic systems and the presence of numerous diversified CAZymes for obtaining energy through polysaccharide metabolism were speculated to help the three novel strains adapt to the utilization of both terrestrial and marine polysaccharides.

KEYWORDS

bare tidal flats, culturable bacteria, CAZymes, polysaccharide utilization loci, bacteroidota

1 Introduction

Tidal flats are located in the intertidal zone between the high- and low-tide levels (Murray et al., 2019; Wang et al., 2020b). Recent research showed that tidal flats occupy at least 127,921 km^2 globally, mainly distributed along the coast of Asia, especially China (Murray et al., 2019). Due to their unique geographical location and periodic changes in environmental factors such as salinity, temperature, dissolved oxygen, light intensity, tides, ocean currents, and human disturbance, tidal flats have become one of the most productive and vulnerable environments in the world (Underwood and Kromkamp, 1999; Mayor et al., 2018; Chang et al., 2022). At the same time, tidal flats play important roles in carbon sequestration (Howard et al., 2014; Sasmito et al., 2020), aquaculture (Ni et al., 2020), microbial diversity, and function research (Mayor et al., 2018; Perillo et al., 2018). Lots of studies mainly focused on the special vegetated tidal flats such as mangrove and salt marsh; however, the studies on bare tidal flats (also referred to unvegetated tidal flats) were relatively limited.

With the rapid development of high-throughput sequencing technologies, our understanding of microbial diversity, structure, and function in bare tidal flats has tremendously expanded in recent years (Gong et al., 2019; Zhang et al., 2021; Rinke et al., 2022). Microbial diversity in mudflats is extremely high and significantly varies with different substrates and depths, playing an essential role in organic matter catabolism and even carbon fixation (Molari et al., 2012; Choi et al., 2018; Gaubert-Boussarie et al., 2020; Mohapatra et al., 2021). The degradation and metabolism process involved by bacteria and archaea in bare tidal flats is an important part of the global cycle of carbon, nitrogen, phosphorus, sulfur, and other elements (Ettwig et al., 2010; Bauer et al., 2013), which has a profound impact on the content of atmospheric greenhouse gases and the rate of element cycling.

Although the well-known hypothesis said "only 1% of microbes are culturable" (Amann et al., 1995; Torsvik and Ovreas, 2002), more and more scientists believe that more than 1% of microbes can be culturable (Martiny, 2019; Steen et al., 2019). High-throughput sequencing technologies provide a comprehensive understanding of microbial diversity; pure culture of microorganisms is also of great importance, which can help us to elucidate the physiological mechanism and ecological function of microorganisms, as well as find new metabolic pathways and metabolites (Guo et al., 2006), such as *Bacteroidota* strains which play important roles in polysaccharide degradation, which account for roughly 75% of the annually renewable biomass (Lichtenthaler and Peters, 2004; Lapebie et al., 2019; Gavriilidou et al., 2020; McKee et al., 2021).

Marine representatives of the phylum *Bacteroidota* possess diverse enzyme repertoires and flexible polysaccharide metabolism, actively participating in numerous biogeochemical processes (Fernández-Gómez et al., 2013). Highly specialized bacterial strains of the phylum *Bacteroidota* exhibit prolific proliferation during phytoplankton blooms and serve as primary degraders of microalgal polysaccharides (Unfried et al., 2018). In phylum *Bacteroidota*, members of the family *Flavobacteriaceae* exhibit a high proportion and diversity of carbohydrate-active enzymes (CAZymes) within their polysaccharide utilization loci (PULs), which supports their ability to utilize a wide range of polysaccharides (Kappelmann et al., 2019). For instance, *Zobellia galactanivorans* Dsij^T has emerged as a model organism for studying polysaccharide degradation in marine flavobacteria (Barbeyron et al., 2016), *Z. amurskyensis* KMM 3526^T and *Z. laminariae* KMM 3676^T possess a relatively high proportion of CAZymes (accounting for 6.49% and 5.93% of all predicted coding sequences, respectively) and are specialized in the degradation of algal polysaccharides (Chernysheva et al., 2019). In this study, we investigated the culturable bacterial proportion in the sediments from 34 sampling stations of bare tidal flats, selected three novel *Bacteroidota* strains for polyphasic taxonomy, and further analyzed their potential in polysaccharide metabolism.

2 Materials and methods

2.1 Sample collection and strain isolation

All samples were collected by a self-made cylindrical plexiglass tube sampler, transferred into sterile sample tubes after being fully homogenized, stored in a 4°C–6°C incubator, and transported to the laboratory as soon as possible. The distribution of samples is presented in Figure 1. The particle size of the sediments was determined using a laser particle size analyzer, and the sediment types were classified according to the modification of Folk's

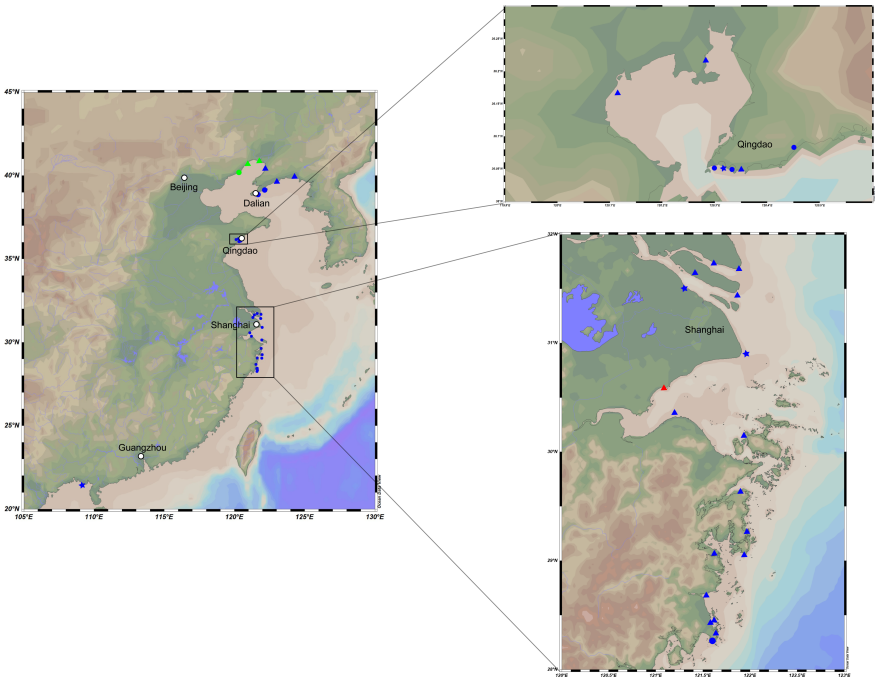

FIGURE 1
Map representing locations of the intertidal sediment sampling stations. Dots in these plots represent different substrate types and sample depths. Triangle, mud flat; circle, sand flat; star, muddy sand flat. Blue, 0–5-cm depth; red, 5–15-cm depth; green, 15–25-cm depth.

classification of sediments: sand (greater than 10% of particles with a diameter less than 63 μm), muddy sand (10%–90% of particles with a diameter less than 63 μm), and mud (less than 10% of particles with a diameter less than 63 μm) (Folk et al., 1970). Strain M17^T was isolated from an intertidal mudflat (0–5 cm) collected from Qingdao, Shandong Provence (36°10′ N, 120°07′ E); strains M82^T and M415^T were isolated from two intertidal mudflats (0–5 cm) collected from Taizhou, Zhejiang Provence (28°27′ N, 121°37′ E and 29°4′ N, 121°37′ E, respectively).

Samples were serially diluted to 10^{-3} with sterile seawater using the standard dilution-plating method (Williams and Davies, 1965). Generally, a 100-μL aliquot of each dilution was spread on modified marine agar (per liter of distilled water: Bacto yeast extract 0.1 g, Bacto peptone 0.5 g, ferric citrate 0.1 g, NaCl 19.45 g, $MgCl_2{\cdot}6H_2O$ 12.6 g, $MgSO_4$ 3.24 g, $CaCl_2$ 1.8 g, KCl 0.55 g, $NaHCO_3$ 0.16 g, KBr 0.08 g, $SrCl_2$ 34.0 mg, $NaSiO_3$ 4.0 mg, NH_4NO_3 1.6 mg, H_3BO_4 22.0 mg, NaF 2.4 mg, Na_2HPO_4 8.0 mg, agar 20 g) and incubated at 30°C for 3–7 days to a simulated oligotrophic environment. Afterward, the strains were isolated from different plates and purified by repeating streaking. All bacterial cultures were stored in Marine Broth 2216 (MB) medium containing 25% glycerol at −80°C. Six type strains, namely, *Mangrovivirga cuniculi* KCTC 72349^T, *Pontibacter actiniarum* KCTC 12367^T, *Pontibacter litorisediminis* KCTC 52252^T, *Poritiphilus flavus* MCCC 1K03853^T, *Eudoraea chungangensis* KCTC 42048^T, and *Zeaxanthinibacter enoshimensis* NBRC 101990^T, were purchased from the Korean Collection for Type Cultures (KCTC), the Marine Culture Collection of China (MCCC), and the NITE Biological Resource Center (NBRC), and used as reference strains in this study.

2.2 Morphological, physiological, and chemotaxonomic characteristics

Strains M17^T, M82^T, and M415^T were cultured on Marine Agar (MA) medium for 3 days to observe their morphological characteristics, including colonial size, shape, edge, bulge, transparency, and color characteristics. Cell morphology, size, and special structure were examined using a transmission electron microscope (JEM-1230; JEOL). Gram staining reaction was performed according to the method described by Dong and Cai (Dong and Cai, 2001). Motility of the strains was assessed in semisolid MB medium containing 0.5% agar. The growth range and optimum temperature of the strains were determined in MB medium at 4°C, 10°C, 20°C, 25°C, 28°C, 30°C, 37°C, 40°C, 45°C, and 50°C, whereas their growth and optimal pH range were measured by adding appropriate buffer (40 mM) to MB medium (0.5 pH unit intervals), which include MES (pH 5.0–5.5), MOPS (pH 6.0–7.5), Tricine buffers (pH 8.0–8.5), and CAPSO (pH 9.0–10.0). By adding 0%, 0.5%, 1%, 1.5%, 2%, 2.5%, 3%, 3.5%, 4%, 6%, 8%, 10%, and 12% (w/v) NaCl to saltness-MB medium, the growth and optimal salinity range were determined. The optimal growth conditions and growth range were determined after 3 days and 1 month of culture, respectively. The growth condition of the strains was measured using a UV/visible spectrophotometer (Ultrospec 6300 Pro, Amersham Biosciences) at OD_{600}.

Sodium nitrate (20 mM) was used as a potential electron acceptor to assess the anaerobic growth of strains in the anaerobic system (AnaeroPack-MicroAero, 2.5 L, MGC, Japan) (Shi et al., 2017). Catalase activity was measured by dripping 3%

(v/v) hydrogen peroxide solution to the colonies placed on sterile slides. Oxidase activity was determined by observing whether the cell color turned red within 1 min after dripping 1% *p*-amino dimethylaniline oxalate solution. Carotenoid was extracted by acetone/methanol (7:2, v/v) solution, and their absorption spectra were determined using a scanning UV/visible spectrophotometer (Bowman and Nichols, 2005). Strains were cultured in suitable medium containing sodium thiosulfate (5 g/L), and their hydrogen sulfide production capacity was determined using sterile filter strips soaked in the solution of lead acetate. Amylase, cellulase, and hydrolysis of Tweens 20, 40, 60, and 80 were carried out according to the previously described methods (Liu et al., 2019). Carbon source oxidation was tested using Biolog GEN III MicroPlates, and activity of other common bacterial enzymes was examined using the API ZYM kit. Other physiological characteristics of the strains were analyzed using the API 20NE kit. All of the BIOLOG and API tests were carried out according to the manufacturer's instructions except for adjusting salinity to 2%.

Strains M17^T, M82^T, and M415^T and the six type strains were cultured on MB medium under optimal conditions, and the cells at the end of exponential growth stage were collected for chemotaxonomic analysis. Bacteria were collected and freeze-dried, then saponified, methylated, extracted, and washed to obtain the bacterial fatty acids (Sasser, 1990). Identification and quantification of the extracted cellular fatty acids of these strains were performed using a gas chromatograph (Agilent G6890N) and the Sherlock Microbial Identification System (MIDI database: Version 6.0). Polar lipids were extracted according to the procedure described by Minnikin et al. (1984), and composition analysis was performed on silica gel 60 F254 plates (10 × 10 cm, Merck) (Komagata and Suzuki, 1988). Isoprenoid quinones were extracted by a mixture of chloroform:methanol (2:1 v/v), and the further identification was performed by the HPLC-MS system.

2.3 16S rRNA gene sequence similarities and phylogenetic analysis

A total of 352 strains were isolated from 34 sampling stations. The 16S rRNA gene was amplified by PCR using the universal primers 27F/1492R and sequenced by Guangdong Magigene Biotechnology Co., Ltd. (Guangzhou, China). The sequences were submitted to NCBI under the accession numbers OQ617539–OQ617890. The complete 16S rRNA gene sequences of strains M17^T, M82^T, and M415^T were extracted from their draft genomes. The similarities of all 16S rRNA gene sequences were identified by aligning these sequences against the National Center for Biotechnology Information (NCBI) database (https://www.ncbi.nlm.nih.gov/) and the EzBioCloud database (https://www.ezbiocloud.net/).

The 16S rRNA gene sequence alignment of strains M17^T, M82^T, and M415^T and their phylogenetically related taxa were performed by the ClustalW algorithm within MEGA11 v11.0.13 (Tamura et al., 2021), and the phylogenetic trees were reconstructed by the neighbor-joining (NJ), maximum-parsimony (MP), and maximum-likelihood (ML) algorithms within the MEGA11 software (Felsenstein, 1981; Saitou and Nei, 1987). The robustness of phylogenetic trees was assessed through bootstrap analysis based on 1,000 replications.

2.4 Genome sequencing and analysis

The genomes of strains M17^T, M82^T, and M415^T were extracted using a bacterial genomic DNA kit (Takara), and draft genomes were sequenced using the Illumina NovaSeq 6000 platform (PE150) in Guangdong Magigene Biotechnology Co., Ltd. (Guangzhou, China). The sequences were assembled using SPAdes v3.10.1 (Zou et al., 2020), and the completeness and contamination of the assembled draft genomes were accessed using CheckM v1.1.3 (Parks et al., 2015).

Phylogenomic analysis based on single-copy orthologous clusters (OCs) of strains M17^T, M82^T, and M415^T and the related type strains were performed as described (Xu et al., 2018). Briefly, the orthologous clusters were filtered based on the blastp+ program and 50% sequence identity using Proteinortho v5.16 (Lechner et al., 2011), and their formats were converted into OrthoMCL for subsequent analysis. The single-copy orthologous clusters were aligned through MAFFT v7.310 (Katoh and Standley, 2013), and the aligned sequences were concatenated after further refining by trimAL v1.4.1 (Capella-Gutierrez et al., 2009). The IQ-TREE v1.6.2 software was used to predict the best-fit models. The phylogenetic trees were constructed by maximum-likelihood algorithms based on the concatenated aligned single-copy orthologous clusters (Lam-Tung et al., 2015), and the best-fit models of strains M17^T, M82^T, and M415^T were LG+F+R6, LG+F+R5, and LG+F+R8, respectively. Finally, MEGA11 software was employed to visualize the phylogenetic trees.

Functional and metabolic pathway predictions were realized by Kyoto Encyclopedia of Genes and Genomes (KEGG) and Evolutionary Genealogy of Genes with enhanced Non-supervised Orthologous Groups (EggNOG) (Kanehisa et al., 2017; Hernández-Plaza et al., 2023). The Average Nucleotide Identity (ANI) was calculated using the online ANI calculator based on the OrthoANIu algorithm, which is an improved iteration of the original OrthoANI algorithm (Yoon et al., 2017). Digital DNA–DNA hybridization (dDDH) and Two-way Average Amino Acid Identity (AAI) were calculated through Genome-to-Genome Distance Calculator 3.0 and the AAI calculator, respectively (Rodriguez-R and Konstantinidis, 2014; Meier-Kolthoff et al., 2022).

As for the potential in polysaccharide metabolism of strains M17^T, M82^T, and M415^T, carbohydrate-active enzymes (CAZymes) were predicted by the HMMER tools within dbCAN2 software based on Carbohydrate-Active enZYmes Database V11 (CAZy database), and SusC/D-like proteins (SusC, outer membrane TonB-dependent transporter; SusD, surface glycan-binding protein) and other auxiliary proteins and genes were predicted and annotated using PROKKA v1.12 and Rapid Annotation using Subsystem Technology (RAST) version 2.0 (Aziz et al., 2008; Seemann, 2014; Zhang et al., 2018; Drula et al., 2022). The PUL prediction relies on the identification in each genome of the PUL markers: the presence of adjacent genes encoding SusC/D-like proteins, and according to the position of CAZymes and SusC/D-

like proteins in the genome, combined with the position of corresponding auxiliary proteins and genes (Terrapon et al., 2015). In addition, the substrates of these PULs were predicted by searching through the PUL database (PULDB) and BLAST the CAZymes through UniProt (Terrapon et al., 2018; Consortium, 2019).

3 Results and discussion

3.1 Diversity of culturable bacteria in bare tidal flats

The sampling stations are widely distributed in the bare tidal flats of China. The samples from 34 sampling stations were used for the isolation of strains (Figure 1). A total of 352 bacterial strains were isolated. Compared with the 16S rRNA gene sequences with validly published species, the isolates were assigned to 180 species, belonging to 4 phyla, 7 classes, 22 orders, 37 families, and 94 genera; among them, 126 species and 52 genera had only one isolate (Table 1 and Figure 2). In our study, a higher number of species were discovered among the culturable strains compared with mangrove sediments (116 pure culture strains distributed in 13 species, 1 sample; Sefrji et al., 2022), plant rhizosphere (59 pure culture strains distributed in 22 species, 4 samples; Brígido et al., 2019), and Tabernas Desert (236 strains distributed in 37 genera, 3 samples; Molina-Menor et al., 2021); our results showed that bare tidal flats had a greater diversity of culturable bacteria. *Flavobacteriales* and *Bacillales* represented two most abundant orders, accounting for approx. 50% of the total isolates (Figure 3). A total of 17 strains were identified as *Fictibacillus phosphorivorans*, which was widely distributed in 12 sampling stations located in the different areas such as Jiangsu Province, Zhejiang Province, Guangxi Zhuang Autonomous Region, and Shanghai City. It became the most abundant and widely distributed culturable species in this study. Recent studies showed that *Fictibacillus phosphorivorans* was able to produce biosurfactant and displayed high nematicidal capability against root-knot nematodes (RKNs), which could infect almost all crops and lead to huge economic losses in agriculture around the world (Zheng et al., 2016; Pandey et al., 2021).

In addition, the effects of different depths and substrates on culturable bacteria were compared (Table 1). *Actinomycetota* strains, a total of 13 species in 5 orders, were isolated only in 0–5-cm non-sandy sediment, some of which were reported to have great ecological functions and economic values; e.g., strains of *Rhodococcus qingshengii* and *Brachybacterium paraconglomeratum* have the ability to repair heavy metal pollution (Du et al., 2022; Harboul et al., 2022) and pesticide contamination (Chuang et al., 2021; Wang et al., 2021), strains of *Arthrobacter pascens*, known as indole-3-acetic acid (IAA)-producing bacteria, could regulate plant growth and development (Li et al., 2021), and strains of *Cellulosimicrobium cellulans* are able to produce ginsenoside Rg3, a known anticancer agent (Hu et al., 2019). Different from *Actinomycetota* species, *Pseudomonadota* species *Psychrobacter nivimaris* was the only species distributed in all three types of sediment (Supplementary Figure 1), and strains in it may have the ecological function of repairing heavy metal pollution (Staloch et al., 2022).

In addition, a large number of novel species were discovered in bare tidal flats; a total of 47 strains showed less than 98.65% sequence similarities of the 16S rRNA gene with validly published species and may represent novel species (Kim et al., 2014). Most of them were assigned to *Cytophagales* and *Flavobacteriales*, both of which belong to the phylum *Bacteroidota*, with ratios of 46.2% and 30.2%, respectively. Three *Bacteroidota* strains (M17^T, M82^T, and M415^T) were chosen for further phylogenetic and functional characterization.

3.2 Morphological, physiological, and chemotaxonomic characteristics

The morphological observations by transmission electron microscopy showed that the cells of strains M17^T, M82^T, and M415^T were slender and long (2.0–10.0 μm × 0.3–0.5 μm), ellipsoidal to ovoid (0.9–3.2 μm × 0.6–1.1 μm), and slender and long (1.8–8.0 μm × 0.3–0.5 μm), respectively (Supplementary Figure 2 - Figure 4). For strain M17^T, after 3 days of cultivation, the colony was round, 1–3 mm in diameter, and orange in color; mobility was not observed in the semisolid MB medium; and anaerobic growth and carotenoid production were not detected. The colony of M82^T was round, 1–2 mm in diameter, and red in color after 3 days of incubation; mobility was not observed in the semisolid MB medium; and anaerobic growth and carotenoid production were both observed. The colony of M415^T was round, 0.5 mm in diameter, and orange in color; mobility was not observed; and anaerobic growth and carotenoid production were detected. All

TABLE 1 Taxonomic profile of isolates in different depths and substrates.

Depth	Phylum	Class	Order	Family	Genus	Species	Strains
0–5 cm	4	7	22	37	88	165	295
5–15 cm	3	5	6	7	8	10	10
15–25cm	3	4	9	9	17	21	47
Substrate							
Mud	4	7	20	32	74	136	254
Sand	3	4	10	14	30	42	64
Muddy sand	4	5	11	13	21	26	34

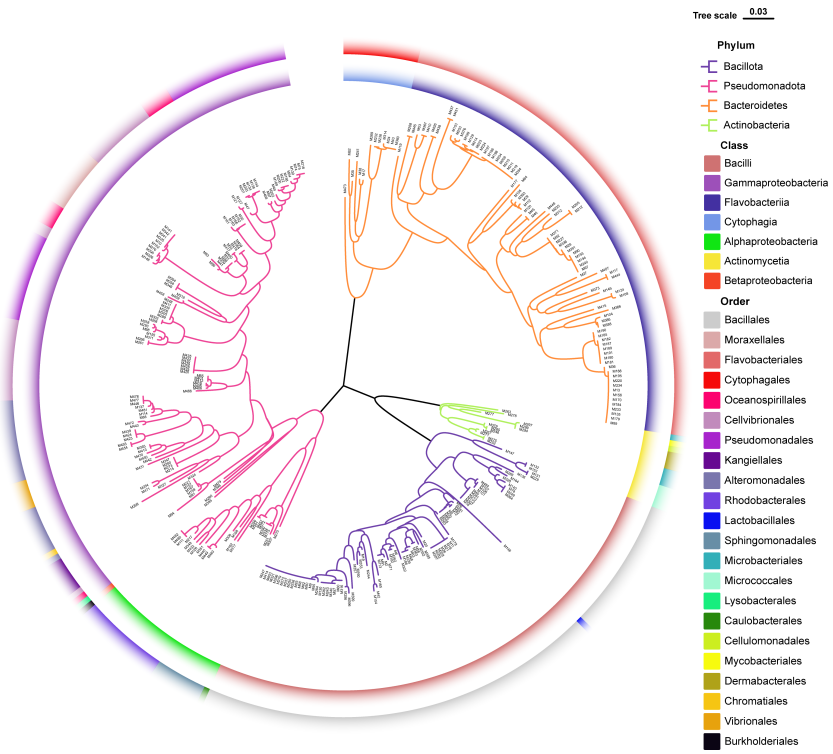

FIGURE 2
Diversity of culturable bacteria from unvegetated tidal flats of China. Neighbor-joining phylogenetic tree reconstructed from 16S rRNA gene sequences of 352 pure culture isolates. Branches in different colors represent different bacterial phyla; colors on the inner ring refer to bacterial classes; and colors on the outer ring refer to bacterial orders.

the three strains were positive in the oxidations of D-fucose, L-galactonic acid lactone, D-glucuronic acid, glucuronamide, and tetrazolium violet. Detailed differences between strains M17^T, M82^T, and M415^T and reference strains are summarized in Table 2 and Supplementary Table 1.

The major respiratory quinone of strains M17^T and M82^T was MK-7, which is consistent with their reference strains *Mangrovivirga cuniculi* KCTC 72349^T, *Pontibacter actiniarum* KCTC 12367^T, and *Pontibacter litoriseditiminis* KCTC 52252^T. The major respiratory quinone of strain M415^T was MK-6, identical with that of

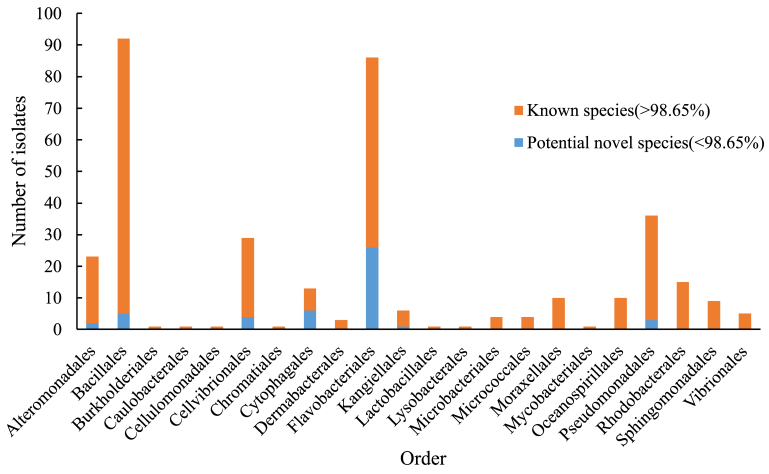

FIGURE 3
Number of isolates in different orders. Blue bar, the number of potential novel species in each order (16S rRNA gene similarity < 98.65%). Orange bar, the number of identified isolates in each order (16S rRNA gene similarity > 98.65%).

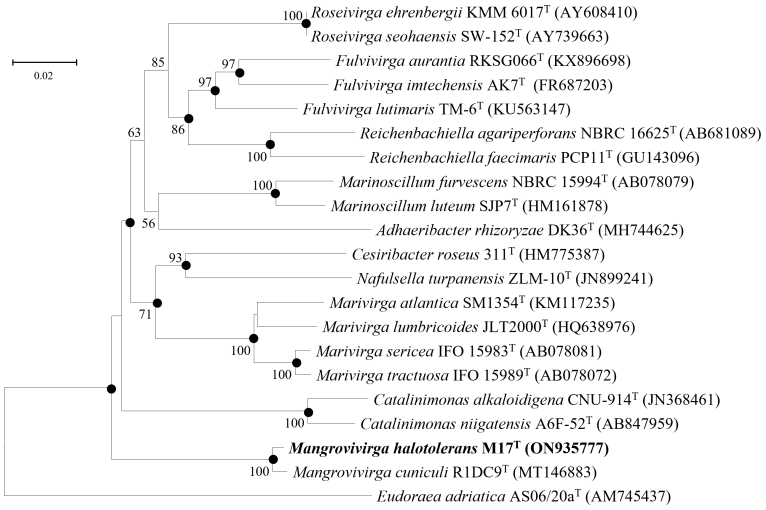

FIGURE 4
Neighbor-joining phylogenetic tree reconstructed from 16S rRNA gene sequences of strains M17^T and related species. Bootstrap values <50% (based on 1,000 replications) are not shown. Filled circles indicate branches that were also recovered using maximum-likelihood and maximum-parsimony methods. *Eudoraea adriatica* AS06/20a^T (AM745437) was used as the outgroup; bar, 0.02 nt substitutions per nucleotide position.

TABLE 2 Differential phenotypic characteristics between strains M17^T, M82^T, and M415^T and their reference strains.

Characteristics	1	2	3	4	5	6	7	8	9
Colony color*	O	R	O	O	O	O	Y	Y	Y
Temp. range (°C)	20-45	20-40	25-37	20-40[a]	6-43[b]	10-45[c]	16-40[d]	20-30[e]	15-33[f]
pH range	6.5-9	6-9	6-8	6-10[a]	NA	5.5-9[c]	5.5-11[d]	6.5-8.5[e]	6-10[f]
NaCl conc. (%)	0.5-10	0-8	1-4	3-11[a]	0-10[b]	0-8[c]	0-8[d]	2-6[e]	2-8[f]
Nitrate reduction	–	–	–	–	+	–	–	+	–
Oxidase	+	+	+	+	+	+	–	+	+
Enzyme activity:									
Chymotrypsin	+	+	+	+	w	+	+	–	+
α-Galactosidase	–	+	–	–	–	+	w	–	+
β-Galactosidase	–	w	–	–	–	+	+	–	+
β-Glucuronidase	+	–	–	+	–	–	+	–	–
α-Glucosidase	–	+	w	–	+	+	+	–	+
β-Glucosidase	+	+	+	w	–	+	+	–	+
N-Acetyl-glucosaminidase	+	+	+	–	+	+	+	+	+
α-Mannosidase	–	–	–	–	–	+	+	–	w
Hydrolysis of:									
Tween 20	–	–	–	–	+	–	–	–	–
Tween 40	–	–	–	–	–	–	w	–	+
Tween 60	–	–	–	–	–	–	+	–	+
Tween 80	–	–	–	+	+	–	+	–	–
Starch	+	–	w	+	–	–	w	+	+

(Continued)

TABLE 2 Continued

Characteristics	1	2	3	4	5	6	7	8	9
Oxidation of:									
D-Maltose	–	+	+	–	+	+	–	–	+
D-Cellobiose	–	+	+	–	+	+	–	–	+
Sucrose	w	+	+	–	–	w	–	–	+
α-D-Lactose	w	+	–	+	–	+	–	–	+
D-Salicin	–	+	+	–	–	+	–	–	+
N-Acetyl-D-glucosamine	–	+	+	–	+	+	–	–	+
L-Fucose	–	+	w	+	–	+	+	+	+
Fusidic acid	+	+	+	–	–	–	+	+	+
D-Glucose-6-PO_4	–	+	+	–	+	–	–	–	w
D-Galacturonic acid	w	+	w	+	+	+	+	+	+
Tetrazolium blue	–	+	–	+	–	–	+	+	–
Bromo-succinic acid	w	–	+	–	+	–	+	+	+
Acetoacetic acid	+	+	–	–	+	+	+	+	+
Acetic acid	+	+	–	–	+	+	–	–	–
Formic acid	+	+	–	–	–	–	–	w	–
Sodium butyrate	+	+	+	–	–	+	+	+	+

Strains: 1, M17^T; 2, M82^T; 3, M415^T; 4, Mangrovivirga cuniculi KCTC 72349^T; 5, Pontibacter actiniarum KCTC 12367^T; 6, Pontibacter litorisediminis KCTC 52252^T; 7, Zeaxanthinibacter enoshimensis NBRC 101990^T; 8, Eudoraea chungangensis KCTC 42048^T; 9, Poritiphilus flavus MCCC 1K03853^T. All data were obtained from this study unless stated otherwise. +, positive reaction; w, weakly positive reaction; -, negative reaction; NA, data not available. *Colony color in orange, red, and yellow are abbreviated as O, R, and Y, respectively. All strains are positive for the following characteristics: catalase, alkaline phosphatase, esterase (C4), esterase lipase (C8), leucine arylamidase, valine arylamidase, cystine arylamidase, trypsin, acid phosphatase, and naphthol-AS-BI-phosphohydrolase. All strains are negative for the following characteristics: Gram-staining, H_2S production, lipase (C14).
Data taken from the following: a, Sefrji et al. (Sefrji et al., 2021); b, Nedashkovskaya et al. (Nedashkovskaya et al., 2005); c, Park et al. (Park et al., 2016); d, Asker et al. (Asker et al., 2007); e, Siamphan et al. (Siamphan et al., 2015); f, Wang et al. (Wang et al., 2020a).

Poritiphilus flavus MCCC 1K03853^T, *Eudoraea chungangensis* KCTC 42048^T, and *Zeaxanthinibacter enoshimensis* NBRC 101990^T.

The main polar lipids of strain M17^T were phosphatidylethanolamine (PE), aminoglycolipid (AGL), one unidentified phospholipid (PL), three unidentified aminolipids (ALs), three unidentified glycolipids (GLs), and six unidentified lipids (L1–6) (Supplementary Figure 5). Compared with its reference strain *M. cuniculi* KCTC 72349^T, they both contained PE as main polar lipids, but strain M17^T comprised more polar lipids such as AGL, ALs, and GLs. The major polar lipids of strain M82^T were PE, two ALs, and nine unidentified lipids (L1–9), in which PE and plenty of unidentified lipids were also detected in other species of the genus *Pontibacter* (Nedashkovskaya et al., 2005; Zhang et al., 2008; Subhash et al., 2013; Park et al., 2016). The major polar lipids detected in M415^T were PE, phosphoglycolipid (PGL), aminophospholipid (APL), one GL, two ALs, and five unidentified lipids (L1–5).

Similar to *M. cuniculi* KCTC 72349^T, iso-$C_{15:0}$ and iso-$C_{17:0}$ 3-OH were the main cellular fatty acids (>10%) in strain M17^T. Meanwhile, strain M82^T contained iso-$C_{15:0}$ and summed feature 4 (SF4) as the major cellular fatty acids (>10%), which was also found in its reference strains. However, some differences in the ratio of main fatty acids (such as iso-$C_{15:0}$) existed between the two novel isolates and their reference strains (Table 3). Similar to its reference strains, strain M415^T contained iso-$C_{15:0}$ and iso-$C_{17:0}$ 3-OH as the main cellular fatty acids, but the relatively higher ratio of iso-$C_{15:1}$ -G and the lower ratio of summed feature 3 (SF3) differed strain M415^T from its reference strains (Table 3).

3.3 Phylogenetic analysis and genomic properties

The 16S rRNA gene sequences between strain M17^T and *M. cuniculi* KCTC 72349^T shared the highest similarity of 99.28%, and less than 90.09% with other species (Table 4). In both of the phylogenetic trees based on the 16S rRNA gene and single-copy orthologous clusters (concatenated protein sequences), strain M17^T formed a closest and robust cluster with *M. cuniculi* KCTC 72349^T (Figure 4 and Supplementary Figure 6), indicating that strain M17^T was affiliated with the genus *Mangrovivirga*. Although sequence similarity of the 16S rRNA gene reached 99.28% between strains M17^T and *M. cuniculi* KCTC 72349^T, the dDDH, ANI, and AAI values between strain M17^T and *M. cuniculi* KCTC 72349^T were 57.9%, 84.0%, and 88.8%, respectively (Table 4), all lower than the thresholds for species delimitation (Konstantinidis and Tiedje, 2005; Tindall et al., 2010; Kim et al., 2014), indicating that strain M17^T

10.3389/fmars.2023.1222157

TABLE 3 Cellular fatty acid composition of strains M17^T, M82^T, and M415^T and their reference strains.

Fatty acid	1	2	3	4	5	6	7	8	9
Saturated straight chain:									
$C_{12:0}$	TR	–	1.9	TR	–	–	–	–	–
$C_{14:0}$	TR	–	1.3	TR	–	–	TR	TR	TR
$C_{16:0}$	TR	TR	2.5	TR	TR	TR	3.1	3.6	4.5
$C_{18:0}$	–	TR	1.7	–	TR	TR	–	–	–
Saturated branched chain:									
iso-$C_{11:0}$	3.4	–	–	3.3	–	–	–	–	–
iso-$C_{13:0}$	1.2	TR	–	TR	TR	–	–	TR	TR
iso-$C_{15:0}$	43.3	25.8	22.7	35.7	32.2	22.3	24.9	18.7	25.1
anteiso-$C_{15:0}$	0.3	TR	TR	TR	TR	TR	3.8	3.2	0.4
iso-$C_{16:0}$	4.6	3.4	5.1	4.1	TR	TR	4.4	TR	1.0
iso-$C_{17:0}$	1.5	2.7	TR	1.5	5.5	2.6	TR	TR	TR
Unsaturated branched chain:									
iso-$C_{15:1}$ -G	9.9	–	24.4	10.9	–	–	7.0	13.0	14.1
iso-$C_{16:1}$ -G	1.0	–	1.2	TR	–	–	–	–	–
iso-$C_{16:1}$ -H	–	2.7	–	–	TR	TR	1.2	–	–
$C_{16:1}$ ω5c	6.2	–	–	4.7	–	3.2	–	–	–
$C_{17:1}$ ω6c	–	2.0	–	–	1.1	2.0	1.5	TR	–
$C_{17:1}$ ω8c	–	–	–	–	–	TR	1.3	TR	–
$C_{18:1}$ ω9c	0.4	1.2	–	TR	1.2	1.0	TR	TR	TR
Hydroxylated:									
iso-$C_{15:0}$ 3-OH	4.1	3.7	6.8	5.3	4.4	3.0	3.6	6.7	6.2
$C_{15:0}$ 2-OH	–	–	–	–	–	–	TR	1.2	TR
$C_{15:0}$ 3-OH	–	–	–	–	–	–	–	1.7	–
$C_{16:0}$ 3-OH	2.8	–	TR	3.7	–	–	TR	2.7	2.2
iso-$C_{16:0}$ 3-OH	1.2	TR	8.6	1.0	TR	TR	4.3	2.7	1.5
$C_{17:0}$ 2-OH	–	TR	–	–	–	TR	1.2	TR	TR
iso-$C_{17:0}$ 3-OH	10.7	10.7	16.4	15.0	10.2	7.9	15.3	14.9	29.9
Summed feature [a]:									
1	–	3.6	–	–	2.1	2.5	–	–	–
3	3.6	7.1	3.5	4.8	12.9	7.7	8.1	20.8	10.9
4	3.7	31.2	–	4.9	26.1	39.9	–	–	–
9	–	TR	–	–	1.1	1.8	13.5	3.3	–

Strains: 1, M17^T; 2, M82^T; 3, M415^T; 4, Mangrovivirga cuniculi KCTC 72349^T; 5, Pontibacter actiniarum KCTC 12367^T; 6, Pontibacter litorisediminis KCTC 52252^T; 7, Zeaxanthinibacter enoshimensis NBRC 101990^T; 8, Eudoraea chungangensis KCTC 42048^T; 9, Porithiphilus flavus MCCC 1K03853^T. All data were obtained from this study unless stated otherwise. Fatty acids representing trace amounts or not detected in all strains are not shown. TR, Trace amount (<1%); -, not detected; Fatty acids more than 10% of total were indicated in bold.

[a]Summed features represent groups of two or three fatty acids that could not be separated by GLC using the MIDI system. Summed feature 1 contains $C_{13:0}$ 3-OH and/or iso-$C_{15:1}$ H; summed feature 3 contains $C_{16:1}$ ω6c and/or $C_{16:1}$ ω7c; summed feature 4 contains ante-iso-$C_{17:1}$ B and/or iso-$C_{17:1}$ I; summed feature 9 contains iso-$C_{17:1}$ ω9c.

represents a new species within the genus *Mangrovivirga*. In addition, the cell morphology of the strain *M. cuniculi* KCTC 72349^T was short rod-shaped (1.0–1.2 μm × 0.3–0.5 μm; Sefrji et al., 2021), which was different from that of strain M17^T, showing a long rod shape (2.0–10.0 μm × 0.3–0.5 μm; Supplementary Figure 2). In addition, there were also a great number of differences between them in phenotypic and genomic properties (Tables 2-5). Therefore, strain M17^T represents a novel species of the genus *Mangrovivirga*.

TABLE 4 16S rRNA gene sequence similarities, digital DNA-DNA hybridization (dDDH), Average Nucleotide Identity (ANI), and Average Amino acid Identity (AAI) of strains M17^T, M82^T, and M415^T and their related type strains.

Reference genome	16S rRNA (%)	dDDH (%)	ANI (%)	AAI (%)
M17^T				
Mangrovivirga cuniculi KCTC 72349^T	99.28	57.9	83.97	88.82
Roseivirga spongicola JCM 13337^T	90.09	12.6	66.96	50.29
Marivirga sericea ATCC 23182^T	90.08	12.6	67.28	50.95
M82^T				
Pontibacter litorisediminis KCTC 52252^T	97.85	35.6	81.08	84.22
Pontibacter korlensis X14-1^T	97.43	23.2	77.89	82.1
Pontibacter actiniarum KCTC 12367^T	96.59	24.1	78.85	80.17
M415^T				
Eudoraea chungangensis KCTC 42048^T	93.68	13.2	68.84	66.94
Robiginitalea biformata KCTC 12146^T	93.08	12.9	69.08	65.37
Zeaxanthinibacter enoshimensis NBRC 101990^T	92.91	13	69.69	67.31
Eudoraea adriatica DSM 19308^T	92.62	13.5	69.43	69.35
Poritiphilus flavus MCCC 1K03853^T	92.44	13.1	70.23	68.33

Strain M82^T shares the highest 16S rRNA gene sequence similarity of 97.85%, 97.43%, and 96.59%, respectively, with *Pontibacter litorisediminis* KCTC 52252^T, *Pontibacter korlensis* X14-1^T, and *Pontibacter actiniarum* KCTC 12367^T, lower than the threshold for species delimitation (Kim et al., 2014). Based on the phylogenetic analysis of 16S rRNA gene sequences and single-copy orthologous clusters, strain M82^T was closely clustered within *Pontibacter* strains (Figure 5 and Supplementary Figure 7). The highest values of dDDH, ANI, and AAI between strain M82^T and the type strains within the genus *Pontibacter* were 35.6%, 81.1%, and 84.2%, respectively, which are lower than the thresholds of species delimitation (Table 4).

Low 16S rRNA gene sequence similarities were found between strain M415^T and its type species of the genera *Eudoraea* (92.62%–93.68%), *Zeaxanthinibacter* (92.02%–92.91%), *Muriicola* (92.21%–92.83%), *Robiginitalea* (91.48%–92.74%), and *Poritiphilus* (92.44%). Phylogenetic analysis based on 16S rRNA gene sequences and single-copy orthologous clusters showed that strain M415^T was clearly separated from the related genera (Figure 6 and Supplementary Figure 8), representing a novel species of a new genus within the family *Flavobacteriaceae*. The highest values of dDDH, ANI, and AAI between strain M415^T and its related species were 13.5%, 70.2%, and 69.4%, respectively (Table 4).

The genomic features of strains M17^T, M82^T, and M415^T and their related strains were analyzed to further confirm the taxonomic status of these three novel strains (Table 5). Strain M17^T showed a similar genome size and GC content with *M. cuniculi* KCTC 72349^T, but the latter has more protein-coding genes and obvious multicopy of the rRNA gene than strain M17^T. The genomic composition of strain M82^T was different from the related species, showing a higher GC content and a lower number of rRNA. Strain M415^T has the smallest genome size and the lowest protein-coding gene number, compared with its related species. According to the annotation result against the COG database, the most abundant category in strains M17^T and M82^T was cell wall/membrane/envelope biogenesis; however, in strain M415^T, it changed to amino acid transport and metabolism (Supplementary Figure 9). The genome sequences of strains M17^T, M82^T, and M415^T were annotated against the KEGG database and 1,614 (39.43%), 1,775 (44.55%), and 1,368 (47.14%) genes were assigned to putative functions, respectively. These functions were mainly composed of carbohydrate metabolism, genetic information processing, signaling and cellular processing, and amino acid metabolism, and notably, strain M82^T contained much more function genes associated with energy metabolism and environmental information processing (Supplementary Figure 10).

As indicated by KEGG pathway annotation, these three strains have many differences in metabolic pathways. As for sulfur metabolism, the assimilatory sulfate reduction (M00176) was devoid only in strain M415^T. In the lipid metabolism, phosphatidylcholine (PC) biosynthesis (M00091) was only found in strain M82^T; nevertheless, strain M82^T and strain M415^T both contained the threonine biosynthesis (M00018) which was not found in strain M17^T. In the metabolism of major nutrients, the complete β-oxidation pathway only existed in strain M17^T; the phosphate acetyltransferase-acetate kinase pathway was complete in strains M17^T and M415^T but incomplete in strain M82^T (Figure 7). In addition, we also found that the glyoxylate cycle was presented in both strains M17^T and M82^T but not in strain M415^T (Figure 7); the activation of the glyoxylate cycle could provide malic acid and

10.3389/fmars.2023.1222157

TABLE 5 Genomic statistics of strains M17^T, M82^T, and M415^T and their related type strains.

	1	2	3	4	5	6	7	8	9	10	11	12	13	14
Genome size (MB)	4.67	4.64	3.13	4.66	4.48	4.74	5.00	5.46	4.97	3.73	3.53	3.34	3.91	4.99
Completeness (%)	99.7	100	99.33	98.74	99.05	100	100	99.7	99.97	98.68	99.01	99.34	99.28	99.67
G+C content (%)	35.9	50.6	44.6	36.1	40.2	36.0	53.2	47.3	53.2	37.2	55.3	46.4	38.3	44.5
Genes (no.)	4,093	3,984	2,902	4,303	4,021	4,127	4,350	4,768	4,411	3,322	3,158	2,970	3,528	4,282
tRNA genes (no.)	38	43	39	43	40	41	43	49	51	36	41	38	37	40
rRNA genes (no.)	3	3	3	12	3	7	5	12	15	3	6	3	5	3
GenBank ID	JAPFQN00	JAPFQO00	JAPFQP00	CP028923	LRPC01	FXAW01	JARDUA00	CP009621	AXBP01	JARDUB00	CP001712	SNYI00	ARNE01	WXYO00

Strains: 1, M17^T; 2, M82^T; 3, M415^T; 4, Mangrovivirga cuniculi KCTC 72349^T; 5, Roseivirga spongicola JCM 13337^T; 6, Marivirga sericea ATCC 23182^T; 7, Pontibacter litoriseditinis KCTC 52252^T; 8, Pontibacter korlensis X14-1^T; 9, Pontibacter actiniarum KCTC 12367^T; 10, Eudoraea chungangensis KCTC 42048^T; 11, Robiginitalea biformata KCTC 12146^T; 12, Zeaxanthinibacter enoshimensis NBRC 101990^T; 13, Eudoraea adriatica DSM 19308^T; 14, Porifiphilus flavus MCCC 1K03853^T.

NADH, which serve as precursors and energy sources for metabolic reactions to sustain cell survival under stress conditions (Schroeter et al., 2011; Yuan et al., 2019). Therefore, the existence of the glyoxylate cycle for resisting the stress condition in tidal flats might indicate the adaptation mechanism of strains M17^T and M82^T to such environment.

3.4 The potential in polysaccharide metabolism

Considering the outstanding polysaccharide metabolic abilities of marine *Bacteroidota* (Krüger et al., 2019), especially *Flavobacteriaceae* strains (Kappelmann et al., 2019; Gavriilidou et al., 2020), and special geographical location of mudflats—the source of strains M17^T, M82^T, and M415^T, we further analyzed their CAZyme profiles and potential polysaccharide substrates. The result showed that strains M17^T, M82^T, and M415^T had 114, 155, and 103 CAZymes, respectively (Figure 8A), which were similar as the KEGG results, where 157, 175, and 153 genes for the carbohydrate metabolism pathway were detected, respectively. The detailed numbers of each CAZyme family presented in three strains are summarized in Supplementary Table 2. GH and GT were the most abundant CAZyme classes, accounting for more than 70% of the total CAZymes; this finding was consistent with studies on carbohydrate-active enzymes in *Flavobacteriaceae* species by Gavriilidou et al., which also indicated that GH and GT were the most abundant CAZyme classes (Gavriilidou et al., 2020). Strain M82^T comprised the highest number of CAZymes assigned to different classes and SusC/D-like proteins, indicating that it may have great potential in polysaccharide metabolism. However, the CAZyme count per Mb genome in strain M415^T was similar with strain M82^T and much higher than that in strain M17^T, even though the total number of CAZymes of strain M415^T was smaller than strains M17^T and M82^T due to the smallest genome size of strain M415^T (Figure 8B). A great number of GT2 and GT4 were present in strain M415^T, and they were involved in critical glycan synthesis, such as cellulose, chitin, and mannan; in addition, a higher number of GH2, GH3, GH16, and GH30 revealed that strain M415^T can metabolize plant polysaccharides and oligosaccharides (Coutinho et al., 2003; Gómez-Silva et al., 2019).

Polysaccharide utilization loci (PULs) are specialized saccharolytic systems that exhibit functional homology to the paradigmatic starch utilization system; the number and type of PULs determine the potential of polysaccharide utilization (Xu et al., 2003; McKee et al., 2021). According to the annotation results of carbohydrate-active enzymes and the SusC/D-like protein complex, we manually sorted the PULs of three novel strains (Figure 9); strains M17^T, M82^T, and M415^T have five, six, and two putative PULs, respectively. The PULs in strains M17^T and M82^T were specific for marine polysaccharide metabolism; for strain M17^T, PUL2 may be associated with the degradation of ulvan as the existence of GH2 (β-xylosidase), PUL3 may be associated with the degradation of laminarin as the existence of GH3 and GH16_3 (Tang et al., 2017; Chen et al., 2018), and PUL4 may be associated with the degradation of chitin as the

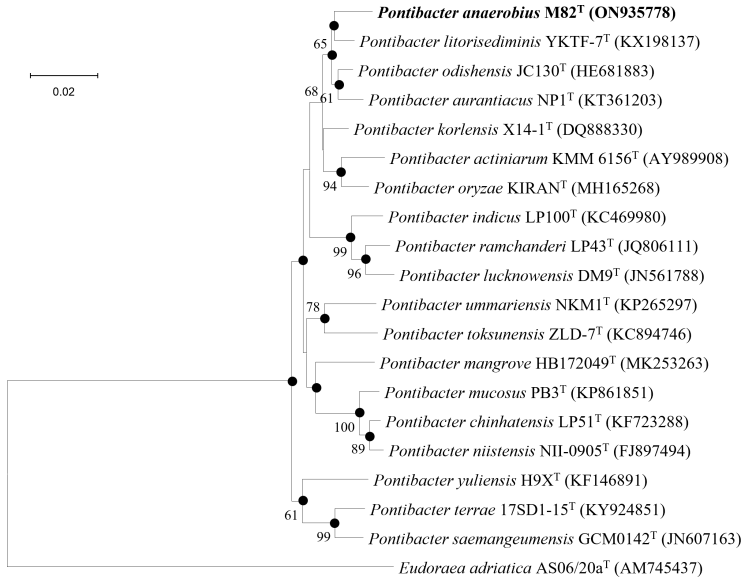

FIGURE 5
Neighbor-joining phylogenetic tree reconstructed from 16S rRNA gene sequences of strains M82^T and related species. Bootstrap values < 50% (based on 1,000 replications) are not shown. Filled circles indicate branches that were also recovered using maximum-likelihood and maximum-parsimony methods. *Eudoraea adriatica* AS06/20a^T (AM745437) was used as the outgroup; bar, 0.02 nt substitutions per nucleotide position.

existence of GH18 (Kappelmann et al., 2019). For strain M82^T, PUL1 may be associated with the degradation of fucoidan as the existence of GH29 (fucosidase) and PUL4 may be associated with the degradation of laminarin as the existence of GH16_3 (Tang et al., 2017; Chen et al., 2018). However, with the ability to utilize marine polysaccharides as strains M17^T and M82^T, strains M415^T can also utilize polysaccharides that are mainly present in land; for instance, it contained more glycogen and starch

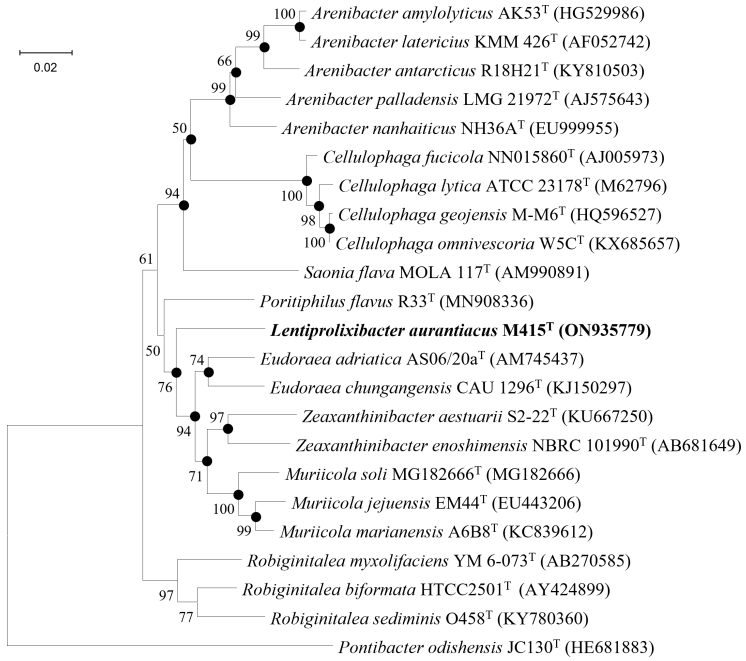

FIGURE 6
Neighbor-joining phylogenetic tree reconstructed from 16S rRNA gene sequences of strains M415^T and related species. Bootstrap values < 50% (based on 1,000 replications) are not shown. Filled circles indicate branches that were also recovered using maximum-likelihood and maximum-parsimony methods. *Pontibacter odishensis* JC130^T (HE681883) was used as the outgroup; bar, 0.02 nt substitutions per nucleotide position.

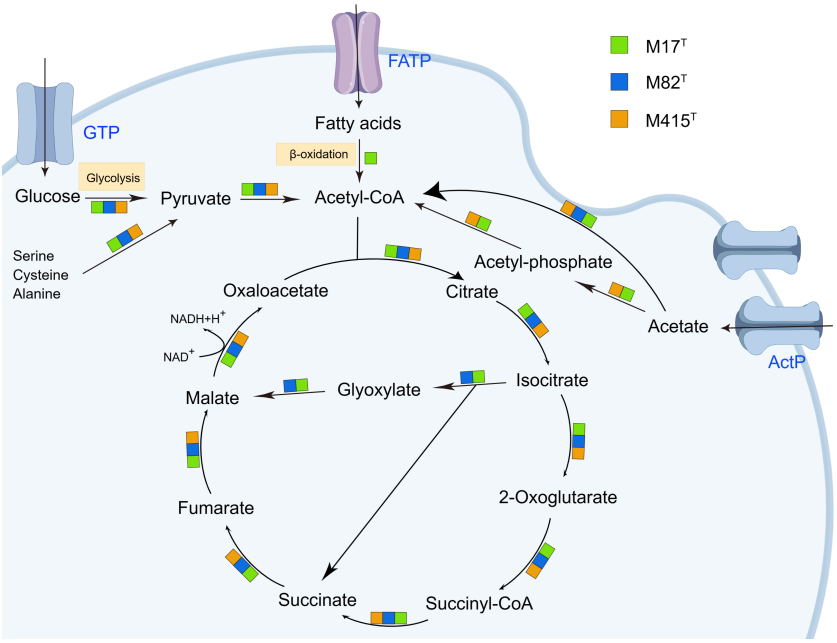

FIGURE 7
The citrate cycle (TCA cycle) and glyoxylate cycle in strains M17^T, M82^T, and M415^T. Color blocks indicated the reaction occurred in specific strains. GTP, glucose transport protein. FATP, fatty acid transport proteins. ActP, acetate permease. Other products have been omitted.

degrading CAZymes compared to another two strains (e.g., GH13, GH13_8; Berlemont and Martiny, 2015), and the PUL1 of strain M415^T may be related to the degradation of glycogen or starch.

3.5 Description of *Lentiprolixibacter* gen. nov.

Lentiprolixibacter (L. masc. adj. *lentus*, slow, delayed; L. masc. adj. *prolixus*, long, extended; N.L. masc. n. *bacter*, a rod; N.L. masc. n. *Lentiprolixibacter*, slowly growing long rod)

Cells are Gram-stain-negative, non-spore-forming, and non-motile aerobic rods. Catalase- and oxidase-positive. Predominant menaquinone is menaquinone 6 (MK-6). Major polar lipids are phosphatidylethanolamine, phosphoglycolipid, aminophospholipid, unidentified glycolipids, aminolipids, and lipids. The type species is *Lentiprolixibacter aurantiacus*.

3.6 Description of Lentiprolixibacter aurantiacus sp. nov.

Lentiprolixibacter aurantiacus (au.ran.ti.a'cus. N.L. masc. adj. *aurantiacus*, orange-colored)

Displays the following characteristics in addition to those given in the genus description. Cells are rod shaped and usually 0.3–0.5 μm wide and 1.8–8.0 μm long. Colonies (0.5 mm in diameter) are circular, convex, smooth, shiny, and orange pigmented after 3 days of incubation. Cells grow at 25°C–37°C (optimum, 25°C–30°C) in a

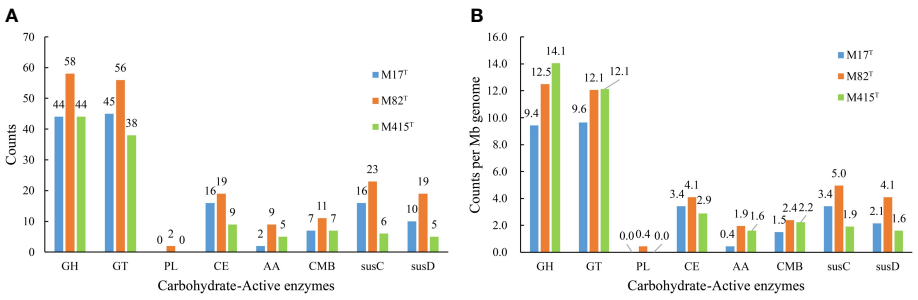

FIGURE 8
The number of predicted carbohydrate-active enzymes in strains M17^T, M82^T, and M415^T. **(A)** number of predicted CAZymes per genome and **(B)** average number of predicted CAZymes per Mb genome. GH, glycoside hydrolases; GT, glycosyltransferases; PL, polysaccharide lyases; CE, carbohydrate esterases; AA, auxiliary activities; CBM, carbohydrate-binding modules.

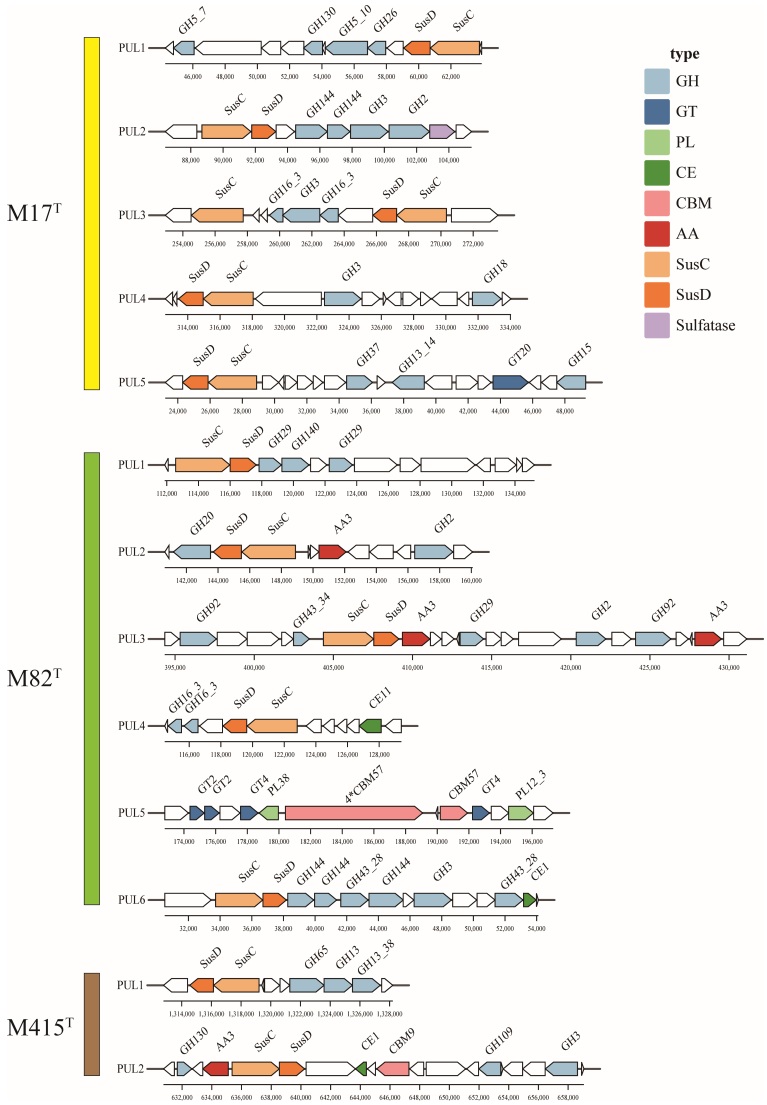

FIGURE 9
The putative polysaccharide utilization loci and genes in strains M17^T, M82^T, and M415^T. GH, glycoside hydrolases; GT, glycosyltransferases; PL, polysaccharide lyases; CE, carbohydrate esterases; AA, auxiliary activities; CBM, carbohydrate-binding modules.

medium of pH 6–8 (optimum, pH 6.5–7) and contain 1%–4% NaCl (optimum, 2%–3%). Catalase and oxidase are positive; nitrate reduction, carotenoid production, and H_2S production are negative. Starch is weakly hydrolyzed, but Tweens 20, 40, 60, and 80 are not. Dextrin, D-maltose, D-trehalose, D-cellobiose, gentiobiose, sucrose, D-turanose, β-methyl-D-glucoside, D-salicin, *N*-acetyl-D-glucosamine, α-D-glucose, fusidic acid, D-serine, D-glucose-6-PO_4, D-fructose-6-PO_4, pectin, glucuronamide, L-malic acid, bromo-succinic acid, nalidixic acid, and sodium butyrate are oxidized. In assays with the API ZYM system, alkaline phosphatase, esterase (C4), esterase lipase (C8), leucine arylamidase, valine arylamidase, cystine arylamidase, trypsin, chymotrypsin, acid phosphatase, naphthol-AS-BI-phosphohydrolase, β-glucosidase, and *N*-acetylglucosaminidase are positive and α-glucosidase is weakly positive. The major cellular fatty acids (>10%) are iso-$C_{15:0}$, iso-$C_{15:1}$ -G, and iso-$C_{17:0}$ 3-OH. The polar lipids are phosphatidylethanolamine, phosphoglycolipid, aminophospholipid, one unidentified glycolipids, two unidentified aminolipids, and five unidentified lipids. The DNA G+C content of the type strain is 44.6%.

The type strain, M415^T (MCCC 1K08058^T = KCTC 92534^T), was isolated from an intertidal mudflat (0–5 cm) collected from Taizhou, Zhejiang Provence, PR China. The GenBank accession numbers for the 16S rRNA gene sequence and the draft genome sequence of strain M415^T are ON935779 and JAPFQP000000000, respectively.

3.7 Description of *Mangrovivirga halotolerans* sp. nov.

Mangrovivirga halotolerans (ha.lo.to'le.rans. Gr. masc. n. *hals*, salt; L. pres. part. *tolerans*, tolerating, enduring; N.L. part. adj. *halotolerans*, salt-tolerating)

Cells are Gram-stain negative, non-motile, strictly aerobic rod-shaped, usually 0.3–0.5 μm wide, and 2–10 μm long, some more than 10 μm in length. Colonies (1–3 mm in diameter) are circular, convex, smooth, shiny, and orange pigmented after 3 days of incubation. Cells grow at 20°C–45°C (optimum, 20°C–28°C) in a medium of pH 6.5–9 (optimum, pH 6.5-7.5) and contain 0.5%–10% NaCl (optimum, 3.5%–6%). Catalase and oxidase activities are positive; nitrate reduction, carotenoid production, and H_2S production are negative. Starch is hydrolyzed, but Tweens 20, 40, 60, and 80 are not. Sucrose, stachyose, D-fucose, fusidic acid, L-alanine, glucuronamide, tetrazolium violet, α-keto-glutaric acid, L-malic acid, nalidixic acid, acetoacetic acid, propionic acid, acetic acid, formic acid, aztreonam, and sodium butyrate are oxidized. In assays with the API ZYM system, alkaline phosphatase, esterase (C4), esterase lipase (C8), leucine arylamidase, valine arylamidase, cystine arylamidase, trypsin, chymotrypsin, acid phosphatase, naphthol-AS-BI-phosphohydrolase, β-glucuronidase, β-glucosidase, and *N*-acetylglucosaminidase are positive. The predominant menaquinone is MK-7. The major cellular fatty acids (>10%) are iso-$C_{15:0}$ and iso-$C_{17:0}$ 3-OH. The polar lipids are phosphatidylethanolamine, aminoglycolipid, one unidentified phospholipid, three unidentified aminolipids, three unidentified glycolipids, and six unidentified lipids. The DNA G+C content of the type strain is 35.9%.

The type strain, M17^T (MCCC 1K08105^T = KCTC 92592^T), was isolated from an intertidal mudflat (0–5 cm) collected from Qingdao, Shandong Provence, PR China. The GenBank accession numbers for the 16S rRNA gene sequence and the draft genome sequence of strain M17^T are ON935777 and JAPFQN000000000, respectively.

3.8 Description of *Pontibacter anaerobius* sp. nov.

Pontibacter anaerobius (an.ae.ro'bi.us. Gr. pref. *an-*, not; Gr. masc. n. *aêr*, air; Gr. masc. n. *bios*, life; N.L. masc. adj. *anaerobius*, able to live in the absence of oxygen)

Cells are Gram-stain negative, non-motile, facultative aerobic rod-shaped, and usually 0.6–1.1 μm wide and 0.9–3.2 μm long. Colonies (1–2 mm in diameter) are circular, convex, smooth, shiny, and red pigmented after 3 days of incubation. Cells grow at 20°C–40°C (optimum, 28°C–37°C) in a medium of pH 6–9 (optimum, pH 6.5–7.5) and contain 0%–8% NaCl (optimum, 2%–3%). Carotenoid production and catalase and oxidase activity are positive. Nitrate reduction and H_2S production are negative. Starch and Tweens 20, 40, 60, and 80 are not hydrolyzed. Dextrin, D-maltose, D-trehalose, D-cellobiose, gentiobiose, sucrose, D-turanose, stachyose, D-raffinose, α-D-lactose, D-melibiose, β-methyl-D-glucoside, D-salicin, *N*-acetyl-D-glucosamine, α-D-glucose, D-mannose, D-galactose, D-fucose, L-fucose, fusidic acid, D-arabitol, myo-inositol, D-glucose-6-PO_4, D-fructose-6-PO_4, gelatin, glycyl-L-proline, L-aspartic acid, L-glutamic acid, L-serine, D-galacturonic acid, glucuronamide, acetoacetic acid, acetic acid, formic acid, and sodium butyrate are oxidized. In assays with the API ZYM system, alkaline phosphatase, esterase (C4), esterase lipase (C8), leucine arylamidase, valine arylamidase, cystine arylamidase, trypsin, chymotrypsin, acid phosphatase, α-galactosidase, α-glucosidase, β-glucosidase, and *N*-acetylglucosaminidase are positive; naphthol-AS-BI-phosphohydrolase and β-galactosidase are weakly positive. The predominant menaquinone is MK-7. The major cellular fatty acids (>10%) are iso-$C_{15:0}$, iso-$C_{17:0}$ 3-OH, and summed feature 4 (ante-iso-$C_{17:1}$ B and/or iso-$C_{17:1}$ I). The polar lipids are phosphatidylethanolamine, two unidentified aminolipids, and nine unidentified lipids. The DNA G+C content of the type strain is 50.6%.

The type strain, M82^T (MCCC 1K08048^T = KCTC 92537^T), was isolated from an intertidal mudflat (0–5 cm) collected from Taizhou, Zhejiang Provence, PR China. The GenBank accession numbers for the 16S rRNA gene sequence and the draft genome sequence of strain M82^T are ON935778 and JAPFQO000000000, respectively.

Data availability statement

The datasets presented in this study can be found in online repositories. The names of the repository/repositories and accession number(s) can be found in the article/Supplementary Material.

Author contributions

K-JM, Y-LY, and Y-HF collected the samples and isolated these strains. K-JM performed data collection and analysis. G-YF performed project guidance. K-JM and CS wrote the manuscript. X-WX and CS performed project guidance and critical revision of manuscripts. All authors contributed to the article and approved the submitted version.

Funding

This work was supported by the National Science and Technology Fundamental Resources Investigation Program of China (2019FY100700), the National Natural Science Foundation of China (No. 31900003), and the Key R&D Program of Zhejiang (#2023C03011).

Acknowledgments

We appreciate the helpful suggestion of Prof. Aharon Oren on the nomenclature and the help of Dr. Zhi-Cheng Wu and Dr. Maripat Xamxidin in sample collection and detection of polar lipids, respectively.

Conflict of interest

Author CS was employed by company Zhejiang Sci-Tech University Shaoxing Academy of Biomedicine Co., Ltd..

The remaining authors declare that the research was conducted in the absence of any commercial or financial relationships that could be construed as a potential conflict of interest.

Publisher's note

All claims expressed in this article are solely those of the authors and do not necessarily represent those of their affiliated organizations, or those of the publisher, the editors and the reviewers. Any product that may be evaluated in this article, or claim that may be made by its manufacturer, is not guaranteed or endorsed by the publisher.

Supplementary material

The Supplementary Material for this article can be found online at: https://www.frontiersin.org/articles/10.3389/fmars.2023.1222157/full#supplementary-material

References

Amann, R. I., Ludwig, W., and Schleifer, K. H. (1995). Phylogenetic identification and in *situ* detection of individual microbial cells without cultivation. *Microbiological Rev.* 59 (1), 143–169. doi: 10.1128/mmbr.59.1.143-169.1995

Asker, D., Beppu, T., and Ueda, K. (2007). *Zeaxanthinibacter enoshimensis* gen. nov., sp nov., a novel zeaxanthin-producing marine bacterium of the family *Flavobacteriaceae*, isolated from seawater off Enoshima Island, Japan. *Int. J. Systematic Evolutionary Microbiol.* 57 (4), 837–843. doi: 10.1099/ijs.0.64682-0

Aziz, R. K., Bartels, D., Best, A. A., DeJongh, M., Disz, T., Edwards, R. A., et al. (2008). The RAST server: Rapid annotations using subsystems technology. *BMC Genomics* 9 (1), 75. doi: 10.1186/1471-2164-9-75

Barbeyron, T., Thomas, F., Barbe, V., Teeling, H., Schenowitz, C., Dossat, C., et al. (2016). Habitat and taxon as driving forces of carbohydrate catabolism in marine heterotrophic bacteria: example of the model algae-associated bacterium Zobellia galactanivorans DsijT. *Environ. Microbiol.* 18 (12), 4610–4627. doi: 10.1111/1462-2920.13584

Bauer, J. E., Cai, W. J., Raymond, P. A., Bianchi, T. S., Hopkinson, C. S., and Regnier, P. A. (2013). The changing carbon cycle of the coastal ocean. *Nature* 504 (7478), 61–70. doi: 10.1038/nature12857

Berlemont, R., and Martiny, A. C. (2015). Genomic potential for polysaccharide deconstruction in bacteria. *Appl. Environ. Microbiol.* 81 (4), 1513–1519. doi: 10.1128/aem.03718-14

Bowman, J. P., and Nichols, D. S. (2005). Novel members of the family *Flavobacteriaceae* from Antarctic maritime habitats including *Subsaximicrobium wynnwilliamsii* gen. nov., sp. nov., *Subsaximicrobium saxinquilinus* sp. nov., *Subsaxibacter broadyi* gen. nov., sp. nov., *Lacinutrix copepodicola* gen. nov., sp. nov., and novel species of the genera *Bizionia*, *Gelidibacter* and *Gillisia*. *Int. J. Systematic Evolutionary Microbiol.* 55 (4), 1471–1486. doi: 10.1099/ijs.0.63527-0

Brígido, C., Singh, S., Menéndez, E., Tavares, M. J., Glick, B. R., Félix, M. D. R., et al. (2019). Diversity and functionality of culturable endophytic bacterial communities in chickpea plants. *Plants* 8 (2), 42. doi: 10.3390/plants8020042

Capella-Gutierrez, S., Silla-Martinez, J. M., and Gabaldon, T. (2009). trimAl: a tool for automated alignment trimming in large-scale phylogenetic analyses. *Bioinformatics* 25 (15), 1972–1973. doi: 10.1093/bioinformatics/btp348

Chang, M. X., Li, P., Li, Z. H., and Wang, H. J. (2022). Mapping tidal flats of the bohai and yellow seas using time series sentinel-2 images and google earth engine. *Remote Sens.* 14 (8), 1789. doi: 10.3390/rs14081789

Chen, J., Robb, C. S., Unfried, F., Kappelmann, L., Markert, S., Song, T., et al. (2018). Alpha- and beta-mannan utilization by marine Bacteroidetes. *Environ. Microbiol.* 20 (11), 4127–4140. doi: 10.1111/1462-2920.14414

Chernysheva, N., Bystritskaya, E., Stenkova, A., Golovkin, I., Nedashkovskaya, O., and Isaeva, M. (2019). Comparative Genomics and CAZyme Genome Repertoires of Marine Zobellia amurskyensis KMM 3526T and Zobellia laminariae KMM 3676T. *Mar. Drugs* 17 (12), 661. doi: 10.3390/md17120661

Choi, H. J., Jeong, T. Y., Yoon, H., Oh, B. Y., Han, Y. S., Hur, M. J., et al. (2018). Comparative microbial communities in tidal flats sediment on Incheon, South Korea. *J. Gen. Appl. Microbiol.* 64 (5), 232–239. doi: 10.2323/jgam.2017.12.007

Chuang, S. C., Yang, H. X., Wang, X., Xue, C., Jiang, J. D., and Hong, Q. (2021). Potential effects of *Rhodococcus qingshengii* strain djl-6 on the bioremediation of carbendazim-contaminated soil and the assembly of its microbiome. *J. Hazardous Materials* 414, 125496. doi: 10.1016/j.jhazmat.2021.125496

Consortium, U. (2019). UniProt: a worldwide hub of protein knowledge. *Nucleic Acids Res.* 47 (D1), D506–D515. doi: 10.1093/nar/gky1049

Coutinho, P. M., Deleury, E., Davies, G. J., and Henrissat, B. (2003). An evolving hierarchical family classification for glycosyltransferases. *J. Mol. Biol.* 328 (2), 307–317. doi: 10.1016/s0022-2836(03)00307-3

Dong, X. Z., and Cai, M. Y. (2001). "Determination of Biochemical Characteristics," in *Manual for the Systematic Identification of General Bacteria*. Eds. X. Z. Dong and M. Y. Cai (Beijing: Science Press), 370–398.

Drula, E., Garron, M. L., Dogan, S., Lombard, V., Henrissat, B., and Terrapon, N. (2022). The carbohydrate-active enzyme database: functions and literature. *Nucleic Acids Res.* 50 (D1), D571–D577. doi: 10.1093/nar/gkab1045

Du, S. T., Lu, Q., Liu, L. J., Wang, Y., and Li, J. X. (2022). *Rhodococcus qingshengii* facilitates the phytoextraction of Zn, Cd, Ni, and Pb from soils by Sedum alfredii Hance. *J. Hazardous Materials* 424, 127638. doi: 10.1016/j.jhazmat.2021.127638

Ettwig, K. F., Butler, M. K., Le Paslier, D., Pelletier, E., Mangenot, S., Kuypers, M. M., et al. (2010). Nitrite-driven anaerobic methane oxidation by oxygenic bacteria. *Nature* 464 (7288), 543–548. doi: 10.1038/nature08883

Felsenstein, J. (1981). Evolutionary trees from DNA sequences: A maximum likelihood approach. *J. Mol. Evol.* 17 (6), 368–376. doi: 10.1007/bf01734359

Fernández-Gómez, B., Richter, M., Schüler, M., Pinhassi, J., Acinas, S. G., González, J. M., et al. (2013). Ecology of marine Bacteroidetes: a comparative genomics approach. *ISME J.* 7 (5), 1026–1037. doi: 10.1038/ismej.2012.169

Folk, R. L., Andrews, P. B., and Lewis, D. W. (1970). Detrital sedimentary rock classification and nomenclature for use in New Zealand. N. Z. *J. Geology Geophysics* 13 (4), 937–968. doi: 10.1080/00288306.1970.10418211

Gaubert-Boussarie, J., Prado, S., and Hubas, C. (2020). An untargeted metabolomic approach for microphytobenthic biofilms in intertidal mudflats. *Front. Mar. Sci.* 7. doi: 10.3389/fmars.2020.00250

Gavriilidou, A., Gutleben, J., Versluis, D., Forgiarini, F., van Passel, M. W., Ingham, C. J., et al. (2020). Comparative genomic analysis of *Flavobacteriaceae*: insights into carbohydrate metabolism, gliding motility and secondary metabolite biosynthesis. *BMC Genomics* 21 (1), 1–21. doi: 10.1186/s12864-020-06971-7

Gómez-Silva, B., Vilo-Muñoz, C., Galetović, A., Dong, Q., Castelán-Sánchez, H. G., Pérez-Llano, Y., et al. (2019). Metagenomics of Atacama lithobiontic extremophile life unveils highlights on fungal communities, biogeochemical cycles and carbohydrate-active enzymes. *Microorganisms* 7 (12), 619. doi: 10.3390/microorganisms7120619

Gong, B., Cao, H. M., Peng, C. Y., Perculija, V., Tong, G. X., Fang, H. Y., et al. (2019). High-throughput sequencing and analysis of microbial communities in the mangrove swamps along the coast of Beibu Gulf in Guangxi, China. *Sci. Rep.* 9, 9377. doi: 10.1038/s41598-019-45804-w

Guo, B., Wu, X. L., and Qian, Y. (2006). Approaches for increasing the culturability of microorganisms. *Weishengwu Xuebao* 46 (3), 504–507. doi: 10.3321/j.issn:0001-6209.2006.03.036

Harboul, K., Alouiz, I., Hammani, K., and El-Karkouri, A. (2022). Isotherm and kinetics modeling of biosorption and bioreduction of the Cr (VI) by *Brachybacterium paraconglomeratum* ER41. *Extremophiles* 26 (3), 30. doi: 10.1007/s00792-022-01278-9

Hernández-Plaza, A., Szklarczyk, D., Botas, J., Cantalapiedra, C. P., Giner-Lamia, J., Mende, D. R., et al. (2023). eggNOG 6.0: enabling comparative genomics across 12 535 organisms. *Nucleic Acids Res.* 51 (D1), D389–D394. doi: 10.1093/nar/gkac1022

Howard, J., Hoyt, S., Isensee, K., Telszewski, M., and Pidgeon, E. (2014). *Coastal blue carbon: methods for assessing carbon stocks and emissions factors in mangroves, tidal salt marshes, and seagrasses* (Arlington, VA: Conservation International, Intergovernmental Oceanographic Commission of UNESCO, International Union for Conservation of Nature).

Hu, Y. B., Wang, N., Yan, X. C., Yuan, Y., Luo, F., Jiang, Z. Y., et al. (2019). Ginsenoside Re impacts on biotransformation products of ginsenoside Rb1 by Cellulosimicrobium cellulans sp. 21 and its mechanisms. *Process Biochem.* 77, 57–62. doi: 10.1016/j.procbio.2018.11.019

Kanehisa, M., Furumichi, M., Tanabe, M., Sato, Y., and Morishima, K. (2017). KEGG: new perspectives on genomes, pathways, diseases and drugs. *Nucleic Acids Res.* 45 (D1), D353–D361. doi: 10.1093/nar/gkw1092

Kappelmann, L., Krüger, K., Hehemann, J. H., Harder, J., Markert, S., Unfried, F., et al. (2019). Polysaccharide utilization loci of North Sea *Flavobacteriia* as basis for using SusC/D-protein expression for predicting major phytoplankton glycans. *ISME J.* 13 (1), 76–91. doi: 10.1038/s41396-018-0242-6

Katoh, K., and Standley, D. M. (2013). MAFFT multiple sequence alignment software version 7: improvements in performance and usability. *Mol. Biol. Evol.* 30 (4), 772–780. doi: 10.1093/molbev/mst010

Kim, M., Oh, H. S., Park, S. C., and Chun, J. (2014). Towards a taxonomic coherence between average nucleotide identity and 16S rRNA gene sequence similarity for species demarcation of prokaryotes. *Int. J. Systematic Evolutionary Microbiol.* 64 (Pt_2), 346–351. doi: 10.1099/ijs.0.059774-0

Komagata, K., and Suzuki, K. I. (1988). 4 Lipid and cell-wall analysis in bacterial systematics. *Methods Microbiol.* 19, 161–207. doi: 10.1016/S0580-9517(08)70410-0

Konstantinidis, K. T., and Tiedje, J. M. (2005). Towards a genome-based taxonomy for prokaryotes. *J. Bacteriology* 187 (18), 6258–6264. doi: 10.1128/jb.187.18.6258-6264.2005

Krüger, K., Chafee, M., Ben Francis, T., Glavina del Rio, T., Becher, D., Schweder, T., et al. (2019). In marine *Bacteroidetes* the bulk of glycan degradation during algae blooms is mediated by few clades using a restricted set of genes. *ISME J.* 13 (11), 2800–2816. doi: 10.1038/s41396-019-0476-y

Lam-Tung, N., Schmidt, H. A., von Haeseler, A., and Bui Quang, M. (2015). IQ-TREE: A fast and effective stochastic algorithm for estimating maximum-likelihood phylogenies. *Mol. Biol. Evol.* 32 (1), 268–274. doi: 10.1093/molbev/msu300

Lapebie, P., Lombard, V., Drula, E., Terrapon, N., and Henrissat, B. (2019). *Bacteroidetes* use thousands of enzyme combinations to break down glycans. *Nat. Commun.* 10, 2043. doi: 10.1038/s41467-019-10068-5

Lechner, M., Findeiss, S., Steiner, L., Marz, M., Stadler, P. F., and Prohaska, S. J. (2011). Proteinortho: Detection of (Co-)orthologs in large-scale analysis. *BMC Bioinf.* 12, 124. doi: 10.1186/1471-2105-12-124

Li, M. S., Li, T., Zhou, M., Li, M. D., Zhao, Y. X., Xu, J. J., et al. (2021). Caenorhabditis elegans extracts stimulate IAA biosynthesis in *Arthrobacter pascens* ZZ21 *via* the indole-3-pyruvic acid pathway. *Microorganisms* 9 (5), 970. doi: 10.3390/microorganisms9050970

Lichtenthaler, F. W., and Peters, S. (2004). Carbohydrates as green raw materials for the chemical industry. *Comptes Rendus Chimie* 7 (2), 65–90. doi: 10.1016/j.crci.2004.02.002

Liu, Y. L., Meng, D., Li, R. R., Gu, P. F., Fan, X. Y., Huang, Z. S., et al. (2019). *Rhodoligotrophos defluvii* sp. nov., isolated from activated sludge. *Int. J. Systematic Evolutionary Microbiol.* 69 (12), 3830–3836. doi: 10.1099/ijsem.0.003691

Martiny, A. C. (2019). High proportions of bacteria are culturable across major biomes. *ISME J.* 13 (8), 2125–2128. doi: 10.1038/s41396-019-0410-3

Mayor, D. J., Thornton, B., Jenkins, H., and Felgate, S. L. (2018). "Chapter 3 microbiota: the living foundation," in *Mudflat ecology*. Ed. P. G. Beninger (Amsterdam, Netherlands: Springer), 43–61.

McKee, L. S., La Rosa, S. L., Westereng, B., Eijsink, V. G., Pope, P. B., and Larsbrink, J. (2021). Polysaccharide degradation by the *Bacteroidetes*: mechanisms and nomenclature. *Environ. Microbiol. Rep.* 13 (5), 559–581. doi: 10.1111/1758-2229.12980

Meier-Kolthoff, J. P., Carbasse, J. S., Peinado-Olarte, R. L., and Goeker, M. (2022). TYGS and LPSN: a database tandem for fast and reliable genome-based classification and nomenclature of prokaryotes. *Nucleic Acids Res.* 50 (D1), D801–D807. doi: 10.1093/nar/gkab902

Minnikin, D., O'donnell, A., Goodfellow, M., Alderson, G., Athalye, M., Schaal, A., et al. (1984). An integrated procedure for the extraction of bacterial isoprenoid quinones and polar lipids. *J. Microbiological Methods* 2 (5), 233–241. doi: 10.1016/0167-7012(84)90018-6

Mohapatra, M., Yadav, R., Rajput, V., Dharne, M. S., and Rastogi, G. (2021). Metagenomic analysis reveals genetic insights on biogeochemical cycling, xenobiotic degradation, and stress resistance in mudflat microbiome. *J. Environ. Manage.* 292, 112738. doi: 10.1016/j.jenvman.2021.112738

Molari, M., Giovannelli, D., d'Errico, G., and Manini, E. (2012). Factors influencing prokaryotic community structure composition in sub-surface coastal sediments. *Estuarine Coast. Shelf Sci.* 97, 141–148. doi: 10.1016/j.ecss.2011.11.036

Molina-Menor, E., Gimeno-Valero, H., Pascual, J., Peretó, J., and Porcar, M. (2021). High culturable bacterial diversity from a European desert: The Tabernas desert. *Front. Microbiol.* 11. doi: 10.3389/fmicb.2020.583120

Murray, N. J., Phinn, S. R., DeWitt, M., Ferrari, R., Johnston, R., Lyons, M. B., et al. (2019). The global distribution and trajectory of tidal flats. *Nature* 565 (7738), 222–225. doi: 10.1038/s41586-018-0805-8

Nedashkovskaya, O. I., Kim, S. B., Suzuki, M., Shevchenko, L. S., Lee, M. S., Lee, K. H., et al. (2005). *Pontibacter actiniarum* gen. nov., sp nov., a novel member of the phylum *'Bacteroidetes'*, and proposal of *Reichenbachiella* gen. nov as a replacement for the illegitimate prokaryotic generic name *Reichenbachia* Nedashkovskaya et al. 2003. *Int. J. Systematic Evolutionary Microbiol.* 55, 2583–2588. doi: 10.1099/ijs.0.63819-0

Ni, M., Yuan, J. L., Hua, J. Q., Lian, Q. P., Guo, A. H., Liu, M., et al. (2020). Shrimp–vegetable rotational farming system: An innovation of shrimp aquaculture in the tidal flat ponds of Hangzhou Bay, China. *Aquaculture* 518, 734864. doi: 10.1016/j.aquaculture.2019.734864

Pandey, R., Sharma, P., Rathee, S., Singh, H. P., Batish, D. R., Krishnamurthy, B., et al. (2021). Isolation and characterization of a novel hydrocarbonoclastic and biosurfactant producing bacterial strain: *Fictibacillus Phosphorivorans* RP3. *3 Biotech.* 11 (2), 105. doi: 10.1007/s13205-021-02655-5

Park, S., Park, J. M., Lee, K. H., and Yoon, J. H. (2016). *Pontibacter litorisediminis* sp. nov., isolated from a tidal flat. *Int. J. Systematic Evolutionary Microbiol.* 66 (10), 4172–4178. doi: 10.1099/ijsem.0.001331

Parks, D. H., Imelfort, M., Skennerton, C. T., Hugenholtz, P., and Tyson, G. W. (2015). CheckM: assessing the quality of microbial genomes recovered from isolates, single cells, and metagenomes. *Genome Res.* 25 (7), 1043–1055. doi: 10.1101/gr.186072.114

Perillo, G., Wolanski, E., Cahoon, D. R., and Hopkinson, C. S. (2018). *Coastal Wetlands: An Integrated Ecosystem Approach* (Amsterdam: Elsevier).

Rinke, M., Maraun, M., and Scheu, S. (2022). Spatial and temporal variations in salt marsh microorganisms of the Wadden Sea. *Ecol. Evol.* 12 (3), e8767. doi: 10.1002/ece3.8767

Rodriguez-R, L. M., and Konstantinidis, K. T. (2014). Bypassing cultivation to identify bacterial species. *Microbe* 9 (3), 111–118. doi: 10.1128/microbe.9.111.1

Saitou, N., and Nei, M. (1987). The neighbor-joining method: a new method for reconstructing phylogenetic trees. *Mol. Biol. Evol.* 4 (4), 406–425. doi: 10.1093/oxfordjournals.molbev.a040454

Sasmito, S. D., Kuzyakov, Y., Lubis, A. A., Murdiyarso, D., Hutley, L. B., Bachri, S., et al. (2020). Organic carbon burial and sources in soils of coastal mudflat and mangrove ecosystems. *Catena* 187, 104414. doi: 10.1016/j.catena.2019.104414

Sasser, M. (1990). *Identification of bacteria by gas chromatography of cellular fatty acids* (Newark, DE: Microbial ID Inc). Available at: http://www.microbialid.com/PDF/TechNote_101.pdf.

Schroeter, R., Voigt, B., Jürgen, B., Methling, K., Pöther, D. C., Schäfer, H., et al. (2011). The peroxide stress response of *Bacillus licheniformis*. *Proteomics* 11 (14), 2851–2866. doi: 10.1002/pmic.201000461

Seemann, T. (2014). Prokka: rapid prokaryotic genome annotation. *Bioinformatics* 30 (14), 2068–2069. doi: 10.1093/bioinformatics/btu153

Sefrji, F. O., Marasco, R., Michoud, G., Seferji, K. A., Merlino, G., and Daffonchio, D. (2022). Insights Into the Cultivable Bacterial Fraction of Sediments From the Red Sea Mangroves and Physiological, Chemotaxonomic, and Genomic Characterization of *Mangrovibacillus cuniculi* gen. nov., sp. nov., a Novel Member of the *Bacillaceae* Family. *Front. Microbiol.* 13. doi: 10.3389/fmicb.2022.777986

Sefrji, F. O., Michoud, G., Marasco, R., Merlino, G., and Daffonchio, D. (2021). *Mangrovivirga cuniculi* gen. nov., sp. nov., a moderately halophilic bacterium isolated from bioturbated Red Sea mangrove sediment, and proposal of the novel family *Mangrovivirgaceae* fam. nov. *Int. J. Systematic Evolutionary Microbiol.* 71 (7), 4866. doi: 10.1099/ijsem.0.004866

Shi, X. L., Wu, Y. H., Jin, X. B., Wang, C. S., and Xu, X. W. (2017). *Alteromonas lipolytica* sp. nov., a poly-beta-hydroxybutyrate-producing bacterium isolated from surface seawater. *Int. J. Systematic Evolutionary Microbiol.* 67 (2), 237–242. doi: 10.1099/ijsem.0.001604

Siamphan, C., Chang, Y. H., and Kim, W. (2015). *Eudoraea chungangensis* sp nov., isolated from an aquafarm waste water sludge. *Antonie Van Leeuwenhoek Int. J. Gen. Mol. Microbiol.* 107 (4), 1009–1015. doi: 10.1007/s10482-015-0393-7

Staloch, B. E. K., Niero, H., de Freitas, R. C., Ballone, P., Rodrigues-Costa, F., Trivella, D. B. B., et al. (2022). Draft genome sequence of *Psychrobacter nivimaris* LAMA 639 and its biotechnological potential. *Data Brief* 41, 107927. doi: 10.1016/j.dib.2022.107927

Steen, A. D., Crits-Christoph, A., Carini, P., DeAngelis, K. M., Fierer, N., Lloyd, K. G., et al. (2019). High proportions of bacteria and archaea across most biomes remain uncultured. *ISME J.* 13 (12), 3126–3130. doi: 10.1038/s41396-019-0484-y

Subhash, Y., Tushar, L., Sasikala, C., and Ramana, C. V. (2013). *Erythrobacter odishensis* sp nov and *Pontibacter odishensis* sp nov isolated from dry soil of a solar saltern. *Int. J. Systematic Evolutionary Microbiol.* 63, 4524–4532. doi: 10.1099/ijs.0.052183-0

Tamura, K., Stecher, G., and Kumar, S. (2021). MEGA11 molecular evolutionary genetics analysis version 11. *Mol. Biol. Evol.* 38 (7), 3022–3027. doi: 10.1093/molbev/msab120

Tang, K., Lin, Y., Han, Y., and Jiao, N. (2017). Characterization of potential polysaccharide utilization systems in the marine bacteroidetes gramella flava JLT2011 using a multi-omics approach. *Front. Microbiol.* 8. doi: 10.3389/fmicb.2017.00220

Terrapon, N., Lombard, V., Drula, E., Lapebie, P., Al-Masaudi, S., Gilbert, H. J., et al. (2018). PULDB: the expanded database of Polysaccharide Utilization Loci. *Nucleic Acids Res.* 46 (D1), D677–D683. doi: 10.1093/nar/gkx1022

Terrapon, N., Lombard, V., Gilbert, H. J., and Henrissat, B. (2015). Automatic prediction of polysaccharide utilization loci in *Bacteroidetes* species. *Bioinformatics* 31 (5), 647–655. doi: 10.1093/bioinformatics/btu716

Tindall, B. J., Rosselló-Móra, R., Busse, H. J., Ludwig, W., and Kämpfer, P. (2010). Notes on the characterization of prokaryote strains for taxonomic purposes. *Int. J. Systematic Evolutionary Microbiol.* 60 (1), 249–266. doi: 10.1099/ijs.0.016949-0

Torsvik, V., and Ovreas, L. (2002). Microbial diversity and function in soil: from genes to ecosystems. *Curr. Opin. Microbiol.* 5 (3), 240–245. doi: 10.1016/s1369-5274(02)00324-7

Underwood, G. J. C., and Kromkamp, J. (1999). Primary production by phytoplankton and microphytobenthos in estuaries. *Adv. Ecol. Res.* 29, 93–153. doi: 10.1016/s0065-2504(08)60192-0

Unfried, F., Becker, S., Robb, C. S., Hehemann, J.-H., Markert, S., Heiden, S. E., et al. (2018). Adaptive mechanisms that provide competitive advantages to marine bacteroidetes during microalgal blooms. *ISME J.* 12 (12), 2894–2906. doi: 10.1038/s41396-018-0243-5

Wang, Y., Nie, M. Q., Diwu, Z. J., Chang, F., Nie, H. Y., Zhang, B., et al. (2021). Toxicity evaluation of the metabolites derived from the degradation of phenanthrene by one of a soil ubiquitous PAHs-degrading strain *Rhodococcus qingshengii* FF. *J. Hazardous Materials* 415, 125657. doi: 10.1016/j.jhazmat.2021.125657

Wang, X. X., Xiao, X. M., Zou, Z. H., Chen, B. Q., Ma, J., Dong, J. W., et al. (2020b). Tracking annual changes of coastal tidal flats in China during 1986–2016 through analyses of Landsat images with Google Earth Engine. *Remote Sens. Environ.* 238, 110987. doi: 10.1016/j.rse.2018.11.030

Wang, G. H., Xu, S. L., Dang, G., Liu, J. F., Su, H. F., Chen, B. A., et al. (2020a). *Poritiphilus flavus* gen. nov., sp. nov., a member of the family Flavobacteriaceae isolated from coral Porites lutea. *Int. J. Systematic Evolutionary Microbiol.* 70 (11), 5620–5626. doi: 10.1099/ijsem.0.004452

Williams, S., and Davies, F. (1965). Use of antibiotics for selective isolation and enumeration of actinomycetes in soil. *Microbiology* 38 (2), 251–261. doi: 10.1099/00221287-38-2-251

Xu, J., Bjursell, M. K., Himrod, J., Deng, S., Carmichael, L. K., Chiang, H. C., et al. (2003). A genomic view of the human-*Bacteroides* thetaiotaomicron symbiosis. *Science* 299 (5615), 2074–2076. doi: 10.1126/science.1080029

Xu, L., Wu, Y. H., Zhou, P., Cheng, H., Liu, Q., and Xu, X. W. (2018). Investigation of the thermophilic mechanism in the genus *Porphyrobacter* by comparative genomic analysis. *BMC Genomics* 19, 385. doi: 10.1186/s12864-018-4789-4

Yoon, S. H., Ha, S. M., Lim, J., Kwon, S., and Chun, J. (2017). A large-scale evaluation of algorithms to calculate average nucleotide identity. *Antonie Van Leeuwenhoek Int. J. Gen. Mol. Microbiol.* 110 (10), 1281–1286. doi: 10.1007/s10482-017-0844-4

Yuan, H. L., Xu, Y., Chen, Y. Z., Zhan, Y. Y., Wei, X. T., Li, L., et al. (2019). Metabolomics analysis reveals global acetoin stress response of *Bacillus licheniformis*. *Metabolomics* 15, 1–12. doi: 10.1007/s11306-019-1492-7

Zhang, R., Sun, M. R., Zhang, H. L., and Zhao, Z. H. (2021). Spatial separation of microbial communities reflects gradients of salinity and temperature in offshore sediments from Shenzhen, south China. *Ocean Coast. Manage.* 214, 105904. doi: 10.1016/j.ocecoaman.2021.105904

Zhang, H., Yohe, T., Huang, L., Entwistle, S., Wu, P. Z., Yang, Z. L., et al. (2018). dbCAN2: a meta server for automated carbohydrate-active enzyme annotation. *Nucleic Acids Res.* 46 (W1), W95–W101. doi: 10.1093/nar/gky418

Zhang, L., Zhang, Q. J., Luo, X. S., Tang, Y. L., Dai, J., Li, Y. W., et al. (2008). *Pontibacter korlensis* sp nov., isolated from the desert of Xinjiang, China. *Int. J. Systematic Evolutionary Microbiol.* 58, 1210–1214. doi: 10.1099/ijs.0.65667-0

Zheng, Z. G., Zheng, J. S., Liu, H. L., Peng, D. H., and Sun, M. (2016). Complete genome sequence of Fictibacillus phosphorivorans G25-29, a strain toxic to nematodes. *J. Biotechnol.* 239, 20–22. doi: 10.1016/j.jbiotec.2016.09.014

Zou, H. Y., Berglund, B., Xu, H., Chi, X. H., Zhao, Q., Zhou, Z. Y., et al. (2020). Genetic characterization and virulence of a carbapenem-resistant *Raoultella ornithinolytica* isolated from well water carrying a novel megaplasmid containing bla (NDM-1). *Environ. pollut.* 260, 114041. doi: 10.1016/j.envpol.2020.114041

frontiers | Frontiers in Marine Science

TYPE Original Research
PUBLISHED 11 August 2023
DOI 10.3389/fmars.2023.1222526

OPEN ACCESS

EDITED BY
Xue-Wei Xu,
Ministry of Natural Resources, China

REVIEWED BY
Min Yu,
Ocean University of China, China
Costantino Vetriani,
The State University of New Jersey, United States
Michael Hügler,
Technologiezentrum Wasser, Germany

*CORRESPONDENCE
Lijing Jiang
jianglijing@tio.org.cn
Zongze Shao
shaozz@163.com

RECEIVED 14 May 2023
ACCEPTED 24 July 2023
PUBLISHED 11 August 2023

CITATION
Wang J, Zheng Q, Wang S, Zeng J, Yuan Q, Zhong Y, Jiang L and Shao Z (2023) Characterization of two novel chemolithoautotrophic bacteria of *Sulfurovum* from marine coastal environments and further comparative genomic analyses revealed species differentiation among deep-sea hydrothermal vent and non-vent origins. *Front. Mar. Sci.* 10:1222526. doi: 10.3389/fmars.2023.1222526

Characterization of two novel chemolithoautotrophic bacteria of *Sulfurovum* from marine coastal environments and further comparative genomic analyses revealed species differentiation among deep-sea hydrothermal vent and non-vent origins

Jun Wang[1,2,3,4], Qiang Zheng[2], Shasha Wang[1,3,4], Jialing Zeng[2], Qing Yuan[1,3,4], Yangsheng Zhong[1,3,4], Lijing Jiang[1,3,4,5]* and Zongze Shao[1,2,3,4]*

[1]Key Laboratory of Marine Genetic Resources, Third Institute of Oceanography, Ministry of Natural Resources of China, Xiamen, China, [2]State Key Laboratory for Marine Environmental Science, Institute of Marine Microbes and Ecospheres, College of Ocean and Earth Sciences, Xiamen University, Xiamen, China, [3]State Key Laboratory Breeding Base of Marine Genetic Resources, Third Institute of Oceanography, Ministry of Natural Resources, Xiamen, China, [4]Key Laboratory of Marine Genetic Resources of Fujian Province, Third Institute of Oceanography, Ministry of Natural Resources, Xiamen, China, [5]School of Marine Biology, Xiamen Ocean Vocational College, Xiamen, China

Bacteria of the genus *Sulfurovum* within the class *Campylobacteria* are widespread in global oceans and are predominant in sulfide-rich environments. However, little is known about their adaptation to such harsh environments owing to their resistance to cultivation. In this study, we obtained three pure cultures of this genus from marine coastal environments and compared them with those obtained from the deep sea. Phylogenetic analysis of 16S rRNA gene sequences indicated that they represent two novel species of the genus, sharing 95.9%–96.1% sequence similarities to *Sulfurovum aggregans* Monchim33^T. Based on the polyphasic classification results, the type strains XTW-4^T and zt1-1^T were proposed to represent two new species: *Sulfurovum xiamenensis* sp. nov. and *Sulfurovum zhangzhouensis* sp. nov., respectively. These coastal isolates were also obligate chemoautotrophs featuring molecular hydrogen as an electron donor and molecular oxygen, thiosulfate, or elemental sulfur as the sole electron acceptor. Comparative genomic analyses based on 11 *Sulfurovum* species further revealed a clear differentiation between hydrothermal vent and non-vent origins. The non-vent *Sulfurovum* can use thiosulfate as an electron acceptor but lacks denitrification pathways, whereas the vent bacteria can respire nitrate through complete denitrification pathways. Moreover, the non-vent *Sulfurovum* contained a nitrogen fixation pathway, implying their adaptation to nitrogen source-deficit niches. In addition, non-

vent *Sulfurovum* species adapted to a higher oxygen concentration *via* multiple antioxidative defense mechanisms. These phenotypic and genotypic features help us to understand the ecological role of *Sulfurovum* bacteria in marine ecosystems.

KEYWORDS

***Sulfurovum xiamenensis*, *Sulfurovum zhangzhouensis*, nitrogen fixation, coastal environment, hydrothermal vent, environmental adaptation**

Introduction

The genus *Sulfurovum* is an important taxon of sulfur-oxidizing bacteria belonging to the family *Sulfurovaceae* of the phylum *Campylobacterota* (Waite et al., 2018) and can be found in various habitats, including mangroves (Lin et al., 2019), nearshore sediments (Marziah et al., 2016), shallow hydrothermal zones (Wang et al., 2017), glaciers (Wright et al., 2013), seagrass beds (Sun Y. Y. et al., 2020), and deep-sea hydrothermal vents (Nakagawa et al., 2006; Dahle et al., 2013; Meier et al., 2017). *Sulfurovum* bacteria are especially abundant in deep-sea hydrothermal vent environments and are widely distributed in various hydrothermal habitats, including chimneys, sediments, plumes, diffuse-flow vent fluids, and symbionts with animals (Akerman et al., 2013; Sheik et al., 2015; Motoki et al., 2020; Moulana et al., 2020; Lee et al., 2021; Chiu et al., 2022). *Sulfurovum* species are strict chemolithoautotrophs that have diverse energy metabolic pathways (Meier et al., 2017; Wang et al., 2023). They usually use hydrogen and reduced sulfur compounds as electron donors and oxygen, nitrate, and elemental sulfur as electron acceptors to fix CO_2, thus contributing to primary productivity in chemosynthetic ecosystems (Wright et al., 2013; Sheik et al., 2015). Recently, *Sulfurovum* was found to have potential applications in environmental remediation by removing hydrogen sulfide and nitrite from industrial wastewater (Li W. et al., 2022; Wang K. Q. et al., 2022; Zheng et al., 2022).

Currently, the genus *Sulfurovum* comprises only five species with validly published names and one provisional species. Five species, *Sulfurovum lithotrophicum* 42BKT^T, *Sulfurovum aggregans* Monchim33^T, *Sulfurovum riftiae* 1812E^T, *Sulfurovum denitrificans* eps51^T, and *Sulfurovum indicum* ST-419^T, were isolated from deep-sea hydrothermal vent environments, including vent sediments, plumes, chimneys, and outer biofilms of the polychaete *Riftia pachyptila* (Inagaki et al., 2004; Mino et al., 2014; Giovannelli et al., 2016; Mori et al., 2018; Xie et al., 2021). One provisional species, "*Candidatus Sulfurovum sediminum*", strain AR, was isolated from a non-vent environment. It was an enrichment culture from 78-m deep marine sediment collected near Svalbard Island in the Arctic Circle (Park et al., 2012). Recently, two strains *Sulfurovum* sp. TSL1 and TSL 6 were isolated from a tsunami-launched marine sediment based only on genomic analysis (Guo et al., 2022). Thus, in view of their widespread distribution and potentially high diversity, more bacteria of this genus are being isolated from different environments.

Although sequences affiliated with genus *Sulfurovum* have been detected from worldwide marine systems (Teske et al., 2002; Takai et al., 2004; Sylvan et al., 2012; Takai et al., 2015), physiological diversity and the ecological role of this genus have not yet been fully elucidated due to the lack of cultivated strains. Compared to vent *Sulfurovum* species, which has been studied extensively, there has been less exploration of non-vent *Sulfurovum* bacteria owing to fewer pure cultures being available from non-vent marine environments. In this study, three strains of the genus *Sulfurovum* were isolated from intertidal sediments, mangrove sediments, and mariculture pond sediments in subtropical estuary areas along the west bank of the Taiwan Strait. To elucidate their ecological roles and environmental adaptations in coastal marine ecosystems, we characterized strains belonging to two novel species using a polyphasic taxonomic approach. In addition, we performed comparative genomic analyses of all members of the genus *Sulfurovum*, including those with vent and non-vent origins, to gain insights into the environmental adaptation mechanisms underlying their widespread distribution.

Materials and methods

Bacterial enrichment and isolation

The marine sediments were sampled from intertidal zone of Xiamen island on April 12, 2021 (11812′25′′E 2429′52′′N), the mangrove garden of Xia-Tan-Wei at the estuary of Xixi River of Xiamen on June 27, 2022 (11812′4′′E 2439′14′′N), and an abandoned pond nearby the mangrove conservation area at the estuary of Zhangjiang River, Zhangzhou on September 14, 2022 (11725′55′′E 2357′18′′N) (Supplementary Figure S1). These samples are black and smell like rotten eggs, implying these sediments are enriched in sulfide. The samples were kept cool and returned to the laboratory. Each of 2 g (wet mass) was suspended with artificial seawater, and then 1 ml was transferred into 50 ml anaerobic bottles respectively containing 10 ml MMJHS medium supplied with 76% H_2/20% CO_2/4% O_2 (200kPa) with hydrogen and thiosulfate as energy sources, or 10 ml of MMJS medium, which contains 76% N_2/20% CO_2/4% O_2 (200 kPa) with thiosulfate as the sole energy source, or 10 ml MMJH medium which contains 76% H_2/20% CO_2/4% O_2 (200 kPa) with hydrogen as the energy source (See supplementary material for medium

composition). All of them were incubated at 32°C according to a method described previously (Jiang et al., 2017). After 3-round enrichment, the cell growth in MMJH medium was observed. Subsequently, cells were purified three times with the dilution-to-extinction technique. The culture in the serum bottle showing growth at the highest dilution was designated as strains XGS-02, XTW-4, and zt1-1. The purity of these cultures was confirmed by microscopic examination and 16S rRNA gene sequencing.

Phenotypic and chemotaxonomic characterization

Cultures were grown in MMJH medium at 30°C for 2 days, cell morphology was observed under transmission electron microscopy (HT7800, Hitachi, Japan). The physiological characterization of three strains was performed in MMJHS medium and growth was measured by direct cell counting using a phase contrast microscope (Eclipse 80i, Nikon) according to the method previously described (Jiang et al., 2017). The temperature range for growth was determined at 4, 10, 15, 20, 25, 28, 30,32, 35, 37, 40, 45, 50 and 60°C. The salinity range for growth was examined by adjusting the concentrations of NaCl between 0 and 9.0% (w/v) at 0.5 (w/v) intervals. Oxygen sensitivity was examined using MMJHS medium with different O_2 concentrations (0%, 1%, 2%, 4%, 6%, 8%, 10%, 15% and 20%) in the headspace gas. In the case of oxygen absence, 10 mM nitrate was added as a potential electron acceptor. The pH range was investigated from 3.5 to 9.0 with a 0.5 pH unit interval by altering pH with several buffers, including 30 mM acetate/acetic acid buffer (pH 3.0–5.0), MES (pH 5.5–6.0), PIPES (pH 6.5–7.0), HEPES (pH 7.5–8.0), Tris and CAPSO (pH 8.0 and above).

To determine the electron donors and acceptors, MMJ synthetic seawater containing 0.1% (w/v) $NaHCO_3$ was used as a basal medium, and H_2 was tested as the electron donor for the growth of three strains, nitrate (0.1%, w/v), nitrite (0.1 and 0.01%, w/v), thiosulfate (0.1%, w/v), sulfite (0.01%, w/v), elemental sulfur (1%, w/v), or molecular oxygen (1%), were tested as the only electron acceptor. The sulfur oxidation was tested with MMJS medium, using sodium thiosulfate (0.1%, w/v) or elemental sulfur (S) (1%, w/v) as sole electron donor, nitrate (0.1%, w/v), nitrite (0.1 and 0.01%, w/v), or molecular oxygen (0.1 and 1%, v/v) were tested as the only electron acceptor. Heterotrophic growth was tested in MMJ medium in the absence of $NaHCO_3$ and in a 94% N_2/6% O_2 (200 kPa) gas phase. The following potential organic carbon compounds were tested: 0.02% (w/v) glucose, galactose and fructose, 0.1% (w/v) peptone, starch and casein, 5 mM formate, acetate, citrate, fumarate and pyruvate.

For fatty acids analysis, cells grown on MMJHS medium at 30C for 24h were saponified, methylated, and extracted following the standard MIDI protocol (Sherlock Microbial Identification System, version 6.0B). The fatty acids were analyzed by gas chromatography (Agilent Technologies 6850), and then the result was identified using the TSBA6.0 database of the Microbial Identification System.

Phylogenetic analysis and genome sequencing

The total DNA of the three strains was extracted and the 16S rRNA gene was amplified as described previously (Jiang et al., 2009). The similarity of 16S rRNA gene sequences was determined using the EzBioCloud server (http://www.ezbiocloud.net/) and NCBI database, and sequences of close strains were downloaded for the phylogenetic analysis. Sequence comparison was performed using CLUSTAL_W (Larkin et al., 2007) and phylogenetic trees were constructed using MEGA X (Kumar et al., 2018) according to the Neighbor-Joining (Tamura et al., 2004), Maximum likelihood and Maximum Parsimony methods (Felsenstein, 1981). The online website TVBOT was used to embellish the phylogenetic tree (Xie et al., 2023). Genetic distance was calculated using Kimura two-parameter model. Bootstrap analysis was calculated based on 1000 replications. The complete genome of strain XGS-02 was sequenced by Tianjin Biochip Corporation (Tianjin, PR China) using the single molecule real-time (SMRT) technology on the Pacific Biosciences (PacBio) sequencing platform. *De novo* assembly was performed using the Hierarchical Genome Assembly Process (Version 4) workflow, and the complete circular genome was derived. Draft genome sequences of strains XTW-4 and zt1-1 were sequenced using Illumina Hiseq 2000 platform (Major Bio-Pharm Technology Co., Ltd, China). Raw reads were clipped and trimmed using Trimmomatic version 0.32 (Bolger et al., 2014). Trimmed reads were assembled using SOAPdenovo (Luo et al., 2015). The G+C content of the genomic DNA was determined from the whole genome sequence. Gene prediction and annotation were performed using NCBI Prokaryotic Genomes Annotation Pipeline (PGAP) (Tatusova et al., 2016) and the Rapid Annotation using Subsystem Technology (RAST) pipeline (Overbeek et al., 2014)

Genomic properties and comparative genomic analysis

We downloaded all culturable *Sulfurovum* genomes available from NCBI database, including four strains *Sulfurovum indicum* ST-419^T, *Sulfurovum riftiae* 1812E^T, *Sulfurovum lithotrophicum* ATCC BAA-797^T, and *Sulfurovum* sp. NBC37-1 from deep-sea hydrothermal vent environments, four strains, *Sulfurovum* sp. TSL1, *Sulfurovum* sp. TSL6, *Candidatus Sulfurovum* sp. AR, and *Sulfurovum* sp. HSL1-3 from coastal sediments. A total of eleven genomic sequences, including three genomes from our newly isolated strains XGS-02, XTW-4, and zt1-1, were checked for completeness and contamination using CheckM (Parks et al., 2015). The phylogenomic tree was constructed based on an up-to-date 92 bacterial core gene sets by UBCG version 3.0 (Na et al., 2018), the ANI was compared using the pyani tool (Pritchard et al., 2016), Pan-genomic analysis was performed with BPGA software (Chaudhari et al., 2016). Protein sequences were identified using PowerBLAST (Zhang and Madden, 1997). Sequence comparison

was performed using MEGA X (Kumar et al., 2018), and phylogenetic trees based on amino acid sequences were constructed using the Maximum Likelihood method with bootstrap values based on 1000 replicates.

Data availability

The GenBank accession numbers for 16S rRNA gene sequence of strains XGS-02, XTW-4 and zt1-1 are OM960633, OP810811 and OP810810, respectively. The genome sequences have been deposited at GenBank under the accession numbers of CP093312, JAQIBC000000000 and JAQIBD000000000, respectively. The three *Sulfurovum* strains were deposited in the Marine Culture Collection of China (MCCC) under collection numbers MCCC 1A18820, MCCC 1A19406, MCCC 1A19490.

Results

Phylogenetic analysis based on 16S rRNA gene and core genome

With enrichments with H_2 as the sole energy source, three strains of *Sulfurovum* were isolated from coastal sediments and designated as strains XGS-02, XTW-4, and zt1-1. In other enriched media, the isolates belonged to genus *Thiomicrorhabdus* and *Sulfurimonas*, which were not the focus of this study. The full-length 16S rRNA gene sequences of strains XGS-02 and zt1-1 retrieved from genomes were 1,503 bp and 1,513 bp, respectively. The 16S rRNA gene sequences of XTW-4 was 1,419 bp. BLAST analysis of the 16S rRNA gene sequences indicated that strains XGS-02, XTW-4, and zt1-1 shared the highest sequence similarity with *S. aggregans* Monchim33^T, which was isolated from a deep-sea hydrothermal vent chimney with similarities of 96.4%, 96.1%, and 95.9%, respectively. They were also closely related to *S. indicum* ST-419^T from the deep-sea hydrothermal plume with 95.6%, 94.6%, and 95.2% similarity, respectively. Furthermore, strains XGS-02 and XTW-4 shared 99.6% sequence similarity with each other and 95.9% and 96.0% similarity with strain zt1-1, respectively. The results indicate that strains XTW-4 and zt1-1 represent two novel species of the genus *Sulfurovum*.

Based on 16S rRNA gene sequences, the phylogenetic tree indicated that strains XGS-02 and XTW-4 clustered with *Sulfurovum* species from non-vent marine habitats, whereas those from vent environments formed separate clusters. Notably, strains zt1-1 and HSL1-3 represented a new branch located differently from other *Sulfurovum* species (Figure 1, Supplementary Figures S2, S3). The phylogeny was confirmed by whole-genome phylogenetic analysis based on 92 core gene sequences (Figure 2), which was consistent with the phylogenetic tree based on the 16S rRNA gene sequences. Combining the phylogenetic tree based on 16S rRNA gene sequences and whole genomes, three different evolutionary branches of the genus *Sulfurovum* were revealed. Correspondingly, three groups were named: Group I, bacteria from intertidal sediments; Group II, bacteria from hydrothermal vent areas; and Group III, bacteria from intertidal sediments (Figure 2).

Phenotypic and chemotaxonomic characterization

Morphological observation by TEM showed that strains XTW-4 and zt1-1 had no flagella. The result was confirmed by a genomic analysis, without genes encoding flagella in their genomes. The cells of strain XTW-4 was short rods, 0.2–0.4 μm wide and 0.4–1.2 μm long (Supplementary Figure S4). The morphology of strain zt1-1 was short rod-shaped, 0.2–0.5 μm wide, and 0.4–1.2 μm long, which was similar to strain XTW-4 (Supplementary Figure S4).

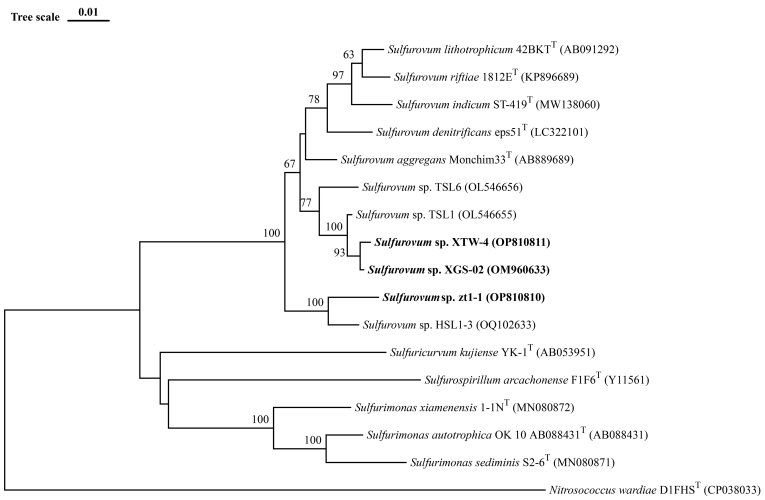

FIGURE 1
Neighbor-Joining phylogenetic tree based on 16S rRNA gene sequences showing the phylogenetic positions of strains XGS-02, XTW-4, zt1-1 and other members of the genus *Sulfurovum*. The tree was rooted using *Nitrosococcus wardiae* as an outgroup. Bootstrap values based on 1000 replicates are shown at branch node. Higher than 50% bootstrap values are shown. Bar, 0.01 substitutions per nucleotide position.

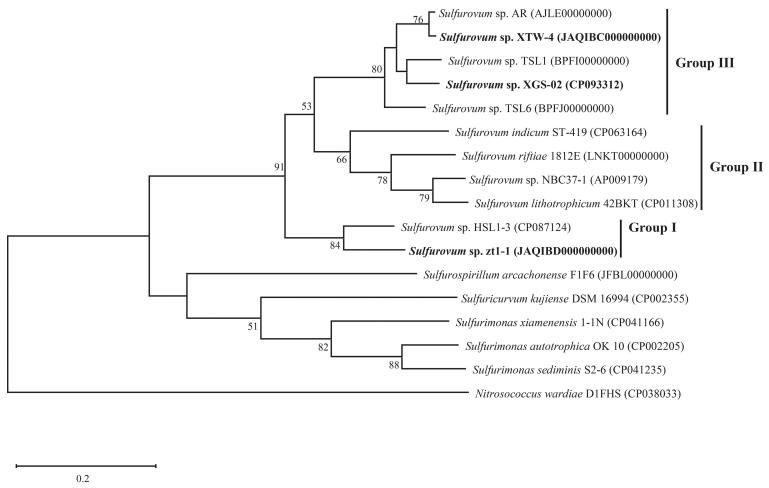

FIGURE 2
Whole genome phylogenetic tree based on 92 core gene sequences showing the position of XGS-02, XTW-4, zt1-1 and closely related taxa within the genus *Sulfurovum* using the maximum-likelihood algorithm. The node is labeled with Gene Support Index (GSI) values. Branch node values below 50% are not shown. The accession numbers of the genomes are shown in parentheses. Bar, 0.2 substitutions per position.

The growth experiment showed that strain XGS-02 could grow at a temperature range of 10–45°C, salinity range of 0.5–4.0% (w/v) NaCl, pH range of 5.5–8.5, and oxygen concentration range of 1–20%. Strain XTW-4 could grow at temperature (15–45°C), salinity (0.5–5.0% (w/v) NaCl), pH (5.0–8.5), and oxygen (1–15%) ranges. Strain zt1-1 could grow at 10–45°C, 0%–7.0% (w/v) NaCl, 4.5–8.5 pH, and 1%–20% O_2. The optimal temperature for the three newly isolated strains was approximately 30°C and the optimum pH was 6.0–6.5. The optimal salinity was 2.5% (w/v) NaCl for strains XGS-02 and XTW-4, and 1.5% (w/v) NaCl for strain zt1-1. The optimum oxygen concentrations were 8% for XGS-02 and XTW-4 and 15% for zt1-1. Chemoautotrophic growth showed that the three strains could utilize hydrogen and thiosulfate as electron donors but fail to oxidize elemental sulfur. They had the highest biomass with hydrogen as the electron donor. Thus, hydrogen may be the preferred energy source for these bacteria. All oxygen, thiosulfate and elemental sulfur can be used as electron acceptors. It is worth mentioning that the strains grew weakly when thiosulfate acted as the electron donor and oxygen acted as electron acceptor. All strains could not use nitrate and nitrite as electron acceptors.

We further compared the physiological characteristics of the three new non-vent strains with those of the vent-type strains, *S. indicum* ST-419^T (Xie et al., 2021), *S. riftiae* 1812E^T (Giovannelli et al., 2016), *S. lithotrophicum* ATCC BAA-797^T (Inagaki et al., 2004), *S. denitrificans* eps51^T (Mori et al., 2018), and *S. aggregans* Monchim33^T (Mino et al., 2014) (Table 1). The results revealed an evident divergence between the vent and non-vent strains. The non-vent strains had an optimal oxygen range of 8–15%, showing higher oxygen adaptation than the vent strains. Moreover, the three non-vent strains could not use nitrate as an electron acceptor, whereas all the vent strains could. All the non-vent *Sulfurovum*-type strains could reduce thiosulfate, but all those of the vent species could not, except for *S. aggregans*. In the case of electron donor utilization, all non-vent strains can utilize hydrogen as an electron donor, while most (3/5) vent strains cannot. In contrast, none of the non-vent strains can grow with elemental sulfur as the sole energy source, whereas most (4/5) vent strains can grow.

The fatty acid profiles of strains XTW-4 and zt1-1 and related type strains are listed in Table 1. Strain XTW-4 contained the predominant cellular fatty acids $C_{18:1}\omega7c$ (35.0%), $C_{16:1}\omega7c$ (24.5%), and $C_{16:0}$ (16.4%), and strain zt1-1 mainly contained $C_{16:1}\omega7c$ (35.9%), $C_{18:1}\omega7c$ (18.1%), and $C_{16:0}$ (17.6%). These profiles are similar to those of *S. indicum* ST-419^T, *S. riftiae* 1812^T, and *S. denitrificans* eps51^T.

Genomic features of the two novel species of *Sulfurovum*

The genome size of strain XTW-4 was 2.20 Mb with a GC content of 39.1%, and the genome size of zt1-1 was 2.18 Mb with a GC content of 39.3%. A total of 2,268 genes were predicted in the genome of strain XTW-4, including 2,203 protein-coding and 65 RNA genes. The genome of strain zt1-1 contains 2,267 genes, including 2,209 protein-coding genes and 58 RNA genes. The genomic similarity of strains XTW-4 and zt1-1 with other species of the genus *Sulfurovum* was determined using ANI values. The paired ANI values between strain XTW-4 and its close relatives, *S. indicum* and *S. riftiae*, were 86.0% and 85.7%, respectively. The paired ANI values between strain zt1-1 and its close relatives, *S. indicum* and *S. riftiae*, were 84.0% and 84.4%, respectively. These findings support the classification of strains XTW-4 and zt1-1 as two distinct species based on the cut-off threshold of ANI (95–96%) for the delineation of prokaryotic species. Strains XTW-4, zt1-1, and others of *Sulfurovum*

TABLE 1 Comparison of physiological characteristics within the genus *Sulfurovum*. .

		Sulfurovum sp. XTW-4	*Sulfurovum* sp. zt1-1	*Sulfurovum* sp. XGS-02	*S.aggregans* Monchim33^T	*S.indicum* ST-419^T	*S.riftiae* 1812^T	*S.lithotrophicum* ATCC BAA-797^T	*S.denitrificans* eps51^T
Source of Isolation		Non-vent	Non-vent	Non-vent	Vent	Vent	Vent	Vent	Vent
Temperature ranges (°C)		15–45	10–45	10–45	15–37	4–45	25–40	10–40	10–35
(Optimum)		(32)	(32)	(30)	(33)	(37)	(35)	(28–30)	(30)
Salinity ranges (%)		0.5–5.0	0–7.0	0.5–4.0	2.0–4.0	1.0–5.0	1.5–4.0	2.0–4.0	2.0–5.0
(Optimum)		(2.5)	(1.50)	(2.5)	(2.5)	(3.0)	(3.0)	(2.5)	(3.0)
Oxygen conditions (%)		1–15	1–20	1–20	3	1–20	–	1–7.5	20
(Optimum)		(8–10)	(15)	(8–10)	ND	(5)	–	ND	ND
pH ranges		5.0–8.5	4.5–8.5	5.5–8.5	5.5–8.6	5.0–8.6	5.0–8.0	5.0–9.0	6.5–7.5
(Optimum)		(6.0–6.5)	(6.0–6.5)	(6.0–6.5)	(6.0)	(6.0)	(6.0)	(6.5–7.0)	(7.0)
Electron donor	H_2	+	+	+	+	+	–	–	–
	$S_2O_3^{2-}$	+	+	+	–	+	+	+	+
	S^0	–	–	–	–	+	+	+	+
Electron acceptor	O_2	+	+	+	ND	+	–	+	+
	NO_3^-	–	–	–	+	+	+	+	+
	$S_2O_3^{2-}$	+	+	+	+	–	–	–	–
	S^0	+	+	+	+	+	–	–	–
Major fatty acids %		$C_{16:1}\omega7c$ (24.47)	$C_{16:1}\omega7c$ (35.9)	ND	$C_{16:1}\omega7c$ (18.1)	$C_{16:1}\omega7c$ (50.3)	$C_{16:1}\omega7c$ (34.3)	$C_{16:1}\omega7c$ (53.7)	$C_{16:1}\omega7c$ (61.1)
		$C_{18:1}\omega7c$ (35.0)	$C_{18:1}\omega7c$ (18.1)		$C_{18:0}$ (18.9)	$C_{18:1}\omega7c$ (19.5)	$C_{18:1}\omega7c$ (28.4)	$C_{16:0}$ (31.3)	$C_{18:1}\omega7c$ (17.4)
		$C_{16:0}$ (16.4)	$C_{16:0}$ (17.6)		$C_{16:0}$ (40.0)	$C_{16:0}$ (11.3)	$C_{16:0}$ (15.4)	$C_{18:0}$ (15.0)	$C_{16:0}$ (13.2)

Data of S.riftiae 1812^T from Donato Giovannelli (Giovannelli et al., 2016), S. lithotrophicum ATCC BAA-797^T from Fumio Inagaki (Inagaki et al., 2004), S.denitrificans eps51^T from Koji Mori (Mori et al., 2018), and S.aggregans Monchim33^T from Sayaka Mino (Mino et al., 2014). +, present; –, absent; ND, no data.

species shared less than 40.0 % DDH values (Table S2). The low DDH values (< 70%) confirmed that strains XTW-4 and zt1-1 represented two novel species within the genus *Sulfurovum* (Stackebrandt and Goebel, 1994; Auch et al., 2010; Meier-Kolthoff et al., 2014).

Comparative genomic analysis within the genus

A total of 11 *Sulfurovum* genomes from hydrothermal vents and intertidal environments were used for comparative analysis in this study. The genome size range of the non-vent *Sulfurovum* species was 2.1–2.6 Mb, and the G+C content ranged from 38.4 to 43.6%, while the genome size range of the vent strain was 2.2–2.6 Mb and the range of G+C content was 42.5–45.7%. The results showed that *Sulfurovum* species from deep-sea hydrothermal vent environments had relatively higher G+C values (Table 2). In addition, comparative genomic analysis revealed 1051 core genes in all *Sulfurovum* genomes (Supplementary Figure S5). The percentage of core genes per genome ranged from 42.8% to 50.9%, and the percentage of unique genes per genome ranged from 5.4% to 19.6%. *Sulfurovum* genomes belonging to Group I had 12.2–19.3% of unique genes, and those genomes from Group II had 11.9–17.9%. Group III from non-vent genomes had the lowest percentage of unique genes (< 9%) (Table S1).

Central metabolisms of *Sulfurovum*

Nitrogen metabolism and its differentiation among vent and non-vent origins

Comparative genomic analysis showed significant differences in nitrogen metabolism between the vent and non-vent *Sulfurovum* species (Table 3). *Sulfurovum* species from hydrothermal vent habitats contain genes required for the complete denitrification pathway, including the *napAB* gene encoding outer membrane nitrate reductase, the *nirS* gene encoding nitrite reductase, the *norBC* gene encoding nitric oxide reductase, and the *nosZ* gene encoding nitric oxide reduction enzyme. In addition, the genes *nrfA* and *napA*, performing a heterotrimeric nitrate reduction pathway, were present in all vent *Sulfurovum* genomes. Intriguingly, the denitrification and dissimilatory nitrate reduction pathways were completely absent in all non-vent *Sulfurovum* genomes, except for strain TSL1, which only has a denitrification-related *nirk* gene.

TABLE 2 Genomic information of all *Sulfurovum* strains available in NCBI database and obtained in this study.

Strains	completeness (%)	contamination (%)	Genome size (Mb)	G + C (%)	CDS	Source of Isolation	NCBI accession No.
S.xiamenensis XGS-02	99.6	2.3	2.2	40.2	2131	coastal sediments	CP093312
S.xiamenensis XTW-4	99.6	2.5	2.2	39.1	2203	mangrove sediments	JAQIBC000000000
S.zhangzhouensis zt1-1	99.0	2.1	2.2	39.4	2209	coastal sediments	JAQIBD000000000
Sulfurovum sp. HSL1-3	99.6	2.7	2.6	43.6	2533	mangrove sediments	CP087124
Candidatus Sulfurovum sp. AR	99.0	1.6	2.1	39.2	2122	marine sediment	NZ_AJLE00000000
Sulfurovum sp. TSL1	99.6	4.7	2.4	40.7	2292	marine sediment	BPFI00000000
Sulfurovum sp. TSL6	99.6	2.7	2.3	38.4	2205	marine sediment	BPFJ00000000
S.indicum ST-419^T	99.2	0.4	2.2	42.5	2155	hydrothermal vent field	CP063164
Sulfurovum sp. NBC37-1	99.6	0.6	2.6	43.9	2546	deep-sea hydrothermal vent	AP009179
S.lithotrophicum ATCC BAA-797^T	98.0	1.6	2.2	44.3	2184	hydrothermal vent sediments	CP011308
S.riftiae 1812E^T	98.6	1	2.4	45.7	2343	hydrothermal polychaete	NZ_LNKT00000000

Interestingly, key genes encoding nitrogen-fixing enzymes were observed for the first time in *Sulfurovum* genomes, including *nifH, nifD*, and *nifK*, but only in the non-vent strains zt1-1 and HSL1-3. In the phylogenetic tree, we found that the *nifH* of *Sulfurovum* represents a different branch from that of *Betaproteobacteria* and *Alphaproteobacteria* (Supplementary Figure S6).

Hydrogen metabolism and the differentiation within the genus

Sulfurovum species contain three types of hydrogenases (Table 3): Type I, Type II, and Type IV. However, *S. lithotrophicum* only contains Type IV hydrogenase. Type I hydrogenases are the most widely distributed among members of the genus *Sulfurovum*. They usually have multiple copies of Type I hydrogenases, and *S. indicum* contains four copies of Type I hydrogenases (Figure 3). Type II was not conserved in *Sulfurovum* species, as in Type I, which was absent in some non-vent isolates, such as *Sulfurovum* sp. AR, TSL1, TSL6, and the vent-type *S. lithotrophicum* strains. Intriguingly, Type IV was only detected in the vent isolates, which belong to the hydrogenase Hyc type, except for *S. indicum* with a Coo type. In addition, phylogenetic analysis based on the large subunit of hydrogenase showed that hydrogenases from vent genomes and non-vent genomes of the genus *Sulfurovum* clustered together.

Differentiation in sulfur metabolism among vent and non-vent origins

For sulfide oxidation, *Sulfurovum* species contain four sulfoquinone oxidoreductase (Sqr) types, including Type II, Type III, Type IV, and Type VI (Supplementary Figure S7). Type II Sqr was present in all strains (Table 3), implying that it is essential for sulfide oxidation in *Sulfurovum* species. Notably, the vent strains contained more copies of Type II Sqr, up to four copies in strain NBC37-1 and *S. riftiae*, in contrast to the single copy in the non-vent strains. Type III Sqr was present only in the non-vent strain HSL1-3, whereas Type VI Sqr was present in all strains in a single copy. Phylogenetic analysis showed that the vent and non-vent branches of Sqr were located in different evolutionary clusters, and Sqr from different groups of *Sulfurovum* clustered together.

In addition, all *Sulfurovum* species encode the complete sox gene cluster (*soxABXYZ* and *soxCDYZ*) for thiosulfate oxidation. The phylogenetic tree based on the SoxB protein showed a topology similar to that of the phylogenomic analysis of *Sulfurovum*, suggesting that the SoxB gene in *Sulfurovum* species is acquired by vertical inheritance within the lineage (Supplementary Figure S8). For elemental sulfur respiration, all *Sulfurovum* strains have polysulfide reductase (Psr) of the three groups, which can reduce elemental sulfur to sulfide (Table 3). Phylogenetic analysis showed that polysulfide reductase Group I was detected in all *Sulfurovum* species from non-vent environments, encoded by five genes, *psrA1B1CDE*. Groups II and III were also present in some non-vent strains, such as TSL6, XGS-02, and HSL1-3 (Supplementary Figure S9).

TABLE 3 Comparison of key enzymes for nitrogen, hydrogen, and sulfur metabolisms in *Sulfurovum* species based on RAST annotations in this study.

		S.xiamenensis XGS-02	*S.xiamenensis* XTW-4	*S.zhangzhouensis* zt1-1	*Sulfurovum* sp. HSL1-3	*Candidatus Sulfurovum* sp. AR	*Sulfurovum* sp. TSL1	*Sulfurovum* sp. TSL6	*S.indicum* ST-419^T	*Sulfurovum* sp. NBC37-1	*S.lithotrophicum* ATCC BAA-797^T	*S.riftiae* 1812E^T
Nitrogen metabolism	Denitrification	-	-	-	-	-	*nirK*	-	*napA,napB,nirS, norB,norC,nosZ*	*napA,napB,nirS, norB,norC,nosZ*	*napA,napB,nirS, norB,norC,nosZ*	*napA,napB,nirS, norB,norC,nosZ*
	Dissimilatory nitrate reduction to ammonium (DNRA)	-	-	-	-	-	-	-	*napA*	*napA,nrfA*	*napA*	*napA,nrfA*
	Nitrogen fixation	-	-	*nifH,nifD,nifK*	*nifH,nifD, nifK*	-	-	-	-	-	-	-
Hydrogen metabolism	Hydrogenases Type I	3	3	3	2	2	2	2	4	2	-	2
	Hydrogenases Type II	+	+	+	+	-	-	-	+	+	-	+
	Hydrogenases Type IV	-	-	-	-	-	-	-	+	+	+	+
Sulfur metabolism	Sulfur oxidation protein (Sox)	SoxABXYZ SoxCDYZ	SoxABXYZ SoxCDYZ	SoxABXYZ SoxCDYZ	SoxABXYZ SoxCDYZ	SoxABXYZ SoxCDYZ	SoxABXYZ SoxCDYZ	SoxABXYZ SoxCDYZ	SoxABXYZ SoxCDYZ	SoxABXYZ SoxCDYZ	SoxABXYZ SoxCDYZ	SoxABXYZ SoxCDYZ
	Sulfide:quinone oxidoreductase (Sqr)	II(1), IV(1), VI(1)	II(1), IV(1), VI(1)	II(1), IV(1),VI(1)	II(1), III(1), IV(1),VI(1)	II(1), IV(1), VI(1)	II(1), IV(1), VI(1)	II(1), VI(1)	II(1), IV(1),VI (1)	II(4), IV(1),VI (1)	II(3), IV(1),VI(1)	II(4), IV(1),VI (1)
	Polysulfide reductase (PsrA)	*$psrA_1B_1CDE$, $psrA_2B_2$*	*$psrA_1B_1CDE$*	*$psrA_1B_1CDE$*	*$psrA_1B_1CDE$, $psrA_3B_3$*	*$psrA_1B_1CDE$*	*$psrA_1B_1CDE$*	*$psrA_1B_1CDE$, $psrA_2B_2$*	*$psrA_1B_1CDE$, $psrA_2B_2$, $psrA_3B_3$, $psrA_4B_4$*	*$psrA_1B_1CDE$, $psrA_2B_2$*	*$psrA_1B_1CDE$, $psrA_2B_2$*	*$psrA_1B_1CDE$, $psrA_2B_2$*
Oxidative stress	Superoxide dismutase	+	+	+	+	+	+	+	2	-	-	-
	Catalase	+	+	+	+	+	+	+	-	+	+	-
	Cytochrome c peroxidase	+	+	+	2	+	+	+	3	3	3	3
	Thiol peroxidase	+	+	+	+	+	+	+	+	+	+	+
Respiratory metabolism	heme-copper oxidase, caa3-type	*coxA,coxB, coxC*	*coxA,coxB, coxC*	*coxA,coxB,coxC*	-	*coxA,coxB, coxC*	*2(coxA, coxB,coxC)*	*coxA,coxB, coxC*	-	-	-	-
	heme-copper oxidase cbb3-type	*ccoN,ccoO, cooP,ccoQ*	*ccoN,ccoO, cooP,ccoQ*	*ccoN,ccoO, cooP, ccoQ*	*ccoN,ccoO, cooP,ccoQ*	*ccoN,ccoO, cooP,ccoQ*	*ccoN,ccoO, cooP,ccoQ*	*ccoN,ccoO, cooP,ccoQ*	*ccoN(2),ccoO(2), cooP,ccoQ*	*ccoN(2),ccoO(2), cooP,ccoQ*	*ccoN,ccoO, cooP, ccoQ*	*ccoN(2),ccoO(2), cooP,ccoQ*
	bd oxidases Superfamily											
	bd-type quinol oxidase	-	-	*cydA,cydB*	*cydA,cydB*	-	*cydA,cydB*	-	*cydA,cydB*	-		

"+" indicated present; "-" indicated absent.

10.3389/fmars.2023.1222526

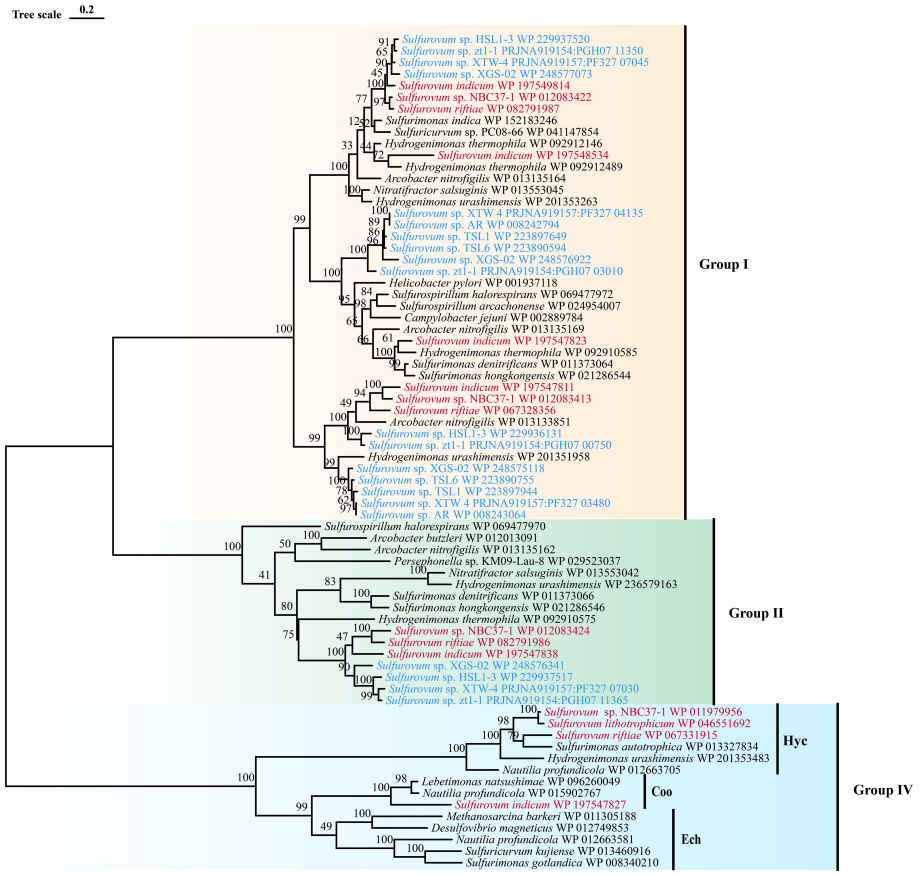

FIGURE 3
Maximum-likelihood tree based on large subunit sequences of hydrogenase from *Sulfurovum*. Bootstrap values shown on each node are based on a total of 1000 bootstrap replicates. Branch node values below 50% are not shown. The isolation source of the *Sulfurovum* species were indicated by different font colors: red, deep-sea hydrothermal vent environments; blue, marine non-vent system.

Differentiation in antioxidation and terminal oxidases

Genes encoding superoxide dismutase and catalase, which are involved in oxidative stress, were found in non-vent strains (Table 3), while superoxide dismutase was absent in vent strains NBC37-1, *S. lithotrophicum* and *S. riftiae*, and catalase was absent in *S. indicum* and *S. riftiae*. In addition, all *Sulfurovum* strains contain genes encoding cytochrome c peroxidase and thiol peroxidase, which scavenge peroxides and provide defense against oxidative damage (Missall et al., 2004). Vent *Sulfurovum* genomes usually have more copies of cytochrome c peroxidase than those from non-vent environments. Multiple terminal oxidases are present in the *Sulfurovum* genomes, all containing cbb3-type cytochrome c oxidase (Table 3). Phylogenetic analysis showed that cbb3 type cytochrome c oxidase clustered into two groups: CcoN I and CcoN II (Supplementary Figure S10). All strains containing CcoN I and CcoN II were of vent origin. The *coxA*-encoded caa3 type terminal oxidase was present in non-vent strains and absent in vent strains (Table 3). In addition, some *Sulfurovum* strains, such as zt1-1, HSL1-3, TSL1, and *S. indicum*, contained genes encoding cytochrome bd ubiquinone oxidase.

Discussion

Sulfurovum spp. in the *Campylobacteria* class are important chemolithoautotrophic bacteria with wide distribution in sulfidic habitats in the ocean, and they play an essential role in marine carbon, nitrogen, and sulfur biogeochemical cycling (Patwardhan et al., 2018; Sun Q. L. et al., 2020; Huang L. B. et al., 2021; Wang Y. et al., 2022). However, knowledge about this important bacterial taxon has been limited to deep-sea hydrothermal vent environments, and little is known about its diversity and ecological role in non-vent environments. In the present study, we isolated these species from coastal sediments. Further comparative analyses revealed the presence of unique metabolic features. Evident diversification was confirmed by phylogenetic analysis of vent and non-vent origins.

Two novel species of non-vent origin of the genus

To our knowledge, this is the first report of a novel species of non-vent origin in *Sulfurovum*. The combined phenotypic, chemotaxonomic, and phylogenetic characteristics demonstrated

that strains XTW-4 and zt1-1 represent two new species in the genus *Sulfurovum*, for which the names *Sulfurovum xiamenensis* sp. nov. and *Sulfurovum zhangzhouensis* sp. nov. are proposed, both of which showed the closest 16S rRNA gene sequence similarity to *S. aggregans* Monchim33^T (95.8% and 95.4%, respectively). They differed from other type strains in phenotypical features, such as optimum salinity and oxygen concentrations and the utilization of electron acceptors. Intriguingly, the two coastal species both respired for thiosulfate, while the vent strains could not; however, while the vent strains could respire nitrate, the two coastal strains could not (Table 1).

Environmental adaptations of Sulfurovum revealed by comparative genomic analyses

To understand their environmental adaptation, we performed comparative genomic analyses between the vent and non-vent *Sulfurovum* strains. Significant differences were observed in key metabolic mechanisms and stress responses between the vent and non-vent strains, implying that their adaptive evolution and species diversification were related to inhabitance.

Correspondingly, we found that all members of the genus *Sulfurovum* from deep-sea hydrothermal vents contained a complete denitrification pathway in addition to some genes involved in dissimilatory nitrate reduction to ammonia (DNRA) in part vent strains. Denitrification and DNRA processes are currently considered to be two competing pathways for nitrate reduction (Bu et al., 2017; Jia et al., 2020; Pandey et al., 2020; Li S. et al., 2022), and few studies have reported their coexistence except for *Pseudomonas* and *Shewanella* (Kuypers et al., 2018; Huang X. J. et al., 2021; Liu et al., 2021). The nitrate reduction pathway (NAP) is considered conserved and widespread in the phylum *Campylobacterota* based on bacteria from deep-sea hydrothermal vent habitats (Vetriani et al., 2014). However, these two processes were absent in our coastal strains. Sulfur oxidation coupled with nitrate reduction is considered the primary source of energy in vent ecosystems (Wang et al., 2009), whereas this process does not occur in coastal *Sulfurovum* species. The genome revealed that the denitrification and DNRA pathways were completely absent, and experimental validation showed that they could not use nitrate as an electron acceptor. To compensate, our two *Sulfurovum* species adapted to higher oxygen concentrations and preferred to use oxygen as an electron acceptor, which is in agreement with the loss of denitrification and DNRA-related genes, as well as other non-vent *Sulfurovum* strains (unpublished data).

Intriguingly, members of the genus *Sulfurovum* from coastal sediments possess genes for nitrogen fixation, which are absent in deep-sea vent *Sulfurovum*. Coastal mangrove sediments are recognized to be nitrogen-limited due to the unbalance of carbon and nitrogen caused by burying of carbon-rich plant litter (Lin et al., 2019; Luo et al., 2021). Nitrogen-fixing bacteria are considered to play a key role in nitrogen amendment (Alfaro-Espinoza and Ullrich, 2015; Tang et al., 2020; Luo et al., 2021). Therefore, *Sulfurovum* containing nitrogenase genes are of competitive advantage in coastal environments. Recently, the expression of Nif genes associated with *Sulfurovum* spp., as well as the presence of the *nifH* gene in a *Sulfurovum* metagenome-assembled genome (MAG) was demonstrated at a coastal gas vent site (Patwardhan et al., 2021). Certainly, not all coastal *Sulfurovum* have nitrogenase genes. This is probably due to highly variable environmental parameters in coastal sediments. In contrast, ammonia is relatively abundant in the vent fluid, which can reach micromolar level *in situ* (Xu et al., 2014), and can be oxidized to nitrate by ammonia-oxidizing archaea (Crepeau et al., 2011; Zhang et al., 2016; Ding et al., 2017). Thus, genes for nitrogen fixation in deep-sea vent may be redundant and lost in all vent *Sulfurovum*. The differentiation of *Sulfurovum* in accordance with unique habitats expands our understanding of the genus in terms of environmental adaptation (Figure 4).

Reduced sulfur compounds, such as sulfides, are important energy sources for chemolithoautotrophs in deep-sea vents. Unexpectedly, we found that coastal isolates of *Sulfurovum* grew best with hydrogen as an electron donor and weakly with thiosulfate and sulfide. Moreover, all members of this genus contain an extensive suite of hydrogenases, including [NiFe]-hydrogenase groups 1b, 2d, and 4 (Hyc and Coo). The most frequently occurring hydrogenases belonged to Group I. Almost all *Sulfurovum* members contained multiple copies of this group, probably in response to different hydrogen concentrations, suggesting that hydrogenase in Group I plays an important role in energy draining to support bacterial growth (Grote et al., 2012; Berney et al., 2014).

Regarding sulfide oxidation, *Sulfurovum* species contain genes encoding different types of Sqr, classified as types II, III, IV, and VI. The diversification of these Sqr genes is thought to play important roles in sulfide oxidation, sulfide assimilation, energy production, heavy metal tolerance, detoxification, and sulfide signaling (Marcia et al., 2010). Additionally, *Sulfurovum* bacteria have one or more copies of Type II Sqr (Table 3), which may compensate for other Sqrs under specific environmental conditions (Wang et al., 2021). Thiosulfate (Figure 4) can commonly be oxidized by *Sulfurovum* of any origin, but as an electron acceptor, it can be used by non-vent *Sulfurovum*, as confirmed by our coastal pure cultures (Table 1).

Sulfurovum usually grows in a mixed zone with unsaturated oxygen concentration (Meier et al., 2017). Antioxidation systems may be essential for traveling across redox gradients to oxic areas. Reactive oxygen species (ROS) are formed by the intermediate products of oxygen reduction and can cause damage to cellular macromolecules (Cabiscol et al., 2000). Superoxide dismutase and catalase are the most well-characterized ROS defense mechanisms (Johnson and Hug, 2019). Interestingly, we found that the genes encoding both superoxide dismutase and catalase were present in the non-vent strains but were partially or completely absent in the vent strains (Table 3). In addition, some terminal oxidases function in the defense against ROS (Kaminski et al., 1996; Hassani et al., 2010; Borisov and Siletsky, 2019), allowing certain strictly anaerobic bacteria to grow in microaerobic environments, such as cbb3-type hemocopper oxidase and cytochrome bd ubiquinone oxidase. All pure culture strains of *Sulfurovum* contain the CcoNOQP operon, which encodes a cbb3-type cytochrome c oxidase that supports bacterial growth under anaerobic and microaerobic conditions

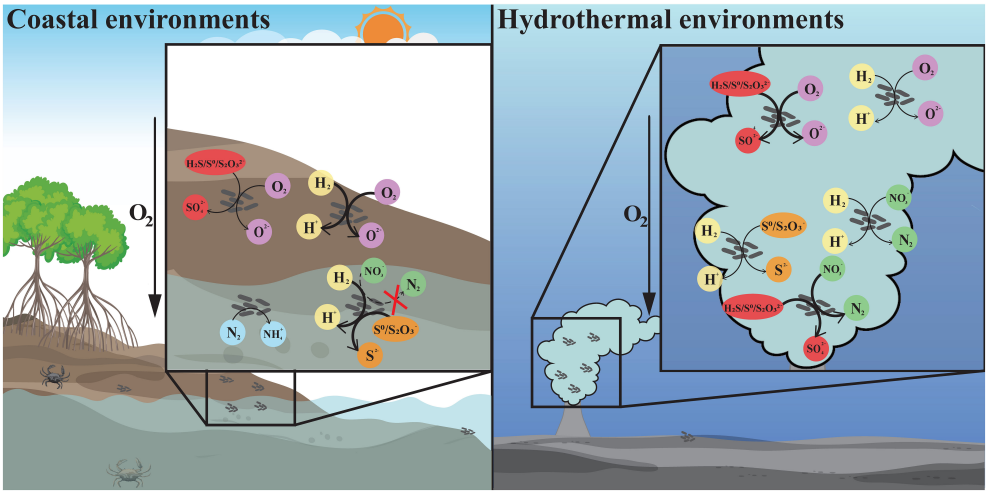

FIGURE 4
The differentiation and adaptation of *Sulfurovum* bacteria in coastal sediment and deep-sea hydrothermal vent environments. Metabolic features of *Sulfurovum* with different origins, including hydrogen oxidation (yellow), sulfur oxidation (red), oxygen reduction (purple), sulfur reduction (orange), denitrification (green), and nitrogen fixation (blue). The arrows with different styles indicate the presence or absence of the related metabolic pathway, and whether it is the major energy-acquiring pathway. Thick solid line: the process is present and probably the main process; thin solid line: the relevant gene is present; thin dashed line: the relevant gene is absent. Left: coastal environments represented by a mangrove ecosystem; right: deep-sea hydrothermal vent environment.

owing to its high affinity for oxygen. Some strains also encode cytochrome bd ubiquinone oxidase, which is an alternative oxidase found in many bacteria that oxidizes ubiquinone and reduces oxygen as part of the electron transport chain. In addition, unlike vent strains, non-vent strains have a caa3-type hemocopper oxidase that catalyzes the reduction of oxygen to water and may play an important role in oxygen adaptation. Hence, it is possible that the ROS defense mechanisms enable coastal *Sulfurovum* bacteria to deal with oxidative stress caused by increased O_2 concentrations in coastal environments. This is consistent with their wider growth ranges with regard to oxygen concentrations (1–15%) and higher optimum oxygen concentration compared the vent *Sulfurovum* bacteria (Table 1).

Conclusions

Two novel *Sulfurovum* species were characterized from coastal marine habitats for the first time, *Sulfurovum xiamenensis* and *Sulfurovum zhangzhouensis*, contributing to the understanding of the ecological role of *Sulfurovum* in marine environments. As summarized in Figure 4, the coastal isolates significantly differed from the vent species of this genus in energy metabolism and environmental adaptation. Non-vent *Sulfurovum* bacteria cannot respire nitrate because of the lack of nitrate reduction pathways but can reduce thiosulfate coupling hydrogen oxidation in addition to high oxygen concentrations. Moreover, non-vent members can perform nitrogen fixation, which might facilitate their survival in niches with limited N sources. These results reveal the diversification among members inhabiting deep-sea vent and non-vent ecosystems and highlight the unique roles of *Sulfurovum* in coastal marine environments.

Description of *Sulfurovum xiamenensis* sp. nov.

Sulfurovum xiamenensis (xia.men.en'sis. N.L. masc. adj. *xiamenensis* of Xiamen, a city in Fujian, China, where the type strain was isolated).

Cells are Gram-negative short rods (0.4-1.2 × 0.2-0.4 μm) without flagella. Optimum oxygen concentration 8%-10%. Growth occurs at 15-45°C (optimum 32°C), pH 5.0-8.5 (optimum pH 6.0-6.5), and 0.5-5.0% (w/v) NaCl (optimum 2.5%). Obligate chemolithoautotrophic growth occurs with H_2 as electron donor, and oxygen, thiosulfate, and S^0 can be utilized as electron acceptors. It also growth occurs with thiosulfate as an electron donor and oxygen as an electron acceptor. Organic substrates are not utilized as carbon sources and energy sources. Major cellular fatty acids are $C_{18:1}\omega7c$, $C_{16:1}\omega7c$ and $C_{16:0}$.

The type strain, XTW-4^T (=MCCC 1A19406), was isolated from mangrove sediments in, Xiamen, Fujian Province, PR China. The genomic G+C content of the type strain is 39.1 mol%.

Description of *Sulfurovum zhangzhouensis* sp. nov.

Sulfurovum zhangzhouensis (zhang.zhou.en'sis. N.L. masc. adj. *zhangzhouensis* of Zhangzhou, a city in Fujian, China, where the type strain was isolated).

Cells are Gram-negative short rods (0.4-1.2 × 0.2-0.5 μm) without flagella. Optimum oxygen concentration 15%. Growth occurs at 10-45°C (optimum 32°C), pH 4.5-8.5 (optimum pH 6.0-6.5), and 0.5-7.0% (w/v) NaCl (optimum 1.5%). Obligate chemolithoautotrophic growth occurs with H_2 as electron donor, and oxygen, thiosulfate, and S^0 can be utilized as electron acceptors. It also growth occurs with thiosulfate

as an electron donor and oxygen as an electron acceptor. Organic substrates are not utilized as carbon sources and energy sources. Major cellular fatty acids are $C_{16:1}\omega7c$, $C_{18:1}\omega7c$ and $C_{16:0}$.

The type strain, zt1-1^T (=MCCC 1A19490), was isolated from the sediment of retirement ponds in Yunxiao County, Zhangzhou City, Fujian Province, PR China. The genomic G+C content of the type strain is 39.4 mol%.

Data availability statement

The datasets presented in this study can be found in online repositories. The names of the repository/repositories and accession number(s) can be found in the article/Supplementary Material.

Author contributions

ZS and LJ conceived the study. JW, LJ, QZ, and ZS designed the experiments. JW, YZ, and QY participated in the sample collection. JW performed the experiments and analyzed the data. JW and JZ drafted the manuscript. SW, QZ, LJ, and ZS revised the manuscript, which was finally read and corrected by ZS. All authors read and approved the final manuscript. All authors contributed to the article.

Funding

Financial support was provided by the National Natural Science Foundation of China (No. 42176134 to LJ; No.42030412 to ZS), the China Ocean Mineral Resources R&D Association (COMRA) program (No. DY135-B2-01 to ZS), National Key Research and Development Program of China (No. 2018YFC0310701 to ZS), the Scientific Research Foundation of Third Institute of Oceanography, MNR (No. 2019021 to ZS).

Acknowledgments

We thank Dr. Ding Li and M.S. Xuying Zhu from the Third Institute of Oceanography for their help in the collection of XGS-02 samples.

Conflict of interest

The authors declare that the research was conducted in the absence of any commercial or financial relationships that could be construed as a potential conflict of interest.

Publisher's note

Supplementary material

The Supplementary Material for this article can be found online at: https://www.frontiersin.org/articles/10.3389/fmars.2023.1222526/full#supplementary-material

References

Akerman, N. H., Butterfield, D. A., and Huber, J. A. (2013). Phylogenetic diversity and functional gene patterns of sulfur-oxidizing subseafloor Epsilonproteobacteria in diffuse hydrothermal vent fluids. *Front. Microbiol.* 4. doi: 10.3389/fmicb.2013.00185

Alfaro-Espinoza, G., and Ullrich, M. S. (2015). Bacterial N-2-fixation in mangrove ecosystems: insights from a diazotroph-mangrove interaction. *Front. Microbiol.* 6. doi: 10.3389/fmicb.2015.00445

Auch, A. F., von Jan, M., Klenk, H.-P., and Goeker, M. (2010). Digital DNA-DNA hybridization for microbial species delineation by means of genome-to-genome sequence comparison. *Stand. Genomic Sci.* 2 (1), 117–134. doi: 10.4056/sigs.531120

Berney, M., Greening, C., Hards, K., Collins, D., and Cook, G. M. (2014). Three different NiFe hydrogenases confer metabolic flexibility in the obligate aerobe Mycobacterium smegmatis. *Environ. Microbiol.* 16 (1), 318–330. doi: 10.1111/1462-2920.12320

Bolger, A. M., Lohse, M., and Usadel, B. (2014). Trimmomatic: a flexible trimmer for Illumina sequence data. *Bioinformatics* 30 (15), 2114–2120. doi: 10.1093/bioinformatics/btu170

Borisov, V. B., and Siletsky, S. A. (2019). Features of organization and mechanism of catalysis of two families of terminal oxidases: Heme-copper and bd-type. *Biochem. (Mosc)* 84 (11), 1390–1402. doi: 10.1134/s0006297919110130

Bu, C., Wang, Y., Ge, C., Ahmad, H. A., Gao, B., and Ni, S.-Q. (2017). Dissimilatory nitrate reduction to ammonium in the yellow river estuary: Rates, abundance, and community diversity. *Sci. Rep.* 7 (1), 6830. doi: 10.1038/s41598-017-06404-8

Cabiscol, E., Tamarit, J., and Ros, J. (2000). Oxidative stress in bacteria and protein damage by reactive oxygen species. *Int. Microbiol.* 3 (1), 3–8.

Chaudhari, N. M., Gupta, V. K., and Dutta, C. (2016).). BPGA- an ultra-fast pan-genome analysis pipeline. *Sci. Rep.* 6, 24373. doi: 10.1038/srep24373

Chiu, L., Wang, M.-C., Tseng, K.-Y., Wei, C.-L., Lin, H.-T., Yang, S.-H., et al. (2022). Shallow-water hydrothermal vent system as an extreme proxy for discovery of microbiome significance in a crustacean holobiont. *Front. Mar. Sci.* 9. doi: 10.3389/fmars.2022.976255

Crepeau, V., Bonavita, M. A. C., Lesongeur, F., Randrianalivelo, H., Sarradin, P. M., Sarrazin, J., et al. (2011). Diversity and function in microbial mats from the Lucky Strike hydrothermal vent field. *FEMS Microbiol. Ecol.* 76 (3), 524–540. doi: 10.1111/j.1574-6941.2011.01070.x

Dahle, H., Roalkvam, I., Thorseth, I. H., Pedersen, R. B., and Steen, I. H. (2013). The versatile in *situ* gene expression of an Epsilonproteobacteria-dominated biofilm from a hydrothermal chimney. *Environ. Microbiol. Rep.* 5 (2), 282–290. doi: 10.1111/1758-2229.12016

Ding, J., Zhang, Y., Wang, H., Jian, H. H., Leng, H., and Xiao, X. (2017). Microbial community structure of deep-sea hydrothermal vents on the ultraslow spreading southwest Indian ridge. *Front. Microbiol.* 8. doi: 10.3389/fmicb.2017.01012

Felsenstein, J. (1981). Evolutionary trees from dna-sequences - A maximum-likelihood approach. *J. Mol. Evol.* 17 (6), 368–376. doi: 10.1007/bf01734359

Giovannelli, D., Chung, M., Staley, J., Starovoytov, V., Le Bris, N., and Vetriani, C. (2016). Sulfurovum riftiae sp nov., a mesophilic, thiosulfate-oxidizing, nitrate-reducing chemolithoautotrophic epsilonproteobacterium isolated from the tube of the deep-sea hydrothermal vent polychaete Riftia pachyptila. *Int. J. Syst. Evol. Microbiol.* 66, 2697–2701. doi: 10.1099/ijsem.0.001106

Grote, J., Schott, T., Bruckner, C. G., Gloockner, F. O., Jost, G., Teeling, H., et al. (2012). Genome and physiology of a model Epsilonproteobacterium responsible for sulfide detoxification in marine oxygen depletion zones. *PNAS* 109 (2), 506–510. doi: 10.1073/pnas.1111262109

Guo, Y., Ihara, H., Aoyagi, T., Hori, T., and Katayama, Y. (2022).). Draft genome sequences of sulfurovum spp. TSL1 and TSL6, two sulfur-oxidizing bacteria isolated from marine sediment. *Microbiol. Resour. Announce.* 11 (1), e0092221. doi: 10.1128/mra.00922-21

Hassani, B. K., Steunou, A. S., Liotenberg, S., Reiss-Husson, F., Astier, C., and Ouchane, S. (2010). Adaptation to oxygen: role of terminal oxidases in photosynthesis initiation in the purple photosynthetic bacterium, Rubrivivax gelatinosus. *J. Biol. Chem.* 285 (26), 19891–19899. doi: 10.1074/jbc.M109.086066

Huang, L. B., Bae, H. S., Young, C., Pain, A. J., Martin, J. B., and Ogram, A. (2021). Campylobacterota dominate the microbial communities in a tropical karst subterranean estuary, with implications for cycling and export of nitrogen to coastal waters. *Environ. Microbiol.* 23 (11), 6749–6763. doi: 10.1111/1462-2920.15746

Huang, X. J., Tie, W. Z., Xie, D. T., and Li, Z. L. (2021). Low C/N Ratios Promote Dissimilatory Nitrite Reduction to Ammonium in Pseudomonas putida Y-9 under Aerobic Conditions. *Microorganisms* 9 (7), 1524. doi: 10.3390/microorganisms9071524

Inagaki, F., Takai, K., Nealson, K. H., and Horikoshi, K. (2004). Sulfurovum lithotrophicum gen. nov., sp nov., a novel sulfur-oxidizing chemolithoautotroph within the epsilon-Proteobacteria isolated from Okinawa Trough hydrothermal sediments. *Int. J. Syst. Evol. Microbiol.* 54, 1477–1482. doi: 10.1099/ijs.0.03042-0

Jia, M. S., Winkler, M. K. H., and Volcke, E. I. P. (2020). Elucidating the competition between heterotrophic denitrification and DNRA using the resource-ratio theory. *Environ. Sci. Technol.* 54 (21), 13953–13962. doi: 10.1021/acs.est.0c01776

Jiang, L. J., Lyu, J., and Shao, Z. Z. (2017). Sulfur metabolism of hydrogenovibrio thermophilus strain S5 and its adaptations to deep-sea hydrothermal vent environment. *Front. Microbiol.* 8. doi: 10.3389/fmicb.2017.02513

Jiang, L., Zheng, Y., Peng, X., Zhou, H., Zhang, C., Xiao, X., et al. (2009). Vertical distribution and diversity of sulfate-reducing prokaryotes in the Pearl River estuarine sediments, Southern China. *FEMS Microbiol. Ecol.* 70 (2), 93–106. doi: 10.1111/j.1574-6941.2009.00758.x

Johnson, L. A., and Hug, L. A. (2019). Distribution of reactive oxygen species defense mechanisms across domain bacteria. *Free Radic. Biol. Med.* 140, 93–102. doi: 10.1016/j.freeradbiomed.2019.03.032

Kaminski, P. A., Kitts, C. L., Zimmerman, Z., and Ludwig, R. A. (1996). Azorhizobium caulinodans uses both cytochrome bd (quinol) and cytochrome cbb3 (cytochrome c) terminal oxidases for symbiotic N2 fixation. *J. Bacteriol* 178 (20), 5989–5994. doi: 10.1128/jb.178.20.5989-5994.1996

Kumar, S., Stecher, G., Li, M., Knyaz, C., and Tamura, K. (2018). MEGA X: Molecular evolutionary genetics analysis across computing platforms. *Mol. Biol. Evol.* 35 (6), 1547–1549. doi: 10.1093/molbev/msy096

Kuypers, M. M. M., Marchant, H. K., and Kartal, B. (2018). The microbial nitrogen-cycling network. *Nat. Rev. Microbiol.* 16 (5), 263–276. doi: 10.1038/nrmicro.2018.9

Larkin, M. A., Blackshields, G., Brown, N. P., Chenna, R., McGettigan, P. A., McWilliam, H., et al. (2007). Clustal W and clustal X version 2.0. *Bioinformatics* 23 (21), 2947–2948. doi: 10.1093/bioinformatics/btm404

Lee, W. K., Juniper, S. K., Perez, M., Ju, S. J., and Kim, S. J. (2021). Diversity and characterization of bacterial communities of five co-occurring species at a hydrothermal vent on the Tonga Arc. *Ecol. Evol.* 11 (9), 4481–4493. doi: 10.1002/ece3.7343

Li, S., Jiang, Z., and Ji, G. (2022). Effect of sulfur sources on the competition between denitrification and DNRA. *Environ. Pollut.* 305, 119322. doi: 10.1016/j.envpol.2022.119322

Li, W., Zhen, Y. M., Li, N., Wang, H. Q., Lin, M. H., Sui, X. T., et al. (2022). Sulfur transformation and bacterial community dynamics in both desulfurization-denitrification biofilm and suspended activated sludge. *Bioresour. Technol.* 343, 126108. doi: 10.1016/j.biortech.2021.126108

Lin, X., Hetharua, B., Lin, L., Xu, H., Zheng, T., He, Z., et al. (2019). Mangrove sediment microbiome: Adaptive microbial assemblages and their routed biogeochemical processes in yunxiao mangrove national nature reserve, China. *Microb. Ecol.* 78 (1), 57–69. doi: 10.1007/s00248-018-1261-6

Liu, S. Y., Dai, J. C., Wei, H. H., Li, S. Y., Wang, P., Zhu, T. B., et al. (2021). Dissimilatory nitrate reduction to ammonium (DNRA) and denitrification pathways are leveraged by cyclic AMP receptor protein (CRP) paralogues based on electron donor/acceptor limitation in shewanella loihica PV-4. *Appl. Environ. Microbiol.* 87 (2), e01964–20. doi: 10.1128/aem.01964-20

Luo, R., Liu, B., Xie, Y., Li, Z., Huang, W., Yuan, J., et al. (2015). Erratum: SOAPdenovo2: an empirically improved memory-efficient short-read *de novo* assembler. *GigaScience* 4, 30. doi: 10.1186/s13742-015-0069-2

Luo, Z. W., Zhong, Q. P., Han, X. G., Hu, R. W., Liu, X. Y., Xu, W. J., et al. (2021). Depth-dependent variability of biological nitrogen fixation and diazotrophic communities in mangrove sediments. *Microbiome* 9 (1), 212. doi: 10.1186/s40168-021-01164-0

Marcia, M., Ermler, U., Peng, G. H., and Michel, H. (2010). A new structure-based classification of sulfide:quinone oxidoreductases. *Proteins-Structure Funct. Bioinf.* 78 (5), 1073–1083. doi: 10.1002/prot.22665

Marziah, Z., Mahdzir, A., Musa, M. N., Jaafar, A. B., Azhim, A., and Hara, H. (2016). Abundance of sulfur-degrading bacteria in a benthic bacterial community of shallow sea sediment in the off-Terengganu coast of the South China Sea. *Microbiologyopen* 5 (6), 967–978. doi: 10.1002/mbo3.380

Meier, D. V., Pjevac, P., Bach, W., Hourdez, S., Girguis, P. R., Vidoudez, C., et al. (2017). Niche partitioning of diverse sulfur-oxidizing bacteria at hydrothermal vents. *ISME J.* 11 (7), 1545–1558. doi: 10.1038/ismej.2017.37

Meier-Kolthoff, J. P., Klenk, H.-P., and Goeker, M. (2014). Taxonomic use of DNA G plus C content and DNA-DNA hybridization in the genomic age. *Int. J. Syst. Evol. Microbiol.* 64, 352–356. doi: 10.1099/ijs.0.056994-0

Mino, S., Kudo, H., Arai, T., Sawabe, T., Takai, K., and Nakagawa, S. (2014). Sulfurovum aggregans sp nov., a hydrogenoxidizing, thiosulfate-reducing chemolithoautotroph within the Epsilonproteobacteria isolated from a deep-sea hydrothermal vent chimney, and an emended description of the genus Sulfurovum. *Int. J. Syst. Evol. Microbiol.* 64, 3195–3201. doi: 10.1099/ijs.0.065094-0

Missall, T. A., Pusateri, M. E., and Lodge, J. K. (2004). Thiol peroxidase is critical for virulence and resistance to nitric oxide and peroxide in the fungal pathogen, Cryptococcus neoformans. *Mol. Microbiol.* 51 (5), 1447–1458. doi: 10.1111/j.1365-2958.2004.03921.x

Mori, K., Yamaguchi, K., and Hanada, S. (2018). Sulfurovum denitrificans sp nov., an obligately chemolithoautotrophic sulfur-oxidizing epsilonproteobacterium isolated from a hydrothermal field. *Int. J. Syst. Evol. Microbiol.* 68 (7), 2183–2187. doi: 10.1099/ijsem.0.002803

Motoki, K., Watsuji, T. O., Takaki, Y., Takai, K., and Iwasaki, W. (2020). Metatranscriptomics by *in situ* RNA stabilization directly and comprehensively revealed episymbiotic microbial communities of deep-sea squat lobsters. *Msystems* 5 (5), e00551–20. doi: 10.1128/mSystems.00551-20

Moulana, A., Anderson, R. E., Fortunato, C. S., and Huber, J. A. (2020). Selection is a significant driver of gene gain and loss in the pangenome of the bacterial genus sulfurovum in geographically distinct deep-sea hydrothermal vents. *Msystems* 5 (2), e00673–19. doi: 10.1128/mSystems.00673-19

Na, S.-I., Kim, Y. O., Yoon, S.-H., Ha, S. M., Baek, I., and Chun, J. (2018). UBCG: Up-to-date bacterial core gene set and pipeline for phylogenomic tree reconstruction. *J. Microbiol.* 56 (4), 280–285. doi: 10.1007/s12275-018-8014-6

Nakagawa, T., Takai, K., Suzuki, Y., Hirayama, H., Konno, U., Tsunogai, U., et al. (2006). Geomicrobiological exploration and characterization of a novel deep-sea hydrothermal system at the TOTO caldera in the Mariana Volcanic Arc. *Environ. Microbiol.* 8 (1), 37–49. doi: 10.1111/j.1462-2920.2005.00884.x

Overbeek, R., Olson, R., Pusch, G. D., Olsen, G. J., Davis, J. J., Disz, T., et al. (2014). The SEED and the Rapid Annotation of microbial genomes using Subsystems Technology (RAST). *Nucleic Acids Res.* 42 (D1), D206–D214. doi: 10.1093/nar/gkt1226

Pandey, C. B., Kumar, U., Kaviraj, M., Minick, K. J., Mishra, A. K., and Singh, J. S. (2020). DNRA: A short-circuit in biological N-cycling to conserve nitrogen in terrestrial. *Sci. Total Environ.* 738, 139710. doi: 10.1016/j.scitotenv.2020.139710

Park, S.-J., Ghai, R., Martin-Cuadrado, A.-B., Rodriguez-Valera, F., Jung, M.-Y., Kim, J.-G., et al. (2012). Draft genome sequence of the sulfur-oxidizing bacterium "Candidatus sulfurovum sediminum" AR, which belongs to the epsilonproteobacteria. *J. Bacteriol.* 194 (15), 4128–4129. doi: 10.1128/jb.00741-12

Parks, D. H., Imelfort, M., Skennerton, C. T., Hugenholtz, P., and Tyson, G. W. (2015). CheckM: assessing the quality of microbial genomes recovered from isolates, single cells, and metagenomes. *Genome Res.* 25 (7), 1043–1055. doi: 10.1101/gr.186072.114

Patwardhan, S., Foustoukos, D. I., Giovannelli, D., Yucel, M., and Vetriani, C. (2018). Ecological succession of sulfur-oxidizing epsilon- and gammaproteobacteria during colonization of a shallow-water gas vent. *Front. Microbiol.* 9. doi: 10.3389/fmicb.2018.02970

Patwardhan, S., Smedile, F., Giovannelli, D., and Vetriani, C. (2021). Metaproteogenomic profiling of chemosynthetic microbial biofilms reveals metabolic flexibility during colonization of a shallow-water gas vent. *Front. Microbiol.* 12. doi: 10.3389/fmicb.2021.638300

Pritchard, L., Glover, R. H., Humphris, S., Elphinstone, J. G., and Toth, I. K. (2016). Genomics and taxonomy in diagnostics for food security: soft-rotting enterobacterial plant pathogens. *Anal. Methods* 8 (1), 12–24. doi: 10.1039/c5ay02550h

Sheik, C. S., Anantharaman, K., Breier, J. A., Sylvan, J. B., Edwards, K. J., and Dick, G. J. (2015). Spatially resolved sampling reveals dynamic microbial communities in rising hydrothermal plumes across a back-arc basin. *ISME J.* 9 (6), 1434–1445. doi: 10.1038/ismej.2014.228

Stackebrandt, E., and Goebel, B. M. (1994). A place for dna-dna reassociation and 16s ribosomal-rna sequence-analysis in the present species definition in bacteriology. *Int. J. Systematic Bacteriology* 44 (4), 846–849. doi: 10.1099/00207713-44-4-846

Sun, Y. Y., Song, Z. L., Zhang, H. K., Liu, P. Y., and Hu, X. K. (2020). Seagrass vegetation affect the vertical organization of microbial communities in sediment. *Mar. Environ. Res.* 162, 105174. doi: 10.1016/j.marenvres.2020.105174

Sun, Q. L., Zhang, J., Wang, M. X., Cao, L., Du, Z. F., Sun, Y. Y., et al. (2020). High-throughput sequencing reveals a potentially novel sulfurovum species dominating the microbial communities of the seawater-sediment interface of a deep-sea cold seep in South China sea. *Microorganisms* 8 (5), 687. doi: 10.3390/microorganisms8050687

Sylvan, J. B., Pyenson, B. C., Rouxel, O., German, C. R., and Edwards, K. J. (2012). Time-series analysis of two hydrothermal plumes at 950′N East Pacific Rise reveals distinct, heterogeneous bacterial populations. *Geobiology* 10 (2), 178–192. doi: 10.1111/j.1472-4669.2011.00315.x

Takai, K., Gamo, T., Tsunogai, U., Nakayama, N., Hirayama, H., Nealson, K. H., et al. (2004). Geochemical and microbiological evidence for a hydrogen-based, hyperthermophilic subsurface lithoautotrophic microbial ecosystem (HyperSLiME) beneath an active deep-sea hydrothermal field. *Extremophiles* 8 (4), 269–282. doi: 10.1007/s00792-004-0386-3

Takai, K., Nakagawa, S., and Nunoura, T. (2015). "Comparative Investigation of Microbial Communities Associated with Hydrothermal Activities in the Okinawa Trough," in *Subseafloor Biosphere Linked to Hydrothermal Systems: TAIGA Concept*. Eds. J. I. Ishibashi, K. Okino and M. Sunamura (Tokyo: Springer Japan), 421–435.

Tamura, K., Nei, M., and Kumar, S. (2004). Prospects for inferring very large phylogenies by using the neighbor-joining method. *PNAS* 101 (30), 11030–11035. doi: 10.1073/pnas.0404206101

Tang, W. Y., Cerdan-Garcia, E., Berthelot, H., Polyviou, D., Wang, S. V., Baylay, A., et al. (2020). New insights into the distributions of nitrogen fixation and diazotrophs revealed by high-resolution sensing and sampling methods. *ISME J.* 14 (10), 2514–2526. doi: 10.1038/s41396-020-0703-6

Tatusova, T., DiCuccio, M., Badretdin, A., Chetvernin, V., Nawrocki, E. P., Zaslavsky, L., et al. (2016). NCBI prokaryotic genome annotation pipeline. *Nucleic Acids Res.* 44 (14), 6614–6624. doi: 10.1093/nar/gkw569

Teske, A., Hinrichs, K.-U., Edgcomb, V., de Vera Gomez, A., Kysela, D., Sylva, S. P., et al. (2002). Microbial diversity of hydrothermal sediments in the guaymas basin: Evidence for anaerobic methanotrophic communities. *Appl. Environ. Microbiol.* 68 (4), 1994–2007. doi: 10.1128/aem.68.4.1994-2007.2002

Vetriani, C., Voordeckers, J. W., Crespo-Medina, M., O'Brien, C. E., Giovannelli, D., and Lutz, R. A. (2014). Deep-sea hydrothermal vent Epsilonproteobacteria encode a conserved and widespread nitrate reduction pathway (Nap). *Isme J.* 8 (7), 1510–1521. doi: 10.1038/ismej.2013.246

Waite, D. W., Vanwonterghem, I., Rinke, C., Parks, D. H., Zhang, Y., Takai, K., et al. (2018). Comparative genomic analysis of the class epsilonproteobacteria and proposed reclassification to epsilonbacteraeota (phyl. nov.). *Front. Microbiol.* 9. doi: 10.3389/fmicb.2018.00772

Wang, Y., Bi, H. Y., Chen, H. G., Zheng, P. F., Zhou, Y. L., and Li, J. T. (2022). Metagenomics reveals dominant unusual sulfur oxidizers inhabiting active hydrothermal chimneys from the Southwest Indian ridge. *Front. Microbiol.* 13, 861795. doi: 10.3389/fmicb.2022.861795

Wang, L., Cheung, M. K., Liu, R., Wong, C. K., Kwan, H. S., and Hwang, J.-S. (2017). Diversity of total bacterial communities and chemoautotrophic populations in sulfur-rich sediments of shallow-water hydrothermal vents off kueishan island, Taiwan. *Microb. Ecol.* 73 (3), 571–582. doi: 10.1007/s00248-016-0898-2

Wang, S., Jiang, L., Hu, Q., Cui, L., Zhu, B., Fu, X., et al. (2021). Characterization of Sulfurimonas hydrogeniphila sp. nov., a Novel Bacterium Predominant in Deep-Sea Hydrothermal Vents and Comparative Genomic Analyses of the Genus Sulfurimonas. *Front. Microbiol.* 12. doi: 10.3389/fmicb.2021.626705

Wang, S. S., Jiang, L. J., Xie, S. B., Alain, K., Wang, Z. D., Wang, J., et al. (2023). Disproportionation of inorganic sulfur compounds by mesophilic chemolithoautotrophic campylobacterota. *Msystems* 8 (1), e0095422. doi: 10.1128/msystems.00954-22

Wang, K. Q., Qaisar, M., Chen, B. L., and Cai, J. (2022). Response difference of simultaneous sulfide and nitrite removal process to different cooling modes. *Bioresour. Technol.* 346. doi: 10.1016/j.biortech.2021.126601

Wang, F., Zhou, H., Meng, J., Peng, X., Jiang, L., Sun, P., et al. (2009). GeoChip-based analysis of metabolic diversity of microbial communities at the Juan de Fuca Ridge hydrothermal vent. *PNAS* 106 (12), 4840–4845. doi: 10.1073/pnas.0810418106

Wright, K. E., Williamson, C., Grasby, S. E., Spear, J. R., and Templeton, A. S. (2013). Metagenomic evidence for sulfur lithotrophy by Epsilonproteobacteria as the major energy source for primary productivity in a sub-aerial arctic glacial deposit Borup Fiord Pass. *Front. Microbiol.* 4. doi: 10.3389/fmicb.2013.00063

Xie, J., Chen, Y., Cai, G., Cai, R., Hu, Z., and Wang, H. (2023). Tree Visualization By One Table (tvBOT): a web application for visualizing, modifying and annotating phylogenetic trees. *Nucleic Acids Res.* 51 (W1), W587–W592. doi: 10.1093/nar/gkad359

Xie, S., Wang, S., Li, D., Shao, Z., Lai, Q., Wang, Y., et al. (2021). Sulfurovum indicum sp. nov., a novel hydrogen- and sulfur-oxidizing chemolithoautotroph isolated from a deep-sea hydrothermal plume in the Northwestern Indian Ocean. *Int. J. Syst. Evol. Microbiol.* 71 (3). doi: 10.1099/ijsem.0.004748

Xu, W., Li, M., Ding, J. F., Gu, J. D., and Luo, Z. H. (2014). Bacteria dominate the ammonia-oxidizing community in a hydrothermal vent site at the Mid-Atlantic Ridge of the South Atlantic Ocean. *Appl. Microbiol. Biotechnol.* 98 (18), 7993–8004. doi: 10.1007/s00253-014-5833-1

Zhang, L. K., Kang, M. Y., Xu, J. J., Xu, J., Shuai, Y. J., Zhou, X. J., et al (2016). Bacterial and archaeal communities in the deep-sea sediments of inactive hydrothermal vents in the Southwest India Ridge. *Sci. Rep.* 6, 25982. doi: 10.1038/srep25982

Zhang, J., and Madden, T. L. (1997). PowerBLAST: a new network BLAST application for interactive or automated sequence analysis and annotation. *Genome Res.* 7 (6), 649–656. doi: 10.1101/gr.7.6.649

Zheng, S. H., Liu, X. Y., Yang, X. J., Zhou, H. E., Fang, J., Gong, S. Y., et al. (2022). The nitrogen removal performance and microbial community on mixotrophic denitrification process. *Bioresour. Technol.* 363, 127901. doi: 10.1016/j.biortech.2022.127901

frontiers | Frontiers in Marine Science

TYPE Original Research
PUBLISHED 27 September 2023
DOI 10.3389/fmars.2023.1256393

OPEN ACCESS

EDITED BY
Zhongzheng Yan,
East China Normal University, China

REVIEWED BY
Bao-zhu Fang,
Chinese Academy of Sciences (CAS), China
Zhaobin Huang,
Quanzhou Normal University, China
Da Huo,
Chinese Academy of Sciences (CAS), China

*CORRESPONDENCE
Xue-Wei Xu
xuxw@sio.org.cn
Cong Sun
michael_sc@sina.com

RECEIVED 10 July 2023
ACCEPTED 08 September 2023
PUBLISHED 27 September 2023

CITATION
Ye Y-L, Ma K-J, Fu Y-H, Wu Z-C, Fu G-Y, Sun C and Xu X-W (2023) The heterogeneity of microbial diversity and its drivers in two types of sediments from tidal flats in Beibu Gulf, China. *Front. Mar. Sci.* 10:1256393. doi: 10.3389/fmars.2023.1256393

The heterogeneity of microbial diversity and its drivers in two types of sediments from tidal flats in Beibu Gulf, China

Yong-Lian Ye[1], Kuo-Jian Ma[1,2], Yun-Han Fu[1,2], Zhi-Cheng Wu[1,2], Ge-Yi Fu[1], Cong Sun[3,4]* and Xue-Wei Xu[1]*

[1]Key Laboratory of Marine Ecosystem Dynamics, Ministry of Natural Resources & Second Institute of Oceanography, Ministry of Natural Resources, Hangzhou, China, [2]Ocean College, Zhejiang University, Zhoushan, China, [3]College of Life Sciences and Medicine, Zhejiang Sci-Tech University, Hangzhou, China, [4]Zhejiang Sci-Tech University Shaoxing Academy of Biomedicine Co., Ltd., Shaoxing, China

Mudflats and sandflats are two common types of coastal tidal flats, the structure and function differences of microbial communities between them are still underappreciated. Beibu Gulf is a diurnal tidal regime located in China, the differences between the two type of tidal flats could be more distinct. In this study, we collected a total of 6 samples from Beibu Gulf, consisting of 3 sandflats samples and 3 mudflats samples, classified based on clay and silt content. Generally, the mudflats samples exhibited higher levels of NH_4^+_N and TOC, but lower in ORP and pH. The microbial diversity of the two types of tidal flats was investigated, revealing great differences existed and sandflats had higher microbial richness and diversity than mudflats. Furthermore, we analyzed the association between microbial communities and environmental factors, finding NH_4^+_N to have the highest contribution to the total variation in microbial community structure, and microbial groups such as Desulfobacterota, Campilobacterota, Chloroflexota, Calditrichota, Spirochaetota, Zixibacteria, Latescibacterota and Sva0485 group in mudflats were positively associated with NH_4^+_N. The functions of microbial community were predicted using metagenomic sequences and metagenome assembled genome (MAG). Mudflats contained more genes for carbon fixation. Nitrate and nitrite reduction were widely existed in mudflats and sandflats, but nitrogen fixation was only existed in mudflats, and *Campilobacterota*, Desulfobacterota and Gammaproteobacteria MAGs were mainly responsible for it. Sandflats composed more genes for ammonium oxidation, but no MAG was found whether in sandflats or mudflats. Microbes in mudflats exhibited a greater abundance of genes related to sulfur cycling, especially in reduction process, unique MAGs in mudflats such as Calditrichota, Chloroflexota, Desulfobacterota and Zixibacteria MAGs are responsible for sulfate and sulfite reduction. Finally, we predicted functions of ammonium related microbes in mudflats based on MAGs and found Campilobacterota and Desulfobacterota MAGs were important for high accumulation of ammonium in mudflats. This study illuminated the structural and functional differences of microbial communities in mudflats and sandflats, providing new insights into the relationship of microbial communities and environment in the tidal flat.

KEYWORDS

tidal flats, microbial diversity, ammonium, mudflat, metagenome, Beibu Gulf

1 Introduction

Tidal flats are important transitional areas that connect the ocean and land, characterized by strong dynamic interactions between tide and river runoff, and between surface water and groundwater (Osland et al., 2016). Tidal flats usually defined as ecosystems including sandflats and mudflats that undergo regular tidal inundation (Healy et al., 2002). These ecosystems play vital roles with biodiversity, ecological services (Murray et al., 2019). However, tidal flats are affected by human and natural activities such as coastal development (Sarukhán et al., 2005), sea-level rise (Passeri et al., 2015), and coastal erosion (Nicholls et al., 2007), which is interfering the ecological structure and function, with significant implications for their ecological services (Zhang et al., 2020).

Microorganisms play a crucial role in the tidal flat ecosystem influencing key ecological processes (Böer et al., 2009), such as energy flow, pollutant degradation, element transformation and migration (Wang et al., 2020a). The diversity and composition of microbial communities in sediment are primarily influenced by various environmental factors, including salinity (Zhang et al., 2021), pH (Zhang et al., 2017), total organic carbon (Du et al., 2011), temperature (Lv et al., 2016), nitrogen (Ki et al., 2018), and the content of silt and clay (Boey et al., 2021). This selective effect of the environment on microorganisms is a central concept in niche theory, which suggests that microbial dispersal is unlimited and community assembly is primarily driven by deterministic factors, such as environmental selection (Webb et al., 2002). Bass-Becking hypothesized that "everything is everywhere, but the environment selects," due to the small size, high rates of population growth, and the vast abundance of microbes. Environmental and nutrient factors were fundamental for microbial growth and development and thus could clearly shape the pattern of microbial communities (Li et al., 2020). Understanding the structure of bacterial communities is crucial for studying tidal flat functions and their response to environmental changes.

Mudflats and sandflats, two common types of tidal flats, exhibit distinct differences in their physical, chemical, and biological characteristics (Thrush et al., 2004; Boey et al., 2021). Research has demonstrated that due to the greater cohesiveness and less permeability of terrigenous sediments (silt and clay, <63 μm on the Wentworth scale), the increase of silt and clay content significantly influences the environmental conditions and biogeochemical processes (Lohrer et al., 2004; Cummings et al., 2009). Compared with sandflat sediments, mudflat sediments are dominated by diffusive transport (Huettel et al., 2014), and may restrict nutrient processing (release, uptake or transformation of organic nutrients by the benthos) facilitating ecosystem shifts toward eutrophication (Douglas et al., 2018), which indicated that mudflat sediments have a higher level of anoxia (Boey et al., 2021). Furthermore, sandier, more permeable sediments are dominated by advective transport (Huettel et al., 2014), are more oxygenated, and metabolites are rapidly exchanged for new substrates, which facilitates higher rates of bacterial carbon uptake compared to mudflat sediments (Woulds et al., 2016). Microbial communities associated with sandy sediments are thus thought t have the ability to quickly adapt to changing biogeochemical conditions (Boey et al., 2021).

The Beibu Gulf, situated in northwest of the South China Sea, is a semi-enclosed tropical and subtropical gulf partially enclosed by the Leizhou Peninsula, Qiongzhou Strait, Hainan Island, Vietnam, and stretches to the Guangxi coast in the north (Ma et al., 2010). One notable characteristic of the Beibu Gulf coast is the presence of numerous estuaries, including the Red River in Vietnam and the Beilun, Maoling, and Dafeng Rivers in China, these rivers serve as significant potential sources of nutrients and pollution that enter the Gulf (Dou et al., 2013). Additionally, the Beibu Gulf experiences a diurnal tidal regime, which is uncommon in other regions of China. Compared with the common semi-diurnal tide, the diurnal tide has a longer continuous submerged time on a single tidal day, and the diurnal and semi-diurnal tidal zones are different in hydrology, climate and soil characteristics (He et al., 2007).

In this study, field investigations were carried out with two types of tidal flat along the coastline of the Beibu Gulf. We aimed to solve the following scientific issues: (1) to determine the differences in microbial structure and diversity between mudflats and sandflats in the Beibu Gulf; (2) to identify the key environmental factors that influence the distribution of microbes in both mudflats and sandflats; (3) to assess the interaction mechanisms between environmental factors and microbial communities.

2 Materials and methods

2.1 Samples collection and strain isolation

The study area encompassed the northern and eastern regions of the Beibu Gulf, spanning across Guangxi and Guangdong Provinces, China (Figure 1). Random collection of sediment samples was carried out from 6 stations along the tidal flats of the Beibu Gulf. The sampling positions were determined using a global positioning system by Ocean data view (Supplementary Table 1) (Schlitzer, 2021). Based on the observations at the sampling sites, the collected samples were classified into two types: mudflats-like

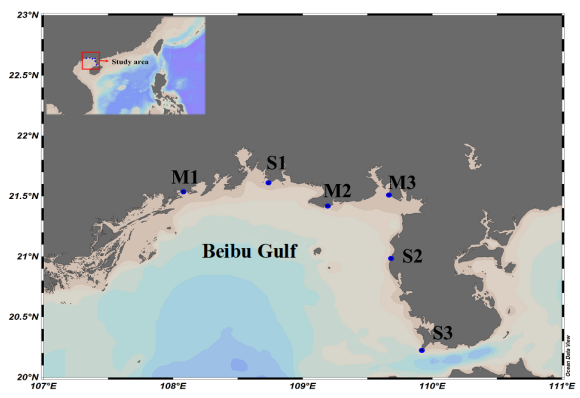

FIGURE 1
Map of the study area showing the location of the sampling stations.

sediment samples (M1, M2, M3) and sandflats-like sediment samples (S1, S2, S3). For each sampling site, three replicates of 0-5 cm soils from the sub-top layer were collected and thoroughly mixed to create a composite sample. The collected samples were transported to the laboratory in an ice box, with some stored at 4°C for strain isolation and culture experiments, while the remaining portion was stored in a -20°C freezer for subsequent sequencing and physical and chemical analysis.

2.2 Physicochemical analysis

Pore water in the sediment samples was extracted using Rhizon CSS pore water technique, followed by *in situ* analysis of salinity (SAL), pH, oxidation-reduction potential (ORP), dissolved oxygen (DO), and temperature (T) using a water quality analyzer (HQ40D, Hach) in combination with salinity (CDC401, Hach), pH (pHC108, Hach), oxidation-reduction potential (MTC101, Hach), and dissolved oxygen (LDO101, Hach) probes. The content of silt and clay (SC) was characterized using a laser particle size analyzer (MS2000, Malvern), in brief, sediments with diameters < 63 μm were defined as mud (a combination of clay and silt according to the Wentworth scale), and those with a mud content ≥10% were categorized as mudflats, while those with ≤10% were classified as sandflats (Folk et al., 1970). The total organic carbon (TOC) was determined using the potassium dichromate volumetric method, total nitrogen (TN) in the sediment was determined using the Kjeldahl method (Kjeldahl, 1883), and total phosphorus (TP) was analyzed using the acidic molybdate–ascorbic acid spectrophotometric method (Ames, 1966). The concentrations of ammonium nitrogen (NH_4^+_N) and nitrate nitrogen (NO_3^-_N) in the sediment were determined using the indophenol blue colorimetric method (Peterson, 1979) and the hydrazine sulfate method (Sims, 1961), respectively. Triplicate samples (n = 3) were analyzed, and the data were presented as mean values ± standard deviations (SD) on a dry weight basis. Statistical significance of the sediment properties was assessed using a two-sided analysis of Welch's t-test (Welch, 1947), with a p-value less than 0.05 considered as significant.

2.3 DNA extraction and sequencing

DNA extraction from the sediment samples (0.5 g each) was performed using the Magnetic Soil and Stool DNA Kit (TIANGEN, China) following the manufacturer's instructions. The extracted environmental DNA served as the template for polymerase chain reaction (PCR), with amplification of bacterial 16S rRNA genes targeting the V4 hypervariable region using Earth Microbiome Project (EMP) standard primers 515F (5′-GTGCCAGC MGCCGCGGTAA-3′) and 806R (5′-GGACTACHVGGGTW TCTAAT-3′) (Thompson et al., 2017). The amplified products were visualized by electrophoresis on a 2% (w/v) agarose gel. PCR products with clear bands were pooled in equal densities and purified using the GeneJET Gel Recovery Kit (Thermo Scientific, China). High-throughput sequencing was performed using the Illumina NovaSeq 6000 sequencing platform (Novogene, China) with paired-end reads. Each sediment sample was sequenced in triplicate.

The extracted environmental DNA was also used for high-throughput sequencing on the Illumina HiSeq platform, and paired-end reads were generated using Magigene (Shenzhen, P.R. China). Sequencing libraries were prepared using the NEBNext® UltraTM DNA Library Prep Kit for Illumina (NEB, Ipswich, U.S.A.) following the manufacturer's recommendations, with index codes assigned to each sample for sequence attribution. The raw reads have been deposited into the NCBI Sequence Read Archive (SRA) database under the accession numbers PRJNA774167 and PRJNA967168.

2.4 16S rRNA gene amplicon sequences and statistical analysis

The raw sequences obtained from Illumina sequencing were processed using QIIME2 version 2021.4 software (Liu et al., 2021). The QIIME2 cutadapt module was utilized to remove adapter and barcode sequences from the raw 16S rRNA gene sequences. Subsequently, the assembled sequences were filtered and de-replicated to obtain representative sequences known as Amplicon Sequence Variants (ASVs) and a feature table (ASVs table) by using DADA2 module in QIIME2. Taxonomy annotation was performed based on the SILVA 132 database (Quast et al., 2012), and the resulting representative sequences and feature tables with taxonomy annotation information were imported into QIIME2 for downstream analysis. To minimize the impact of sequencing depth on treatment effects, the sediment samples were randomly resampled to the same sequence depth based on the sample with the fewest number of sequences. Alpha-diversity indices, including observed_features, Faith's phylogenetic diversity (faith_pd), Shannon index, and Chao1 value, were calculated for each sample using QIIME2. Principal coordinate analysis (PCoA) based on weighted UniFrac distance (Lozupone and Knight, 2005) and Bray-Curtis similarity (Bray and Curtis, 1957) were conducted to explore differences in bacterial community structures among the sampling sites. Differences in species abundances between the two groups were compared using Welch's t-test with the Statistical Analysis of Metagenomic Profiles (STAMP version 2.1.3) software (Parks et al., 2014). Spearman's rank correlation coefficient was employed to analyze the correlation between microbial communities and different environmental factors (Spearman, 1987). Redundancy analysis (RDA) was used to identify key factors influencing bacterial community structure (McArdle and Anderson, 2001), and envfit analysis in the 'vagan' package was performed to evaluate the explanatory ability of environmental factors on the community.

2.5 Metagenomic analysis

The total of 1,283,967,682 metagenomic raw reads (430,455,448 raw reads in sandflat samples and 853,512,234 raw reads in mudflat

samples, Supplementary Table 5) were filtered and trimmed using Trimmomatic version 0.39 (Bolger et al., 2014) to generate clean reads. *De novo* assembly of metagenomes was performed for each sample (Supplementary Table 6) using the MEGAHIT module implemented in MetaWRAP pipeline software version 1.2.1 (Uritskiy et al., 2018). QUAST was used to evaluate the quality of each assembly (Gurevich et al., 2013). High- and medium-quality metagenome-assembled genomes (MAGs) were binned using modules implemented in MetaWRAP pipeline software version 1.2.1 (Uritskiy et al., 2018), with completeness and contamination thresholds set at >50% and <10%, respectively (Bowers et al., 2017). The abundance of MAGs in different samples was calculated using the quant_bins module in MetaWRAP pipeline software version 1.2.1 (Uritskiy et al., 2018). Duplicate MAGs with an average nucleotide identity (ANI) ≥95% were removed using the dereplicate module in dRep version 3.4.2 (Olm et al., 2017). Prior to detailed metabolic analysis, the MAGs were assigned initial taxonomy using the GTDB-Tk classify pipeline and a phylogenomic tree was constructed using the GTDB-Tk infer pipeline (Chaumeil et al., 2019). The final trees were visualized using Interactive Tree of Life (iTOL) v.5 (Letunic and Bork, 2021). Open reading frames (ORFs) were predicted using Prodigal v.2.6.3 (Hyatt et al., 2010) with the parameter "-p meta", and then annotated using KOfam (Aramaki et al., 2020) and custom HMM profiles within METABOLIC v.4.0 (Zhou et al., 2022) with default settings. Functional genes first characterized by METABOLIC were additionally testified using the MEROPS database release 12.3 (Rawlings et al., 2018), CAZy database (Zhang et al., 2018; Drula et al., 2022), PSORTb v.3.0 (Yu et al., 2010), FeGenie (Garber et al., 2020), and HydDB (Søndergaard et al., 2016). All statistical analyses were performed using R software (version 4.0.4), SPSS Statistics (version 26.0), online cloud computing platform (https://www.bioincloud.tech/), and online drawing platform (https://www.chiplot.online/tvbot.html).

3 Results

3.1 Physicochemical properties of sediments

The main physical and chemical properties of sediment at different sampling points are presented in Supplementary Table 2. The silt and clay contents (<63 μm) in the mudflat-like sediment samples (M1-M3) ranged from 33.791% to 98.637%, while in the sandflat-like sediment samples (S1-S3), they ranged from 0% to 7.798%. According to Folk's classification of sediments, the silt and clay contents indicate that samples M1-M3 correspond to mudflat sediments, while samples S1-S3 correspond to sandflat sediments (Supplementary Figure 1). Compared the environmental factors of sediments, NH_4^+_N was great significantly higher ($p< 0.01$) and TOC was significantly higher ($p< 0.05$) in mudflat than sandflat, on the other hand, ORP was great significantly higher ($p< 0.01$) and pH was significantly higher ($p< 0.05$) in sandflat than mudflat. Meanwhile, some factors were not different significantly including the content of TN in mudflats were higher and NO_3^-_N, TP, DO and SAL were lower compared to sandflat (Supplementary Table 3). Correlation analysis revealed that the content of silt and clay (SC) was positively correlated with TOC, NH_4^+_N, and TN ($r> 0.5$, $p< 0.05$), but negatively correlated with SAL, pH, ORP and DO ($r< -0.5$, $p< 0.05$) (Supplementary Table 4).

3.2 Microbial diversity and community structure

A total of 18 amplicon sequencing data (6 sediment samples, with 3 replicates for each sample) were retained after trimming and checking for chimera. In total, there were 959,821 sequences, with a mean sequence number of 53,323 in each sample. For each sample, four alpha diversity indices (shannon, observed_features, Faith's phylogenetic diversity (faith_pd), and chao1) were analyzed. Except for the shannon index which show relative higher values in sandflat, other three indexes in sandflat were significantly higher than those in mudflat (Wilcox-test, $p<0.05$), indicated that sandflat had higher microbial richness and diversity than mudflat in the Beibu Gulf (Figure 2A). To assess the microbial community distributions, a PCoA based on weighted_unifrac distance analysis was performed. The results showed that all sediment samples were clearly separated into two groups. This suggested that the type of tidal flats in the Beibu Gulf region had an important influence on the microbial community composition (Figure 2B).

A total of 2816 ASVs were identified from mudflat sediments, while 2716 ASVs were identified from sandflat sediments. Among these, 677 ASVs were unique to mudflats and 577 ASVs were unique to sandflats (Figure 3A). The dominant phyla in mudflats were Pseudomonadota, Desulfobacterota, Campilobacterota, Bacteroidota and Chloroflexota, whereas in sandflats, the dominant phyla were Pseudomonadota, Actinomycetota, Bacteroidota, Acidobacteria and Crenarchaeota (Figure 3B). A significant difference was observed in the distribution of phyla between the two sediment types, with higher abundance of Desulfobacterota, Campilobacterota, Chloroflexota, Calditrichota, Spirochaetota, Zixibacteria, Latescibacterota, Sva0485 and Deferrisomatota in mudflats, and higher abundance of Pseudomonadota, Actinomycetota, Crenarchaeota, Acidobacteriota, NB1_j, Planctomycetota, PAUC34f and AncK6 in sandflats (Supplementary Figure 2).

3.3 The association of microbial community structure and environmental factors

We used redundancy analysis (RDA) and envfit analysis to examine the contribution of environmental factors to variations in microbial community structure in tidal flats. The results of RDA revealed that the first two axes explained 69.35% of the total variables, with RDA1 accounting for 42.13% and RDA2 accounting for 18.9%. Between the two types of tidal flats, mudflats showed positive correlations between the abundance of

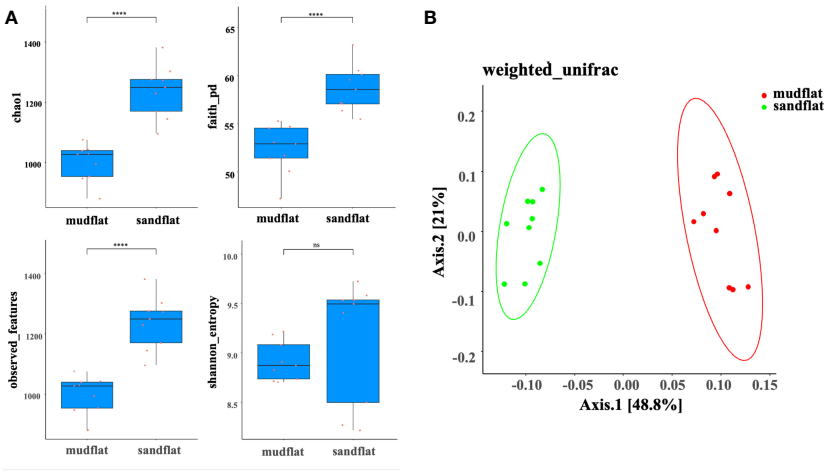

FIGURE 2
(A) Alpha diversity indexes of mudflat and sandflat sediments. The values of chao1, faith_pd, observed_features and Shannon_entropy. **(B)** Differences in microbial community distribution between mudflat and sandflat sediments assessed using principle coordinate analysis (PCoA) based on weighted_unifrac distance. ****: significance at the $p < 0.05$ level. ns, not significant.

microbial community and NH_4^+_N, TN, TOC and SC, while sandflats showed positive correlations between the abundance of microbial community and pH, ORP, and DO (Figure 4A). In which, NH_4^+_N (envfit analysis, $r^2 = 0.95$), pH (envfit analysis, $r^2 = 0.90$), TN (envfit analysis, $r^2 = 0.78$), ORP (envfit analysis, $r^2 = 0.72$), DO (envfit analysis, $r^2 = 0.68$), TOC (envfit analysis, $r^2 = 0.67$) and SC (envfit analysis, $r^2 = 0.60$) made a significant ($p< 0.01$) contribution on the total variation of the microbial community structure. These findings highlighted the important role of the environment in shaping microbial communities, and the observed differences in environmental factors between mudflats and sandflats likely contributed to the variations in their microbial groups.

The correlation between microbial communities and environmental factors was analyzed using Spearman's rank correlation coefficient. As shown in Figure 4B, the microbial groups including Desulfobacterota, Campilobacterota, Chloroflexota, Calditrichota, Spirochaetota, Zixibacteria, Latescibacterota and Sva0485, shown higher abundance in mudflat sediments, were positively associated with environmental factors including NH_4^+_N, TN, TOC and SC (Spearman'Rs > 0.5, q-value < 0.01), and negatively associated with pH, ORP and DO (Spearman'Rs < -0.5, q-value < 0.01), however, Chloroflexota was not negatively associated with DO (Spearman'Rs < -0.5, q-value > 0.05). Similarly, microbial groups with higher abundance in sandflat sediments, including Acidobacteriota, Crenarchaeota, Planctomycetota, Actinomycetota, NB1_j, Alphaproteobacteria and Gammaproteobacteria were positively associated with DO and pH (Spearman'Rs > 0.5, q-value < 0.05), but negatively

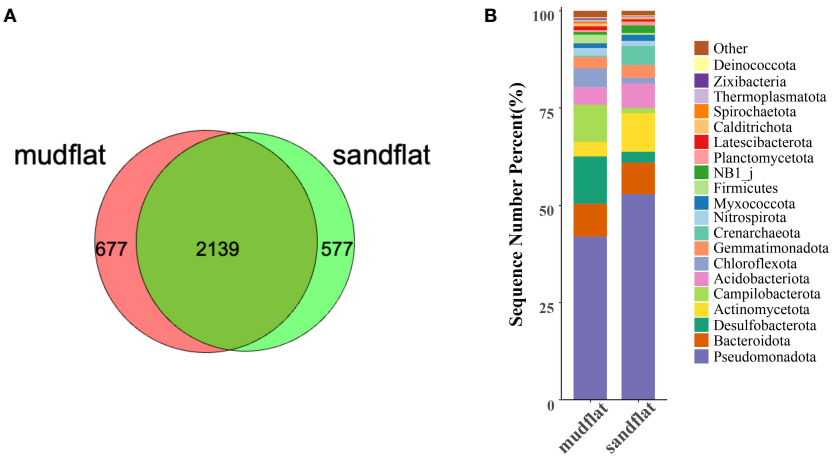

FIGURE 3
(A) The number of ASVs from mudflat and sandflat samples. **(B)** The microbial community structures and taxonomic compositions based on classifications at phylum level.

10.3389/fmars.2023.1256393

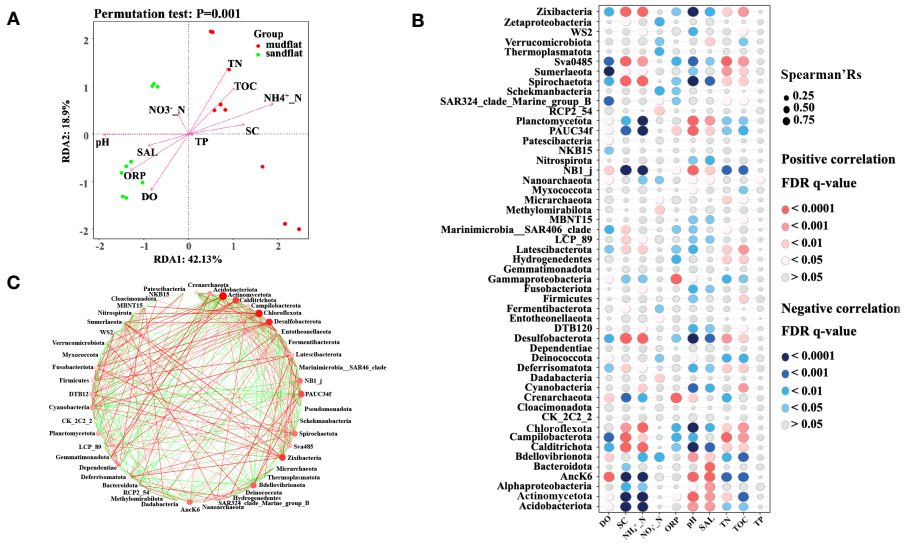

FIGURE 4
(A) The results of redundancy analysis (RDA) between environmental factors and microbial abundance/diversity in these two types of tidal flats. **(B)** The results of Spearman correlation analysis between microbial community and environmental factors. The Spearman correlation ecoefficiency is shown on the x axis and the bar are color coded by FDR q-value. The color of the bar represents the FDR (q-value) level. **(C)** Co-occurrence networks of the phyla in tidal flats. Notes: The size of each node indicates the abundances of the phylum, and the color of each node indicates different phyla taxa. Red and green lines represent positive and negative correlations, respectively (Spearman, $p < 0.05$, $r > 0.5$).

associated with SC, NH4+_N, and TOC (Spearman'Rs < -0.5, q-value < 0.05), all of these groups, except Acidobacteriota and AncK6, showed a positively association with ORP (Spearman'Rs > 0.5, q-value < 0.05),

After evaluating the interpretive ability of environmental factors to the microbe community, we found that NH_4^+_N (envfit analysis, r^2 = 0.95) played the most important role to the tidal flat samples. For instance, Desulfobacterota, Campilobacterota, Chloroflexota, Calditrichota, Spirochaetota, Zixibacteria, Latescibacterota and Sva0485 in mudflats were positively associated with NH_4^+_N (Spearman'Rs > 0.5, q-value < 0.01), on the contrary, Acidobacteriota, Crenarchaeota, Planctomycetota, Actinomycetota, NB1_j, Alphaproteobacteria and Gammaproteobacteria in sandflats were negatively associated with NH_4^+_N (Spearman'Rs < -0.5, q-value < 0.01). Network analysis was used to explore the co-occurrence pattern between microorganisms (Barberán et al., 2012). The network diagrams revealed 49 nodes ($p < 0.05$, $r > 0.5$) (Figure 4C). Furthermore, there were 181 edges with positive correlations and 164 edges with negative correlations. The phyla shown a significant correlation with NH_4^+_N, including Calditrichota, Campilobacterota, Chloroflexota, Desulfobacterota, Spirochaetota and Zixibacteria, exhibited positive correlations with each other but negative correlations with Acidobacteriota, Actinomycetota, Alphaproteobacteria and Gammaproteobacteria. The phylum Actinomycetota had the largest number of interactional nodes, with 9 positive correlations and 17 negative correlations. Pseudomonadota, the most abundant phylum, was only directly linked to the other 3 phyla. Therefore, there was a significant correlation among the interaction, the abundance of the microbial community, and environmental factors.

3.4 The differences among mudflats and sandflats in microbial biogeochemical cycles and antibiotic resistance genes

The metagenomic sequencing data was used to detect the biogeochemical functions of microbial communities in two different sediment types: mudflats and sandflats. Key genes involved in sulfur, nitrogen, and carbon cycling were annotated to analyze these functions. Although both mudflats and sandflats had similar overall functions, there were notable differences in the specific processes of sulfur, nitrogen, and carbon cycling (Figure 5). In the carbon cycling, it was observed that mudflats exhibited a significantly higher presence of genes associated with carbon fixation. The primary carbon

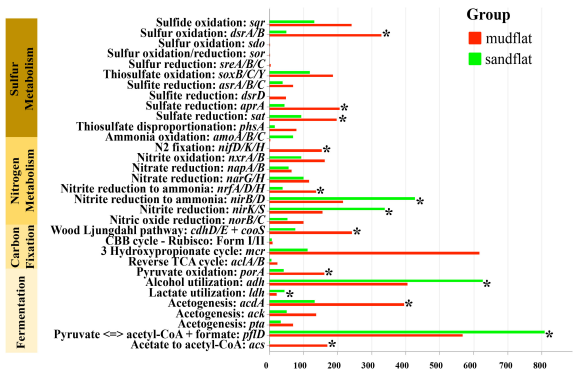

FIGURE 5
The abundance (TPM) of metabolic genes for these two types of tidal flats. *Significant differences ($p < 0.05$).

sequestration pathways identified were the Wood-Ljungdahl pathway and the 3-Hydroxypropionate cycle. When considering fermentation, sandflats displayed a greater abundance of genes related to alcohol utilization (*adh*) and acetate to acetyl-CoA (*acs*). On the other hand, mudflats exhibited a higher prevalence of genes involved in acetate synthesis (*acdA*, *ack*, *pta*), pyruvate oxidation (*porA*) and the breakdown/synthesis of pyruvate (*pflD*). In the nitrogen cycling, the genes responsible for nitrogen fixation (*nifD/K/H*) were only found in mudflats and not in sandflats. This suggested that the process of nitrogen fixation (N_2 to NH_4^+) only occurs in mudflats, potentially leading to higher levels of ammonium input in mudflats compared to sandflats. Conversely, the genes for ammonium oxidation (*amoA/B/C*) were more abundant in sandflats, indicating that microbes in sandflats might prefer to oxidize ammonium to nitrite (NH_4^+ to NO_2^-). Regarding the processes of nitrite oxidation (NO_2^- to NO_3^-) and nitrate reduction (NO_3^- to NO_2^-), the abundance of corresponding genes (*nxrA/B* for nitrite oxidation; *napA/B* and *narG/H* for nitrate reduction) in mudflats and sandflats were similar. The abundance of genes involved in nitrite ammonification (NO_2^- to NH_4^+) (*nrfA/D/H* and *nirB/D*) were also similar in both sandflats and mudflats. However, *nrfA/D/H* genes were relatively more abundant in mudflats, while *nirB/D* genes were relatively more abundant in sandflats. In the sulfur cycling, microbes in mudflats exhibited a higher abundance of functional genes in all processes, particularly in sulfur oxidation (*sdo* and *dsr A/B*), sulfate reduction (*apr A* and *sat*), sulfite reduction (*dsrD*) and thiosulfate disproportionation (*phsA*). In summary, sandflats showed a greater potential for ammonium oxidation, while mudflats demonstrated a stronger potential for sulfur metabolism, nitrogen fixation and carbon fixation.

The metagenomic assemblies data was used to identify and define the ARGs in these two types of tidal flats (Supplementary Figure 3). A total of 129 ARGs subtypes (50 ARGs subtypes in sandflats samples and 79 ARGs subtypes in mudflat samples) were retained and those ARGs belonged to 14 different ARG types. Multidrug, Fluoroquinolone and Tetracycline antibiotic were the main ARG types in these two types of tidal flat. Elfamycin, Cephem, Acridinedye, Rifamycin, Triclosan, Phenicol and Diaminopyrimidine antibiotic were unique ARG types in sandflats, in which, Phenicol and Diaminopyrimidine antibiotic were abundant ones. The resistance mechanisms in both sandflats and mudflats were mainly based on antibiotic efflux (resistance-nodulation-cell division (RND) antibiotic efflux pump), antibiotic target alteration and antibiotic target protection,but antibiotic inactivation was only found in sandflats.

3.5 Phylogenetic, metabolic and functional diversity of metagenome-assembled genomes in tidal flats

In this study, we obtained 185 bacterial and 17 archaeal draft MAGs (58 MAGs from sandflat sediments, 144 MAGs from mudflat sediments). After dereplication, we had a total of 197 MAGs (180 bacterial and 17 archaeal draft MAGs) for further analysis. The MAGs were initially characterized phylogenetically using GTDB-TK, compared with the result of 16S rRNA amplicon, all of them could be assigned to a known phylum, but some archaeal MAGs like Aenigmatarchaeota and Asgardarchaeota were only found by metagenomic assembled analysis from mudflat samples (Figure 6A; Supplementary Table 7). As shown in Figure 6B, sandflat and mudflat were not very similar in MAGs profiles under phyla level, which illuminated their difference in microbial diversity. To explore the metabolic and functional diversity of the MAGs, we summarized the functions of each MAG at the phylum level. As the results, we found genes involved in carbon, nitrogen and sulfur metabolism were widespread and shared in MAGs across all tidal flats, but distinct features also existed between different sediment types (Figure 7; Supplementary Table 8; Supplementary Figures 4–6). In the carbon cycle, the majority of MAGs contain pathways for oxidative phosphorylation and oxygen metabolism. Additionally, some MAGs had the potential for substrate-level phosphorylation through acetate formation. All samples exhibit heterotrophy, autotrophy, and mixotrophy metabolism. Notably, MAGs from mudflat samples showed potential for carbon fixation, particularly in Campilobacterota, Chloroflexota, Desulfobacterota,

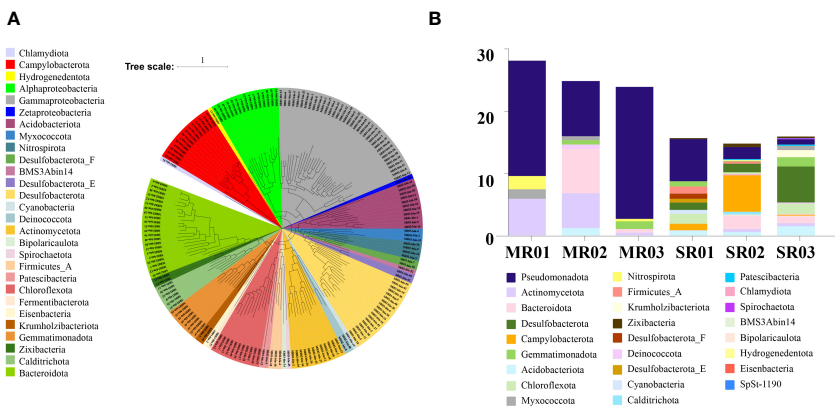

FIGURE 6
(A) Maximum-likelihood phylogenomic reconstruction of bacterial metagenome-assembled genomes generated in GTDB-Tk. The tree was generated with 120 bacterial marker genes. Taxa are shown at the phylum level, except for the *Pseudomonadota* shown at the class level. **(B)** Relative abundance of MAG phyla, based on normalized read coverage.

10.3389/fmars.2023.1256393

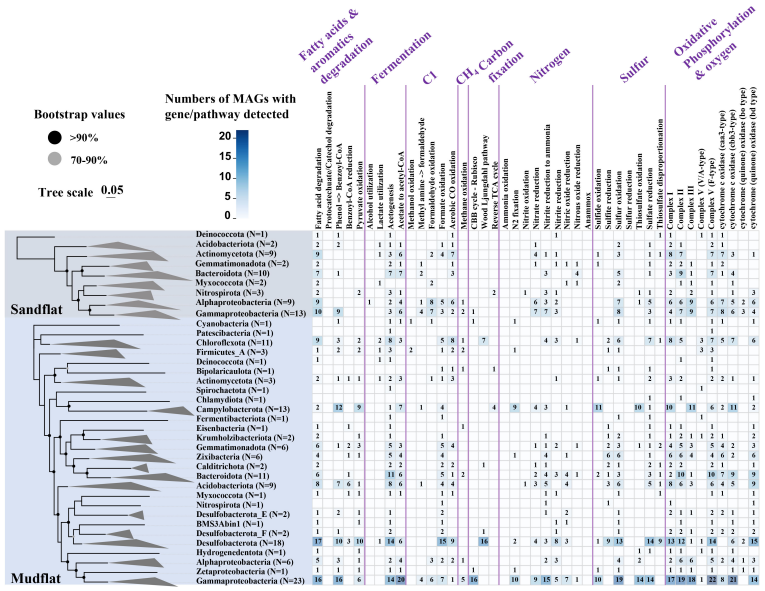

FIGURE 7
Core metabolic gene presence across phylogenetic clusters in these two types of tidal flats. The number of MAGs in each clade is shown in parentheses. Bacterial clades are shown at the phylum level expect for Pseudomonadota shown in class. Nodes with ultrafast bootstrap support ≥ 70% are shown with filled circles.

Gammaproteobacteria, Asgardarchaeota, Micrarchaeota, Thermoproteota and Thermoplasmatota. In the nitrogen cycle, nitrogen fixation was only identified in the mudflat, with Campilobacterota, Desulfobacterota and Gammaproteobacteria MAGs being primarily responsible for this process. Ammonium oxidation was only observed in Thermoproteota MAG from sandflat samples. Nitrate reduction was found to be widespread in both the mudflat and sandflat, with Bacteroidota, Calditrichota, Campilobacterota, Chloroflexota and Desulfobacterota MAGs being specific workers in the mudflat, while Alphaproteobacteria and Actinomycetota MAGs were specific workers in the sandflat. Nitrite reduction to ammonia was also found to be widespread in both the mudflat and sandflat, with additional specific workers including Acidobacteriota, Bacteroidota, Calditrichota, Chloroflexota, Campilobacterota, Desulfobacterota, Myxococcota and Zixibacteria MAGs being identified in the mudflat. In the sulfur cycle, the reduction process was more prevalent in mudflats. Specifically, sulfite reduction was only found in mudflats, while sulfate reduction occurs in both sediments. However, there was a greater diversity and abundance of MAGs associated with sulfate reduction in mudflats. Alphaproteobacteria, Gammaproteobacteria, Bacteroidota and Thermoproteota were common MAGs playing these functions in both sandflats or mudflats. Notably, unique MAGs like Calditrichota, Chloroflexota, Desulfobacterota and Zixibacteria MAGs were found to perform both functions in mudflats.

3.6 The predicted function of ammonium related microbes in mudflats based on MAGs

Based on the Spearman's rank correlation analysis shown in Figure 4B, some microbes assembled in MAGs including Calditrichota, Campylobacterota, Chloroflexota, Desulfobacterota and Zixibacteria exhibited a higher abundance in the mudflat and were significantly positively correlated with NH_4^+_N. We selected these MAGs for further analysis to investigate their relationship with NH_4^+_N and their specific functions (Figure 8). As for the sulfur cycle, the reduction of sulfite (SO_3^{2-} to H_2S) was observed in Calditrichota (2/2 MAGs), Desulfobacterota (9/18 MAGs) and Zixibacteria (6/6 MAGs). Additionally, sulfite was produced by the process of sulfur oxidation (S to SO_3^{2-}), sulfate reduction (SO_4^{2-} to SO_3^{2-}) and thiosulfate disproportionation ($S_2O_3^{2-}$ to SO_3^{2-} and H_2S) and the main microbes responded for these processes above were Calditrichota (1/2, 2/2 and 1/2 MAGs, respectively), Chloroflexota (6/11, 7/11 and 1/11 MAGs, respectively), Desulfobacterota (13/18, 14/18 and 9/18 MAGs, respectively) and

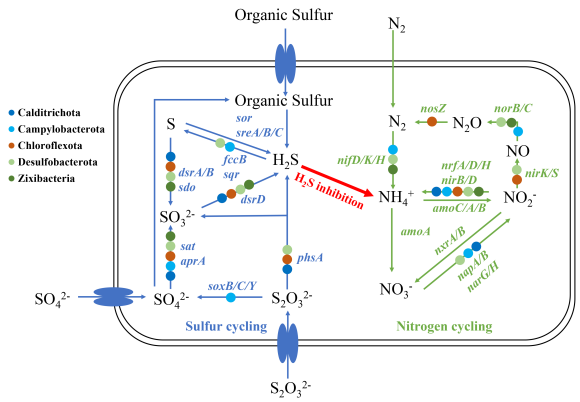

FIGURE 8
Potential scheme of microbial nitrogen and sulfur metabolisms and associated interactions in mudflats.

Zixibacteria (6/6, 1/6 and 1/6 MAGs, respectively). Campylobacterota (10/13 MAGs) predominantly participated in thiosulfate oxidation ($S_2O_3^{2-}$ to SO_4^{2-}). Sulfur reduction (S to H_2S) was not observed in the identified MAGs, however, certain microbes like Campylobacterota (11/13 MAGs) might capable of oxidizing sulfide (H_2S to S), leading to a decrease in H_2S levels. For the nitrogen cycle, nitrogen fixation (N_2 to NH_4^+) was found in Campylobacterota (9/13 MAGs), Desulfobacterota (2/18 MAGs) and Zixibacteria (1/6 MAGs). Nitrite reduction to ammonia (NO_2^- to NH_4^+) was detected in Calditrichota (1/2 MAGs), Campylobacterota (3/13 MAGs), Chloroflexota (3/11 MAGs), Desulfobacterota (3/18 MAGs) and Zixibacteria (4/6 MAGs). Nitrate reduction (NO_3^- to NO_2^-) was found in Calditrichota (1/2 MAGs), Campylobacterota (4/13 MAGs) and Desulfobacterota (4/18 MAGs). Nitrite reduction (NO_2^- to NO) and nitric oxide reduction (NO to N_2O) were both found in Desulfobacterota (8/18 and 3/18 MAGs, respectively). The genes for nitrous oxide reduction (N_2O to N_2) was only found in Chloroflexota (1/13 MAGs). However, no MAGs were found to be involved in nitrification (NH_4^+ to NO_3^-/NO_2^-).

4 Discussion and conclusion

4.1 Two types of tidal flats in Beibu Gulf were distinct in environmental factors including TOC, NH_4^+_N and ORP

Mudflats and sandflats, two common types of tidal flats, are distinguished by their grain size and sediment composition, low-grain mudflat sediments and large-grain sandflat sediments are easily formed by the influence of erosion and sedimentation processes (Thrush et al., 2004). During sampling, we found that mangroves *Avicennia marina* were present near all sampled mudflats, and the presence of seedlings indicated that the mangroves were actively expanding. This suggested that the mudflats we studied primarily consist of terrestrial sediments with a high sedimentation rate, while in the sandflats, tidal processes and the deposition of coarse-grained sediments dominated (Lovelock et al., 2007; Swales et al., 2007; Flemming, 2011). The contents of TOC ($p < 0.05$) and NH_4^+_N ($p < 0.01$) in mudflats were significantly higher than those in sandflats (Supplementary Table 3). The high concentration of TOC was consistent with the previous results (Trimmer et al., 2000; Rauch and Denis, 2008), and the high concentration of TOC was, on the one hand, due to the input of terrestrial sediments and carbon fixation by plants, algae and microbes, on the other hand, as the result of the small charged particles enhanced the adsorption of TOC (Yang et al., 2015; Arias-Ortiz et al., 2021; Boey et al., 2021). Meanwhile, increasingly anaerobic, cohesive and impermeable conditions in mudflat sediments also encouraged the accumulation of NH_4^+_N (Gooday et al., 2009; Moseman-Valtierra et al., 2010; Douglas et al., 2018). In contrast, our result that ORP was higher in sandflat (Supplementary Table 3), indicating mudflat sediments exhibit strong reducibility, the reason for this differences could be due to high permeability and aerobic environments in sandflat (Woulds et al., 2016).

4.2 Mudflats had lower microbial diversity than sandflats

The environment is a significant factor in the selection of microorganisms (Webb et al., 2002). Various environmental factors, such as sediment properties and nutrient availability, can either promote or inhibit bacterial community structure and function to some extent (Buyer et al., 2010; Wang et al., 2020b). Our results showed that in the alpha diversity, the species abundance and diversity in sandflat were higher than those in mudflat, mudflats and sandflats was different in microbial diversity and microbial community structure (Figure 2). This result is not consistent with previous studies which mudflat had higher microbial diversity than sandflat (Boey et al., 2021). This discrepancy may be attributed to the higher oxygen content and ORP found in the sandflat, which is a result of its stronger permeability and heterogeneous physicochemical gradients (Huettel et al., 2014; Woulds et al., 2016). Higher oxygen content and ORP could increase heterotrophic activity and boost higher biomass such as Actinomycetota, Bacteroidota and Pseudomonadota (Hou et al., 2017). On the contrary, the lower oxygen content and ORP would lead to the environment in a state of hypoxia/anoxia, resulting in changes in microbial community structure, some anaerobic bacteria like Desulfobacterota would produce H_2S through sulfate reduction and interrupt the growth of other microorganisms (Pett-Ridge and Firestone, 2005; Sinkko et al., 2019). Meanwhile, the higher diversity in the sandflat may be attributed to the influence of tides, the occurrence of a large number of transient species and/or the continuous aerobic degradation of organic carbon providing broader ecological niche (Boey et al., 2021).

4.3 The differences of microbial functions between sandflat and mudflat in Beibu Gulf

The distinct environmental factors between sandflat and mudflat result in significant differences in biodiversity, which in turn leads to variations in microbial functions. Through the analysis of metagenome sequences, it was observed that mudflats had a higher abundance of genes related to carbon fixation through the Wood-Ljungdahl pathway and 3-Hydroxypropionate cycle (Figure 5). The Wood-Ljungdahl pathway was identified in Calditrichota, Chloroflexota and Desulfobacterota MAGs, while no MAGs were found to be responsible for the 3-Hydroxypropionate cycle (Figure 7). Consequently, further study should focus on the strains responsible for the 3-Hydroxypropionate cycle. Furthermore, nitrogen fixation was only existed in mudflat and annotated in Campilobacterota, Desulfobacterota, Firmicutes, Gammaproteobacteria, Zetaproteobacteria and Zixibacteria,

combined with the proportion of most of these microbes were also higher in mudflat (Figure 3B), indicating that these microbes might mainly contribute to the high NH_4^+_N shown in the mudflat. The ratio of genes for ammonium oxidation were higher in sandflat, even MAGs responsible for it was not found, it was also illuminated that ammonium oxidation was the unique feature of sandflat (Figures 5, 7). In addition, mudflats had a stronger potential in sulfur metabolism, Acidobacteriota, Bacteroidota, Campilobacterota, Calditrichota, Chloroflexota, Desulfobacterota, Gammaproteobacteria, Gemmatimonadota and Zixibacteria MAGs were mainly participated in it (Figures 5, 7). Mudflats were dominated by diffusion transport, which promoted the fermentation of organic matter (Douglas et al., 2018), the traditional biogeochemical processes such as microbial fermentation were related to the rapid metabolism of sulfur in sediments (Bowles et al., 2014). It had also shown that the sulfur cycle was mainly driven by sulfate reduction (Wasmund et al., 2017), and among the oxidants consumed by reoxidation and reduction, microorganisms in mudflats tended to use sulfate and metal ions as electron acceptors (Braker et al., 2001). These illuminated sulfur related MAGs may also function in fermentation and metal cycle of mudflats.

4.4 The unique microbial community in mudflats played an important role in high ammonium accumulation

Based on the result of Spearman's rank correlation, RDA and envfit analysis, the content of NH_4^+_N was the most important environmental factor to the microbial community in mudflats, this feature could be attributed to several potential factors. On the one hand, mudflat was an anoxic, organic-matter-rich environment with strong reducible property. In such environment, the nitrification would be inhibited due to the lack of oxygen, and the sufficient organic matter would be oxidized and stimulate sulfate reduction to produce H_2S, which was then passed through blocking the necessary intermediate step of nitrification and separated nitrogen regeneration from denitrification (Lovley and Klug, 1986). In addition, some of the microbes like nitrate reducing and nitrite ammoniating microbial groups prefer high-reduction anoxic environments would not grow well in it (Gao et al., 2010). On the other hand, it relied on the unique microbial community in mudflats. For example, Desulfobacterota, typically occurred in hypoxic place, traditionally regarded as bacteria that both reduce and oxidize sulfates in wetland systems, it could produce H_2S through sulfite reduction and thiosulfate disproportionation and high concentration of H_2S would inhibit the oxidation of NH_4^+_N (Joye and Hollibaugh, 1995; Joye and Anderson, 2008). In addition, Calditrichota and Zixibacteria could also be attributed to the production of H_2S. Campilobacterota in mudflats encoded genes including nitrogen fixation, nitrate reduction, nitrite reduction to ammonium, and thiosulfate oxidation, it produced NH_4^+_N by nitrogen fixation, nitrate reduction and nitrite reduction to ammonium, and helped other microbial groups like Desulfobacterota by providing sulfate which could link and regulate the S and N cycles, and stratify the microbial communities (Huang et al., 2021). In summary, the high accumulation of ammonium in mudflat would be the result of strong reductive and anoxic conditions, and the unique microbial groups such as Calditrichota, Campilobacterota, Desulfobacterota and Zixibacteria.

Data availability statement

The original contributions presented in the study are publicly available. This data can be found here: NCBI-BioProject, PRJNA774167 and PRJNA967168.

Author contributions

Y-LY: Data curation, Formal Analysis, Investigation, Methodology, Software, Writing – original draft. K-JM: Data curation, Investigation, Methodology, Software, Writing – review & editing. Y-HF: Formal Analysis, Investigation, Writing – review & editing. Z-CW: Data curation, Investigation, Software, Writing – review & editing, Conceptualization, Formal Analysis. G-YF: Project administration, Supervision, Writing – review & editing. CS: Conceptualization, Funding acquisition, Methodology, Project administration, Supervision, Writing – review & editing, Writing – original draft. X-WX: Conceptualization, Funding acquisition, Project administration, Supervision, Writing – review & editing.

Funding

This study was supported by National Science and Technology Fundamental Resources Investigation Program of China (2019FY100700), Zhejiang Provincial Natural Science Foundation of China (LDT23D06025D06), the Key R&D Program of Zhejiang (#2023C03011), National Natural Science Foundation of China (No. 31900003) and the Fundamental Research Funds of Zhejiang Sci-Tech University (22042315-Y).

Acknowledgments

We appreciate the help of Dr. Lin Xu in the guide of metagenome analysis.

Conflict of interest

CS was employed by Zhejiang Sci-Tech University Shaoxing Academy of Biomedicine Co., Ltd.

The remaining authors declare that the research was conducted in the absence of any commercial or financial relationships that could be construed as a potential conflict of interest.

The authors declared that they were an editorial board member of Frontiers, at the time of submission. This had no impact on the peer review process and the final decision

Publisher's note

All claims expressed in this article are solely those of the authors and do not necessarily represent those of their affiliated organizations, or those of the publisher, the editors and the reviewers. Any product that may be evaluated in this article, or claim that may be made by its manufacturer, is not guaranteed or endorsed by the publisher.

Supplementary material

The Supplementary Material for this article can be found online at: https://www.frontiersin.org/articles/10.3389/fmars.2023.1256393/full#supplementary-material

References

Ames, B. N. (1966). Assay of inorganic phosphate, total phosphate and phosphatase. *Meth. Enzymol.* 8, 115–118. doi: 10.1016/0076-6879(66)08014-5

Aramaki, T., Blanc-Mathieu, R., Endo, H., Ohkubo, K., Kanehisa, M., Goto, S., et al. (2020). KofamKOALA: KEGG ortholog assignment based on profile HMM and adaptive score threshold. *Bioinformatics* 36 (7), 2251–2252. doi: 10.1093/bioinformatics/btz859

Arias-Ortiz, A., Masqué, P., Glass, L., Benson, L., Kennedy, H., Duarte, C. M., et al. (2021). Losses of soil organic carbon with deforestation in mangroves of Madagascar. *Ecosystems* 24 (1), 1–19. doi: 10.1007/s10021-020-00500-z

Barberán, A., Bates, S. T., Casamayor, E. O., and Fierer, N. (2012). Using network analysis to explore co-occurrence patterns in soil microbial communities. *ISME J.* 6 (2), 343–351. doi: 10.1038/ismej.2011.119

Böer, S. I., Hedtkamp, S. I., Van Beusekom, J. E., Fuhrman, J. A., Boetius, A., and Ramette, A. (2009). Time-and sediment depth-related variations in bacterial diversity and community structure in subtidal sands. *ISME J.* 3 (7), 780–791. doi: 10.1038/ismej.2009.29

Bolger, A. M., Lohse, M., and Usadel, B. (2014). Trimmomatic: a flexible trimmer for illumina sequence data. *Bioinformatics* 30 (15), 2114–2120. doi: 10.1093/bioinformatics/btu170

Boey, J. S., Mortimer, R., Couturier, A., Worrallo, K., and Handley, K. M. (2021). Estuarine microbial diversity and nitrogen cycling increase along sand–mud gradients independent of salinity and distance. *Environ. Microbiol.* 24, 50–65. doi: 10.1111/1462-2920.15550

Bowers, R. M., Kyrpides, N. C., Stepanauskas, R., Harmon-Smith, M., Doud, D., Reddy, T., et al. (2017). Minimum information about a single amplified genome (MISAG) and a metagenome-assembled genome (MIMAG) of bacteria and archaea. *Nat. Biotechnol.* 35 (8), 725–731. doi: 10.1038/nbt.3893

Bowles, M. W., Mogollón, J. M., Kasten, S., Zabel, M., and Hinrichs, K.-U. (2014). Global rates of marine sulfate reduction and implications for sub–sea-floor metabolic activities. *Science* 344(6186), 889–891. doi: 10.1126/science.1249213

Braker, G., Ayala-del-Río, H. L., Devol, A. H., Fesefeldt, A., and Tiedje, J. M. (2001). Community structure of denitrifiers, Bacteria, and Archaea along redox gradients in Pacific Northwest marine sediments by terminal restriction fragment length polymorphism analysis of amplified nitrite reductase (nirS) and 16S rRNA genes. *Appl. Environ. Microbiol.* 67 (4), 1893–1901. doi: 10.1128/AEM.67.4.1893-1901.2001

Bray, J. R., and Curtis, J. T. (1957). An ordination of the upland forest communities of southern wisconsin. *Ecol. Monogr.* 27 (4), 326–349. doi: 10.2307/1942268

Buyer, J. S., Teasdale, J. R., Roberts, D. P., Zasada, I. A., and Maul, J. E. (2010). Factors affecting soil microbial community structure in tomato cropping systems. *Soil Boil Biochem.* 42 (5), 831–841. doi: 10.1016/j.soilbio.2010.01.020

Chaumeil, P.-A., Mussig, A. J., Hugenholtz, P., and Parks, D. H. (2019). GTDB-Tk: a toolkit to classify genomes with the Genome Taxonomy Database. *Bioinformatics* 36 (6), 1925–1927. doi: 10.1093/bioinformatics/btz848

Cummings, V., Vopel, K., and Thrush, S. (2009). Terrigenous deposits in coastal marine habitats: influences on sediment geochemistry and behaviour of post-settlement bivalves. *Mar. Ecol. Prog. Ser.* 383, 173–185. doi: 10.3354/meps07983

Dou, Y., Li, J., Zhao, J., Hu, B., and Yang, S. (2013). Distribution, enrichment and source of heavy metals in surface sediments of the eastern Beibu Bay, South China Sea. *Mar. pollut. Bull.* 67 (1-2), 137–145. doi: 10.1016/j.marpolbul.2012.11.022

Douglas, E. J., Pilditch, C. A., Lohrer, A. M., Savage, C., Schipper, L. A., and Thrush, S. F. (2018). Sedimentary environment influences ecosystem response to nutrient enrichment. *Estuar. Coast.* 41 (7), 1994–2008. doi: 10.1007/s12237-018-0416-5

Drula, E., Garron, M.-L., Dogan, S., Lombard, V., Henrissat, B., and Terrapon, N. (2022). The carbohydrate-active enzyme database: functions and literature. *Nucleic Acids Res.* 50 (D1), D571–D577. doi: 10.1093/nar/gkab1045

Du, J., Xiao, K., Huang, Y., Li, H., Tan, H., Cao, L., et al. (2011). Seasonal and spatial diversity of microbial communities in marine sediments of the South China Sea. *Anton Leeuw* 100 (3), 317–331. doi: 10.1007/s10482-011-9587-9

Flemming, B. (2011). 3.02-geology, morphology, and sedimentology of estuaries and coasts. *Waltham: Acad. Press* 3, 7–38. doi: 10.1016/B978-0-12-374711-2.00302-8

Folk, R. L., Andrews, P. B., and Lewis, D. W. (1970). Detrital sedimentary rock classification and nomenclature for use in New Zealand. *New Zealand J. Geol. Geophys.* 13 (4), 937–968. doi: 10.1080/00288306.1970.10418211

Gao, H., Schreiber, F., Collins, G., Jensen, M. M., Kostka, J. E., Lavik, G., et al. (2010). Aerobic denitrification in permeable wadden sea sediments. *ISME J.* 4 (3), 417–426. doi: 10.1038/ismej.2009.127

Garber, A. I., Nealson, K. H., Okamoto, A., McAllister, S. M., Chan, C. S., Barco, R. A., et al. (2020). FeGenie: a comprehensive tool for the identification of iron genes and iron gene neighborhoods in genome and metagenome assemblies. *Front. Microbiol.* 37. doi: 10.3389/fmicb.2020.00037

Gooday, A., Jorissen, F., Levin, L., Middelburg, J., Naqvi, S., Rabalais, N., et al. (2009). Historical records of coastal eutrophication-induced hypoxia. *Biogeosciences* 6 (8), 1707–1745. doi: 10.5194/bg-6-1707-2009

Gurevich, A., Saveliev, V., Vyahhi, N., and Tesler, G. (2013). QUAST: quality assessment tool for genome assemblies. *Bioinformatics* 29 (8), 1072–1075. doi: 10.1093/bioinformatics/btt086

He, B., Lai, T., Fan, H., Wang, W., and Zheng, H. (2007). Comparison of flooding-tolerance in four mangrove species in a diurnal tidal zone in the Beibu Gulf. *Estuar. Coast. Shelf S* 74 (1-2), 254–262. doi: 10.1016/j.ecss.2007.04.018

Healy, T., Wang, Y., and Healy, J.-A. (2002). *Muddy coasts of the world: processes, deposits and function* (Amsterdam: Elsevier).

Hou, Z., Nelson, W. C., Stegen, J. C., Murray, C. J., Arntzen, E., Crump, A. R., et al. (2017). Geochemical and microbial community attributes in relation to hyporheic zone geological facies. *Sci. Rep.* 7 (1), 12006. doi: 10.1038/s41598-017-12275-w

Huang, L., Bae, H. S., Young, C., Pain, A. J., Martin, J. B., and Ogram, A. (2021). Campylobacterota dominate the microbial communities in a tropical karst subterranean estuary, with implications for cycling and export of nitrogen to coastal waters. *Environ. Microbiol.* 23 (11), 6749–6763. doi: 10.1111/1462-2920.15746

Huettel, M., Berg, P., and Kostka, J. E. (2014). Benthic exchange and biogeochemical cycling in permeable sediments. *Annu. Rev. Mar. Sci.* 6, 23–51. doi: 10.1146/annurev-marine-051413-012706

Hyatt, D., Chen, G.-L., LoCascio, P. F., Land, M. L., Larimer, F. W., and Hauser, L. J. (2010). Prodigal: prokaryotic gene recognition and translation initiation site identification. *BMC Bioinf.* 11 (1), 1–11. doi: 10.1186/1471-2105-11-119

Joye, S. B., and Anderson, I. C. (2008). Nitrogen cycling in coastal sediments. *Nitrogen Mar. Environ.* 2, 868–915. doi: 10.1016/B978-0-12-372522-6.00019-0

Joye, S. B., and Hollibaugh, J. T. (1995). Influence of sulfide inhibition of nitrification on nitrogen regeneration in sediments. *Science* 270, 623–625. doi: 10.1126/science.270.5236.62

Ki, B.-M., Huh, I. A., Choi, J.-H., and Cho, K.-S. (2018). Relationship of nutrient dynamics and bacterial community structure at the water–sediment interface using a benthic chamber experiment. *J. Environ. Sci. Heal A* 53 (5), 482–491. doi: 10.1080/10934529.2017.1412191

Kjeldahl, J. (1883). A new method for the determination of nitrogen in organic matter. *Z. für Analytische Chemie* 22, 366–382 . doi: 10.1007/BF01338151

Letunic, I., and Bork, P. (2021). Interactive tree of life (iTOL) v5: an online tool for phylogenetic tree display and annotation. *Nucleic Acids Res.* 49 (W1), W293–W296. doi: 10.1093/nar/gkab301

Li, N., Chen, X., Zhao, H., Tang, J., Jiang, G., Li, Z., et al. (2020). Spatial distribution and functional profile of the bacterial community in response to eutrophication in the subtropical Beibu Gulf, China. *Mar. pollut. Bull.* 161, 111742. doi: 10.1016/j.marpolbul.2020.111742

Liu, Y.-X., Qin, Y., Chen, T., Lu, M., Qian, X., Guo, X., et al. (2021). A practical guide to amplicon and metagenomic analysis of microbiome data. *Protein Cell* 12 (5), 315–330. doi: 10.1007/s13238-020-00724-8

Lohrer, A. M., Thrush, S. F., Hewitt, J. E., Berkenbusch, K., Ahrens, M., and Cummings, V. J. (2004). Terrestrially derived sediment: response of marine macrobenthic communities to thin terrigenous deposits. *Mar. Ecol. Prog. Ser.* 273, 121–138. doi: 10.3354/meps273121

Lovelock, C. E., Feller, I. C., Ellis, J., Schwarz, A. M., Hancock, N., Nichols, P., et al. (2007). Mangrove growth in New Zealand estuaries: the role of nutrient enrichment at sites with contrasting rates of sedimentation. *Oecologia* 153 (3), 633–641. doi: 10.1007/s00442-007-0750-y

Lovley, D. R., and Klug, M. J. (1986). Model for the distribution of sulfate reduction and methanogenesis in freshwater sediments. *Geochimica Cosmochimica Acta* 50 (1), 11–18. doi: 10.1016/0016-7037(86)90043-8

Lozupone, C., and Knight, R. (2005). UniFrac: a new phylogenetic method for comparing microbial communities. *Appl. Environ. Microbiol.* 71 (12), 8228–8235. doi: 10.1128/AEM.71.12.8228-8235.2005

Lv, X., Ma, B., Yu, J., Chang, S. X., Xu, J., Li, Y., et al. (2016). Bacterial community structure and function shift along a successional series of tidal flats in the Yellow River Delta. *Sci. Rep-UK* 6 (1), 1–10. doi: 10.1038/srep36550

Ma, F., Wang, Y., Li, Y., Ye, C., Xu, Z., and Zhang, F. (2010). The application of geostatistics in grain size trend analysis: a case study of eastern Beibu Gulf. *J. Geogr. Sci.* 20 (1), 77–90. doi: 10.1007/s11442-010-0077-1

McArdle, B. H., and Anderson, M. J. (2001). Fitting multivariate models to community data: a comment on distance-based redundancy analysis. *Ecology* 82 (1), 290–297. doi: 10.1890/0012 9658(2001)082[0290:FMMTCD]2.0.CO;2

Moseman-Valtierra, S., Armaiz-Nolla, K., and Levin, L. (2010). Wetland response to sedimentation and nitrogen loading: diversification and inhibition of nitrogen-fixing microbes. *Ecol. Appl.* 20 (6), 1556–1568. doi: 10.1890/08-1881.1

Murray, N. J., Phinn, S. R., DeWitt, M., Ferrari, R., Johnston, R., Lyons, M. B., et al. (2019). The global distribution and trajectory of tidal flats. *Nature* 565 (7738), 222–225. doi: 10.1038/s41586-018-0805-8

Nicholls, R. J., Wong, P., Burkett, V., Codignotto, J., Hay, J., McLean, R., et al. (2007). *Climate change 2007: impacts, adaptation and vulnerability. Contribution of working group II to the fourth assessment report of the intergovernmental panel on climate change* (Cambridge: Cambridge University Press).

Olm, M. R., Brown, C. T., Brooks, B., and Banfield, J. F. (2017). dRep: a tool for fast and accurate genomic comparisons that enables improved genome recovery from metagenomes through de-replication. *ISME J.* 11 (12), 2864–2868. doi: 10.1038/ismej.2017.126

Osland, M. J., Enwright, N. M., Day, R. H., Gabler, C. A., Stagg, C. L., and Grace, J. B. (2016). Beyond just sea-level rise: Considering macroclimatic drivers within coastal wetland vulnerability assessments to climate change. *Global Change Biol.* 22 (1), 1–11. doi: 10.1111/gcb.13084

Parks, D. H., Tyson, G. W., Hugenholtz, P., and Beiko, R. G. (2014). STAMP: statistical analysis of taxonomic and functional profiles. *Bioinformatics* 30 (21), 3123–3124. doi: 10.1093/bioinformatics/btu494

Passeri, D. L., Hagen, S. C., Medeiros, S. C., Bilskie, M. V., Alizad, K., and Wang, D. (2015). The dynamic effects of sea level rise on low-gradient coastal landscapes: A review. *Earths Future* 3 (6), 159–181. doi: 10.1002/2015EF000298

Peterson, G. L. (1979). Review of the folin phenol protein quantitation method of lowry, rosebrough, farr and randall. *Anal. Biochem.* 100 (2), 201–220. doi: 10.1016/0003-2697(79)90222-7

Pett-Ridge, J., and Firestone, M. (2005). Redox fluctuation structures microbial communities in a wet tropical soil. *Appl. Environ. Microbiol.* 71 (11), 6998–7007. doi: 10.1128/AEM.71.11.6998-7007.2005

Quast, C., Pruesse, E., Yilmaz, P., Gerken, J., Schweer, T., Yarza, P., et al. (2012). The SILVA ribosomal RNA gene database project: improved data processing and web-based tools. *Nucleic Acids Res.* 41 (D1), D590–D596. doi: 10.1093/nar/gks1219

Rauch, M., and Denis, L. (2008). Spatio-temporal variability in benthic mineralization processes in the eastern English Channel. *Biogeochemistry* 89 (2), 163–180. doi: 10.1007/s10533-008-9191-x

Rawlings, N. D., Barrett, A. J., Thomas, P. D., Huang, X., Bateman, A., and Finn, R. D. (2018). The MEROPS database of proteolytic enzymes, their substrates and inhibitors in 2017 and a comparison with peptidases in the PANTHER database. *Nucleic Acids Res.* 46 (D1), D624–D632. doi: 10.1093/nar/gkx1134

Sarukhán, J., Whyte, A., Hassan, R., Scholes, R., Ash, N., Carpenter, S., et al. (2005). *Millenium ecosystem assessment: Ecosystems and human well-being* (Washington, DC: Island Press).

Schlitzer, R. (2021) *Ocean data view*. Available at: https://odv.awi.de.

Sims, R. P. A. (1961). Formation of heteropoly blue by some reduction procedures used in the micro-determination of phosphorus. *Analyst* 86 (1026), 584–590. doi: 10.1039/AN9618600584

Sinkko, H., Hepolehto, I., Lyra, C., Rinta-Kanto, J. M., Villnäs, A., Norkko, J., et al. (2019). Increasing oxygen deficiency changes rare and moderately abundant bacterial communities in coastal soft sediments. *Sci. Rep.* 9 (1), 1–14. doi: 10.1038/s41598-019-51432-1

Søndergaard, D., Pedersen, C. N., and Greening, C. (2016). HydDB: a web tool for hydrogenase classification and analysis. *Sci. Rep.* 6 (1), 1–8. doi: 10.1038/srep34212

Spearman, C. (1987). The proof and measurement of association between two things. *Am. J. Psychol.* 100 (3/4), 441–471. doi: 10.2307/1422689

Swales, A., Bentley, S. J., Lovelock, C., and Bell, R. G. (2007). "Sediment processes and mangrove-habitat expansion on a rapidly-prograding muddy coast, New Zealand," in *Coastal sediments* (Virginia: Amer Society of Civil Engineers), 1441–1454.

Thompson, L. R., Sanders, J. G., McDonald, D., Amir, A., Ladau, J., Locey, K. J., et al. (2017). A communal catalogue reveals Earth's multiscale microbial diversity. *Nature* 551 (7681), 457–463. doi: 10.1038/nature24621

Thrush, S., Hewitt, J., Cummings, V., Ellis, J., Hatton, C., Lohrer, A., et al. (2004). Muddy waters: elevating sediment input to coastal and estuarine habitats. *Front. Ecol. Environ.* 2 (6), 299–306. doi: 10.2307/3868405

Trimmer, M., Nedwell, D. B., Sivyer, D. B., and Malcolm, S. J. (2000). Seasonal benthic organic matter mineralisation measured by oxygen uptake and denitrification along a transect of the inner and outer River Thames estuary, UK. *Mar. Ecol. Prog. Ser.* 197, 103–119. doi: 10.3354/meps197103

Uritskiy, G. V., DiRuggiero, J., and Taylor, J. (2018). MetaWRAP–a flexible pipeline for genome-resolved metagenomic data analysis. *Microbiome* 6 (1), 1–13. doi: 10.1186/s40168-018-0541-1

Wang, X., Yang, J., Xie, X., Chen, X., Pu, L., and Zhang, X. (2020b). Soil microbial succession with soil development since costal reclamation. *Catena* 187, 104393. doi: 10.1016/j.catena.2019.104393

Wang, W., Yang, Y., Zhou, Y., Zhang, S., Wang, X., and Yang, Z. (2020a). Impact of anthropogenic activities on the sediment microbial communities of Baiyangdian shallow lake. *Int. J. Sediment Res.* 35 (2), 180–192. doi: 10.1016/j.ijsrc.2019.10.006

Wasmund, K., Mußmann, M., and Loy, A. (2017). The life sulfuric: microbial ecology of sulfur cycling in marine sediments. *Environ. Microbiol. Rep.* 9 (4), 323–344. doi: 10.1111/1758-2229.12538

Webb, C. O., Ackerly, D. D., McPeek, M. A., and Donoghue, M. J. (2002). Phylogenies and community ecology. *Annu. Rev. Ecol. Evol. S* 33 (1), 475–505. doi: 10.1146/annurev.ecolsys.33.010802.150448

Welch, B. L. (1947). The generalization of 'student's' problem when several different population varlances are involved. *Biometrika* 34 (1-2), 28–35. doi: 10.1093/biomet/34.1-2.28

Woulds, C., Bouillon, S., Cowie, G. L., Drake, E., Middelburg, J. J., and Witte, U. (2016). Patterns of carbon processing at the seafloor: the role of faunal and microbial communities in moderating carbon flows. *Biogeosciences* 13 (15), 4343–4357. doi: 10.5194/bg-13-4343-2016

Yang, B., Cao, L., Liu, S.-M., and Zhang, G.-S. (2015). Biogeochemistry of bulk organic matter and biogenic elements in surface sediments of the Yangtze River Estuary and adjacent sea. *Mar. pollut. Bull.* 96 (1-2), 471–484. doi: 10.1016/j.marpolbul.2015.05.003

Yu, N. Y., Wagner, J. R., Laird, M. R., Melli, G., Rey, S., Lo, R., et al. (2010). PSORTb 3.0: improved protein subcellular localization prediction with refined localization subcategories and predictive capabilities for all prokaryotes. *Bioinformatics* 26 (13), 1608–1615. doi: 10.1093/bioinformatics/btq249

Zhang, H., Yohe, T., Huang, L., Entwistle, S., Wu, P., Yang, Z., et al. (2018). dbCAN2: a meta server for automated carbohydrate-active enzyme annotation. *Nucleic Acids Res.* 46 (W1), W95–W101. doi: 10.1093/nar/gky418

Zhang, G., Bai, J., Tebbe, C. C., Zhao, Q., Jia, J., Wang, W., et al. (2021). Salinity controls soil microbial community structure and function in coastal estuarine wetlands. *Environ. Microbiol.* 23 (2), 1020–1037. doi: 10.1111/1462-2920.15281

Zhang, Z., Guo, Y., Guo, L., Hu, F., Zhao, Y., Jin, C., et al. (2020). Elucidating salinity adaptation and shock loading on denitrification performance: focusing on microbial community shift and carbon source evaluation. *Bioresour. Technol.* 305, 123030. doi: 10.1016/j.biortech.2020.123030

Zhang, H., Zheng, S., Ding, J., Wang, O., and Liu, F. (2017). Spatial variation in bacterial community in natural wetland-river-sea ecosystems. *J. Basic Microbiol.* 57 (6), 536–546. doi: 10.1002/jobm.201700041

Zhou, Z., Tran, P. Q., Breister, A. M., Liu, Y., Kieft, K., Cowley, E. S., et al. (2022). METABOLIC: high-throughput profiling of microbial genomes for functional traits, metabolism, biogeochemistry, and community-scale functional networks. *Microbiome* 10 (1), 33. doi: 10.1186/s40168-021-01213-8

frontiers | Frontiers in Marine Science

TYPE Original Research
PUBLISHED 20 October 2023
DOI 10.3389/fmars.2023.1244849

OPEN ACCESS

EDITED BY
Xue-Wei Xu,
Ministry of Natural Resources, China

REVIEWED BY
Dao-Feng Zhang,
Hohai University, China
Graciela Dias,
Federal University of Rio de Janeiro, Brazil

*CORRESPONDENCE
Bao-Zhu Fang
fangbaozhu2009@126.com
Wen-Jun Li
liwenjun3@mail.sysu.edu.cn

†These authors have contributed equally to this work

RECEIVED 23 June 2023
ACCEPTED 10 October 2023
PUBLISHED 20 October 2023

CITATION
Gao L, Fang B-Z, Lu C-Y, Hong K-H, Huang X-Y, She T-T, Xiao M and Li W-J (2023) Unraveling the genomic diversity and ecological potential of the genus *Demequina*: insights from comparative analysis of different saline niche strains. *Front. Mar. Sci.* 10:1244849. doi: 10.3389/fmars.2023.1244849

Unraveling the genomic diversity and ecological potential of the genus *Demequina*: insights from comparative analysis of different saline niche strains

Lei Gao[1,2†], Bao-Zhu Fang[1*†], Chun-Yan Lu[3†], Kun-Hui Hong[4], Xin-Yu Huang[4], Ting-Ting She[4], Min Xiao[3] and Wen-Jun Li[1,3*]

[1]State Key Laboratory of Desert and Oasis Ecology, Key Laboratory of Ecological Safety and Sustainable Development in Arid Lands, Xinjiang Institute of Ecology and Geography, Chinese Academy of Sciences, Urumqi, China, [2]University of Chinese Academy of Sciences, Beijing, China, [3]State Key Laboratory of Biocontrol, Guangdong Provincial Key Laboratory of Plant Resources and Southern Marine Science and Engineering Guangdong Laboratory (Zhuhai), School of Life Sciences, Sun Yat-Sen University, Guangzhou, Guangdong, China, [4]Guangdong University of Education, Guangzhou, Guangdong, China

During an investigation of the culturable microbial diversity of sediments with salinity from tidal flats and saline lake, seven strains of the genus *Demequina* were harvested. The genomic analysis and physiological characteristics of strains of this genus have unveiled their significant potential in degrading complex carbon source such as lignin, hemicellulose, chitin, and oligosaccharides. In addition, these strains show potential abilities in nitrite ammonification and sulfide oxidation. These findings not only improved our understanding of their metabolic model, but also provided valuable insights into their ecological roles. Four new species of the genus *Demequina* are described: *Demequina litoralis* sp. nov., with SYSU T00192^T designated as the type species; *Demequina zhanjiangensis* sp. nov., with SYSU T00b26^T as the type species; *Demequina lignilytica* sp. nov., with SYSU T00068^T as the type species; and *Demequina muriae* sp. nov., with EGI L300058^T as the type species. Additionally, strains SYSU T0a273, SYSU T00039-1, and SYSU T00039 are identified as different strains of *Demequina lignilytica*. Our study thus sheds light on the diversity, biological significance, and ecological contribution of the *Demequina* genus in different habitats.

KEYWORDS

***Demequina*, comparative genomic analysis, diversity and identification, tidal flat, saline lake**

1 Introduction

Demequina was a genus in the family *Demequinaceae* of the phylum *Actinomycetota* (Ue et al., 2011; Oren and Garrity, 2021). The genus *Demequina*, a group of Gram-stain positive bacteria, was first discovered from tidal flats sediment by Yi et al., 2007 (Yi et al., 2007) and currently comprises 21 known species (https://lpsn.dsmz.de/genus/demequina, accessed on 15 May 2023). Then, the description of the genus *Demequina* is amended by Ue et al., 2011 and Park et al., 2016 Species of the genus *Demequina* exhibited diverse morphologies, including short rod-shaped, oval, coccoid forms and were widely distributed in tidal flats sediment (Yi et al., 2007), mangrove (Matsumoto et al., 2010; Hamada et al., 2015b), soil (Finster et al., 2009), and marine related niches (Hamada et al., 2013). The species within the genus *Demequina* displayed diverse morphologies and biochemical characteristics and were found to be widely distributed in natural environments. These traits provided interesting objects for researchers to explore their genomes and biological properties (Chao et al., 2021).

With technological advances, more researches had been conducted on the genomics (Hamada et al., 2015a) and biological properties of strains of the genus *Demequina*, revealing their ability to perform ecological functions in various niches (Meng et al., 2009; Al-Naamani et al., 2015; Peruzzi et al., 2017; Wei et al., 2018; Duan et al., 2019). Comparative genome analysis was an effective approach to decipher the genetic diversity and evolutionary relationships of microorganisms (Wei et al., 2002). However, the lack of understanding genomic data on *Demequina* strains hindered our comprehension of their ecological roles and potential applications. Comparative genome analysis of species in the genus *Demequina* would therefore make an important contribution to the field of microbial genomics and could have practical implications for biotechnology and human health.

In our study, we obtained seven strains of the genus *Demequina*. Our research has three main objectives: first, to determine the taxonomic status of these new strains; second, to compare the metabolic potential of the genus *Demequina*; and finally, to evaluate the potential ecological and physiological functions of the genus *Demequina*. Overall, our efforts have resulted in a successful expansion of diversity within the genus *Demequina*, which will be critical for future implementation of industrial applications.

2 Materials and methods

2.1 Strain source

During our investigation into the culturable microbial diversity of saline aquatic environments, we successfully isolated a strain (EGI L300058) from sediment samples of Dabancheng saline lake in Xinjiang, PR China. In the meantime, tidal flats as other saline niche, we also obtained six strains (SYSU T0a273, SYSU T00068, SYSU T00039-1, SYSU T00039, SYSU T00192, and SYSU T00b26) from sediment samples of tidal flats from Zhanjiang city in Guangdong. All strains were routinely maintained on marine agar 2216 (28°C, 1 week) and biomass of these strains for the later experiment was collected under the same conditions.

2.2 Genome sequencing, assembly, and annotation

DNA extraction from all strains was carried out using the TIANamp Bacteria DNA kit, following the kit instructions. The DNA library was prepared according to the instructions of the NGS Fast DNA Library Prep Set for Illumina. The genomes of these strains were sequenced using paired-end sequencing on the Illumina Hiseq X platform, which was performed at the Guangdong Institute of Microbiology. The reads obtained from each dataset were trimmed using Sickle (Joshi and Fass, 2011) and subsequently, the high-quality paired-end reads were assembled using the SPAdes program (Bankevich et al., 2012) with options "-k 21, 33, 55, 77, 99, 121 -careful" in Unicycler software (Wick et al., 2017). The identification of protein-coding sequences within the assembled sequences was carried out using Prodigal (Hyatt et al., 2010). Meanwhile, tRNA-scan (Chan and Lowe, 2019) and RNAmmer (Lagesen et al., 2007) were utilized to identify tRNA and rRNA, respectively. To identify the gene functions, we applied an E-value cut-off of 1e-5 and filtered for the best hit using the Clusters of Orthologous Groups (COG) (Galperin et al., 2019), Kyoto Encyclopedia of Genes and Genomes (KEGG) (Kanehisa et al., 2016), and carbohydrate-active enzymes (CAZy) databases (Drula et al., 2021). We determined the G + C content from the genome sequences and constructed genome maps with the GenoVi: Genome Visualizer (Cumsille et al., 2023).

2.3 Phylogenetic analysis

16S rRNA gene sequences were amplified using genomic DNA as the template with universal bacterial primers 27F and 1492R following the protocol described by Fang et al., 2020. Almost full-length 16S rRNA gene sequences were compared to related sequences in the EzBioCloud (Yoon et al., 2017) and NCBI (Sayers et al., 2021) databases, respectively (Altschul et al., 1990). To conduct phylogenetic analysis, 16S rRNA gene sequences of related species within the genus *Demequina* were downloaded from the above-mentioned databases and aligned using the CLustalW MEGAX (Thompson et al., 1994; Kumar et al., 2018). The Kimura 2-parameter model (Casanellas et al., 2020) was used to calculate genetic distances and clustering, and phylogenetic trees were constructed using the neighbor-joining (Saitou and Nei, 1987) and maximum likelihood (Felsenstein, 1981) methods. The phylogenomic tree of the genus *Demequina* was constructed according to the method described before (Jiao et al., 2021) and shown in brief below. Multiple sequence alignments (MSAs) of 120 bacterial marker genes were generated using GTDB-Tk (Chaumeil et al., 2019), and the maximum-likelihood phylogeny of the MSAs was calculated using IQ-Tree (Nguyen et al., 2015) with the parameters -alrt 1000, -bb 1000, and -nt AUTO.

2.4 Comparative genomics and metabolic potential analysis

Nineteen *Demequina* genomes were retrieved from NCBI databases for comparative analysis. Average nucleotide identity (ANI) and amino acid identity (AAI) were computed using IPGA (Liu et al., 2022) and CompareM software (https://github.com/dparks1134/CompareM, ver. 3), respectively. To perform comparative analysis of orthologous and unique genes among species of the genus *Demequina*, we filtered out low-quality protein sequences based on length (10 AA) and percent stop codons (20%) in FASTA format and then used the OrthoFinder program (Emms and Kelly, 2019) within the PGCGAP pipeline (Liu et al., 2020) to cluster the proteomes and generate gene families based on reciprocal DIAMOND best hits of predicted amino acid sequences. We also leveraged the IPGA pipeline to perform pan- and core-genome analyses of species of the genus *Demequina* with a minimum sequence identity threshold of 70% (https://nmdc.cn/ipga/, accessed on 8 April 2023). Metabolic and biogeochemical functional trait profiles for the genome datasets were further predicted using the METABOLIC software (Zhou et al., 2022). The antiSMASH (ver. 6.0) was used for the analysis of biosynthetic gene clusters (BGCs) in all genomes (Blin et al., 2021). All plots were generated using the ggplot2 package in R (https://www.r-project.org/, ver. 4.1.2).

2.5 Phenotypic and physiological analysis

The physiological characteristics of these strains were determined by the methods previously described (Xu et al., 2005; Gao et al., 2022). We also analyzed the morphology of our strains by negative staining with ammonium molybdate and transmission electron microscopy. After seven days of incubation on marine agar 2216, we recorded the size, shape, and color of the colonies, and conducted Gram staining to examine the bacterial cell wall. We assessed the utilization of substrates by the target strain at 30°C using GEN III Microplates (BIOLOG Inc., Hayward, California, United States) and measured oxidase activity using the Oxidase Reagent kit (bioMerieux SA). We also evaluated the ability of strains to peptonize and coagulate milk, as well as their urease activity, starch and Tween degradation, and liquefaction of gelatin, following Smibert and Krieg's instructions (Smibert and Krieg, 1994). We measured protease activity by spot inoculating strains onto a 5% (v/v) skim milk agar medium (Rohban et al., 2009). Additionally, we analyzed nitrate and nitrite reduction and other biochemical properties using API 20NE and API ZYM kits (manufactured by bioMérieux in France). The production for ligninase, cellulase, chitinase, IAA (indole-3-acetic acid), ACC (1-Aminocyclopropane-1-carboxylic Acid) deaminase of *Demequina* strains were tested by following protocols of manufacturer for the Microbial Ligninase Detection Kit (JINMEI, China), Microorganism Cellulase (CE) ELISA Kit (JINMEI, China), Microbial Chitinase ELISA Kit (JINMEI, China), Microbial Indoleacetic Acid (IAA) ELISA Kit (JINMEI, China), and Microbial ACC Deaminase (ACCD) ELISA Kit (JINMEI, China), respectively.

Biomasses for the chemotaxonomic analysis of seven strains were obtained from cultures grown on the marine agar 2216 at 30 °C for 7 days. The cellular fatty acids of both strains were extracted from the collected biomasses, methylated, and analyzed by the Microbial Identification System (Sherlock Version 6.1; MIDI database: TSBA6). The respiratory quinones were extracted and purified from lyophilized cells (Collins et al., 1977; Minnikin et al., 1984) and the extracts were analyzed by using HPLC (High Performance Liquid Chromatography) (Kroppenstedt, 1982; Groth et al., 1997). After extraction, the polar lipids were analyzed by the two-dimensional TLC (thin-layer chromatography) method on silica gel G 60 plates (Merck; Germany) (Hasegawa et al., 1983; Yin et al., 2021).

3 Results

3.1 Genome characteristics of the species of the genus *Demequina*

The genome size of species in the genus *Demequina* displayed a range of 2,359,865 bp to 3,228,371 bp, with a corresponding GC content range of 62.73% to 72.39%, and numbers of predicted genes varied from 2172 to 3013 (Dataset S1). For a strain form saline lake, genome size of strain EGI L300058^T was 2,359,865 bp with a GC content of 69.41% and contained 8 contigs, 2172 genes, 3 rRNAs, and 39 tRNAs. For six strains from tidal flats, strain SYSU T00192^T had a genome size of 3,024,536 bp and a GC content of 72.26%, consisting of 21 contigs, 2804 genes, 3 rRNAs, and 52 tRNAs. Strain SYSU T00b26^T had a genome size of 3,125,962 bp and a GC content of 69.58%, consisting of 17 contigs, 2882 genes, 3 rRNAs, and 49 tRNAs. Strain SYSU T00068^T had a genome size of 2,927,318 bp and a GC content of 71.88%, consisting of 23 contigs, 2705 genes, 4 rRNAs, and 52 tRNAs (Supplementary Figures 1A–D). Strain SYSU T0a273 had a genome size of 2,838,212 bp and a GC content of 72.08%, consisting of 16 contigs, 2626 genes, 3 rRNAs, and 53 tRNAs. Strain SYSU T00039-1 had a genome size of 2,896,852 bp and a GC content of 71.95%, consisting of 15 contigs, 2677 genes, 3 rRNAs, and 45 tRNAs. Strain SYSU T00039 had a genome size of 2,482,171 bp and a GC content of 71.93%, consisting of 17 contigs, 2309 genes, 3 rRNAs, and 52 tRNAs (Supplementary Figure 1E).

The results of KEGG annotation revealed that the species in this genus were classified into 22 KEGG level two pathways. In particular, the metabolic pathways, including carbohydrate metabolism, amino acid metabolism, and overview, exhibited high abundance (Figure 1A). The results of COG annotation revealed that species were classified into 22 functional categories, including A, C-V, and Z (Figure 1B). The most abundant COGs of the genomes in this genus were exclusively assigned to general function prediction, closely followed by CDSs dedicated to carbohydrate transport and metabolism, amino acid transport and metabolism, function unknown, and transcription. Notably, the COG annotation results were also enriched for genes associated with metabolism, which was largely consistent with the KEGG annotation results. Functional annotation of the *Demequina* strains revealed a high degree of similarity in their functional repertoire, as indicated by the relatively concentrated distribution of similar functions across different strains. These new strains

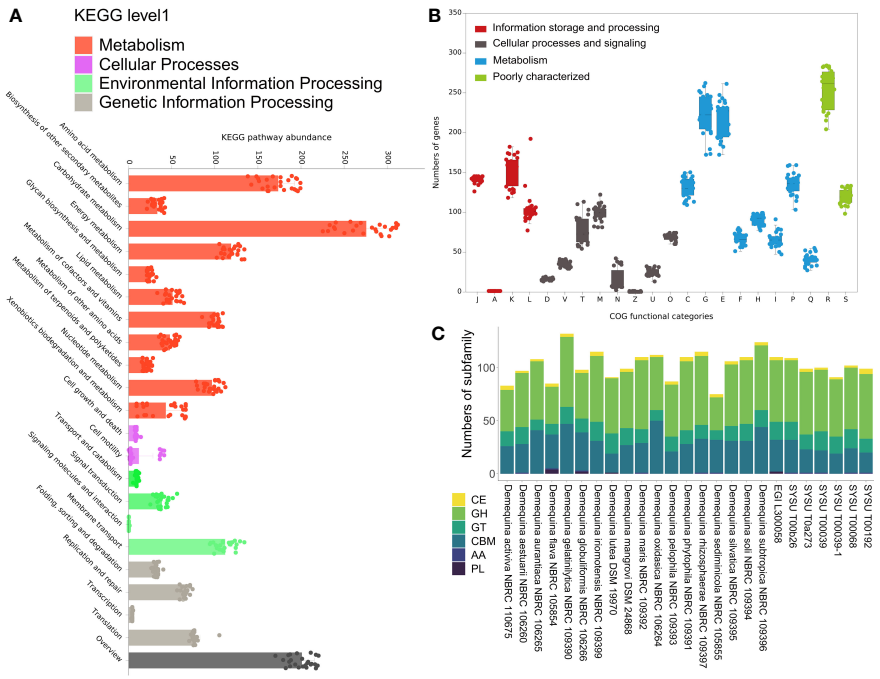

FIGURE 1
Metabolic potentials of *Demequina* strains. **(A)** KEGG pathway abundance of species of the genus *Demequina*. **(B)** COG functional categories of Demequina strains. **(C)** Carbohydrate-active enzymes (CAZymes) family associated with the CAZy database. (A), RNA processing and modification; (B), Chromatin structure and dynamics; (C), Energy production and conversion; (D), Cell cycle control, cell division, chromosome partitioning; (E), Amino acid transport and metabolism; (F), Nucleotide transport and metabolism; (G), Carbohydrate transport and metabolism; (H), Coenzyme transport and metabolism; (I), Lipid transport and metabolism; (J), Translation, ribosomal structure and biogenesis; (K), Transcription; (L), Replication, recombination and repair; (M), Cell wall/membrane/envelope biogenesis; (N), Cell motility; (O), Posttranslational modification, protein turnover; (P), Inorganic ion transport and metabolism; (Q), Secondary metabolites biosynthesis, transport and catabolism; (R), General function prediction only; (S), Function unknown; (T), Signal transduction mechanisms; (U), Intracellular trafficking, secretion, and vesicular transport; (V), Defense mechanisms; (W), Extracellular structures; (X), Mobilome: prophages, transposons; (Z), Cytoskeleton.

contained 6 families of carbohydrate-active enzymes involved in glycosidic bond degradation, modification, and generation. These enzyme families include Carbohydrate Esterases (CEs), Glycoside Hydrolases (GHs), Auxiliary Activities (AAs), Polysaccharide Lyases (PLs), Glycoside Transferases (GTs), and Carbohydrate Binding Modules (CBMs) (Figure 1C). Glycoside Hydrolases, which were present in the highest amounts, were a ubiquitous group of enzymes that catalyze the hydrolysis of glycosidic bonds between two or more carbohydrates or between a carbohydrate and a non-carbohydrate moiety (Li et al., 2021). CBMs in CAZymes, which ranked third in quantity, bind specifically to carbohydrates and played critical roles in enzyme targeting, activity enhancement, facilitation of recycling, assembly of multi-enzyme complex, and modulation of substrate specificity and catalytic activity of associated enzymes (Attia and Brumer, 2021). GTs, which ranked third in terms of quantity, had also been identified and were involved in the biosynthesis of disaccharides, oligosaccharides, and polysaccharides (Sánchez-Rodríguez et al., 2014). In addition, our analysis revealed there were few PLs in the genomes of this genus that removed uronic acid from polysaccharide chains via a β-elimination mechanism, resulting in the formation of an unsaturated hexenuronic acid residue and a new reducing end (MacDonald and Berger, 2014). This suggested that species of the genus *Demequina* might have a versatile substrate utilization ability.

In addition, the nearly-complete 16S rRNA gene sequences of related species of this genus were submitted to the IMNGS platform and 1513 OTUs with a high sequence similarity cutoff value (99%) were discovered (Lagkouvardos et al., 2016). Our analysis revealed the global distribution of strains of the genus *Demequina* in various sample types worldwide, including soil, rhizosphere, and plant samples, and suggested that related strains of this genus might be more abundant in aquatic environments (Supplementary Figure 2).

3.2 Phylogenetic relationship of strains of the genus *Demequina*

The EZBioCloud comparison results based on almost complete16S rRNA gene sequences indicated that these sequences shared significant similarity with bacteria of the genus *Demequina*. The highest sequence similarity was found between strain EGI L300058^T and *D. aestuarii* NBRC 106260^T (97.74%). Strain SYSU T00b26^T had the highest homology of 99.22% with *D. salsinemoris* NBRC 105323^T, while strain SYSU T00192^T had a homology of 98.45% with *D. maris* NBRC 109392^T. *D. iriomotensis* NBRC 109399^T had the highest homology with strains SYSU T00068^T, SYSU T00039, SYSU T00039-1 and SYSU T00a273 with homology of 97.82%, 98.16%, 97.87%, and 97.96%, respectively. The

phylogenetic trees constructed by the neighbor-joining and maximum likelihood methods using the 16S rRNA gene also confirmed the above relationship and similarity results for the seven novel strains (Supplementary Figures 3, 4). The phylogenomic tree (Figure 2) based on the genomes of seven strains and their related species of the genus *Demequina* also confirmed the above results of the phylogenetic analysis.

3.3 Unveiling *Demequina* genomic and potential functional variations through comparative genomics

Based on average nucleotide identity (ANI), average amino acid identity (AAI), and digital DNA-DNA hybridization (dDDH), we found that strains EGI L300058^T, SYSU T00b26^T, SYSU T00192^T and SYSU T00068^T were genetically distinct from related type species of this genus, indicating that they belonged to different species. Furthermore, values of ANI, AAI, and dDDH showed that strains SYSU T00039, SYSU T00039-1, SYSU T00a273 and SYSU T00068^T were closely related, indicating that they were different strains of the same species (Figures 3A, B and Dataset S2).

The extent of genetic variation among species of the genus *Demequina*, consisting of 19 type species and 7 novel strains genomes, was investigated by analyzing the distribution of conserved (core) and species-specific (unique) genes using a pan-genome analysis. A limited number of core gene clusters, involved in various basic biological processes such as metabolism, information storage and processing, cellular processes and signaling, were identified in these genomes. Nevertheless, numerous strain-specific genes involved in metabolism, information storage and processing, cellular processes, and signal transduction, as well as uncharacterized and insufficiently annotated genes contributing to the unique metabolic functions of each strain in this genus (Figure 3C). Comparative genomic analysis based on the orthologs of the recovered genomes revealed that all strains of the genus *Demequina* possessed 1002 core proteins, whereas each strain contained more than 1000 unique proteins (Supplementary Figure 5A). Besides, core/pan genome analysis also showed that there were significant genomic differences among the species of the genus *Demequina* (Supplementary Figure 5B).

3.4 Revealing the functional diversity and differences of *Demequina* through comparative genomics

Genome annotation of genus *Demequina* revealed that they might play a vital role in the biogeochemical cycles of various crucial elements such as nitrogen, sulfur, and carbon, which was crucial for maintaining the stability of aquatic ecosystem.

Members of the genus *Demequina* were able to convert nitrite, the intermediate compound of dissimilatory nitrate reduction, to ammonia via the *nrfADH* and *nirBD* pathways under different oxygen concentrations (Figure 4). In particular, many species of this genus had been isolated from different marine niches that could express nitrite reductase encoded by *nrfADH* genes to adapt to low-oxygen environments. At the same time, members of this genus played important roles in various steps of sulfur cycling in aquatic ecosystems. In our study, we predicted the presence of some functional genes (*fccB*, *sqr*) responsible for sulfide oxidation from the genomes of this genus (Figure 4). The process of sulfide oxidation, in which the key genes *fccB* and *sqr* were involved, was of critical ecological importance for maintaining the sulfur cycle in aquatic ecosystems. The *fccB* gene, a subunit of the flavocytochrome c complex, facilitated the transfer of electrons from reduced sulfur compounds to oxygen. Similarly, the *sqr* gene, encoding a sulfide: quinone oxidoreductase, catalyzed the oxidation of sulfide to elemental sulfur, transferring electrons to quinones. In summary, the presence of these two genes was critical for detoxification of sulfide in the oxic-anoxic interface of aquatic habitats, thereby preventing potential damage to other organisms and generating elemental sulfur as an energy source for sulfur-oxidizing bacteria. Furthermore, genome annotation results revealed that strains of the

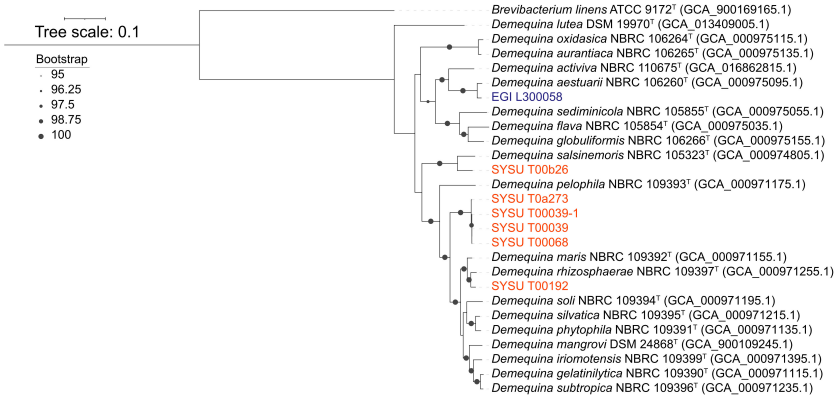

FIGURE 2
Phylogenomic tree of species of the genus *Demequina*. Bootstrap values (>95) based on 1000 resamplings are marked gray points at the nodes. *Brevibacterium linens* ATCC 9172^T (GCA_900169165.1) was used as an outgroup. ModelFinder used the Akaike Information Criterion (AIC), Corrected Akaike Information Criterion (Correct AIC), and Bayesian Information Criterion (BIC) to select the best-fit model (LG+F+R3).

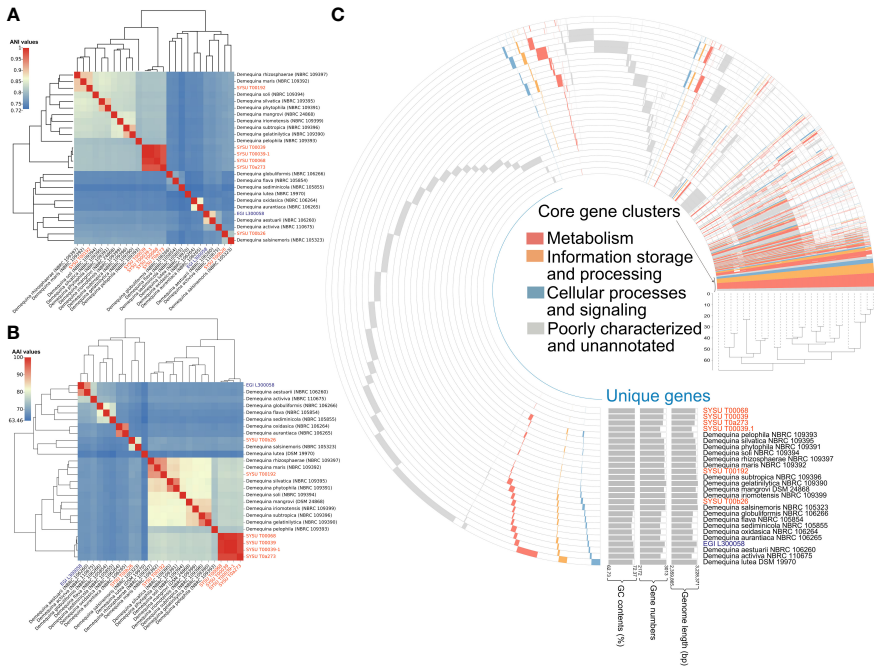

FIGURE 3
Comparative genomic of species of the genus *Demequina*. **(A)**, Average nucleotide identity (ANI) values shared among the related type species; **(B)**, Average amino acid identity (AAI) values shared among the related type species; **(C)**, The pan-genome profile of all *Demequina* strains. "GC," "Gene number," and "Genome length" represent GC content, gene number, genome length, respectively.

genus *Demequina* had the ability to reduce iron. The iron reduction process encompasses various genes and proteins, such as *CytC3* and *CytC4* genes, Fe (III) reductase proteins, electron transfer chain genes, thiol-containing proteins, and electron carrier protein genes, working collaboratively to convert iron oxides into soluble iron. Iron-reducing bacteria (FeRB) not only contributed to the reduction of minerals and humus, but also participated in the oxidation of sulfur compounds and organic matter. FeRB played a crucial role in many engineering applications, such as wastewater treatment, bioremediation, and bioelectrochemical systems (Garber et al., 2020).

Species of the genus *Demequina* from aquatic environments also played critical roles in metabolic and energy cycles and showed the ability to oxidize organic carbon or acetate as a substrate for fermentation. Annotation of these genomes revealed a diverse repertoire of complex carbon degradation enzymes, including

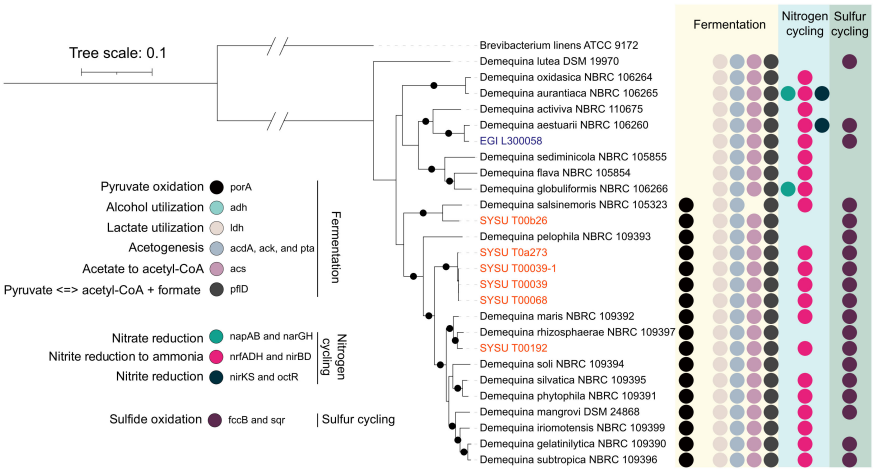

FIGURE 4
Complex carbon degradation potentials of species of the genus *Demequina*. Bootstrap values (>95) based on 1000 resamplings are marked gray points at the nodes. *Brevibacterium linens* ATCC 9172^{T} (GCA_900169165.1) was used as an outgroup. ModelFinder used the Akaike Information Criterion (AIC), Corrected Akaike Information Criterion (Correct AIC), and Bayesian Information Criterion (BIC) to select the best-fit model (LG+F +R3). Different colored stripes show different metabolisms. Various colored circles represent different metabolic genes.

cellobiosidase, cellulase, and β-glucosidase for cellulose degradation, and arabinosidase, β-glucuronidase, α-L-rhamnosidase for hemicellulose debranching, and mannan endo-1,4-β-mannosidase, α-D-xyloside xylohydrolase for endohemicellulase degradation; β-xylosidase, β-mannosidase, and β-galactosidase for degradation of other oligosaccharides; α-amylase, glucoamylase, pullulanase, and isoamylase for amylolytic enzymes; and chitinase and hexosaminidase for chitin degradation (Figures 4, 5, and Dataset S3). In addition, species of this genus harbored the Embden-Meyerhof pathway for glycolysis, as well as the pentose phosphate pathway and genes responsible for phosphoribosyl diphosphate (PRPP) biosynthesis and facilitating the metabolism of purine, pyrimidine, and histidine. For energy metabolism, the genome had a complete oxidative phosphorylation pathway, including an NADH dehydrogenase (*nuoABCDEFGHIJKLMN*) for proton shift, a ubiquinol-cytochrome c reductase (*qerABC*), a cytochrome c oxidase (*ctaCDE*), and an F-type ATPase (*atpABCDEFGH*) (Dataset S3). Finally, basic organic substrate utilization processes such as pyruvate metabolism and the tricarboxylic acid cycle were also found in their genomes, representing the metabolic pathways of the three major nutrients (sugars, lipids, and amino acids) and serving as metabolic hubs for their cross-linking. In summary, the species of the genus *Demequina* were involved in the main carbon cycle processes and played an important role in the carbon cycle of the aquatic ecosystem (Dataset S4).

Comparative analysis of genes related to salt tolerance revealed that species of the genus *Demequina* had the ability to regulate extracellular osmotic balance through outer membrane pore proteins (*OmpR*), maintained optimal potassium ion concentrations (Hasan et al., 2023), and excreted excessive sodium ions via ion transport proteins (*NhaA*) (Tan et al., 2019; Quick et al., 2021). It also synthesized the osmoregulatory substance proline via *ProA*, *ProB*, *glnA* (Wu et al., 2018), and relied on chaperones and proteases (*DnaK*, *GroEL*, *ClpP*) (Susin et al., 2006; Nouri et al., 2020) to ensure proper protein folding and repair in response to osmotic stress (Supplementary Figure 6). These functional systems allowed species in this genus to adapt to different osmotic niches, maintained cellular homeostasis, and ensured optimal physiological function and survival.

Furthermore, secondary metabolites of species in this genus were categorized into eight types of biosynthetic gene clusters (BGCs), including terpenes, RRE-containing, betalactones, NAP-AA, T3PKS, NRPS-like, resorcinol, and lanthipeptide-class-v. Differences in the type and abundance of BGCs were observed among these species, but some BGCs were present in most strains (Supplementary Figure 7). This diversity of BGCs suggests that *Demequina* strains might have the potential to be resistant to pathogens, which could have various functions in defending against pathogens in different niches.

3.5 Exploring physiological characteristics of novel strains

Seven novel strains were characterized as Gram-stain positive, non-motile, and aerobic. The colony morphology of these strains was characterized by a large, circular shape with a smooth and moist texture, well-defined edges, and yellow. The electron micrograph of seven strains showed the short-rod structure with a length of roughly 0.71-1.37 μm and a width of approximately 0.34-0.45 μm (Supplementary Figure 8). The seven strains exhibited a wide range of growth temperatures, from 4-37 °C, and could tolerate different pH values between 6-9 and salt concentrations of 0-8% (w/v). According to results of Biolog Gen III, strain SYSU T0a273 could utilize D-fructose, D-fructose-6-PO_4, D-glucuronic acid, glucuronamide, nalidixic acid, lithium chloride, and potassium tellurite. Strain SYSU T00039-1 was able to utilize 33 different substrates, while strain SYSU T00039 was capable of utilizing 29 substrates, and SYSU T00068^T was capable of utilizing 31

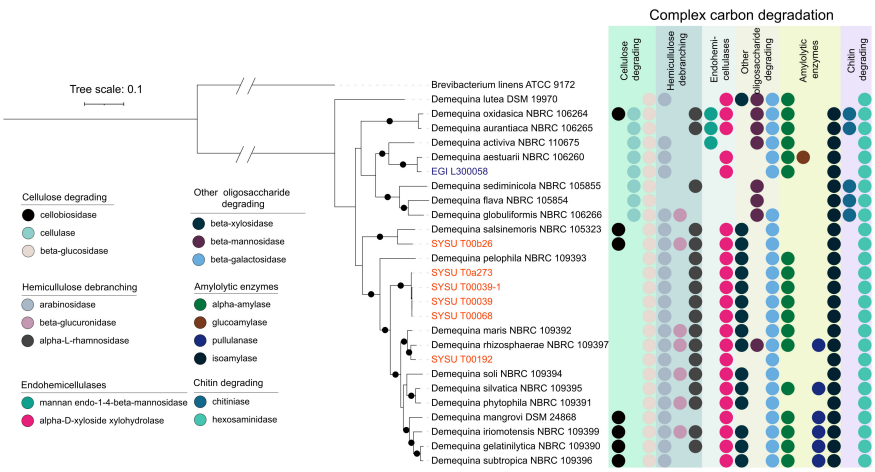

FIGURE 5
Fermentation, nitrogen, sulfur metabolism of species of the genus *Demequina*. Bootstrap values (>95) based on 1000 resamplings are marked gray points at the nodes. *Brevibacterium linens* ATCC 9172^T (GCA_900169165.1) was used as an outgroup. ModelFinder used the Akaike Information Criterion (AIC), Corrected Akaike Information Criterion (Correct AIC), and Bayesian Information Criterion (BIC) to select the best-fit model (LG+F +R3). Different colored stripes show different metabolisms. Various colored circles represent different metabolic genes.

substrates. SYSU T00039-1, SYSU T00039, and SYSU T00068^T shared the ability to utilize 16 substrates, including dextrin, D-maltose, D-trehalose, D-cellobiose, gentiobiose, sucrose, D-turanose, stachyose, α-D-lactose, D-melibiose, β-methyl-D-glucoside, D-fructose, D-galactose, inosine, lithium chloride, and sodium butyrate. Significant differences in substrate utilization were observed between the above four strains of the same species. Strains SYSU T00192^T, SYSU T00b26^T, and EGI L300058^T showed the ability to utilize different substrates by using 27, 28, and 50 substrates, respectively. These results demonstrated the metabolic versatility of these strains and indicated their potential applications in biotechnology and environmental fields. The API 20NE experiments showed that SYSU T0a273, SYSU T00039-1, SYSU T00039, and SYSU T00068^T produced only a single enzyme, β-galactosidase. Although SYSU T0a273, SYSU T00039, and SYSU T00068^T produced β-glucosidase, SYSU T00039-1 was found to have other abilities, including hydrolysis of gelatin, production of urease and indole, and the ability to assimilate glucose, arabinose, mannose, and N-acetyl-β-glucosamine. SYSU T00192^T produced both β-glucosidase and β-galactosidase and was able to assimilate glucose, arabinose, and maltose. SYSU T00b26^T was found to produce β-galactosidase and assimilate glucose, arabinose, and maltose. EGI L300058^T produced both β-glucosidase and β-galactosidase. According to the results of experiments conducted by API ZYM, these strains shared the following enzyme activities: (C4) esterase, (C8) esterase lipase, leucine arylamidase, valine arylamidase, naphthol-AS-BI-phosphohydrolase, β-galactosidase, and α-glucosidase. Substantial variations in enzyme activities were observed within the *Demequina* strains. However, the results of the H_2S production, starch degradation, Tween (60 and 80) degradation, and gelatin liquefaction assays showed that these novel strains could not perform these activities.

Upon analysis with Microbial Ligninase Detection Kit analysis, all seven strains showed the ability to produce ligninase, with EGI L300058^T producing the highest amount of up to 800 ng/mL, while SYSU T00b26^T had the lowest production at 500 ng/mL (Figure 6A). When analyzed with the Microbial Cellulase Detection Kit, all seven strains showed the ability to produce cellulase, with EGI L300058^T and SYSU T00068^T producing the highest amount of up to 1200 pg/mL, while SYSU T00b26^T and SYSU T00039-1 exhibited the lowest production at 600 pg/mL (Figure 6B). According to Microbial Chitinase Detection Kit analysis, all seven strains showed the ability to produce chitinase, with SYSU T00068^T producing the highest amount of up to 60 pg/mL, while SYSU T00b26^T exhibited the lowest production 3 to 30 pg/mL (Figure 6C). Analysis of the microbial indoleacetic acid (IAA) with ELISA kit showed that all novel strains were able to produce IAA (SYSU T00068^T with the highest IAA production of 28.5 µg/L on average) (Figure 6D), suggesting that these strains had the potential to promote plant growth. ACC is one of the precursors involved in the synthesis of ethylene in plants. The enzyme ACC deaminase degrades ACC into ammonia and α-keto butyric acid, thereby lowering the ethylene levels in plants and promoting plant growth (Glick et al., 2007). In addition, the *Demequina* strains exhibited high-yielding ACC deaminase properties (SYSU T00039 with the highest ACCD production on average: 17.9 ng/L), as shown by the result of the physiological experiment (Figure 6E).

The major fatty acids (>5%) of *Demequina* strains were anteiso-$C_{15:0}$, iso-$C_{19:0}$, anteiso-$C_{17:1}$ $\omega 9c$, iso-$C_{16:0}$, iso-$C_{14:0}$, and iso-$C_{15:0}$ (Supplementary Table 1). MK-9 (H_4) was found to be the respiratory quinone of these strains. The polar lipids of these novel strains were found to consist of diphosphatidylglycerol (DPG), phosphoglyceride (PG), phosphatidylinositol (PI), phosphatidylinositol mannosides (PIMs), and unidentified lipid (L) (Supplementary Figure 9). Detailed phenotypic and physiological characteristics of novel strains from the genus of *Demequina* were listed in Dataset S5.

4 Discussion

4.1 Deciphering evolutionary lineage and taxonomic discrimination through phylogenomic analysis and comparative genomics

As previous studies description, numerous species of the genus *Demequina* were isolated from marine related niches such as marine, tidal flat, arctic permafrost soil, rhizosphere of a mangrove, etc. In our study, six strains of the genus *Demequina* (SYSU T00068^T, SYSU T0a273, SYSU T00039, SYSU T00039-1, SYSU T00192^T and SYSU T00b26^T) were isolated from tidal flats and one strain (EGI L300058^T) was isolated from saline lake. Strains EGI L300058^T and SYSU T00192^T displayed the low 16S rRNA gene homologies with their most related type species, which were satisfied the species delineation (98.65%) (Kim et al., 2014). The phylogenetic analysis of the 16S rRNA genes and genomes, along with comparative genomics (specifically ANI and AAI values below species delimitation thresholds), confirmed that EGI L300058^T and SYSU T00192^T represented two novel species of this genus. Although the 16S rRNA gene sequence of strain SYSU T00b26^T showed a high homology of 99.22% with *D. salsinemoris* NBRC 105323^T, phylogenetic analysis of the 16S rRNA gene and genome, as well as comparative genomics (especially ANI and AAI values below the species delimitation thresholds) confirmed that SYSU T00b26^T represented a novel species of this genus (Richter and Rosselló-Móra, 2009). The 16S rRNA gene homologies between *D. iriomotensis* NBRC 109399^T and strains SYSU T00068^T, SYSU T00039, SYSU T00039-1 and SYSU T00a273 were lower than the species delineation threshold. Furthermore, based on the phylogenetic analysis of the 16S rRNA genes and genomes, as well as comparative genomics using ANI, AAI, dDDH values below the species delimitation thresholds (Richter and Rosselló-Móra, 2009), it was confirmed that SYSU T00068^T, SYSU T00039, SYSU T00039-1and SYSU T00a273 were seen as one novel species of this genus. Additionally, the comparative genomic results demonstrated that these four strains belong to different strains within the same species. In summary, we acquired seven strains from different salinity niches that could be classified into 4 novel species, and expended our understanding of microbial biodiversity in the genus *Demequina*.

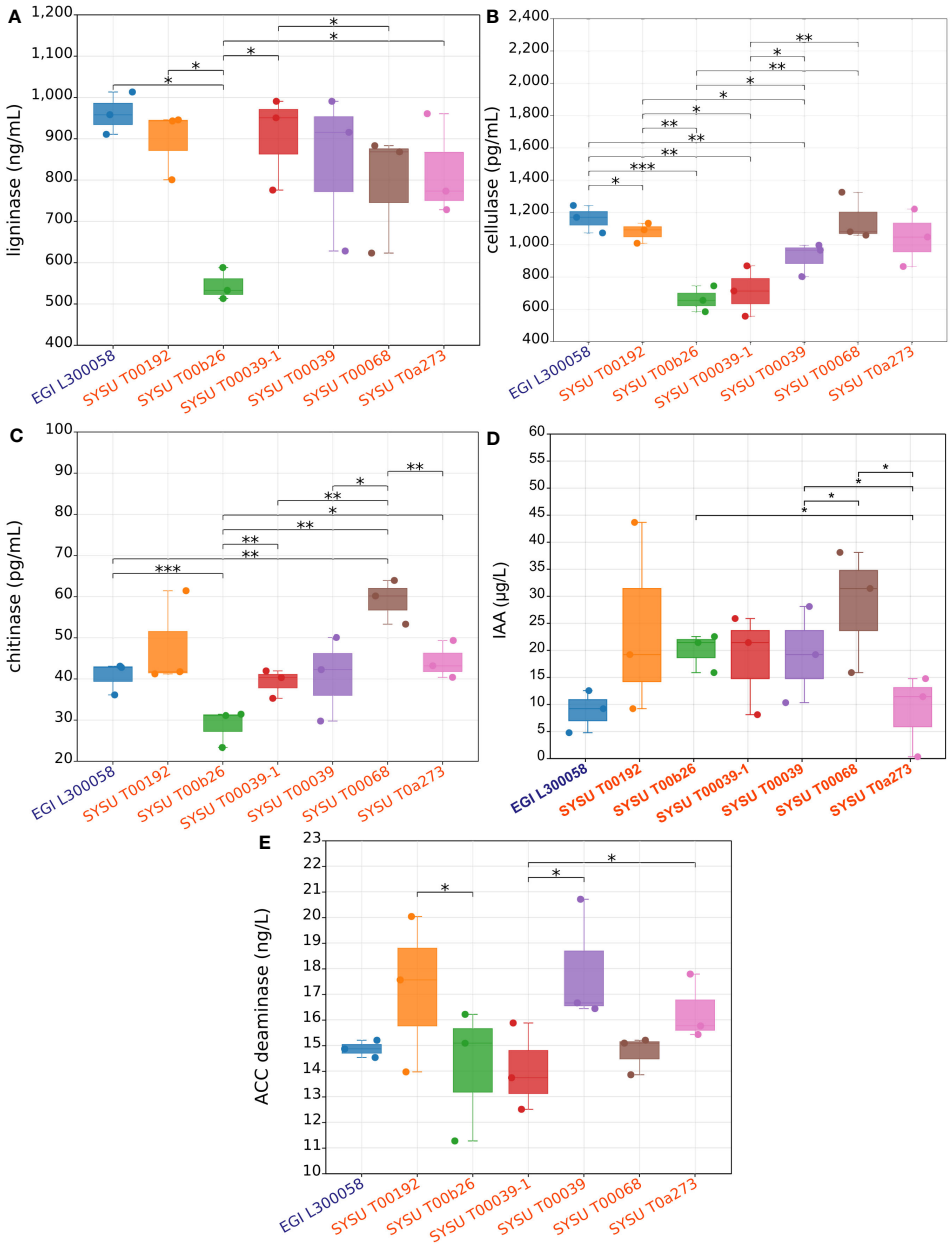

FIGURE 6
Ligninase, cellulase, chitinase, IAA, and ACCD production species of the genus *Demequina*. **(A)**, comparison of ligninase production capacity among tested *Demequina* strains; **(B)**, comparison of cellulase production capacity among tested *Demequina* strains; **(C)**, comparison of chitinase production capacity among tested *Demequina* strains; **(D)**, comparison of indole-3-acetic acid (IAA) production capacity among tested *Demequina* strains; **(E)**, comparison of ACC (1-aminocyclopropane-1-carboxylate) deaminase production capacity among tested *Demequina* strains. The method employed for the differential comparison was the t-test. * refers to $p < 0.05$; ** refers to $p < 0.01$; *** refers to $p < 0.001$.

4.2 Exploring the biogeochemical significance and physiological characteristics of *Demequina* in living ecosystem

The genus *Demequina* from the order *Micrococcales* played a vital role in the nitrogen cycle of aquatic ecosystems, particularly in the reduction of nitrite to ammonia via the *nrfADH* and *nirBD* pathways (as shown in Figure 4). The *nrfADH* pathway utilized the *nrfA* and *nrfH* genes, which encoded key enzymes for the reduction of nitrite to ammonia, particularly in oxygen deficient aquatic niches (Rütting et al., 2011). The *nirBD* pathway, on the other hand, used the *nirB* and *nirD* genes to reduce nitrite to ammonia, which was critical in high-oxygen environments (Akhtar et al., 2013). This implied that strains of this genus could express different functional genes for the conversion of nitrite to ammonia to expand habitat with different oxygen concentrations. Our study also shed light on the possible involvement of strains of this genus in the sulfur cycle in aquatic ecosystems. The sulfur cycle was an important biogeochemical process that involved the conversion of

sulfur compounds between different oxidation states. Sulfide, a reduced form of the sulfur element, was toxic to most organisms and could cause severe ecological damage if not properly detoxified (Lamers et al., 2013). Our research revealed that most strains of the genus *Demequina* possessed key genes, namely *fccB* and *sqr*, which were involved in sulfide oxidation. *fccB*, a subunit of the flavocytochrome c complex, could transfer electrons from reduced sulfur compounds to oxygen (Friedrich et al., 2001), while *sqr*, a sulfide: quinone oxidoreductase, catalyzed the oxidation of sulfide to elemental sulfur and transferred electrons to quinones (Cherney et al., 2012). Taken together, these genes were essential for detoxification of sulfide in the aquatic environment and prevented other organisms from being harmed. Moreover, sulfide oxidation contributes to the production of elemental sulfur, which serves as an energy source for sulfur-oxidizing bacteria, supporting the diversity of microbial communities in aquatic ecosystems. The presence of these key genes in *Demequina* strains suggested that they were actively involved in sulfur cycling of aquatic ecosystems, which was a significant finding because the role of *Demequina* strains in sulfur cycling had not been previously reported. Overall, our study highlights the ecological importance of *Demequina* strains in maintaining the balance of nitrogen and sulfur cycling in aquatic ecosystems, thereby maintaining the diversity of microbial communities in these environments. *Demequina* strains had also been shown to have the ability to reduce Fe^{3+} to Fe^{2+}. This process, known as iron reduction, was an important biogeochemical process that occurs in both soil and aquatic environments. The reduction of Fe^{3+} to Fe^{2+} can be carried out by a variety of microorganisms, including *Demequina* strains, and can play a significant role in the cycling of iron in ecosystems. This process was important because Fe^{2+} was more soluble than Fe^{3+} and more easily taken up by plants and other organisms (Morrissey and Guerinot, 2009). In addition, Fe^{2+} could react with other compounds in the environment and lead to the formation of minerals such as magnetite and siderite, which could affect the composition and stability of soil and sediments environments (Huang et al., 2021; Shen et al., 2021). Therefore, the ability of *Demequina* strains to reduce Fe^{3+} to Fe^{2+} was of ecological importance to the biogeochemical cycling of iron and the maintenance of ecosystem functions.

Our study also revealed that strains of the genus *Demequina* had the potential for antagonistic activity against pathogens, as evidenced by genome annotations. In particular, the strains were found to contain a number of biosynthetic gene clusters (BGCs) involved in antifungal activities, including terpenes, RRE-containing, betalactones, NAP-AA, T3PKS, NRPS-like, resorcinol or lanthipeptide-class-V. Previous researches had revealed that these types of secondary metabolites might exhibit various biological activities such as antibacterial, antioxidant, and anti-inflammatory properties (Modjinou et al., 2017; Shimizu et al., 2017; Lima et al., 2020; Xu et al., 2020; Shi et al., 2021). Overall, these results suggested that strains of this genus had a role in biocontrol and bioremediation in various environments and might be suitable for the pharmaceutical industry.

Our results showed that genomes of the genus *Demequina* had diverse complex carbon degradation enzymes, including cellulose and hemicellulose degradation, oligosaccharide degradation, amylolytic enzymes, and chitin degradation. The presence of these enzymes suggested that strains of this genus, as heterotrophic microorganisms, were capable of degrading a variety of complex organic compounds, which was essential for maintaining the balance of carbon and nutrient cycling to sustain life and stabilize microbial communities in different aquatic niches. Hence wood or herbs as a carbon source for aquatic niches consisted of lignocellulose, lignin, chitin, or other compounds that made them resistant to the degradation of these complex carbohydrates (Janusz et al., 2017; Zoghlami and Paës, 2019; Börcsök and Pásztory, 2021). Wood-degrading enzymes, especially lignin-degrading enzymes, played a critical role in the utilization of wood or herbs as a renewable energy and carbon source (Ayuso-Fernández et al., 2018). Our research results had shown that strains of the genus *Demequina* possessed a significant amount of ligninase, cellulase, chitinase, IAA, and ACCD related genes and were capable of utilizing a wide range of substrates based on genomic and physiological evidences. These results might shed a light on the reason for the distribution of most species of this genus from mangrove or tidal flat niches, where lignin or cellulose had normally been enriched. Further studies of the ligninase produced by strains of the genus *Demequina* could lead to a better understanding of its function and potential applications in the biorefinery and bioenergy industries.

These research findings have greatly improved our understanding of the diversity and potential functions of *Demequina*, which are abundant in aquatic environments, and facilitate study of microorganisms in more complex ecosystems.

5 Conclusion

Our research results showed that seven novel strains of the genus *Demequina* were isolated from different salinity aquatic niches (tidal flats and saline lake). Phylogenetic relationships, based on 16S rRNA gene sequences and genomes, comparative genomics (ANI, AAI, and dDDH values), and physiological characteristics, showed that the seven isolated strains could be classified into 4 novel species. In particular, SYSU T00039, SYSU T00039-1, SYSU T00a273, and SYSU T00068^T were different strains of the same novel species. However, EGI L300058^T, SYSU T00192^T, and SYSU T00b26^T belonged to three different species in the genus *Demequina*. Genomic analysis and physiological characteristics of these strains had led to the development of a metabolic model that showed their ability to degrade various polysaccharides such as lignin, hemicellulose, and chitin, as well as oligosaccharides, and to participate in nitrite ammonification and sulfide oxidation. These results shed light on the potential ecological role of strains from the genus *Demequina*. Therefore, we propose four novel strains of the genus *Demequina*, namely *Demequina muriae* sp. nov. with strain EGI L300058^T (=GDMCC 1.3270^T=KCTC 59052^T) as the type species, *Demequina litoralis* sp. nov. with strain SYSU T00192^T (=GDMCC 1.3840^T=KCTC 49956^T) as the type species, *Demequina zhanjiangensis* sp. nov. with strain SYSU T00b26^T (=GDMCC 1.3841^T =KCTC 49950^T) as the type species, and *Demequina*

lignilytica sp. nov. with strain SYSU T00068^T (=GDMCC 1.3838^T= KCTC 49954^T) as the type species, while SYSU T0a273, SYSU T00039-1, and SYSU T00039 were different strains of *Demequina lignilytica*.

Description of *Demequina muriae* sp. nov.

Demequina muriae (mu'ri.ae. L. gen. n. *muriae*, of a brine).

Each cell is about 0.80 μm in length and 0.39 μm in width, giving them a short rod-like shape. Cells are not motile and have no flagella. Cells are Gram-stain positive and aerobic. Cells grow at pH values of 8 to 9, temperatures between 25 and 37°C, as well as NaCl concentration at 0-5%. The organism exhibits negative activity for urease, milk peptonization and coagulation, gelatin liquefaction and coagulation, and degradation of Tweens (40, 60, and 80) and starch, while positive activity is observed for indole-3-acetic acid production, 1-aminocyclopropane-1-carboxylic acid (ACC) deaminase production, catalase, esterase, β-glucosidase, ligninase, cellulase, chitinase, and other enzymes. The major fatty acids (>5%) were anteiso-$C_{15:0}$, iso-$C_{19:0}$, anteiso-$C_{17:1}$ $\omega9c$, iso-$C_{16:0}$, iso-$C_{14:0}$, and iso-$C_{15:0}$. The predominant menaquinone is MK-9 (H_4). The polar lipid profile consists of diphosphatidylglycerol, phosphoglyceride, phosphatidylinositol, phosphatidylinositol mannosides, and unidentified lipid. The G+C content of the genomic DNA is 69.41%.

The type strain, EGI L300058^T (=GDMCC 1.3270^T=KCTC 59052^T), was isolated from the Dabancheng saline lake in Xinjiang, PR China. The G+C content is 69.41%. The GenBank accession numbers for the 16S rRNA gene and genome sequences of strain EGI L300058^T are OR098447 and NMDC60064244 respectively.

Description of *Demequina litoralis* sp. nov.

Demequina litoralis (lit.to.ra.lis. L. fem. adj. *litoralis*, coastal).

Each cell is about 0.92 μm in length and 0.42 μm in width, giving them a short rod-like shape. Cells are not motile and have no flagella. Cells are Gram-stain positive and aerobic. Cells grow at pH values of 6 to 7, temperatures between 25 and 37°C, as well as NaCl concentration at 0-4%. The organism exhibits negative activity for urease, milk peptonization and coagulation, gelatin liquefaction and coagulation, and degradation of Tweens (40, 60, and 80) and starch, while positive activity is observed for indole-3-acetic acid production, 1-aminocyclopropane-1-carboxylic acid (ACC) deaminase production, esterase, lipase, β-glucosidase, ligninase, cellulase, chitinase, and other enzymes. The major fatty acids (>5%) were anteiso-$C_{15:0}$, iso-$C_{19:0}$, anteiso-$C_{17:1}$ $\omega9c$, iso-$C_{16:0}$, iso-$C_{14:0}$, and iso-$C_{15:0}$. The predominant menaquinone is MK-9 (H_4). The polar lipid profile consists of diphosphatidylglycerol, phosphoglyceride, phosphatidylinositol, phosphatidylinositol mannosides, and unidentified lipid. The G+C content of the genomic DNA is 72.26%.

The type strain, SYSU T00192^T (=GDMCC 1.3840^T=KCTC 49956^T), was isolated from tidal flats sediments of Zhanjiang city in Guangdong, PR China. The G+C content is 72.26%. The GenBank accession numbers for the 16S rRNA gene and genome sequences of strain SYSU T00192^T are OR098449 and NMDC60064242 respectively.

Description of *Demequina zhanjiangensis* sp. nov.

Demequina zhanjiangensis (zhan.jiang.en'sis. N.L. fem. adj. *zhanjiangensis*, from Zhanjiang, China).

Each cell is about 0.73 μm in length and 0.34 μm in width, giving them a short rod-like shape. Cells are not motile and have no flagella. Cells are Gram-stain positive and aerobic. Cells grow at pH values of 6 to 8, temperatures between 25 and 37°C, as well as NaCl concentration at 0-8%. The organism exhibits negative activity for urease, milk peptonization and coagulation, gelatin liquefaction and coagulation, and degradation of Tweens (40, 60, and 80) and starch, while positive activity is observed for indole-3-acetic acid production, 1-aminocyclopropane-1-carboxylic acid (ACC) deaminase production, esterase, lipase, β-glucosidase, β-mannosidase, ligninase, cellulase, chitinase, and other enzymes. The major fatty acids (>5%) were anteiso-$C_{15:0}$, iso-$C_{19:0}$, anteiso-$C_{17:1}$ $\omega9c$, iso-$C_{16:0}$, iso-$C_{14:0}$, and iso-$C_{15:0}$. The predominant menaquinone is MK-9 (H_4). The polar lipid profile consists of diphosphatidylglycerol, phosphoglyceride, phosphatidylinositol, phosphatidylinositol mannosides, and unidentified lipid. The G+C content of the genomic DNA is 69.58%.

The type strain, SYSU T00b26^T (=GDMCC 1.3841^T =KCTC 49950^T), was isolated from tidal flats sediments of Zhanjiang city in Guangdong, PR China. The G+C content is 69.58%. The GenBank accession numbers for the 16S rRNA gene and genome sequences of strain SYSU T00b26^T are OR098448 and NMDC60064243 respectively.

Description of *Demequina lignilytica* sp. nov.

Demequina lignilytica (lig.ni.ly'ti.ca. L. neut. n. lignum, wood; Gr. masc. adj. lytikos, loosening, dissolving; N.L. fem. adj. *lignilytica*, splitting lignin).

Each cell is about 1.37 μm in length and 0.49 μm in width, giving them a short rod-like shape. Cells are not motile and have no flagella. Cells are Gram-stain positive and aerobic. Cells grow at pH values of 6 to 7, temperatures between 25 and 37°C, as well as NaCl concentration at 0-8%. The organism exhibits negative activity for urease, milk peptonization and coagulation, gelatin liquefaction and coagulation, and degradation of Tweens (40, 60, and 80) and starch, while positive activity is observed for indole-3-acetic acid production, 1-aminocyclopropane-1-carboxylic acid (ACC) deaminase production, esterase, lipase, β-glucosidase, ligninase, cellulase, chitinase, and other enzymes. The major fatty acids (>5%) were anteiso-$C_{15:0}$, iso-$C_{19:0}$, anteiso-$C_{17:1}$ $\omega9c$, iso-$C_{16:0}$, iso-$C_{14:0}$, and iso-$C_{15:0}$. The predominant menaquinone is MK-9 (H_4). The polar lipid profile consists of diphosphatidylglycerol, phosphoglyceride, phosphatidylinositol, phosphatidylinositol mannosides, and unidentified lipid. The G+C content of the genomic DNA is 71.88%.

The type strain, SYSU T00068^T (=GDMCC 1.3838^T= KCTC 49954^T), was isolated from tidal flats sediments of Zhanjiang city in Guangdong, PR China. The G+C content is 71.88%. The GenBank accession numbers for the 16S rRNA gene and genome sequences of strain SYSU T00068^T are OR098453 and NMDC60064239 respectively.

Data availability statement

The datasets presented in this study can be found in online repositories. The names of the repository or repositories

and accession number(s) can be found in the article or Supplementary Material.

Author contributions

W-JL and B-ZF designed research and project outline. B-ZF and C-YL obtained samples. LG, K-HH, and X-YH performed isolation, deposition, and other experiments. LG and T-TS performed genome analysis. LG, B-ZF, MX, and W-JL drafted the manuscript. All authors contributed to the article and approved the submitted version.

Funding

The author(s) declare that no financial support was received for the research, authorship, and/or publication of this article.

Acknowledgments

This research was supported by National Science and Technology Fundamental Resources Investigation Program of China (Nos 2019FY100701 and 2021FY100900), The Third Xinjiang Scientific Expedition Program (No.2022xjkk1204), Natural Science Foundation of Xinjiang Uygur Autonomous Region (2022D01A154), Xinjiang Uygur Autonomous Region regional coordinated innovation project (Shanghai cooperation organization science and technology partnership program) (No. 2021E01018). We thank Prof. Aharon Oren for his recommendations on the nomenclature of these novel strains in this study.

Conflict of interest

The authors declare that the research was conducted in the absence of any commercial or financial relationships that could be construed as a potential conflict of interest.

Publisher's note

Supplementary material

The Supplementary Material for this article can be found online at: https://www.frontiersin.org/articles/10.3389/fmars.2023.1244849/full#supplementary-material

References

Akhtar, S., Khan, A., Sohaskey, C. D., Jagannath, C., and Sarkar, D. (2013). Nitrite reductase NirBD is induced and plays an important role during in *vitro* dormancy of Mycobacterium tuberculosis. *J. Bacteriol* 195, 4592–4599. doi: 10.1128/JB.00698-13

Al-Naamani, L., Dobretsov, S., Al-Sabahi, J. N., and Soussi, B. (2015). Identification and characterization of two amylase producing bacteria Cellulosimicrobium sp. and Demequina sp. isolated from marine organisms. *J. Agric. Mar. Sci.* 20, 8–15. doi: 10.24200/jams.vol20iss0pp8-15

Altschul, S. F., Gish, W., Miller, W., Myers, E. W., and Lipman, D. J. (1990). Basic local alignment search tool. *J. Mol. Biol.* 215, 403–410. doi: 10.1016/S0022-2836(05)80360-2

Attia, M. A., and Brumer, H. (2021). New family of carbohydrate-binding modules defined by a galactosyl-binding protein module from a cellvibrio japonicus endo-xyloglucanase. *Appl. Environ. Microbiol.* 87, e0263420. doi: 10.1128/AEM.02634-20

Ayuso-Fernández, I., Ruiz-Dueñas, F. J., and Martínez, A. T. (2018). Evolutionary convergence in lignin-degrading enzymes. *Proc. Natl. Acad. Sci. U.S.A.* 115, 6428–6433. doi: 10.1073/pnas.1802555115

Bankevich, A., Nurk, S., Antipov, D., Gurevich, A. A., Dvorkin, M., Kulikov, A. S., et al. (2012). SPAdes: a new genome assembly algorithm and its applications to single-cell sequencing. *J. Comput. Biol.* 19, 455–477. doi: 10.1089/cmb.2012.0021

Blin, K., Shaw, S., Kloosterman, A. M., Charlop-Powers, Z., Van Wezel, G. P., Medema, M. H., et al. (2021). antiSMASH 6.0: improving cluster detection and comparison capabilities. *Nucleic Acids Res.* 49, W29–w35. doi: 10.1093/nar/gkab335

Börcsök, Z., and Pásztory, Z. (2021). The role of lignin in wood working processes using elevated temperatures: an abbreviated literature survey. *Eur. J. Wood Wood Products* 79, 511–526. doi: 10.1007/s00107-020-01637-3

Casanellas, M., Fernández-Sánchez, J., and Roca-Lacostena, J. (2020). Embeddability and rate identifiability of Kimura 2-parameter matrices. *J. Math Biol.* 80, 995–1019. doi: 10.1007/s00285-019-01446-0

Chan, P. P., and Lowe, T. M. (2019). tRNAscan-SE: searching for tRNA genes in genomic sequences. *Methods Mol. Biol.* 1962, 1–14. doi: 10.1007/978-1-4939-9173-0_1

Chao, S., Xiang, Z., Guangyu, L., Yaping, D., Zhaoshou, W., and Zongze, S. (2021). Diversity of anaerobic degrading bacteria for natural organic polymers in mangrove sediments and isolation of novel groups of bacteria. *Acta Microbiologica Sin.* 61, 987–1001. doi: 10.13343/j.cnki.wsxb.20200715

Chaumeil, P. A., Mussig, A. J., Hugenholtz, P., and Parks, D. H. (2019). GTDB-Tk: a toolkit to classify genomes with the Genome Taxonomy Database. *Bioinformatics* 36, 1925–1927. doi: 10.1093/bioinformatics/btz848

Cherney, M. M., Zhang, Y., James, M. N., and Weiner, J. H. (2012). Structure-activity characterization of sulfide:quinone oxidoreductase variants. *J. Struct. Biol.* 178, 319–328. doi: 10.1016/j.jsb.2012.04.007

Collins, M. D., Pirouz, T., Goodfellow, M., and Minnikin, D. E. (1977). Distribution of menaquinones in actinomycetes and corynebacteria. *J. Gen. Microbiol.* 100, 221–230. doi: 10.1099/00221287-100-2-221

Cumsille, A., Durán, R. E., Rodríguez-Delherbe, A., Saona-Urmeneta, V., Cámara, B., Seeger, M., et al. (2023). GenoVi, an open-source automated circular genome visualizer for bacteria and archaea. *PloS Comput. Biol.* 19, e1010998. doi: 10.1371/journal.pcbi.1010998

Drula, E., Garron, M.-L., Dogan, S., Lombard, V., Henrissat, B., and Terrapon, N. (2021). The carbohydrate-active enzyme database: functions and literature. *Nucleic Acids Res.* 50, D571–D577. doi: 10.1093/nar/gkab1045

Duan, Y., Wang, Y., Liu, Q., Xiong, D., and Zhang, J. (2019). Transcriptomic and microbiota response on Litopenaeus vannamei intestine subjected to acute sulfide exposure. *Fish Shellfish Immunol.* 88, 335–343. doi: 10.1016/j.fsi.2019.02.021

Emms, D. M., and Kelly, S. (2019). OrthoFinder: phylogenetic orthology inference for comparative genomics. *Genome Biol.* 20, 238. doi: 10.1186/s13059-019-1832-y

Fang, B. Z., Han, M. X., Jiao, J. Y., Xie, Y. G., Zhang, X. T., Liu, L., et al. (2020). *Streptomyces cavernae* sp. nov., a novel actinobacterium isolated from a karst cave sediment sample. *Int. J. Syst Evol. Microbiol.* 70, 120–125. doi: 10.1099/ijsem.0.003724

Felsenstein, J. (1981). Evolutionary trees from DNA sequences: a maximum likelihood approach. *J. Mol. Evol.* 17, 368–376. doi: 10.1007/BF01734359

Finster, K. W., Herbert, R. A., Kjeldsen, K. U., Schumann, P., and Lomstein, B. A. (2009). Demequina lutea sp. nov., isolated from a high Arctic permafrost soil. *Int. J. Syst. Evol. Microbiol.* 59, 649–653. doi: 10.1099/ijs.0.004929-0

Friedrich, C. G., Rother, D., Bardischewsky, F., Quentmeier, A., and Fischer, J. (2001). Oxidation of reduced inorganic sulfur compounds by bacteria: emergence of a common mechanism? *Appl. Environ. Microbiol.* 67, 2873–2882. doi: 10.1128/AEM.67.7.2873-2882.2001

Galperin, M. Y., Kristensen, D. M., Makarova, K. S., Wolf, Y. I., and Koonin, E. V. (2019). Microbial genome analysis: the COG approach. *Brief Bioinform.* 20, 1063–1070. doi: 10.1093/bib/bbx117

Gao, L., Fang, B. Z., Liu, Y. H., Jiao, J. Y., Li, M. M., Antunes, A., et al. (2022). Rhabdothermincola salaria sp. nov., a novel actinobacterium isolated from a saline lake sediment. *Int. J. Syst. Evol. Microbiol.* 72, 005361. doi: 10.1099/ijsem.0.005361

Garber, A. I., Nealson, K. H., Okamoto, A., Mcallister, S. M., Chan, C. S., Barco, R. A., et al. (2020). FeGenie: A comprehensive tool for the identification of iron genes and iron gene neighborhoods in genome and metagenome assemblies. *Front. Microbiol.* 11. doi: 10.3389/fmicb.2020.00037

Glick, B. R., Cheng, Z., Czarny, J., and Duan, J. (2007). Promotion of plant growth by ACC deaminase-producing soil bacteria. *Eur. J. Plant pathology.* 119, 329–339. doi: 10.1007/s10658-007-9162-4

Groth, I., Schumann, P., Rainey, F. A., Martin, K., Schuetze, B., and Augsten, K. (1997). Demetria terragena gen. nov., sp. nov., a New Genus of Actinomycetes Isolated from Compost Soil. *Int. J. Systematic Evolutionary Microbiol.* 47, 1129–1133. doi: 10.1099/00207713-47-4-1129

Hamada, M., Ichikawa, N., Oguchi, A., Komaki, H., Tamura, T., and Fujita, N. (2015a). Draft genome sequences of eight type strains of the genus demequina. *Genome Announcements* 3, e00281–15. doi: 10.1128/genomeA.00281-15

Hamada, M., Shibata, C., Saitou, S., Tamura, T., Komaki, H., Ichikawa, N., et al. (2015b). Proposal of nine novel species of the genus Lysinimicrobium and emended description of the genus Lysinimicrobium. *Int. J. Syst. Evol. Microbiol.* 65, 4394–4402. doi: 10.1099/ijsem.0.000587

Hamada, M., Tamura, T., Yamamura, H., Suzuki, K. I., and Hayakawa, M. (2013). Demequina flava sp. nov. and Demequina sediminicola sp. nov., isolated from sea sediment. *Int. J. Syst. Evol. Microbiol.* 63, 249–253. doi: 10.1099/ijs.0.039297-0

Hasan, M. K., Scott, N. E., Hays, M. P., Hardwidge, P. R., and El Qaidi, S. (2023). Salmonella T3SS effector SseK1 arginine-glycosylates the two-component response regulator OmpR to alter bile salt resistance. *Sci. Rep.* 13, 9018. doi: 10.1038/s41598-023-36057-9

Hasegawa, T., Takizawa, M., and Tanida, S. (1983). A rapid analysis for chemical grouping of aerobic actinomycetes. *J. Gen. Appl. Microbiol.* 29, 319–322. doi: 10.2323/jgam.29.319

Huang, J., Jones, A., Waite, T. D., Chen, Y., Huang, X., Rosso, K. M., et al. (2021). Fe (II) redox chemistry in the environment. *Chem. Rev.* 121, 8161–8233. doi: 10.1021/acs.chemrev.0c01286

Hyatt, D., Chen, G. L., Locascio, P. F., Land, M. L., Larimer, F. W., and Hauser, L. J. (2010). Prodigal: prokaryotic gene recognition and translation initiation site identification. *BMC Bioinf.* 11, 119. doi: 10.1186/1471-2105-11-119

Janusz, G., Pawlik, A., Sulej, J., Swiderska-Burek, U., Jarosz-Wilkolazka, A., and Paszczynski, A. (2017). Lignin degradation: microorganisms, enzymes involved, genomes analysis and evolution. *FEMS Microbiol. Rev.* 41, 941–962. doi: 10.1093/femsre/fux049

Jiao, J. Y., Fu, L., Hua, Z. S., Liu, L., Salam, N., Liu, P. F., et al. (2021). Insight into the function and evolution of the Wood-Ljungdahl pathway in Actinobacteria. *ISME J.* 15, 3005–3018. doi: 10.1038/s41396-021-00935-9

Joshi, N. A., and Fass, J. N. (2011). Sickle: A sliding-window, adaptive, quality-based trimming tool for FastQ files (Version 1.33) [Software]. Available at: https://github.com/najoshi/sickle.

Kanehisa, M., Sato, Y., Kawashima, M., Furumichi, M., and Tanabe, M. (2016). KEGG as a reference resource for gene and protein annotation. *Nucleic Acids Res.* 44, D457–D462. doi: 10.1093/nar/gkv1070

Kim, M., Oh, H. S., Park, S. C., and Chun, J. (2014). Towards a taxonomic coherence between average nucleotide identity and 16S rRNA gene sequence similarity for species demarcation of prokaryotes. *Int. J. Syst. Evol. Microbiol.* 64, 346–351. doi: 10.1099/ijs.0.059774-0

Kroppenstedt, R. M. (1982). Separation of bacterial menaquinones by HPLC using reverse phase (RP18) and a silver loaded ion exchanger as stationary phases. *J. Liquid Chromatogr.* 5, 2359–2367. doi: 10.1080/01483918208067640

Kumar, S., Stecher, G., Li, M., Knyaz, C., and Tamura, K. (2018). MEGA X: molecular evolutionary genetics analysis across computing platforms. *Mol. Biol. Evol.* 35, 1547–1549. doi: 10.1093/molbev/msy096

Lagesen, K., Hallin, P., Rødland, E. A., Staerfeldt, H. H., Rognes, T., and Ussery, D. W. (2007). RNAmmer: consistent and rapid annotation of ribosomal RNA genes. *Nucleic Acids Res.* 35, 3100–3108. doi: 10.1093/nar/gkm160

Lagkouvardos, I., Joseph, D., Kapfhammer, M., Giritli, S., Horn, M., Haller, D., et al. (2016). IMNGS: A comprehensive open resource of processed 16S rRNA microbial profiles for ecology and diversity studies. *Sci. Rep.* 6, 33721. doi: 10.1038/srep33721

Lamers, L. P., Govers, L. L., Janssen, I. C., Geurts, J. J., van der Welle, M. E., Van Katwijk, M. M., et al. (2013). Sulfide as a soil phytotoxin-a review. *Front. Plant Sci.* 4, 268. doi: 10.3389/fpls.2013.00268

Li, D. D., Wang, J. L., Liu, Y., Li, Y. Z., and Zhang, Z. (2021). Expanded analyses of the functional correlations within structural classifications of glycoside hydrolases. *Comput. Struct. Biotechnol. J.* 19, 5931–5942. doi: 10.1016/j.csbj.2021.10.039

Lima, L. M., Silva, B., Barbosa, G., and Barreiro, E. J. (2020). β-lactam antibiotics: An overview from a medicinal chemistry perspective. *Eur. J. Med. Chem.* 208, 112829. doi: 10.1016/j.ejmech.2020.112829

Liu, H., Xin, B., Zheng, J., Zhong, H., Yu, Y., Peng, D., et al. (2020). Build a bioinformatics analysis platform and apply it to routine analysis of microbial genomics and comparative genomics. *Protoc Exch.* doi: 10.21203/rs.2.21224/v3

Liu, D., Zhang, Y., Fan, G., Sun, D., Zhang, X., Yu, Z., et al. (2022). IPGA: A handy integrated prokaryotes genome and pan-genome analysis web service. *iMeta* 1, e55. doi: 10.1002/imt2.55

MacDonald, L. C., and Berger, B. W. (2014). A polysaccharide lyase from Stenotrophomonas maltophilia with a unique, pH-regulated substrate specificity. *J. Biol. Chem.* 289, 312–325. doi: 10.1074/jbc.M113.489195

Matsumoto, A., Nakai, K., Morisaki, K., Ōmura, S., and Takahashi, Y. (2010). Demequina salsinemoris sp. nov., isolated on agar media supplemented with ascorbic acid or rutin. *Int. J. Syst. Evol. Microbiol.* 60, 1206–1209. doi: 10.1099/ijs.0.012617-0

Meng, X., Shao, Z., Hong, Y., Lin, L., Li, C., and Liu, Z. (2009). A novel pH-stable, bifunctional xylanase isolated from a deep-sea microorganism, Demequina sp. JK4. *J. Microbiol. Biotechnol.* 19, 1077–1084. doi: 10.4014/JMB.0901.0017

Minnikin, D. E., O'donnell, A. G., Goodfellow, M., Alderson, G., Athalye, M., Schaal, A., et al. (1984). An integrated procedure for the extraction of bacterial isoprenoid quinones and polar lipids. *J. Microbiological Methods* 2, 233–241. doi: 10.1016/0167-7012(84)90018-6

Modjinou, T., Versace, D.-L., Abbad-Andaloussi, S., Langlois, V., and Renard, E. (2017). Antibacterial and antioxidant photoinitiated epoxy co-networks of resorcinol and eugenol derivatives. *Materials Today Commun.* 12, 19–28. doi: 10.1016/j.mtcomm.2017.03.005

Morrissey, J., and Guerinot, M. L. (2009). Iron uptake and transport in plants: the good, the bad, and the ionome. *Chem. Rev.* 109, 4553–4567. doi: 10.1021/cr900112r

Nguyen, L. T., Schmidt, H. A., Von Haeseler, A., and Minh, B. Q. (2015). IQ-TREE: a fast and effective stochastic algorithm for estimating maximum-likelihood phylogenies. *Mol. Biol. Evol.* 32, 268–274. doi: 10.1093/molbev/msu300

Nouri, K., Feng, Y., and Schimmer, A. D. (2020). Mitochondrial ClpP serine protease-biological function and emerging target for cancer therapy. *Cell Death Dis.* 11, 841. doi: 10.1038/s41419-020-03062-z

Oren, A., and Garrity, G. M. (2021). Valid publication of the names of forty-two phyla of prokaryotes. *Int. J. Systematic Evolutionary Microbiol.* 71, 005056. doi: 10.1099/ijsem.0.005056

Park, S., Jung, Y.-T., Won, S.-M., and Yoon, J.-H. (2016). Demequina litorisediminis sp. nov., isolated from a tidal flat, and emended description of the genus Demequina. *Int. J. Systematic Evolutionary Microbiol.* 66, 4197–4203. doi: 10.1099/ijsem.0.001335

Peruzzi, E., Franke-Whittle, I. H., Kelderer, M., Ciavatta, C., and Insam, H. (2017). Microbial indication of soil health in apple orchards affected by replant disease. *Appl. Soil Ecol.* 119, 115–127. doi: 10.1016/j.apsoil.2017.06.003

Quick, M., Dwivedi, M., and Padan, E. (2021). Insight into the direct interaction of Na+ with NhaA and mechanistic implications. *Sci. Rep.* 11, 7045. doi: 10.1038/s41598-021-86318-8

Richter, M., and Rosselló-Móra, R. (2009). Shifting the genomic gold standard for the prokaryotic species definition. *Proc. Natl. Acad. Sci. U.S.A.* 106, 19126–19131. doi: 10.1073/pnas.0906412106

Rohban, R., Amoozegar, M. A., and Ventosa, A. (2009). Screening and isolation of halophilic bacteria producing extracellular hydrolyses from Howz Soltan Lake, Iran. *J. Ind. Microbiol. Biotechnol.* 36, 333–340. doi: 10.1007/s10295-008-0500-0

Rütting, T., Boeckx, P., Müller, C., and Klemedtsson, L. (2011). Assessment of the importance of dissimilatory nitrate reduction to ammonium for the terrestrial nitrogen cycle. *Biogeosciences* 8, 1779–1791. doi: 10.5194/bg-8-1779-2011

Saitou, N., and Nei, M. (1987). The neighbor-joining method: a new method for reconstructing phylogenetic trees. *Mol. Biol. Evol.* 4, 406–425. doi: 10.1093/oxfordjournals.molbev.a040454

Sánchez-Rodríguez, A., Tytgat, H. L. P., Winderickx, J., Vanderleyden, J., Lebeer, S., and Marchal, K. (2014). A network-based approach to identify substrate classes of bacterial glycosyltransferases. *BMC Genomics* 15, 349. doi: 10.1186/1471-2164-15-349

Sayers, E. W., Beck, J., Bolton, E. E., Bourexis, D., Brister, J. R., Canese, K., et al. (2021). Database resources of the national center for biotechnology information. *Nucleic Acids Res.* 49, D10–d17. doi: 10.1093/nar/gkaa892

Shen, X., Dong, W., Wan, Y., Feng, K., Liu, Y., and Wei, Y. (2021). Influencing mechanisms of siderite and magnetite, on naphthalene biodegradation: Insights from degradability and mineral surface structure. *J. Environ. Manage* 299, 113648. doi: 10.1016/j.jenvman.2021.113648

Shi, J., Xu, X., Liu, P. Y., Hu, Y. L., Zhang, B., Jiao, R. H., et al. (2021). Discovery and biosynthesis of guanipiperazine from a NRPS-like pathway. *Chem. Sci.* 12, 2925–2930. doi: 10.1039/D0SC06135B

Shimizu, Y., Ogata, H., and Goto, S. (2017). Type III polyketide synthases: functional classification and phylogenomics. *ChemBioChem* 18, 50–65. doi: 10.1002/cbic.201600522

Smibert, R., and Krieg, N. (1994). "Phenotypic characterization. In: *Methods for General and Molecular Bacteriology* P. Gerhardt, R. G. E. Murray, W. A. Wood and N. R. Krieg Eds. American Society for Microbiology, Washington, DC, 607–654.

Susin, M. F., Baldini, R. L., Gueiros-Filho, F., and Gomes, S. L. (2006). GroES/GroEL and DnaK/DnaJ have distinct roles in stress responses and during cell cycle progression in Caulobacter crescentus. *J. Bacteriol* 188, 8044–8053. doi: 10.1128/JB.00824-06

Tan, S., Liu, J., Fang, Y., Hedlund, B. P., Lian, Z.-H., Huang, L.-Y., et al. (2019). Insights into ecological role of a new deltaproteobacterial order Candidatus Acidulodesulfobacterales by metagenomics and metatranscriptomics. *ISME J.* 13, 2044–2057. doi: 10.1038/s41396-019-0415-y

Thompson, J. D., Higgins, D. G., and Gibson, T. J. (1994). CLUSTAL W: improving the sensitivity of progressive multiple sequence alignment through sequence weighting, position-specific gap penalties and weight matrix choice. *Nucleic Acids Res.* 22, 4673–4680. doi: 10.1093/nar/22.22.4673

Ue, H., Matsuo, Y., Kasai, H., and Yokota, A. (2011). Demequina globuliformis sp. nov., Demequina oxidasica sp. nov. and Demequina aurantiaca sp. nov., actinobacteria isolated from marine environments, and proposal of Demequinaceae fam. nov. *Int. J. Systematic Evolutionary Microbiol.* 61, 1322–1329. doi: 10.1099/ijs.0.024299-0

Wei, L., Liu, Y., Dubchak, I., Shon, J., and Park, J. (2002). Comparative genomics approaches to study organism similarities and differences. *J. BioMed. Inform* 35, 142–150. doi: 10.1016/S1532-0464(02)00506-3

Wei, H., Wang, L., Hassan, M., and Xie, B. (2018). Succession of the functional microbial communities and the metabolic functions in maize straw composting process. *Bioresource Technol.* 256, 333–341. doi: 10.1016/j.biortech.2018.02.050

Wick, R. R., Judd, L. M., Gorrie, C. L., and Holt, K. E. (2017). Unicycler: Resolving bacterial genome assemblies from short and long sequencing reads. *PloS Comput. Biol.* 13, e1005595. doi: 10.1371/journal.pcbi.1005595

Wu, Z., Li, Y., Gu, Z., Ding, Z., Zhang, L., and Shi., G. (2018). Function of glnA, proB and proA genes in L-proline anabolic pathway of Bacillus subtilis. *Acta Microbiologica Sin.* 58, 39–50. doi: 10.13343/j.cnki.wsxb.20170011

Xu, P., Li, W. J., Tang, S. K., Zhang, Y. Q., Chen, G. Z., Chen, H. H., et al. (2005). Naxibacter alkalitolerans gen. nov., sp. nov., a novel member of the family 'Oxalobacteraceae' isolated from China. *Int. J. Syst. Evol. Microbiol.* 55, 1149–1153. doi: 10.1099/ijs.0.63407-0

Xu, M., Zhang, F., Cheng, Z., Bashiri, G., Wang, J., Hong, J., et al. (2020). Functional genome mining reveals a class V lanthipeptide containing a d-amino acid introduced by an F(420) H(2) -dependent reductase. *Angew Chem. Int. Ed Engl.* 59, 18029–18035. doi: 10.1002/anie.202008035

Yi, H., Schumann, P., and Chun, J. (2007). Demequina aestuarii gen. nov., sp. nov., a novel actinomycete of the suborder Micrococcineae, and reclassification of Cellulomonas fermentans Bagnara et al. 1985 as Actinotalea fermentans gen. nov., comb. nov. *Int. J. Systematic Evolutionary Microbiol.* 57, 151–156. doi: 10.1099/ijs.0.64525-0

Yin, L. Z., Liu, Z. T., Li, J. L., Wang, P. D., Dong, L., Duan, L., et al. (2021). Agilicoccus flavus gen. nov., sp. nov., a novel member of the family Dermatophilaceae isolated from the Pearl River. *Int. J. Syst. Evol. Microbiol.* 71, 005076. doi: 10.1099/ijsem.0.005076

Yoon, S. H., Ha, S. M., Kwon, S., Lim, J., Kim, Y., Seo, H., et al. (2017). Introducing EzBioCloud: a taxonomically united database of 16S rRNA gene sequences and whole-genome assemblies. *Int. J. Syst. Evol. Microbiol.* 67, 1613–1617. doi: 10.1099/ijsem.0.001755

Zhou, Z., Tran, P. Q., Breister, A. M., Liu, Y., Kieft, K., Cowley, E. S., et al. (2022). METABOLIC: high-throughput profiling of microbial genomes for functional traits, metabolism, biogeochemistry, and community-scale functional networks. *Microbiome* 10, 33. doi: 10.1186/s40168-021-01213-8

Zoghlami, A., and Paës, G. (2019). Lignocellulosic biomass: understanding recalcitrance and predicting hydrolysis. *Front. Chem.* 7. doi: 10.3389/fchem.2019.00874

frontiers | Frontiers in Marine Science

TYPE Original Research
PUBLISHED 20 October 2023
DOI 10.3389/fmars.2023.1248754

OPEN ACCESS

EDITED BY
Feng-Yan Bai,
Chinese Academy of Sciences (CAS), China

REVIEWED BY
Heng-Lin Cui,
Jiangsu University, China
Min Yu,
Ocean University of China, China

*CORRESPONDENCE
Cong Sun
michael_sc@sina.com

RECEIVED 27 June 2023
ACCEPTED 26 September 2023
PUBLISHED 20 October 2023

CITATION
Gao J-W, Ying J-J, Dong H, Liu W-J, He D-Y, Xu L and Sun C (2023) Characterization of *Maribacter polysaccharolyticus* sp. nov., *Maribacter huludaoensis* sp. nov., and *Maribacter zhoushanensis* sp. nov. and illumination of the distinct adaptative strategies of the genus *Maribacter*. *Front. Mar. Sci.* 10:1248754. doi: 10.3389/fmars.2023.1248754

Characterization of *Maribacter polysaccharolyticus* sp. nov., *Maribacter huludaoensis* sp. nov., and *Maribacter zhoushanensis* sp. nov. and illumination of the distinct adaptative strategies of the genus *Maribacter*

Jia-Wei Gao[1,2], Jun-Jie Ying[1,2], Han Dong[1], Wen-Jia Liu[1,2], Dong-Yan He[1], Lin Xu[1,2] and Cong Sun[1,2]*

[1]College of Life Sciences and Medicine, Zhejiang Sci-Tech University, Hangzhou, China, [2]Shaoxing Biomedical Research Institute of Zhejiang Sci-Tech University Co., Ltd, Zhejiang Engineering Research Center for the Development Technology of Medicinal and Edible Homologous Health Food, Shaoxing, China

Polysaccharides are complex carbohydrates and are abundant in the marine environment. Microbes degrade and utilize them using Carbohydrate-active enzymes (CAZymes), which mediate polysaccharides into the marine carbon cycle. With the continued supply of polysaccharides from the marine environment, tidal flats are also abundant in polysaccharides, resulting in an abundance of marine polysaccharide degrading strains. In this study, three novel strains, designated as D37^T, M208^T, and SA7^T, were isolated from the intertidal sediment samples located in Zhoushan, Zhejiang and Huludao, Liaoning, PR China. The phylogenetic trees using the 16S rRNA gene and genome sequences showed that the three novel strains belonged to the genus *Maribacter*. The highest 16S rRNA gene sequence similarities between the three novel strains and other strains of the genus *Maribacter* were 98.7%, 99.2%, and 98.8%, respectively, while the ANI, AAI, and dDDH values between the three strains and the other strains of the genus *Maribacter* were 70-86%, 67-91%, and 17-30%, respectively, supporting their affiliation as novel species. Combined with other phenotypic and genotypic characterization in this study, three novel species are proposed as *Maribacter polysaccharolyticus* sp. nov., *Maribacter huludaoensis* sp. nov., and *Maribacter zhoushanensis* sp. nov., respectively, for the three strains. Furthermore, we compared all available genomes of *Maribacter* representatives and found that *Maribacter* strains could be divided into two groups (A and B). The two groups are different in genome size and G + C content and gene densities of CAZyme, peptidase, and sulfatase. Group A possesses

more CAZymes which are related to degrading laminarin, fucoidan, mannan, xylose, and xylan. This result suggests that the two groups may have different niche adaptation strategies. Our study contributes to a better understanding of the role of marine flavobacteria in biogeochemical cycles and niche specialization.

KEYWORDS

tidal flats, bacteroidota, *Maribacter*, CAZyme, PUL, ecological niches

1 Introduction

Tidal flats, the boundary between the terrestrial and marine habitats, are well-known ecosystems for their productivity and possession of one of the most abundant and diverse microbial community (Schuerch et al., 2019; Niu et al., 2022). *Bacteroidota* is considered as a major part of bacterial communities in the tidal flats and plays an important role, participating in complex polysaccharides degradation, cycling of nutrients, carbon sequestration, and other functions (Zhang et al., 2018b). *Flavobacteriaceae*, one of the most important and largest components of this phylum, contains more than 160 validly published genera (Gavriilidou et al., 2020). *Maribacter*, of family *Flavobacteriaceae*, was initially identified and established with *Maribacter sedimenticola* (Nedashkovskaya et al., 2004). Based on the LPSN (https://lpsn.dsmz.de/genus/maribacter), there are 32 validly published species in the genus *Maribacter*. *Maribacter* species have been isolated from different marine environments such as tidal flats (Lo et al., 2013; Jung et al., 2014; Park et al., 2016; Thongphrom et al., 2016; Liu et al., 2020), seawater (Yoon et al., 2005; Barbeyron et al., 2008; Nedashkovskaya et al., 2010; Jin et al., 2017; Kang et al., 2018), marine sponges (Jackson et al., 2015), deep-sea sediment (Fang et al., 2017), and marine alga (Nedashkovskaya et al., 2007; Zhang et al., 2009; Weerawongwiwat et al., 2013; Khan et al., 2020; Zhang et al., 2020). *Maribacter* strains share similar characteristics such as containing menaquinone-6 (MK-6) as the major isoprenoid quinone (Zhang et al., 2020).

Algal polysaccharide is one of the most important components of marine organic carbon (Barbeyron et al., 2016). *Bacteroidota* usually utilizes algal polysaccharides through polysaccharide utilization loci (PUL), which are mainly comprised of carbohydrate-active enzymes (CAZymes), TonB-dependent receptor-like transporter (susC), and polysaccharide binding protein (susD) (Bennke et al., 2016). Besides, CAZymes encompass glycoside hydrolases (GH), polysaccharide lyases (PL), carbohydrate esterases (CE), auxiliary activity (AA), carbohydrate-binding modules (CBM), and glycosyl transferases (GT). The frequent transfer of CAZyme-encoding genes among microorganisms is an effective mechanism for strains to adapt to different environments and related niches (Arnosti et al., 2021). Recent studies suggest that *Flavobacteriaceae* is a major contributor to marine polysaccharide degradation and related carbon cycling in the marine environment (Klippel et al., 2011; Mann et al., 2013; Sun et al., 2020). For example, *Zobellia galactanivorans* is able to degrade diverse marine polysaccharides including alginate, carrageenan, and laminarin and is capable of complex degradation and regulatory mechanisms for the species that have been revealed (Ficko-Blean et al., 2017; Zhu et al., 2017). *Formosa agariphila* can degrade ulvan through related PUL (Reisky et al., 2019). *Maribacter* is one of the recurrent genera in a highly dynamic fashion of a bacterial community in the North Sea spring blooms (Bartlau et al., 2022). The analysis of CAZyme and PUL in a novel strain *Maribacter dokdonensis* 62-1 indicated that it was specialized to certain "polysaccharide niches" such as alginate and ulvan (Wolter et al., 2021).

In this study, three novel isolates D37^T, M208^T, and SA7^T were discovered in the intertidal sediments of Zhoushan and Huludao, China, and subject to polyphasic taxonomic identification. We also compared the genomes of the three novel isolates with all available strains of the genus *Maribacter* to clarify their similarities and differences in algal polysaccharide degradation, and tried to illuminate their preference in carbon cycles and niche specialization. Through this study, we provide novel resources of the genus *Maribacter* and further evidence for its evolution. The result is valuable for our understanding of the role of marine flavobacteria in biogeochemical cycles and niche specialization.

2 Materials and methods

2.1 Strain isolation and cultivation

A self-manufactured columnar tube sampler was used to collect and stratify the sediment samples, collected samples at varying depths (0-5, 5-15, and 15-30 cm) were immediately kept at 4°C in sterile self-sealing bags before reservation (Wu et al., 2021). The sediment samples were preserved at 4°C for short-term preservation and preserved at -20°C for long-term preservation. The sediment sample was 10-fold serially diluted to 10^{-3} with 3% NaCl solution, and 50 µl diluent was coated on the marine agar 2216 with 1/10 strength of yeast extract and peptone (MA; Becton Dickinson) to minimize the isolation of fast-growing strains, which usually belong to well-studied species, and maximize the isolation of rarely studied strains in the samples. The strains were picked out after five days of

incubation at 25°C and purified by subcultivation on marine agar 2216 at 25°C. The novel strains were frozen at -80°C, supplemented with glycerol (25%, v/v) for long-term preservation, and cultivated in marine broth (MB, Becton Dickinson) for three days for further experiments. Strains D37^T and SA7^T were isolated from intertidal sediments collected in Zhoushan, Zhejiang, PR China (21°35′ N, 109°80′ E) and strain M208^T was isolated from an intertidal sediment sample collected in Huludao, Liaoning, PR China (40° 41′ N, 120°56′ E).

2.2 Morphological, physiological, biochemical, and chemotaxonomic features

The colony morphology was viewed by scribing on MA after 3 days. Transmission electron microscopy (TEM, JEM-1400Flash) was used to examine the cell morphology of novel isolates incubated at MA after 3 days. The Gram staining method was used to detect the Gram reaction. (Romero et al., 1988). Motility was observed by dipping a small amount of bacterial solution into a semi-solid culture medium (MA, reduce 0.5% agar content) with an inoculation needle and cultivating the bacterial solution under optimal conditions for 3 days. Anaerobic growth was tested using the formulated anaerobic culture medium as described (Xu et al., 2021). The activities of catalase and oxidase were tested as described (Sun et al., 2018). To determine the growth ranges and optimal conditions, the temperature ranges (4, 10, 15, 20, 25, 27, 30, 37, 40, 42, 45, 50 °C), pH range (5.0 to 10.0), and different NaCl concentrations (0, 0.5, 1.0, 1.5, 2.0, 2.5, 3.0, 3.5, 4.0, 6.0, 8.0, 10.0, and 12.0%, w/v) for growth were investigated as described (Gao et al., 2023). Hydrolysis of starch, tyrosine, cellulose, Tween 20, 40, 60, and 80, and casein were tested in modified MA (MA medium without peptidase and with reduced yeast extract of 0.1 g/L) and then with added 2g/L starch, 5g/L tyrosine, 10g/L Tween 20, 40, 60, and 80 each, 2g/L cellulose and 10g/L casein, respectively (Sun et al., 2018). API 20NE, API ZYM, and API 50CH strips (bioMérieux) were utilized for physiological, biochemical and acid production, respectively, according to the instruction manuals.

The cells of strains D37^T, M208^T, and SA7^T for the analysis of fatty acids were collected after being cultivated on MA at optimum temperature for 3 days, then subjected to gas chromatography (Agilent 8860). The results were analyzed with the Sherlock microbial identification system (MIDI) and the standard MIS library generation software (version 6.5) (Gao et al., 2023). Polar lipids were extracted following the described procedure (Ying et al., 2021), separated on the TLC silica gel plate (60 F254, Merck, 10 x 10 cm, activate in 55 °C oven for 30 minutes) by two-dimensional TLC, and finally visualized by spraying staining agents including phosphomolybdic acid for total lipids, ninhydrin for amino lipids, molybdenum blue for phospholipids, alpha-naphthol with sulfuric acid for glycolipids to distinguish different polar lipids (Sun et al., 2019; Ying et al., 2021). The respiratory quinones were analyzed using one-dimensional TLC and High Performance Liquid Chromatography (HPLC; Agilent 1200) and Mass Spectrometry (MS; Thermo Finnigan LCQ DECA XP MAX) as described (Sun et al., 2014).

2.3 Genome sequencing and phylogenetic analyses

Genomic DNA was extracted as described (Sun et al., 2016) and sent to Guangdong Magigene Biotechnology Co. Ltd. (Guangzhou, PR China) for genome sequencing. Illumina Hiseq platform (Novaseq 6000) and SPAdes v.3.10.1 were used for the genome sequencing and assembly, respectively. CheckM v.1.0.7 was used to estimate the quality of the spliced genome (Parks et al., 2015). The complete 16S rRNA gene sequences were extracted from the genome data by the RNAmmer v.1.2 (Lagesen et al., 2007), and further confirmed using Sanger sequencing by Tsingke Biotechnology Co., Ltd. (Beijing, PR China). Sequence similarities were compared by using the EzBioCloud (www.ezbiocloud.net) and the 16S rRNA genes of closely related type strains were downloaded from NCBI and analyzed using the MEGA 11.0 software with ClustalW program (Tamura et al., 2021) for sequence alignment. The neighbor-joining (NJ) (Saitou and Nei, 1987), maximum-likelihood (ML) (Felsenstein, 1981), maximum-parsimony (MP) (Fitch, 1971), and minimum-evolution (ME) (Rzhetsky and Nei, 1992) methods were used for the reconstruction of phylogenetic trees. For all methods, the Kimura's two-parameter model (Kimura, 1980) and 1000 replications were employed (Do, 1992). *Zeaxanthinibacter aestuarii* S2-22^T was used as an outgroup.

For phylogenomic analysis, twenty-two genomes of type strains in the genus *Maribacter* were downloaded from NCBI (https://www.ncbi.nlm.nih.gov), *Zeaxanthinibacter enoshimensis* DSM 18435^T was used as an outgroup. Together with the draft genomes of strains D37^T, M208^T, and SA7^T, all genomes (Table S1) were annotated by the RAST server (Aziz et al., 2008). OrthoFinder v.2.5.4 was used for the extraction of orthologous clusters (OCs) of all genomes based on protein sequences, single-copy orthologous clusters were unified by MAFFT v.7.490 (Katoh and Standley, 2013), and then refined with trimAL v.1.2rev59 (Capella-Gutierrez et al., 2009). The Local Perl script "concatenate.pl" was used for sequence concatenation. The '-m MFP' was served as a predictive command of the best amino acid substitution model of concatenated sequences in IQ-TREE v.1.6.12, for which, 'LG+F+I+R5' was used as the best amino acid model in this study. Based on the amino acid model 'LG+F+I+R5', the maximum-likelihood phylogenomic tree with ultrafast bootstraps set to 1,000 was reconstructed by IQ-TREE. tvBOT web application was applied for visualizing and modifying phylogenetic trees (Xie et al., 2023). The values of average nucleotide identity (ANI), the digital DNA-DNA hybridization (dDDH) and Average Amino acid Identity (AAI) were analyzed by OrthoANI Tool version 0.93.1 (Kim et al., 2014) (Lee et al., 2016), Genome-to-Genome Distance Calculator 3.0 web server (https://ggdc.dsmz.de/ggdc.php#) (Meier-Kolthoff et al., 2013), and the AAI Calculator (http://enve-omics.ce.gatech.edu/aai/) (Chun et al., 2018), respectively.

2.4 Comparative genomic analyses

The metabolic genes and pathways were annotated and analyzed in the KEGG website (https://www.kegg.jp/blastkoala/) (Kanehisa et al., 2017). Functional annotations assigned to Clusters of Orthologous groups (COG) were performed with the eggnog-mapper version 2 (Cantalapiedra et al., 2021). CAZyme was identified using dbCAN2 (https://bcb.unl.edu/dbCAN2/blast.php) (Zhang et al., 2018a). Peptidase was annotated against MEROPS (https://www.ebi.ac.uk/merops/) (Rawlings et al., 2018) and the local server BLASTP (only considering values e<1e-15). Sulfatase was identified using the database of Sulfatases SulfAtlas version 2.3.1 (https://sulfatlas.sb-roscoff.fr/sulfatlas/) (Stam et al., 2023) and the local server BLASTP (only considering values of e<1e-15). PUL and its function genes were predicted based on the PULDB databases (http://www.cazy.org/PULDB/) (Terrapon et al., 2018). Data were visualized by chiplot (https://www.chiplot.online). The principal component analysis (PCA) was performed in RStudio using R v4.1.2 and visualized using the package prompts.

3 Results and discussion

3.1 Morphological, physiological, biochemical, and chemotaxonomic characteristics

Strains D37^T, M208^T, and SA7^T were all Gram-stain-negative, rod-shaped, aerobic, and non-motile, which were similar to other *Maribacter* strains. The cells of strains D37^T, M208^T, and SA7^T were rod-shaped with 1.8-3.3, 1.7-2.7, and 1.5-3 μm in length, and 0.4-0.8, 0.3-0.4, and 0.6-0.8 μm in width, respectively (Figure S1). The three strains all formed yellow, round, opaque, border smooth, and convex colonies after scribing on MA medium and cultivated for 3 days. Strain D37^T was observed to be oxidase-positive and catalase-positive as most *Maribacter* strains, but strain M208^T and SA7^T were both weakly positive in oxidase and negative in catalase. Strains D37^T, M208^T, and SA7^T could all hydrolyze tyrosine and Tween 20, and none of them could hydrolyze casein. Besides, the three strains showed different reactions in starch, cellulose, and Tween 40, 60, and 80 hydrolysis. Strains M208^T and SA7^T could hydrolyze cellulose, Tween 40, 60, and 80, but strain D37^T could not. On the contrary, only strain D37^T could hydrolyze starch. Moreover, the three strains also differed in other biochemical characteristics, including the fermentation of glucose, esterase (C4), esterase lipase (C8), cysteine arylamidase, trypsin, chymotrypsin, α-galactosidase, α-mannosidase, α-glucosidase, β-galactosidase, β-fucosidase, glycerol, D-arabinose, L-fucose, D-fructose, D-mannose, N-acetyl-glucosamine, D-mannitol, starch, and so on. In general, strain D37^T exhibited stronger enzyme activity and carbohydrate acid production ability. The detailed features differentiatiating strains D37^T, M208^T, and SA7^T from their closely related *Maribacter* strains are shown in Table 1.

The major fatty acids (>10%) of strains D37^T, M208^T, and SA7^T were iso-$C_{15:0}$ (16.7%, 14.4%, 13.2%, respectively) and iso-$C_{17:0}$ 3-OH (16.3%, 16.6%, 25.3%, respectively), which were all detected in other members of the genus *Maribacter* as the major fatty acids (Table 2). Meanwhile, fatty acids $C_{16:0}$, iso-$C_{13:0}$, iso-$C_{14:0}$, anteiso-$C_{15:0}$, iso-$C_{15:1}$ G, $C_{16:0}$ 3-OH, iso-$C_{15:0}$ 3-OH, iso-$C_{16:0}$ 3-OH, Summed Feature 3, and Summed Feature 9 were determined for strains D37^T, M208^T, and SA7^T as the minor fatty acids (>1% but <10%, Summed Feature 3 in strain M208^T was >10%). Strain D37^T had more differences to strains M208^T and SA7^T including iso-$C_{15:1}$ G, anteiso-$C_{15:0}$,and Summed Feature 1. The fatty acid iso-$C_{15:1}$ G was only detected in strain D37^T, and the content of anteiso-$C_{15:0}$ in strain D37^T was clearly more than the other two strains. The fatty acids profiles of strains M208^T and SA7^T were quite similar. Summed Feature 1 was only detected in strains M208^T and SA7^T, while these two strains also had minor differences such as $C_{16:0}$ and $C_{15:0}$ 3-OH. The detailed fatty acid results of strains D37^T, M208^T and SA7^T with their closely related taxa of the genus *Maribacter* are in Table 2. The major polar lipids of strains D37^T, M208^T, and SA7^T all comprised phosphatidylethanolamine (PE), unidentified glycolipids (GL), unidentified aminolipids (AL), and unidentified lipids (L), which resembled the majority of *Maribacter* strains (Table 1, Figure S2). Strain D37^T and its reference strain *M. luteus* RZ05^T both consisted of PE, two GLs, and one AL, and *M. luteus* RZ05^T had one additional unidentified lipid compared to strain D37^T. Like its reference strain *M. dokdonensis* DSW-8^T, strain M208^T also contained PE and one AL, but compared with each other, *M. dokdonensis* DSW-8^T had two additional unidentified phospholipids (PL) and strain M208^T had one GL. The polar lipid profile of strain SA7^T was also similar to its reference strain *M. caenipelagi* HD-44^T. However, strain *M. caenipelagi* HD-44^T was absent of GL and had an extra unidentified lipid. Similar to the majority of bacteria in the genus *Maribacter*, the major respiratory quinone of strains D37^T, M208^T, and SA7^T was MK-6.

According to the above phenotypical features, these three strains showed common features of the genus *Maribacter* but also features that are distinct from them. Three strains shared similar chemotaxonomic features such as MK-6 as the major respiratory quinone, iso-$C_{15:0}$ and iso-$C_{17:0}$ 3-OH as the major fatty acids, and PE as the main polar lipid with *Maribacter* strains, while the oxidase, catalase, hydrolysis of starch, cellulose, Tween 40, 60, and 80, and other physiological and biochemical characteristics indicated that these three strains as well as the genus *Maribacter* were clearly distinct. Therefore, these three strains could be classified as novel species of the genus *Maribacter* based on their phenotypical characteristics.

3.2 Phylogenetic analyses based on 16S rRNA gene and genome sequences

The lengths of the complete 16S rRNA gene of strains D37^T, M208^T, and SA7^T were 1535, 1537, and 1533 bp, respectively. Strain D37^T showed the highest 16S rRNA gene sequence identities with *M. luteus* RZ05^T (98.76%), followed by *M. polysiphoniae* LMG 23671^T (97.24%), *M. arenosus* CAU 1321^T (96.93%), *M. maritimus* HMF 3635^T (96.83%), and the rest of *Maribacter* type strains (<95.85%). The 16S rRNA gene sequence of strain M208^T was most closely similar with *M. dokdonensis* DSW-8^T (99.17%), then

TABLE 1 Characteristics that differentiate strains D37^T, M208^T, and SA7^T from closely related taxa of the genus.

Characteristic	1	2	3	4[a]	5[b]	6[c]	7[d]
Temperature range (°C) for growth	15-37	4-35	4-30	7-40	4-35	4-32	4-35
pH range for growth	5.5-8.5	6.0-8.5	5.5-9	5.5-9	5.5-8	5.5-8.5	5.5-8
NaCl concentration (%) for growth	0-6	0.5-6	0.5-6	0.5-6	0.5-10	0-9	0-10
Oxidase	+	w	w	+	+	–	+
Catalase	+	–	–	+	+	+	–
Hydrolysis of							
starch	+	–	–	+	–	–	–
cellulose	–	+	+	–	ND	ND	ND
Tween 40	–	+	+	+	+	+	+
Tween 60	–	+	+	+	+	ND	+
Tween 80	–	+	+	+	+	+	+
API 20NE:							
fermentation of glucose	+	–	–	+	ND	ND	ND
API ZYM:							
Esterase (C4) and Esterase lipase (C8)	w	w	+	+	+	+	+
cysteine arylamidase	w	w	–	+	–	+	–
trypsin	+	w	–	+	–	–	–
chymotrypsin	w	+	w	+	–	+	+
α-galactosidase	–	w	w	+	–	+	+
β-galactosidase and α-glucosidase	–	+	+	+	–	+	+
β-fucosidase	w	–	–	ND	ND	ND	ND
API 50CH							
Glycerol, D-arabinose and L-fucose	+	–	–	ND	ND	ND	ND
D-fructose, D-mannose and N-acetyl-glucosamine	+	w	+	ND	ND	ND	ND
D-mannitol, starch and potassium 2-ketogluconate	+	–	+	ND	ND	ND	ND
methyl- αD-mannopyranoside, inulin and D-melezitose	+	w	w	ND	ND	ND	ND
glycogen and xylitol	+	–	w	ND	ND	ND	ND
potassium gluconate	–	+	+	ND	ND	ND	ND
L-rhamnose	–	+	–	ND	ND	ND	ND
Methyl-βD-xylopyranoside	–	w	w	ND	ND	ND	ND
Polar lipids	PE, GL (2), AL, L (3)	PE, GL (2), AL, L (2)	PE, GL (3), AL, L (2)	PE, GL (2), AL, L (4)	PE, GL (1), PL (2), AL	ND	PE, AL, L (5)
DNA G+C% content (%)	41.7	35.9	34.8	38.9	36.1	34.4	37.6

Strains: 1, strain D37^T; 2, strain M208^T; 3, strain SA7^T; 4, M. luteus RZ05^T; 5, M. dokdonensis DSW-8^T; 6, M. forsetti KT02ds18-4^T.
+, Positive; –, Negative; w, weakly positive; ND, not detected; PE, phosphatidylethanolamine; GL, glycolipids; AL, aminolipid; PL, phospholipid; L, Lipid.
Data were cited from [a]Liu et al. (2020), [b]Yoon et al. (2005),[c]Barbeyron et al. (2008), [d]Jung et al. (2014).

M. confluentis SSK2-2^T (97.73%), *M. litoralis* SDRB-Phe2^T (97.69%), *M. stanieri* KMM 6046^T (97.58%), and less than 97.51% with other type species. Strain SA7^T was identified to have the highest identities of 98.69% 16S rRNA gene sequence with *M. forsetii* KT02ds18-6^T, followed by *M. litoralis* SDRB-Phe2^T (98.67%), *M. spongiicola* W15M10^T (98.35%), *M. ulvicola* KMM 3951^T (98.34%), and the rest of the strains of *Maribacter* (<98.13%). From the above results, the similarity of 16S rRNA gene sequence

TABLE 2 Comparison of cellular fatty acid compositions of novel isolates and closely related taxa of the genus *Maribacter*.

Fatty acids	1	2	3	4[a]	5[b]	6[c]
Straight-chain						
$C_{14:0}$	TR	1.5	TR	–	2.0	TR
$C_{16:0}$	5.3	6.0	1.8	TR	5.2	3.4
Unsaturated						
$C_{15:1}$ ω6c	TR	TR	1.7	3.1	–	1.6
$C_{17:1}$ ω6c	TR	TR	1.1	TR	–	TR
Branched-chain						
iso-$C_{13:0}$	1.6	1.5	1.4	–	TR	1.2
iso-$C_{14:0}$	3.4	5.7	5.3	–	–	4.8
iso-$C_{15:0}$	**16.7**	**14.4**	**13.2**	**19.6**	**26.7**	**10.3**
iso-$C_{15:1}$ G	**9.0**	–	–	**18.9**	**16.0**	–
iso-$C_{16:0}$	1.2	1.2	TR	–	–	1.1
anteiso-$C_{14:0}$	1.1	TR	TR	–	–	2.2
anteiso-$C_{15:0}$	6.8	1.9	1.0	5.2	1.3	–
Hydroxy						
$C_{15:0}$ 3-OH	–	TR	1.9	1.7	1.4	1.6
$C_{16:0}$ 3-OH	1.5	5.7	2.7	TR	5.4	4.3
$C_{17:0}$ 2-OH	2.7	TR	TR	1.7	–	–
iso-$C_{14:0}$ 3-OH	TR	TR	–	–	–	–
iso-$C_{15:0}$ 3-OH	5.4	5.3	5.8	7.5	4.2	4.3
iso-$C_{16:0}$ 3-OH	5.0	3.2	3.6	7.8	1.0	4.4
iso-$C_{17:0}$ 3-OH	**16.3**	**16.6**	**25.3**	**10.5**	**26.4**	**20.4**
Summed Feature 1	–	**14.4**	**14.2**	–	–	**13.5**
Summed Feature 3	8.9	**10.2**	7.9	6.4	9.5	**13.0**
Summed Feature 9	5.2	1.9	4.3	7.9	2.2	4.8

Data of strains were taken from [a]Liu et al. (2020), [b]Jung et al. (2014), [c]Zhang et al. (2020).
Summed feature 1 contains iso-$C_{15:1}$ H and/or $C_{13:0}$ 3-OH; Summed feature 3 contains $C_{16:1}$ ω7c and/or $C_{16:1}$ ω6c; Summed feature 9 contains 10-methyl $C_{16:0}$ and/or iso-$C_{17:1}$ ω9c.
Strains: 1, strain D37^T; 2, strain M208^T; 3, strain SA7^T; 4, M. luteus RZ05^T; 5, M. dokdonensis DSW-8^T; 6, M. spongiicola DSM 25233^T.
Values are percentages of total fatty acids. Fatty acids representing >10% of the total are in bold type. -, not detected. TR, traces (<0.5%).

between the three strains and the type species of the genus *Maribacter* were higher than the recommended species delineation (98.65%), so we compared their ANI, AAI, and dDDH values with the other strains of the genus *Maribacter* (Figure 1). The ANI values between strains D37^T, M208^T, SA7^T and the species of the genus *Maribacter* ranged from 70% to 80%, 70% to 85%, and 70% to 86%, respectively. The AAI values and dDDH values of the three novel strains with other members of the genus *Maribacter* ranged from 17% to 23% and 66% to 83%, 17% to 29% and 67% to 90%, as well as 17% to 30% and 67% to 91%, respectively. According to the threshold values of recommended species delineation (ANI of < 95%; AAI of < 95%; dDDH of < 70%), the above results undoubtedly indicate that the three strains represent the new members of the genus *Maribacter* and are different species.

The phylogenetic trees reconstructed based on 16S rRNA gene sequences showed that strains D37^T, M208^T, and SA7^T were clustered with the members of the genus *Maribacter*, which firmly suggested that these three strains should be the new species of the genus *Maribacter* (Figure 2; Figures S3–S5). In the phylogenomic tree based on the single-copy orthologous proteins, the three strains were still situated in the genus *Maribacter*, supporting the affiliation of the three strains as the novel species of the genus *Maribacter* (Figure S6). Besides, these three strains were far apart from each other in the 16S rRNA phylogenetic trees, but in the phylogenomic tree, strains M208^T and SA7^T had a closer genetic relationship and were clustered in a clade far away from strain D37^T.

Although the highest similarity of 16S rRNA was higher than 98.65%, the value of recommended species delineation, their ANI,

10.3389/fmars.2023.1248754

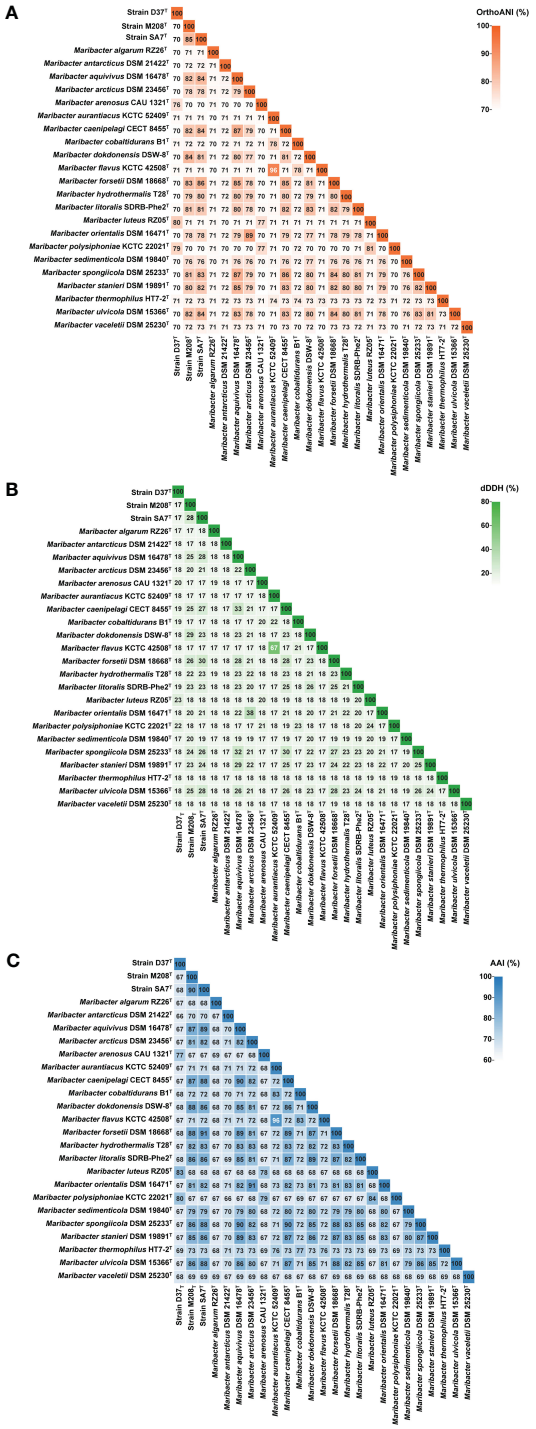

FIGURE 1
OrthoANI **(A)**, dDDH **(B)**, and AAI **(C)** values among the twenty-five genomes of the genus *Maribacter*.

AAI, and dDDH were below the threshold. Together with the 16S rRNA gene and genomic phylogenetic analysis above, strains D37^T, M208^T, and SA7^T could be assigned as the novel species of the genus *Maribacter*.

3.3 General genomic features

The draft genome sequences of strains D37^T (GCF_014610845.1), M208^T (GCF_029350945.1), and SA7^T (GCF_029350975.1) had 21 contigs with 4,760,098 bp length and the N_{50} value was 577,838 bp, 16 contigs with a length of 4,243,569 bp and the N_{50} value was 341,292 bp, and 18 contigs with a length of 4,257,159 bp and the N_{50} value was 844,229 bp, respectively. The genomic completeness and contamination values of strains D37^T, M208^T, and SA7^T were estimated to be 99.67% and 1.67%, 99.67% and 1.67%, and 99.67% and 0.33%, respectively. The genome size of strain D37^T was larger than strains M208^T and SA7^T, which were 4.8 Mb, 4.2 Mb, and 4.2 Mb, respectively, which were similar to the genome size of *Maribacter* species (ranges from 3.9 Mb to 5.1 Mb). The DNA G + C contents of strains D37^T, M208^T, and SA7^T calculated from the genome sequences were 41.7%, 35.9%, and 34.8%, respectively. Although the DNA G + C content of strain D37^T was higher than that of strains M208^T and SA7^T, it was still within the range for the genus *Maribacter* (31.7% ~ 41.8%). The detailed results of the genus *Maribacter* are shown in Supplementary Table S1.

Metabolic pathway analysis based on the KEGG database indicated that these three strains all had metabolism pathways that could maintain the most basic life activities of organisms like the other *Maribacter* strains, including glycolysis, trichloroacetic acid (TCA) cycle, and fatty acid biosynthesis (Figure S7). Besides, strain D37^T had additional different metabolic pathways including nicotinamide adenine dinucleotide (NAD) biosynthesis, pyruvate metabolism, and cysteine biosynthesis. For example, only strain D37^T contained *nadA* and *nadB* genes that could biosynthesize the NAD from aspartate as well as *ppdk* genes that enabled the transformation of malate to phosphoenolpyruvate (PEP) (Figure S8). Strain SA7^T had a unique metabolic pathway that could degrade D-galacturonate, which was different from strain M208^T. The detailed results of clusters of orthologous groups (COG) are shown in Figure 3. The top five gene functions with the highest proportion of the three strains were cell wall/membrane/envelope biogenesis (M), carbohydrate transport and metabolism (G), inorganic ion transport and metabolism (P), amino acid transport and metabolism (E), and energy production and conversion (C). However, strain D37^T contained more genes in energy production and conversion (C), carbohydrate transport and metabolism (G), inorganic ion transport and metabolism (P), and defense mechanisms (V). The number counts of CAZyme, sulfatase, and peptidase in strain D37^T were higher than those in strains M208^T and SA7^T (226 vs 156 vs 115, 377 vs 267 vs 212, 286 vs 235 vs 245, respectively). In addition, the quantities of CAZyme and sulfatase of strain D37^T were the highest and the second highest among the genus *Maribacter*, respectively and strain SA7^T had the lowest number counts of CAZyme and sulfatase (Supplementary Table S2). The number counts of peptidase of the genus *Maribacter* ranged from 189 to 380 and the three strains were all within the range.

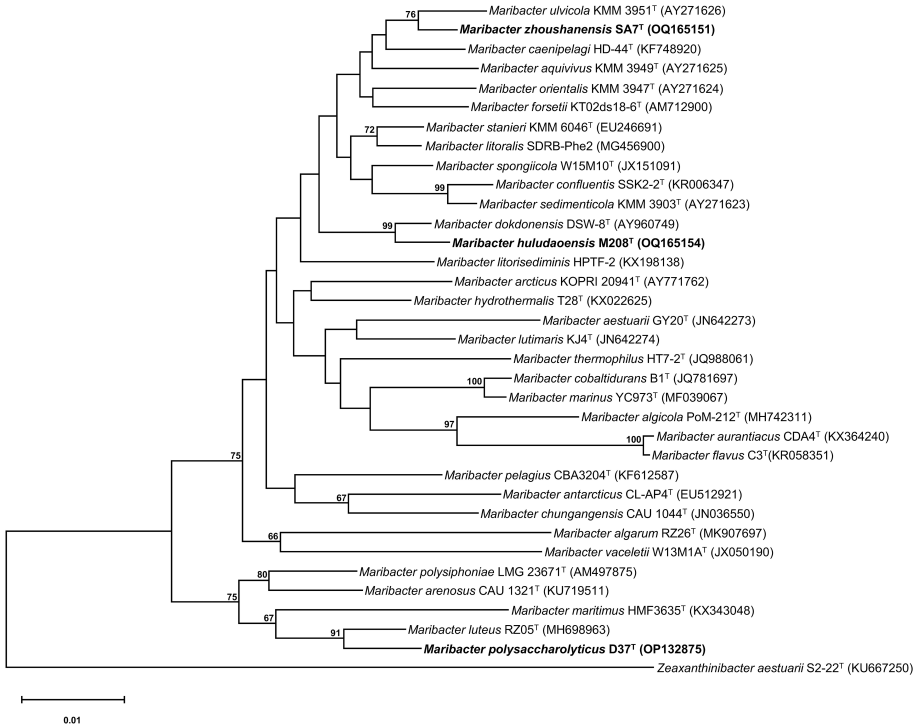

FIGURE 2
Neighbor-joining phylogenetic tree reconstructed with 16S rRNA gene sequences showing the relationships between strains D37^T, M208^T, and SA7^T and related taxa. Filled circles indicate branches recovered with both two methods (neighbor-joining and maximum-likelihood). Bootstrap values are based on 1000 replicates and values less than 65% are not shown. Bar, 0.01 substitutions per amino acid position. *Zeaxanthinibacter aestuarii* S2-22^T (KU667250) was used as an outgroup.

3.4 Comparative genomic analyses

3.4.1 *Maribacter* strains could be separated into two groups based on the genomic features

We performed a comparative genomic analysis of the genus *Maribacter*, including annotating the CAZyme, peptidase, and sulfatase in this genus and calculated their gene densities, which were the ratios of CAZyme, peptidase, and sulfatase to genome size, respectively. (Supplementary Table S2). The CAZyme gene densities of the twenty-five *Maribacter* members ranged from 28 to 56 per/Mb. Among them, four strains including *M. arenosus* CAU121^T, *M. polysiphoniaae* KCTC 22021^T, strain D37^T, and *M. luteus* RZ05^T, showed higher CAZyme gene densities which were 45, 44, 47, and 56 per/Mb, respectively. The CAZyme gene densities of the other eighteen strains ranged from 28 to 39 per/Mb except *M. algarum* RZ26^T, *M. vaceletti* DSM 25230^T, and *M.antarcticus* DSM

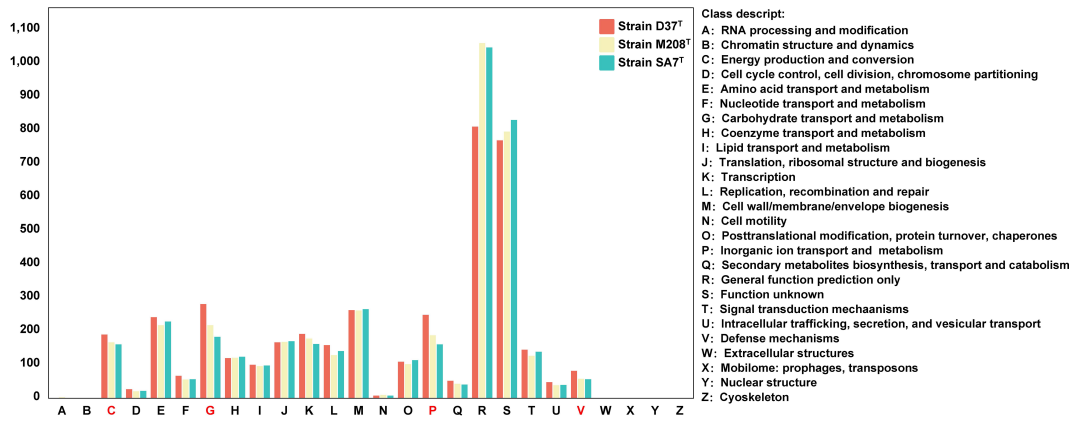

FIGURE 3
The annotation results of clusters of orthologous groups (COG) of the three novel strains. Groups in red means significant differences between three novel strains.

21422^T. The peptidase gene densities of the twenty-five *Maribacter* strains ranged from 48 to 78 per/Mb. Among them, four strains including *M. arenosus* CAU121^T, *M. polysiphoniaae* KCTC 22021^T, strain D37^T, and *M. luteus* RZ05^T showed lower peptidase gene densities which were 55, 56, 60, and 56 per/Mb, respectively. The peptidase gene densities of the other eighteen strains ranged from 55 to 66 per/Mb except *M. algarum* RZ26^T, *M. vaceletti* DSM 25230^T, and *M. antarcticus* DSM 21422^T. The sulfatase gene densities of the twenty-five *Maribacter* strains ranged from 52 to 83 per/Mb. Among them, four strains including *M. arenosus* CAU121^T, *M. polysiphoniaae* KCTC 22021^T, strain D37^T, *M. luteus* RZ05^T showed higher sulfatase gene densities which were 62, 69, 79, and 79 per/Mb, respectively. The sulfatase gene densities of the other eighteen strains ranged from 52 to 69 per/Mb except *M. algarum* RZ26^T, *M. vaceletti* DSM 25230^T, and *M.antarcticus* DSM 21422^T. According to the above results, the genus *Maribacter* strains were mainly divided into two groups. Four strains (*M. arenosus* CAU121^T, *M. polysiphoniaae* KCTC 22021^T, strain D37^T, *M. luteus* RZ05^T) were classified as group A, and except *M. algarum* RZ26^T, *M. vaceletii* DSM 25230^T, and *M. antarcticus* DSM 21422^T which were considered as transition strains, another 18 strains were clustered as group B (Figure 4). The principal component analysis (PCA) based on the number counts of CAZyme and peptidase in the twenty-five *Maribacter* strains supported this classification: all eighteen group B members were clearly clustered together and separated from four group A members (Figure 5) and the phylogenetic trees based on 16S rRNA genes also presented a similar phenomenon, in which four group A strains were clearly set apart from eighteen group B strains (Figure S9). The average gene densities of CAZyme and sulfatase in group A were higher than group B (48 vs 33 and 72 vs 61 per/Mb, Mann-Whitney *U* test; $p < 0.001$ for CAZyme and $p < 0.05$ for sulfatase). Furthermore, other genome features of these three groups including the genome size and the DNA G + C content also indicated that group A was different from group B (Figure 4). For example, the genome sizes of group B (4.0-4.6 Mb, average 4.3 Mb) were significantly smaller than that of group A (4.2-5.1 Mb, average 4.7 Mb) (t-test, $p < 0.05$). Meanwhile, the DNA G + C contents of group B (34.4%-41.8%, average 36.5%) were also significantly lower than that of group A (38.9%-41,7%, average 40.2%) (t-test, $p < 0.01$).

3.4.2 The composition of CAZyme was different between group A and group B

We further analyzed the composition and distribution of CAZyme after dividing *Maribacter* strains into two groups (Figure 6). Group A had more CAZyme than group B, in particular, group A encoded more GH families than group B (average 134 vs 63; t-test, $p < 0.001$), almost twice as much as group B. But the differences of CAZyme in PL, GT, AA, CE, and CBM were not so significant. The number counts of the CAZyme families including GH3, GH29, GH30, GH43, GH92, and GH130 in group A were significantly higher than group B, and GH76, GH94, and PL8 families were unique in group A. Besides, although the number counts of CAZyme families in group B were less than those in group A, GH74 family only existed in group B.

GH3 family has diverse functions that are usually related to degrading β-glucan in brown algae as exo-β-glucosidase activity

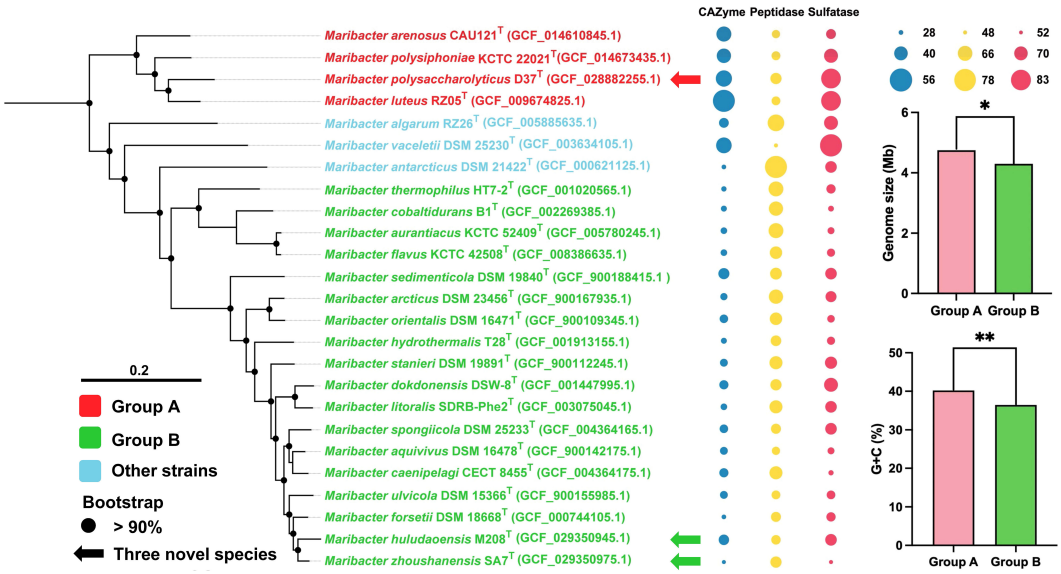

FIGURE 4
IQ-TREE reconstructed from single-copy orthologous protein sequences extracted from genome sequences showing the relationships between strains D37^T, M208^T, and SA7^T and related taxa (left panel). Bootstrap values are based on 1000 replicates and values less than 90% are not shown. Bar, 0.20 substitutions per amino acid position. The arrows represent novel species proposed in this study. Group A strains are in red and group B strains are in green. The bubbles chart (middle panel) shows the ratios of CAZyme (blue), peptidase (yellow) and sulfatase (red) to genome size, respectively and the bubble size represents the size of the ratios. The bar chart (right panel) shows the genome sizes and G + C contents of strains in the two groups. *, significant (t-test, $p < 0.05$); **, very significant (t-test, $p < 0.01$).

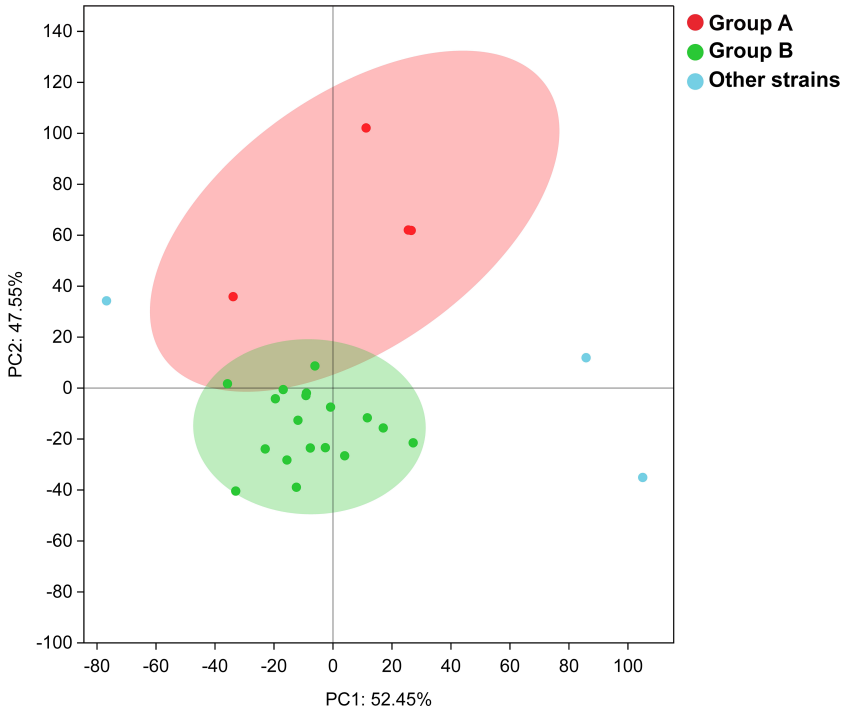

FIGURE 5
The PCA analysis result for the twenty-five *Maribacter* strains based on the number counts of CAZyme and peptidase.

(Tamura et al., 2017). GH3 family usually participates in laminarin degradation with GH17 family which has endo-β-glucosidase activity (Kappelmann et al., 2019). GH29 family mainly showed fucosidase activity and is related to the degradation of fucoidan (Grootaert et al., 2020). GH30 and GH43 families are broader in degradation capacities and both have β-xylosidase activity to degrade xylan, they can be more specific to mixed xylose-containing substrates (Qeshmi et al., 2020). The main function of GH92 family is exo-α-mannosidases activity (Chen et al., 2018), and it also has an exo-mode of action with mannosidase activities (Zhu et al., 2010; Teeling et al., 2016; Chen et al., 2018). GH130 family is a glycoside phosphorylase, which always degrades mannan with GH26 family (Cuskin et al., 2015). GH76 family shows the activity of endo-α-1,6-mannanase and usually hydrolyzes mannan with GH92 family (Solanki et al., 2022). GH94 family is a glycoside phosphorylase that may work with some other GH families to

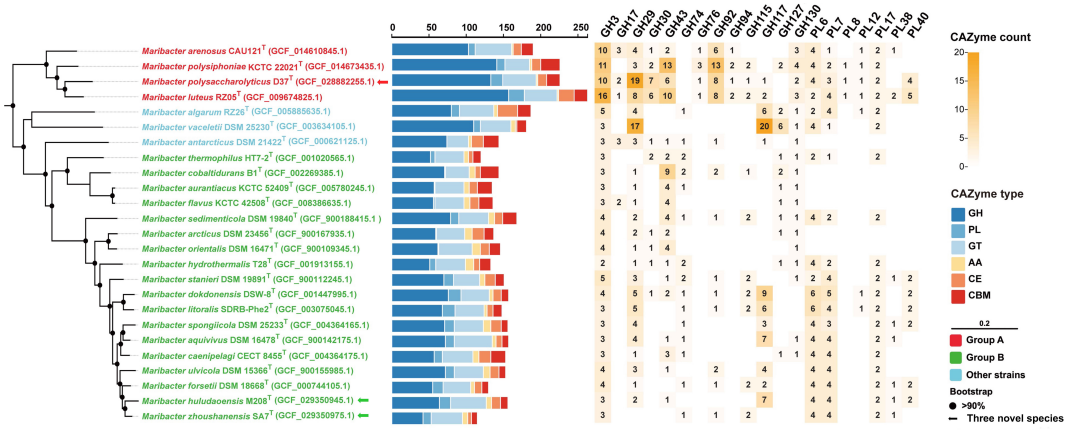

FIGURE 6
The phylogenomic tree based on single-copy orthologous protein sequences showing the relationships between strains D37^T, M208^T, and SA7^T and related taxa (left panel). Bootstrap values are based on 1000 replicates and values less than 90% are not shown. Bar, 0.20 substitutions per amino acid position. The arrows represent novel species proposed in this study. The quantities and categories sum of CAZymes (middle panel) includes GH (dark blue), PL (blue), GT (light blue), AA (yellow), CE (orange), and CBM (red). The numbers and the shade (right panel) means the number counts and relative abundance of selected CAZyme families in twenty-five members of the genus *Maribacter*.

degrade certain oligosaccharides of mannan (Senoura et al., 2011). PL8 family is usually predicted as hyaluronan and chondroitin activities, but it also shows exogenous specificity and synergy which indicates it may be a new type of alginate lyase family (Garron and Cygler, 2014; Pilgaard et al., 2019). Besides, GH74 family is generally considered as xyloglucanase e.g. endo-β-1,4-glucanases (Chen et al., 2022).

3.4.3 The unique PUL in group A is mannan-specific

In *Bacteroidota*, the polysaccharides degradation is usually carried out with distinct PULs. For example, GH92 family is always associated with the degradation of mannan, but the existence of sole GH92 family in the genome cannot fully explain whether it is truly able to degrade mannan. The existence of related PUL can further indicate that a strain has a relatively comprehensive degradation ability for a certain type of substrate. We found the number counts of GH92 family in group A was far higher than group B, and mannan-specific PULs were predicted only in group A strains including *M. arenosus* CAU121^T (1 PUL), *M. polysiphoniae* KCTC 22021^T (3 PULs), strain D37^T (2 PULs), and *M. luteus* RZ05^T (2 PULs), no mannan-specific PUL was found in group B. (Figure 7).

Mannan can be divided into α-mannan and β-mannan. α-mannan has the α-1, 6-D-mannose backbone, and most of the predicted mannan-specific PULs of group A degrade α-mannan, which were shown as three types: (1) PUL consists of transport proteins SusC/D, multiple GH92, one GH130 with certain other GH families, transcriptional regulator *LuxR* but with no sulfatase; the typical PULs were *M. arenosus* CAU121^T PUL1, *M. polysiphoniae* KCTC 22021^T PUL1, and *M. luteus* RZ05^T PUL2; (2) PUL with transport proteins SusC/D, α-mannan related CAZymes which had α-1,6-mannosidases activity or α-mannosidases activity such as GH76, GH125, or GH38; the typical PULs were *M. polysiphoniae* KCTC 22021^T PUL2, and *M. luteus* RZ05^T PUL1; (3) PUL contains transport proteins SusC/D, multiple GH92 with several other GH families, transcriptional regulator *LuxR* and abundant sulfatases; the typical PULs were PUL1 and PUL2 in strain D37^T. β-mannan contains β-1, 4-linked backbone with mannose as the major component, only one type of β-mannan-specific PUL was predicted in group A, which contained transport proteins SusC/D, GH130, and GH26 (endo-β-1,4-mannanases activity). The typical PUL was *M. luteus* RZ05^T PUL3.

3.4.4 The differences between group A and group B indicate their different niches

Marine bacteria exist in distinct environments, while marine *Bacteroidota* is considered to have two types of existing modes (Fernández-Gómez et al., 2013). For instance, marine *Bacteroidota* emerges as important responders during algal blooms, many of them exhibit a significant portion of macroalgae-related representatives (Kruger et al., 2019). The number of *Polaribacter* strains are associated with algae degradation, it has shown a significant increase during North Sea algal blooms (Avci et al., 2020). Besides marine *Bacteroidota*, certain marine heterotrophic bacteria also have evolved the capability to thrive on algal polysaccharides, such as *Pseudoalteromonas* strains which are mainly isolated from red algae, the analysis of the genomes of these strains revealed a high abundance of carbohydrate-active enzymes (Gobet et al., 2018). Meanwhile, marine flavobacterium *Dokdonia donghaensis* MED134^T prefers low-nutrition environments and possesses a small genome size, and it encodes more peptidase rather than CAZyme for growth through genome analysis, which reveals that this strain has few potentials for degrading algal polysaccharides (Gonzalez et al., 2011). The genome analysis for *Polaribacter* sp. MED152 reveals multitudinous presence genes associated with motility and proteorhodopsin, and these genetic traits potentially contribute to its ability to thrive in nutrient-poor marine surface environments (Gonzalez et al., 2008).

The ratio of CAZyme combined with peptidase can be utilized for niche assessment (Fernández-Gómez et al., 2013; Mann et al., 2013;

FIGURE 7
PULs related to mannan degradation in group A. The function genes in PULs included SusC/D genes (yellow), GH family (red), transcriptional regulator (purple), sulfatase (blue), and the GH families (red font).

Unfried et al., 2018). The high proportion of CAZyme and low proportion of peptidase are considered to be a "particle-associated" mode of existence, and the abundant presence of peptidase in the genome is considered to be one of the indicators for a "free-living" mode of existence (Gonzalez et al., 2011; Fernández-Gómez et al., 2013; Xing et al., 2015; Xue et al., 2020). Some marine bacteria contain certain numbers of CAZymes (not in high proportion) in the genome, and they may also prefer an oligotrophic marine environment and "free-living" mode (Xu et al., 2015; Arnosti et al., 2021). In addition, the algal polysaccharides are the primary constituent of the cell wall in marine algae and encompass a wide range of sulfated polysaccharides such as fucoidan, carrageenan and ulvan (Ramanan et al., 2016; Hentati et al., 2020). The abundant presence of sulfatase in the genome can also reflect the preference of strains to algal abundant environments. Our study found the gene densities of CAZyme and sulfatase in group A were high, while the gene densities of peptidase were relatively low. On the contrary, group B possessed higher gene densities of peptidase than CAZyme and sulfatase. Nevertheless, smaller genomes may enhance the adaptability of strains to oligotrophic marine environments (Qin et al., 2019; Liang et al., 2022). A smaller genome may be an adaptation strategy to reduce costs in microbial DNA replication, and the lower DNA G + C content can reduce the energy consumption in the process of bacterial replication in the oligotrophic environment (Luo and Moran, 2015). As a result, particle-associated bacteria prefer to have larger genome sizes than free-living bacteria which are usually found in oligotrophic environments (Luo et al., 2014). Our results indicate that the genome size and the DNA G + C content of group A are much higher than those of group B. Therefore, through the average gene densities of CAZyme, peptidase and sulfatase, and other genomic features, we propose that two groups may have different niche adaptation strategies to different marine environments. Group A can be assigned as the "particle-associated" mode of existence, while group B is the "free-living" mode of existence.

We further analyzed the detailed profiles of CAZyme in different groups. The results show that group A had more CAZyme than group B whether in total number count or diversity, including GH3, GH29, GH30, GH43, GH92, and GH130 families, which are related to the degradation of laminarin, fucoidan, mannan, xylose, and xylan, respectively. This phenomenon is similar to other algae-associated paradigms observed in other well-studied marine flavobacteria strains in the genus *Gramellai* and *Polaribacter* (Kabisch et al., 2014; Xing et al., 2015). Furthermore, mannan mainly comes from various algae, including red and green algae. For example, sulfated α-1,3-linked D-mannan is found in red alga *Nothogenia fastigiate* (Kolender et al., 1997) and mixed-linkage mannan exists in green alga *Codium fragile* (Tabarsa et al., 2013). GH92 family is considered as the specific CAZyme related to mannan degradation and widely occurs in *Flavobacteriaceae* (Teeling et al., 2012; Zeugner et al., 2021). Our research also showed that GH92 family was abundant in group A and the mannan-specific PUL only appeared in this group. This can be further evidence for the proposed "particle-associated" mode of existence of group A.

4 Conclusions

Phenotypic and genotypic characterization analysis of strains D37^T, M208^T, and SA7^T in this study shows unequivocally that the three strains should be assigned as novel species of the genus *Maribacter*, for which the names are proposed as *Maribacter polysaccharolyticus* sp. nov., *Maribacter huludaoensis* sp. nov., and *Maribacter zhoushanensis* sp. nov., respectively. Furthermore, we compared all available genomes of *Maribacter* representatives and determined that they could be divided into two groups (A and B). Two groups are different in gene densities of CAZyme, peptidase and sulfatase, genome size and G + C content. Group A possesses more CAZymes and sulfatases than group B, especially in GH families including GH3, GH29, GH30, GH43, GH92, and GH130 which are related to degrading laminarin, fucoidan, mannan, xylose, and xylan, respectively. In addition, mannan-specific PUL is only found in group A. These results indicate that two groups have different niche adaptation strategies, and we consider that group A uses the "particle-associated" strategy of existence and prefers the niche in environments with enriched marine polysaccharides, while group B uses the "free-living" strategy of existence and prefers the niche in oligotrophic marine.

4.1 Description of *Maribacter polysaccharolyticus* sp. Nov.

Maribacter polysaccharolyticus (po.ly.sac.cha.ro.ly'ti.cus. Gr. Masc. adj. *polys*, many; Gr. Neut. N. *sakcharon*, sugar; Gr. Masc. adj.*lytikos*, dissolving; N.L. masc. adj. *polysaccharolyticus*, many sugars dissolving).

Cells are Gram-stain-negative, strictly aerobic, non-motile, oxidase-positive and catalase-positive. Cells are rod-shaped with 1.8-3.3 μm in length and 0.6-0.8 μm in width. Colonies are orange, 1-2mm in diameter, round, opaque, border smooth, and convex. Growth can be observed at 15-37 °C (optimum, 28 °C), pH 5.5-8.5 (optimum, pH 7.0), and with 0-6% (w/v) NaCl (optimum, 2.0-3.5%). In the API 20NE test, cells were positive for reduction of nitrate to nitrite, fermentation of glucose, hydrolyzation of esculin and β-galactosidase. In the API ZYM test, alkaline phosphatase, leucine arylamidase, valine arylamidase, trypsin, acid phosphatase, napthol-AS-BI-phosphorylase, and N-acetyl-β-glucosaminidase are positive. esterase (C4), esterase lipase (C8), cysteine arylamidase, chymotrypsin, and β-fucosidase are weak. Acid is produced from glycerol, D-arabinose, D-xylose, D-galactose, D-glucose, D-fructose, D-mannose, D-mannitol, methyl-αD-mannopyranoside, methyl-αD-glucopyranoside, N-acetyl-glucosamine, amygdalin, arbutin, esculin ferric citrate, salicin, D-cellobiose, D-maltose, D-lactose, D-melibiose, D-saccharose, D-trehalose, inulin, D-melezitose, D-raffinose, starch, glycogen, xylitol, gentiobiose, D-turanose, L-fucose, and potassium 2-ketogluconate. The major fatty acids (>10%) are iso-$C_{15:0}$ and iso-$C_{17:0}$ 3-OH. The major respiratory quinone is MK-6. The major polar lipids contain phosphatidylethanolamine, two unidentified glycolipids, one unidentified aminolipid, and three unidentified lipids. The G+C content based on the genome sequence is 41.7%.

The strain D37^T (=MCCC 1K06123^T =KCTC 82772^T) was isolated from an intertidal sediment sample collected from Zhoushan, Zhejiang, PR China (21°35′ N, 109°9′ E). The GenBank accession numbers for the 16S rRNA gene and genome sequences of strain D37^T are OP132875 and GCF_014610845.1, respectively.

4.2 Description of *Maribacter huludaoensis* sp. nov.

Maribacter huludaoensis (hu.lu.dao.en'sis. N.L. masc./fem. adj. *huludaoensis*, pertaining to Huludao, PR China, where the strain was isolated).

Cells are Gram-stain-negative, strictly aerobic, non-motile, oxidase-weakly, and catalase-negative. Cells are rod-shaped with 1.7-2.7 μm in length and 0.3-0.4 μm in width. Colonies are orange, 1-2mm in diameter, round, opaque, border smooth and convex. Growth can be observed at 4-35°C (optimum, 28°C), pH 6.0-8.5 (optimum, pH 6.5) and with 0.5-6.0% (w/v) NaCl (optimum, 1.5-2.5%). Cellulose, tyrosine, Tween 20, 40, 60, and 80 are hydrolyzed, but starch and casein are not hydrolyzed. In the API 20NE test, cells were positive for reduction of nitrate to nitrite, hydrolyzation of esculin and *β*-galactosidase. In the API ZYM test, alkaline phosphatase, leucine arylamidase, valine arylamidase, chymotrypsin, acid phosphatase, napthol-AS-BI-phosphorylase, *β*-galactosidase, *α*-glucosidase, and N-acetyl-*β*-glucosaminidase are positive. Esterase (C4), esterase lipase (C8), cysteine arylamidase, trypsin, α-galactosidase, *β*-fucosidase, and α-mannosidase are weak. Acid is produced from D-xylose, methyl-*β*D-xylopyranoside (weakly), D-galactose, D-glucose, D-fructose (weakly), D-mannose (weakly), L-rhamnose, methyl-*α*D-mannopyranoside (weakly), methyl-*α*D-glucopyranoside, N-acetyl-glucosamine (weakly), amygdalin, arbutin, esculin ferric citrate, salicin, D-cellobiose, D-maltose, D-lactose, D-melibiose, D-saccharose, D-trehalose, inulin (weakly), D-melezitose (weakly), D-raffinose, gentiobiose, D-turanose, and potassium gluconate. The major fatty acids (>10%) are iso-$C_{15:0}$, iso-$C_{17:0}$ 3-OH, Summed Feature 1, and Summed Feature 3. The major respiratory quinone is MK-6. The major polar lipids comprise phosphatidylethanolamine, two unidentified glycolipids, one unidentified aminolipid, and two unidentified lipids. The G+C content based on the genome sequence is 35.9%.

The strain M208^T (=MCCC 1K08510^T =KCTC 82763^T) is an intertidal sediment sample taken from the coastal zone of Huludao, Liaoning, PR China (40°41′ N, 120°56′ E). The GenBank accession numbers for the 16S rRNA gene and genome sequences of strain M208^T are OQ165154 and GCF_029350945.1, respectively.

4.3 Description of *Maribacter zhoushanensis* sp. nov.

Maribacter zhoushanensis (zhou.shan.en'sis. N.L. masc./fem. adj. *zhoushanense*, pertaining to Zhoushan, eastern China, where the strain was isolated)

Cells are Gram-stain-negative, strictly aerobic, non-motile, oxidase-weakly, and catalase-negative. Cells are rod-shaped with 1.5-3 μm in length and 0.6-0.8 μm in width. Colonies are orange, 0.5-1mm in diameter, round, opaque, border smooth, and convex. Growth can be observed at 4-30°C (optimum, 25°C), pH 5.5-9.0 (optimum, pH 7.0), and with 0.5-6.0% (w/v) NaCl (optimum, 1-3%). Cellulose, tyrosine, Tween 20, 40, 60, and 80 are hydrolyzed, but starch and casein are not hydrolyzed. In the API 20NE test, cells were positive for reduction of nitrate to nitrite, hydrolyzation of esculin and *β*-galactosidase. In the API ZYM test, alkaline phosphatase, esterase (C4), esterase lipase (C8), leucine arylamidase, valine arylamidase, acid phosphatase, napthol-AS-BI-phosphorylase, *α*-glucosidase, and N-acetyl-*β*-glucosaminidase are positive. Chymotrypsin, *α*-galactosidase and *α*-mannosidase are weak. Acid is produced from D-xylose, methyl-*β*D-xylopyranoside (weakly), D-galactose, D-glucose, D-fructose, D-mannose, D-mannitol, methyl- *α*D-mannopyranoside (weakly), methyl-*α*D-glucopyranoside, N-acetyl-glucosamine, amygdalin, arbutin, esculin ferric citrate, salicin, D-cellobiose, D-maltose, D-lactose, D-melibiose, D-saccharose, D-trehalose, inulin (weakly), D-melezitose (weakly), D-raffinose, starch, glycogen (weakly), xylitol (weakly), gentiobiose, D-turanose, potassium gluconate, and potassium 2-ketogluconate. The major fatty acids (>10%) are iso-$C_{15:0}$, iso-$C_{17:0}$ 3-OH, and Summed feature 1. The major respiratory quinone is MK-6. The major polar lipids consist of phosphatidylethanolamine, three unidentified glycolipids, one unidentified aminolipid, and three unidentified lipids. The G+C content based on the genome sequence is 34.8%.

The strain SA7^T (=MCCC 1K08511^T =KCTC 82773^T) was isolated from an intertidal sediment sample collected from Zhoushan, Zhejiang, PR China (21°35′ N, 109°9′ E). The GenBank accession numbers for the 16S rRNA gene and genome sequences of strain SA7^T are OQ165151 and GCF_029350975.1, respectively.

Data availability statement

The original contributions presented in the study are publicly available. This data can be found here: https://www.ncbi.nlm.nih.gov/, accession number: OP132875, OQ165154, OQ165151, JARBUY000000000, JARKMS000000000 and JARKMR000000000.

Author contributions

J-WG and HD collected the samples and isolated these strains. J-WG, J-JY, W-JL, and D-YH performed data collection and analysis. J-WG and CS wrote the manuscript. LX and CS performed project guidance and critical revision of manuscripts. All authors contributed to the article and approved the submitted version.

Funding

This study was supported by National Science and Technology Fundamental Resources Investigation Program of China

(2019FY100700), Zhejiang Provincial Natural Science Foundation of China (LDT23D06025D06), the Key R&D Program of Zhejiang (#2023C03011), National Natural Science Foundation of China (No. 31900003), and the Fundamental Research Funds of Zhejiang Sci-Tech University (22042315-Y).

Conflict of interest

Authors J-WG, J-JY, W-JL, LX, and CS are employed by Shaoxing Biomedical Research Institute of Zhejiang Sci-Tech University Co., Ltd.

The remaining authors declare that the research was conducted in the absence of any commercial or financial relationships that could be construed as a potential conflict of interest.

Publisher's note

Supplementary material

The Supplementary Material for this article can be found online at: https://www.frontiersin.org/articles/10.3389/fmars.2023.1248754/full#supplementary-material

References

Arnosti, C., Wietz, M., Brinkhoff, T., Hehemann, J. H., Probandt, D., Zeugner, L., et al. (2021). The biogeochemistry of marine polysaccharides: sources, inventories, and bacterial drivers of the carbohydrate cycle. *Ann. Rev. Mar. Sci.* 13, 81–108. doi: 10.1146/annurev-marine-032020-012810

Avci, B., Kruger, K., Fuchs, B. M., Teeling, H., and Amann, R. I. (2020). Polysaccharide niche partitioning of distinct *Polaribacter* clades during North Sea spring algal blooms. *ISME J.* 14, 1369–1383. doi: 10.1038/s41396-020-0601-y

Aziz, R. K., Bartels, D., Best, A. A., DeJongh, M., Disz, T., Edwards, R. A., et al. (2008). The RAST Server: rapid annotations using subsystems technology. *BMC Genomics* 75, 1–15. doi: 10.1186/1471-2164-9-75

Barbeyron, T., Carpentier, F., L'Haridon, S., Schuler, M., Michel, G., and Amann, R. (2008). Description of Maribacter forsetii sp. nov., a marine *Flavobacteriaceae* isolated from North Sea water, and emended description of the genus *Maribacter*. *Int. J. Syst. Evol. Microbiol.* 58, 790–797. doi: 10.1099/ijs.0.65469-0

Barbeyron, T., Thomas, F., Barbe, V., Teeling, H., Schenowitz, C., Dossat, C., et al. (2016). Habitat and taxon as driving forces of carbohydrate catabolism in marine heterotrophic bacteria: example of the model algae-associated bacterium *Zobellia galactanivorans* Dsij(T). *Environ. Microbiol.* 18, 4610–4627. doi: 10.1111/1462-2920.13584

Bartlau, N., Wichels, A., Krohne, G., Adriaenssens, E. M., Heins, A., Fuchs, B. M., et al. (2022). Highly diverse flavobacterial phages isolated from North Sea spring blooms. *ISME J.* 16, 555–568. doi: 10.1038/s41396-021-01097-4

Bennke, C. M., Kruger, K., Kappelmann, L., Huang, S., Gobet, A., Schuler, M., et al. (2016). Polysaccharide utilisation loci of Bacteroidetes from two contrasting open ocean sites in the North Atlantic. *Environ. Microbiol.* 18, 4456–4470. doi: 10.1111/1462-2920.13429

Cantalapiedra, C. P., Hernandez-Plaza, A., Letunic, I., Bork, P., and Huerta-Cepas, J. (2021). eggNOG-mapper v2: Functional Annotation, Orthology Assignments, and Domain Prediction at the Metagenomic Scale. *Mol. Biol. Evol.* 38, 5825–5829. doi: 10.1093/molbev/msab293

Capella-Gutierrez, S., Silla-Martinez, J. M., and Gabaldon, T. (2009). trimAl: a tool for automated alignment trimming in large-scale phylogenetic analyses. *Bioinformatics* 25, 1972–1973. doi: 10.1093/bioinformatics/btp348

Chen, J., Robb, C. S., Unfried, F., Kappelmann, L., Markert, S., Song, T., et al. (2018). Alpha- and beta-mannan utilization by marine Bacteroidetes. *Environ. Microbiol.* 20, 4127–4140. doi: 10.1111/1462-2920.14414

Chen, M., Ropartz, D., Mac-Bear, J., Bonnin, E., and Lahaye, M. (2022). New insight into the mode of action of a GH74 xyloglucanase on tamarind seed xyloglucan: Action pattern and cleavage site. *Carbohydr Res.* 521, 108661. doi: 10.1016/j.carres.2022.108661

Chun, J., Oren, A., Ventosa, A., Christensen, H., Arahal, D. R., da Costa, M. S., et al. (2018). Proposed minimal standards for the use of genome data for the taxonomy of prokaryotes. *Int. J. Syst. Evol. Microbiol.* 68, 461–466. doi: 10.1099/ijsem.0.002516

Cuskin, F., Basle, A., Ladeveze, S., Day, A. M., Gilbert, H. J., Davies, G. J., et al. (2015). The GH130 family of mannoside phosphorylases contains glycoside hydrolases that target beta-1,2-mannosidic linkages in candida mannan. *J. Biol. Chem.* 290, 25023–25033. doi: 10.1074/jbc.M115.681460

Do, K.-A. (1992). A simulation study of balanced and antithetic bootstrap resampling methods. *J. Stat. Comput. Simulation* 40, 153–166. doi: 10.1080/00949659208811373

Fang, C., Wu, Y. H., Xamxidin, M., Wang, C. S., and Xu, X. W. (2017). *Maribacter cobaltidurans* sp. nov., a heavy-metal-tolerant bacterium isolated from deep-sea sediment. *Int. J. Syst. Evol. Microbiol.* 67, 5261–5267. doi: 10.1099/ijsem.0.002458

Felsenstein, J. (1981). Evolutionary trees from DNA sequences: a maximum likelihood approach. *J. Mol. Evol.* 17, 368–376. doi: 10.1007/bf01734359

Fernández-Gómez, B., Richter, M., Schüler, M., Pinhassi, J., Acinas, S. G., González, J. M., et al. (2013). Ecology of marine Bacteroidetes: a comparative genomics approach. *ISME J.* 7, 1026–1037. doi: 10.1038/ismej.2012.169

Ficko-Blean, E., Prechoux, A., Thomas, F., Rochat, T., Larocque, R., Zhu, Y., et al. (2017). Carrageenan catabolism is encoded by a complex regulon in marine heterotrophic bacteria. *Nat. Commun.* 8, 1685. doi: 10.1038/s41467-017-01832-6

Fitch, W. M. (1971). Toward defining the course of evolution: minimum change for a specific tree topology. *Systematic Biol.* 20, 406–416. doi: 10.1093/sysbio/20.4.406

Gao, J. W., He, D. Y., Zhang, W. W., Wang, Y. R., Su, Y., Ying, J. J., et al. (2023). *Aestuariibaculum lutulentum* sp. nov., a marine bacterium isolated from coastal sediment in Beihai. *Arch. Microbiol.* 187, 205. doi: 10.1007/s00203-023-03535-7

Garron, M. L., and Cygler, M. (2014). Uronic polysaccharide degrading enzymes. *Curr. Opin. Struct. Biol.* 28, 87–95. doi: 10.1016/j.sbi.2014.07.012

Gavriilidou, A., Gutleben, J., Versluis, D., Forgiarini, F., van Passel, M. W. J., Ingham, C. J., et al. (2020). Comparative genomic analysis of *Flavobacteriaceae*: insights into carbohydrate metabolism, gliding motility and secondary metabolite biosynthesis. *BMC Genomics* 569, 1–21. doi: 10.1186/s12864-020-06971-7

Gobet, A., Barbeyron, T., Matard-Mann, M., Magdelenat, G., Vallenet, D., Duchaud, E., et al. (2018). Evolutionary evidence of algal polysaccharide degradation acquisition by *pseudoalteromonas carrageenovora* 9(T) to adapt to macroalgal niches. *Front. Microbiol.* 9, 2740. doi: 10.3389/fmicb.2018.02740

Gonzalez, J. M., Fernandez-Gomez, B., Fernandez-Guerra, A., Gomez-Consarnau, L., Sanchez, O., Coll-Llado, M., et al. (2008). Genome analysis of the proteorhodopsin-containing marine bacterium Polaribacter sp. MED152 (*Flavobacteria*). *Proc. Natl. Acad. Sci. U.S.A.* 105, 8724–8729. doi: 10.1073/pnas.0712027105

Gonzalez, J. M., Pinhassi, J., Fernandez-Gomez, B., Coll-Llado, M., Gonzalez-Velazquez, M., Puigbo, P., et al. (2011). Genomics of the proteorhodopsin-containing marine flavobacterium Dokdonia sp. strain MED134. *Appl. Environ. Microbiol.* 77, 8676–8686. doi: 10.1128/AEM.06152-11

Grootaert, H., Van Landuyt, L., Hulpiau, P., and Callewaert, N. (2020). Functional exploration of the GH29 fucosidase family. *Glycobiology* 30, 735–745. doi: 10.1093/glycob/cwaa023

Hentati, F., Tounsi, L., Djomdi, D., Pierre, G., Delattre, C., Ursu, A. V., et al. (2020). Bioactive polysaccharides from seaweeds. *Molecules.* 25, 3152. doi: 10.3390/molecules25143152

Jackson, S. A., Kennedy, J., Morrissey, J. P., O'Gara, F., and Dobson, A. D. W. (2015). *Maribacter spongiicola* sp. nov. and Maribacter vaceletii sp. nov., isolated from marine sponges, and emended description of the genus *Maribacter*. *Int. J. Syst. Evol. Microbiol.* 65, 2097–2103. doi: 10.1099/ijs.0.000224

Jin, M., Kim, M., Kim, J. Y., Song, H. S., Cha, I. T., Roh, S. W., et al. (2017). *Maribacter pelagius* sp. nov., isolated from seawater. *Int. J. Syst. Evol. Microbiol.* 67, 3834–3839. doi: 10.1099/ijsem.0.002203

Jung, Y. T., Lee, J. S., and Yoon, J. H. (2014). *Maribacter caenipelagi* sp. nov., a member of the Flavobacteriaceae isolated from a tidal flat sediment of the Yellow Sea in Korea. *Antonie Van Leeuwenhoek* 106, 733–742. doi: 10.1007/s10482-014-0243-z

Kabisch, A., Otto, A., Konig, S., Becher, D., Albrecht, D., Schuler, M., et al. (2014). Functional characterization of polysaccharide utilization loci in the marine Bacteroidetes '*Gramella forsetii*' KT0803. *ISME J.* 8, 1492–1502. doi: 10.1038/ismej.2014.4

Kanehisa, M., Furumichi, M., Tanabe, M., Sato, Y., and Morishima, K. (2017). KEGG: new perspectives on genomes, pathways, diseases and drugs. *Nucleic Acids Res.* 45, D353–D361. doi: 10.1093/nar/gkw1092

Kang, H., Cha, I., Kim, H., and Joh, K. (2018). Maribacter maritimus sp. nov., isolated from seawater. *Int. J. Syst. Evol. Microbiol.* 68, 2431–2436. doi: 10.1099/ijsem.0.002843

Kappelmann, L., Kruger, K., Hehemann, J. H., Harder, J., Markert, S., Unfried, F., et al. (2019). Polysaccharide utilization loci of North Sea Flavobacteriia as basis for using SusC/D-protein expression for predicting major phytoplankton glycans. *ISME J.* 13, 76–91. doi: 10.1038/s41396-018-0242-6

Katoh, K., and Standley, D. M. (2013). MAFFT multiple sequence alignment software version 7: improvements in performance and usability. *Mol. Biol. Evol.* 30, 772–780. doi: 10.1093/molbev/mst010

Khan, S. A., Jeong, S. E., Baek, J. H., and Jeon, C. O. (2020). Maribacter algicola sp. nov., isolated from a marine red alga, Porphyridium marinum, and transfer of Maripseudobacter aurantiacus Chen et al. 2017 to the genus Maribacter as Maribacter aurantiacus comb. nov. *Int. J. Syst. Evol. Microbiol.* 70, 797–804. doi: 10.1099/ijsem.0.003828

Kim, M., Oh, H.-S., Park, S.-C., and Chun, J. (2014). Towards a taxonomic coherence between average nucleotide identity and 16S rRNA gene sequence similarity for species demarcation of prokaryotes. *Int. J. Systematic Evolutionary Microbiol.* 64, 346–351. doi: 10.1099/ijs.0.059774-0

Kimura, M. (1980). A simple method for estimating evolutionary rates of base substitutions through comparative studies of nucleotide sequences. *J. Mol. Evol.* 16, 111–120. doi: 10.1007/bf01731581

Klippel, B., Lochner, A., Bruce, D. C., Davenport, K. W., Detter, C., Goodwin, L. A., et al. (2011). Complete genome sequences of Krokinobacter sp. strain 4H-3-7-5 and *Lacinutrix* sp. strain 5H-3-7-4, polysaccharide-degrading members of the family *Flavobacteriaceae*. *J. Bacteriol* 193, 4545–4546. doi: 10.1128/JB.05518-11

Kolender, A. A., Pujol, C. A., Damonte, E. B., Matulewicz, M. C., and Cerezo, A. S. (1997). The system of sulfated alpha-(1–>3)-linked D-mannans from the red seaweed *Nothogenia fastigiata*: structures, antiherpetic and anticoagulant properties. *Carbohydr. Res.* 304, 53–60. doi: 10.1016/s0008-6215(97)00201-2

Kruger, K., Chafee, M., Ben Francis, T., Glavina Del Rio, T., Becher, D., Schweder, T., et al. (2019). In marine Bacteroidetes the bulk of glycan degradation during algae blooms is mediated by few clades using a restricted set of genes. *ISME J.* 13, 2800–2816. doi: 10.1038/s41396-019-0476-y

Lagesen, K., Hallin, P., Rodland, E. A., Staerfeldt, H. H., Rognes, T., and Ussery, D. W. (2007). RNAmmer: consistent and rapid annotation of ribosomal RNA genes. *Nucleic Acids Res.* 35, 3100–3108. doi: 10.1093/nar/gkm160

Lee, I., Ouk Kim, Y., Park, S. C., and Chun, J. (2016). OrthoANI: An improved algorithm and software for calculating average nucleotide identity. *Int. J. Syst. Evol. Microbiol.* 66, 1100–1103. doi: 10.1099/ijsem.0.000760

Liang, J. C., Liu, J. W., Wang, X. L., Sun, H., Zhang, Y. L., Ju, F., et al. (2022). Genomic analysis reveals adaptation of *vibrio campbellii* to the hadal ocean? *Appl. Environ. Microbiol.* 88, 00575–22. doi: 10.1128/aem.00575-22

Liu, A., Zhang, Y. J., Liu, D. K., and Li, X. Z. (2020). *Maribacter luteus* sp. nov., a marine bacterium isolated from intertidal sand of the Yellow Sea. *Int. J. Syst. Evol. Microbiol.* 70, 3497–3503. doi: 10.1099/ijsem.0.004206

Lo, N., Jin, H. M., and Jeon, C. O. (2013). *Maribacter aestuarii* sp. nov., isolated from tidal flat sediment, and an emended description of the genus *Maribacter*. *Int. J. Syst. Evol. Microbiol.* 63, 3409–3414. doi: 10.1099/ijs.0.050054-0

Luo, H., and Moran, M. A. (2015). How do divergent ecological strategies emerge among marine bacterioplankton lineages? *Trends Microbiol.* 23, 577–584. doi: 10.1016/j.tim.2015.05.004

Luo, H., Swan, B. K., Stepanauskas, R., Hughes, A. L., and Moran, M. A. (2014). Evolutionary analysis of a streamlined lineage of surface ocean Roseobacters. *ISME J.* 8, 1428–1439. doi: 10.1038/ismej.2013.248

Mann, A. J., Hahnke, R. L., Huang, S., Werner, J., Xing, P., Barbeyron, T., et al. (2013). The genome of the alga-associated marine flavobacterium *Formosa agariphila* KMM 3901T reveals a broad potential for degradation of algal polysaccharides. *Appl. Environ. Microbiol.* 79, 6813–6822. doi: 10.1128/AEM.01937-13

Meier-Kolthoff, J. P., Auch, A. F., Klenk, H. P., and Goker, M. (2013). Genome sequence-based species delimitation with confidence intervals and improved distance functions. *BMC Bioinf.* 14, 1–14. doi: 10.1186/1471-2105-14-60

Nedashkovskaya, O. I., Kim, S. B., Han, S. K., Lysenko, A. M., Rohde, M., Rhee, M. S., et al. (2004). *Maribacter* gen. nov., a new member of the family *Flavobacteriaceae*, isolated from marine habitats, containing the species Maribacter sedimenticola sp. nov., *Maribacter aquivivus* sp. nov., *Maribacter orientalis* sp. nov. and *Maribacter ulvicola* sp. nov. *Int. J. Syst. Evol. Microbiol.* 54, 1017–1023. doi: 10.1099/ijs.0.02849-0

Nedashkovskaya, O. I., Kim, S. B., and Mikhailov, V. V. (2010). *Maribacter stanieri* sp. nov., a marine bacterium of the family Flavobacteriaceae. *Int. J. Syst. Evol. Microbiol.* 60, 214–218. doi: 10.1099/ijs.0.012286-0

Nedashkovskaya, O. I., Vancanneyt, M., De Vos, P., Kim, S. B., Lee, M. S., and Mikhailov, V. V. (2007). *Maribacter polysiphoniae* sp. nov., isolated from a red alga. *Int. J. Syst. Evol. Microbiol.* 57, 2840–2843. doi: 10.1099/ijs.0.65181-0

Niu, L., Xie, X., Li, Y., Hu, Q., Wang, C., Zhang, W., et al. (2022). Effects of nitrogen on the longitudinal and vertical patterns of the composition and potential function of bacterial and archaeal communities in the tidal mudflats. *Sci. Total Environ.* 806, 151210. doi: 10.1016/j.scitotenv.2021.151210

Park, S., Jung, Y. T., Won, S. M., and Yoon, J. H. (2016). *Maribacter litorisediminis* sp. nov., isolated from a tidal flat. *Int. J. Syst. Evol. Microbiol.* 66, 4236–4242. doi: 10.1099/ijsem.0.001341

Parks, D. H., Imelfort, M., Skennerton, C. T., Hugenholtz, P., and Tyson, G. W. (2015). CheckM: assessing the quality of microbial genomes recovered from isolates, single cells, and metagenomes. *Genome Res.* 25, 1043–1055. doi: 10.1101/gr.186072.114

Pilgaard, B., Wilkens, C., Herbst, F. A., Vuillemin, M., Rhein-Knudsen, N., Meyer, A. S., et al. (2019). Proteomic enzyme analysis of the marine fungus *Paradendryphiella salina* reveals alginate lyase as a minimal adaptation strategy for brown algae degradation. *Sci. Rep.* 9, 12338. doi: 10.1038/s41598-019-48823-9

Qeshmi, F. I., Homaei, A., Fernandes, P., Hemmati, R., Dijkstra, B. W., and Khajeh, K. (2020). Xylanases from marine microorganisms: A brief overview on scope, sources, features and potential applications. *Biochim. Biophys. Acta Proteins Proteom* 1868, 140312. doi: 10.1016/j.bbapap.2019.140312

Qin, Q. L., Li, Y., Sun, L. L., Wang, Z. B., Wang, S., Chen, X. L., et al. (2019). Trophic specialization results in genomic reduction in free-living marine idiomarina bacteria.*Mbio*. 10, 02545–18. doi: 10.1128/mBio.02545-18

Ramanan, R., Kim, B. H., Cho, D. H., Oh, H. M., and Kim, H. S. (2016). Algae-bacteria interactions: Evolution, ecology and emerging applications. *Biotechnol. Adv.* 34, 14–29. doi: 10.1016/j.bioteChadv.2015.12.003

Rawlings, N. D., Barrett, A. J., Thomas, P. D., Huang, X., Bateman, A., and Finn, R. D. (2018). The MEROPS database of proteolytic enzymes, their substrates and inhibitors in 2017 and a comparison with peptidases in the PANTHER database. *Nucleic Acids Res.* 46, D624–D632. doi: 10.1093/nar/gkx1134

Reisky, L., Prechoux, A., Zuhlke, M. K., Baumgen, M., Robb, C. S., Gerlach, N., et al. (2019). A marine bacterial enzymatic cascade degrades the algal polysaccharide ulvan. *Nat. Chem. Biol.* 15, 803–812. doi: 10.1038/s41589-019-0311-9

Romero, S., Schell, R. F., and Pennell, D. R. (1988). Rapid method for the differentiation of gram-positive and gram-negative bacteria on membrane filters. *J. Clin. Microbiol.* 26, 1378–1382. doi: 10.1128/jcm.26.7.1378-1382.1988

Rzhetsky, A., and Nei, M. (1992). Statistical properties of the ordinary least-squares, generalized least-squares, and minimum-evolution methods of phylogenetic inference. *J. Mol. Evol.* 35, 367–375. doi: 10.1007/bf00161174

Saitou, N., and Nei, M. (1987). The neighbor-joining method: a new method for reconstructing phylogenetic trees. *Mol. Biol. Evol.* 4, 406–425. doi: 10.1093/oxfordjournals.molbev.a040454

Schuerch, M., Spencer, T., and Evans, B. (2019). Coupling between tidal mudflats and salt marshes affects marsh morphology. *Mar. Geology* 412, 95–106. doi: 10.1016/j.margeo.2019.03.008

Senoura, T., Ito, S., Taguchi, H., Higa, M., Hamada, S., Matsui, H., et al. (2011). New microbial mannan catabolic pathway that involves a novel mannosylglucose phosphorylase. *Biochem. Biophys. Res. Commun.* 408, 701–706. doi: 10.1016/j.bbrc.2011.04.095

Solanki, V., Kruger, K., Crawford, C. J., Pardo-Vargas, A., Danglad-Flores, J., Hoang, K. L. M., et al. (2022). Glycoside hydrolase from the GH76 family indicates that marine Salegentibacter sp. Hel_I_6 consumes alpha-mannan from fungi. *ISME J.* 16, 1818–1830. doi: 10.1038/s41396-022-01223-w

Stam, M., Lelievre, P., Hoebeke, M., Corre, E., Barbeyron, T., and Michel, G. (2023). SulfAtlas, the sulfatase database: state of the art and new developments. *Nucleic Acids Res.* 51, D647–D653. doi: 10.1093/nar/gkac977

Sun, C., Fu, G. Y., Zhang, C. Y., Hu, J., Xu, L., Wang, R. J., et al. (2016). Isolation and Complete Genome Sequence of Algibacter alginolytica sp. nov., a Novel Seaweed-Degrading *Bacteroidetes* Bacterium with Diverse Putative Polysaccharide Utilization Loci. *Appl. Environ. Microbiol.* 82, 2975–2987. doi: 10.1128/AEM.00204-16

Sun, H., Gao, L., Xue, C., and Mao, X. (2020). Marine-polysaccharide degrading enzymes: Status and prospects. *Compr. Rev. Food Sci. Food Saf.* 19, 2767–2796. doi: 10.1111/1541-4337.12630

Sun, C., Huo, Y. Y., Liu, J. J., Pan, J., Qi, Y. Z., Zhang, X. Q., et al. (2014). *Thalassomonas eurytherma* sp. nov., a marine proteobacterium. *Int. J. Syst. Evol. Microbiol.* 64, 2079–2083. doi: 10.1099/ijs.0.058255-0

Sun, C., Xamxidin, M., Wu, Y. H., Cheng, H., Wang, C. S., and Xu, X. W. (2019). *Alteromonas alba* sp. nov., a marine bacterium isolated from seawater of the West Pacific Ocean. *Int. J. Syst. Evol. Microbiol.* 69, 278–284. doi: 10.1099/ijsem.0.003151

Sun, C., Xu, L., Yu, X. Y., Zhao, Z., Wu, Y. H., Oren, A., et al. (2018). *Minwuia thermotolerans* gen. nov., sp. nov., a marine bacterium forming a deep branch in the *Alphaproteobacteria*, and proposal of *Minwuiaceae* fam. nov. and *Minwuiales* ord. nov. *Int. J. Syst. Evol. Microbiol.* 68, 3856–3862. doi: 10.1099/ijsem.0.003073

Tabarsa, M., Karnjanapratum, S., Cho, M., Kim, J. K., and You, S. (2013). Molecular characteristics and biological activities of anionic macromolecules from *Codium fragile*. *Int. J. Biol. Macromol* 59, 1–12. doi: 10.1016/j.ijbiomac.2013.04.022

Tamura, K., Hemsworth, G. R., Dejean, G., Rogers, T. E., Pudlo, N. A., Urs, K., et al. (2017). Molecular mechanism by which prominent human gut bacteroidetes utilize mixed-linkage beta-glucans, major health-promoting cereal polysaccharides. *Cell Rep.* 21, 417–430. doi: 10.1016/j.celrep.2017.09.049

Tamura, K., Stecher, G., and Kumar, S. (2021). MEGA11: molecular evolutionary genetics analysis version 11. *Mol. Biol. Evol.* 38, 3022–3027. doi: 10.1093/molbev/msab120

Teeling, H., Fuchs, B. M., Becher, D., Klockow, C., Gardebrecht, A., Bennke, C. M., et al. (2012). Substrate-controlled succession of marine bacterioplankton populations induced by a phytoplankton bloom. *Science* 336, 608–611. doi: 10.1126/science.1218344

Teeling, H., Fuchs, B. M., Bennke, C. M., Kruger, K., Chafee, M., Kappelmann, L., et al. (2016). Recurring patterns in bacterioplankton dynamics during coastal spring algae blooms. *Elife* 5, e11888. doi: 10.7554/eLife.11888

Terrapon, N., Lombard, V., Drula, E., Lapebie, P., Al-Masaudi, S., Gilbert, H. J., et al. (2018). PULDB: the expanded database of Polysaccharide Utilization Loci. *Nucleic Acids Res.* 46, D677–D683. doi: 10.1093/nar/gkx1022

Thongphrom, C., Kim, J. H., and Kim, W. (2016). *Maribacter arenosus* sp. nov., isolated from marine sediment. *Int. J. Syst. Evol. Microbiol.* 66, 4826–4831. doi: 10.1099/ijsem.0.001436

Unfried, F., Becker, S., Robb, C. S., Hehemann, J. H., Markert, S., Heiden, S. E., et al. (2018). Adaptive mechanisms that provide competitive advantages to marine bacteroidetes during microalgal blooms. *ISME J.* 12, 2894–2906. doi: 10.1038/s41396-018-0243-5

Weerawongwiwat, V., Kang, H., Jung, M. Y., and Kim, W. (2013). *Maribacter chungangensis* sp. nov., isolated from a green seaweed, and emended descriptions of the genus *Maribacter* and *Maribacter arcticus*. *Int. J. Syst. Evol. Microbiol* 63, 2553–2558. doi: 10.1099/ijs.0.039628-0

Wolter, L. A., Mitulla, M., Kalem, J., Daniel, R., Simon, M., and Wietz, M. (2021). CAZymes in *maribacter dokdonensis* 62-1 from the patagonian shelf: genomics and physiology compared to related flavobacteria and a co-occurring *alteromonas* strain. *Front. Microbiol.* 12, 628055. doi: 10.3389/fmicb.2021.628055

Wu, Z. C., Zhang, X. Y., Sun, C., Xu, L., Fu, G. Y., and Xu, X. W. (2021). *Aestuariibaculum sediminum* sp. nov., a marine bacterium isolated from a tidal flat in Zhoushan. *Arch. Microbiol.* 203, 2953–2960. doi: 10.1007/s00203-021-02262-1

Xie, J., Chen, Y., Cai, G., Cai, R., Hu, Z., and Wang, H. (2023). Tree Visualization By One Table (tvBOT): a web application for visualizing, modifying and annotating phylogenetic trees. *Nucleic Acids Res.* 51, W587–W592. doi: 10.1093/nar/gkad359

Xing, P., Hahnke, R. L., Unfried, F., Markert, S., Huang, S., Barbeyron, T., et al. (2015). Niches of two polysaccharide-degrading *Polaribacter* isolates from the North Sea during a spring diatom bloom. *ISME J.* 9, 1410–1422. doi: 10.1038/ismej.2014.225

Xu, L., Ying, J. J., Fang, Y. C., Zhang, R., Hua, J., Wu, M., et al. (2021). *Halomonas populi* sp. nov. isolated from Populus euphratica. *Arch. Microbiol.* 204, 86. doi: 10.1007/s00203-021-02704-w

Xu, T., Yu, M., Lin, H., Zhang, Z., Liu, J., and Zhang, X. H. (2015). Genomic insight into *Aquimarina longa* SW024 T: its ultra-oligotrophic adapting mechanisms and biogeochemical functions. *BMC Genomics* 16, 772. doi: 10.1186/s12864-015-2005-3

Xue, C. X., Zhang, H., Lin, H. Y., Sun, Y., Luo, D., Huang, Y., et al. (2020). Ancestral niche separation and evolutionary rate differentiation between sister marine flavobacteria lineages. *Environ. Microbiol.* 22, 3234–3247. doi: 10.1111/1462-2920.15065

Ying, J. J., Fang, Y. C., Ye, Y. L., Wu, Z. C., Xu, L., Han, B. N., et al. (2021). *Marinomonas vulgaris* sp. nov., a marine bacterium isolated from seawater in a coastal intertidal zone of Zhoushan island. *Arch. Microbiol.* 203, 5133–5139. doi: 10.1007/s00203-021-02500-6

Yoon, J. H., Kang, S. J., Lee, S. Y., Lee, C. H., and Oh, T. K. (2005). *Maribacter dokdonensis* sp. nov., isolated from sea water off a Korean island, Dokdo. *Int. J. Syst. Evol. Microbiol.* 55, 2051–2055. doi: 10.1099/ijs.0.63777-0

Zeugner, L. E., Krüger, K., Barrero-Canosa, J., Amann, R. I., and Fuchs, B. M. (2021). *In situ* visualization of glycoside hydrolase family 92 genes in marine *flavobacteria*. *ISME Commun.* 1, 81. doi: 10.1038/s43705-021-00082-4

Zhang, X., Hu, B. X., Ren, H., and Zhang, J. (2018b). Composition and functional diversity of microbial community across a mangrove-inhabited mudflat as revealed by 16S rDNA gene sequences. *Sci. Total Environ.* 633, 518–528. doi: 10.1016/j.scitotenv.2018.03.158

Zhang, G. I., Hwang, C. Y., Kang, S. H., and Cho, B. C. (2009). *Maribacter antarcticus* sp. nov., a psychrophilic bacterium isolated from a culture of the Antarctic green alga *Pyramimonas gelidicola*. *Int. J. Syst. Evol. Microbiol.* 59, 1455–1459. doi: 10.1099/ijs.0.006056-0

Zhang, J. Y., Xia, Y., Feng, X., Mu, D. S., and Du, Z. J. (2020). *Maribacter algarum* sp. nov., a new member of the family *Flavobacteriaceae* isolated from the red alga *Gelidium amansii*. *Int. J. Syst. Evol. Microbiol.* 70, 3679–3685. doi: 10.1099/ijsem.0.004220

Zhang, H., Yohe, T., Huang, L., Entwistle, S., Wu, P., Yang, Z., et al. (2018a). dbCAN2: a meta server for automated carbohydrate-active enzyme annotation. *Nucleic Acids Res.* 46, W95–W101. doi: 10.1093/nar/gky418

Zhu, Y., Suits, M. D., Thompson, A. J., Chavan, S., Dinev, Z., Dumon, C., et al. (2010). Mechanistic insights into a Ca2+-dependent family of alpha-mannosidases in a human gut symbiont. *Nat. Chem. Biol.* 6, 125–132. doi: 10.1038/nchembio.278

Zhu, Y., Thomas, F., Larocque, R., Li, N., Duffieux, D., Cladiere, L., et al. (2017). Genetic analyses unravel the crucial role of a horizontally acquired alginate lyase for brown algal biomass degradation by *Zobellia galactanivorans*. *Environ. Microbiol.* 19, 2164–2181. doi: 10.1111/1462-2920.13699

frontiers | Frontiers in Marine Science

TYPE Original Research
PUBLISHED 17 November 2023
DOI 10.3389/fmars.2023.1288142

OPEN ACCESS

EDITED BY
Xue-Wei Xu,
Ministry of Natural Resources, China

REVIEWED BY
Jiapeng Wu,
Guangzhou University, China
Heng-Lin Cui,
Jiangsu University, China
Hongchen Jiang,
China University of Geosciences Wuhan, China

*CORRESPONDENCE
Ping Han
phan@geo.ecnu.edu.cn

RECEIVED 03 September 2023
ACCEPTED 03 November 2023
PUBLISHED 17 November 2023

CITATION
Zhao Q, Sun D, Tang X, Hou L, Liu M and Han P (2023) An investigation of *Nitrospira* bacteria in coastal wetlands of China: distribution pattern and related environmental driving factors. *Front. Mar. Sci.* 10:1288142. doi: 10.3389/fmars.2023.1288142

An investigation of *Nitrospira* bacteria in coastal wetlands of China: distribution pattern and related environmental driving factors

Qiang Zhao[1], Dongyao Sun[1,2], Xiufeng Tang[1], Lijun Hou[3], Min Liu[1] and Ping Han[1,3,4]*

[1]Key Laboratory of Geographic Information Science (Ministry of Education), School of Geographic Sciences, East China Normal University, Shanghai, China, [2]School of Geography Science and Geomatics Engineering, Suzhou University of Science and Technology, Suzhou, China, [3]State Key Laboratory of Estuarine and Coastal Research, East China Normal University, Shanghai, China, [4]Institute of Eco-Chongming, East China Normal University, Shanghai, China

Nitrate is mainly converted via aerobic nitrite oxidation during the second step of nitrification, which is catalyzed by nitrite-oxidizing bacteria (NOB) and the recently discovery complete ammonia oxidizers (comammox). Members of the genus *Nitrospira* are the most diverse and widespread known NOB and comammox. However, the community assembly of *Nitrospira* in estuary and coastal wetland and the major environmental shaping factors remain understudied. Here in this study, we investigated the geographical distribution pattern of *Nitrospira* along the large-scale coastal wetlands of China. The results showed that the abundance of *Nitrospira* ranged from 4.96×10^6 - 3.88×10^7 copies/g dry sediment, significantly (more than one order of magnitude) higher than *amoA* gene of ammonia-oxidizers. The identified *Nitrospira* belong to *Nitrospira* lineage IV (50%), lineage I and II. The adaptability of the three lineages to environmental factors (such as temperature, pH, salinity and particle size) are different, which leads to the diversity of its distribution composition in different estuaries. Network analysis showed that the cooperation takes greater portion than competition in the relationship of *Nitrospira* population. This study revealed the abundance and community composition of *Nitrospira* bacteria, as well as the major environmental driving factors in coastal wetland ecosystems, which deepens our understanding of the niche separation of *Nitrospira* with the nitrogen cycling.

KEYWORDS

coastal wetlands, *Nitrospira*, nitrification, distribution pattern, environmental driving factors

Introduction

Nitrogen is an essential component of all living organism and considered as a growth limiting factor in many ecosystems. As a major source of bioavailable nitrogen, nitrate is mainly converted by aerobic nitrite oxidation during the second step of nitrification, which is catalyzed by chemolithoautotrophic nitrite-oxidizing bacteria (NOB) (Kuypers et al., 2018).

To date, the known NOB were found in seven genera (*Nitrobacter*, *Nitrococcus*, *Nitrospina*, *Nitrospira*, *Nitrotoga*, *Nitrolancea*, and *Candidatus* Nitromaritima) (Daims et al., 2016). Among these NOB, *Nitrospira* is the most diverse genus and consists of six phylogenetically diverged sub-lineages (Daims et al., 2016). *Nitrospira* is globally distributed in natural and engineered ecosystems, including soil (Pester et al., 2014), ocean (Watson et al., 2004; Pachiadaki et al., 2017), freshwater habitats (Altmann et al., 2003), geothermal springs (Lebedeva et al., 2005; Edwards et al., 2013), wastewater treatment plants (WWTPs) (Daims et al., 2001; Kruse et al., 2013; Ushiki et al., 2013; Daims et al., 2015; Gruber-Dorninger et al., 2015; Annavajhala et al., 2018), saline-alkaline lakes (Daebeler et al., 2020), and aquaculture biofilters (Keuter et al., 2011; van Kessel et al., 2015). The *Nitrospira* lineage I and II exhibited dominance in WWTPs (Okabe and Watanabe, 1999; Daims et al., 2001; Kruse et al., 2013), with ventilation intensity emerging as a significant factor influencing their relative abundance (Park and Noguera, 2008). Furthermore, within marine ecosystems, it is the linage IV rather than linage II that assumes dominance among NOB (Pester et al., 2014).

Nevertheless, *Nitrospira* have a reputation for being difficult to isolate and grow under laboratory conditions so that progress in *Nitrospira*-related research is lagging (Daims et al., 2016). Remarkably, the hitherto known lineage I *Nitrospira* were mainly detected in the activated sludge of WWTPs (Lucker et al., 2010; Fujitani et al., 2014).

Nitrospira had been regarded as obligate chemolithoautotrophic organisms that gain growth energy solely from nitrite oxidation for a long time. However, the discovery of complete ammonia oxidizers (comammox) belonging to *Nitrospira* lineage II challenged our perception (Daims et al., 2015; van Kessel et al., 2015). Meanwhile, some *Nitrospira* were physiologically confirmed of being able to grow with various organic substrates. For example, nitrite oxidizers of the genus *Nitrospira* can hydrolyze urea or cyanate to NH_3 and CO_2, then provides ammonia-oxidizing bacteria (AOB) with ammonia. Subsequently, they can acquire nitrite from the AOB. This interaction between NOB and AOB called "reciprocal feeding" (Koch et al., 2015; Palatinszky et al., 2015). Moreover, genomic analysis and physiological experiment prove that several *Nitrospira* can grow aerobically with hydrogen or formate as sole energy source. Meanwhile, under anoxic conditions, they are capable of reducing nitrate to nitrite with hydrogen or formate as electron donor (Koch et al., 2014; Koch et al., 2015). All of these studies revealed previously unrevealed metabolic potentials of *Nitrospira* beyond the autotrophic nitrite-oxidizing lifestyle.

Due to the sea-land interaction, estuaries are highly productive environments that harbor active and diverse microbial communities so that have always been a hotspot for the study of biochemical cycles. Meanwhile, estuaries also continuously enrich reactive nitrogen from the upstream of the rivers (Hou et al., 2015; Osburn et al., 2016; Hou et al., 2018b). Therefore, the process and mechanism of nitrogen biogeochemical cycling are the focus of estuarine research. China has a wide latitude range of eastern coastline, the researching to *Nitrospira* of the coastal wetlands may expand our knowledge of ecological niche differentiation among *Nitrospira* genus. In this study, we aimed to examine the diversity and distribution of *Nitrospira* in the eastern estuaries of China, and determine the key environmental factors shaping the community structure of *Nitrospira*.

Experimental procedures

Sample collection

Sediment samples were collected from 16 estuarine intertidal zones of China in May 2019 (Sun et al., 2020), including LH, BDH, HH, YR, SYH, BCYH, CJ, JJ, OJ, MJ, MLX, JLJ, YFX, ZJ, YJ and NLJ (Figure 1). The collected sediment samples were sealed in sterile plastic bags, subsequently refrigerated and transported back to the laboratory. Then aliquots of the sediment samples were used for enrichment cultures and physicochemical properties analyses, the others were stored at -20°C for molecular analyses.

DNA extraction and quantitative PCR

DNA was extracted in duplicate from the sediment samples according to the standard protocol of the FastDNA Spin Kit for Soil (QBIOgene, Carlsbad, CA, United States). The *nxrB* gene of *Nitrospira* was amplified using nxrB169F (TACATGTGG TGGAACA and nxrB638R (CGGTTCTGGTCRATCA) primers. Reactors for quantitative PCR were prepared with Maxima SYBR Green qPCR Master Mix (Thermo Fisher Scientific, Waltham, MA, USA). The reaction comprised 10 μL Hieff ® qPCR SYBR Green Master Mix with Low Rox Plus (Yeasan, China), 1 μL template DNA (approximately 5 ng), 0.4 μL of forward and reverse mixed primers (10 μM) and 9.2 μL of ddH_2O. Samples were run in triplicates on an ABI 7500 sequence detection system (Applied Biosystems, Canada). Standard curve for quantitative PCR (qPCR) was created by purifying PCR products containing the target gene fragments with the QIAquick PCR Purification Kit (Qiagen, Germany) according to manufacturer's instructions, the concentration was measured with the Nanodrop-2000 Spectrophotometer (Thermo, United States) and serially 10-fold diluted before qPCR was conducted. The correlation coefficient (r^2) value for standard curve was greater than 0.99, and the amplification efficiency was between 96% and 105%. The amplicon specificity was assessed by the melting curve. The qPCR results were showed as the copy numbers calculated as: Copy number = $(C \times 10^{-9}/MW) \times NA$ (C represents template concentration (ng/μL); MW indicates template molecular weight in Daltons; NA indicates Avogadro's constant, 6.022×10^{23}). For

FIGURE 1
Sampling site and *Nitrospira nxrB* Gene abundance in the coastal wetlands of China. This figure illustrates the geographical location of our sampling site within the coastal wetlands of China, as referenced in Sun et al. (2020). The pie chart inset depicts the relative abundance of the *nxrB* gene across three lineages of *Nitrospira*: Lineage I, Lineage II, and Lineage IV. Each segment of the pie chart is proportionally representative of the respective lineage's abundance within the sampled population.

each qPCR assay, negative controls were performed by the no-template DNA for ruling out any possible contamination.

Phylogenetic analysis

For amplicon sequencing, DNA was extracted from sedimental samples and used as template for PCR with primers targeting the *nxrB* gene of *Nitrospira*. Then PCR products for Illumina MiSeq sequencing were performed at Shanghai Majorbio Biomedical Technology Company (Shanghai, China). The processing of raw data was performed by Quantitative Insight into Microbial Ecology (QIIME) (Caporaso et al., 2010). Paired-end reads were stitched with FLASH plugin based on matched overlapping regions. Then the sequences were grouped into operational taxonomic units (OTU) with a similarity threshold of 95% (Schloss, 2013). The closest reference strain to each OTU was searched using the NCBI Web BLASTn program. All of the sequences we obtained were aligned using ClusalX (Thompson et al., 1997). Neighbor-joining phylogenetic trees from one representative OTU sequence and its closest reference sequence retrieved from GenBank (Kumar et al., 2004) were created using MEGA 7.0 with 1000 bootstrap replicates to confirm the tree topologies (Tamura et al., 2007).

Statistical analysis

The alpha diversity was calculated for the numbers of OTU, richness estimator (Chao1) and diversity indices (Shannon-Weiner and Simpson) using the Vegan packages V2.5-4 in R V3.4 (Okasen et al., 2007; R Core Team, 2020). Non-metric multidimensional scaling (NMDS) ordination was performed in R (R Core Team, 2020), and principal coordinate analysis (PCoA) was conducted in QIIME, both of them were employed to explore the community

classification of *Nitrospira*. The correlation between community structure and environmental parameters was determined by canonical correspondence analysis (CCA) using Canoco 4.5 (Braak and Šmilauer, 2002). Pearson correlation in SPSS 22.0 was used to uncover the relationship between the abundance, diversity and sediment physiochemical parameters. For network analysis, the highly representative OTUs were selected. The network analysis was conducted using the "Hmisc" package in R and was visualized in Gephi V0.9.2.

Results

Abundance and diversity of Nitrospira in coastal wetlands of China

Based on the qPCR results, *Nitrospira* was discovered in all of the sediment samples from 16 sites, and the *nxrB* gene of *Nitrospira* with an abundance between 4.96×10^6 - 3.88×10^7 copies/g dry sediment (Figure 1), was significantly (more than one magnitude) higher than *amoA* gene of ammonia-oxidizers (Sun et al., 2020). Among these studied areas, MLX has the most copy number of *nxrB* gene, similar as comammox *Nitrospira amoA* gene (Sun et al., 2020). Meanwhile, the abundance of the *Nitrospira nxrB* gene was lower in the southern than in the northern and middle estuaries.

Overall, 141,688 high-quality were generated from the 16 sediment samples after trimming and chimera moving. There *Nitrospira nxrB* gene sequences were further clustered into 451 OTUs based on 95% nucleotide similarity cutoff threshold, and the number of OTUs for each sample ranges from 53 to 201 (Table S1). The richness of Chao1 ranged from 64.14 (for the NLJ site) to 234.39 (for the JLJ site). For diversity indices, the Shannon indices ranged from 1.01 (for the BCYH site) to 3.39 (for the JLJ site) and Simpson indices ranged from 0.32 (for the BCYH site) to 0.93 (for the JLJ site).

Phylogeny of Nitrospira *nxrB* gene

The neighbor-joining tree based amino acid was constructed with 25 representative OTUs which are more than 0.5% abundance together constituting 85.26% of the total sequences (Figure 2). In sediment samples from 16 estuaries, we detected diverse *Nitrospira* phylotypes affiliated within lineage I, II and IV. *Nitrospira* lineage II and IV were more prevalent and abundant than lineage I, with the lineage I mainly present in 5 samples (YR, CJ, MJ, MLX and JLJ).

OTU 526 was mainly presented in YR and was the major OTU in lineage I, closely related to *Ca. Nitrospira* defluvii. Besides, the remaining four representative OTUs of lineage I clustered without any reported *Nitrospira* species, among them, OTU 830 and OTU 832 possessed a relatively low abundance and were only detected at YR. OTU 1005 was the most abundant OTU in *Nitrospira* lineage II and was related to Pearl River estuary clone NprPB841, similarly, OTU 1005 reached high relative abundance in Nanliu River (NLJ) and Pearl River (ZJ) estuaries. However, OTU 602, which is also closely related to Pearl River Estuary Clone NprPS979, was nearly absent in all sample sites. OTU 562 was dominant in *Nitrospira* lineage IV and was detected in most sample sites but YR. Interestingly, lineage I was not detected in the samples with higher relative abundance of lineage IV, such as BDH, HH, SYH, BCYH and MLX. Conversely, lineage IV was absent at YR and MJ, where lineage I was more abundant.

Community structure of Nitrospira

PCoA and NMDS analyses based on the Bray-Curtis distances of *Nitrospira* OTUs were performed to evaluate the differences of *Nitrospira* community structure in acidic areas (pH: 6-7) versus alkaline areas (pH: 7-9), and both of them exhibited a significant separation of *Nitrospira* community (Figure 3). In order to illustrate the occurrence pattern among *Nitrospira*, network was constructed according to the significance (Spearman, $p<0.05$) and correlation coefficients (Spearman, $|x|>0.6$) of highly representative *Nitrospira* OTUs. The network showed a complicated structure containing 42 nodes and 100 edges with the average degree of 4.762 and the average clustering coefficient of 0.573. In general, majority of the nodes belonged to *Nitrospira* lineage IV (50%), and the ratio of positive edges was higher (66%). Therein, the correlation between lineage I and lineage II was mainly positive, while both of them competed with lineage IV. Especially, there were no positive edges in OTU 622 belonging to *Nitrospira* lineage IV, suggesting the different physiological characteristics from most *Nitrospira*.

The effects of physiochemical parameters

The environmental factors of the sample sites refer to previous studies (Table S2). The correlations of *Nitrospira* community structure with physiochemical parameters were tested by CCA (Figure 4). The first two CCA dimensions explained 44.06% of the cumulative variance of the *Nitrospira* community-environment correlation. The results confirmed that *Nitrospira* community structures had significant correlation with pH (P=0.004, F=2.9), salinity (P=0.028, F=1.6) and particle size (P=0.046, F=2.5), theseparameters provided 38.3% of total CCA explanatory power. By contrast, other parameters had little effect on community structure (P>0.064), and they accounted for 50.9% of CCA explanatory power.

Environmental impacts on *Nitrospira* diversity indices including the Chao1, Shannon, Simpson and OTU numbers were evaluated by Pearson correlation analysis (Table S3). The results demonstrated that Chao1 richness varied with salinity, but other indices seemed stable among different salinity. In addition, Shannon index, Simpson index and OTU numbers were negatively correlated to temperature, the lower diversity at higher temperature indicating that only a few *Nitrospira* species could tolerate high temperature. Shannon index and Simpson index also showed negative correlation with nitrate concentration, but no significant correlation with nitrite concentration. Meanwhile, OTU numbers were significantly correlated to ammonia and ferric ion content, additionally, the correlation between other

10.3389/fmars.2023.1288142

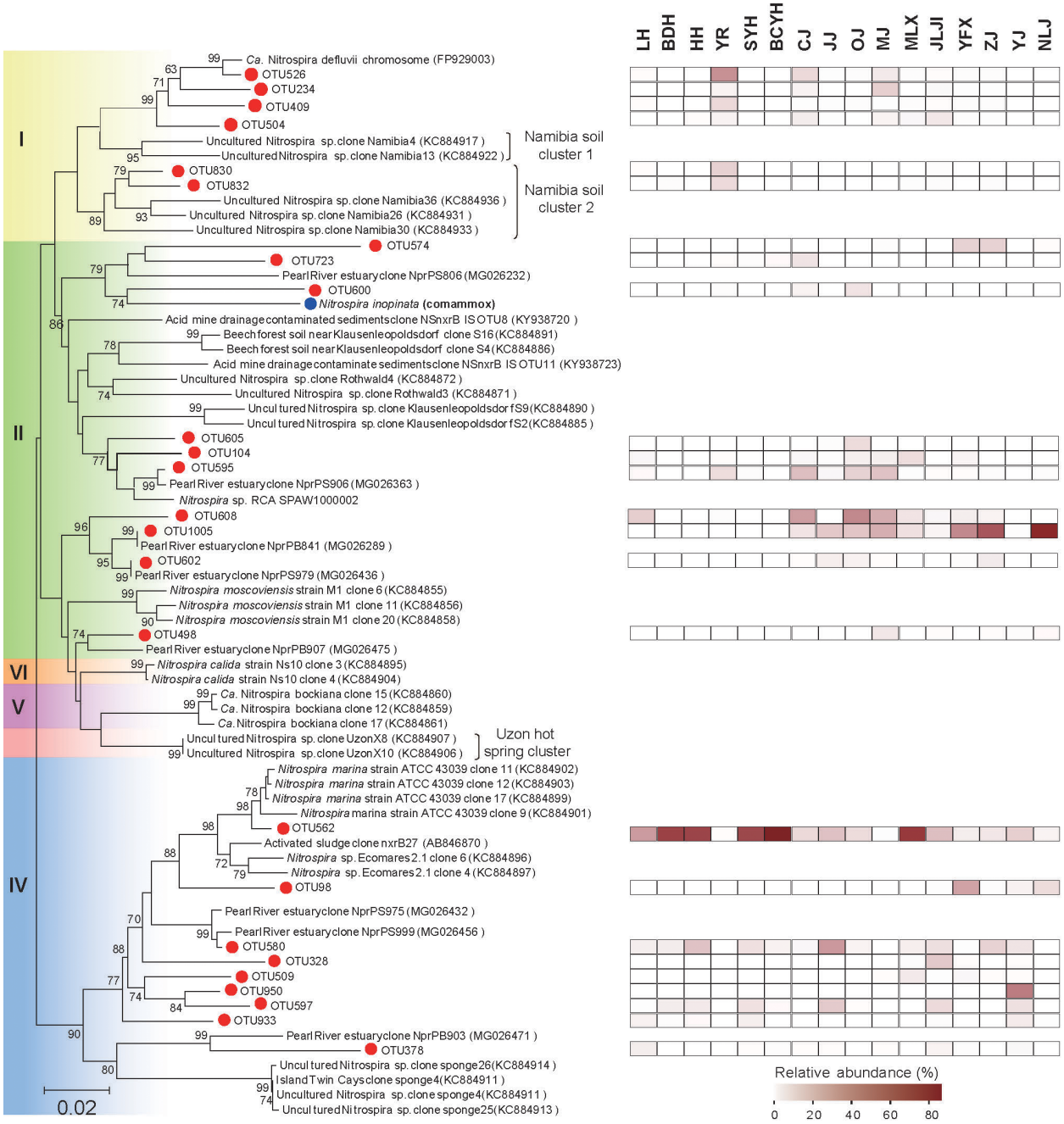

FIGURE 2
Neighbor-joining phylogenetic tree of *Nitrospira nxrB* genes. Sequences were collected from this study and the GenBank database. Bootstrap values were given on the branches of the tree. The scale bar represents 2% nucleic acid sequence divergence.

parameters we studied and *Nitrospira* diversity indices was not significant.

Correlation between abundance of 12 dominant *Nitrospira* OTUs and environment parameters was performed by Spearman correlation analysis (Figure 5), which showed a strong association between the representative OTUs and selective physiochemical properties such as temperature, pH value, particle size, moisture and Fe^{3+}. In general, the correlation of abundance with environment parameters was inverse between *Nitrospira* lineage I and lineage II. For example, OTUs affiliating with lineage II were negatively correlated with pH value, particle size and the content of sulfur, while the correlation with lineage I was positive. The content of Fe^{3+}, total nitrogen, total organic carbon showed positive correlation with the relative abundance of lineage II, but negative correlation with lineage I. Besides, temperature was positively correlated to the OTUs belonging to lineage IV but negatively correlated to lineage I, suggesting the different adaptations to temperature among them.

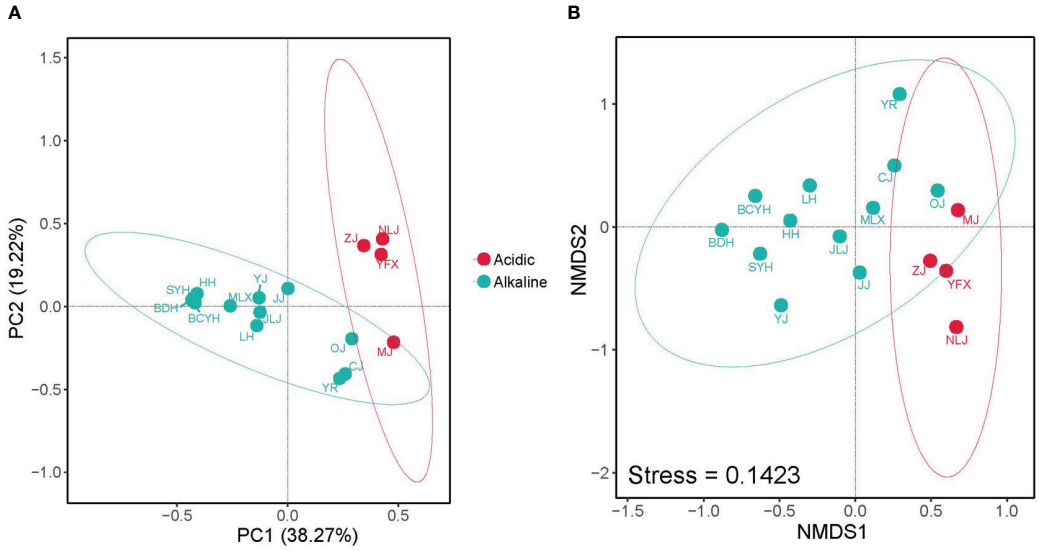

FIGURE 3
(A) PCoA plots of *Nitrospira* community dissimilarities among sampling sites based on Bray-Curtis distance; **(B)** NMDS plots showing the *Nitrospira* community composition separation. Red solid circle, acidic (pH: 6-7); Green solid circle, alkaline (pH: 7-9).

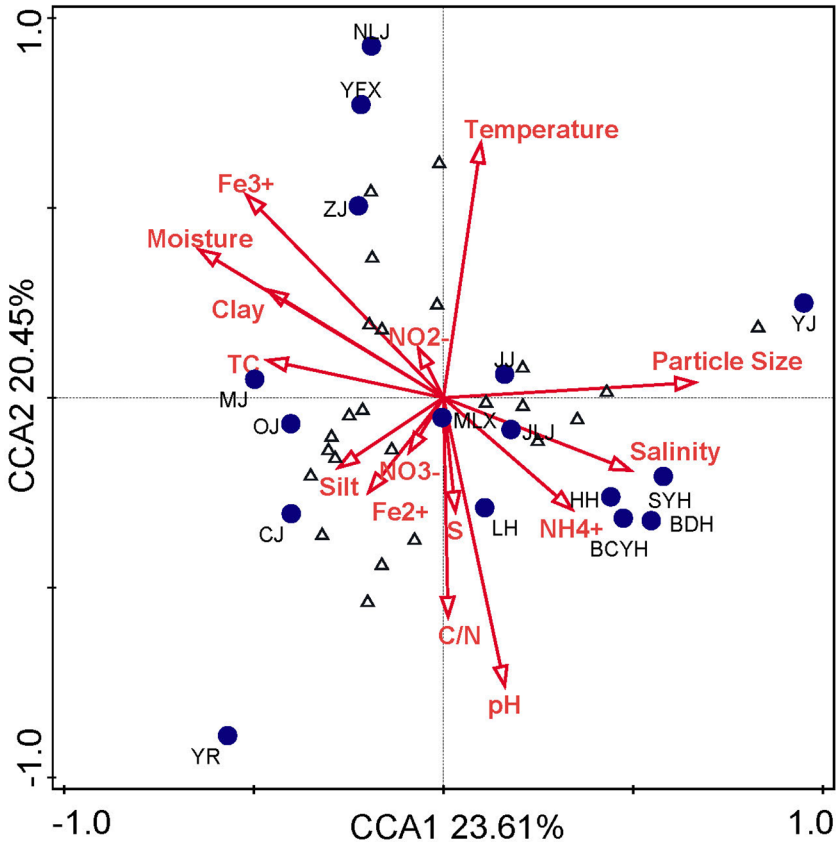

FIGURE 4
CCA plots for the first two principal dimensions of the relationship between the *Nitrospira* community pattern and the environmental parameters. Blue circles, samples; Blue triangles, *Nitrospira* OTUs; Red arrows, environmental factors.

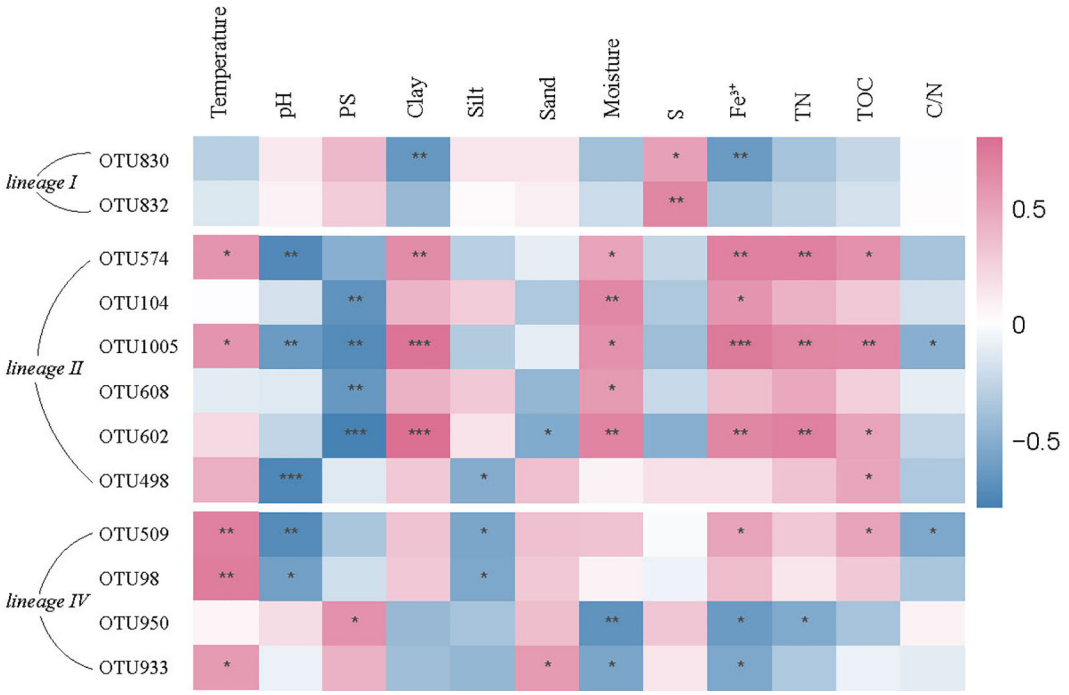

FIGURE 5
Correlation of relative abundance of 12 dominant *Nitrospira* OTUs with environment parameters. *P<0.05, **P<0.01, ***P<0.001. PS, particle size; S, sulfur; TN, total nitrogen; TOC, total organic carbon; C/N, ratio of carbon to nitrogen.

Discussion

Community pattern of Nitrospira bacteria in coastal wetlands of China

Members of the *Nitrospira* bacteria were considered as the most diverse and widespread known NOB. However, distribution pattern of *Nitrospira* in large-scale coastal wetland are missing, and a systematic assessment of multi-factor effects their different niche adaptation strategies is scarce (Daims et al., 2016). In this study, we investigated the abundance, diversity and community pattern of *Nitrospira* in sediments along the eastern estuary and coastal line of China and identified the major driving environmental factors of their niche partitions.

Quantification results showed that the *nxrB* gene of *Nitrospira* was detected in all of the sediment samples, and was more abundant than ammonia oxidizers (Sun et al., 2020). This result was in line with one previous study showing the high proportion of NOB in the detected environment (Winkler et al., 2012), and the growth on alternative energy source from hydrogen or formate utilization may sometimes explain higher *in situ* abundances of NOB than their ammonia-oxidizing counterparts (Koch et al., 2014; Koch et al., 2015). According to the phylogenetic analysis, *Nitrospira* lineage IV was present at all sites except YR at which lineage I was dominant. Meanwhile, the relative abundance of lineage IV was higher than other two lineage at most sites, suggesting a dominant but fluctuating role of lineage IV in the nitrite oxidizing of coastal wetlands. Hitherto, strains belonging to *Nitrospira* lineage I and lineage II were mainly obtained from engineering systems, but rarely founded in marine (Ushiki et al., 2013; Fujitani et al., 2014; Gruber-Dorninger et al., 2015). In contrast, *Nitrospira* lineage IV was usually present in marine or hypersaline systems (Watson et al., 2004; Daebeler et al., 2020; Bayer et al., 2021). Due to the influence of the ocean, most of the sample sites we studied showed significant marine characteristics, therefore lineage IV was more abundant. As a large amount of sediment from the upstream deposited in the estuary, the riverbed at the YR site uplifted and turned into the elevated stream, thus was relatively less affected by seawater, this may be the reason why lineage IV was not found here. In addition to the large amount of nutrients carried by sediment, the excessive application of fertilizers in the downstream of the Yellow River caused inorganic nitrogen was enriched in the estuary, therefore lineage I was dominant here.

The network analysis showed that the positive correlations were more dominant among *Nitrospira* (Figure 6), suggesting the cooperation is more than competition in the relationship of *Nitrospira* population. Interestingly, OTU 622 belonging to *Nitrospira* lineage IV was negatively corelated with the OTUs of lineage I, II and IV, suggesting its unique characteristic in *Nitrospira*.

Influence of environmental factors on the distribution of Nitrospira bacteria in coastal wetlands of China

Previous study proved that the concentration of nitrite was a key factor affecting the population and niche separation, the growth

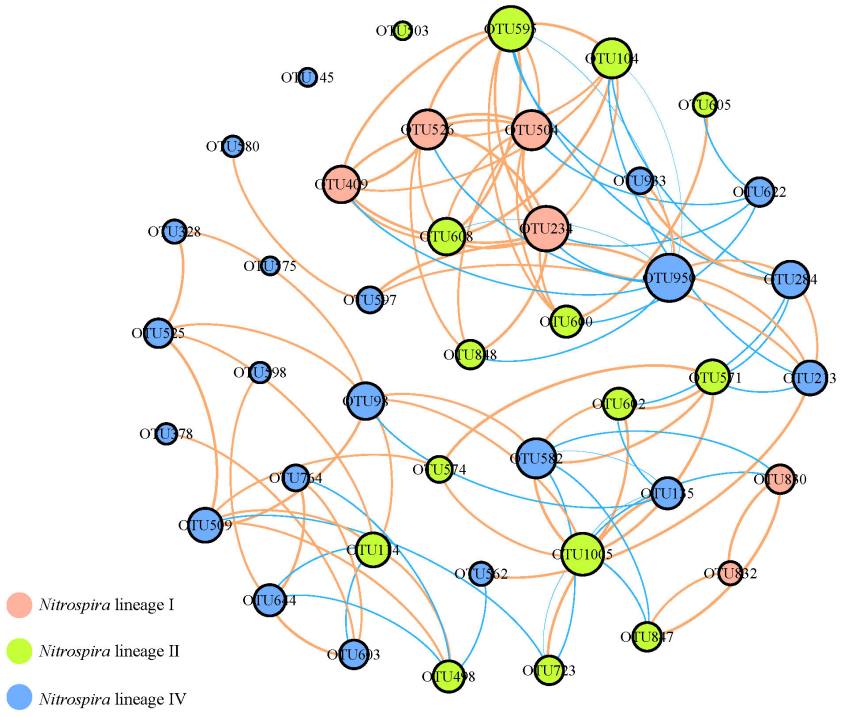

FIGURE 6
Co-occurrence network analysis of representative *Nitrospira* OTUs. The size of circles means relative abundance; orange lines represent negative interactions; blue lines represent positive interactions.

of some *Nitrospira* would suspend with the increasing nitrite concentration (Wagner et al., 2002). However, the correlation between nitrite concentration with abundance or diversity was not significant in this study, which may be explained by the limited accumulation of nitrite in natural environment. Besides, we investigated more other physicochemical parameters contributing to the community construction, which broaden our understanding of niche differentiation of *Nitrospira*.

It is generally accepted that *Nitrospira* strains grew in the optimum temperature between 25 and 31 (Spieck and Lipski, 2011), while nitrite oxidation by these organisms was still detected in a broad temperature range (10 to 65 °C) (Alawi et al., 2009). Comparatively, *Nitrospira* lineage I has weak tolerance to higher temperature, and *Nitrospira* found in geothermal springs was mainly affiliated with lineage II and lineage IV (Lebedeva et al., 2011; Marks et al., 2012; Edwards et al., 2013). Additionally, the studies performed in the Yangtze River showed that, with the increase of ambient temperature, the relative abundance of NOB-*Nitrospira* lineage I or lineage II decreased, while that of comammox-*Nitrospira* increased (Liu et al., 2020). *Nitrospira* showed different adaptation characteristics to temperature, only a few strains were able to tolerate the higher temperature (Alawi et al., 2009). Similarly, *Nitrospira* diversity tended to decrease with the elevating temperature in this study. Meanwhile, the positive correlation between the relative abundance of lineage IV OTUs and temperature suggesting lineage IV was more adaptable to higher temperature conditions.

The recent study reported that *Nitrospira* population was decreased with the salinity gradient (Cébron and Garnier, 2005), whereas another study showed the richness of *Nitrospira* in the high saline regions of Pearl River estuary (Hou et al., 2018a). Members of *Nitrospira* lineage IV were mostly detected in marine and hypersaline environments so far (Watson et al., 2004; Foesel et al., 2008; Keuter et al., 2011; Haaijer et al., 2013; Daebeler et al., 2020), but there were no members of lineage I and II found in these habitats (Santos et al., 2017; Sun et al., 2020), suggesting the different adaption of *Nitrospira* lineage to salinity condition. Here, we discovered a higher abundance of *Nitrospira* lineage I and II in the estuaries that salinity was low, while lower than lineage IV when the salinity was above 1 ppt. The result might guarantee the tolerance of *Nitrospira* lineage IV to hypersaline habitats and the role of salinity in niche separation between *Nitrospira* lineage IV and lineage I, II.

In addition to salinity, pH was another environmental factor that affects the abundance and diversity of *Nitrospira*. Previous study reported that *Nitrospira* defluvii belonging to lineage I grew best at pH 7.3 (Hupeden et al., 2016). Besides, study of *Nitrospira* community in the saline-alkaline lakes showed the decrease of *Nitrospira* diversity with the increasing pH and the *Nitrospira* lineage IV enrichment cultures, "Candidatus *Nitrospira* alkalitolerans", could oxidize nitrite at the condition of neutral to pH 10.5 (Daebeler et al., 2020). In this study, both PCoA and NMDS analysis showed a clear separation of the *Nitrospira* communities with the pH conditions (Figure 3). According to the results of CCA

analysis, the relative abundance of *Nitrospira* OTUs was significantly correlated with pH. The result of Pearson correlation showed that OTUs number was significantly negative corelated with pH value, indicating that only specific *Nitrospira* species tolerate the highly alkaline conditions. The negative correlation between relative abundance of *Nitrospira* lineage II and pH might explain the vacancies of *Nitrospira* lineage II detected in alkaline environments. These results suggested a strong influence of pH on the community pattern of *Nitrospira* bacteria.

As a chemical catalyst, iron could enhance the cell membrane permeability and hence accelerate the nutrients transmission rate. Meanwhile, iron presents in the center of various active enzymes which function in the molecular oxygen transportation and the nitrogen species' transformation in nitrifying microbes. Fe^{3+} in NOB also was hypothesized to act as alternative terminal electron acceptors for nitrite oxidation in the oxygen minimum zone (Lam and Kuypers, 2011). Here, our study showed that Fe^{3+} content was positively correlated with the relative abundance of *Nitrospira* lineage II (Figure 5), whereas this correlation tended to be negative with lineage I. Besides, the significantly negative correlation between Fe^{3+} content and *Nitrospira* OTUs was showed by the Pearson correlation. All of the results suggested Fe^{3+} might play different role in *Nitrospira* lineages, and further physiological verification is needed.

Particle size directly influences the physicochemical property of the sediments and thereby affects the distribution of microbial community (Dang et al., 2010). We found that *Nitrospira* lineage II abundance was negatively correlated with particle size of sediments. In addition, growth of *Nitrospira* could be inhibited under high concentration of nitrate. For instance, growth of *N.moscoviensis* ceased to grow in the presence of 75mM nitrate (Ehrich et al., 1995), and the marine lineage IV *Nitrospira ecomares* 2.1 80mM nitrate (Keuter et al., 2011). Consistently, our study showed that *Nitrospira* diversity decreased with the increasing nitrate concentration. Moreover, previous study showed the high concentration of TOC would mutually strengthen the effect on nitrification in low oxygen conditions (Ling and Chen, 2005). Here, with the low oxygen concentration of estuarine tidal flats, there were a positive correlation between TOC and the relative abundance of *Nitrospira* lineage II, suggesting the community composition of *Nitrospira* was affected by TOC, whereas the interaction mechanism requires further research. As for any other parameters, clay and moisture had a remarkable influence on the abundance of *Nitrospira* OTUs, whereas sulfur content seemed to only significantly effect *Nitrospira* lineage I. These factors might exhibit a role in niche differentiation of *Nitrospira* lineage I and II, therefore the experimental tests are needed.

Concluding remarks

Nitrospira was prevalent and abundant in the estuarine tidal flat wetlands of China and was higher than ammonia oxidizers in abundance. Meanwhile, *Nitrospira* phylotypes were affiliated with *Nitrospira* lineage I, II and IV, in which lineage IV was dominant but fluctuating at different sites.

Data availability statement

The datasets presented in this study can be found in online repositories. The names of the repository/repositories and accession number(s) can be found in the article/Supplementary Material.

Author contributions

QZ: Conceptualization, Data curation, Formal analysis, Investigation, Software, Visualization, Writing - original draft, Writing - review & editing. DS: Conceptualization, Formal analysis, Investigation, Methodology, Visualization, Writing - review & editing. XT: Data curation, Formal analysis, Investigation, Software, Validation, Visualization, Writing - review & editing. LH: Conceptualization, Data curation, Funding acquisition, Investigation, Resources, Writing - review & editing. ML: Conceptualization, Funding acquisition, Investigation, Resources, Writing - review & editing. PH: Conceptualization, Data curation, Formal analysis, Funding acquisition, Investigation, Methodology, Project administration, Resources, Supervision, Validation, Writing - original draft, Writing - review & editing.

Funding

The author(s) declare financial support was received for the research, authorship, and/or publication of this article. This work was financially supported by the National Natural Science Foundation of China (Nos. 42371064, 41807465 and 42030411) and the Starting Research Program of Suzhou University of Science and Technology (No. 332214803).

Conflict of interest

The authors declare that the research was conducted in the absence of any commercial or financial relationships that could be construed as a potential conflict of interest.

Publisher's note

Supplementary material

The Supplementary Material for this article can be found online at: https://www.frontiersin.org/articles/10.3389/fmars.2023.1288142/full#supplementary-material

References

Alawi, M., Off, S., Kaya, M., and Spieck, E. (2009). Temperature influences the population structure of nitrite-oxidizing bacteria in activated sludge. *Env. Microbiol. Rep.* 1, 184–190. doi: 10.1111/j.1758-2229.2009.00029.x

Altmann, D., Stief, P., Amann, R., De Beer, D., and Schramm, A. (2003). *In situ* distribution and activity of nitrifying bacteria in freshwater sediment. *Environ. Microbiol.* 5, 798–803. doi: 10.1046/j.1469-2920.2003.00469.x

Annavajhala, M. K., Kapoor, V., Santo-Domingo, J., and Chandran, K. (2018). Comammox functionality identified in diverse engineered biological wastewater treatment systems. *Environ. Sci. Technol. Lett.* 5, 110–116. doi: 10.1021/acs.estlett.7b00577

Bayer, B., Saito, M. A., Mcilvin, M. R., Lucker, S., Moran, D. M., Lankiewicz, T. S., et al. (2021). Metabolic versatility of the nitrite-oxidizing bacterium Nitrospira marina and its proteomic response to oxygen-limited conditions. *ISME J.* 15, 1025–1039. doi: 10.1038/s41396-020-00828-3

Braak, C. J. F. T., and Šmilauer, P. (2002). *CANOCO Reference Manual and CanoDraw for Windows User's Guide: Software for Canonical Community Ordination (version 4.5)*. Ithaca: Microcomputer Power, p500.

Caporaso, J. G., Kuczynski, J., Stombaugh, J., Bittinger, K., Bushman, F. D., Costello, E. K., et al. (2010). QIIME allows analysis of high-throughput community sequencing data. *Nat. Methods* 7, 335–336. doi: 10.1038/nmeth.f.303

Cébron, A., and Garnier, J. (2005). *Nitrobacter* and *Nitrospira* genera as representatives of nitrite-oxidizing bacteria: detection, quantification and growth along the lower Seine River (France). *Water Res.* 39 20, 4979–4992. doi: 10.1016/j.watres.2005.10.006

Daebeler, A., Kitzinger, K., Koch, H., Herbold, C. W., Steinfeder, M., Schwarz, J., et al. (2020). Exploring the upper pH limits of nitrite oxidation: diversity, ecophysiology, and adaptive traits of haloalkalitolerant *Nitrospira*. *ISME J.* 14, 2967–2979. doi: 10.1038/s41396-020-0724-1

Daims, H., Lebedeva, E. V., Pjevac, P., Han, P., Herbold, C., Albertsen, M., et al. (2015). Complete nitrification by *Nitrospira* bacteria. *Nature* 528, 504–509. doi: 10.1038/nature16461

Daims, H., Lucker, S., and Wagner, M. (2016). A new perspective on microbes formerly known as nitrite-oxidizing bacteria. *Trends Microbiol.* 24, 699–712. doi: 10.1016/j.tim.2016.05.004

Daims, H., Nielsen, J. L., Nielsen, P. H., Schleifer, K. H., and Wagner, M. (2001). *In situ* characterization of *Nitrospira*-like nitrite-oxidizing bacteria active in wastewater treatment plants. *Appl. Environ. Microbiol.* 67, 5273–5284. doi: 10.1128/AEM.67.11.5273-5284.2001

Dang, H., Li, J., Chen, R., Wang, L., Guo, L., Zhang, Z., et al. (2010). Diversity, abundance, and spatial distribution of sediment ammonia-oxidizing Betaproteobacteria in response to environmental gradients and coastal eutrophication in Jiaozhou Bay, China. *Appl. Environ. Microbiol.* 76, 4691–4702. doi: 10.1128/AEM.02563-09

Edwards, T. A., Calica, N. A., Huang, D. A., Manoharan, N., Hou, W., Huang, L., et al. (2013). Cultivation and characterization of thermophilic *Nitrospira* species from geothermal springs in the US Great Basin, China, and Armenia. *FEMS Microbiol. Ecol.* 85, 283–292. doi: 10.1111/1574-6941.12117

Ehrich, S., Behrens, D., Lebedeva, E., Ludwig, W., and Bock, E. (1995). A new obligately chemolithoautotrophic, nitrite-oxidizing bacterium, *Nitrospira moscoviensis* sp. nov. and its phylogenetic relationship. *Arch. Microbiol.* 164, 16–23. doi: 10.1007/BF02568729

Foesel, B. U., Gieseke, A., Schwermer, C., Stief, P., Koch, L., Cytryn, E., et al. (2008). *Nitrosomonas* Nm143-like ammonia oxidizers and *Nitrospira marina*-like nitrite oxidizers dominate the nitrifier community in a marine aquaculture biofilm. *FEMS Microbiol. Ecol.* 63, 192–204. doi: 10.1111/j.1574-6941.2007.00418.x

Fujitani, H., Ushiki, N., Tsuneda, S., and Aoi, Y. (2014). Isolation of sublineage I *Nitrospira* by a novel cultivation strategy. *Environ. Microbiol.* 16, 3030–3040. doi: 10.1111/1462-2920.12248

Gruber-Dorninger, C., Pester, M., Kitzinger, K., Savio, D. F., Loy, A., Rattei, T., et al. (2015). Functionally relevant diversity of closely related *Nitrospira* in activated sludge. *ISME J.* 9, 643–655. doi: 10.1038/ismej.2014.156

Haaijer, S. C., Ji, K., Van Niftrik, L., Hoischen, A., Speth, D., Jetten, M. S., et al. (2013). A novel marine nitrite-oxidizing *Nitrospira* species from Dutch coastal North Sea water. *Front. Microbiol.* 4, 60. doi: 10.3389/fmicb.2013.00060

Hou, L. J., Wang, R., Yin, G. Y., Liu, M., and Zheng, Y. L. (2018b). Nitrogen fixation in the intertidal sediments of the Yangtze Estuary: occurrence and environmental implications. *J. Geophys. Res.-Biogeo.* 123, 936–944. doi: 10.1002/2018JG004418

Hou, L., Xie, X. B., Wan, X. H., Kao, S. J., Jiao, N. Z., and Zhang, Y. (2018a). Niche differentiation of ammonia and nitrite oxidizers along a salinity gradient from the Pearl River estuary to the South China Sea. *Biogeosciences* 15, 5169–5187. doi: 10.5194/bg-2018-189

Hou, L., Yin, G., Liu, M., Zhou, J., Zheng, Y., Gao, J., et al. (2015). Effects of sulfamethazine on denitrification and the associated N_2O release in estuarine and coastal sediments. *Environ. Sci. Technol.* 49, 326–333. doi: 10.1021/es504433r

Hupeden, J., Wegen, S., Off, S., Lucker, S., Bedarf, Y., Daims, H., et al. (2016). Relative abundance of *Nitrotoga* spp. in a biofilter of a cold-freshwater aquaculture plant appears to be stimulated by slightly acidic pH. *Appl. Environ. Microbiol.* 82, 1838–1845. doi: 10.1128/AEM.03163-15

Keuter, S., Kruse, M., Lipski, A., and Spieck, E. (2011). Relevance of *Nitrospira* for nitrite oxidation in a marine recirculation aquaculture system and physiological features of a Nitrospira marina-like isolate. *Environ. Microbiol.* 13, 2536–2547. doi: 10.1111/j.1462-2920.2011.02525.x

Koch, H., Galushko, A., Albertsen, M., Schintlmeister, A., Gruber-Dorninger, C., Lucker, S., et al. (2014). Growth of nitrite-oxidizing bacteria by aerobic hydrogen oxidation. *Science* 345, 1052–1054. doi: 10.1126/science.1256985

Koch, H., Lucker, S., Albertsen, M., Kitzinger, K., Herbold, C., Spieck, E., et al. (2015). Expanded metabolic versatility of ubiquitous nitrite-oxidizing bacteria from the genus *Nitrospira*. *Proc. Natl. Acad. Sci. U.S.A.* 112, 11371–11376. doi: 10.1073/pnas.1506533112

Kruse, M., Zumbragel, S., Bakker, E., Spieck, E., Eggers, T., and Lipski, A. (2013). The nitrite-oxidizing community in activated sludge from a municipal wastewater treatment plant determined by fatty acid methyl ester-stable isotope probing. *Syst. Appl. Microbiol.* 36, 517–524. doi: 10.1016/j.syapm.2013.06.007

Kumar, S., Tamura, K., and Nei, M. (2004). MEGA3: Integrated software for Molecular Evolutionary Genetics Analysis and sequence alignment. *Brief Bioinform.* 5, 150–163. doi: 10.1093/bib/5.2.150

Kuypers, M. M. M., Marchant, H. K., and Kartal, B. (2018). The microbial nitrogen-cycling network. *Nat. Rev. Microbiol.* 16, 263–276. doi: 10.1038/nrmicro.2018.9

Lam, P., and Kuypers, M. M. (2011). Microbial nitrogen cycling processes in oxygen minimum zones. *Ann. Rev. Mar. Sci.* 3, 317–345. doi: 10.1146/annurev-marine-120709-142814

Lebedeva, E. V., Alawi, M., Fiencke, C., Namsaraev, B., Bock, E., and Spieck, E. (2005). Moderately thermophilic nitrifying bacteria from a hot spring of the Baikal rift zone. *FEMS Microbiol. Ecol.* 54, 297–306. doi: 10.1016/j.femsec.2005.04.010

Lebedeva, E. V., Off, S., Zumbragel, S., Kruse, M., Shagzhina, A., Lucker, S., et al. (2011). Isolation and characterization of a moderately thermophilic nitrite-oxidizing bacterium from a geothermal spring. *FEMS Microbiol. Ecol.* 75, 195–204. doi: 10.1111/j.1574-6941.2010.01006.x

Ling, J., and Chen, S. L. (2005). Impact of organic carbon on nitrification performance of different biofilters. *Aquacult. Eng.* 33, 150–162. doi: 10.1016/j.aquaeng.2004.12.002

Liu, S. F., Wang, H. Y., Chen, L. M., Wang, J. W., Zheng, M. S., Liu, S. T., et al. (2020). Comammox *Nitrospira* within the Yangtze River continuum: community, biogeography, and ecological drivers. *ISME J.* 14, 2488–2504. doi: 10.1038/s41396-020-0701-8

Lucker, S., Wagner, M., Maixner, F., Pelletier, E., Koch, H., Vacherie, B., et al. (2010). A *Nitrospira* metagenome illuminates the physiology and evolution of globally important nitrite-oxidizing bacteria. *Proc. Natl. Acad. Sci. U.S.A.* 107, 13479–13484. doi: 10.1073/pnas.1003860107

Marks, C. R., Stevenson, B. S., Rudd, S., and Lawson, P. A. (2012). *Nitrospira*-dominated biofilm within a thermal artesian spring: a case for nitrification-driven primary production in a geothermal setting. *Geobiology* 10, 457–466. doi: 10.1111/j.1472-4669.2012.00335.x

Okabe, S., and Watanabe, H. S. Y. (1998). *In situ* analysis of nitrifying biofilms as determined by *in situ* hybridization and the use of Microelectrodes. *Appl. Environ. Microbiol.* 65, 3182–3191. doi: 10.1128/AEM.65.7.3182-3191.1999

Okasen, J., Kindt, R., Legendre, P., and O'Hara, R. B. (2007). Vegan: community ecology package version. 1.8–6. Available at: https://cran.rproject.org/web/packages/vegan.

Osburn, C. L., Handsel, L. T., Peierls, B. L., and Paerl, H. W. (2016). Predicting sources of dissolved organic nitrogen to an estuary from an agro-urban coastal watershed. *Environ. Sci. Technol.* 50, 8473–8484. doi: 10.1021/acs.est.6b00053

Pachiadaki, M. G., Sintes, E., Bergauer, K., Brown, J. M., Record, N. R., Swan, B. K., et al. (2017). Major role of nitrite-oxidizing bacteria in dark ocean carbon fixation. *Science* 358, 1046–1051. doi: 10.1126/science.aan8260

Palatinszky, M., Herbold, C., Jehmlich, N., Pogoda, M., Han, P., Von Bergen, M., et al. (2015). Cyanate as an energy source for nitrifiers. *Nature* 524, 105–108. doi: 10.1038/nature14856

Park, H.-D., and Noguera, D. R. (2008). *Nitrospira* community composition in nitrifying reactors operated with two different dissolved oxygen levels. *J. Microbiol. Biotechnol.* 18, 1470–1474. doi: 10.1007/s10295-008-0366-1

Pester, M., Maixner, F., Berry, D., Rattei, T., Koch, H., Lucker, S., et al. (2014). NxrB encoding the beta subunit of nitrite oxidoreductase as functional and phylogenetic marker for nitrite-oxidizing *Nitrospira*. *Environ. Microbiol.* 16, 3055–3071. doi: 10.1111/1462-2920.12300

Santos, J. P., Mendes, D., Monteiro, M., Ribeiro, H., Baptista, M. S., Borges, M., et al. (2017). Salinity impact on ammonia oxidizers activity and *amoA* expression in estuarine sediments. *Estuar. Coast. Shelf S.* 211, 177–187. doi: 10.1016/j.ecss.2017.09.001

Schloss, P. D. (2013). Secondary structure improves OTU assignments of 16S rRNA gene sequences. *ISME J.* 7, 457–460. doi: 10.1038/ismej.2012.102

Spieck, E., and Lipski, A. (2011). Cultivation, growth physiology, and chemotaxonomy of nitrite-oxidizing bacteria. *Methods Enzymology: Res. Nitrification Related Processes* 486, 109–130. doi: 10.1016/B978-0-12-381294-0.00005-5

Sun, D., Tang, X., Zhao, M., Zhang, Z., Hou, L., Liu, M., et al. (2020). Distribution and diversity of comammox *Nitrospira* in coastal wetlands of China. *Front. Microbiol.* 11, 589268. doi: 10.3389/fmicb.2020.589268

Tamura, K., Dudley, J., Nei, M., and Kumar, S. (2007). MEGA4: Molecular Evolutionary Genetics Analysis (MEGA) software version 4.0. *Mol. Biol. Evol.* 24, 1596–1599. doi: 10.1093/molbev/msm092

R. Core Team. (2020). R: A language and environment for statistical computing. Vienna, Austria: R Foundation for Statistical Computing.

Thompson, J. D., Gibson, T. J., Plewniak, F., Jeanmougin, F., and Higgins, D. G. (1997). The CLUSTAL_X windows interface: flexible strategies for multiple sequence alignment aided by quality analysis tools. *Nucleic Acids Res.* 25, 4876–4882. doi: 10.1093/nar/25.24.4876

Ushiki, N., Fujitani, H., Aoi, Y., and Tsuneda, S. (2013). Isolation of *Nitrospira* belonging to sublineage II from a wastewater treatment plant. *Microbes Environ.* 28, 346–353. doi: 10.1264/jsme2.ME13042

van Kessel, M. A., Speth, D. R., Albertsen, M., Nielsen, P. H., Op Den Camp, H. J., Kartal, B., et al. (2015). Complete nitrification by a single microorganism. *Nature* 528, 555–559. doi: 10.1038/nature16459

Wagner, M., Loy, A., Nogueira, R., Purkhold, U., Lee, N., and Daims, H. (2002). Microbial community composition and function in wastewater treatment plants. *Anton. Leeuw. Int. J. G.* 81, 665–680. doi: 10.1023/A:1020586312170

Watson, S. W., Bock, E., Valois, F., Waterbury, J., and Schlosser, U. (2004). *Nitrospira marina* gen. nov. sp. nov.: a chemolithotrophic nitrite-oxidizing bacterium. *Arch. Microbiol.* 144, 1–7. doi: 10.1007/BF00454947

Winkler, M. K., Bassin, J. P., Kleerebezem, R., Sorokin, D. Y., and Van Loosdrecht, M. C. (2012). Unravelling the reasons for disproportion in the ratio of AOB and NOB in aerobic granular sludge. *Appl. Microbiol. Biotechnol.* 94, 1657–1666. doi: 10.1007/s00253-012-4126-9

frontiers | Frontiers in Microbiology

TYPE Original Research
PUBLISHED 20 November 2023
DOI 10.3389/fmicb.2023.1291242

OPEN ACCESS

EDITED BY
Xue-Wei Xu,
Ministry of Natural Resources, China

REVIEWED BY
Ajaya Kumar Rout,
Rani Lakshmi Bai Central Agricultural University, India
Pandeng Wang,
Sun Yat-sen University, China

*CORRESPONDENCE
Qichao Tu
✉ tuqichao@sdu.edu.cn

†These authors have contributed equally to this work

RECEIVED 08 September 2023
ACCEPTED 01 November 2023
PUBLISHED 20 November 2023

CITATION
Song W, Li H, Zhou Y, Liu X, Li Y, Wang M, Li D-d and Tu Q (2023) Discordant patterns between nitrogen-cycling functional traits and taxa in distant coastal sediments reveal important community assembly mechanisms. *Front. Microbiol.* 14:1291242. doi: 10.3389/fmicb.2023.1291242

Discordant patterns between nitrogen-cycling functional traits and taxa in distant coastal sediments reveal important community assembly mechanisms

Wen Song[1†], Hongjun Li[2†], Yuqi Zhou[1], Xia Liu[1], Yueyue Li[1], Mengqi Wang[1], Dan-dan Li[1] and Qichao Tu[1*]

[1]Institute of Marine Science and Technology, Shandong University, Qingdao, China, [2]State Environmental Protection Key Laboratory of Coastal Ecosystem, National Marine Environmental Monitoring Center, Dalian, China

A central question in microbial ecology is how immense microbes are assembled in changing natural environments while executing critical ecosystem functions. Over the past decade, effort has been made to unravel the contribution of stochasticity and determinism to the compositional of microbial communities. However, most studies focus on microbial taxa, ignoring the importance of functional traits. By employing shotgun metagenomic sequencing and state-of-the-art bioinformatics approaches, this study comprehensively investigated the microbially mediated nitrogen (N) cycling processes in two geographically distant coastal locations. Both shotgun and 16S rRNA gene amplicon sequencing demonstrated significantly differed taxonomic compositions between the two sites. The relative abundance of major microbial phyla, such as *Pseudomonadota*, *Thaumarchaeota*, and *Bacteroidota*, significantly differed. In contrast, high homogeneity was observed for N-cycling functional traits. Statistical analyses suggested that N-cycling taxonomic groups were more related to geographic distance, whereas microbial functional traits were more influenced by environmental factors. Multiple community assembly models demonstrated that determinism strongly governed the microbial N-cycling functional traits, whereas their carrying taxonomic groups were highly stochastic. Such discordant patterns between N-cycling functional traits and taxa demonstrated an important mechanism in microbial ecology in which essential ecosystem functions are stably maintained despite geographic distance and stochastic community assembly.

KEYWORDS

nitrogen cycling, community assembly, microbial communities, functional traits, taxonomic groups, coastal sediments

Introduction

Nitrogen (N) is an essential element of nutrition in the Earth biosphere, making up critical life components such as proteins and nucleic acids (Kuypers et al., 2018). The regulation of N supply constrains the primary productivity of many natural ecosystems (Falkowski et al., 1998). In nature, the cycling of N is primarily driven by microorganisms, by whom N is converted among different redox states (Nelson et al., 2016), closely linked to biogeochemical cycles such

as carbon, sulphur, phosphorus, and others, influencing the structure and functioning of ecosystems (Qian et al., 2023). Specifically, N-cycling microorganisms constitute an important part of biodiversity in natural ecosystems and ultimately affect ecosystem function by mediating a series of processes, including nitrogen fixation, nitrification, denitrification, ammonium oxidation, dissimilatory/assimilatory nitrate reduction to ammonium, and ammonification (Damashek and Francis, 2018). A critical question in microbial ecology is how different microorganisms are assembled into complex communities to execute these essential ecological processes.

Over the past years, much progress has been made toward our understanding of the microbially driven N-cycling processes on Earth. Novel discoveries have been continuously made, such as the discovery of complete nitrification of ammonia via nitrite to nitrate by a single microorganism (Daims et al., 2015; van Kessel et al., 2015), the regulatory and metabolic adaptations in the nitrogen assimilation of marine *Picocyanobacteria* (Díez et al., 2023), and widespread and abundant nitrogen-fixing populations of *Pseudomonadota* and *Planctomycetota* in marine and river ecosystems (Delmont et al., 2018; Behera et al., 2021b). By employing high-throughput amplicon sequencing technologies, recent studies have revealed surprisingly high genetic diversity of N-cycling marker genes in various ecosystems (Damashek and Francis, 2018; Li et al., 2023), suggesting high redundancy of N-cycling functional traits. For instance, using the Pearl River Estuary (PRE) as a study system, researchers have delineated the diversity and abundance of key microbial nitrogen cycling gene families and their carrying taxa (Wang et al., 2021). However, our understanding regarding the ecological perspectives of the whole N-cycling community remains fragmented. Questions such as how different microorganisms collaboratively maintain the stability of N-cycling function in different ecosystems require further attention.

Although high-throughput amplicon sequencing approaches provide novel insights into the genetic diversity of N-cycling gene families, technical barriers exist in cross-linking whole N-cycling processes with taxonomic compositions, limiting systematic understanding of the N-cycling pathway in complex ecosystems. Notably, technical advances in metagenomic sequencing have more or less overcome the barriers in amplicon sequencing approaches. By employing accurate functional gene databases (Tu et al., 2018; Wang et al., 2021; Mosley et al., 2022), the linkage between N-cycling microbial functional traits and taxa can be accurately and efficiently resolved (Wang et al., 2021; Song et al., 2022), providing a technological basis for disentangling the underlying ecological mechanisms at the whole pathway level.

The coastal sediments comprise a major part of the ocean ecosystem, serving as the transition zone between the terrestrial and open ocean. The high community diversity and immense biogeochemical cycling processes they mediate in coastal sediments make them an ideal place to investigate the ecological mechanisms underlying complex biogeochemical cycling processes, including N cycling. In this study, the microbial communities involved in N-cycling processes in two distant coastal sediments were investigated, aiming to address the following two ecological questions: (1) Do geographically distant coastal sediments harbor distinct N-cycling communities? (2) What ecological mechanisms mediate the diversity patterns of N-cycling communities? As previously described in other ecosystems (Nelson et al., 2016; Sunagawa et al., 2020), we expected vast diverse microbial taxa in mediating different N-cycling processes. As a critical ecosystem function, N-cycling functional traits show relatively stable distributions across space, but their carrying microbial taxa may vary greatly. Consequently, we expected the assembly of N-cycling functional traits to be highly deterministic, while the taxonomic groups would be more stochastic. The results supported our expectation and demonstrated a microbial community assembly mechanism in which essential ecosystem functions are stably maintained despite geographic distance differences and stochastic community assembly.

Materials and methods

Coastal sediment collection

Two coastal sediments were surveyed in this study, including temperate (Yalu River, YLR) and tropical (Beibu Gulf, BBG) coastal sediments in the North and South China Sea. The BBG sampling site is located at 21°07′54″ ± 8′67″N, 108°91′08″ ± 8′58″E, covering an area of approximately 16,136 km^2. The YLR sampling site is located at 39°68′83″ ± 1′10″N, 123°93′14″ ± 3′44″E, covering an area of approximately 472.57 km^2 (Figure 1). A total of 29 and 18 sedimental samples were collected for the YLR and BBG locations, respectively, during the cruises conducted by the National Marine Environmental Monitoring Center of Dalian on 16 July 2020 and 8 September 2020 (Supplementary Table S1). For each sampling site, three sediment replicates were collected using a van Veen grab measuring 0.05 m^2 and subsequently combined to achieve homogenization. Each site yielded a 500 g sediment sample, which was preserved on ice and promptly transported to the laboratory within 24 h and stored at −80°C before measuring physiochemical properties and DNA extraction.

Measuring physiochemical properties of sediment samples

The collected sediment samples were freeze-dried before analyzing their geochemical characteristics. The pH and salinity values were measured using probes (ORION STRAR A212 and EUTECH SALT 6+; Thermo Scientific, USA) with a 1:2.5 (m/v) and 1:5 (m/v) ratio of sediment to water. The concentrations of total phosphorus (TP), total nitrogen (TN), nitrate (NO_3^--N), nitrite (NO_2^--N), ammonium (NH_4^+-N), and water-soluble sulphates (SO_4^{2-}) in sediment solutions were determined by ultraviolet spectrophotometry. Sedimental NH_4^+-N, NO_3^--N, and NO_2^--N were extracted by adding 12 mL of 1 M KCl to 2 g sediment, and the sediment SO_4^{2-} was extracted by adding 10 mL deionized water to 2 g sediment, vortexed at maximum speed for 20 min, and spun at 5,000 × *g* for 5 min. The supernatants were taken to determine the concentrations with an automated procedure (CYTATION™5; BIOTEK, USA) by measuring the absorbance at 630 nm, 410 nm, 543 nm and 420 nm (Cawse, 1967; Nelson, 1983). The DIN concentration was calculated as the sum of NH_4^+-N, NO_3^--N and NO_2^--N. The TN and TP were analyzed by weighing 2.5 g sediment, adding 35 mL alkaline $K_2S_2O_8$ oxidizer solution, mixing well and digestion in an autoclave at 121°C for 60 min. The supernatants were taken to determine the concentrations with an automated procedure (CYTATION™5; BIOTEK, USA) to measure absorbance at 630 nm

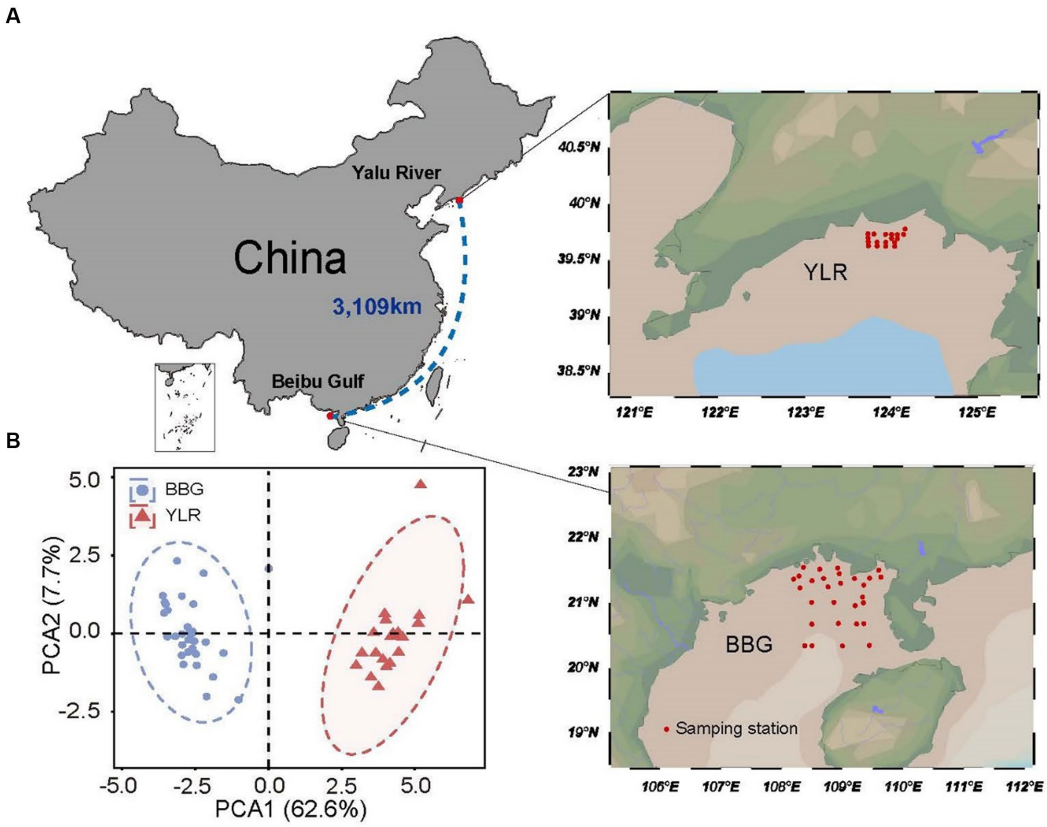

FIGURE 1
Locations of the 47 sampling stations on the temperate and subtropical coasts of China investigated in this study. **(A)** Sedimental samples were collected in two coastal sediments, including Beibu Gulf (BBG) and Yalu River (YLR). The geographic distance between the two sampling sites is 3,109 km. **(B)** Principal component analysis for environmental heterogeneity between the two sampling sites based on the environmental factor data.

and 700 nm. The organic carbon was determined by the potassium dichromate approach (Mebius, 1960). The NH_4^+-N, NO_3^--N, NO_2^--N, SO_4^{2-}, TN, TP and petroleum hydrocarbon (PH) variables were measured following methods based on the National Standard of China (GB17378.3–2007). Moreover, inductively coupled plasma–mass spectrometry (ICP–MS, Optima, 2000 DV, PerkinElmer, USA) was used to measure the contents of seven heavy metals, including Hg, Cd, Pb, Cr, As, Cu, and Zn (Yuan et al., 2004).

DNA extraction and sequencing

For each sample, approximately 0.5 g of thoroughly mixed sediment was used to extract genomic DNA using the DNeasy® PowerSoil Kit (QIAGEN, GERMANY, USA), following the manufacturer's protocols. The quantity of DNA was assessed by a NanoDrop ONE (Thermo Scientific, USA) with a range of 40–60 ng/μL and stored at −80°C. An aliquot (50 ng) of purified DNA from each sample was sent to Novogene (Novogene Inc., Tianjin, China) for shotgun metagenomic sequencing and amplicon sequencing of the V3–V4 region (338F-806R) of bacterial 16S rRNA genes. The universal primers 338F (5′-ACTCCTACGGGAGGCAGCA-3′) and 806 R (5′-GGACTACHVGGGTWTCTAAT-3′) were used for PCR amplification of 16S rRNA genes. For both shotgun metagenomic and amplicon sequencing, the Illumina HiSeq PE2500 platform was used for paired-end sequencing. The 16S rRNA gene amplicon sequencing was performed for all 47 samples, while shotgun metagenome sequencing was performed for a total of 27 samples (14 for BBG and 13 for YLR).

Metagenomic profiling of N-cycling microbial communities

In order to profile microbially mediated N-cycling processes from the shotgun metagenome sequencing data, the manually curated functional gene database NCycDB[1] (Tu et al., 2018) was used. Briefly, shotgun metagenomic sequences were searched against NCycDB databases using DIAMOND (v 0.9.25) (Buchfink et al., 2015) in blastx mode using parameters "-k 1 -e 0.0001." Sequences matched to NCycDB were extracted to generate functional gene profiles of N-cycling microbial communities. The Perl script in NCycDB was used to obtain functional profiles. A random subsampling procedure was applied to normalize the total number of sequences for each sample to the minimum sequencing depth. To acquire the taxonomic profiles for N-cycling microbial communities, the seqtk program was

1 https://github.com/qichao1984/NCyc

used to extract the sequences mapped by NCycDB. Taxonomic assignment was then carried out using Kraken 2 (Wood et al., 2019). A taxonomic profile was generated for the N-cycling pathway at various taxonomic levels using a standard local Kraken2 database. In this study, we defined each microbially mediated N-cycling gene family as one functional trait for mediating a specific process/function (Violle et al., 2007), whereas the corresponding microbial species as taxa. The abundance of each N-cycling gene family was calculated as the proportion of each nitrogen cycling gene to the total number of all nitrogen cycling genes in each sample. The total number of sequences referred to all N-cycling gene related reads.

16S rRNA gene amplicon sequencing analysis

The 16S rRNA gene amplicon sequence data were processed using the DADA2 pipeline (Callahan et al., 2016). The raw data was first demultiplexed according to the barcode, followed by primer removal. Longer sequences were obtained by merging forward and reverse reads for subsequent analysis. Chimeras were identified and removed. Then, these sequences were filtered to remove chimeras and sequences of nonbacterial origin. These sequences were further clustered into amplicon sequence variants (ASVs), resulting in 15,735 ASVs. The ASV abundance profile was then subjected to a random subsampling effort of 7,944 per sample. Taxonomy assignment was carried out against the Ribosomal Database Project (RDP) 16S rRNA gene training set online database[2] (Wang et al., 2007). The default confidence interval cutoff of 80% was used for the RDP classifier.

MiTAG profiling of microbial communities

In addition to 16S rRNA gene amplicons, the miTAG approach (Logares et al., 2014) was also employed to profile bacterial community composition from metagenome sequences, providing complementary information to 16S rRNA gene amplicon data without potential bias caused by PCR amplification. Here, SortMeRNA (Kopylova et al., 2012) was used to extract 16S rRNA sequences from shotgun metagenomes by searching the metagenomic reads against the Silva SSU database (V138) (Yilmaz et al., 2014). Reads matching the Silva SSU database with an e-value $<10^{-4}$ were further filtered with custom Perl and R scripts. A total of 88,987 MiTAG sequences were recovered from the shotgun metagenomes, resulting in 7,490 sequences per sample. The RDP classifier was then employed for taxonomic assignment of the extracted sequences. Microbial profiles were generated at different taxonomic levels.

Statistical analyses of community diversity and structure

The non-metric multidimensional scaling (NMDS) ordination was performed to explore the compositional differences in microbial functional traits and taxonomic groups between BBG and YLR. The Bray–Curtis dissimilarity index was employed to quantify the differences among different samples. Response ratio analysis (Lajeunesse, 2011) was employed to evaluate the differences in the relative abundance of N-cycling microbial functional traits and taxonomic groups present in BBG and YLR sediments.

$$\mathrm{RR} = \ln\left(\frac{\bar{X}_B}{\bar{X}_Y}\right) = \ln\left(\bar{X}_B\right) - \ln\left(\bar{X}_Y\right)$$

where RR is the natural-log proportional change in the mean relative abundance ($\bar{X}$) of BBG and YLR sediments.

Correlating environmental factors with N-cycling communities

Multiple statistical tests were conducted to investigate the potential environmental factors that affect the variations in the composition and diversity of N-cycling functional traits and taxa. First, the effects of environmental factors on N-cycling functional traits and taxa were evaluated using the partial Mantel test. The distance matrices for N-cycling functional traits and taxa were, respectively, correlated with environmental parameters. Second, to determine the potential correlation between community similarity and environmental heterogeneity, a thorough assessment was conducted. The environmental factors that we used to calculate environmental distance included temperature, pH, salinity, NH_4^+-N, NO_3^--N, NO_2^--N, SO_4^{2-}, TN, TP, petroleum hydrocarbons (PHs), organic carbon (OC), organic matter (OM), Hg, Cd, Pb, Cr, As, Cu, and Zn. Here, the pairwise environment distances between different samples were calculated using Euclidean distance. The Bray–Curtis community similarity of N-cycling communities (functional traits and taxa) was correlated with the Euclidean distance of environmental conditions based on Spearman's rank correlations. Third, to include potential nonlinear relationships and multivariate interactions, a random-forest machine-learning approach was used to estimate the important predictors for both N-cycling functional traits and taxonomic groups (Liaw and Wiener, 2002). The relative importance of environmental factors in explaining the compositional differences in N-cycling microbial functional traits and taxa (phylum level) were investigated. To conduct the above analyses, R packages such as "vegan," "randomForest," and "relaimpo" were used.

Inferring community assembly mechanisms

In addition to investigating the effects of environmental factors on N-cycling communities, we also compared the relative contributions of deterministic and stochastic processes to N-cycling processes. Three complementary analyses were carried out for N-cycling microbial functional traits and taxa. First, variation partitioning analysis (VPA) was employed to evaluate the relative importance of environmental factors and geographic distance in shaping the compositional variations in N-cycling communities. We calculated spatial variables based on the longitude and latitude coordinates of

2 http://rdp.cme.msu.edu/classifier/classifier.jsp

each sampling station using the principal coordinates of neighbor matrices (PCNMs) (Lear et al., 2014; Righetti et al., 2019). The canonical correlation analysis (CCA) model was employed to select spatial and environmental variables using a forward selection procedure. VPA factors were chosen based on significance levels ($p < 0.05$) until no improvement in VPA was observed with additional new variables. After selection based on forward selection and Arch Effect *p*-values. The final VPA model includes PCNM14, PCNM16, PCNM18, PCNM24, pH, salinity, NH_4^+-N, SO_4^{2-}, TN, TP, Zn, Hg, and Cr. Second, a null-model approach was used to quantify the relative importance of deterministic vs. stochastic processes. Using Bray–Curtis distance, a null distribution of beta diversity was obtained by shuffling the original communities randomly (1,000 randomizations), on the basis of which we calculated the normalized stochasticity ratio (NST) (Ning et al., 2019). During the assembly process, a ratio of 50% was chosen as the cutoff to distinguish between more deterministic (50% or less) and more stochastic assembly (over 50%) processes. Third, in addition to the null-model approach, a neutral community model (NCM) was also employed to determine the potential importance of stochastic processes on community assembly (Sloan et al., 2006). It was predicted that species frequency and relative abundance across the wider metacommunity would be correlated in the NCM. The parameter R^2 represents the overall fit to the neutral model within the 95% confidence interval of the NCM predictions. R packages including vegan (e.g., pcnm, bioenv), NST, and tidyverse were used for the above analyses. All statistical analyses were performed in R software (v.4.3.2) (Oksanen et al., 2013).

Results

Overall community characteristics in BBG and YLR sediments

A total of 29 and 18 sediment samples were collected from the BBG and YLR sampling sites, respectively. These two sampling sites were geographically distant (3,109 km) and distinctly different in environmental conditions (Figures 1A,B). All samples were subjected to 16S rRNA gene amplicon sequencing, while 27 of them (13 from BBG and 14 from YLR) were subjected to shotgun metagenomic sequencing (Supplementary Table S2). For each sample, an average of 53,780 high-quality 16S rRNA sequences and 20 Gb shotgun metagenome sequences were obtained. Random subsampling of 7,944 16S rRNA gene sequences resulted in 2,903 and 9,221 ASVs per sample for BBG and YLR, respectively. In addition, these two sampling sites were found to have distinctly different microbial compositions, as revealed by both 16S rRNA gene amplicon sequencing and 16S rRNA gene extraction from shotgun metagenomes (i.e., miTAG microbial profiles, Supplementary Figure S1).

Interestingly, distinct microbial taxa carried homogeneous N-cycling functional traits. Microbial communities involved in N-cycling processes were extracted by searching shotgun metagenomes against NCycDB (Tu et al., 2018), a manually curated functional gene database targeting N-cycling pathways. An average of 131,752,546 sequences were found to be N-cycling genes in each sample, occupying 0.54% of the total sequences. Taxonomic assignment of these N-cycling genes using Kraken2 showed an assignment rate of 38.7% to currently known microbial taxa, suggesting that a high portion of N-cycling genes were still taxonomically unknown. In total, 53 N-cycling functional traits and 5,588 taxonomic groups were found to be present in at least one sample. The relative abundances of functional traits were highly similar and compositionally not distinguishable (Figure 2A). In contrast, consistent with the whole community level, a significantly different taxonomic composition was observed for the N-cycling communities (Figure 2B).

Functionally, microbial functional traits mediating N-cycling processes were relatively evenly and stably distributed across different sampling sites in BBG and YLR, regardless of their locations (Figures 2A, 3A). Among the various N-cycling processes, only assimilatory nitrate reduction to nitrite (ANRN) showed significantly differed relative abundances between BBG and YLR (Figure 3A). Consequently, gene families including *nasA*, *nasB* and *narB* were more abundant in BBG (Supplementary Table S2). This suggested that the southern sampling site BBG could be more functional in assimilatory conversion of ammonia into nitrite. Bacterial *amo* gene families were more abundantly detected in the YLR sediment than in the BBG sediment, suggesting that AOB taxa may favor lower temperature in the ocean sediment (Supplementary Table S2). In addition, gene families including *napA*, *narHIZ*, *nirK*, and *norC* involved in denitrification and DNRN (dissimilatory nitrate reduction to nitrite) also showed significant differences in relative abundance between BBG and YLR (Supplementary Table S2). The different patterns in the relative abundance of *nap* (e.g., *napAB*) and *nar* (e.g., *narHIZ*) between BBG and YLR suggested that these two sites favored different gene families in dissimilatory nitrate reduction to nitrite. In both BBG and YLR, the relative abundances of archaeal *amo* gene families were all significantly higher than those of bacterial *amo* gene families (Supplementary Figure S2A), suggesting that archaea rather than bacteria dominated ammonia oxidization to hydroxylamine in the investigated coastal sediments.

Taxonomically, much more complex information was observed than functional traits. First, the N-cycling communities were dramatically different from the whole prokaryotic communities, based on either the 16S amplicon or miTAG results (Figure 2B; Supplementary Figure S3). Taxonomic assignment against the RDP database identified a total of 54 phyla for the MiTAG dataset. In contrast, for the 16S rRNA gene amplicon dataset, 36 phyla were identified. Not surprisingly, these two different approaches generated substantially different microbial profiles, even at the phylum level (Supplementary Figure S3). For instance, the relative abundance for the major phyla dramatically differed using these two approaches, which was especially evident for the YLR samples (Supplementary Figure S3). Nonetheless, both approaches demonstrated dramatically different community compositions between BBG and YLR. *Actinomycetota* was overall more abundantly detected in YLR than in BBW, but with a similarly high contribution to N-cycling processes. Microbial taxa belonging to *Acidobacteriota* and *Chloroflexota* were rarely found in N-cycling communities but were abundantly observed in the sediments. *Pseudomonadota* and *Actinomycetota* dominated the N-cycling communities at both sites, contributing 65.9–84.4% and 9.1–17.8% of the relative abundance, respectively (Figure 2B). *Pseudomonadota* taxa were significantly more abundant in BBG, whereas *Bacteroidota*, *Thaumarchaeota*, and *Methanobacteriota* taxa were more abundant in YLR (Figure 2B; Supplementary Figure S4). Of these, *Thaumarchaeota* was mainly

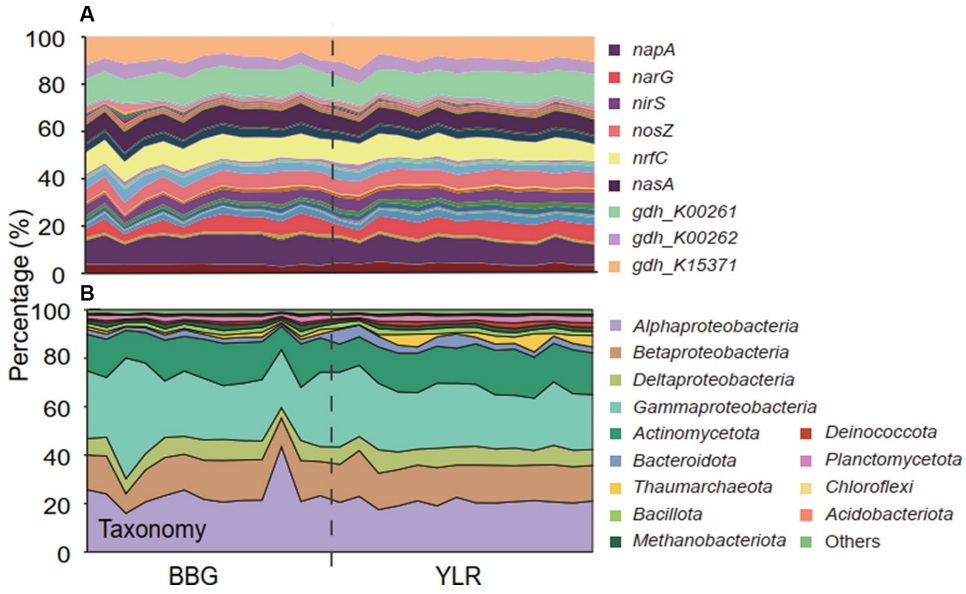

FIGURE 2
The composition of microbial N-cycling functional traits and taxa (phylum-level, class-level for *Pseudomonadota*) in BBG and YLR. **(A)** Relative abundances of microbial N-cycling functional traits. Color codes were displayed for the top 9 most abundant gene families. Supplementary Table S2 contains the exact relative abundance and corresponding color for each functional trait. **(B)** Relative abundances of different taxonomic groups.

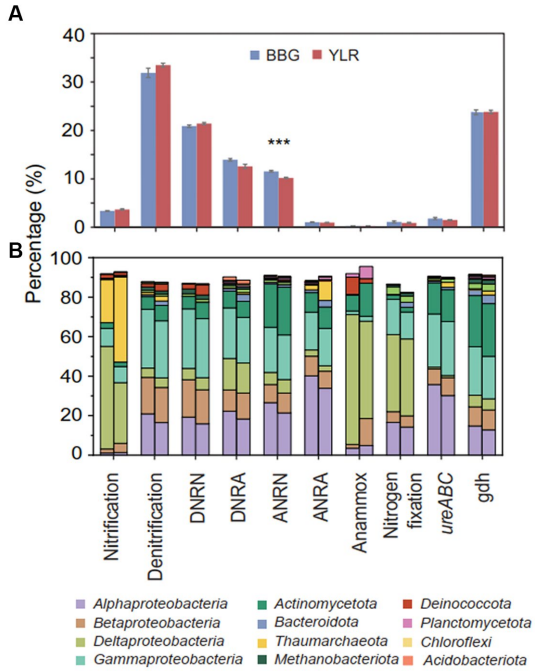

FIGURE 3
(A) Relative abundances of different N-cycling pathways. Significant differences between the two sampling sites were displayed by asterisks (***$p < 0.001$). **(B)** The left (BBG) and right (YLR) bars represent the average relative abundance of N-cycling microbial communities at the phylum (top 10 in abundance) and class (top 4 in abundance) levels. Different N-cycling pathways were shown. DNRN, dissimilatory nitrate reduction to nitrite; DNRA, dissimilatory nitrite reduction to ammonia; ANRN, assimilatory nitrate reduction to nitrite; ANRA, assimilatory nitrite reduction to ammonia.

detected in nitrification (21.8% in BBG and 43.1% in YLR) and assimilatory nitrite reduction to ammonia (ANRA) (2.52% in BBG and 9.75% in YLR, Figure 2D). Second, different N-cycling processes and functional traits were mediated by highly different microbial taxonomic groups (Figure 3B; Supplementary Figure S2B). For instance, nitrification, the process that converts ammonia into nitrate, was mainly mediated by *Deltaproteobacteria* and *Thaumarchaeota* in this study. Anammox, which converts ammonium into dinitrogen and was low in relative abundance, was mainly mediated by *Deltaproteobacteria* and *Actinomycetota*. Almost all denitrification gene families were dominated by *Pseudomonadota* (71 to 98.4%), except *nirK*, for which *Thaumarchaeota* (49.5%) was the dominant phylum. Third, different N-cycling processes were generally similar in relative abundance between BBG and YLR. However, their taxonomic composition between BBG and YLR was considerably different (Figure 3B). For instance, the relative contribution of *Deltaproteobacteria* and *Thaumarchaeota* to nitrification dramatically differed between BBG and YLR. For anammox, in addition to the major and different contributions of *Deltaproteobacteria* and *Actinomycetota* to anammox in BBG and YLR, BBG was also enriched by *Methanobacteriota*, whereas YLR was enriched by *Planctomycetota* and *Betaproteobacteria*. Such results suggested that geographically distant coastal sediments were similar in N-cycling functional traits but dramatically different in their carrying microbial taxa.

Environmental drivers of sedimental N-cycling communities

Dramatically different diversity patterns in composition were observed between the N-cycling functional traits and their carrying

microbial taxonomy. First, the taxonomic composition of N-cycling microbial communities between BBG and YLR sediments was clearly different, whereas the structure of N-cycling microbial functional traits was compositionally not distinguishable (Figures 4A,B). Second, for both BBG and YLR, functional traits showed much lower between-sample community similarity than taxonomic groups (Figure 4C). We therefore expected different effects of environmental conditions on N-cycling functional traits and taxonomy.

We first investigated the overall influence of environmental variables on N-cycling communities. Here, the Euclidean distance of

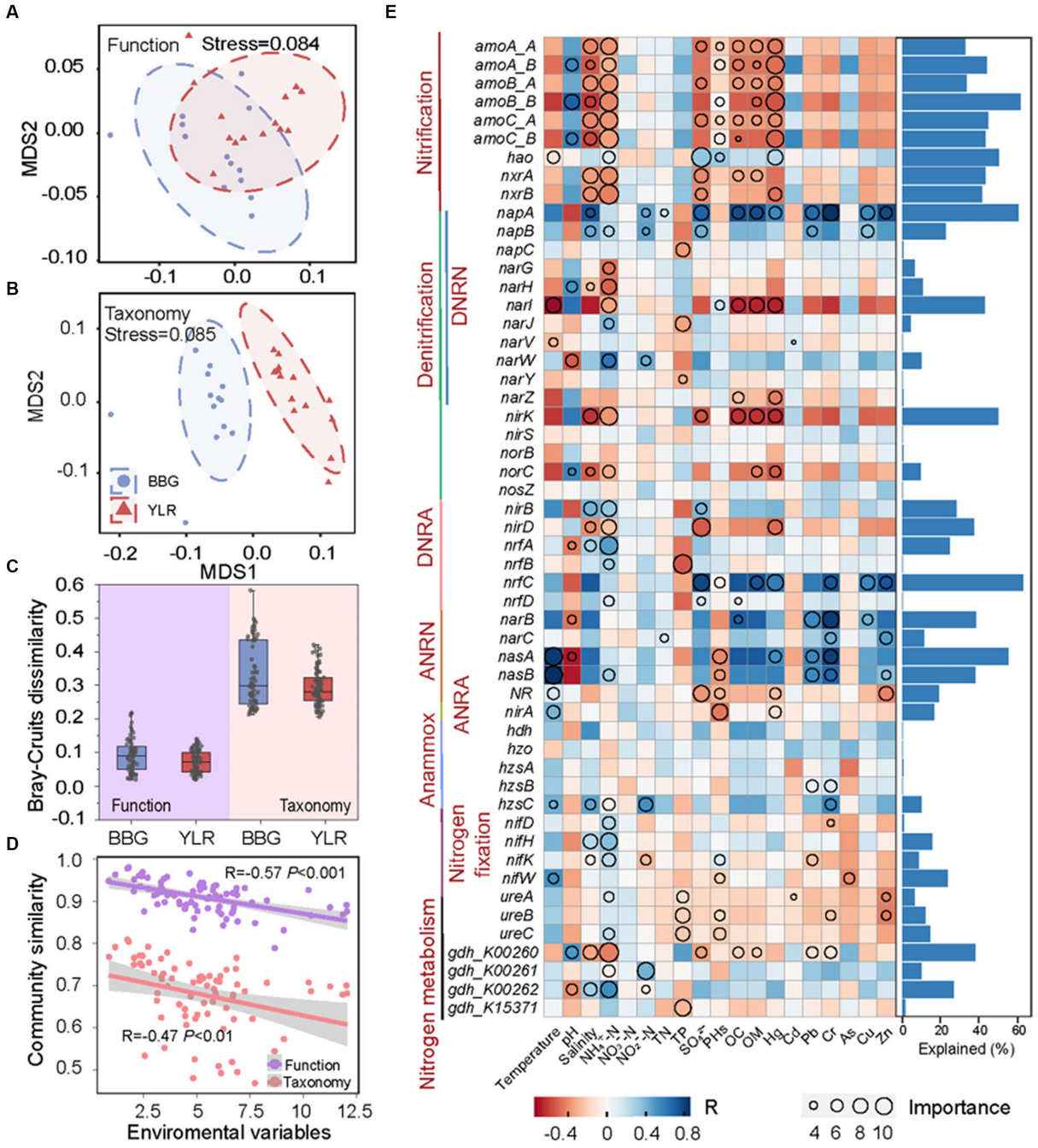

FIGURE 4
Relationship between N-cycling communities and environmental factors in BBG and YLR sampling sites. In order to assess the distance compositional variation of N-cycling functional trait **(A)** and taxa **(B)**, a non-metric multidimensional scaling (NMDS) was applied based on Bray–Curtis dissimilarity. **(C)** Bray–Curtis dissimilarity of N-cycling functional trait and taxa in BBG and YLR. **(D)** Spearman's rank correlations between the Bray–Curtis similarity of N-cycling communities and the Euclidean distance of environmental variables. **(E)** Explainable variations by different environmental factors for different functional traits. As indicated by the heatmap (on the left panel), environmental factors were important in explaining the variations in functional traits based on random forest analysis, whereas the circle size indicated the degree to which environmental factors played a role. In the right panel, bar plots represent the variations explained by the best environmental factor (the circle with the largest diameter). DNRN, dissimilatory nitrate reduction to nitrite; DNRA, dissimilatory nitrite reduction to ammonia; ANRN, assimilatory nitrate reduction to nitrite; ANRA, assimilatory nitrite reduction to ammonia.

19 environmental conditions was calculated as a measurement of environmental heterogeneity and was correlated with N-cycling community similarity based on functional traits and taxonomic groups. Strong negative associations between environmental heterogeneity and N-cycling community similarity were observed (Figure 4D). Notably, a stronger association was observed between environmental heterogeneity and N-cycling functional traits ($R = -0.57$, $p < 0.001$) than taxonomic groups ($R = -0.47$, $p < 0.01$). In addition, the partial Mantel test by sequentially excluding individual environmental parameters showed that four environmental factors were significantly associated with the N-cycling taxonomic composition, while the number of significantly associated environmental parameters was eight for functional traits (Supplementary Table S3). This suggested that environmental heterogeneity exerted a stronger influence on the compositional difference of N-cycling functional traits than taxonomic groups, although N-cycling functional traits harbored weaker compositional variation than microbial taxa. The influence of environmental factors on individual N-cycling functional traits and taxonomic groups was also investigated using a multiple stepwise regression model and a machine learning approach random forest. As a result, multiple N-cycling functional traits can be well explained by one or more environmental factors (Figure 4E). The effects of different environmental variables on the functional traits belonging to the same process were generally similar, suggesting that microorganisms performing the same function tended to be involved in the same ecological niche. For instance, functional traits involved in nitrification were strongly associated with salinity, NH_4^+-N, and Hg, with explanation rates larger than 40%. In addition, functional traits involved in ANRN were strongly associated with heavy metal contamination, such as Pb and Cr. Among various environmental factors, NH_4^+-N was the major factor affecting multiple functional traits involved in different processes. In contrast, the association between environmental factors and taxonomic groups was relatively weak, especially for abundant phyla. Notably, *Thaumarchaeota* and *Methanobacteriota*, which are two representative phyla involved in nitrification and anammox, were best explained by NH_4^+-N (Supplementary Figure S5). This was consistent with the fact that both nitrification and anammox were intermediated with ammonia.

Community assembly mechanisms for N-cycling communities

Both deterministic and stochastic processes shape the compositional variations of complex microbial communities. Here, multiple approaches were used to quantify the role that deterministic and stochastic processes play in shaping the functional and taxonomic composition of the sedimental N-cycling communities. First, the contributions of geographic distance and environmental variables in explaining N-cycling communities were quantified (Figure 5A). The total explained ratios by geographic distance and environmental variables were similar for N-cycling microbial functional traits (84.6%) and taxa (81.6%). However, the ratios of geographic distance and environmental variables were dramatically different. The pure explanation ratio of environmental variables was 44% for functional trait composition, but was only 16.8% for taxonomic composition. This indicated that N-cycling functional traits were more strongly affected by environmental conditions, consistent with the above results obtained by partial Mantel tests and random forest modeling. Second, which is consistent with the VPA results, analyses of stochastic ratios indicated a high degree of determinism in the assembly of N-cycling functional traits (0.36), whereas the assembly of N-cycling taxonomic groups was more stochastic (0.81, Figure 5B). Third, the NCM was used to estimate and predict the frequency distribution of N-cycling functional traits and taxonomic groups. The frequency of N-cycling functional traits was poorly predicted by the NCM (Figure 5C). In contrast, the frequency of microbial taxonomic groups that occurred in communities was well described by the NCM, explaining as much as 91.4% of compositional variations (Figure 5D), suggesting that neutral processes governed the frequency and occurrence of N-cycling taxonomic groups. Integrating all of the above lines of evidence, the results demonstrated that N-cycling functional traits were highly deterministic, whereas their carrying microbial taxa were relatively stochastic.

Discussion

Microbial communities mediating N-cycling processes

Linking microbial function with taxonomy has been challenging in the field of microbial ecology due to the vast diversity and unknown majority of microbial taxa in natural ecosystems (Fierer, 2017). The emerging shotgun metaghenome sequencing technology has been routinely used to elucidate the structure, function, and ecology of microbiota in evolving climates and ecosystems (Behera et al., 2021a,b). In this study, by employing shotgun metagenome sequencing and the current state-of-the-art curated functional gene database (NCycDB) (Tu et al., 2018), the diversity and compositional variations of microbial communities responsible for N cycling were investigated in two geographically distant coastal sediments. Comparative analyses were conducted from two different perspectives, including functional traits and taxonomic groups. Several interesting findings were obtained. First, despite the fact that different techniques generate different microbial profiles (e.g., 16S amplicon vs. miTAG) (Logares et al., 2012, 2014). However, the taxonomic composition of N-cycling communities was dramatically different from that of the whole microbial communities. Similar findings were obtained from other ecosystems, such as the Ganges ecosystem (Parida et al., 2022), suggesting that N-cycling processes occurred in selective microbial taxa (Strom, 2008). Second, although lowly detected in the overall communities, microbial phyla such as *Bacteroidota*, *Thaumarchaeota*, and *Methanobacteriota* played critical roles in N-cycling and were significantly enriched in YLR sediments, especially *Thaumarchaeota*, which was found to be the major phyla responsible for nitrification and nitrite reduction by *nirK* (Reji et al., 2019). Such results suggested that rare and less abundant microbial taxa may have executed critical ecosystem functions in natural environments (Jousset et al., 2017). Third, consistent with several previous studies (He et al., 2012; Kozlowski et al., 2016; Kitzinger et al., 2019), archaea (more specifically *Thaumarchaeota*) rather than bacteria dominated the process of ammonia oxidization to hydroxylamine. All these results demonstrated that whole N cycling is a result of collaborative effort by the vast diverse microbial taxa in the ecosystem (Huber et al., 2007; Nelson et al., 2016).

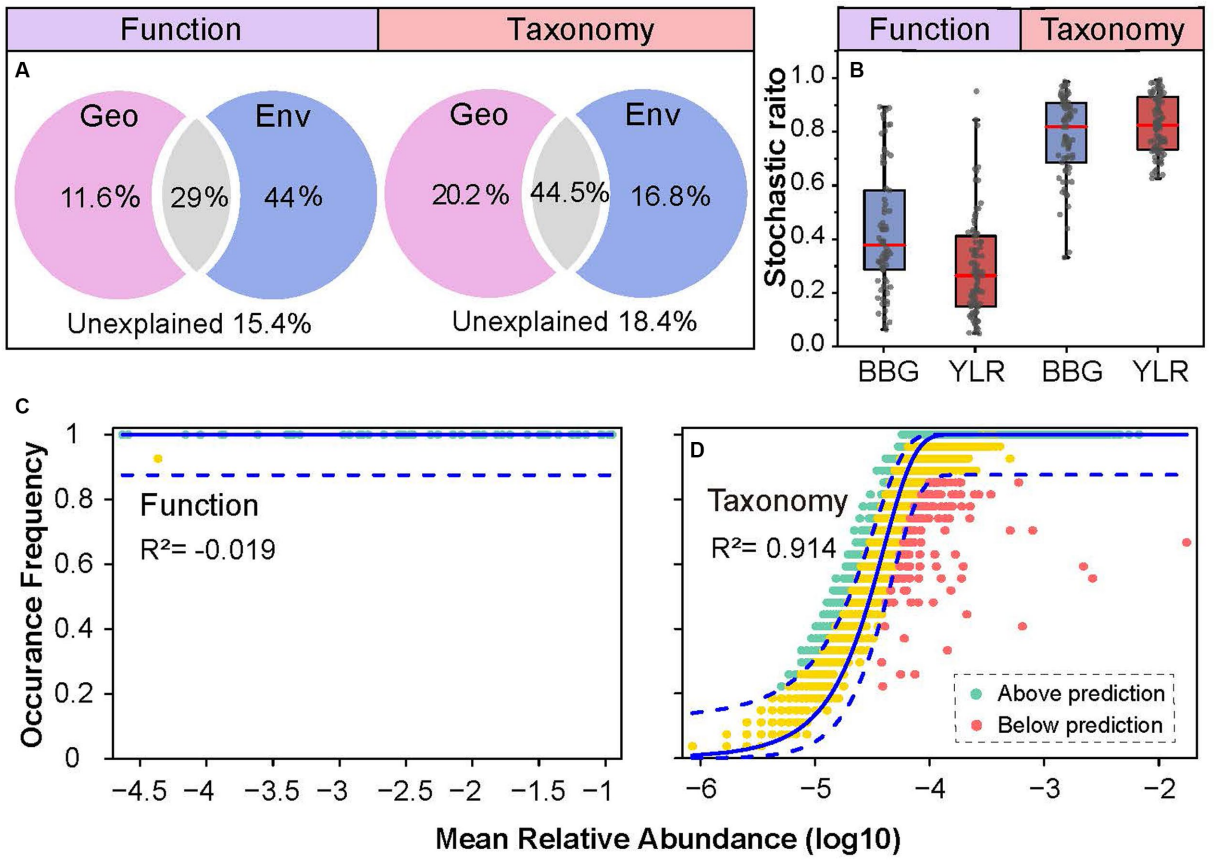

FIGURE 5
Community assembly mechanisms governing N-cycling microbial functional traits and taxa. **(A)** Contribution of geo-environmental factors to N-cycling microbial taxa and functional traits as revealed by variation partitioning analysis. **(B)** Stochastic ratio analyses using a null model showing the relative contribution of stochastic and deterministic processes in the assembly of N-cycling communities. **(C,D)** NCM analyses of community assembly for N-cycling functional traits **(C)** and taxonomic groups **(D)**. The predicted occurrence frequencies for N-cycling functional traits and taxonomic groups communities were analyzed. The model prediction has 95% confidence intervals around it, represented by the dashed blue lines. Community compositions that occurred more or less frequently than predicted by the NCM are shown in different colors.

Discordant patterns between N-cycling functional traits and taxonomy

Divergent trends were identified for the N-cycling functional traits and carrying taxa in the BBG and YLR sediments. Consistent with our expectation, N-cycling functional traits were relatively stably distributed in the two geographically distant coastal sediments, while their carrying microbial taxa dramatically varied. Similar discordant patterns between microbial functional traits and taxonomy have also been observed at much larger scales in different ecosystems, e.g., the global ocean (Sunagawa et al., 2015; Song et al., 2022), global soil (Bahram et al., 2018), polluted river sediment (Behera et al., 2021b; Rout et al., 2022), and human microbiome (Tian et al., 2020). Different microbial ecological principles underlie this phenomenon. First, thousands of different microbial taxa may carry the same functional trait, as revealed by amplicon sequencing studies (Bru et al., 2011; Tu et al., 2016), resulting in high functional redundancy in microbial systems (Allison and Martiny, 2008; Louca et al., 2018; Tian et al., 2020). Therefore, the taxonomic composition of microbial communities executing the same function may vary. Second, the ecosystem selects microbial functional traits rather than taxonomy (Burke et al., 2011). Although species are the basic unit of the life forms in the Earth's biosphere and directly interact with the environment, this study, together with several others (Stilianos et al., 2016; Escalas et al., 2019), suggests that the functional traits carried by microbial taxa are more important in the ecosystem. Variations in microbial taxonomic composition are constrained by the ecosystem to maintain essential ecosystem function, such as N-cycling. Therefore, functional redundancy and ecosystem selection of functional traits jointly shape the variation in N-cycling taxonomic composition and maintain the stability of functional traits.

Perspectives for ecological mechanisms driving microbial community assembly

One of the most critical questions in microbial ecology is how such complex microbial assemblages, consisting of thousands of different taxa, are formed in natural ecosystems (DeLong et al., 2006; Burke et al., 2011; Behera et al., 2021a), performing crucial ecosystem functions and maintaining ecosystem equilibrium. Over the past decade, machine learning algorithms have been conducted by researchers to categorize newly identified and unidentified microorganisms in metagenomic datasets (Choudhury et al., 2023). In addition, many studies have been carried out to disentangle the mechanisms governing complex microbial community assembly

(Stegen et al., 2015; Zhou and Ning, 2017; Wu et al., 2023). A general consensus was that microbial community composition is shaped by a combination of deterministic and stochastic processes (Stegen et al., 2012; Tripathi et al., 2018). Notably, previous studies solely rely on microbial taxonomic composition to infer the relative importance of stochastic vs. deterministic processes (Chen et al., 2019; Huang et al., 2022), ignoring the functional traits carried by microbial taxa. In this study, the relative importance of stochastic vs. deterministic processes was investigated from both taxonomic and functional trait angles. Similar to what has been observed in the global ocean (Song et al., 2022), multiple lines of empirical evidence have indicated that the composition of microbial N-cycling functional traits is predominantly governed by deterministic factors, while N-cycling microbial taxa exhibit a high degree of stochasticity.

Taking together the above evidence and prior knowledge in microbial systems (Goldford et al., 2018), we propose the following explanation for how microbial communities are assembled in natural ecosystems. Essential ecosystem functions are executed and maintained by various microbial taxa in natural ecosystems. Due to functional redundancy in microbial systems (Louca et al., 2018; Biggs et al., 2020), the same functional traits may be carried by many different microbial taxa. Only the microbial taxa executing the required functions and adapting to the environmental conditions were selected by the ecosystem. For instance, despite the extensive release of varied polluted wastewater into the Ganges, abundant phages executing similar functions actively combat harmful pathogens, preserving the river's self-purification capability (Behera et al., 2023). Therefore, microbial functional traits are more important than taxa, especially for functionally redundant communities. The formation of complex microbial assemblages is constrained to guarantee ecosystem multifunctioning and stability. Consequently, the microbial functional trait composition is strongly deterministic, while the taxonomic composition is more stochastic. However, the stochasticity of microbial taxonomic composition may depend on environmental conditions. In light of this, we propose that the ecosystem prioritizes the selection of microbial functional traits over taxonomy, with functional redundancy serving as the foundation for the stochastic composition of microbial taxa.

Conclusion

In this study, the microbially mediated N-cycling processes in two geographically distant coastal sediments were characterized using shotgun metagenome sequencing approaches. By employing state-of-the-art bioinformatics approaches, the composition and diversity patterns of N-cycling microbial functional traits and their carrying taxa were comparatively investigated. Discordant patterns were observed between N-cycling functional traits and taxa. N-cycling functional traits were highly homogeneous between the two distant coastal sediments, while their carrying microbial taxa varied greatly. Further investigation suggested that the compositional variations in N-cycling functional traits were more affected by environmental factors and subjected to deterministic processes. In contrast, the differences in the composition of microbial taxa carrying N-cycling functional traits were highly stochastic. Additionally, this study reveals basic information regarding N-cycling processes mediated by microbes as well as demonstrating an essential ecological mechanism explaining the assembly of complex microbial community assembly in natural ecosystems, whose essential ecosystem functions are maintained despite of geographic distance and stochastic community assembly.

Data availability statement

Sequencing data generated in this study is deposited at the NCBI SRA portal under project ID PRJNA842863 and PRJNA857996, as well as at NODE (https://www.biosino.org/node/) under project ID OEP003498.

Author contributions

WS: Conceptualization, Data curation, Formal analysis, Investigation, Methodology, Writing – original draft. HL: Data curation, Writing – review & editing. YZ: Data curation, Methodology, Writing – review & editing. XL: Methodology, Writing – review & editing. YL: Data curation, Methodology, Writing – review & editing. MW: Investigation, Methodology, Writing – review & editing. D-dL: Writing – review & editing. QT: Conceptualization, Funding acquisition, Project administration, Writing – review & editing.

Funding

The author(s) declare financial support was received for the research, authorship, and/or publication of this article. This study was supported by the National Key Research and Development Program of China (2019YFA0606700, 2020YFA0607600), by the National Natural Science Foundation of China (92051110, 31971446, 32371598), and by the Taishan Young Sholarship of Shandong Province. The funders had no role in the study design, data collection and interpretation, or the decision to submit the work for publication.

Conflict of interest

The authors declare that the research was conducted in the absence of any commercial or financial relationships that could be construed as a potential conflict of interest.

Publisher's note

Supplementary material

The Supplementary material for this article can be found online at: https://www.frontiersin.org/articles/10.3389/fmicb.2023.1291242/full#supplementary-material

References

Allison, S. D., and Martiny, J. B. H. (2008). Resistance, resilience, and redundancy in microbial communities. *Proc. Natl. Acad. Sci. U. S. A.* 105, 11512–11519. doi: 10.1073/pnas.0801925105

Bahram, M., Hildebrand, F., Forslund, S. K., Anderson, J. L., Soudzilovskaia, N. A., Bodegom, P. M., et al. (2018). Structure and function of the global topsoil microbiome. *Nature* 560, 233–237. doi: 10.1038/s41586-018-0386-6

Behera, B. K., Dehury, B., Rout, A. K., Patra, B., Mantri, N., Chakraborty, H. J., et al. (2021a). Metagenomics study in aquatic resource management: recent trends, applied methodologies and future needs. *Gene Reports* 25:101372. doi: 10.1016/j.genrep.2021.101372

Behera, B. K., Patra, B., Chakraborty, H. J., Rout, A. K., Dixit, S., Rai, A., et al. (2023). Bacteriophages diversity in India's major river ganga: a repository to regulate pathogenic bacteria in the aquatic environment. *Environ. Sci. Pollut. Res.* 30, 34101–34114. doi: 10.1007/s11356-022-24637-7

Behera, B. K., Sahu, P., Rout, A. K., Parida, P. K., Sarkar, D. J., Kaushik, N. K., et al. (2021b). Exploring microbiome from sediments of river ganga using a metagenomic approach. *Aquat. Ecosyst. Health Manage.* 24, 12–22. doi: 10.14321/aehm.024.04.04

Biggs, C. R., Yeager, L. A., Bolser, D. G., Bonsell, C., Dichiera, A. M., Hou, Z., et al. (2020). Does functional redundancy affect ecological stability and resilience? A review and meta-analysis. *Ecosphere* 11:03184. doi: 10.1002/ecs2.3184

Bru, D., Ramette, A., Saby, N. P. A., Dequiedt, S., Ranjard, L., Jolivet, C., et al. (2011). Determinants of the distribution of nitrogen-cycling microbial communities at the landscape scale. *ISME J.* 5, 532–542. doi: 10.1038/ismej.2010.130

Buchfink, B., Xie, C., and Huson, D. H. (2015). Fast and sensitive protein alignment using DIAMOND. *Nat. Methods* 12, 59–60. doi: 10.1038/nmeth.3176

Burke, C., Steinberg, P., Rusch, D., Kjelleberg, S., and Thomas, T. (2011). Bacterial community assembly based on functional genes rather than species. *Proc. Natl. Acad. Sci. U. S. A.* 108, 14288–14293. doi: 10.1073/pnas.1101591108

Callahan, B. J., Mcmurdie, P. J., Rosen, M. J., Han, A. W., Johnson, A. J. A., and Holmes, S. P. (2016). DADA2: high-resolution sample inference from Illumina amplicon data. *Nat. Methods* 13, 581–583. doi: 10.1038/nmeth.3869

Cawse, P. A. (1967). The determination of nitrate in soil solutions by ultraviolet spectrophotometry. *Analyst* 92, 311–315. doi: 10.1039/AN9679200311

Chen, W., Ren, K., Isabwe, A., Chen, H., Liu, M., and Yang, J. (2019). Stochastic processes shape microeukaryotic community assembly in a subtropical river across wet and dry seasons. *Microbiome* 7:138. doi: 10.1186/s40168-019-0749-8

Choudhury, N., Sahu, T. K., Rao, A. R., Rout, A. K., and Behera, B. K. (2023). An improved machine learning-based approach to assess the microbial diversity in major North Indian River ecosystems. *Genes* 14:1082. doi: 10.3390/genes14051082

Daims, H., Lebedeva, E. V., Pjevac, P., Han, P., Herbold, C., Albertsen, M., et al. (2015). Complete nitrification by Nitrospira bacteria. *Nature* 528, 504–509. doi: 10.1038/nature16461

Damashek, J., and Francis, C. A. (2018). Microbial nitrogen cycling in estuaries: from genes to ecosystem processes. *Anal. Chim. Acta* 41, 626–660. doi: 10.1007/s12237-017-0306-2

Delmont, T. O., Quince, C., Shaiber, A., Esen, Ö. C., Lee, S. T. M., Rappé, M. S., et al. (2018). Nitrogen-fixing populations of Planctomycetes and Proteobacteria are abundant in surface ocean metagenomes. *Nat. Microbiol.* 3, 804–813. doi: 10.1038/s41564-018-0176-9

Delong, E. F., Preston, C. M., Mincer, T., Rich, V., Hallam, S. J., Frigaard, N. U., et al. (2006). Community genomics among stratified microbial assemblages in the Ocean's interior. *Science* 311, 496–503. doi: 10.1126/science.1120250

Díez, J., López-Lozano, A., Domínguez-Martín, M. A., Gómez-Baena, G., Muñoz-Marín, M. C., Melero-Rubio, Y., et al. (2023). Regulatory and metabolic adaptations in the nitrogen assimilation of marine picocyanobacteria. *FEMS Microbiol. Rev.* 47:fuac043. doi: 10.1093/femsre/fuac043

Escalas, A., Hale, L., Voordeckers, J. W., Yang, Y., Firestone, M. K., Alvarez-Cohen, L., et al. (2019). Microbial functional diversity: from concepts to applications. *Ecol. Evol.* 9, 12000–12016. doi: 10.1002/ece3.5670

Falkowski, P. G., Barber, R. T., and Smetacek, V. (1998). Biogeochemical controls and feedbacks on ocean primary production. *Science* 281, 200–206. doi: 10.1126/science.281.5374.200

Fierer, N. (2017). Embracing the unknown: disentangling the complexities of the soil microbiome. *Nat. Rev. Microbiol.* 15, 579–590. doi: 10.1038/nrmicro.2017.87

Goldford, J. E., Lu, N., Bajic, D., Estrela, S., Tikhonov, M., Sanchez-Gorostiaga, A., et al. (2018). Emergent simplicity in microbial community assembly. *Science* 361, 469–474. doi: 10.1126/science.aat1168

He, J., Hu, H., and Zhang, L. (2012). Current insights into the autotrophic thaumarchaeal ammonia oxidation in acidic soils. *Soil Biol. Biochem.* 55, 146–154. doi: 10.1016/j.soilbio.2012.06.006

Huang, L., Bai, J., Wang, J., Zhang, G., Wang, W., Wang, X., et al. (2022). Different stochastic processes regulate bacterial and fungal community assembly in estuarine wetland soils. *Soil Biol. Biochem.* 167:108586. doi: 10.1016/j.soilbio.2022.108586

Huber, J. A., Mark Welch, D. B., Morrison, H. G., Huse, S. M., Neal, P. R., Butterfield, D. A., et al. (2007). Microbial population structures in the deep marine biosphere. *Science* 318, 97–100. doi: 10.1126/science.1146689

Jousset, A., Bienhold, C., Chatzinotas, A., Gallien, L., Gobet, A., Kurm, V., et al. (2017). Where less may be more: how the rare biosphere pulls ecosystems strings. *ISME J.* 11, 853–862. doi: 10.1038/ismej.2016.174

Kitzinger, K., Padilla, C. C., Marchant, H. K., Hach, P. F., Herbold, C. W., Kidane, A. T., et al. (2019). Cyanate and urea are substrates for nitrification by Thaumarchaeota in the marine environment. *Nat. Microbiol.* 4, 234–243. doi: 10.1038/s41564-018-0316-2

Kopylova, E., Noé, L., and Touzet, H. (2012). SortMeRNA: fast and accurate filtering of ribosomal RNAs in metatranscriptomic data. *Bioinformatics* 28, 3211–3217. doi: 10.1093/bioinformatics/bts611

Kozlowski, J. A., Stieglmeier, M., Schleper, C., Klotz, M. G., and Stein, L. Y. (2016). Pathways and key intermediates required for obligate aerobic ammonia-dependent chemolithotrophy in bacteria and Thaumarchaeota. *ISME J.* 10, 1836–1845. doi: 10.1038/ismej.2016.2

Kuypers, M. M. M., Marchant, H. K., and Kartal, B. (2018). The microbial nitrogen-cycling network. *Nat. Rev. Microbiol.* 16, 263–276. doi: 10.1038/nrmicro.2018.9

Lajeunesse, M. J. (2011). On the meta-analysis of response ratios for studies with correlated and multi-group designs. *Ecology* 92, 2049–2055. doi: 10.1890/11-0423.1

Lear, G., Bellamy, J., Case, B. S., Lee, J. E., and Buckley, H. L. (2014). Fine-scale spatial patterns in bacterial community composition and function within freshwater ponds. *ISME J.* 8, 1715–1726. doi: 10.1038/ismej.2014.21

Li, Y., Ma, K., Song, W., Zhou, J., Liu, X., Wang, M., et al. (2023). Environmental heterogeneity and dispersal limitation simultaneously determine the spatial scaling of different microbial functional groups. *Sci. Total Environ.* 885:163854. doi: 10.1016/j.scitotenv.2023.163854

Liaw, A., and Wiener, M. (2002). Classification and regression by randomForest. *R news* 2, 18–22.

Logares, R., Haverkamp, T. H. A., Kumar, S., Lanzén, A., Nederbragt, A. J., Quince, C., et al. (2012). Environmental microbiology through the lens of high-throughput DNA sequencing: synopsis of current platforms and bioinformatics approaches. *J. Microbiol. Methods* 91, 106–113. doi: 10.1016/j.mimet.2012.07.017

Logares, R., Sunagawa, S., Salazar, G., Cornejo-Castillo, F. M., Ferrera, I., Sarmento, H., et al. (2014). Metagenomic 16S rDNA Illumina tags are a powerful alternative to amplicon sequencing to explore diversity and structure of microbial communities. *Environ. Microbiol.* 16, 2659–2671. doi: 10.1111/1462-2920.12250

Louca, S., Polz, M. F., Mazel, F., Albright, M. B. N., Huber, J. A., O'connor, M. I., et al. (2018). Function and functional redundancy in microbial systems. *Nature Ecol. Evol.* 2, 936–943. doi: 10.1038/s41559-018-0519-1

Mebius, L. J. (1960). A rapid method for the determination of organic carbon in soil. *Anal. Chim. Acta* 22, 120–124. doi: 10.1016/S0003-2670(00)88254-9

Mosley, O., Gios, E., Close, M., Weaver, L., Daughney, C., and Handley, K. (2022). Nitrogen cycling and microbial cooperation in the terrestrial subsurface. *ISME J.* 16, 2561–2573. doi: 10.1038/s41396-022-01300-0

Nelson, D. W. (1983). Determination of ammonium in KCl extracts of soils by the salicylate method. *Commun. Soil Sci. Plant Anal.* 14, 1051–1062. doi: 10.1080/00103628309367431

Nelson, M. B., Martiny, A. C., and Martiny, J. B. H. (2016). Global biogeography of microbial nitrogen-cycling traits in soil. *Proc. Natl. Acad. Sci. U. S. A.* 113, 8033–8040. doi: 10.1073/pnas.1601070113

Ning, D., Deng, Y., Tiedje, J. M., and Zhou, J. (2019). A general framework for quantitatively assessing ecological stochasticity. *Proc. Natl. Acad. Sci. U. S. A.* 116, 16892–16898. doi: 10.1073/pnas.1904623116

Oksanen, J., Blanchet, F. G., Kindt, R., Legendre, P., Minchin, P., O'hara, R., et al. (2013). Community ecology package. *R Package Version* 2, 321–326.

Parida, P. K., Behera, B. K., Dehury, B., Rout, A. K., Sarkar, D. J., Rai, A., et al. (2022). Community structure and function of microbiomes in polluted stretches of river Yamuna in New Delhi, India, using shotgun metagenomics. *Environ. Sci. Pollut. Res.* 29, 71311–71325. doi: 10.1007/s11356-022-20766-1

Qian, L., Yu, X., Gu, H., Liu, F., Fan, Y., Wang, C., et al. (2023). Vertically stratified methane, nitrogen and Sulphur cycling and coupling mechanisms in mangrove sediment microbiomes. *Microbiome* 11:71. doi: 10.1186/s40168-023-01501-5

Reji, L., Tolar, B. B., Smith, J. M., Chavez, F. P., and Francis, C. A. (2019). Depth distributions of nitrite reductase (nirK) gene variants reveal spatial dynamics of thaumarchaeal ecotype populations in coastal Monterey Bay. *Environ. Microbiol.* 21, 4032–4045. doi: 10.1111/1462-2920.14753

Righetti, D., Vogt, M., Gruber, N., Psomas, A., and Zimmermann, N. E. (2019). Global pattern of phytoplankton diversity driven by temperature and environmental variability. *Sci. Adv.* 5:eaau6253. doi: 10.1126/sciadv.aau6253

Rout, A. K., Dehury, B., Parida, P. K., Sarkar, D. J., Behera, B., Das, B. K., et al. (2022). Taxonomic profiling and functional gene annotation of microbial communities in sediment of river ganga at Kanpur, India: insights from whole-genome metagenomics study. *Environ. Sci. Pollut. Res.* 29, 82309–82323. doi: 10.1007/s11356-022-21644-6

Sloan, W. T., Lunn, M., Woodcock, S., Head, I. M., Nee, S., and Curtis, T. P. (2006). Quantifying the roles of immigration and chance in shaping prokaryote community structure. *Environ. Microbiol.* 8, 732–740. doi: 10.1111/j.1462-2920.2005.00956.x

Song, W., Liu, J., Qin, W., Huang, J., Yu, X., Xu, M., et al. (2022). Functional traits resolve mechanisms governing the assembly and distribution of nitrogen-cycling microbial communities in the Global Ocean. *mBio* 13, e03832–e03821. doi: 10.1128/mbio.03832-21

Stegen, J. C., Lin, X., Fredrickson, J. K., and Konopka, A. E. (2015). Estimating and mapping ecological processes influencing microbial community assembly. *Front. Microbiol.* 6:370. doi: 10.3389/fmicb.2015.00370

Stegen, J. C., Lin, X., Konopka, A. E., and Fredrickson, J. K. (2012). Stochastic and deterministic assembly processes in subsurface microbial communities. *ISME J.* 6, 1653–1664. doi: 10.1038/ismej.2012.22

Stilianos, L., Laura, W. P., and Michael, D. (2016). Decoupling function and taxonomy in the global ocean microbiome. *Science* 353, 1272–1277. doi: 10.1126/science.aaf4507

Strom, S. L. (2008). Microbial ecology of ocean biogeochemistry: a community perspective. *Science* 320, 1043–1045. doi: 10.1126/science.1153527

Sunagawa, S., Acinas, S. G., Bork, P., Bowler, C., Acinas, S. G., Babin, M., et al. (2020). Tara Oceans: towards global ocean ecosystems biology. *Nat. Rev. Microbiol.* 18, 428–445. doi: 10.1038/s41579-020-0364-5

Sunagawa, S., Coelho, L. P., Chaffron, S., Kultima, J. R., Labadie, K., Salazar, G., et al. (2015). Ocean plankton. Structure and function of the global ocean microbiome. *Science* 348:1261359. doi: 10.1126/science.1261359

Tian, L., Wang, X. W., Wu, A. K., Fan, Y., Friedman, J., Dahlin, A., et al. (2020). Deciphering functional redundancy in the human microbiome. *Nat. Commun.* 11:6217. doi: 10.1038/s41467-020-19940-1

Tripathi, B. M., Stegen, J. C., Kim, M., Dong, K., Adams, J. M., and Lee, Y. K. (2018). Soil pH mediates the balance between stochastic and deterministic assembly of bacteria. *ISME J.* 12, 1072–1083. doi: 10.1038/s41396-018-0082-4

Tu, Q., Deng, Y., Yan, Q., Shen, L., Lin, L., He, Z., et al. (2016). Biogeographic patterns of soil diazotrophic communities across six forests in the North America. *Mol. Ecol.* 25, 2937–2948. doi: 10.1111/mec.13651

Tu, Q., Lin, L., Cheng, L., Deng, Y., and He, Z. (2018). NCycDB: a curated integrative database for fast and accurate metagenomic profiling of nitrogen cycling genes. *Bioinformatics* 35, 1040–1048. doi: 10.1093/bioinformatics/bty741

van Kessel, M. A. H. J., Speth, D. R., Albertsen, M., Nielsen, P. H., op den Camp, H. J. M., Kartal, B., et al. (2015). Complete nitrification by a single microorganism. *Nature* 528, 555–559. doi: 10.1038/nature16459

Violle, C., Navas, M.-L., Vile, D., Kazakou, E., Fortunel, C., Hummel, I., et al. (2007). Let the concept of trait be functional! *Oikos* 116, 882–892. doi: 10.1111/j.0030-1299.2007.15559.x

Wang, Q., Garrity, G. M., Tiedje, J. M., and Cole, J. R. (2007). Naive Bayesian classifier for rapid assignment of rRNA sequences into the new bacterial taxonomy. *Appl. Environ. Microbiol.* 73, 5261–5267. doi: 10.1128/AEM.00062-07

Wang, P. D., Li, J. L., Luo, X. Q., Ahmad, M., Duan, L., Yin, L. Z., et al. (2021). Biogeographical distributions of nitrogen-cycling functional genes in a subtropical estuary. *Funct. Ecol.* 36, 187–201. doi: 10.1111/1365-2435.13949

Wood, D. E., Lu, J., and Langmead, B. (2019). Improved metagenomic analysis with kraken 2. *Genome Biol.* 20, 257–213. doi: 10.1186/s13059-019-1891-0

Wu, L., Yang, Y., Ning, D., Gao, Q., Yin, H., Xiao, N., et al. (2023). Assessing mechanisms for microbial taxa and community dynamics using process models. *mLife* 2, 239–252. doi: 10.1002/mlf2.12076

Yilmaz, P., Parfrey, L. W., Yarza, P., Gerken, J., Pruesse, E., Quast, C., et al. (2014). The SILVA and "all-species living tree project (LTP)" taxonomic frameworks. *Nucleic Acids Res.* 42, D643–D648. doi: 10.1093/nar/gkt1209

Yuan, C., Shi, J. B., He, B., Liu, J. F., Liang, L. N., and Jiang, G. B. (2004). Speciation of heavy metals in marine sediments from the East China Sea by ICP-MS with sequential extraction. *Environ. Int.* 30, 769–783. doi: 10.1016/j.envint.2004.01.001

Zhou, J., and Ning, D. (2017). Stochastic community assembly: does it matter in microbial ecology? *Microbiol. Mol. Biol. Rev.* 81, e00002–e00017. doi: 10.1128/MMBR.00002-17

frontiers | Frontiers in Marine Science

TYPE Original Research
PUBLISHED 07 December 2023
DOI 10.3389/fmars.2023.1286511

OPEN ACCESS

EDITED BY
Chenyu Du,
University of Huddersfield,
United Kingdom

REVIEWED BY
Darren Greetham,
University of Leeds, United Kingdom
Bao-zhu Fang,
Chinese Academy of Sciences (CAS), China

*CORRESPONDENCE
Feng-Yan Bai
baify@im.ac.cn

†These authors have contributed equally to this work

RECEIVED 31 August 2023
ACCEPTED 13 November 2023
PUBLISHED 07 December 2023

CITATION
Zhu H-Y, Han D-Y, Guo L-C, Li J-N, Wei X-Y, Zhang R-P, Wang Q-M, Shang Y-J, Luo L-J, Wei Y-H, Liu X-Z and Bai F-Y (2023) Diversity and distribution of yeasts in intertidal zones of China. *Front. Mar. Sci.* 10:1286511. doi: 10.3389/fmars.2023.1286511

Diversity and distribution of yeasts in intertidal zones of China

Hai-Yan Zhu[1,2†], Da-Yong Han[1†], Liang-Chen Guo[1,2], Jun-Ning Li[1], Xu-Yang Wei[1,3], Ri-Peng Zhang[1,2], Qi-Ming Wang[4], Yu-Jie Shang[1], Lu-Jun Luo[1], Yu-Hua Wei[1,2], Xin-Zhan Liu[1] and Feng-Yan Bai[1,2*]

[1]State Key Laboratory of Mycology, Institute of Microbiology, Chinese Academy of Sciences, Beijing, China, [2]College of Life Sciences, University of Chinese Academy of Sciences, Beijing, China, [3]Department of Biological Sciences & Biotechnology, Faculty of Science & Technology, Universiti Kebangsaan Malaysia, Selangor, Malaysia, [4]Engineering Laboratory of Microbial Breeding and Preservation of Hebei Province, School of Life Sciences, Institute of Life Sciences and Green Development, Hebei University, Baoding, China

China has the second greatest extent of intertidal zones in the world. The intertidal zone is the most dynamic environments in the biosphere and potentially supports high biodiversity. Marine yeasts show excellent performance in various industrial, environmental and medical applications, however, the marine yeast diversity has rarely been studied in China. In this study, we collected 1241 samples including marine sediments, marine water, plants, and benthos at 161 GPS sites in different types of intertidal zones along the Chinese coastline from north to south. A total of 4436 strains were isolated from these samples using different methods and 286 species including 39 potential novel species were identified from these strains based on the internal transcribed spacer (ITS) region or the D1/D2 domain of the large subunit rRNA gene sequence analysis. The majority of the yeast species in different geographical locations belong to the five orders *Serinales*, *Saccharomycetales*, *Tremellales*, *Sporidiobolales*, and *Pichiales*. The yeast species diversity varied depending on sample types, depth of marine sediments, intertidal zone types and geographical locations. Mean annual temperature (MAT), salinity and pH had the greatest effect on the community structures of the yeasts isolated from the intertidal zones. This study represents one of the most comprehensive surveys of marine yeasts in China to date and provides a better understanding of marine yeast diversity and distribution.

KEYWORDS

marine yeasts, species diversity, ecology, intertidal zones, China

Abbreviations: 1/5MEA, 1/5 malt extract agar; CMA, corn meal agar; DO, dissolved oxygen; ITS, the internal transcribed spacer region; NMDS, Non-metric multidimensional scaling; ORP, oxidation reduction potential; PDA, potato dextrose agar; RDA, Redundancy analysis; RM, *Rhodotorula* isolation medium; YM, Yeast malt medium; YPD, yeast extract peptone dextrose.

1 Introduction

Tidal flat, or intertidal zone refers to the area above the low and below the high tide line, which provides a broad range of habitats such as mangrove, mud flat, sandy beach, rocky shore, coral reef and aquaculture area. China has the second largest intertidal zone in the world, extending from the tropical to the temperate climate zones (Liu, 2013; Murray et al., 2019). The Chinese intertidal zones potentially harbour high biodiversity of microorganisms. Marine yeasts are ubiquitous in marine environments and some of them show better growth in seawater than in fresh water (Chi et al., 2010; Kaewkrajay et al., 2020). Due to their high pressure tolerance ability, marine yeasts show outstanding performance in various industrial and medical applications, and remediation of marine environments. In industrial applications, marine yeasts not only play a significant role in the production of various enzymes (Chi et al., 2009; Chi et al., 2010), but also possess enormous potential for bioethanol and biodiesel production (Zaky et al., 2014; Wang et al., 2017). In addition, marine yeasts also exhibit high potentials in the production of single cell protein, polysaccharides, vitamins, killer toxins, pigments etc. In medical applications, marine yeasts can be used to produce pharmaceutical products including astaxanthin, siderophore and riboflavin (Wang et al., 2008; Wang et al., 2009; Nath Ushakumari and Ramanujan, 2013; Zaky et al., 2014). A previous study showed that *Yarrowia lipolytica* isolated from marine environments can produce nanoparticles (Chi et al., 2010). Many marine yeasts can remove organic pollutants and heavy metals, so they can be applied to the remediation of marine environments (Chi et al., 2010).

However, yeast diversity in marine environments has been much less studied compared to that in terrestrial environments in China. Yeast diversity in terrestrial natural habitats has been extensively studied in China, for examples, on the surface and gut of insects (Lou et al., 2014), sediments or soil related to glacier, forest, orchard, and desert (Luo et al., 2019; Li et al., 2020; Zhu et al., 2021; Wei et al., 2022), on the surface of the grapes and plant leaves (Li et al., 2010; Li et al., 2020; Wei et al., 2022), oral cavity (Wang et al., 2007), samples associated with Chinese Baijiu fermentation environments (Wu et al., 2012; Lei et al., 2022) and rotting wood (Gao et al., 2017; Lu et al., 2017; Zheng et al., 2017; Gao et al., 2018; Huang et al., 2018; Huang et al., 2019; Ke et al., 2019; Xi et al., 2019; Chai et al., 2020; Jia et al., 2020; Gao et al., 2021; Shi et al., 2021). Compared to the studies on terrestrial environments, only limited studies focused on yeasts in marine environments in China. Yang et al. (2011); Chi et al. (2012); Zhu et al. (2023a), and Zhu et al. (2023b) described some known and novel marine yeast species in diverse marine environments of China. Wang et al. (2017) found one marine yeast strain which possesses the capability for biodiesel production from renewable feedstocks.

In the course of microbial resource investigation in intertidal zones of China performed in recent years, we collected more than 1200 diversified marine samples along the Chinese coastline from north to south. Based on cultivation-dependent method, we revealed species diversity and distribution of yeasts in Chinese intertidal zones. We also identified key environmental factors affecting the yeast diversity in these intertidal zones.

2 Materials and methods

2.1 Samples collection

A total of 1241 marine samples including marine sediments, marine water, plants, and benthos were collected from different types of intertidal zones, including sand beach, rocky beach, mud flat, grass lands with different dominant plants, and mangrove (Figure 1) along the coastline of China during July 2019 to July 2023. A total of 161 GPS sites covering 11 coastal provinces of China, including Fujian, Guangdong, Guangxi, Hainan, Hebei, Jiangsu, Liaoning, Shandong, Shanghai, Tianjin, and Zhejiang were sampled (Figure 2). The samples were collected using sterile plastic bags and transferred in ice boxes to the laboratory for yeast isolation and physicochemical property measurement (Table S1).

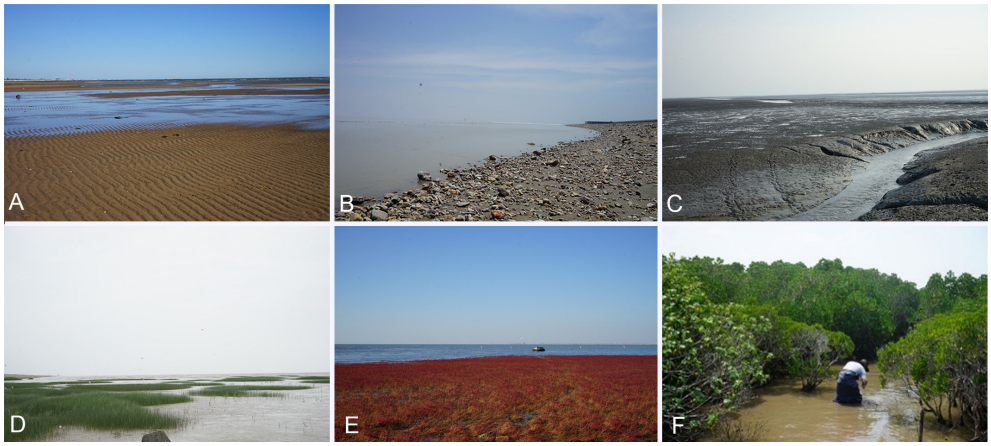

FIGURE 1
Different types of intertidal zones in China sampled in this study. **(A)** sand beach; **(B)** rocky beach; **(C)** mud flat; **(D)** grass land with plant *Phragmites australis*; **(E)** grass land with plant *Suaeda salsa*; **(F)** mangrove.

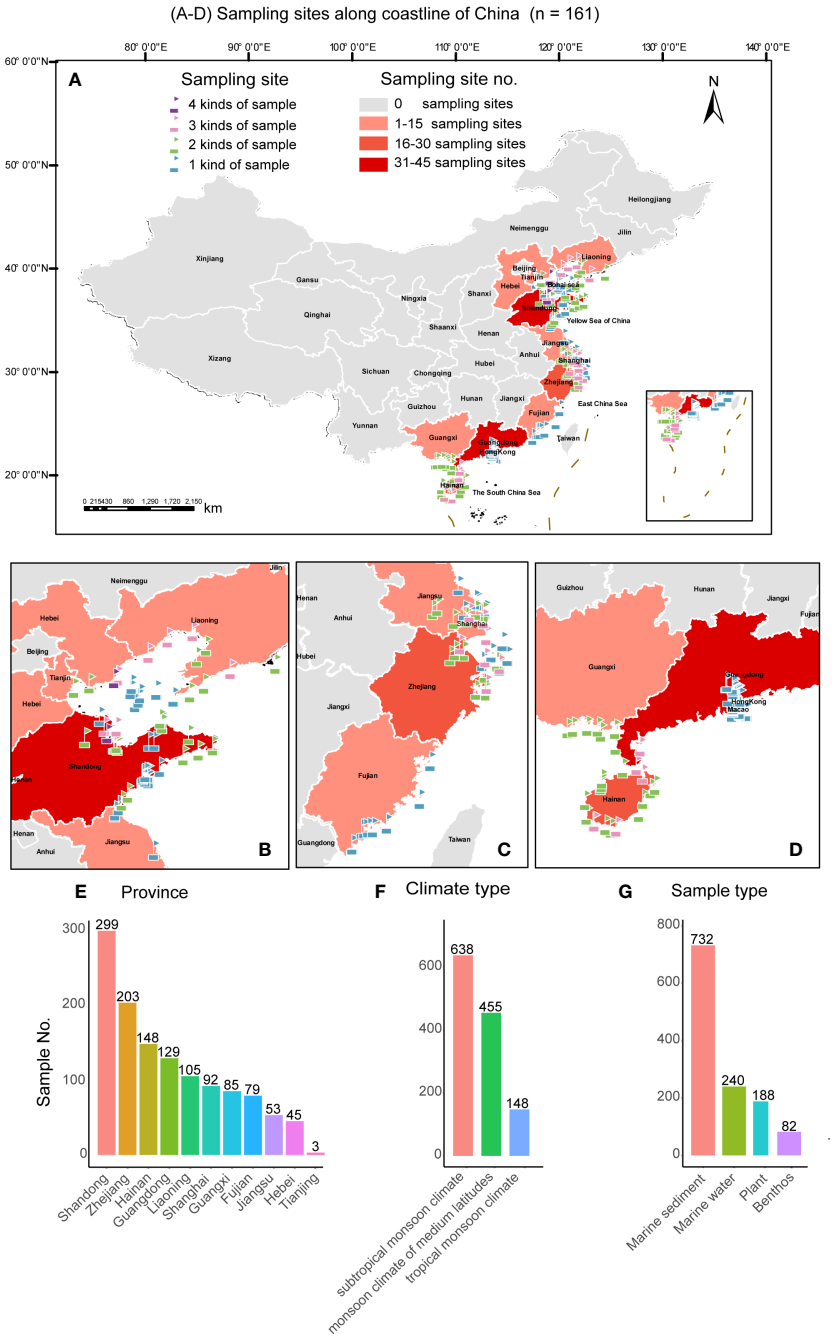

FIGURE 2
The geographic locations of the sampling sites in this study. **(A)** Map showing the distribution of all the sampling sites in 11 provinces in China; **(B)** Map showing the distribution of the samples collected from the Bohai Wan (BHW) Bay; **(C)** Map showing the distribution of the samples collected from the Hangzhou Wan (HZW) Bay; **(D)** Map showing the distribution of the samples collected from the Beibu Wan (BBW) Bay; **(E–G)** Characteristics of collected marine samples. In **(A–D)**, Maps were generated by the ArcGIS v. 10.8 software (Esri, Redlands, CA, USA).

For the marine sediment samples aiming to detailed and extensive yeast diversity and ecological analyses, four to six replicates with the same distance (>50 m) between adjacent samples were collected and mixed together for each site. To reveal the vertical profile of culturable marine yeast communities, at each sampling site, a marine sediment column with 10 cm diameter and 50 cm length was collected using a plastic sampler. The column was separated into three samples with different depth layers (oxic zone, 0 to 5 cm; anoxic zones, 5 to 15cm and 15 to 25 cm). For each marine water sample, 300 ml was collected in a sterile bag.

2.2 Yeast isolation

For the benthos, marine sediment and water samples, yeast strains were isolated using the enrichment method described

previously by Zaky et al. (2016), but additional media were used in this study. For each marine sediment or benthos sample, two grams were suspended in 20 ml sterile water and shaken at 200 rpm for 30 minutes at 25°C. Then each suspension was diluted to 1×10^{-1} and 1×10^{-2} and 200 µl of each dilution was respectively plated on 1/5 malt extract agar (1/5MEA, 0.4% glucose, 0.4% malt extract, 0.02% peptone, 2% agar), corn meal agar (CMA, 2.5% corn starch, 2% agar), potato dextrose agar (PDA, 20% potato infusion, 2% glucose, 2% agar), *Rhodotorula* isolation agar (RM, 1% glucose, 0.1% yeast extract, 0.2% peptone, 2% agar, 1 mg/L sodium glutamate), Yeast malt agar (YM, 1% glucose, 0.3% yeast extract, 0.3% malt extract, 0.5% peptone, 2% agar), and yeast extract peptone dextrose (YPD, 2% glucose, 1% yeast extract, 2% peptone, 2% agar) plates containing 1.5% sea salt, 500 mg/L penicillin and 500 mg/L streptomycin sulphate. For each medium, two plates were inoculated and incubated at 17°C and 25°C, respectively, for 3–5 days. For each marine water sample, 200 ml was filtered through a filter membrane with 100 mm diameter and then one-fourth of the filter was put in 20 ml sterile water and then treated in the same way as the soil suspension. For the plant leaves and stems, yeast strains were isolated by an enrichment method according to Bai et al. (2002) and Wang et al. (2012) with minor modifications. Specifically, two grams of each sample were placed into 10 ml YM broth supplemented with 7% ethanol and 200 mg/L chloramphenicol in a 15 ml sterile centrifuge tube and then incubated at 25 °C for one week. Then 100 µl enrichment culture and appropriate decimal dilutions were spread on YM agar plates supplemented with 200 mg/L chloramphenicol and then incubated at 25 °C for 3–4 days. In the meantime, for the plant leaves, yeast strains were also isolated using ballistoconidia-fall method described by Nakase and Takashima (1993). Yeast and yeast like colonies that appeared on the plates were picked, purified, and preserved in 25% glycerol at –80 °C.

2.3 Measurement of environmental factors and physiochemical properties

The pH, salinity, dissolved oxygen (DO) and oxidation reduction potential (ORP) for marine water were determined using the HQ40d Portable Meter (Hach Company, Loveland, CO, USA). The mean annual temperature (MAT) and mean annual precipitation (MAP) of the sampling areas were obtained from the WorldClim database (http://www.worldclim.org).

2.4 DNA extraction, sequencing and yeast identification

Nuclear DNA of the yeast strains was extracted using the method described previously (Wang and Bai, 2008). The D1/D2 domain of the 26S ribosomal RNA gene and the internal transcribed spacer (ITS) region was amplified and sequenced using the method described by Bai et al. (2002). Yeasts were identified by analysis of the sequence similarity of the D1/D2 domain using the BLASTn search program (https://blast.ncbi.nlm.nih.gov). For the identification of yeasts, the strains with 0–3 nucleotide substitutions in the D1/D2 domain were designated as conspecific, while the strains showing greater than 1% nucleotide substitutions (six or more nucleotides) were considered as different species (Kurtzman and Robnett, 1998; Fell et al., 2000; Scorzetti et al., 2002; Vu et al., 2016). When a strain showed more than three nucleotide substitutions from the type strain of the most closely related known species, the ITS sequence was compared further. If more than 1% mismatch was found, the strain was treated as a "potential novel species" in this study.

2.5 Phylogenetic analyses

Phylogenetic analysis based on the D1/D2 domain or ITS region was performed to verify the identification using sequence similarity analysis. The sequences of representative strains were aligned by MAFFT v. 7 (Katoh and Standley, 2013) and manually improved where necessary using MEGA v.7 (Kumar et al., 2016). A phylogenetic tree was constructed from Kimura's two parameter model (Kimura, 1980) using the neighbour-joining algorithm executed in MEGA v.7 (Kumar et al., 2016; Lachance, 2022). Confidence levels of the clades were estimated from bootstrap analysis (1000 replicates) (Felsenstein, 1985). The phylogenetic trees were visualized and annotated using the online open-source tool Interactive Tree of Life (iTOL) (Letunic and Bork, 2019).

2.6 Statistical analysis

Alpha diversity analysis was calculated in R using the package vegan (Oksanen et al., 2022). Beta diversity analysis was conducted based on Sørensen dissimilarity. This analysis was performed among different collection sites based on the yeast species using the R packages vegan and ape (Paradis and Schliep, 2019). The statistical significance was calculated using the ANOVA or Kruskal–Wallis test executed by the aov function and kruskal.test function of R package multcomp and FSA, respectively. Non-metric multidimensional scaling (NMDS) plot was created using a Bray–Curtis dissimilarity matrix of samples in the R package phyloseq version 1.25.2 (McMurdie and Holmes, 2013). Redundancy analysis (RDA) was used to explore effect of environmental factors on the yeast community. Correlation between yeast species and environmental factors as well as physiochemical properties profiles was analyzed using Spearman's ρ with Padj < 0.05 (Best and Roberts, 1975). Differences in environmental factors, physiochemical property profiles, and yeast species across different sites were assessed using a two-way ANOVA, with the Bonferroni *post hoc* test used for repeated measurements. All significant yeast species and environmental factors, along with the physicochemical properties, were visualized by heatmap graphs. All statistical analyses were performed using R, version v.4.3.1 (R Core Team, 2023).

3 Results

3.1 The overall yeast diversity from all the samples collected in intertidal zones of China

The 1241 marine samples collected in this study yielded a total of 4436 yeast strains. Altogether, 286 yeast species including 141 ascomycetous and 145 basidiomycetous species were identified from these strains (Figures 3 and 4; Table S2). Among them, 39 are potential novel species (Table S3). Among the species discovered, 41 yeast species were isolated from more than thirty samples and 33 species were isolated from more than five provinces in this study (Figures 3 and 4; Table S2). A total of 21 yeast species were the most frequently isolated yeasts, including 15 ascomycetous species, namely *Candida parapsilosis*, *Candida pseudolambica*, *Candida tropicalis*, *Diutina catenulate*, *Geotrichum candidum*, *Kluyveromyces siamensis*, *Kodamaea ohmeri*, *Meyerozyma caribbica*, *Meyerozyma guilliermondii*, *Nakaseomyces glabratus*, *Pichia kudriavzevii*, *Saccharomyces cerevisiae*, *Saccharomycopsis fibuligera*, *Scheffersomyces spartinae*, and *Wickerhamomyces anomalus*; and six basidiomycetous species, namely, *Cystobasidium minutum*, *Cystobasidium slooffiae*, *Moesziomyces aphidis*, *Papiliotrema laurentii*, *Saitozyma podzolica*, *Trichosporon asahii* (Figures 3 and 4; Table S2). Furthermore, three ascomycetous yeast species, *Candida parapsilosis*, *Candida tropicalis*, and

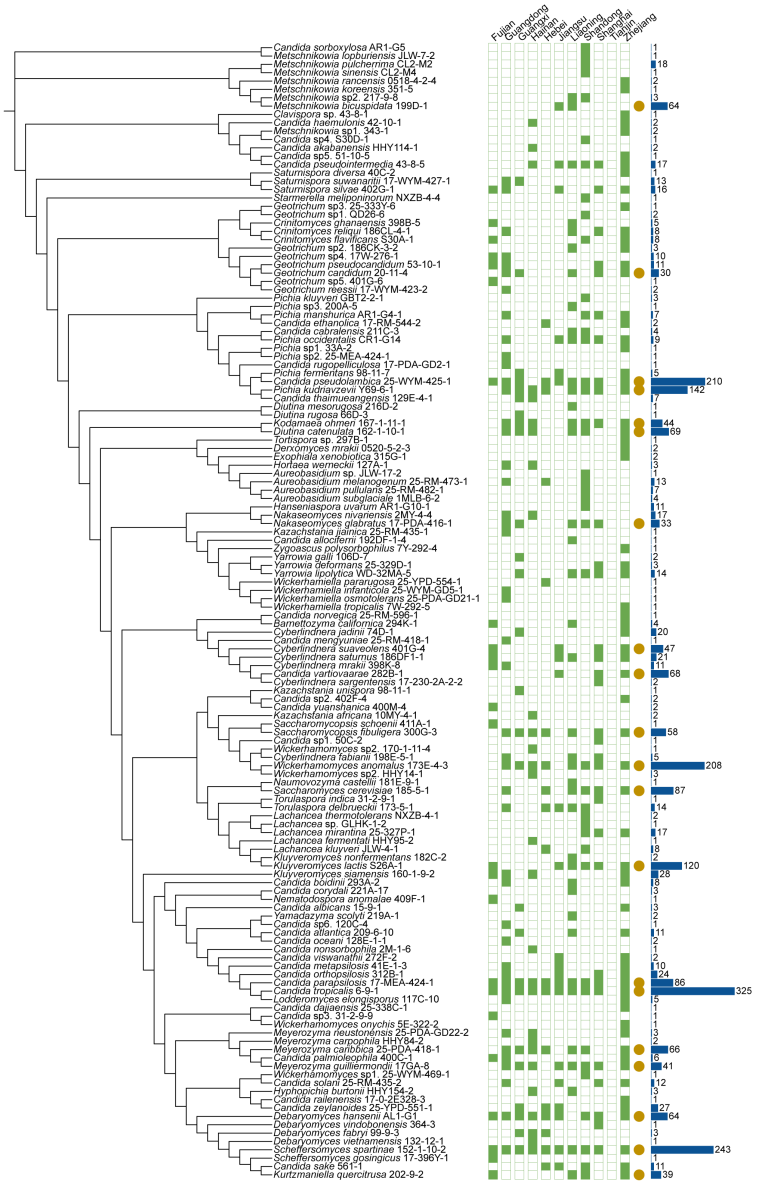

FIGURE 3
Phylogenies and geographic distributions of the ascomycetous yeast species discovered in this study. The trees were constructed based on the D1/D2 sequences. The green squares represent the 11 sampling provinces in this study. Solid and hollow squares indicate the presence and absence of the species in the locations, respectively. Yellow solid circles that each of indicate the species was isolated more than 30 samples. The blue bar charts indicate the number of strains isolated.

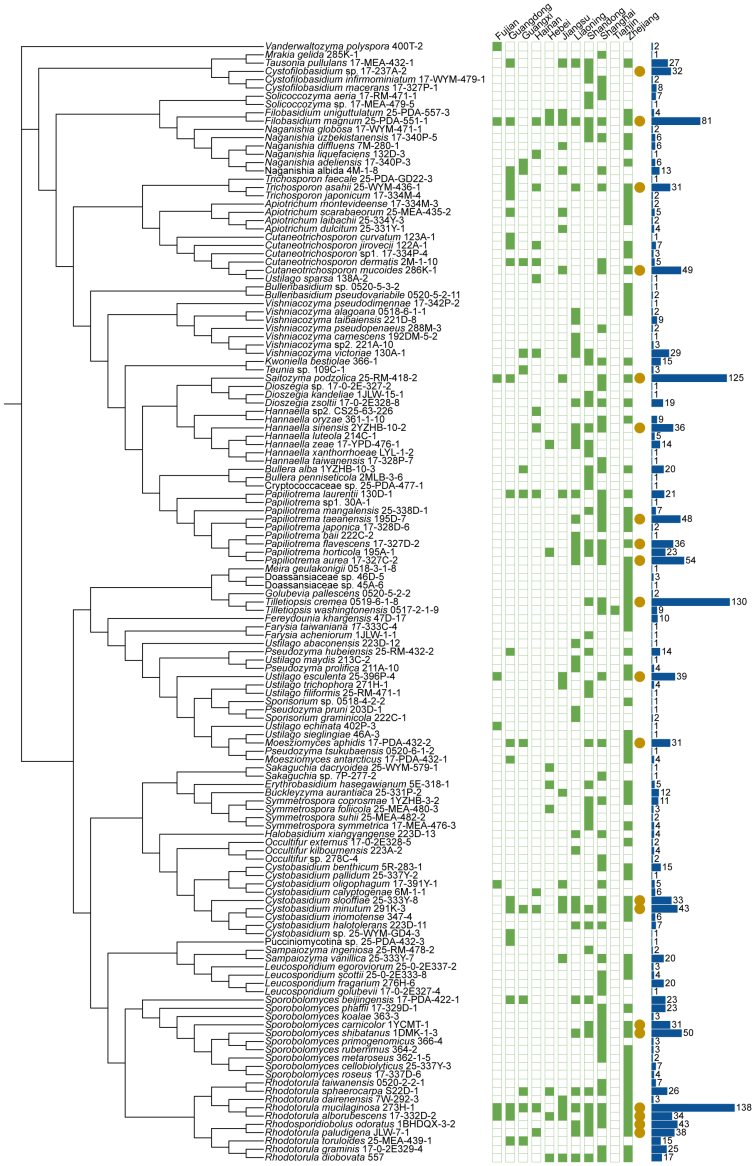

FIGURE 4
Phylogenies and geographic distributions of the basidiomycetous yeast species discovered in this study. The trees were constructed based on the D1/D2 sequences. The green squares represent 11 sampling provinces in this study. Solid and hollow squares indicate the presence and absence of the species in the locations, respectively. Yellow solid circles indicate the species were isolated more than 30 samples. The blue bar charts indicate the number of strains isolated.

Scheffersomyces spartinae were isolated from all the provinces sampled except Tianjin. Only three samples were collected from Tianjin and one yeast strain identified as *Tilletiopsis washingtonensis* was isolated from the Tianjin samples (Figure 2E; Table S2).

3.2 Yeast diversity in representative GPS sites from intertidal zones of China

In order to perform detailed biodiversity analyses of yeasts in depth, we selected 41 representative GPS sites from intertidal zones of China. The samples from these sites were collected using the same sampling method and strategy and were subjected to yeast isolation using the same media and the same processing procedure. Three marine samples including one surface sediment (0–5cm), one subsurface sediment (5–25cm), and one water samples were isolated from per representative GPS site. We divided all the samples from these 41 sites into three groups according to their geographical locations. The Beibu Wan (BBW) Bay group included 17 GPS sites located in the Beibu Gulf, South China (Figure 2D; Table S4); the Hangzhou Wan (HZW) Bay group included 15 GPS sites located in the Hangzhou Bay, East China (Figure 2C; Table S4); and the Bohai Wan (BHW) Bay group included 9 GPS sites located in the Bohai Bay, Northeast China (Figure 2B; Table S4). These samples were subjected to yeast isolation using the same media

PDA, RM and YM at 25°C. A total of 776 yeast strains belonging to 115 species and 63 genera were isolated from these samples. Specifically, 117 strains of 49 species were isolated from HZW; 324 strains of 42 species from BBW; and 335 strains of 58 species from BHW (Figure 5A).

3.3 Yeast species distributions vary depending on geographic regions, substrates and intertidal zone types

Different regions, media, substrates, and tidal flats harbored their own yeast species (Figure 5). Although only nine GPS sites in BHW were selected (Table S4), 68 yeast species were isolated from this region, while 42 species from 17 GPS sites in BBW and 49 species from 15 GPS sites in HZW were discovered. Only eight species were shared by the three regions. BHW possesses the highest yeast species diversity among these three regions (Figure 5A). Although 42 species were commonly found in three different media, each medium yielded its own unique species. Specifically, 18, 12, and 24 unique species were obtained using YM, PDA, and RM, respectively (Figure 5B). A total of 75 species were isolated from marine water samples, while 48 and 40 species were isolated from surface and subsurface sediment samples, respectively (Figure 5C). Different types of intertidal zones also harbour different yeast diversities. A total of 57 species were isolated from mud flat samples, 51 species from sand beach, 48 species from grass land, 25 species from mangrove, and only 10 from rocky beach samples. The yeast species shared by different types of intertidal zones were limited (Figure 5D).

3.4 Yeast community composition in different intertidal zones of China

At the order level, the five orders *Serinales*, *Saccharomycetales*, *Tremellales*, *Sporidiobolales*, and *Pichiales* were the dominant orders in all the three groups, collectively accounting for 84.11% in BBW group, 78.55% in BHW group, and 52.84% in HZW group (Figure 6A; Table S5). The order *Saccharomycetales* was much more abundant in the BBW group (25.23%) than in the BHW group (8.00%) and HZW group (18.18%); the order *Serinales* was much more abundant in the BHW group (26.18%) than in the BBW group (14.64%) and HZW group (9.66%) (Figure 6A; Table S5). At

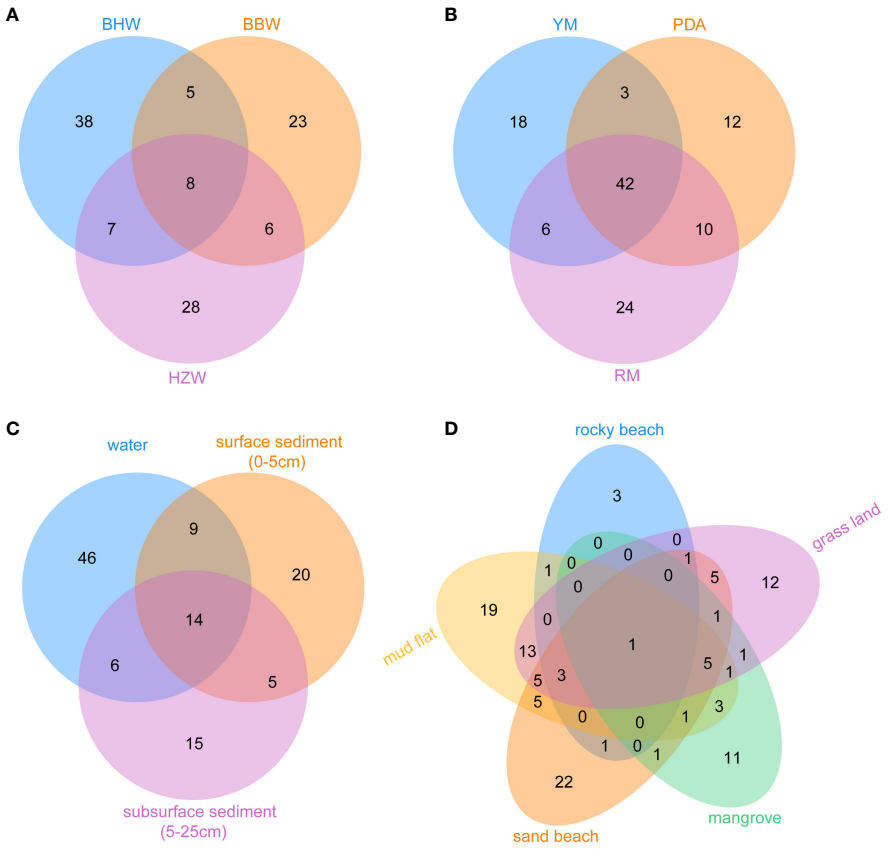

FIGURE 5
The number of unique and shared yeast species from 41 representative GPS sites of intertidal zones in different locations (BBW, the Beibu Wan Bay; BHW, the Bohai Wan Bay; and HZW, the Hangzhou Wan Bay) **(A)**, different media (PDA, potato dextrose agar; RM, *Rhodotorula* isolation magar; YM, yeast malt agar) **(B)**, different substrates **(C)** and different intertidal zone types **(D)**.

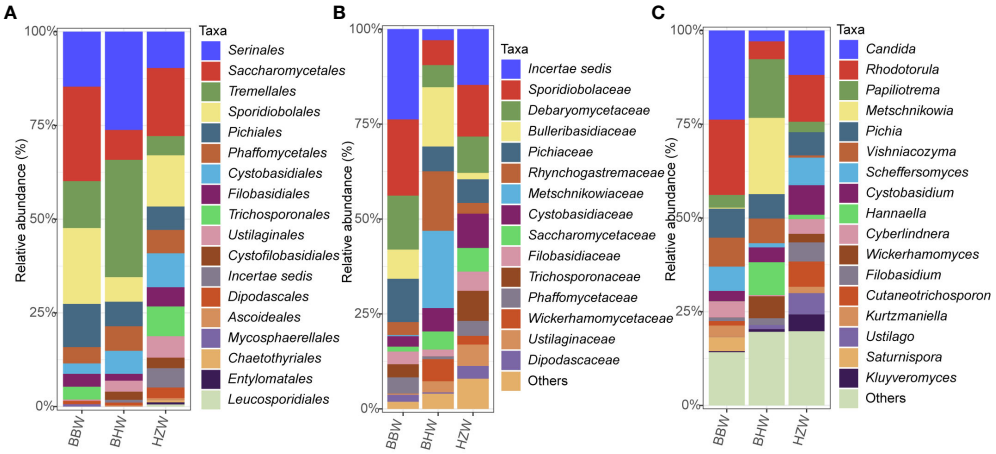

FIGURE 6
Relative abundances of yeast species in different locations at the order **(A)**, family **(B)** and genus **(C)** levels. BBW, the Beibu Wan Bay; BHW, the Bohai Wan Bay; HZW, the Hangzhou Wan Bay.

the family level, *Sporidiobolaceae* was the dominant family in both BBW (20.66%) and HZW groups (13.56%), meanwhile, *Bulleribasidiaceae* is the dominant family in BHW (15.64%) (Figure 6B; Table S5). At the genus level, the dominant genera were also different among the three groups (Figure 6C; Table S5). Both *Candida* and *Rhodotorula* accounted for over 20% each in the BBW group, whereas in the BHW group, only *Metschnikowia* accounted for over 20%. *Rhodotorula* was the dominant genus in HZW group but with a less ratio (15%) (Figure 6C; Table S5).

3.5 Alpha and beta diversities of yeasts in different intertidal zones of China

The alpha diversity analysis showed that the Shannon index of yeasts was higher in BHW group than those in BBW and HZW groups, but the difference was not statistically significant (Figure 7A). The estimated richness (ACE index) of yeasts in BHW group was significantly higher than those in BBW and HZW groups ($P < 0.05$) (Figure 7B), suggesting that the number of yeast species found in BHW group was significantly higher than those in the latter regions.

Comparative yeast diversity analysis was performed after the strain numbers were normalized. NMDS analysis based on Bray-Curtis dissimilarity distances revealed that the yeast communities in BBW, BHW and HZW groups were separated with limited intersection (Figure 7C), indicating that the yeast species compositions in different geographic locations are different.

The RDA analysis based on yeast species and environmental factors and physico-chemical properties of the samples from different regions showed that the first and second RDA components explained 56.53% of the total variation (Figure 7D). MAT, salinity and pH were significantly associated with the yeast community ($P < 0.05$) (Figure 7D; Table S6). The results suggest a significant correlation between the yeast community and physicochemical property and environmental climate, particularly MAT in the sampling regions.

3.6 Influence of physiochemical and environmental factors on the occurrence of yeast species in intertidal zones of China

To identify the preliminary factors affecting the occurrence of yeast species in intertidal zones of China, the top 30 most frequently isolated yeast species were selected and the Spearman correlation coefficients between the isolation frequencies of these yeast species and four physicochemical properties and two environmental factors were calculated (Table S4). The result showed that nine yeast species were significantly influenced by MAT and MAP. Among these species, *Rhodotorula toruloides* and *Papiliotrema laurentii* showed a significantly positive correlation with MAP and MAT ($P < 0.05$); while *Wickerhamomyces anomalus*, *Geotrichum candidum*, *Cyberlindnera jadinii*, *Kluyveromyces lactis*, *Rhodotorula mucilaginosa*, *Tausonia pullulans*, and *Pichia pseudolambica* exhibited a negative correlation with MAP and MAT ($P < 0.05$) (Figure 8). pH positively affected the occurrence of *Candida tropicalis* but negatively affected the occurrence of *Hannaella zeae*, *Papiliotrema aurea*, *Papiliotrema flavescens*, and *Saccharomyces cerevisiae* ($P < 0.05$). Limited species were significantly influenced by DO, ORP and salinity (Figure 8). Among the 30 yeast species analyzed, nine species, including *Cutaneotrichosporon mucoides*, *Filobasidium magnum*, *Saturnispora suwanaritii*, *Ustilago esculenta*, *Vishniacozyma taibaiensis*, *Hannaella sinensis*, *Pichia kudriavzevii*, and *Candida parapsilosis*, did not show any significant correlation with the physiochemical and environmental factors analyzed (Figure 8).

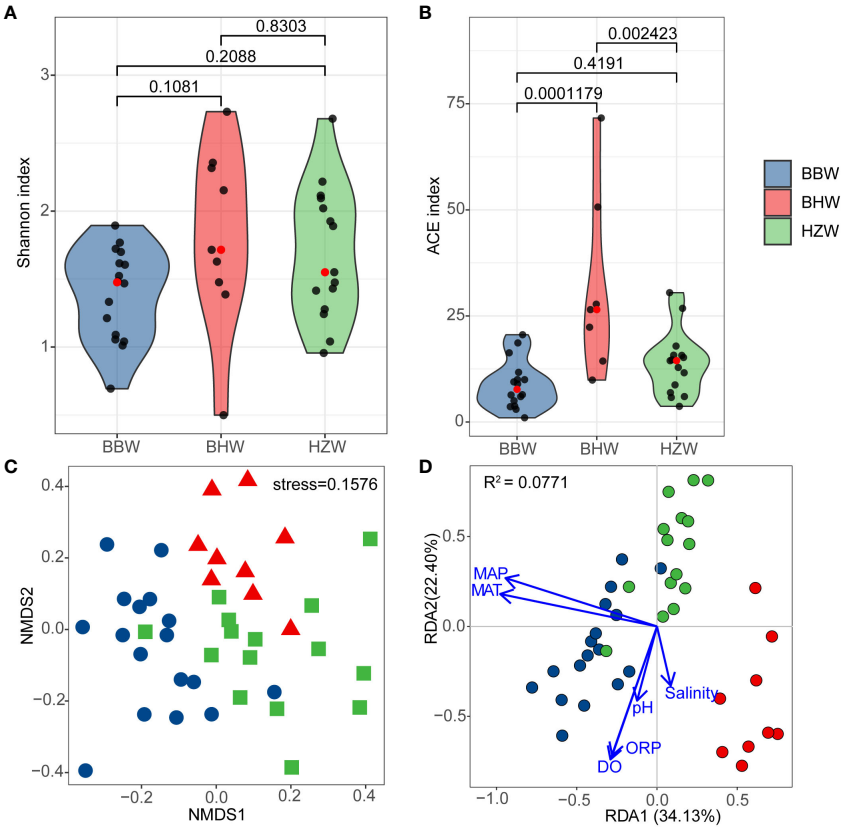

FIGURE 7
Alpha and Beta diversity of marine yeasts from 41 representative GPS sites of intertidal zones of China. **(A)** Shannon index; **(B)** ACE index; **(C)** Non-metric multidimensional scaling; **(D)** Redundancy analysis based on four physiochemical properties, pH, salinity, dissolved oxygen (DO) and oxidation reduction potential (ORP) and two environmental factors, the mean annual temperature (MAT) and mean annual precipitation (MAP). BBW, the Beibu Wan Bay; BHW, the Bohai Wan Bay; HZW, the Hangzhou Wan Bay.

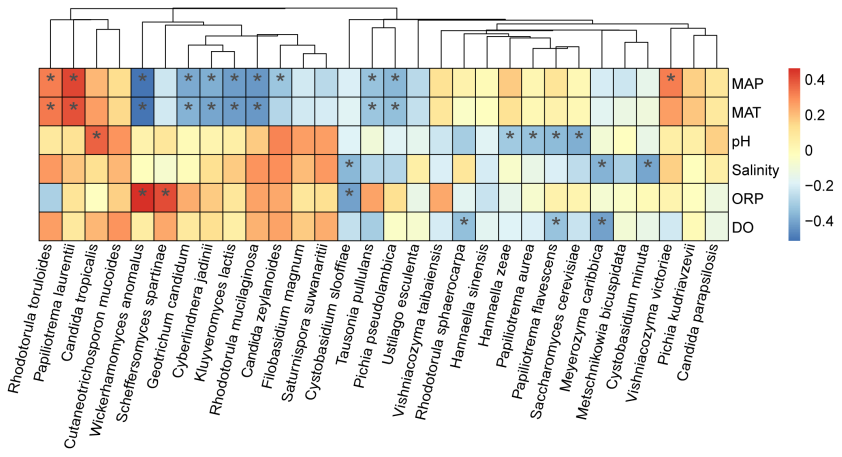

FIGURE 8
Correlation of the occurrence of marine yeast species with physiochemical properties pH, salinity, dissolved oxygen (DO) and oxidation reduction potential (ORP) and environmental factors mean annual temperature (MAT) and mean annual precipitation (MAP). Heatmaps were created based on Spearman correlation coefficients with $P < 0.05$ between the isolation frequency of the yeast species accounting for > 1% of the yeast strains isolated and physiochemical properties and environmental factors. Heat map colors reflect different degrees of negative (blue) and positive (red) correlations according to the scale on the right. * $0.01 < P < 0.05$.

4 Discussion

To our knowledge, this the most extensive study on yeast diversity in marine environment, especially in intertidal regions, in terms of the sample number collected and the yeast strains isolated and the geographic regions covered. In this study, we obtained 286 yeast species, including 140 ascomycetous and 146 basidiomycetous species associated with intertidal zones of China (Table S2). Boekhout et al. (2022) summarized that at least 782 yeast species have been recorded from China recorded until 2020 and 49 additional yeast species were reported from China in the past three years (Gao et al., 2021; Shi et al., 2021; Chai et al., 2022a; Chai et al., 2022b; Chai et al., 2022c; Chu et al., 2022; Li et al., 2022; Wei et al., 2022; Chai et al., 2023; Liu et al., 2023; Qiao et al., 2023; Yu et al., 2023; Zhu et al., 2023a; Zhu et al., 2023b). The number of yeast species discovered in this study accounts for 34.7% in the total yeast species that have been found from China, indicating that there are abundant resources of culturable yeasts in the intertidal zones of China. Jones et al. (2015) summarized that there are 213 marine yeasts, including 138 ascomycetous species, 75 basidiomycetous species, which were reported from marine habitats and even if they are facultative. Our study provides a wider perspective to know the marine yeast species.

Many of the taxa isolated in this study were previously known as opportunistic pathogens of human, including *Candida albicans*, *Candida parapsilosis*, *Candida tropicalis*, *Pichia kudriavzeveii*, *Nakaseomyces glabrata* which are recorded in the WHO fungal priority pathogens list (World Health Organization, 2022). Among these five yeast species, *Candida parapsilosis* and *Candida tropicalis* were the most prevalent which were distributed in 10 of the 11 provinces samples in this study (Figure 3; Table S2). Only the samples from Tianjin showed negative isolation of these two species most probably because of the very limited samples collected from this region. *Pichia kudriavzeveii* distributed in eight provinces was the second prevalent species (Figure 3; Table S2). *Candida albicans* and *Nakaseomyces glabrata* were discovered in five and two provinces, respectively (Figure 3; Table S2). All five species were discovered in more than one province, suggesting their existence in intertidal zone is not a one-off event. Besides the above-mentioned five yeast species, there are many species which are opportunistic pathogenic yeast in previous publications, for example, *Aureobasidium melanogenum* (Chen et al., 2016), *A. pullulans* (Pikazis et al., 2009), *Candida allociferrii* (Soki et al., 2015), *Geotrichum candidum* (Keene et al., 2019), *Wickerhamomyces anomalus* (Aboutalebian et al., 2023), *Yarrowia lipolytica* (Desnos-Ollivier et al., 2020) and so on. Every coin has two sides. For instance, although *Pichia kudriavzeveii* is a globally distributed opportunistic pathogenic yeast (Pfaller et al., 2008), whose infections frequently acquired from the environment was verified by Douglass et al. (2018), it plays a significant role in bioethanol production (Hoppert et al., 2022), cocoa fermentation (Pereira et al., 2017), single–cell protein production (Hashem et al., 2022). Meanwhile, high resistance to fluconazole is common in environmental and clinical isolates without distinction in *Pichia kudriavzeveii* (Douglass et al., 2018), which make the treatment for fungal infections more difficult undoubtedly. There is a question that whether the fungal resistance is common in other opportunistic pathogenic yeasts. In search of the solution, our study maybe could provide vast environmental isolates.

Apart from the dominant species *Pichia kudriavzeveii*, many other dominant species demonstrate remarkable performance in numerous industrial and medical applications. For instance, *Candida tropicalis*, *Debaryomyces hansenii*, and *Saccharomyces cerevisiae* were frequently utilized in the production of bio-ethanol (Zaky et al., 2014). The two species *Candida tropicalis* and *Debaryomyces hansenii* also play a significant role in the biomaterial industry in producing silver nanoparticles. The *Rhodotorula mucilaginosa* can be utilized not only in biodiesel industries for the production of microbial oil, but also in food colorings to generate carotene and feed industries for the production of protease (Zaky et al., 2014). Despite their small size, yeast cells possess a boundless potential. Our study could provide the support for the marine yeast application.

As China is one of the largest coastal countries in the world, our sampling still exists the room for extending sampling, which is requiring us to conduct research continuously in the intertidal zones in the future. Although our representative sampling sites from south (BBW) to north (BHW) are gradually decreasing (from 17 to nine) (Table S2), the number of yeasts isolated is gradually increasing (Figure 5A). With the rise of the latitude, the MAT is gradually increasing (Table S4). RDA analysis results indicates that MAT, salinity and pH had the significant effect on the community structure of the yeasts isolated from the intertidal zones, especially the MAT, which is consistent with Zhou et al. (2016) (Figure 7D). Climate warming is increasingly leading to marked changes in biodiversity, including plant, animal, and microorganism (Zhou et al., 2016). Meanwhile, with the climate warming, the change of carbon dioxide in marine water will dramatically change, which could lead to Ocean acidification (Anand et al. 2021). It will affect the growth of microorganisms. The above-mentioned results are reminding us that it is urgent to rescue the lost microbial resources, including the yeasts.

Yeast species distributions vary depending on geographic regions, isolation media, substrates and intertidal zone types. During the initial medium screening stage, we utilized not only YM, PDA, and RM, but also other three media, namely, YPD, CMA, and 1/5MEA (data not shown). Different media yielded their own unique yeast species, among these media tested, and the three media YM, PDA and RM had the best isolation results. Therefore, these three media were used throughout our entire research. The isolation results from different substrates, including marine water and marine sediment with different depth, show that the marine water possesses more yeast species. Our study provides valuable suggestions and clues for sampling and yeast isolation from marine environments in the future.

Data availability statement

The sequence data of the study are deposited in the NCBI database with accession numbers which can be found in the article/Supplementary Material.

Author contributions

H-YZ: Investigation, Data curation, Visualization, Writing original draft. D-YH: Investigation, Data curation, Visualization. L-CG: Investigation, Data curation, Visualization. J-NL: Investigation. X-YW: Investigation. R-PZ: Investigation. Q-MW: Investigation, Data curation. Y-JS: Investigation. L-JL: Investigation. Y-HW: Data curation, Visualization. X-ZL: Investigation. F-YB: Funding acquisition, Investigation, Supervision, Writing review & editing.

Funding

The author(s) declare financial support was received for the research, authorship, and/or publication of this article. This study was supported by the National Science & Technology Fundamental Resources Investigation Program of China (grant No. 2019FY100700).

Acknowledgments

We thank Fang Liu and Chang Liu from the Institute of Microbiology, Chinese Academy of Sciences, Wen-Jun Li from Sun Yat-sen University, Cong Sun and Jun-Jie Ying from Zhejiang Sci-Tech University, Zhi-Cheng Wu from Zhejiang University and Du-Qiang Luo from Hebei University for providing some marine samples.

Conflict of interest

The authors declare that the research was conducted in the absence of any commercial or financial relationships that could be construed as a potential conflict of interest.

Publisher's note

Supplementary material

The Supplementary Material for this article can be found online at: https://www.frontiersin.org/articles/10.3389/fmars.2023.1286511/full#supplementary-material

References

Aboutalebian, S., Mirhendi, H., Eshaghi, H., Nikmanesh, B., and Charsizadeh, A. (2023). The first case of *Wickerhamomyces anomalus* fungemia in Iran in an immunedeficient child, a review on the literature. *J. Med. Mycology* 33, 101351. doi: 10.1016/j.mycmed.2022.101351

Anand, M., Rangesh, K., Maruthupandy, M., Jayanthi, G., Rajeswari, B., and Priya, R. J. (2021). Effect of CO_2 driven ocean acidification on calcification, physiology and ovarian cells of tropical sea urchin Salmacis virgulata – A microcosm approach. *Heliyon* 7, e05970. doi: 10.1016/j.heliyon.2021.e05970

Bai, F. Y., Zhao, J. H., Takashima, M., Jia, J. H., Boekhout, T., and Nakase, T. (2002). Reclassification of the *Sporobolomyces roseus* and *Sporidiobolus pararoseus* complexes, with the description of *Sporobolomyces phaffii* sp. nov. *Int. J. Syst. Evol. Microbiol.* 52, 2309–2314. doi: 10.1099/00207713-52-6-2309

Best, D. J., and Roberts, D. E. (1975). Algorithm AS 89: the upper tail probabilities of spearman's *Rho*. *Appl. Stat.* 24, 377. doi: 10.2307/2347111

Boekhout, T., Amend, A. S., El Baidouri, F., Gabaldón, T., Geml, J., Mittelbach, M., et al. (2022). Trends in yeast diversity discovery. *Fungal Divers* 114, 491–537. doi: 10.1007/s13225-021-00494-6

Chai, C. Y., Gao, W. L., Li, Y., Yan, Z. L., and Hui, F. L. (2022a). *Kodamaea hongheensis* f.a., sp. nov., *Kodamaea ovata* f.a., sp. nov. and *Kodamaea yamadae* f.a., sp. nov., three new yeast species of *Kodamaea* (*Saccharomycetales, Debaryomycetacae*) from China. *MycoKeys* 89, 121–137. doi: 10.3897/mycokeys.89.81119

Chai, C. Y., Gao, W. L., Yan, Z. L., and Hui, F. L. (2022c). Four new species of Trichomonascaceae (*Saccharomycetales, Saccharomycetes*) from Central China. *MycoKeys* 90, 1–18. doi: 10.5962/bhl.part.10003

Chai, C. Y., Jia, R. R., Chen, C. Y., and Hui, F. L. (2020). *Blastobotrys baotianmanensis* sp. nov. and *Blastobotrys xishuangbannaensis* f.a., sp. nov., two novel yeast species associated with insects and rotting wood. *Int. J. Syst. Evol. Microbiol.* 70, 4217–4223. doi: 10.1099/ijsem.0.004275

Chai, C. Y., Lei, T., Chu, X. Y., and Hui, F. L. (2023). Multi-gene phylogeny and taxonomy of the genus *Bannoa* with the addition of three new species from central China. *Front. Microbiol.* 14. doi: 10.3389/fmicb.2023.1143156

Chai, C. Y., Li, Y., Yan, Z. L., and Hui, F. L. (2022b). Phylogenetic and genomic analyses of two new species of *Clavispora* (*Metschnikowiaceae, Saccharomycetales*) from Central China. *Front. Microbiol.* 13. doi: 10.3389/fmicb.2022.1019599

Chen, W. T., Tu, M. E., and Sun, P. L. (2016). Superficial phaeohyphomycosis caused by *Aureobasidium melanogenum* mimicking tinea nigra in an immunocompetent patient and review of published reports. *Mycopathologia* 181, 555–560. doi: 10.1007/s11046-016-9989-3

Chi, Z., Chi, Z., Zhang, T., Liu, G., Li, J., and Wang, X. (2009). Production, characterization and gene cloning of the extracellular enzymes from the marine-derived yeasts and their potential applications. *Biotechnol. Adv.* 27, 236–255. doi: 10.1016/j.bioteChadv.2009.01.002

Chi, Z. M., Liu, T. T., Chi, Z., Liu, G. L., and Wang, Z. P. (2012). Occurrence and diversity of yeasts in the mangrove ecosystems in Fujian, Guangdong and Hainan Provinces of China. *Indian J. Microbiol.* 52, 346–353. doi: 10.1007/s12088-012-0251-5

Chi, Z. M., Liu, G., Zhao, S., Li, J., and Peng, Y. (2010). Marine yeasts as biocontrol agents and producers of bio-products. *Appl. Microbiol. Biotechnol.* 86, 1227–1241. doi: 10.1007/s00253-010-2483-9

Chu, S. B., Hu, W. T., and Hui, F. L. (2022). *Torulaspora jiuxiensis* sp. nov., a novel yeast species isolated from rotting wood. *Int. J. Syst. Evol. Microbiol.* 72, 005629. doi: 10.1099/ijsem.0.005629

Desnos-Ollivier, M., Letscher-Bru, V., Neuvéglise, C., and Dromer, F. (2020). *Yarrowia lipolytica* causes sporadic cases and local outbreaks of infections and colonisation. *Mycoses* 63, 737–745. doi: 10.1111/myc.13095

Douglass, A. P., Offei, B., Braun-Galleani, S., Coughlan, A. Y., Martos, A. A. R., Ortiz-Merino, R. A., et al. (2018). Population genomics shows no distinction between

pathogenic *Candida krusei* and environmental *Pichia kudriavzevii*: one species, four names. *PloS Pathog.* 14, 1–27. doi: 10.1371/journal.ppat.1007138

Fell, J. W., Boekhout, T., Fonseca, A., Scorzetti, G., and Statzell-Tallman, A. (2000). Biodiversity and systematics of basidiomycetous yeasts as determined by large-subunit rDNA D1/D2 domain sequence analysis. *Int. J. Syst. Evol. Microbiol.* 50, 1351–1371. doi: 10.1099/00207713-50-3-1351

Felsenstein, J. (1985). Confidence limits on phylogenies: an approach using the bootstrap. *Evolution* 39, 783–791. doi: 10.1111/j.1558-5646.1985.tb00420.x

Gao, W. L., Li, Y., Chai, C. Y., Yan, Z. L., and Hui, F. L. (2021). New species of *Yamadazyma* from rotting wood in China. *MycoKeys* 83, 69. doi: 10.3897/MYCOKEYS.83.71156

Gao, W. L., Liu, K. F., Yao, L. G., and Hui, F. L. (2018). *Pichia nanzhaoensis* sp. nov. and *Pichia paraexigua* f.a., sp. nov., two yeast species isolated from rotting wood. *Int. J. Syst. Evol. Microbiol.* 68, 3311–3315. doi: 10.1099/ijsem.0.002989

Gao, W. L., Liu, T. T., Zheng, J., and Hui, F. L. (2017). *Kodamaea neixiangensis* f.a., sp. nov. and *Kodamaea jinghongensis* f.a., sp. nov., two yeast species isolated from rotting wood. *Int. J. Syst. Evol. Microbiol.* 67, 3358–3362. doi: 10.1099/ijsem.0.002117

Hashem, M., Al-Qahtani, M. S., Alamri, S. A., Moustafa, Y. S., Lyberatos, G., and Ntaikou, I. (2022). Valorizing food wastes: assessment of novel yeast strains for enhanced production of single-cell protein from wasted date molasses. *Biomass Convers Biorefin* 12, 4491–4502. doi: 10.1007/s13399-022-02415-2

Hoppert, L., Kölling, R., and Einfalt, D. (2022). Investigation of stress tolerance of *Pichia kudriavzevii* for high gravity bioethanol production from steam–exploded wheat straw hydrolysate. *Bioresour. Technol.* 364, 128079. doi: 10.1016/j.biortech.2022.128079

Huang, L. N., Xi, Z. W., Li, Y., and Hui, F. L. (2018). *Sugiyamaella xiaguanensis* f.a., sp. nov., a yeast species isolated from rotting wood. *Int. J. Syst. Evol. Microbiol.* 68, 3307–3310. doi: 10.1099/ijsem.0.002988

Huang, L. N., Xi, Z. W., Zhai, Y. C., Chai, C. Y., and Hui, F. L. (2019). *Saturnispora galanensis* sp. nov., a yeast species isolated from rotting wood. *Int. J. Syst. Evol. Microbiol.* 69, 2658–2661. doi: 10.1099/ijsem.0.003501

Jia, R., Lv, S., Chai, C., and Hui, F. L. (2020). Three new *Scheffersomyces* species associated with insects and rotting wood in China. *MycoKeys* 71, 87–99. doi: 10.3897/mycokeys.87.56168

Jones, E. B. G., Suetrong, S., Sakayaroj, J., Bahkali, A. H., Abdel-Wahab, M. A., Boekhout, T., et al. (2015). Classification of marine *ascomycota, basidiomycota, blastocladiomycota and chytridiomycota*. *Fungal Divers.* 73, 1–72. doi: 10.1007/s13225-015-0339-4

Kaewkrajay, C., Chanmethakul, T., and Limtong, S. (2020). Assessment of diversity of culturable marine yeasts associated with corals and zoanthids in the Gulf of Thailand, south China sea. *Microorganisms* 8, 474. doi: 10.3390/microorganisms8040474

Katoh, K., and Standley, D. M. (2013). MAFFT multiple sequence alignment software version 7: Improvements in performance and usability. *Mol. Biol. Evol.* 30, 772–780. doi: 10.1093/molbev/mst010

Ke, T., Zhai, Y. C., Yan, Z. L., and Hui, F. L. (2019). *Kazachstania jinghongensis* sp. nov. and *Kazachstania menglunensis* f.a., sp. nov., two yeast species isolated from rotting wood. *Int. J. Syst. Evol. Microbiol.* 69, 3623–3628. doi: 10.1099/ijsem.0.003670

Keene, S., Sarao, M. S., McDonald, P. J., and Veltman, J. (2019). Cutaneous geotrichosis due to *Geotrichum candidum* in a burn patient. *Access Microbiol.* 1, 1–6. doi: 10.1099/acmi.0.000001

Kimura, M. (1980). A simple method for estimating evolutionary rates of base substitutions through comparative studies of nucleotide sequences. *J. Mol. Evol.* 16, 111–120. doi: 10.1007/BF01731581

Kumar, S., Stecher, G., and Tamura, K. (2016). MEGA7: Molecular Evolutionary Genetics Analysis version 7.0 for bigger datasets. *Nordic Hydrology* 34, 281–294. doi: 10.2166/nh.2003.0008

Kurtzman, C. P., and Robnett, C. J. (1998). Identification and phylogeny of ascomycetous yeasts from analysis of nuclear large subunit (26S) ribosomal DNA partial sequences. *Antonie Van Leeuwenhoek* 98, 331–371. doi: 10.1023/A:1001761008817

Lachance, M. A. (2022). Phylogenies in yeast species descriptions: In defense of neighbor-joining. *Yeast* 39, 513–520. doi: 10.1002/yea.3812

Lei, X., Zheng, J., Zhao, D., Qiao, Z., An, M., and Zhang, X. (2022). *Moniliella aeria* sp. nov., a novel yeast isolated from the air of a Wuliangye baijiu-making workshop. *Int. J. Syst. Evol. Microbiol.* 72, 005464. doi: 10.1099/ijsem.0.005464

Letunic, I., and Bork, P. (2019). Interactive Tree of Life (iTOL) v4: recent updates and new developments. *Nucleic Acids Res.* 47, 256–259. doi: 10.1093/nar/gkz239

Li, S. S., Cheng, C., Li, Z., Chen, J. Y., Yan, B., Han, B. Z., et al. (2010). Yeast species associated with wine grapes in China. *Int. J. Food Microbiol.* 138, 85–90. doi: 10.1016/j.ijfoodmicro.2010.01.009

Li, Y. Y., Wang, M. M., Groenewald, M., Li, A. H., Guo, Y. T., Wu, F., et al. (2022). Proposal of two new combinations, twenty new species, four new genera, one new family, and one new order for the anamorphic basidiomycetous yeast species in *Ustilaginomycotina*. *Front. Microbiol.* 12. doi: 10.3389/fmicb.2021.777338

Li, A. H., Yuan, F. X., Groenewald, M., Bensch, K., Yurkov, A. M., Li, K., et al. (2020). Diversity and phylogeny of basidiomycetous yeasts from plant leaves and soil: proposal of two new orders, three new families, eight new genera and one hundred and seven new species. *Stud. Mycol* 96, 17–140. doi: 10.1016/j.simyco.2020.01.002

Liu, J. Y. (2013). Status of marine biodiversity of the China seas. *PloS One* 8, 1–24. doi: 10.1371/journal.pone.0050719

Liu, S., Guo, Q. C., An, Z. R., and Hui, F. L. (2023). Danielozyma pruni sp. nov., an asexual yeast species isolated from insect frass. *Int. J. Syst. Evol. Microbiol.* 73, 006124. doi: 10.1099/ijsem.0.006124

Lou, Q. Z., Lu, M., and Sun, J. H. (2014). Yeast diversity associated with invasive dendroctonus valens killing *Pinus tabuliformis* in China using culturing and molecular methods. *Microb. Ecol.* 68, 397–415. doi: 10.1007/s00248-014-0413-6

Lu, Y. F., Wang, M., Zheng, J., and Hui, F. L. (2017). *Ogataea neixiangensis* sp. nov. and *Ogataea paraovalis* f.a., sp. nov., two methanol-assimilating yeast species isolated from rotting wood. *Int. J. Syst. Evol. Microbiol.* 67, 3038–3042. doi: 10.1099/ijsem.0.002075

Luo, B., Sun, H., Zhang, Y., Gu, Y., Yan, W., Zhang, R., et al. (2019). Habitat-specificity and diversity of culturable cold-adapted yeasts of a cold-based glacier in the Tianshan Mountains, northwestern China. *Appl. Microbiol. Biotechnol.* 103, 2311–2327. doi: 10.1007/s00253-018-9512-5

McMurdie, P. J., and Holmes, S. (2013). Phyloseq: an R package for reproducible interactive analysis and graphics of microbiome census data. *PloS One* 8, e61217. doi: 10.1371/journal.pone.0061217

Murray, N. J., Phinn, S. R., DeWitt, M., Ferrari, R., Johnston, R., Lyons, M. B., et al. (2019). The global distribution and trajectory of tidal flats. *Nature* 565, 222–225. doi: 10.1038/s41586-018-0805-8

Nakase, T., and Takashima, M. (1993). A simple procedure for the high frequency isolation of new taxa of ballistosporous yeasts living on the surfaces of plants. *Riken Rev.* 3, 33–34.

Nath, U. U., and Ravi, R. (2013). Isolation of astaxanthin from marine yeast and study of its pharmacological activity. *Int. curr. pharm. j.* 2, 67–69. doi: 10.3329/icpj.v2i3.13584

Oksanen, r J., Simpson, G. L., Blanchet, F. G., Solymos, P., Stevens, M. H. H., Szoecs, E., et al. (2022). *vegan: community ecology package. Available at: https://github.com/vegandevs/vegan*.

Paradis, E., and Schliep, K. (2019). Ape 5.0: An environment for modern phylogenetics and evolutionary analyses in R. *Bioinformatics* 35, 526–528. doi: 10.1093/bioinformatics/bty633

Pereira, G. V. M., Alvarez, J. P., Neto, D. P., de, C., Soccol, V. T., Tanobe, V. O. A., et al. (2017). Great intraspecies diversity of *Pichia kudriavzevii* in cocoa fermentation highlights the importance of yeast strain selection for flavor modulation of cocoa beans. *Lwt* 84, 290–297. doi: 10.1016/j.lwt.2017.05.073

Pfaller, M. A., Diekema, D. J., Gibbs, D. L., Newell, V. A., Nagy, E., Dobiasova, S., et al. (2008). *Candida krusei*, a multidrug-resistant opportunistic fungal pathogen: geographic and temporal trends from the ARTEMIS DISK Antifungal Surveillance Progra to 2005. *J. Clin. Microbiol.* 46, 515–521. doi: 10.1128/JCM.01915-07

Pikazis, D., Xynos, I. D., Xila, V., Velegraki, A., and Aroni, K. (2009). Extended fungal skin infection due to *Aureobasidium pullulans*. *Clin. Exp. Dermatol.* 34, 892–894. doi: 10.1111/j.1365-2230.2009.03663.x

Qiao, Y. Z., Chen, X., and Hui, F. L. (2023). *Barnettozyma menglunensis* f.a., sp. nov., a novel yeast species isolated from rotting wood. *Int. J. Syst. Evol. Microbiol.* 73, 1–5. doi: 10.1099/ijsem.0.005711

R Core Team (2023) *R: A language and environment for statistical computing* (RVienna, Austria: Foundation for Statistical Computing). Available at: https://www.R-project.org (Accessed 16 June 2023).

Scorzetti, G., Fell, J. W., Fonseca, A., and Statzell-Tallman, A. (2002). Systematics of basidiomycetous yeasts: A comparison of large subunit D1/D2 and internal transcribed spacer rDNA regions. *FEMS Yeast Res.* 2, 495–517. doi: 10.1016/S1567-1356(02)00128-9

Shi, C. F., Zhang, K. H., Chai, C. Y., Yan, Z. L., and Hui, F. L. (2021). Diversity of the genus *Sugiyamaella* and description of two new species from rotting wood in China. *MycoKeys* 77, 27–39. doi: 10.3897/MYCOKEYS.77.60077

Soki, H., Abo, K., Yamazaki, K., Kojima, T., Oda, T., Uzawa, Y., et al. (2015). First report of intraorbital abscess caused by *Candida allociferrii* and specific PCR for differentiating *Stephanoascus ciferrii* complex species. *Med. Mycol J.* 56, E9–E14. doi: 10.3314/mmj.56.E9

Vu, D., Groenewald, M., Szöke, S., Cardinali, G., Eberhardt, U., Stielow, B., et al. (2016). DNA barcoding analysis of more than 9 000 yeast isolates contributes to quantitative thresholds for yeast species and genera delimitation. *Stud. Mycol.* 85, 91–105. doi: 10.1016/j.simyco.2016.11.007

Wang, Q. M., and Bai, F. Y. (2008). Molecular phylogeny of basidiomycetous yeasts in the *Cryptococcus luteolus* lineage (*Tremellales*) based on nuclear rRNA and mitochondrial cytochrome b gene sequence analyses: Proposal of *Derxomyces* gen. nov. and *Hannaella* gen. nov., and description of eight novel *Derxomyces* species. *FEMS Yeast Res.* 8, 799–814. doi: 10.1111/j.1567-1364.2008.00403.x

Wang, W. L., Chi, Z. M., Chi, Z., Li, J., and Wang, X. H. (2009). Siderophore production by the marine-derived *Aureobasidium pullulans* and its antimicrobial activity. *Bioresour. Technol.* 100, 2639–2641. doi: 10.1016/j.biortech.2008.12.010

Wang, L., Chi, Z., Wang, X., Ju, L., Chi, Z., and Guo, N. (2008). Isolation and characterization of *Candida membranifaciens* subsp. *flavinogenie* W14-3, a novel riboflavin-producing marine yeast. *Microbiol. Res.* 163, 255–266. doi: 10.1016/j.micres.2007.12.001

Wang, Q., Cui, Y., Sen, B., Ma, W., Zheng, R. L., Liu, X., et al. (2017). Characterization and robust nature of newly isolated oleaginous marine yeast *Rhodosporidium* spp. from coastal water of Northern China. *AMB Expr.* 7, 30. doi: 10.1186/s13568-017-0329-x

Wang, H., Wang, Y., Chen, J., Zhan, Z., Li, Y., and Xu, J. (2007). Oral yeast flora and its ITS sequence diversity among a large cohort of medical students in Hainan, China. *Mycopathologia* 164, 65–72. doi: 10.1007/s11046-007-9028-5

Wang, Q. M., Liu, W. Q., Liti, G., Wang, S. A., Bai, F. Y., et al. (2012). Surprisingly diverged populations of Saccharomyces cerevisiae in natural environments remote from human activity. *Mol. Ecol.* 21, 54045417. doi: 10.1111/j.1365-294X.2012.05732.x

Wei, X. Y., Zhu, H. Y., Song, L., Zhang, R. P., Li, A. H., Niu, Q. H., et al. (2022). Yeast diversity in the Qaidam basin desert in China with the description of five new yeast species. *J. Fungi* 8, 858. doi: 10.3390/jof8080858

World Health Organization (2022) *WHO fungal priority pathogens list to guide research, development and public health action*. Available at: https://www.who.int/publications/i/item/9789240060241 (Accessed October 25, 2022).

Wu, Q., Xu, Y., and Chen, L. (2012). Diversity of yeast species during fermentative process contributing to chinese maotai-flavour liquor making. *Lett. Appl. Microbiol.* 55, 301–307. doi: 10.1111/j.1472-765X.2012.03294.x

Xi, Z. W., Huang, L. N., Li, Y., and Hui, F. L. (2019). *Vanrija jinghongensis* sp. nov., an asexual basidiomycetous yeast from rotting wood. *Int. J. Syst. Evol. Microbiol.* 69, 105–108. doi: 10.1099/ijsem.0.003108

Yang, S. P., Wu, Z. H., and Jian, J. C. (2011). Distribution of marine red yeasts in shrimps and the environments of shrimp culture. *Curr. Microbiol.* 62, 1638–1642. doi: 10.1007/s00284-011-9910-8

Yu, H. T., Shang, Y. J., Zhu, H. Y., Han, P. J., Wang, Q. M., Santos, A. R. O., et al (2023). Yueomyces silvicola sp. nov., a novel ascomycetous yeast species unable to utilize ammonium, glutamate, and glutamine as sole nitrogen sources. *Yeast* 110. doi: 10.1002/yea.3901

Zaky, A. S., Greetham, D., Louis, E. J., Tucker, G. A., and Du, C. (2016). A new isolation and evaluation method for marine-derived yeast spp. with potential applications in industrial biotechnology. *J. Microbiol. Biotechnol.* 26, 1891–1907. doi: 10.4014/jmb.1605.05074

Zaky, A. S., Tucker, G. A., Daw, Z. Y., and Du, C. (2014). Marine yeast isolation and industrial application. *FEMS Yeast Res.* 14, 813–825. doi: 10.1111/1567-1364.12158

Zheng, J., Lu, Y. F., Liu, X. J., and Hui, F. L. (2017). *Cyberlindnera xishuangbannaensis* f.a., sp. nov., a yeast isolated from rotting wood. *Int. J. Syst. Evol. Microbiol.* 67, 5051–5055. doi: 10.1099/ijsem.0.002411

Zhou, J., Deng, Y., Shen, L., Wen, C., Yan, Q., Ning, D., et al. (2016). Temperature mediates continental-scale diversity of microbes in forest soils. *Nat. Commun.* 7, 12083. doi: 10.1038/ncomms12083

Zhu, S. S., Lei, Y. H., Wang, C., Wei, Y. M., Wang, C. C., and Sun, Y. F. (2021). Patterns of yeast diversity distribution and its drivers in rhizosphere soil of Hami melon orchards in different regions of Xinjiang. *BMC Microbiol.* 21, 1–18. doi: 10.1186/s12866-021-02222-1

Zhu, H. Y., Wei, Y. H., Guo, L. C., Wei, X. Y., Li, J. N., Zhang, R. P., et al. (2023a). *Vishniacozyma pseudocarnescens* sp. nov., a new anamorphic tremellomycetous. *Int. J. Syst. Evol. Microbiol.* 73, 6076. doi: 10.1099/ijsem.0.006076

Zhu, H. Y., Wei, X. Y., Liu, X. Z., and Bai, F. Y. (2023b). *Cystofilobasidium josepaulonis* sp. nov., a novel basidiomycetous yeast species. *Int. J. Syst. Evol. Microbiol.* 73, 5865. doi: 10.1099/ijsem.0.005865

frontiers | Frontiers in Microbiology

TYPE Original Research
PUBLISHED 14 December 2023
DOI 10.3389/fmicb.2023.1265676

OPEN ACCESS

EDITED BY
Xue-Wei Xu,
Ministry of Natural Resources, China

REVIEWED BY
Shuting Liu,
Kean University, United States
Shenghui Li,
Puensum Genetech Institute, China

*CORRESPONDENCE
Song-Gun Kim
✉ sgkim@kribb.re.kr

RECEIVED 23 July 2023
ACCEPTED 23 November 2023
PUBLISHED 14 December 2023

CITATION
Muhammad N, Avila F, Nedashkovskaya OI and Kim S-G (2023) Three novel marine species of the genus *Reichenbachiella* exhibiting degradation of complex polysaccharides. *Front. Microbiol.* 14:1265676.
doi: 10.3389/fmicb.2023.1265676

Three novel marine species of the genus *Reichenbachiella* exhibiting degradation of complex polysaccharides

Neak Muhammad[1,2], Forbes Avila[1,2], Olga I. Nedashkovskaya[3] and Song-Gun Kim[1,2]*

[1]Biological Resource Center/Korean Collection for Type Cultures (KCTC), Korea Research Institute of Bioscience and Biotechnology, Daejeon, Republic of Korea, [2]Department of Environmental Biotechnology, KRIBB School of Biotechnology, University of Science and Technology (UST), Daejeon, Republic of Korea, [3]G.B. Elyakov Pacific Institute of Bioorganic Chemistry of the Far-Eastern Branch of the Russian Academy of Sciences, Vladivostok, Russia

Three novel strains designated ABR2-5^T, BKB1-1^T, and WSW4-B4^T belonging to the genus *Reichenbachiella* of the phylum *Bacteroidota* were isolated from algae and mud samples collected in the West Sea, Korea. All three strains were enriched for genes encoding up to 216 carbohydrate-active enzymes (CAZymes), which participate in the degradation of agar, alginate, carrageenan, laminarin, and starch. The 16S rRNA sequence similarities among the three novel isolates were 94.0%–94.7%, and against all three existing species in the genus *Reichenbachiella* they were 93.6%–97.2%. The genome sizes of the strains ABR2-5^T, BKB1-1^T, and WSW4-B4^T were 5.5, 4.4, and 5.0 Mb, respectively, and the GC content ranged from 41.1%–42.0%. The average nucleotide identity and the digital DNA–DNA hybridization values of each novel strain within the isolates and all existing species in the genus *Reichenbachiella* were in a range of 69.2%–75.5% and 17.7–18.9%, respectively, supporting the creation of three new species. The three novel strains exhibited a distinctive fatty acid profile characterized by elevated levels of iso-$C_{15:0}$ (37.7%–47.4%) and $C_{16:1}$ ω5c (14.4%–22.9%). Specifically, strain ABR2-5^T displayed an additional higher proportion of $C_{16:0}$ (13.0%). The polar lipids were phosphatidylethanolamine, unidentified lipids, aminolipids, and glycolipids. Menaquinone-7 was identified as the respiratory quinone of the isolates. A comparative genome analysis was performed using the KEGG, RAST, antiSMASH, CRISPRCasFinder, dbCAN, and dbCAN-PUL servers and CRISPRcasIdentifier software. The results revealed that the isolates harbored many key genes involved in central metabolism for the synthesis of essential amino acids and vitamins, hydrolytic enzymes, carotenoid pigments, and antimicrobial compounds. The KEGG analysis showed that the three isolates possessed a complete pathway of dissimilatory nitrate reduction to ammonium (DNRA), which is involved in the conservation of bioavailable nitrogen within the ecosystem. Moreover, all the strains possessed genes that participated in the metabolism of heavy metals, including arsenic, copper, cobalt, ferrous, and manganese. All three isolated strains contain the class 2 type II subtype C1 CRISPR-Cas system in their genomes. The distinguished phenotypic, chemotaxonomic, and genomic characteristics led us to propose that the three strains represent three novel species in the genus *Reichenbachiella*: *R. ulvae* sp. nov. (ABR2-5^T = KCTC 82990^T = JCM 35839^T), *R. agarivorans* sp. nov. (BKB1-1^T = KCTC 82964^T = JCM 35840^T), and *R. carrageenanivorans* sp. nov. (WSW4-B4^T = KCTC 82706^T = JCM 35841^T).

KEYWORDS

Bacteroidota, genome analyses, polysaccharide degradation, carbohydrate-active enzymes, CRISPRCas

1 Introduction

The marine ecosystem is one of the largest and most intricate aquatic systems on the planet. The marine microbes participate in the maintenance and regulation of the biogeochemical cycles of the sea (Falkowski et al., 2008; Murillo et al., 2019). Marine microbes degrade dead plants, animals, and algae and turn them into useful nutrients that can allow further growth of these organisms. Furthermore, the genomes of these microbes are highly enriched with genes for the breakdown of complex molecules such as pollutants, peptides, and polysaccharides (Gao et al., 2017; McKee et al., 2021).

There are very different types of polysaccharides, such as agar, alginate, chitin, carrageenan, cellulose, fucoidans, laminarin, pectin, porphyrin, ulvane, and xylan (Helbert, 2017). Polysaccharides are different based on their isolation sources, chemical composition, and structure. Agar, alginate, carrageenan, fucoidan, laminarin, and ulvan originate mainly from diverse algae and phytoplankton, while cellulose, pectin, and xylan are derived from plants, and the remaining are from animals and fungi (de Jesus Raposo et al., 2015; Helbert, 2017). Among them, carrageenan, fucoidan, and ulvan, are classified as sulfated polysaccharides (Bhuyan et al., 2023). Polysaccharides are made of sugar monomers connected through glycosidic linkages, including but not limited to β-1,3, β-1,4, β-1,6, α-1,3, and α-1,4 linkages (Bäumgen et al., 2021). The cell walls of macroalgae and phytoplankton serve as readily accessible sources of these polysaccharides (Ehrlich et al., 2018; Shao and Duan, 2022). Macroalgae consist of three main groups, such as red, brown, and green, which are vital parts of the marine food chain (Øverland et al., 2019). Furthermore, macroalgae provide a solid attachment for many groups of marine bacteria to form a mutually benefit interaction between macroalgae and bacteria or for bacteria to invade macroalgae and breakdown the complex polysaccharides of macroalgae (Singh and Reddy, 2014; Brunet et al., 2022). Numerous groups of algal polysaccharide-degrading bacteria have been isolated in marine environments, contributing to algal biomass recycling and the carbon cycle (Martin et al., 2015). The oligosaccharides produced from degradation of the polysaccharides have been reported to exhibit various biological activities, making them applicable in the functional food, cosmetic, and medical sectors (de Jesus Raposo et al., 2015; Ruocco et al., 2016). For example, carrageenan and alginate oligosaccharides show a wide range of biological activities, including antiviral, anticancer, antioxidant, anti-angiogenic, immunomodulation, antimicrobial, antihypertensive, and antidiabetic activities (Liu et al., 2019; Zhao et al., 2021). Consequently, there is a strong demand to explore novel bacterial strains that can effectively degrade complex polysaccharides. The microbial degradation of polysaccharides for the production of oligosaccharides offers significant advantages over chemical methods. Microbial degradation procedures are environmentally friendly, highly specific, biodegradable, and cost and energy-efficient (Deng et al., 2023).

The marine microbes are enriched with genes encoding enzymes that potentially participate in polysaccharide degradation, known as carbohydrate-active enzymes (CAZymes; McKee et al., 2021). In the bacterial genome, these CAZymes, transporters and regulator proteins are organized into a system called polysaccharide utilization loci (PUL; Terrapon et al., 2015). Currently, there are approximately 300 CAZymes protein families that categorized into five classes: glycoside hydrolases (GHs), glycosyltransferases (GTs), polysaccharide lyases (PLs), carbohydrate esterases (CEs), and carbohydrate-binding modules (CBMs; Cantarel et al., 2009). There are numerous strains belonging to the phylum *Bacteroidota* that are highly enriched with CAZymes and have the potential to degrade diverse types of polysaccharide (Hehemann et al., 2012; Mann et al., 2013; McKee et al., 2021).

The phylum *Bacteroidota*, formerly recognized as *Bacteroidetes*, is considered as a major group of marine heterotrophic bacterioplankton (Paster et al., 1994). At the time of writing, the phylum *Bacteroidota*[1] comprises six classes and six orders. The class *Cytophagia* consist of single order called *Cytophagales*[2] which mainly composed of 20 families. Among these, the family *Reichenbachiellaceae* comprises only three validly published genera.[3] The genus *Reichenbachia* was originally proposed by Nedashkovskaya in 2003 in the family *Flammeovirgaceae* (Nedashkovskaya et al., 2003). The name *Reichenbachia* was subsequently changed to *Reichenbachiella* and separated into the family *Reichenbachiellaceae* (Nedashkovskaya et al., 2005; García-López et al., 2019). Over the past few years, a total of three *Reichenbachiella* species have been described,[4] namely, *R. agariperforans* (Nedashkovskaya et al., 2005) *R. faecimaris* (Cha et al., 2011), and *R. versicolor* (Shi et al., 2018). They have been isolated from sea coelenterate, tidal-flat sediment, and red algae, respectively. The species of genus *Reichenbachiella* are characterized as heterotrophic, Gram-stain-negative, aerobe, non-motile, non-spore producer, rod-shaped bacteria. The menaquinone-7 (MK-7) is common among the species of genus *Reichenbachiella* (Shi et al., 2018). Menaquinone-7 (MK-7) is a type of quinone molecule which is essential cofactor in electron transport chains and plays crucial roles in bacterial physiology and metabolism Menaquinone can also be used as a chemotaxonomic marker in the field of microbial taxonomy (Hiraishi, 1999). To date, relative few studies on the comprehensive genome analysis for applications of the genus *Reichenbachiella* are available.

While investigating the microbial diversity of the tidal flats in the West Sea, Korea, a high number of novel bacteria capable of degrading complex polysaccharides were isolated (Muhammad et al., 2023; Nguyen et al., 2023). Three novel strains, ABR2-5^T,

1 https://lpsn.dsmz.de/phylum/bacteroidota
2 https://lpsn.dsmz.de/order/cytophagales
3 https://lpsn.dsmz.de/family/reichenbachiellaceae
4 https://lpsn.dsmz.de/genus/reichenbachiella

BKB1-1^T, and WSW4-B4^T, were isolated from macroalgae and sea mud. On the basis of a taxonomic study using a polyphasic approach, we propose that these three strains should be included in the genus *Reichenbachiella* as representatives of three novel species. Furthermore, we report the polysaccharide-degrading abilities of these three isolates. The strains possess the ability to degrade various complex polysaccharides of agar, alginate, carrageenan, laminarin, and starch and carry a high number of genes for CAZymes in their genomes. Moreover, the strains carry genes for the production of secondary metabolites, the synthesis of essential amino acids and vitamins, class 2 type II subtype C1 CRISPR-Cas system, heavy metal metabolism, and important pathways that participate in the nitrogen cycle of coastal ecosystems.

2 Materials and methods

2.1 Isolation and identification of gliding bacterial strains

Three samples were collected from different locations in the West Sea, Korea. In late autumn 2022, 100 gram red alga *Chondrus* sp. was collected from a beach in Byeonsan (35° 40′ 53.76″ N 126° 31′ 51.96″ E). One hundred gram green alga *Ulva* sp. was collected from Aphae Island (34° 49′ 52.8″ N 126° 22′ 48.5″ E) on June 2021. Fifty gram sea mud was collected from an estuary at Bigeum Island (34° 41′ 23.3″ N 125° 55′ 13.4″ E) on June 2021. The specimens were taken to the lab immediately and processed.

To isolate gliding bacteria, we used low-nutrient media composed of 60% (v/v) seawater, 1.5% (w/v) agar, and 50 mg/L cycloheximide. To isolate novel strains, we aimed to replicate natural conditions for the bacteria. Therefore, seawater from the same sampling area was collected and used in media preparation. The low-nutrient media, prepared with seawater, enabled us to isolate marine gliding bacteria. We used 60% (v/v) seawater for all media preparation instead of 100% because the samples were collected from tidal flats where salinity could be lower.

One gram of each algae was diced into small pieces and placed at the center of solid media. The sea mud sample was also placed in the same medium. All plates were incubated for 7 days at 15°C and then regularly observed for gliding bacteria using a stereo microscope (ZEISS Stemi 508; Nguyen et al., 2023). The gliding colonies at the margin were transferred with a sterile needle onto marine agar 2,216 (MA; BD) and modified VY/2 agar media [MVY; 60% (v/v) seawater, 5 g/L baker's yeast (Sigma) and 25 mg/L filtered sterile vitamin B_{12}] until pure cultures were obtained. A strain of a circular, smooth, orange-pigmented colony was designated as strain ABR2-5^T, while a strain of an orange-pigmented colony that hydrolyzed agar was designated as strain BKB1-1^T, and a strain of smooth circular pale-yellow colonies was designated as strain WSW4-B4^T. Bacterial strains isolated were preserved in 20% glycerol at-80°C and in lyophilized ampoules at 4°C.

The genomic DNA, extracted from cells cultivated on MA, was used for the amplification of 16S rRNA genes using four universal primers (27F, 518F, 805R, and 1492R; Pheng et al., 2020). These primers are designed to determine a nearly complete sequence of the 16S rRNA gene. The complete sequences were then assembled by using Vector NTI software (Invitrogen). The 16S rRNA sequence were queried to search the similar sequences from the EzBioCloud server[5] (Yoon et al., 2017a). The similar sequences downloaded from the EzBioCloud server were used to construct neighbor-joining (NJ; Saitou and Nei, 1987), maximum-likelihood (ML; Felsenstein, 1981), and maximum parsimony (MP) phylogenetic trees (Fitch, 1971) in Molecular Evolutionary Genetics Analysis (MEGA X) software (Kumar et al., 2018). The robustness of the sequence clustering was evaluated using the bootstrap resampling method with 1,000 replicates. *Flammeovirga aprica* NBRC 15941^T was incorporated into the analysis as an outgroup.

2.2 Phenotypic characterization

The colonies' shapes were observed on MA plates after 3 days of cultivation. We used the BBL™ Gram Stain Kit (BD, USA) for Gram-staining. The shape and size of the bacterial strains was observed by a scanning electron microscope (Regulus 8,100, Hitachi; Jeon et al., 2022). Motility was observed by using a hanging-drop technique, and gliding activity was observed by growing the strain on low-nutrient media composed of sea water and 0.7% (w/v) agar (Tittsler and Sandholzer, 1936). The optimal temperature and salt tolerance for the growth was determined by using MA (Muhammad et al., 2022) while the optimal pH for the growth was tested in MB (Muhammad et al., 2023). To determine the growth under an anaerobic condition, all three strains were tested on a solid medium composed of 0.2% (w/v) glucose, 2% (w/v) NaCl, 0.1% (w/v) polypeptone, 0.1% (w/v) KH_2PO_4, 0.1% (w/v) K_2HPO_4, 0.2% (w/v) NH_4Cl, 0.14% (w/v) MgSO4, $NaNO_3$ (w/v) 0.17, 1.5% (w/v) agar, 0.1% (w/v) resazurin, 0.05% (w/v) cysteine HCl, 1 mL trace elements, and 1 mL multivitamins (Wolin et al., 1963; Kim et al., 2001; Bae et al., 2020).

Catalase and oxidase activities were tested by using 3% (v/v) H_2O_2 and 1% (w/v) tetramethyl-*p*-phenylenediamine reagents, respectively (Ueno et al., 2021). The Cowan & Steel protocol was used to test the hydrolysis of Tweens 20, 40, 80, and casein (Phillips, 1993). The activities of DNase were determined using DNase agar (Difco; Jeffries et al., 1957). The 20% (w/v) KOH solution was used to assess the presence of flexirubin-type pigments (Lin et al., 2020). The enzymatic activities were tested using the API ZYM kit (bioMérieux), and the ability to utilize various carbon sources was assessed using the API 20E and API 50CH kits (bioMérieux), and GEN III Microplates (from Biolog; Jeong et al., 2020).

The cellular fatty acids, quinones, and polar lipids were determined for the three strains. For the fatty acid analysis, cells grown on MA of the same growth stage were collected. The fatty acid was extracted using a standard MIDI protocol (version 6.2; Sasser, 1990). For the determination of respiratory quinones, Komagata and Suzuki protocol was used (Komagata and Suzuki, 1988). For the analysis of polar lipids, Komagata and Suzuki method was used to extract the compound from the cell biomass using chloroform/methanol followed by two-dimensional TLC (Komagata and Suzuki, 1988). Finally, the TLC plates were dried and sprayed with 0.2% ninhydrin, α-naphthol, molybdenum blue, and 0.5% phosphomolybdic acid to detect amino

5 http://www.ezbiocloud.net

lipids, glycollipids, phospholipids, and total lipids (Komagata and Suzuki, 1988).

2.3 Genome sequencing and analysis

The genomic DNA of the three strains ABR2-5^T, BKB1-1^T, and WSW4-B4^T was extracted using NucleoSpin Microbial DNA kit (Macherey-Nagel, Germany). The concentration and purity of the genomic DNA was determined using a NanoDrop spectrophotometer (ThermoScientific, United States), and the fragmentation of DNA was visualized by gel electrophoresis using 1% (w/v) agarose gel.

Oxford Nanopore Technologies (ONT, United Kingdom) platform was used for genome sequencing. Ligation sequencing kit (SQK-LSK112), native barcoding kit (SQK-NBD112.24), R10.4 FLO-MIN112 flow cells, and MinION device were used in the sequencing process. Basecalling was carried out with default parameters using MinKNOW software version 22.10.7 and Guppy 6.3.8 (Wick et al., 2019). *De novo* assembly was done by Flye version 2.9.1[6] (Kolmogorov et al., 2019). To assess the completeness and contamination of the assembled genomes, we used CheckM version 1.2.2[7] and Busco version 5.4.4[8] (Parks et al., 2015; Manni et al., 2021).

2.4 Genome based phylogeny

To determine the taxonomic position of strains ABR2-5^T, BKB1-1^T, and WSW4-B4^T, we calculated the average nucleotide identity (ANI) and digital DNA–DNA hybridization (dDDH) using EZBiocloud's ANI calculator[9] (Yoon et al., 2017b) and DSMZ's Genome to Genome Distance Calculator version 3.0[10] (Meier-Kolthoff et al., 2013). We generated the genomic phylogenetic tree using the 92 prokaryotic core-genes according to the up-to-date bacterial core gene (UBCG) pipeline (Na et al., 2018) with *Flammeovirga aprica* JL-4^T (GCF012844305) as an outgroup.

2.5 Genome functional analysis

First, the three genomes of strains ABR2-5^T, BKB1-1^T, and WSW4-B4^T were annotated using NCBI's Prokaryotic Genome Annotation Pipeline (PGAP; Li W. et al., 2021). Metabolic pathways were predicted using the KEGG and RAST databases. The KEGG pathways were predicted using BlastKOALA server.[11] The protein sequences from each genome were uploaded, and metabolic pathways were predicted for each isolate and reference strains using the prokaryotic database option. Subsequently, the BlastKOALA results were then processed using KEGG-decoder,[12] employing the default parameters (Graham et al., 2018). From the KEGG pathway data, a heatmap was constructed using GraphPad Prism version 8.0.2. To compare the metabolic diversity among novel isolates and reference strains, we used the RAST server version 2.0[13](Aziz et al., 2008). For the RAST annotation (see text footnote 13), we used the genome fasta nucleic acid file and applied the 'RASTtk' tool with the 'automatically fix errors' options on the RAST server. The annotated pathways of the three strains and reference strains from the RAST server were compared using two-tailed one-sample T-test method. Additionally, antiSMASH 6.01 was used to identify biosynthesis gene clusters (BGCs) and metabolic gene clusters (MGCs) within the genomes (Blin et al., 2019). The CRISPRCasFinder and CRISPRcasIdentifier[14] servers were used to annotate the CRISPR Cas system (Couvin et al., 2018; Padilha et al., 2020). The presence of Cas enzymes were further confirmed by blasting each sequence in the UniProt database (The UniProt Consortium, 2023). The genomes of the three novel strains ABR2-5^T, BKB1-1^T, and WSW4-B4^T and three reference strains *R. agariperforans* DSM 26134^T, *R. faecimaris* DSM 26133^T, and *R. versicolor* DC003^T were analyzed to detect carbohydrate active enzymes (CAZymes) using the dbCAN2 meta server (Zhang et al., 2018). To detect polysaccharide utilization loci (PUL) in strains ABR2-5^T and BKB1-1^T, we utilized the dbCAN-PUL database. For the identification of functional genes (*susC* and *susD*), the Prokka server was employed (Ausland et al., 2021). For the strain WSW4-B4^T, we employed the dbCAN-PUL and PULDB databases[15] to identify PUL and the presence of *susC* and *susD* genes. The PULDB database confirmed the existence of functional genes (*susC* and *susD*) in the proximity of CAZymes within PUL. Since the genomes of strains ABR2-5^T and BKB1-1^T were not available in the PULDB, we manually annotated them using the Prokka server.

2.6 Polysaccharide degradation testing

We tested the abilities of three strains to degrade complex polysaccharide by two methods. First, we cultivated three strains on solid media containing 60% (v/v) seawater, 0.01% (w/v) polypeptone, 1% (w/v) of each test polysaccharide, including cellulose, chitin, κ-carrageenan, λ-carrageenan, ι-carrageenan, inulin, laminarin, sodium alginate, starch, and xylan (Gao et al., 2017). For solidification, we used 0.6% (w/v) gellan gum instead of agar. For the degradation of agar and κ-carrageenan, agar and κ-carrageenan were used as solidifying agents instead of gellan gum. All three strains were inoculated on the media containing each test polysaccharide and then cultivated at 30°C for 7 days. The degradation of polysaccharides was detected by the production of a clear zone around the colonies or by the hydrolysis of solid media for the media containing agar and κ-carrageenan as solidifying agents. We used an iodine solution for the determination of starch hydrolysis. The hydrolysis of other polysaccharides was assessed by the development of a clear zone around the colonies.

Second, the degradation of the polysaccharide was further tested in liquid media with the same composition as the solid agar method, except that the media contained 0.2% (w/v) of each test polysaccharide

6 github.com/fenderglass/Flye
7 github.com/Ecogenomics/CheckM
8 busco.ezlab.org/
9 www.ezbiocloud.net/tools/ani
10 https://ggdc.dsmz.de/ggdc.php
11 kegg.jp/blastkoala/
12 github.com/bjtully/BioData/tree/master/KEGGDecoder
13 rast.nmpdr.org/
14 https://github.com/BackofenLab/CRISPRcasIdentifier
15 http://www.cazy.org/PULDB/

(cellulose, chitin, κ-carrageenan, λ-carrageenan, ι-carrageenan, inulin, laminarin, sodium alginate, starch, and xylan). We inoculated two-day-old cultures of the three strains and cultivated them at 30°C in a shaking incubator. The cultures were harvested by centrifugation at 0, 3, and 7 days and then treated with 3,5-dinitrosalicylic acid (DNS) reagents, which reacted with the reducing sugars released from the degradation of polysaccharides. The change of color was measured by a microplate reader (Synergy H1, BioTek) at 570 nm after color development (Gao et al., 2017; Deshavath et al., 2020).

3 Results and discussion

3.1 Isolation and identification

The strains ABR2-5^T, BKB1-1^T, and WSW4-B4^T were isolated from a green algae of the *Ulva* sp., sea mud, and a red algae of the *Chondrus* sp., respectively (Figures 1A–C). All three strains grew well on MA and MVY. Colonies of strain ABR2-5^T and BKB1-1^T were orange, while the colonies of strain WSW4-B4^T were pale-yellow. All three strains produced round, smooth colonies with a diameter in a range of 9.8–16 mm. The size of the cells ranged from 2.1–3.8 μm in length and 0.22–0.31 μm in width (Figures 1D–F).

3.2 16S rRNA gene analysis

The phylogenetic position of the strains ABR2-5^T, BKB1-1^T, and WSW4-B4^T was determined based on the 16S rRNA gene sequences. All three strains were phylogenetically placed within the genus *Reichenbachiella*, which contains three species currently. The analysis of the 16S rRNA genes showed that the closest relatives of strains ABR2-5^T and BKB1-1^T were *R. agariperforans* DSM 26134^T with similarity values of 96.5% and 96.9%, respectively. Strain WSW4-B4^T was closest to *R. faecimaris* DSM 26133^T with a similarity value of 97.2%. In addition, the 16S rRNA gene similarity values among the three novel strains were less than 95%, while the values between the three novel strains and all three type strains in the genus *Reichenbachiella* were under 97% (Supplementary Table S1). These findings support the creation of three novel species. The threshold of the 16S rRNA gene similarity value is typically around 98.7% for species, 94.5% for genera, and 86.5% for families (Yarza et al., 2014). The phylogenetic tree based on 16S rRNA gene sequences (Figure 2) showed the clustering of three isolates (strains ABR2-5^T, BKB1-1^T, and WSW4-B4^T) with three existing species of the genus *Reichenbachiella*: *R. agariperforans* DSM 26134 ^{T}, *R. faecimaris* DSM 26133^T, and *R. versicolor* DC003^T. Interestingly, all the *Reichenbachiella* strains, including the three isolates formed a monophyletic clade with high bootstrap values (>70%). The strains *R. agariperforans* KCTC 12369^T, *R. faecimaris* KCTC 82811^T, and *R. versicolor* KCTC 82854^T were selected as the reference strains for the comparative taxonomic studies for three isolates. The 16S rRNA gene sequences of strains ABR2-5^T, BKB1-1^T, and WSW4-B4^T were registered in GenBank/EMBL/DDBJ with the accession numbers OP473986, OP473987, and OP458510, respectively.

3.3 Phenotypic analysis

All three isolates were Gram-staining-negative, long rod-shaped, and showed gliding motility. All three strains grew optimally at 15°C–30°C, but the strains ABR2-5^T and BKB1-1^T also grew at 37°C. Strain ABR2-5^T grew optimally at pH 6.0–9.0, while the optimum pH for the strains BKB1-1^T and WSW4-B4^T was 6.5–8.5. The NaCl concentration

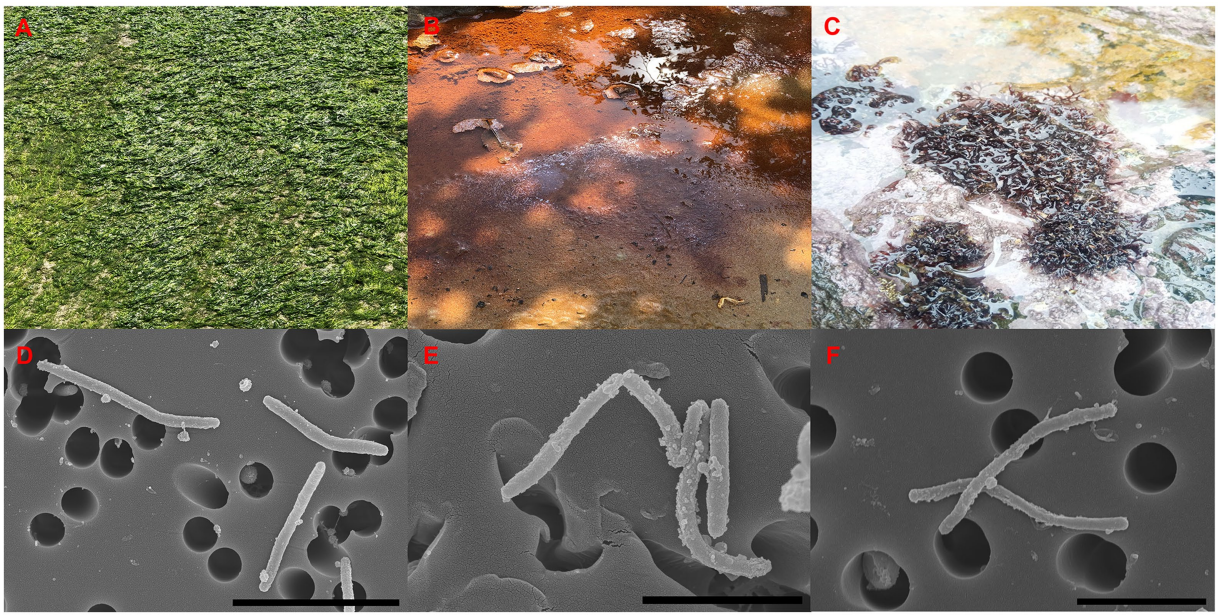

FIGURE 1
Sources of isolation **(A–C)**, and SEM images **(D–F)** of three isolates. Strain: ABR2-5^T **(A,D)**; BKB1-1^T, **(B,E)**; WSW4-B4^T **(C,F)**. Scale bar: 4 μm **(D)**, 2 μm **(E,F)**.

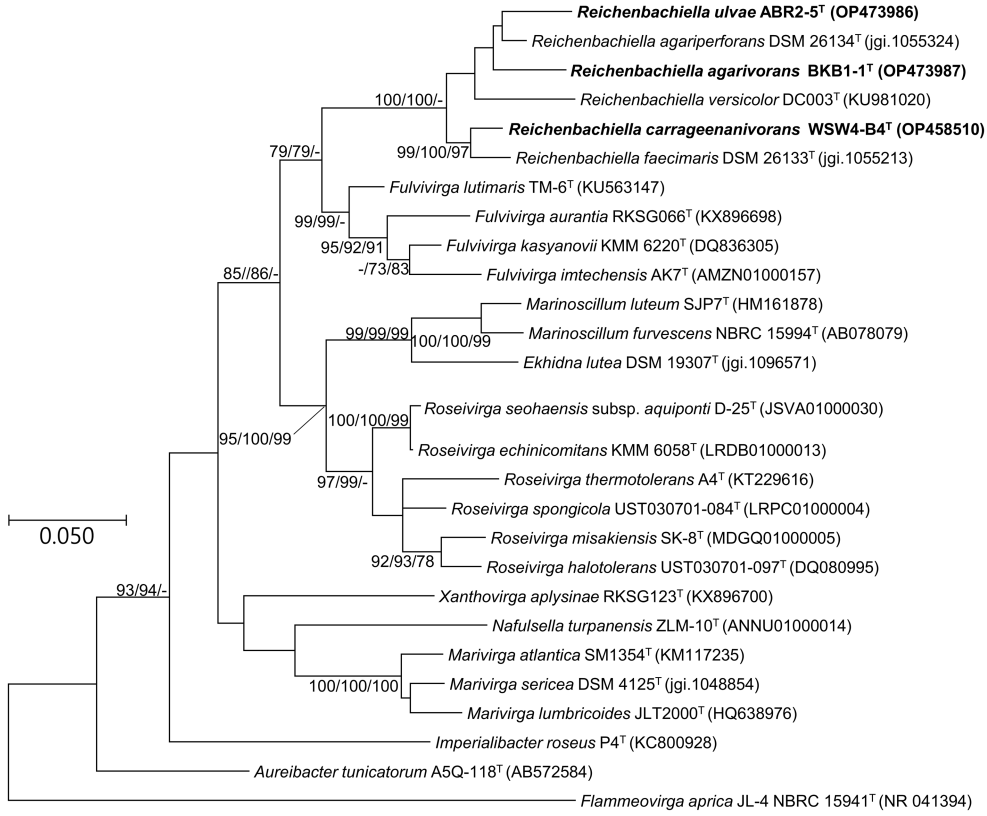

FIGURE 2
Maximum likelihood tree based on 16S rRNA gene sequences showing the phylogenetic relationship of three novel isolates and closely related genus belonging to the order Cytophagales. Bootstrap values (>70%) in the order of ML/NJ/MP are shown at the branch points based on 1,000 replications. GenBank accession numbers are shown in parentheses. Bar, 0.05 substitutions per nucleotide position. *Flammeovirga aprica* JL-4 NBRC 15941^T was used as an outgroup.

for the growth of all three isolates ranged from 0.5–4.0% (w/v), but only the strain ABR2-5^T showed growth up to 7% (w/v) NaCl and only the strain BKB1-1^T showed weak growth in the absence of NaCl. The strains ABR2-5^T and WSW4-B4^T could grow under only aerobic conditions, while strain BKB1-1^T could grow under both aerobic and anaerobic conditions. The detailed physiological characteristics of three novel strain and their reference strains are summarized in Table 1.

Cells of all three strains hydrolyzed Tween 20, not Tweens 40 and 80, and casein. The strains ABR2-5^T and BKB1-1^T were DNase-positive, while strain WSW4-B4^T was DNase-negative. Among the three strains only strains ABR2-5^T and BKB1-1^T contained flexirubin-type pigments. In API ZYM test, all three isolates showed activities of acid phosphatase, alkaline phosphatase, cystine arylamidase, α-chymotrypsin, esterase (C4), esterase lipase (C8), leucine arylamidase, naphthol-AS-BI-phosphohydrolase, trypsin, and valine arylamidase. All three strains were negative for α-fucosidase, α-glucosidase, and α-mannosidase. Among the three novel isolates only strain ABR2-5^T was positive for the activities of α-galactosidase and β-glucuronidase. The API 50CH tests were performed to differentiate the strains by determining their abilities to utilize sugars and produce acid molecules. A total of 50 sugar molecules were tested for hydrolysis, resulting in a color change due to acid production if the strains had the ability to metabolize it. The three novel strains possessed metabolic capabilities that distinguish them from the reference strains. All three strains produced acid from N-acetylglucosamine, L-fucose, D-galactose, and D-mannose, while the strain ABR2-5^T produced acid from additional amidon (starch), amygdalin, D-cellobiose, gentibiose, D-lactose, D-maltose, and L-rhamnose. Furthermore, in a GEN III MicroPlate (Biolog) test, all three novel strains utilized acetoacetic acid, D-cellobiose, L-fucose, gentiobiose, L-glutamic acid, D-mannose, and sodium butyrate. Although all three novel isolates and the three reference strains shared some biochemical characteristics, there are certain biochemical tests that were different between the three novel strains and also with the reference strains, as summarized in Supplementary Table S2.

The predominant fatty acids of the three novel strains and the three reference strains were iso-$C_{15:0}$ in a range of 35.0–47.4%, $C_{16:1}$ ω5c 8.9%–22.9%, and summed feature 3 ($C_{16:1}$ ω7c/$C_{16:1}$ ω6c) 9.0%–19.5%. Interestingly, among the three novel isolates only the strain ABR2-5^T had additional higher components of fatty acids $C_{16:0}$ (13.0%), $C_{18:1}$ ω9c (6.4%) and $C_{18:0}$ (5.0%) as major fatty acids and the strain WSW4-B4^T had iso-$C_{15:1}$\u00B0F (9.7%). The minor fatty acids of all three novel isolates and the reference strains were $C_{14:0}$ (1.5%–2.7%), anteiso-$C_{15:0}$ (1.0%–4.2%), $C_{16:0}$ 3-OH (1.1%–3.0%), and iso-$C_{17:0}$ 3-OH (1.7%–3.5%). Although the fatty acids among all three novel strains and the three reference strains were similar, the uniqueness and differentiation of fatty acids among all six strains are found and presented in Supplementary Table S3. The menaquinone 7

TABLE 1 Differential physiological characteristics of three novel isolates: ABR2-5^T, BKB1-1^T, and WSW4-B4^T and three existing type strains in the genus *Reichenbachiella: R. agariperforans* KCTC 12369^T, *R. faecimaris* KCTC 82811^T, and *R. versicolor* KCTC 82854^T Strains: 1, ABR2-5^T; 2, BKB1-1^T; 3, WSW4-B^T; 4, *R. agariperforans* KCTC 12369^T; 5, *R. faecimaris* KCTC 82811^T; 6, *R. versicolor* KCTC 82854^T.

Characteristics	1	2	3	4	5	6
Cell shape	Long rod	Rod	Rod	Rod	Rod	Rod
Colony morphology	Orange, smooth, circular, convex	Orange, colonies sunken into the agar	Pale yellow, colonies sunken into the agar	Orange, colonies sunken into the agar	Beige circular with regular edges	Circular, convex, translucent, dark brown
Width and length of cells (μm)	3.3–4.7	1.8–2.8	3.5–3.6	5.0–15.0	3.0–5.0	4.0–25.5
	0.3–0.4	0.2–0.3	0.2–0.3	0.5–0.7	0.3–0.5	0.2–0.4
Gliding motility	+	+	+	+	+	+
Flexirubin-type pigment	+	+	–	+	–	–
NaCl range (optimal) (%)	0.5–7	0.0–5	0.5–5	1.0–6.0	1.0–5.0	0.5–7.0
	(0.5–5.0)	(0.5–4.0)	(0.5–4.0)	(2.0)	(3.0)	(2.0–3.0)
Range of temperature (optimal) (°C)	10–37	10–37	(10–30)	4–35	5.0–35	10–37
	(15–37)	(15–30)	(15–30)	(25–28)	(28–30)	–28
Range of pH (optimal)	5.5–9.5	5.5–9.5	5.5–9.0	5.5–10.0	5.5–8.5	6.0–8.5
	(6.0–9.0)	(6.5–8.5)	(6.5–8.5)			(7.0–7.5)
Oxygen requirement	Aerobic	Facultative anaerobic	Aerobic	Aerobic	Aerobic	Aerobic

All the data are from this study except for the reference strains *R. agariperforans* DSM 26134^T (Nedashkovskaya et al., 2005), *R. faecimaris* DSM 26133^T (Cha et al., 2011), and *R. versicolor* DC003^T (Shi et al., 2018), which were obtained from the literature.

(MK-7) was detected as respiratory quinone which was also found in the reference strains in the genus *Reichenbachiella*. The quinone patterns are often conserved within genera or families of microorganisms. Thus, provide an important information for microbial classification and identification. Furthermore, quinones are essential cofactor in electron transport chains and participate in aerobic respiration.

The polar lipid profiles of the three novel isolates were similar to those of the type strains of the three-existing species of the genus *Reichenbachiella*. The three novel strains and the reference strains contained phosphatidylethanolamine (PE). In addition to PE, the strain ABR2-5^T had one aminophospholipid, one unidentified glycolipid, and seven unidentified lipids. The strain BKB1-1^T had two unidentified glycolipids and five unidentified lipids, while the strain WSW4-B4^T contained two aminophospholipids, two unidentified aminolipids, and five unidentified lipids. Among the three novel isolates, only the strain WSW4-B4^T had both aminophospholipid and aminolipid, the strain ABR2-5^T had only aminophospholipid, and strain BKB1-1^T had neither aminophospholipid nor aminolipid (Supplementary Figure S1).

3.4 Genomic general features and phylogeny

The complete genomes of the strains ABR2-5^T, BKB1-1^T, and WSW4-B4^T were determined using the Nanopore platform (Oxford Nanopore Technology, ONT). A CheckM analysis of three genomes of the novel isolates showed that the completeness of the three genomes ranged from 98.2–98.6%. The genome of the strain ABR2-5^T had 12 contigs with a total genome size 5.5 Mbp, among which contig 1 was the largest contig (5.4 Mbp), while the remaining 11 were short unassembled sequences. The strains BKB1-1^T and WSW4-B4^T each had one circular chromosome with sizes of 4.4 and 5.0 Mbp, respectively. The G + C contents of the three novel strains ranged from 41.8% to 42.0%, matching those of other species in the genus *Reichenbachiella*, which range from 37.1% to 43.4%. The genome was annotated with NCBI's PGAP pipeline to annotate the total number of genes, CDS, rRNAs, and tRNAs, as summarized in Supplementary Table S4. The genomes of the strains ABR2-5^T, BKB1-1^T, and WSW4-B4^T are available in the NCBI with the GenBank accession numbers GCA_025833875, GCA_025502585, and GCA_025639805, respectively.

To further confirm the taxonomic position of the three novel isolates, average nucleotide identity (ANI) and digital DNA–DNA hybridization (dDDH) were calculated among the isolates and the type strains of the existing species in the genus *Reichenbachiella*. The ANI and the dDDH values among the three novel strains and the three existing species were in ranges of 69.2%–75.5% and 17.7%–23.2% (Supplementary Table S5), respectively, which were significantly lower than the cut-off values of 95%–96% for the ANI value (Yoon et al., 2017b) and 70% for the dDDH value (Auch et al., 2010). Interestingly, the ANI and dDDH values among the three novel isolates were also lower than the cut-off values of ANI and dDDH for species differentiation, supporting the contention that all three novel isolates could be considered novel species. The genome-based phylogenetic tree also shows the robust clustering of the novel isolates with the three existing species: *R. agariperforans* DSM 26134^T, *R. faecimaris* DSM 26133^T, and *R. versicolor* DC003^T (Figure 3).

3.5 Genome functional analysis

The whole genomes of the three novel strains and the three type strains of existing species were analyzed using various databases. First, the metabolic pathways were constructed using the BlastKOALA

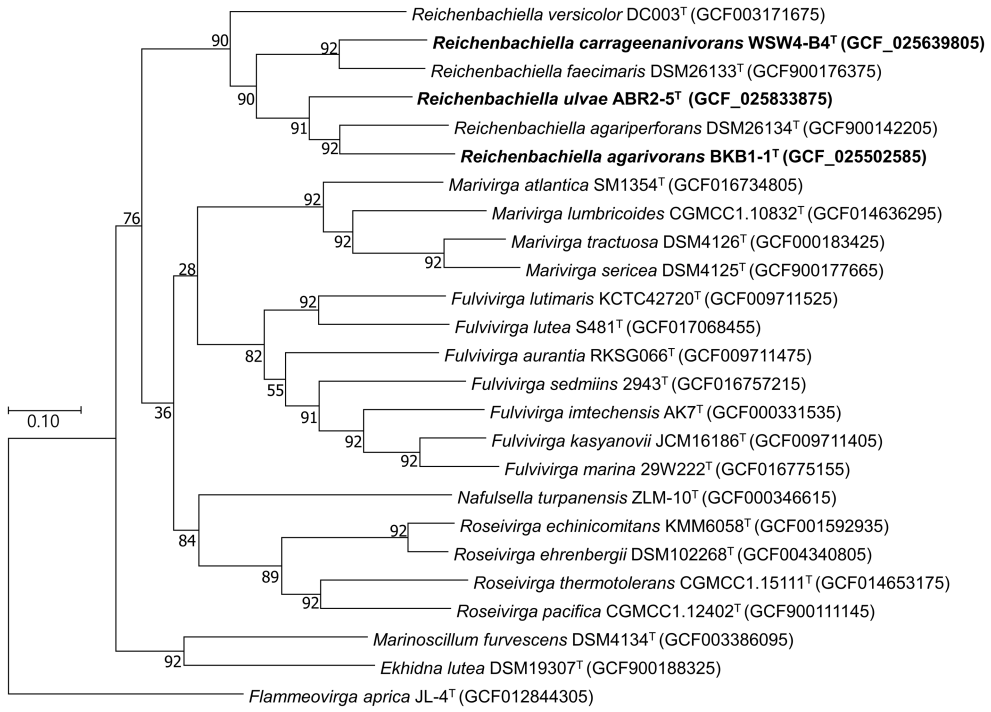

FIGURE 3
Maximum-likelihood phylogenetic tree exhibiting the relationships among the novel isolates ABR2-5^T, BKB1-1^T, WSW4-B4^T and closely related species, based on 92 core genes identified using the UBCG pipeline. GenBank accession numbers of the whole genome sequences are given in parentheses. *Flammeovirga aprica* JL-4^T (GCF012844305) was used as outgroups. Bootstrap values based on 1,000 replicates are indicated at the branch nodes. Bar, 0.1 substitutions per site.

server, which utilizes the Kyoto Encyclopedia of Genes and Genomes (KEGG) pathway database. Then, only the enriched functions were plotted in the heatmap (Figure 4). The KEGG annotation showed that the strain ABR2-5^T had 71 pathways, which was the highest among the isolates. In contrast, the strains BKB1-1^T and WSW4-B4^T had 64 and 62 pathways, respectively. The presence of the highest number of metabolic pathways in the strain ABR2-5^T can be attributed to its larger genome size and the highest number of genes (Supplementary Table S4). Figure 4 shows that the central metabolic pathways, which commonly include aerobic respiration, sugar metabolism, and amino acid synthesis, displayed similarities among these strains. All six strains contained genes that participate in the synthesis of essential amino acids of leucine, methionine, phenylalanine, tryptophan, and valine, while interestingly none of the strains could synthesize tyrosine. The synthesis of essential amino acids in bacteria is crucial for their growth, survival, and adaptation to diverse environments. The KEGG analysis further highlighted that the strains also harbor genes for enzymes such as amylase, chitinase, and epimerase.

The genomes of the three strains ABR2-5^T, BKB1-1^T, and WSW4-B4^T carried three genes of heavy metal transporters: *CorA, CopA*, and *FeoB*, which is associated with cobalt, copper, and iron transportation (Zhang et al., 2009; Lau et al., 2016; Li et al., 2022). All three strains carried a part of pathway for reduction of arsenic. Moreover, the strains ABR2-5^T and WSW4-B4^T possessed additional *MntH* transporter genes, which play a role in the transportation of manganese and iron (Porcheron et al., 2013). The presence of heavy metal transporter genes in the genomes of three novel *Reichenbachiella* strains may confer advantages in terms of heavy metal tolerances, including arsenic, cobalt, copper, and manganese (Altimira et al., 2012).

The KEGG pathways further showed that the strains of the genus *Reichenbachiella* carry certain pathways that are important for the nitrogen cycle of coastal ecosystems. All the strains carry a complete pathway of dissimilatory nitrate reduction to ammonium (DNRA). The DNRA pathway is used by microbes to convert nitrate into ammonium, which is helpful to conserve bioavailable nitrogen within the ecosystem (Liu et al., 2023). DNRA is observed in various ecosystems, encompassing agricultural soils, marine sediments, and wastewater. DNRA not only conserves nitrogen within these ecosystems but also decreases the release of toxic greenhouse gases, such as nitrous oxide (Liu et al., 2021). Furthermore, the stimulation of DNRA has often been proposed as a strategy to improve fertilizer efficiency. In addition to DNRA pathways, the strain ABR2-5^T had additional pathways for reducing nitrate and nitrous oxide, which further highlights its role in the nitrogen cycle (Suenaga et al., 2018; Figure 4).

In the RAST system, the distribution of functional genes among the novel isolates and the type strains of existing species was similar. In all six strains, the largest number of genes were allocated to the metabolism of amino acids and its derivatives (211–253) and carbohydrates (122–168), followed by protein metabolism (109–170). Interestingly, the strain ABR2-5^T carries significantly higher numbers of genes for the metabolism of protein (170), carbohydrates (168), phosphorous (26), and potassium (13), whose p values were less than 0.05. The strains ABR2-5^T and WSW4-B4^T have four and one gene for iron acquisition and metabolism, respectively, while the strain

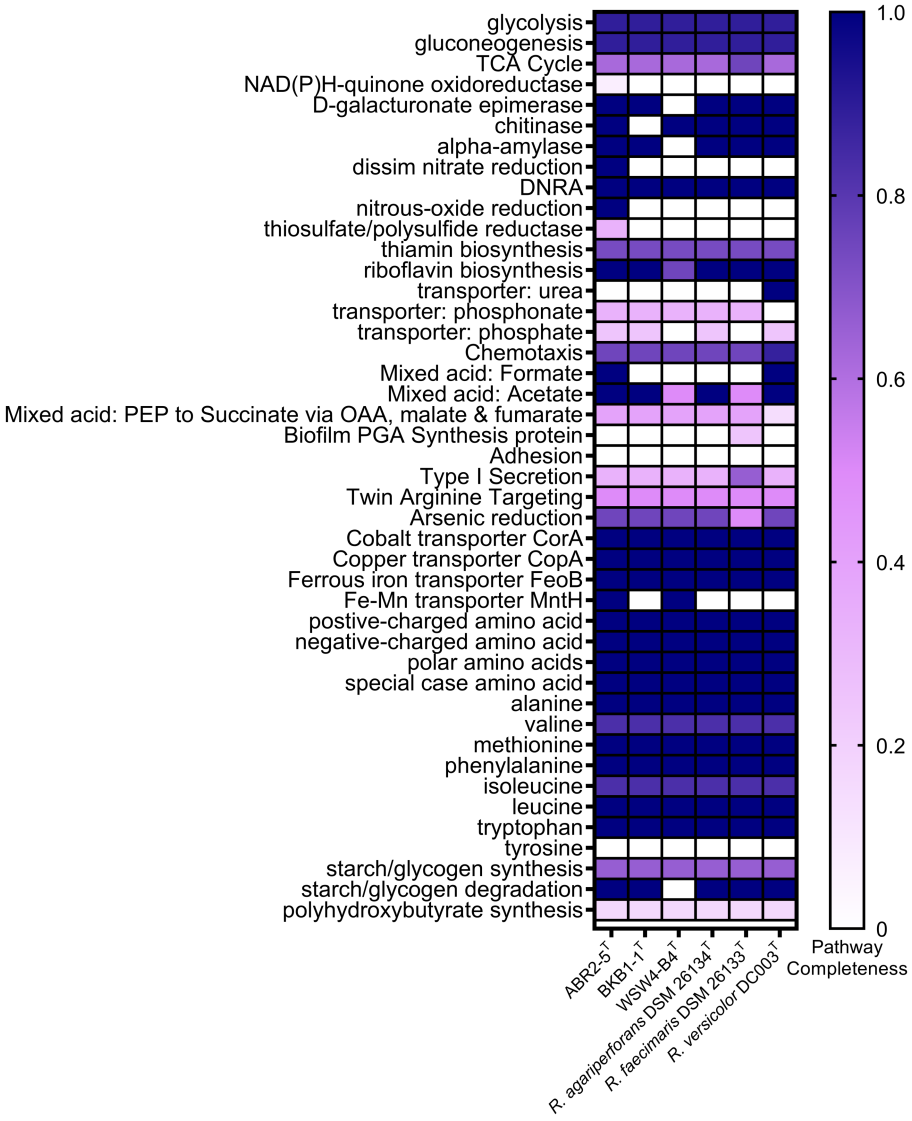

FIGURE 4
Heatmap of discriminated metabolic pathways within the genome of the three novel isolates and the reference strains in genus *Reichenbachiella*. The scale bar indicates that the intensity of color change reflects the completeness of pathways.

BKB1-1^T lacks genes for iron acquisition and metabolism. Among the three novel isolates, the strain WSW4-B4^T has the most genes (15 genes) for regulation and cell signaling (Supplementary Table S6).

The antiSMASH analysis showed that the strains ABR2-5^T, BKB1-1^T, and WSW4-B4^T carry seven, six, and four biosynthetic gene clusters (BGCs) in their genomes, respectively (Table 2). All the novel isolates and reference strains carry type III polyketide synthases and terpenes except *R. faecimaris* DSM 26133^T. The polyketide synthases constitute a group of multi-domain enzymes responsible for synthesizing polyketides, which are diverse group of secondary metabolites (Hochmuth and Piel, 2009), while terpenes are named for the number of five-carbon units that form their hydrocarbon skeleton that had significant biological activities (Helfrich et al., 2019). Among the three novel isolates, only the strains ABR2-5^T and BKB1-1^T have ectoine and arylpolyene type of BGCs, which may protect the bacterial strains under extreme conditions of salinity, drought, irradiation, pH, and temperature (Schöner et al., 2016; Bilstein et al., 2021).

3.6 CRISPR-Cas analysis

The CRISPR-Cas system consists of a CRISPR array and Cas cascade. The Cas cascade is a circuit of CRISPR-associated (Cas) enzymes (Brouns et al., 2008). The Cas cascade of all three isolated strains contains Cas9, Cas1, and Cas2 in order of upstream to downstream. According to the current guideline of CRISPR-Cas classification, all the isolated strains contain the class 2 type II subtype C1 CRISPR-Cas system (Makarova et al., 2020). The Cas1 and Cas2 of all three isolated strains were similar. According to the UniProt database it shows highest similarity to *Reichenbachiella* sp. 5 M10, which was isolated from Japan's West Sea. It can be inferred that Cas1 and Cas2 are conserved in the genus *Reichenbachiella*.

Meanwhile, the Cas9 of each isolate was varied. According to the UniProt database the highest similarity of ABR2-5^T was with *Aquaticitalea lipolytica* (the class *Flavobacteriia*; Supplementary Table S7); BKB1-1^T showed highest similarity with *Acidiluteibacter ferrifornacis* (the class

TABLE 2 Biosynthetic gene clusters for secondary metabolites identified by antiSMASH of three isolates and three existing type strains in genus *Reichenbachiella*.

Strain	Metabolites	From (nt)	To (nt)	Most similar known cluster	Similarity (%)
1	Terpene	554,222	575,058	Carotenoid and Terpene	28
	Arylpolyene	2,734,426	2,780,398	Flexirubin and polyketide	22
	Phosphonate	2,808,331	2,841,707	Polysaccharide B and Saccharide	6
	Ectoine	3,977,552	3,987,941	Ectoine and Other	50
	Type III PKS	4,310,043	4,351,131	o and K-antigen, Saccharide	4
	Type I PKS	5,338,720	5,385,913		
	Resorcinol	5,934,952	5,481,028	Flexirubin and polyketide	13
2	Arylpolyene & Resorcinol	206,645	251,834	Flexirubin and Polyketide	16
	RRE-containing domain	375,672	396,118		
	Ectoine	1,240,170	1,250,568	Ectoine and Other	50
	Type III PKS	1,582,227	1,623,315		
	Type I PKS	2,141,220	2,188,521		
	Arylpolyene	2,474,320	2,520,790	Flexirubin and Polyketide	25
	Terpene	4,207,889	4,228,725	Carotenoid and Terpene	28
3	Type III PKS	903,303	944,394		
	RRE-containing domain	1,686,875	1,707,312		
	Terpene	3,200,818	3,221,654	Carotenoid and Terpene	28
	Phosphonate	3,757,063	3,771,651	Polysaccharide B and Saccharide	6
4	Arylpolyene & Resorcinol	1	32,142	Flexirubin and Polyketide	16
	Terpene	619,422	640,258	Carotenoid and Terpene	28
	Ectoine	684,849	695,250	Ectoine and Other	50
	Arylpolyene	95,289	141,558	Flexirubin and Other	44
	Type III PKS	242,032	283,120		
	Type I PKS	94,015	141,178		
5	Phosphonate	53,093	67,561	Polysaccharide B and Saccharide	6
	Type III PKS	1,011,891	1,052,988		
	Arylpolyene	589,135	625,381	Flexirubin and Polyketide	22
6	Other	839,401	880,930		
	Terpene	924,027	944,866	Carotenoid and Terpene	28
	NRPS-independent-siderophore	16,275	31,047	Bisucaberin	83
	NRPS-like	414,939	459,927		
	Terpene	224,736	245,515		

Nucleotide positions with each genome are presented. Strains: 1, ABR2-5^T; 2, BKB1-1^T; 3, WSW4-B4^T; 4, *R. agariperforans* DSM 26134^T; 5, *R. faecimaris* DSM 26133^T; 6, *R. versicolor* DC003^T
NRPS, Nonribosomal Peptide Synthetase; PKS, Polyketide Synthases; RRE, RiPP (Ribosomally Synthesized and Post-Translationally Modified Peptides) Recognition Element.
*From, indicates the gene's initiation position of biosynthetic gene cluster (BGC). **To, indicates the gene's termination positions of biosynthetic gene cluster (BGC).

Flavobacteriia; Supplementary Table S8); and WSW4-B4^T showed highest similarity with *Reichenbachiella* sp. 5M10 (the class *Cytophagia*; Supplementary Table S9).

3.7 Polysaccharide degradation

3.7.1 Prediction of CAZyme gene clusters and carbohydrate-active enzymes using dbCAN meta server

CAZyme gene cluster (CGC) is a genomic region that consists of carbohydrate-active enzymes (CAZymes), transporter, signal transduction, and transcription factor genes (Ameri et al., 2022). The CGCs within the genomes of the strains were identified using the CGC finder tool in the dbCAN meta server. The CGC finder tool detected a total of 67 CGCs in the genome of the strain ABR2-5^T, while 49 and 66 CGCs were detected in the genomes of the strains BKB1-1^T and WSW4-B4^T, respectively. Next to CGCs detection, the number of CAZymes was predicted in all three isolates and reference strains of the genus *Reichenbachiella*. The genome of the strain ABR2-5^T contains 216 CAZymes, which is a higher number than other strains in the genus *Reichenbachiella*. The 216 CAZymes consist of 146 glycoside hydrolases (GHs), 13 polysaccharide lyases (PLs), 16 carbohydrate esterases (CEs), 25 glycosyltransferases (GTs), and 16 carbohydrate-binding modules

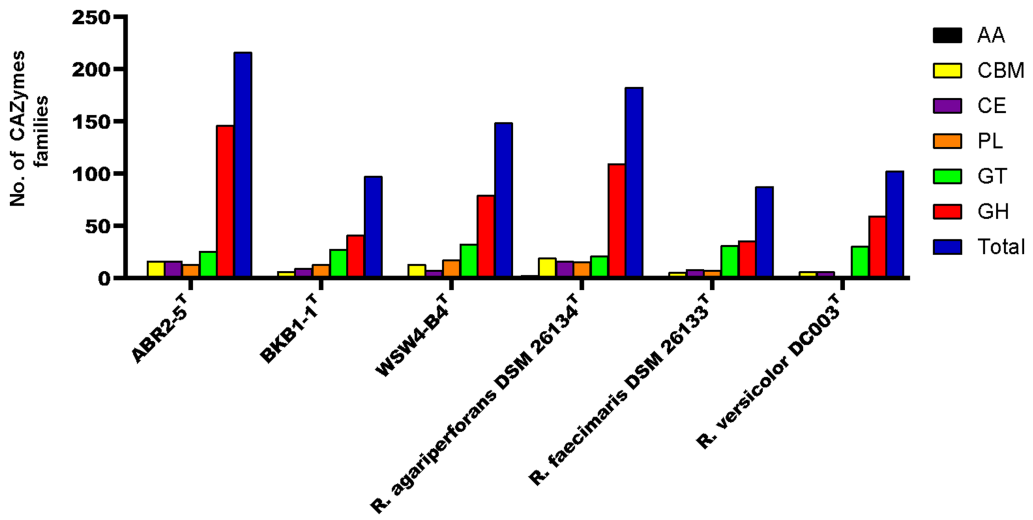

FIGURE 5
The carbohydrate-active enzyme (from dbCAN2 meta server) compositions of three novel isolates and reference strains in genus *Reichenbachiella*.

(CBM). The genomes of the strains BKB1-1^T and WSW4-B4^T contain 97 and 148 CAZymes that are distributed to 41 GHs, 13 Pls, 9 CEs, 27 GTs, and 3 CBMs in the strain BKB1-1^T and 109 GHs, 15 PLs, 7 CEs, 21 GTs, and 13 CBMs in the strain WSW4-B4^T. The distribution of CAZymes in the novel and the reference type strains is presented in Figure 5. The percentage of CAZyme genes out of the total genes and the ratio of glycoside hydrolases (GHs) per Mbp genome were calculated. Among the three isolates, the strain ABR2-5^T carries a higher amount (4.68%) of CAZymes, while the strains BKB1-1^T and WSW4-B4^T carry 2.61% and 3.84% CAZymes in their genomes, respectively. The strain ABR2-5^T carries 26.55 GHs per Mbp in the genome, while the strains BKB1-1^T and WSW4-B4^T carry 9.32 and 15.80 GHs per Mbp in the genome (Supplementary Table S10). The number of CAZymes in the stain ABR2-5^T was significantly higher than that of the other strains in the phylum *Bacteroidota*, such as *Formosa agariphila* KMM 3901^T, totaling 193 CAZymes (Mann et al., 2013), and *Cellulophaga algicola* IC166^T, totaling 101 CAZymes (Abt et al., 2011), while being closest to *Zobellia* sp. (257–315 CAZymes), which is a known polysaccharide degrader (Thomas et al., 2017; Chernysheva et al., 2019).

3.7.2 Prediction of polysaccharide utilization loci using dbCAN-PUL server and PULDB

PULs refer to the cluster of genes consisting of CAZymes and other genes that participate in the digestion and utilization of complex polysaccharides. The prediction of PUL regions in the genome was confirmed by a BLASTX search against the dbCAN-PUL database, which contains experimentally verified PULs from 173 bacterial species of 10 different bacterial phyla (Ausland et al., 2021). By using a BLASTX search, the genomes of isolates for those with PULs % sequence identity values ranging from 18 to 91% were detected. Among the predicted PULs, only those PULs that had % sequence identity values greater than 74% were selected for further analysis (Wu et al., 2021). The analysis showed that strains WSW4-B4^T and BKB1-1^T have nine and seven PULs, respectively, whose similarity values were above 74%, while the remaining strains in the genus *Reichenbachiella* have PULs whose value of identity was less than 74%.

Interestingly, both the strains BKB1-1^T and WSW4-B4^T could degrade agar and alginate (see below section 3.8.3) and harbor 3–4 PULs (PUL0316, PUL0460) for the degradation of agar and 1–3 PULs (PUL0151, PUL0235, PUL0313) for the degradation of alginate, respectively.[16] The strain WSW4-B4^T additionally degraded κ-carrageenan and carries PUL (PUL0148), which may be involved in the degradation of κ-carrageenan (Gobet et al., 2018). All three novel isolates could degrade laminarin, but only the strains BKB1-1^T and WSW4-B4^T have PULs (PUL0005, PUL0314) that may participate in the degradation of laminarin (Thomas et al., 2017; Table 3).

PULs were also identified by the presence of iconic functional genes such as *susC* and *susD* in the vicinity of CAZymes. For the strains ABR2-5^T and BKB1-1^T, we used the Prokka server to search PULs. The analysis revealed the presence of *susC* and *susD* upstream of one GH13 in the genome of strain ABR2-5^T. However, *susC* and *susD* were not detected in the proximity of the other GH16. It is possible that laminarin degradation occurred through the action of GH16, utilizing *susC* and *susD* from other PULs via cross-utilization of transport systems. In case of strain BKB1-2^T, multiple instances of *susC* and *susD* were detected within its genome. However, these transport genes were not organized in a circuitry, indicating that the transport gene were not found next to each other in the same direction.

To detect PULs based on functional genes (*susC* and *susD*) in the strain WSW4-B4^T, we used the PULDB database. The analysis revealed the presence of *sucC* and *susD* in the vicinity of CAZymes. Specifically, *sucC* and *susD* were detected in the proximity of GH50, GH16, GH110, and PL6, enabling the strain to degrade agarose, laminarin, κ-carrageenan, λ-carrageenan, and alginate, respectively.

3.7.3 *In vitro* polysaccharide degradation

The degradation of polysaccharides of agar, cellulose, chitin, κ-carrageenan, λ-carrageenan, ι-carrageenan, laminarin, sodium

16 https://bcb.unl.edu/dbCAN_PUL/Repository

10.3389/fmicb.2023.1265676

TABLE 3 Number of polysaccharide-degrading genes based on dbCAN meta server and dbCAN-PUL, and *in vitro* activities of three novel strains of genus *Reichenbachiella* Strains: 1, ABR2-5^T; 2, BKB1-1^T; 3, WSW4-B4^T.

Strain	Polysaccharides	CAZyme families*	PUL**	*In vitro* degradation
1	Agarose	GH50 (0)		–
	Alginate	PL6 (0), PL7 (0)		–
	Cellulose	GH5 (9), GH9 (1)		–
	Chitin	GH18 (2) GH20 (3)		–
	k-Carrageenan	GH16 (2)		–
	λ-Carrageenan	GH110 (5)		–
	ι-Carrageenans	GH82 (0)		–
	Laminarin	GH16 (2),		+
	Starch	GH13 (3) GH57 (0)		+
	Xylan	GH3 (16)		–
2	Agarose	GH50 (2), GH86 (1)	PUL0316 (2), PUL0460 (1)	+
	Alginate	PL6 (1), PL7 (3),	PUL0151 (1)	+
	Cellulose	GH5 (0), GH9 (0)		–
	Chitin	GH20 (1)		–
	k-Carrageenan	GH16 (4)		–
	λ-Carrageenan	GH110 (0)		–
	ι-Carrageenans	GH82 (0)		–
	Laminarin	GH16 (4),	PUL0314 (1)	+
	Starch	GH13 (1) GH57 (0)		+
	Xylan	GH3 (3)		+
3	Agarose	GH50 (2), GH86 (2)	PUL0316 (3), PUL0460 (1)	+
	Alginate	PL6 (3), PL7 (3),	PUL0151 (1), PUL0235(1), PUL0313 (1)	+
	Cellulose	GH5 (0), GH9 (0)		–
	Chitin	GH18 (2) GH20 (2)		–
	k-Carrageenan	GH16 (6)	PUL0148 (1)	+
	λ-Carrageenan	GH110 (5)		+
	ι-Carrageenans	GH82 (0)		–
	Laminarin	GH16 (6),	PUL0005 (1)	+
	Starch	GH13 (0) GH57 (1)		–
	Xylan	GH3 (5)		–

*CAZyme families with the number of genes in parentheses that are expected to participate in degradation of polysaccharides. **PULs (polysaccharide utilization loci) with the number of PULs in parentheses that are expected to participate in degradation of polysaccharides.

alginate, starch, and xylan was tested both in solid and liquid media. First, degradation of the test polysaccharides was evaluated on solid media by detecting a clear zone around the colonies and by liquefaction of the solid media. Among the three novel isolates, the strain WSW4-B4^T could degrade agar, sodium alginate, laminarin, κ-carrageenan and, λ-carrageenan; the strain BKB1-1^T could degrade agar, starch, sodium alginate, and laminarin while the strain ABR2-5^T degraded only laminarin and starch (Table 3). The enzyme assay for the degradation of cellulose, chitin, κ-carrageenan, λ-carrageenan, ι-carrageenan, laminarin, sodium alginate, starch, and xylan were performed by detecting reducing sugars in the culture broth by a 3, 5-dinitrosalicylic acid assay. The assay was conducted over three time points of cultivation: at the start (day 0), after 3 days, and after 7 days. The changes in optical density were measured using a microplate reader. The increase of optical density indicated the presence of reducing sugars. The results showed that the strain WSW4-B4^T degraded sodium alginate, laminarin, κ-carrageenan, and λ-carrageenan. The strain BKB1-1^T produced reducing sugars from the degradation of sodium alginate, laminarin, and starch, while the strain ABR2-5^T produced reducing sugars only from the degradation of laminarin and starch.

The *in vitro* degradation of each test polysaccharide was supported by the *in silico* detection of CAZymes and PULs in the genomes of all three novel isolates. First, the degradation of starch and laminarin was supported by the presence of a high abundance of GH13, which is primarily responsible for α-amylase (Janeček et al., 2014) and GH57 and GH13 for laminarin (Cantarel et al., 2009). The strains BKB1-1^T and WSW4-B4^T could degrade sodium alginate. Interestingly, in the genome of the strain BKB1-1^T there were one PL6 and three PL7, while WSW4-B4^T had three PL6 and three PL7, which may have role in the breakdown of alginate (Li Q. et al., 2021). Furthermore, strains BKB1-1^T and

WSW4-B4^T carry one GH16, GH50, and GH86, which may participate in the degradation of agar (Gao et al., 2017). Among all the novel isolates, strain WSW4-B4^T was able to degrade κ-carrageenan and λ-carrageenan. Interestingly, in the genome of strain WSW4-B4 ^{T}, we found six GH16 and five GH110 genes, which indicate the strain's capability for the degradation of κ-carrageenan and λ-carrageenan, respectively (Gao et al., 2017; McGuire et al., 2020). The details of each test polysaccharide, the CAZyme families, the numbers of PULs, and *in vitro* test activities are summarized in Table 3.

The three novel strains possessed the ability to degrade various complex polysaccharides such as agar, alginate, carrageenan, laminarin, and starch. Genome analysis further highlighted that all three novel strains carry a high number of CAZymes for the degradation of complex polysaccharides. The degradation of these complex polysaccharides can produce oligosaccharides with practical applications in biomedicine, cosmetics and food industry (Jutur et al., 2016). For example, alginate and laminarin oligosaccharides exhibit various biological activities, including antioxidant, antitumor, and immunomodulatory effects (Zargarzadeh et al., 2020). Our study isolated and characterized three new *Reichenbachiella* strains which harbor various carbohydrate active enzymes that can be utilized for the production of biologically active oligosaccharides.

In conclusion, during a study on the microbial diversity of the West Sea, Korea, three novel stains were isolated from algae and sea mud samples. Through a polyphasic approach, the three strains were determined to be affiliated with the genus *Reichenbachiella* of the phylum *Bacteroidota*. The presence of a high number of CAZymes in the genomes of these strains, which enable the degradation of complex polysaccharides, suggests that they have the potential to serve as effective polysaccharide degraders. Furthermore, the strains carry certain genes involved in the synthesis of essential amino acids and vitamins, secondary metabolites, and also carry important pathways for heavy metal metabolism and for the nitrogen cycle.

3.8 Description of *Reichenbachiella ulvae* sp. nov.

Reichenbachiella ulvae (ul'vae. L. gen. n. *ulvae*, of the seaweed genus *Ulva*)

Cells are Gram-strain-negative, rod-shaped, strictly aerobic, and oxidase-and catalase-positive. The colonies of MA are circular, smooth, and orange in color. The strain grows at temperature 10–37°C (optimum, 30°C), at pH 5.5–9.5 (optimum, pH 7.0), and with 0.5–7% NaCl (optimum, 2%). Positive for the degradation of laminarin and starch. Positive for fexirubin-type pigment. The predominant fatty acid components are iso-$C_{15:0}$, $C_{16:1}$ ω5c, and $C_{16:0}$.

The type strain, ABR2-5^T (=KCTC 82990^T = JCM 35839^T), was isolated from the green alga *Ulva* sp. For the type stain the G + C content is 42.0%.

3.9 Description of *Reichenbachiella agarivorans* sp. nov.

Reichenbachiella agarivorans (a.ga.ri.vo'rans. N.L. neut. n. *agarum*, agar; L. pres. part. *vorans*, devouring; N.L. part. Adj. *agarivorans*, agar-devouring)

Cells are Gram-strain-negative, rod-shaped, facultative anaerobe, and oxidase and catalase positive. The colonies are orange in color and sunken into on MA. The strain grows at temperature 10–37°C (optimum, 30°C), at pH 5.5–9.5 (optimum, pH 7.0), and with 0.5–5% NaCl (optimum, 2%). Positive for the degradation of agar, alginate, laminarin, and starch. Positive for fexirubin-type pigment. The predominant fatty acid components are iso-$C_{15:0}$, $C_{16:1}$ ω5c, and summed feature 3 ($C_{16:1}$ ω7c/$C_{16:1}$ ω6c).

The type strain, BKB1-1^T (=KCTC 82964^T = JCM 35840^T), was isolated from sea mud. For the type stain the G + C content is 42.1%.

3.10 Description of *Reichenbachiella carrageenanivorans* sp. nov.

Reichenbachiella carrageenanivorans (car.ra.gee.na.ni.vo'rans. N.L. neut. n. *carrageenanum*, carrageenan; L. v. *voro*, to devour; N.L. part. Adj. *carrageenanivorans*, carrageenan-devouring)

Cells are Gram-strain-negative, rod-shaped, strictly aerobe, and oxidase and catalase positive. The colonies are pale-yellow and sunken into the agar. The strain grows at temperature 10°C–30°C (optimum, 30°C), at pH 5.5–9.0 (optimum, pH 7.0), and with 0.5%–5% NaCl (optimum, 2%). Positive for the degradation of agar, alginate, κ-carrageenan, λ-carrageenan, and laminarin. Negative for fexirubin-type pigments production. The predominant fatty acid components are iso-$C_{15:0}$, summed feature 3 ($C_{16:1}$ ω7c/$C_{16:1}$ ω6c), $C_{16:1}$ ω5c, and iso-$C_{16:0}$\u00B0F. The type strain, WSW4-B4^T (=KCTC 82706^T = JCM 35841^T), was isolated from the red algae *Chondrus* sp. For the type stain the G + C content is 41.8%.

Data availability statement

The original contributions presented in the study are included in the article/Supplementary material, further inquiries can be directed to the corresponding author.

Author contributions

NM: Conceptualization, Investigation, Methodology, Writing – original draft, Writing – review & editing. FA: Formal Analysis, Investigation, Visualization, Writing – original draft. ON: Formal Analysis, Validation, Writing – review & editing. S-GK: Conceptualization, Funding acquisition, Methodology, Project administration, Supervision, Writing – review & editing.

Funding

The author(s) declare financial support was received for the research, authorship, and/or publication of this article. The Korea Research Institute of Bioscience and Biotechnology (KRIBB) Research Initiative Program (KGM5232322) and a National Research Foundation of Korea (NRF) grant funded by the Korean government (MSIT; no. NRF-2021M3H9A1030164) supported this research.

Acknowledgments

The authors thank Aharon Oren from the Hebrew University of Jerusalem for his help with the nomenclature of the novel strain. The sampling of the bacterial strains was made possible by the support and collaboration of the National Science Museum of Korea through the Joint Academic Survey of the Federation of National Biodiversity Organizations in 2021.

Conflict of interest

The authors declare that the research was conducted in the absence of any commercial or financial relationships that could be construed as a potential conflict of interest.

Publisher's note

All claims expressed in this article are solely those of the authors and do not necessarily represent those of their affiliated organizations, or those of the publisher, the editors and the reviewers. Any product that may be evaluated in this article, or claim that may be made by its manufacturer, is not guaranteed or endorsed by the publisher.

Supplementary material

The Supplementary material for this article can be found online at: https://www.frontiersin.org/articles/10.3389/fmicb.2023.1265676/full#supplementary-material

References

Abt, B., Lu, M., Misra, M., Han, C., Nolan, M., Lucas, S., et al. (2011). Complete genome sequence of *Cellulophaga algicola* type strain (IC166^T). *Stand Genomic Sci.* 4, 72–80. doi: 10.4056/sigs.1543845

Altimira, F., Yanez, C., Bravo, G., Gonzalez, M., Rojas, L. A., and Seeger, M. (2012). Characterization of copper-resistant bacteria and bacterial communities from copper-polluted agricultural soils of Central Chile. *BMC Microbiol.* 12:193. doi: 10.1186/1471-2180-12-193

Ameri, R., García, J. L., Derenfed, A. B., Pradel, N., Neifar, S., Mhiri, S., et al. (2022). Genome sequence and carbohydrate active enzymes (CAZymes) repertoire of the thermophilic Caldicoprobacter algeriensis TH7C1^T. *Microb. Cell Fact.* 21:91. doi: 10.1186/s12934-022-01818-0

Auch, A. F., von Jan, M., Klenk, H. P., and Göker, M. (2010). Digital DNA-DNA hybridization for microbial species delineation by means of genome-to-genome sequence comparison. *Stand Genomic Sci.* 2, 117–134. doi: 10.4056/sigs.531120

Ausland, C., Zheng, J., Yi, H., Yang, B., Li, T., Feng, X., et al. (2021). dbCAN-PUL: a database of experimentally characterized CAZyme gene clusters and their substrates. *Nucleic Acids Res.* 49, D523–D528. doi: 10.1093/nar/gkaa742

Aziz, R. K., Bartels, D., Best, A. A., DeJongh, M., Disz, T., Edwards, R. A., et al. (2008). The RAST server: rapid annotations using subsystems technology. *BMC Genomics* 9:75. doi: 10.1186/1471-2164-9-75

Bae, S. S., Jung, Y. H., and Baek, K. (2020). Shewanella maritima sp. nov., a facultative anaerobic marine bacterium isolated from seawater, and emended description of Shewanella intestini. *Int. J. Syst. Evol. Microbiol.* 70, 1288–1293. doi: 10.1099/ijsem.0.003916

Bäumgen, M., Dutschei, T., and Bornscheuer, U. T. (2021). Marine polysaccharides: occurrence, enzymatic degradation and utilization. *Chembiochem* 22, 2247–2256. doi: 10.1002/cbic.202100078

Bhuyan, P. P., Nayak, R., Patra, S., Abdulabbas, H. S., Jena, M., and Pradhan, B. (2023). Seaweed-derived sulfated polysaccharides; the new age chemopreventives: a comprehensive review. *Cancer* 15:715. doi: 10.3390/cancers15030715

Bilstein, A., Heinrich, A., Rybachuk, A., and Mösges, R. (2021). Ectoine in the treatment of irritations and inflammations of the eye surface. *Biomed. Res. Int.* 2021:8885032. doi: 10.1155/2021/8885032

Blin, K., Shaw, S., Steinke, K., Villebro, R., Ziemert, N., Lee, S. Y., et al. (2019). antiSMASH 5.0: updates to the secondary metabolite genome mining pipeline. *Nucleic Acids Res.* 47, W81–W87. doi: 10.1093/nar/gkz310

Brouns, S. J. J., Jore, M. M., Lundgren, M., Westra, E. R., Slijkhuis, R. J. H., Snijders, A. P. L., et al. (2008). Small CRISPR RNAs guide antiviral defense in prokaryotes. *Science* 321, 960–964. doi: 10.1126/science.1159689

Brunet, M., Le Duff, N., Barbeyron, T., and Thomas, F. (2022). Consuming fresh macroalgae induces specific catabolic pathways, stress reactions and type IX secretion in marine flavobacterial pioneer degraders. *ISME J.* 16, 2027–2039. doi: 10.1038/s41396-022-01251-6

Cantarel, B. L., Coutinho, P. M., Rancurel, C., Bernard, T., Lombard, V., and Henrissat, B. (2009). The carbohydrate-active enzymes database (CAZy): an expert resource for glycogenomics. *Nucleic Acids Res.* 37, D233–D238. doi: 10.1093/nar/gkn663

Cha, I. T., Oh, Y. S., Park, S. J., Park, B. J., Lee, J. K., Lim, C. S., et al. (2011). *Reichenbachiella faecimaris* sp. nov., isolated from a tidal flat, and emended descriptions of the genus Reichenbachiella and *Reichenbachiella agariperforans*. *Int. J. Syst. Evol. Microbiol.* 61, 1994–1999. doi: 10.1099/ijs.0.026849-0

Chernysheva, N., Bystritskaya, E., Stenkova, A., Golovkin, I., Nedashkovskaya, O., and Isaeva, M. (2019). Comparative genomics and CAZyme genome repertoires of marine *Zobellia amurskyensis* KMM 3526^T and *Zobellia laminariae* KMM 3676^T. *Mar. Drugs* 17:661. doi: 10.3390/md17120661

Couvin, D., Bernheim, A., Toffano-Nioche, C., Touchon, M., Michalik, J., Néron, B., et al. (2018). CRISPRCasFinder, an update of CRISRFinder, includes a portable version, enhanced performance and integrates search for Cas proteins. *Nucleic Acids Res.* 46, W246–W251. doi: 10.1093/nar/gky425

de Jesus Raposo, M. F., de Morais, A. M., and de Morais, R. M. (2015). Marine polysaccharides from algae with potential biomedical applications. *Mar. Drugs* 13, 2967–3028. doi: 10.3390/md13052967

Deng, C., Zhao, M., Zhao, Q., and Zhao, L. (2023). Advances in green bioproduction of marine and glycosaminoglycan oligosaccharides. *Carbohydr. Polym.* 300:120254. doi: 10.1016/j.carbpol.2022.120254

Deshavath, N. N., Mukherjee, G., Goud, V. V., Veeranki, V. D., and Sastri, C. V. (2020). Pitfalls in the 3, 5-dinitrosalicylic acid (DNS) assay for the reducing sugars: interference of furfural and 5-hydroxymethylfurfural. *Int. J. Biol. Macromol.* 156, 180–185. doi: 10.1016/j.ijbiomac.2020.04.045

Ehrlich, H., Shaala, L. A., Youssef, D. T. A., Żółtowska-Aksamitowska, S., Tsurkan, M., Galli, R., et al. (2018). Discovery of chitin in skeletons of non-verongiid Red Sea demosponges. *PloS One* 13:e0195803. doi: 10.1371/journal.pone.0195803

Falkowski, P. G., Fenchel, T., and Delong, E. F. (2008). The microbial engines that drive earth's biogeochemical cycles. *Science* 320, 1034–1039. doi: 10.1126/science.1153213

Felsenstein, J. (1981). Evolutionary trees from DNA sequences: a maximum likelihood approach. *J. Mol. Evol.* 17, 368–376. doi: 10.1007/bf01734359

Fitch, W. M. (1971). Toward defining the course of evolution: minimum change for a specific tree topology. *Syst. Zool.* 20, 406–416. doi: 10.2307/2412116

Gao, B., Jin, M., Li, L., Qu, W., and Zeng, R. (2017). Genome sequencing reveals the complex polysaccharide-degrading ability of novel deep-sea bacterium *Flammeovirga pacifica* WPAGA1. *Front. Microbiol.* 8:600. doi: 10.3389/fmicb.2017.00600

García-López, M., Meier-Kolthoff, J. P., Tindall, B. J., Gronow, S., Woyke, T., Kyrpides, N. C., et al. (2019). Analysis of 1,000 type-strain genomes improves taxonomic classification of Bacteroidetes. *Front. Microbiol.* 10:2083. doi: 10.3389/fmicb.2019.02083

Gobet, A., Barbeyron, T., Matard-Mann, M., Magdelenat, G., Vallenet, D., Duchaud, E., et al. (2018). Evolutionary evidence of algal polysaccharide degradation acquisition by *Pseudoalteromonas carrageenovora* 9^T to adapt to macroalgal niches. *Front. Microbiol.* 9:2740. doi: 10.3389/fmicb.2018.02740

Graham, E. D., Heidelberg, J. F., and Tully, B. J. (2018). Potential for primary productivity in a globally-distributed bacterial phototroph. *ISME J.* 12, 1861–1866. doi: 10.1038/s41396-018-0091-3

Hehemann, J. H., Correc, G., Thomas, F., Bernard, T., Barbeyron, T., Jam, M., et al. (2012). Biochemical and structural characterization of the complex agarolytic enzyme system from the marine bacterium *Zobellia galactanivorans*. *J. Biol. Chem.* 287, 30571–30584. doi: 10.1074/jbc.M112.377184

Helbert, W. (2017). Marine polysaccharide sulfatases. *Front. Mar. Sci.* 4:6. doi: 10.3389/fmars.2017.00006

Helfrich, E. J. N., Lin, G. M., Voigt, C. A., and Clardy, J. (2019). Bacterial terpene biosynthesis: challenges and opportunities for pathway engineering. *Beilstein J. Org. Chem.* 15, 2889–2906. doi: 10.3762/bjoc.15.283

Hiraishi, A. (1999). Isoprenoid quinones as biomarkers of microbial populations in the environment. *J. Biosci. Bioeng.* 88, 449–460. doi: 10.1016/s1389-1723(00)87658-6

Hochmuth, T., and Piel, J. (2009). Polyketide synthases of bacterial symbionts in sponges--evolution-based applications in natural products research. *Phytochemistry* 70, 1841–1849. doi: 10.1016/j.phytochem.2009.04.010

Janeček, Š., Svensson, B., and MacGregor, E. A. (2014). α-Amylase: an enzyme specificity found in various families of glycoside hydrolases. *Cell. Mol. Life Sci.* 71, 1149–1170. doi: 10.1007/s00018-013-1388-z

Jeffries, C. D., Holtman, D. F., and Guse, D. G. (1957). Rapid method for determining the activity of microorganisms on nucleic acids. *J. Bacteriol.* 73, 590–591. doi: 10.1128/jb.73.4.590-591.1957

Jeon, D., Jiang, L., Peng, Y., Seo, J., Li, Z., Park, S. H., et al. (2022). Sphingomonas cannabina sp. nov., isolated from *Cannabis sativa* L. 'Cheungsam'. *Int. J. Syst. Evol. Microbiol.* 72:5566. doi: 10.1099/ijsem.0.005566

Jeong, Y. S., Kang, W., Sung, H., Lee, J. Y., Yun, J. H., Shin, N. R., et al. (2020). Flammeovirga pectinis sp. nov., isolated from the gut of the Korean scallop, Patinopecten yessoensis. *Int. J. Syst. Evol. Microbiol.* 70, 499–504. doi: 10.1099/ijsem.0.003783

Jutur, P., Nesamma, A. A., Shaikh, M. K., et al. (2016). Algae-derived marine oligosaccharides and their biological applications. *Front. Mar. Sci.* 3:83. doi: 10.3389/fmars.2016.00083

Kim, S. G., Bae, H. S., and Lee, S. T. (2001). A novel denitrifying bacterial isolate that degrades trimethylamine both aerobically and anaerobically via two different pathways. *Arch. Microbiol.* 176, 271–277. doi: 10.1007/s002030100319

Kolmogorov, M., Yuan, J., Lin, Y., and Pevzner, P. A. (2019). Assembly of long, error-prone reads using repeat graphs. *Nat. Biotechnol.* 37, 540–546. doi: 10.1038/s41587-019-0072-8

Komagata, K., and Suzuki, K.-I. (1988). Lipid and cell-wall analysis in bacterial systematics. *Methods Microbiol.* 19, 161–207. doi: 10.1016/S0580-9517(08)70410-0

Kumar, S., Stecher, G., Li, M., Knyaz, C., and Tamura, K. (2018). MEGA X: molecular evolutionary genetics analysis across computing platforms. *Mol. Biol. Evol.* 35, 1547–1549. doi: 10.1093/molbev/msy096

Lau, C. K., Krewulak, K. D., and Vogel, H. J. (2016). Bacterial ferrous iron transport: the Feo system. *FEMS Microbiol. Rev.* 40, 273–298. doi: 10.1093/femsre/fuv049

Li, W., O'Neill, K. R., Haft, D. H., DiCuccio, M., Chetvernin, V., Badretdin, A., et al. (2021). RefSeq: expanding the prokaryotic genome annotation pipeline reach with protein family model curation. *Nucleic Acids Res.* 49, D1020–D1028. doi: 10.1093/nar/gkaa1105

Li, W., Wang, L., Li, X., Zheng, X., Cohen, M. F., and Liu, Y. X. (2022). Sequence-based functional metagenomics revals noel natural diversity of functioning CopA in environmental microbiomes. *Genomics Proteomics Bioinformatics*. 22, 101–112. doi: 10.1016/j.gpb.2022.08.006

Li, Q., Zheng, L., Guo, Z., Tang, T., and Zhu, B. (2021). Alginate degrading enzymes: an updated comprehensive review of the structure, catalytic mechanism, modification method and applications of alginate lyases. *Crit. Rev. Biotechnol.* 41, 953–968. doi: 10.1080/07388551.2021.1898330

Lin, S. Y., Chen, W. M., Huang, G. H., Hameed, A., Chang, C. T., Tsai, C. F., et al. (2020). Flavobacterium supellecticarium sp. nov., isolated from an abandoned construction timber. *Int. J. Syst. Evol. Microbiol.* 70, 3731–3739. doi: 10.1099/ijsem.0.004227

Liu, S., Dai, J., Wei, H., Li, S., Wang, P., Zhu, T., et al. (2021). Dissimilatory nitrate reduction to ammonium (DNRA) and denitrification pathways are leveraged by cyclic AMP receptor protein (CRP) paralogues based on electron donor/acceptor limitation in *shewanella loihica* PV-4^{T}. *Appl. Environ. Microbiol.* 87:20. doi: 10.1128/aem.01964-20

Liu, J., Yang, S., Li, X., Yan, Q., Reaney, M. J. T., and Jiang, Z. (2019). Alginate oligosaccharides: production, biological activities, and potential applications. *Compr. Rev. Food Sci. Food Saf.* 18, 1859–1881. doi: 10.1111/1541-4337.12494

Liu, Y., Zhang, Y., Huang, Y., Niu, J., Huang, J., Peng, X., et al. (2023). Spatial and temporal conversion of nitrogen using Arthrobacter sp. 24S4-2, a strain obtained from Antarctica. *Front. Microbiol.* 14:1040201. doi: 10.3389/fmicb.2023.1040201

Makarova, K. S., Wolf, Y. I., Iranzo, J., Shmakov, S. A., Alkhnbashi, O. S., Brouns, S. J. J., et al. (2020). Evolutionary classification of CRISPR–Cas systems: a burst of class 2 and derived variants. *Nat. Rev. Microbiol.* 18, 67–83. doi: 10.1038/s41579-019-0299-x

Mann, A. J., Hahnke, R. L., Huang, S., Werner, J., Xing, P., Barbeyron, T., et al. (2013). The genome of the alga-associated marine flavobacterium *Formosa agariphila* KMM 3901^{T} reveals a broad potential for degradation of algal polysaccharides. *Appl. Environ. Microbiol.* 79, 6813–6822. doi: 10.1128/aem.01937-13

Manni, M., Berkeley, M. R., Seppey, M., and Zdobnov, E. M. (2021). BUSCO: assessing genomic data quality and beyond. *Curr Protoc.* 1:e323. doi: 10.1002/cpz1.323

Martin, M., Barbeyron, T., Martin, R., Portetelle, D., Michel, G., and Vandenbol, M. (2015). The cultivable surface microbiota of the brown alga *Ascophyllum nodosum* is enriched in macroalgal-polysaccharide-degrading bacteria. *Front. Microbiol.* 6:1487. doi: 10.3389/fmicb.2015.01487

McGuire, B. E., Hettle, A. G., Vickers, C., King, D. T., Vocadlo, D. J., and Boraston, A. B. (2020). The structure of a family 110 glycoside hydrolase provides insight into the hydrolysis of α-1,3-galactosidic linkages in λ-carrageenan and blood group antigens. *J. Biol. Chem.* 295, 18426–18435. doi: 10.1074/jbc.RA120.015776

McKee, L. S., La Rosa, S. L., Westereng, B., Eijsink, V. G., Pope, P. B., and Larsbrink, J. (2021). Polysaccharide degradation by the Bacteroidetes: mechanisms and nomenclature. *Environ. Microbiol. Rep.* 13, 559–581. doi: 10.1111/1758-2229.12980

Meier-Kolthoff, J. P., Auch, A. F., Klenk, H. P., and Göker, M. (2013). Genome sequence-based species delimitation with confidence intervals and improved distance functions. *BMC Bioinformatics.* 14:60. doi: 10.1186/1471-2105-14-60

Muhammad, N., Avila, F., Lee, Y.-J., Le Han, H., Kim, K.-H., and Kim, S.-G. (2023). Chondrinema litorale gen. Nov., sp. nov., of the phylum Bacteroidota, carrying multiple megaplasmids isolated from a tidal flat in the West Sea, Korea. *Front. Mar. Sci.* 10:6809. doi: 10.3389/fmars.2023.1186809

Muhammad, N., Le Han, H., Lee, Y. J., Ko, J., Nguyen, T. T. H., and Kim, S. G. (2022). Flavobacterium litorale sp. nov., isolated from red alga. *Int. J. Syst. Evol. Microbiol.* 72:5458. doi: 10.1099/ijsem.0.005458

Murillo, A. A., Molina, V., Salcedo-Castro, J., and Harrod, C. (2019). Editorial: marine microbiome and biogeochemical cycles in marine productive areas. *Front. Mar. Sci.* 6:657. doi: 10.3389/fmars.2019.00657

Na, S. I., Kim, Y. O., Yoon, S. H., Ha, S. M., Baek, I., and Chun, J. (2018). UBCG: up-to-date bacterial core gene set and pipeline for phylogenomic tree reconstruction. *J. Microbiol.* 56, 280–285. doi: 10.1007/s12275-018-8014-6

Nedashkovskaya, O. I., Kim, S. B., Suzuki, M., Shevchenko, L. S., Lee, M. S., Lee, K. H., et al. (2005). *Pontibacter actiniarum* gen. Nov., sp. nov., a novel member of the phylum 'Bacteroidetes', and proposal of Reichenbachiella gen. Nov. as a replacement for the illegitimate prokaryotic generic name Reichenbachia. *Int. J. Syst. Evol. Microbiol.* 55, 2583–2588. doi: 10.1099/ijs.0.63819-0

Nedashkovskaya, O. I., Suzuki, M., Vysotskii, M. V., and Mikhailov, V. V. (2003). *Reichenbachia agariperforans* gen. Nov., sp. nov., a novel marine bacterium in the phylum Cytophaga-Flavobacterium-Bacteroides. *Int. J. Syst. Evol. Microbiol.* 53, 81–85. doi: 10.1099/ijs.0.02128-0

Nguyen, T. T., Vuong, T. Q., Han, H. L., Li, Z., Lee, Y.-J., Ko, J., et al. (2023). Three marine species of the genus Fulvivirga, rich sources of carbohydrate-active enzymes degrading alginate, chitin, laminarin, starch, and xylan. *Sci. Rep.* 13:6301. doi: 10.1038/s41598-023-33408-4

Øverland, M., Mydland, L. T., and Skrede, A. (2019). Marine macroalgae as sources of protein and bioactive compounds in feed for monogastric animals. *J. Sci. Food Agric.* 99, 13–24. doi: 10.1002/jsfa.9143

Padilha, V. A., Alkhnbashi, O. S., Shah, S. A., de Carvalho, A., and Backofen, R. (2020). CRISPRcasIdentifier: machine learning for accurate identification and classification of CRISPR-Cas systems. *Gigascience*. 9:giaa062. doi: 10.1093/gigascience/giaa062

Parks, D. H., Imelfort, M., Skennerton, C. T., Hugenholtz, P., and Tyson, G. W. (2015). CheckM: assessing the quality of microbial genomes recovered from isolates, single cells, and metagenomes. *Genome Res.* 25, 1043–1055. doi: 10.1101/gr.186072.114

Paster, B. J., Dewhirst, F. E., Olsen, I., and Fraser, G. J. (1994). Phylogeny of Bacteroides, Prevotella, and Porphyromonas spp. and related bacteria. *J. Bacteriol.* 176, 725–732. doi: 10.1128/jb.176.3.725-732.1994

Pheng, S., Han, H. L., Park, D. S., Chung, C. H., and Kim, S. G. (2020). Lactococcus kimchii sp. nov., a new lactic acid bacterium isolated from kimchi. *Int. J. Syst. Evol. Microbiol.* 70, 505–510. doi: 10.1099/ijsem.0.003782

Phillips, I. (1993). Cowan and steel's manual for the identification of medical bacteria. *J. Clin. Pathol.* 46:975. doi: 10.1017/CBO9780511527104

Porcheron, G., Garénaux, A., Proulx, J., Sabri, M., and Dozois, C. M. (2013). Iron, copper, zinc, and manganese transport and regulation in pathogenic Enterobacteria: correlations between strains, site of infection and the relative importance of the different metal transport systems for virulence. *Front. Cell. Infect. Microbiol.* 3:90. doi: 10.3389/fcimb.2013.00090

Ruocco, N., Costantini, S., Guariniello, S., and Costantini, M. (2016). Polysaccharides from the marine environment with pharmacological, cosmeceutical and nutraceutical potential. *Molecules* 21:551. doi: 10.3390/molecules21050551

Saitou, N., and Nei, M. (1987). The neighbor-joining method: a new method for reconstructing phylogenetic trees. *Mol. Biol. Evol.* 4, 406–425. doi: 10.1093/oxfordjournals.molbev.a040454

Sasser, M. (1990) *Identification of bacteria by gas chromatography of cellular fatty acids. MIDI technical note 101* (Newark, DE: MIDI inc).

Schöner, T. A., Gassel, S., Osawa, A., Tobias, N. J., Okuno, Y., Sakakibara, Y., et al. (2016). Aryl polyenes, a highly abundant class of bacterial natural products, are functionally related to antioxidative carotenoids. *Chembiochem* 17, 247–253. doi: 10.1002/cbic.201500474

Shao, Z., and Duan, D. (2022). The cell wall polysaccharides biosynthesis in seaweeds: a molecular perspective. *Front. Plant Sci.* 13:902823. doi: 10.3389/fpls.2022.902823

Shi, M. J., Wang, C., Liu, Z. Y., Jiang, L. X., and Du, Z. J. (2018). Reichenbachiella versicolor sp. nov., isolated from red alga. *Int. J. Syst. Evol. Microbiol.* 68, 3523–3527. doi: 10.1099/ijsem.0.003023

Singh, R. P., and Reddy, C. R. (2014). Seaweed-microbial interactions: key functions of seaweed-associated bacteria. *FEMS Microbiol. Ecol.* 88, 213–230. doi: 10.1111/1574-6941.12297

Suenaga, T., Riya, S., Hosomi, M., and Terada, A. (2018). Biokinetic characterization and activities of N(2)O-reducing bacteria in response to various oxygen levels. *Front. Microbiol.* 9:697. doi: 10.3389/fmicb.2018.00697

Terrapon, N., Lombard, V., Gilbert, H. J., and Henrissat, B. (2015). Automatic prediction of polysaccharide utilization loci in Bacteroidetes species. *Bioinformatics* 31, 647–655. doi: 10.1093/bioinformatics/btu716

The UniProt Consortium (2023). UniProt: the universal protein knowledge base in 2023. *Nucleic Acids Res.* 51, D523–D531. doi: 10.1093/nar/gkac1052

Thomas, F., Bordron, P., Eveillard, D., and Michel, G. (2017). Gene expression analysis of *zobellia galactanivorans* during the degradation of algal polysaccharides reveals both substrate-specific and shared transcriptome-wide responses. *Front. Microbiol.* 8:1808. doi: 10.3389/fmicb.2017.01808

Tittsler, R. P., and Sandholzer, L. A. (1936). The use of semi-solid agar for the detection of bacterial motility. *J. Bacteriol.* 31, 575–580. doi: 10.1128/jb.31.6.575-580.1936

Ueno, A., Tamazawa, S., Tamamura, S., Murakami, T., Kiyama, T., Inomata, H., et al. (2021). Desulfovibrio subterraneus sp. nov., a mesophilic sulfate-reducing deltaproteobacterium isolated from a deep siliceous mudstone formation. *Int. J. Syst. Evol. Microbiol.* 71:4683. doi: 10.1099/ijsem.0.004683

Wick, R. R., Judd, L. M., and Holt, K. E. (2019). Performance of neural network basecalling tools for Oxford Nanopore sequencing. *Genome Biol.* 20:129. doi: 10.1186/s13059-019-1727-y

Wolin, E., Wolin, M. J., and Wolfe, R. (1963). Formation of methane by bacterial extracts. *J. Biol. Chem.* 238, 2882–2886. doi: 10.1016/S0021-9258(18)67912-8

Wu, J., Liu, M., Zhou, M., Wu, L., Yang, H., Huang, L., et al. (2021). Isolation and genomic characterization of five novel strains of Erysipelotrichaceae from commercial pigs. *BMC Microbiol.* 21:125. doi: 10.1186/s12866-021-02193-3

Yarza, P., Yilmaz, P., Pruesse, E., Glöckner, F. O., Ludwig, W., Schleifer, K. H., et al. (2014). Uniting the classification of cultured and uncultured bacteria and archaea using 16S rRNA gene sequences. *Nat. Rev. Microbiol.* 12, 635–645. doi: 10.1038/nrmicro3330

Yoon, S. H., Ha, S. M., Kwon, S., Lim, J., Kim, Y., Seo, H., et al. (2017a). Introducing EzBioCloud: a taxonomically united database of 16S rRNA gene sequences and whole-genome assemblies. *Int. J. Syst. Evol. Microbiol.* 67, 1613–1617. doi: 10.1099/ijsem.0.001755

Yoon, S. H., Ha, S. M., Lim, J., Kwon, S., and Chun, J. (2017b). A large-scale evaluation of algorithms to calculate average nucleotide identity. *Anton Leeuw. Int. J. G.* 110, 1281–1286. doi: 10.1007/s10482-017-0844-4

Zargarzadeh, M., Amaral, A., Custódio, J. R., and Mano, J. F. (2020). Biomedical applications of laminarin. *Carbohydr. Polym.* 232:115774. doi: 10.1016/j.carbpol.2019.115774

Zhang, Y., Rodionov, D. A., Gelfand, M. S., and Gladyshev, V. N. (2009). Comparative genomic analyses of nickel, cobalt and vitamin B12 utilization. *BMC Genomics* 10:78. doi: 10.1186/1471-2164-10-78

Zhang, H., Yohe, T., Huang, L., Entwistle, S., Wu, P., Yang, Z., et al. (2018). dbCAN2: a meta server for automated carbohydrate-active enzyme annotation. *Nucleic Acids Res.* 46, W95–W101. doi: 10.1093/nar/gky418

Zhao, D., Jiang, B., Zhang, Y., Sun, W., Pu, Z., and Bao, Y. (2021). Purification and characterization of a cold-adapted κ-carrageenase from Pseudoalteromonas sp. ZDY3. *Protein Exper Purif.* 178:105768. doi: 10.1016/j.pep.2020.105768

frontiers | Frontiers in Microbiology

TYPE Original Research
PUBLISHED 08 January 2024
DOI 10.3389/fmicb.2023.1220239

OPEN ACCESS

EDITED BY
Manoj Kumar Solanki,
University of Silesia in Katowice, Poland

REVIEWED BY
Alain Isabwe,
University of Michigan, United States
Hafiz Sohaib Ahmed Saqib,
Fujian Agriculture and Forestry University, China

*CORRESPONDENCE
Jianxin Wang
✉ jxwang@zjou.edu.cn

†These authors have contributed equally to this work

RECEIVED 10 May 2023
ACCEPTED 11 December 2023
PUBLISHED 08 January 2024

CITATION
Qu W, Zuo Y, Zhang Y and Wang J (2024) Structure and assembly process of fungal communities in the Yangtze River Estuary. *Front. Microbiol.* 14:1220239. doi: 10.3389/fmicb.2023.1220239

Structure and assembly process of fungal communities in the Yangtze River Estuary

Wu Qu†, Yaqiang Zuo†, Yixuan Zhang and Jianxin Wang*

Marine Science and Technology College, Zhejiang Ocean University, Zhoushan, China

Marine fungi are essential for the ecological function of estuarine ecosystems. However, limited studies have reported on the structure and assembly pattern of the fungal communities in estuaries. The purpose of this study is to reveal the structure and the ecological process of the fungal community in the Yangtze River Estuary (YRE) by using the amplicon sequencing method. Phyla of Ascomycota, Basidiomycota, and Chytridiomycota were dominant in the seawater and sediment samples from YRE. The null model analysis, community-neutral community model (NCM), and phylogenetic normalized stochasticity ratio (pNST) showed that the stochastic process dominated the assembly of fungal communities in YRE. Drift and homogeneous dispersal were the predominant stochastic processes for the fungal community assembly in seawater and sediment samples, respectively. The co-occurrence network analysis showed that fungal communities were more complex and closely connected in the sediment than in the seawater samples. Phyla Ascomycota, Basidiomycota, and Mucoromycota were the potential keystone taxa in the network. These findings demonstrated the importance of stochastic processes for the fungal community assembly, thereby widening our knowledge of the community structure and dynamics of fungi for future study and utilization in the YRE ecosystem.

KEYWORDS

fungal community, stochastic process, community assembly, Yangtze River Estuary, keystone taxa

Highlights

- Stochastic processes dominated the assembly of fungal communities in the Yangtze River Estuary (YRE).
- The fungal communities in YRE showed a distance–decay pattern.
- Ascomycota, Basidiomycota, and Mucoromycota were the keystone taxa for the fungal networks.

Introduction

Estuaries, which are located at the interface between land and ocean, provide high ecological productivity, goods, and services to humans (Beck et al., 2001), and this particular ecological location is often used as the nursery, sanctuary, and growth areas for many species, thereby playing considerable roles in food webs and energy flux (Chevillot et al., 2019). The Yangtze River Estuary (YRE) and the adjacent East China Sea have an effective and particular function

in the mutual interactions of the land and sea life in East Asia (Zhang J. et al., 2016). In the YRE, material inputs from terrestrial and marine sources are mixed by the hydrodynamic processes, and the resulting distributions have important implications for regulating food web structure and ecosystem function (Zhang J. et al., 2016).

Fungi are an integral part of marine ecosystems and can exist in almost all the explored marine habitats, from the ocean surface to the deep sea (Amend et al., 2019), such as seawater columns (Taylor and Cunliffe, 2016), sediments (Orsi et al., 2013), and estuaries (Mohamed and Martiny, 2011). Diverse fungi are detected in the estuary ecosystem (e.g., Ascomycota, Basidiomycota, Glomeromycota, and Chytridiomycota; Mohamed and Martiny, 2011), and these communities of estuarine fungi contribute to the element cycles, biological carbon pumps, commensal enzymes, and bio-pathogenicity in estuaries due to their special properties (Amend et al., 2019). Hence, the knowledge of fungal communities is of great significance for understanding the ecological functions of estuary ecosystems, including carbon sink, resource development, and biological interaction (Tsui and Hyde, 2004).

The study on the community assembly is a crucial component of the research on fungal communities. The ecological processes, including deterministic and stochastic, are crucial to explain the assembly of microbial communities (Logares et al., 2013; Nemergut et al., 2013b; Isabwe et al., 2022). The deterministic processes is are primarily interactions between biotic and abiotic factors, such as the interactions that exist between species (e.g., competition, predation, mutualism, and tradeoff) and environmental filtering (e.g., salinity, pH, temperature), which together shape community compositions (Chesson, 2000; Fargione et al., 2003), stochastic processes that consider all species as ecologically equivalent, and community structures that are shaped by random factors, such as random births, deaths, dispersal, extinction, and speciation (Chave, 2004; Hubbell, 2011).

The environmental DNA metabarcoding technology typically includes the 18S rRNA (Zuo et al., 2022), ITS (Yu et al., 2022), and 16S rRNA (Huang Y. et al., 2022) amplicons by using special primers. This technology has been widely used in studies on the assembly mechanisms of bio-communities with the development of high-throughput sequencing. For instance, previous studies have shown that stochastic processes have a strong effect on bacterial community assembly in Yellow River Estuary (Huang L. et al., 2022), Pearl River Estuary (Wu et al., 2020), and YRE (Shi et al., 2022). Therefore, stochastic processes might also impact the fungal community assembly in the YRE; however, this hypothesis has not been tested until now. The current study aims to assess the importance of the stochastic processes for the assembly of fungal communities in the YRE by using the 18S rRNA amplicon sequencing method, thereby elucidating the dynamics of the fungal communities in the YRE.

Materials and methods

Sample collection

This study was carried out in the East China Sea across the YRE and its adjacent waters (125°–126°E, 30°–31°N) in August 2020 (Figure 1). Water samples were collected from the surface, middle, and bottom layers at 21 stations by using an SBE32 CTD (Washington,

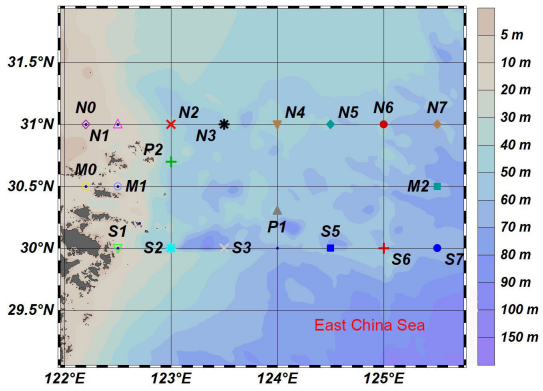

FIGURE 1
The sampling sites of this study in the Yangtze River Estuary (YRE).

Sea-Bird Electronics). Seawater was pre-filtered through the 3.0-μm-pore size polycarbonate membranes and then was filtered through the 0.22-μm-pore size polycarbonate membranes (47 mm diameter; Millipore, Germany; Wu et al., 2020). Sediment samples were taken directly from the topsoil of each site. Each water sample was named with the location name, followed by the abbreviation of the layer and the membranes, and each sediment sample was named by the site. The water samples were divided into three groups: surface, middle, and bottom. For example, the M0SP sample means the water sample in the surface seawater at the M0 site. The M0 sample means the sediment sample collected at the M0 site.

Measurement of the environmental factors

The ammonia nitrogen (NH_4-N), nitrite nitrogen (NO_2-N), and phosphorus (PO_4-P) of seawater were determined by SmartChem automatic nutrient analyzer (Seabird Company, Washington). The nitrate (NO_3-N) of seawater was manually analyzed and determined by the Cu–Cd reduction method (del Carmen et al., 2006). The analysis of the pH of seawater was conducted using a pH meter (Leici, Shanghai). The sediment pH, NH_4-N, NO_2-N, NO_3-N, and PO4-P were measured by Nanjing Yanke Testing Technology Co., Ltd. (Nanjing, China).

Extraction of environmental DNA and sequencing of 18S rRNA genes

The DNA in samples was extracted using a FastDNA Spin Kit (MP Biomedicals, United States) according to the instructions. The integrity and quality of DNA were measured by 1% agarose gel, and the DNA concentration and purity were verified using a NanoDrop 2000 UV–vis spectrophotometer (Thermo Scientific, Wilmington, United States). Primer pairs of SSU0817F (5′-TTAGCATGGAATAATRRAATAGGA-3′) and 1196R (5′-TCTGGACCTGGTGAGTTTCC-3′; Zheng et al., 2020) were used to amplify the 18S rRNA genes from the DNA solution by using the ABI GeneAmp 9700 PCR thermocycler (ABI, CA, United states). The sequencing was conducted using the Illumina Miseq PE300 platform/NovaSeq PE250 platform (Illumina, San Diego, United States)

by Majorbio Bio-Pharm Technology Co. Ltd. (Shanghai, China). Raw sequence data are deposited at the NCBI Sequence Read Archive under the accession numbers SRR21079128–SRR21079264.

Sequence processing and fungal community analysis

The VSEARCH v.2.15.1 was used to perform the merge of the pair-end FASTQ sequences (Rognes et al., 2016). The *fastx_filter* command was used to delete the tags and primers of the original sequence, and the error rate was controlled to be less than 0.01. The *Derep_fulllength* command was used for the de-redundancy of the sequence, and the unoise3 feature in the USEARCH tool was used to de-noise in order to obtain single-base accuracy amplicon sequence variants (ASV; Edgar, 2010). Then, the sequences were de-chimerized using VSEARCH and the Silva database (SILVA_18s_v138.fa). Then, the fungi taxonomy of each ASV representative sequence was analyzed using SINA version 1.2.11 against the Silva 138 database at a confidence threshold of 0.7 (Pruesse et al., 2012). Finally, 280 high-quality sequences of fungi were obtained from 137 samples.

The correlations between environmental factors and alpha-diversity indices were calculated using the "corrplot" package of R software. Diversity indices, including Shannon and Chao1, were calculated using the "picante" package of R software (Kembel et al., 2010) and were visualized using the "ggpubr" package of R software. A one-way analysis of variance (ANOVA) was used for multiple-group comparison of the data. Heatmaps were visualized using R packages of "psych" (Revelle and Revelle, 2015). The environmental factor with variance inflation factor value of <10, calculated using the function vif() in the "car" package of R (Fox et al., 2007), was selected for the linear regression to avoid the multilinearity among the factors (Craney and Surles, 2002; Abadura et al., 2015). The importance of each environmental variable for the community was assessed with the multiple linear regression (Jiao et al., 2020) using calc.relimp() in the relaimpo package of R (Grömping, 2007). R package of "ggalluvial" (Brunson, 2020) was used for visualizing the fungal community composition at the phylum level. The constrained principal coordinate analysis (CPCoA) was used to reveal the fungal community using the package "amplicon" of R software (Liu et al., 2021). An unweighted pair-group method with arithmetic means (UPGMA) clustering analysis was performed to display the dissimilarity among different groups based on the Jaccard dissimilarity index, Bray–Curtis dissimilarity index, Euclidean dissimilarity index, and Manhattan dissimilarity index using "vegan" package of R software (Oksanen et al., 2007).

Beta-diversity of the samples was partitioned into richness difference components (Sørensen dissimilarities) and replaced using the packages "BAT" (Cardoso et al., 2014) and "betapart" of R software (Baselga and Orme, 2012; Si et al., 2017). The de-trend correspondence analysis (DCA) was performed using decorana() of the vegan package of R software. Based on the gradient length along the axis (<4) of the DCA result, the distance-based redundancy analysis (db-RDA) was used to fit the fungal community matrix with the environmental variables using the "vegan" package (Oksanen et al., 2007) to reveal their relationships.

Assembly process analysis of fungal community

Community similarity was used to express the relationship between community dissimilarity and geographic distance. The geographic distances between different samples based on the latitude and longitude coordinates were calculated using the "vegdist" function in the R "vegan" (Oksanen et al., 2007) package. For both latitudinal diversity gradient and distance decay relationships, a linear regression analysis was carried out to calculate the slope, *R*-value, and significance values. A neutral community model (NCM) was used to predict the potential importance of stochastic processes in fungal assembly by determining the relationships between the detection frequency of fungal taxa in a set of local communities (Sloan et al., 2006; Chen et al., 2019) using the minpack.lm (Elzhov et al., 2016) and HMisc (Harrell and Harrell, 2019) packages.

The fungal community assembly patterns including stochastic and deterministic processes (Zhang et al., 2021) were determined as follows: the beta nearest-taxon index (βNTI) was calculated based on the phylogenetic distance and ASV abundances, which indicated the number of the deviation degree of the beta mean nearest taxon distance (βMNTD) of the null model developed by Stegen et al. (2013). Bray–Curtis-based Raup-Crick (RCBray) and βNTI were used to assess the ecological processes. The $|\beta NTI| \geq 2$ indicated that deterministic processes including homogeneous selection (the βNTI value < -2) and variable selection (the βNTI value > 2; Stegen et al., 2012; Zhou and Ning, 2017) played a more significant role than the stochastic process, whereas $|\beta NTI| < 2$ represented a more important role of stochastic processes. Furthermore, $|\beta NTI| < 2$ and $|RCBray| < -0.95$ showed that homogenizing dispersal dominated the fungal community assembly. $|\beta NTI| < 2$ and $|RCBray| > 0.95$ indicated a crucial impact of dispersal limitation, and $|\beta NTI| < 2$ and $|RCBray| < 0.95$ suggested the significant role of the drift. The βNTI and RCBray values were calculated by R script "bNTI_Local_Machine.r" (Stegen et al., 2012). The phylogenetic normalized stochasticity ratio (pNST) was used to quantify the relative importance of deterministic and stochastic processes in community assembly based on the phylogenetic beta diversity index and phylogenetic randomization. pNST < 0.5 indicates a significant role in deterministic processes, while pNST > 0.5 indicates that stochastic processes dominated the community assembly (Ning et al., 2019).

Co-occurrence network analysis

The rcorr() function of R software was used to perform the pairwise correlations based on ASV relative abundance and the R package "Hmisc" was used to build the co-occurrence network of the microbial community (Harrell and Harrell, 2019). The false discovery rate correction was conducted to adjust the *p*-value. The ASVs with an R^2 value > 0.7 and a *p*-value < 0.05 remained for the network. The R package of "igraph" (Csardi and Nepusz, 2006) and Gephi v0.92 (Bastian and Heymann, 2009) were used to build and visualize the network diagram, respectively. The calculation of topology characteristics of the community networks (including degree, clustering coefficient, and average path length) and the analysis of the

network modules were also performed using Gephi v0.92 with default parameters. The ASVs with Zi ≥ 2.5 and/or Pi ≥ 0.62 in the networks were identified as the keystone taxa (Deng et al., 2012).

Results

Environmental parameters

Environmental properties in the current study are listed in Supplementary Table S1. Among these factors, NH_4-N was significantly and positively correlated with PO_4-P, and NO_2-N ($p < 0.01$) and was negatively correlated with NO_3-N and pH ($p < 0.01$). In addition, NO_2-N and PO_4-P was negatively correlated with NO_3-N ($p < 0.01$; Supplementary Figure S1).

Community composition

A total of 7 phyla were annotated in 137 samples (Figure 2). Ascomycota was the most abundant phylum in all samples, followed by Basidiomycota and Chytridiomycota. The relative abundance of Ascomycota was higher in the surface layer of seawater than in the middle layer and bottom layer of the seawater and sediment. In addition, the relative abundance of Chytridiomycota was higher in the sediment layer than in the different layers of seawater.

Alpha- and beta diversity of the fungal communities

The alpha-diversity index of Chao1 was not significantly different among various layers of seawater and sediment (ANOVA, $p > 0.05$; Figure 3A), except that the Chao1 index of the middle layer was significantly lower than the bottom layer of seawater (ANOVA, $p < 0.05$; Figure 3A). The Shannon index of sediment was significantly higher than different layers of seawater (ANOVA, $p < 0.01$; Figure 3B). The Shannon index of the middle layer was significantly lower than the bottom layer of seawater (ANOVA, $p < 0.01$; Figure 3B), and no significant difference was found among other seawater layers (ANOVA, $p > 0.05$; Figure 3B). The results showed that NH_4-N was positively correlated with abundance indices (Richness, ACE, and Chao1) and diversity indices (Shannon and Simpson). In addition, NH_4-N had a higher effect on the abundance index but had little effect on the diversity index (Figure 3C).

The result of UPGMA showed that the sediment could be separated from the seawater samples of different layers regardless of distance algorithms including Jaccard (Figure 4A), Bray–Curtis (Figure 4B), Euclidean (Figure 4C), and Manhattan distances (Figure 4D). The CPCoA result showed that only the fungal communities in the sediment samples were significantly separated from the seawater samples, and the seawater samples with different depths were not separated according to the 95% confidence ellipse, as shown in Figure 4E. The beta-diversity partitioning results showed that the species replacement was the main contributor for the community composition differences, which contributed 54.72% (surface layer), 56.61% (middle layer), 56.95% (bottom layer), and 67.60% (sediment) for the samples, respectively. However, the contribution of richness difference to the beta-diversity dissimilarity was relatively low, which were 45.18% (surface layer), 43.38% (middle layer), 43.05% (bottom layer), and 32.40% (sediment), respectively (Figure 4F).

Influence of environmental variables on the structure of fungal communities in YRE

Owing to that the gradient length along the axis was less than 4 in the results of DCA, db-RDA was selected to describe the relationship between environmental factors and fungal communities. The results

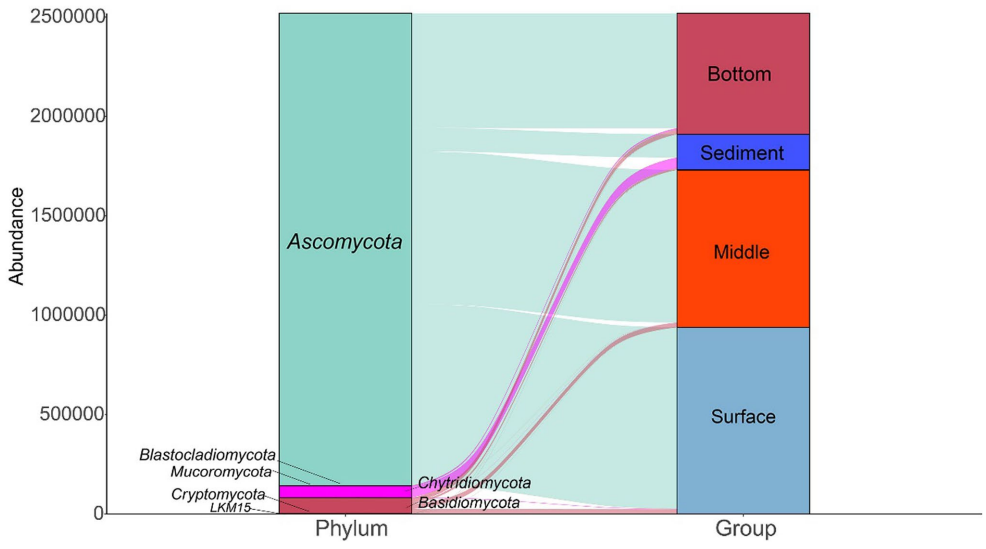

FIGURE 2
The fungal community compositions at the phylum level in the seawater and sediment samples.

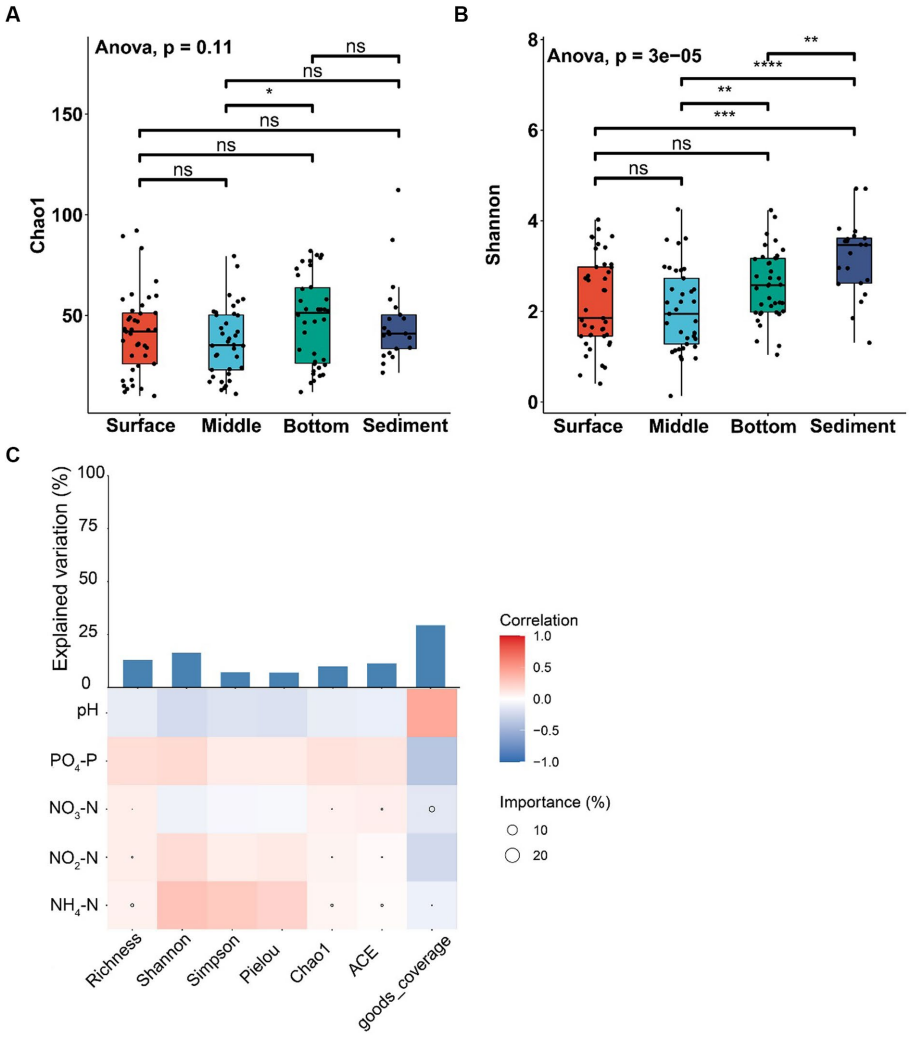

FIGURE 3
Alpha-diversity analysis of fungal communities among the samples from different depths of seawater (surface, middle, and bottom) and sediment in YRE. Panels **(A,B)** represent the Chao1 and Shannon indices of different samples, respectively; Panel **(C)** represents the Spearman correlation coefficient between the environmental factors and the alpha-diversity indices. The circle sizes in heatmaps represent the importance of the environmental factors on the alpha-diversity indices based on the multiple linear regression and variance decomposition analysis. The bar chart represents the explanation degrees in the multiple linear regression of the environmental factors and the alpha-diversity indices. The symbols "*", "**", "***", and "****" represent $0.01 \leq p < 0.05$, $0.005 \leq p < 0.01$, $0.001 \leq p < 0.005$, and $p < 0.001$, respectively.

showed that all the environmental factors had significant effects on fungal communities ($p < 0.001$; Figure 5A). NH_4-N was the most influential environmental factor ($p < 0.001$; $R^2 = 0.5169$) for the fungal community structure (Supplementary Table S2). The NH_4-N was negatively correlated with the relative abundance of Ascomycota and was positively correlated with the relative abundances of other phyla (Figure 5B).

Distance–decay pattern analysis

The distance–decay patterns of the fungal communities in seawater (Figures 6A–C) and sediment (Figure 6D) samples were analyzed. A significant and negative distance–decay pattern was found in the samples from the surface (Figure 6A), bottom (Figure 6B) seawater, and sediment (Figure 6D; $p < 0.01$); however, the distance–decay pattern was not significant in the middle seawater (Figure 6C). In addition, the slope of the sediment's community dissimilarity (slope = 5.29E-07) was higher than those of the seawater samples, indicating the spatial turnover rate of the fungal communities of sediment was higher than the seawater. The slope of seawater from the surface layer (slope = 2.77E-07) was higher than the middle (slope = 3.18E-08) and bottom layers (slope = 2.49E-07). Hence, the dispersal of fungi community in the surface layer was more restricted than that in other layers in the seawater of YRE (Figures 6A–D).

The NCM analysis of the fungal communities in YRE

The NCM was used to predict the relationship between the occurrence frequency of ASV and its relative abundance in fungal

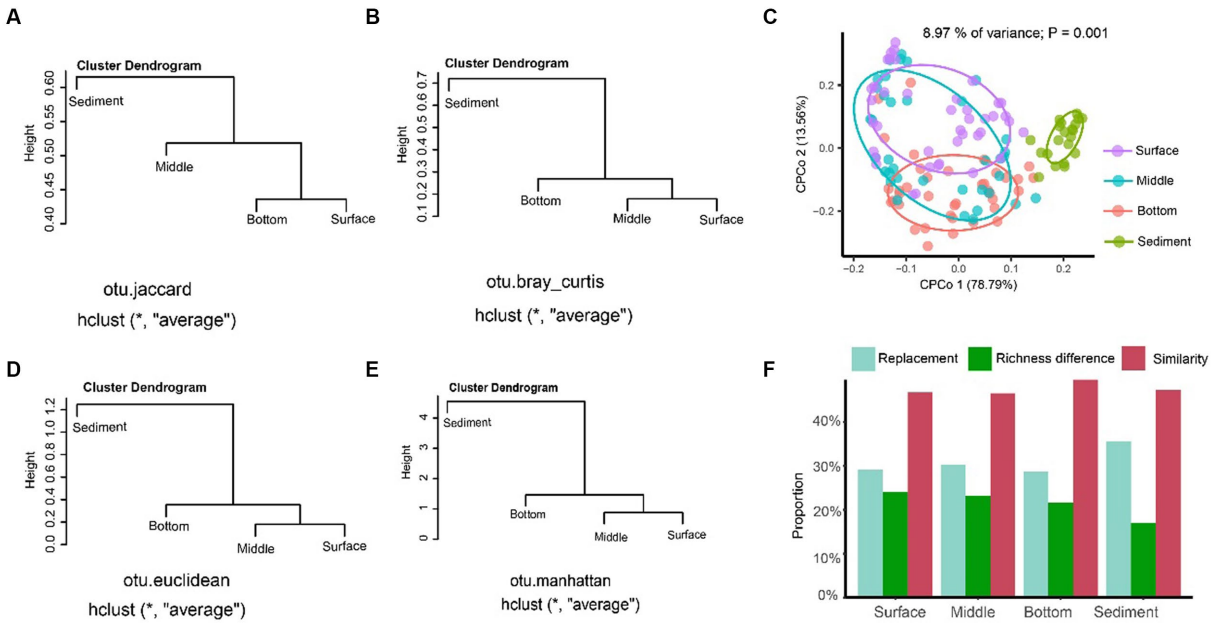

FIGURE 4
The beta-diversity analysis of the fungal communities in YRE. Panels **(A–D)** represent the results of the unweighted pair-group method with arithmetic means (UPGMA) clustering analysis based on the Jaccard, Bray-Curtis, Euclidean, and Manhattan distances, respectively. Panel **(E)** is the constrained principal coordinate analysis (CPCoA) based on the Bray-Curtis distance of the fungal communities from the seawater and sediment samples. Panel **(F)** is the result of the proportion of the replacement and richness difference components of fungal community dissimilarity from the seawater and sediment samples.

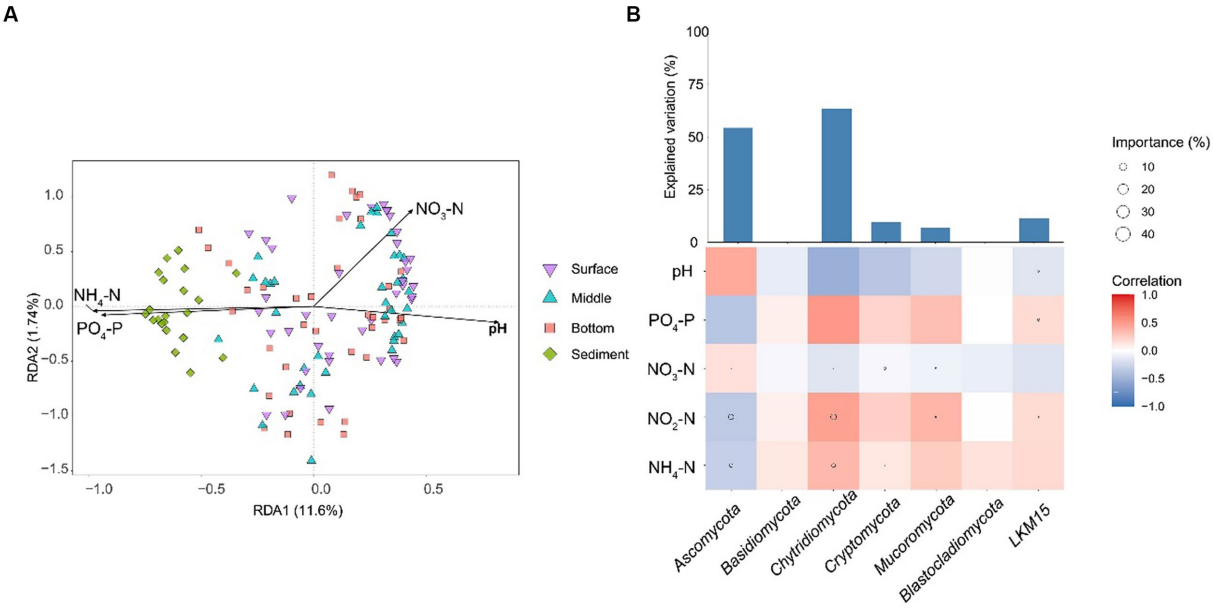

FIGURE 5
(A) db-RDA displays the relationship between fungal community structures and environmental factors. **(B)** The influence of environmental factors on the relative abundances of fungal phyla. The heatmap represents the Spearman correlation coefficient between the environmental factors and the relative abundances of fungal phyla. The circle size in heatmaps represents the importance of the environmental factors on the relative abundances of fungal phyla based on the multiple linear regression and variance decomposition analysis. The bar chart represents the explanation degrees in the multiple linear regression of the environmental factors and the relative abundances of fungal phyla. NH_4-N, ammonia nitrogen; NO_2-N, nitrite nitrogen; PO_4-P, phosphorus; NO_3-N, nitrate.

communities from the different layers of seawater and sediment (Figures 6E–H). The relative contribution of stochastic processes increased gradually with the water depth, explaining 51.6% (Figure 6E), 52.1% (Figure 6F), and 63.1% (Figure 6G) of the fungal community variation in the surface, middle, and bottom layers of seawater, respectively. The explained community variation of fungal

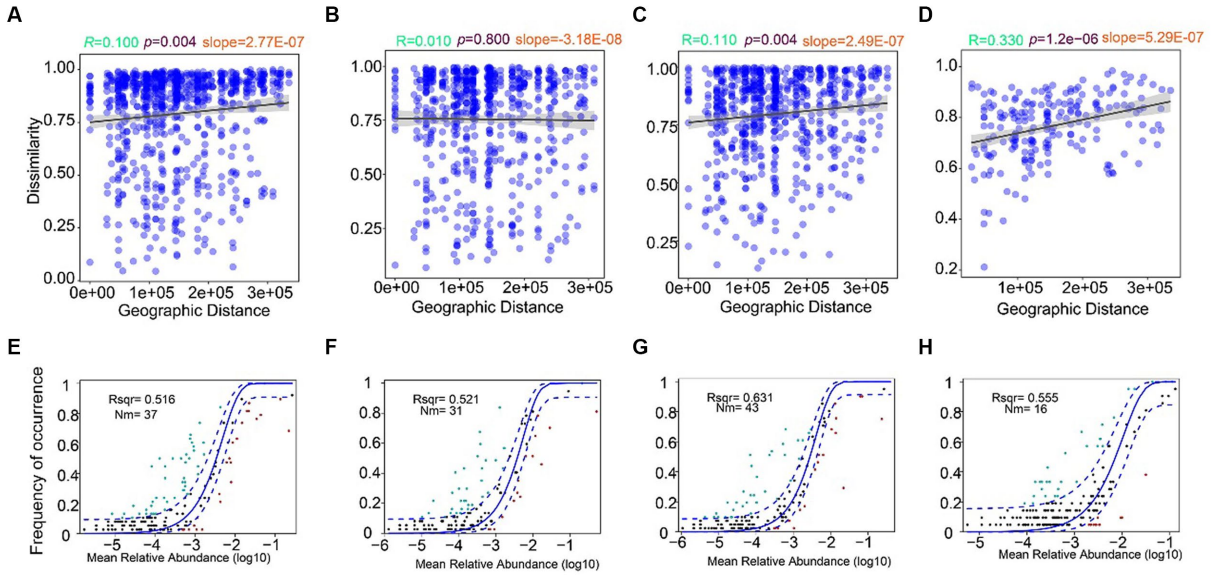

FIGURE 6
Distance–decay patterns of the fungal communities in YRE. Panels **(A–D)** represent the distance–decay curves of dissimilarity for the fungal communities in YRE from surface, middle, bottom, and sediment samples, respectively. Panels **(E–H)** represent the fit of the neutral community model (NCM) of fungal community assembly in the surface, middle, bottom, and sediment samples, respectively. The solid blue lines indicate the best fit to the NCM as in Sloan et al. (2006), and the dashed blue lines represent the 95% confidence intervals in the model prediction. ASVs that occurred more and less frequently than the predicted values in the NCM are shown in green and red, respectively. Nm indicates the products of metacommunity size and migration rate; Rsqr indicates the fit goodness of this model.

community in sediment was 55.5% (Figure 6H), thereby the effect of the stochastic process in sediment was lower than in bottom seawater but higher than in the surface and middle seawater. Furthermore, the Nm value of sediment (16) was lower than those of the seawater from different depths (surface = 37, middle = 31, and bottom = 43). These results indicated that dispersal limitation was more dominant in the fungal community assembly processes in the sediment than in the seawater samples, and the dispersal limitation was more dominant in the fungal community assembly processes in the middle layer seawater than in the surface and bottom layers.

The null model analysis of the fungal communities in YRE

The null model analysis showed that the βNTI values in all the samples were between −2 and 2, suggesting that stochastic processes were more important than deterministic processes (Figure 7A). Most of the RCBray values ranged from −0.95 to 0.95 (Figure 7B), indicating the drift was the significant player for the assembly process of the fungal community. The drift (55.02%), being the predominant stochastic process, dominated the fungal community assembly in the seawater and sediment samples (Figure 7C). The pNST was used to quantify the relative importance of deterministic and stochastic processes in community assembly. The results showed that the pNST values of fungal communities in different groups were mainly distributed in the interval > 0.5 (Figure 7D), showing that the stochastic processes were dominant in this fungal community assembly.

Co-occurrence network analysis

A co-occurrence network consisting of 458 nodes and 134 edges was generated for the surface layer of the seawater (Figure 8A). The nodes in the network were assigned into 6 phyla (Figure 8B). The middle layer network contained 16 modules (Figure 8C), and the nodes in the network were assigned into 6 phyla (Figure 8D). The bottom layer network contained 14 modules (Figure 8E), and the nodes in the network were assigned into 5 phyla (Figure 8F). The sediment network contained 8 modules (Figure 8G), and the nodes in the network were assigned into 7 phyla (Figure 8H). The relative abundances of Ascomycota and Basidiomycota were higher than others in all networks (Figures 8B,D,F,H). The average clustering coefficient of the sediment network was higher than that of the seawater networks, indicating that ASVs from the sediment samples were more closely related to each other (Supplementary Table S3). The topological properties are summarized in Supplementary Table S3.

The Zi-Pi plot showed that 30, 26, 27, and 37 Ascomycota ASVs served as the calculated keystone taxa in the fungal networks of surface (Supplementary Figure S2A), middle (Supplementary Figure S2B), bottom (Supplementary Figure S2C), and sediment (Supplementary Figure S2D) samples. The community composition of the keystone taxa in different groups (Supplementary Figure S3) showed that the relative abundance of Ascomycota was higher in sediment than those in surface, middle, and bottom samples. Basidiomycota with high relative abundances and Mucoromycota with low relative abundances was identified as the calculated keystone taxon.

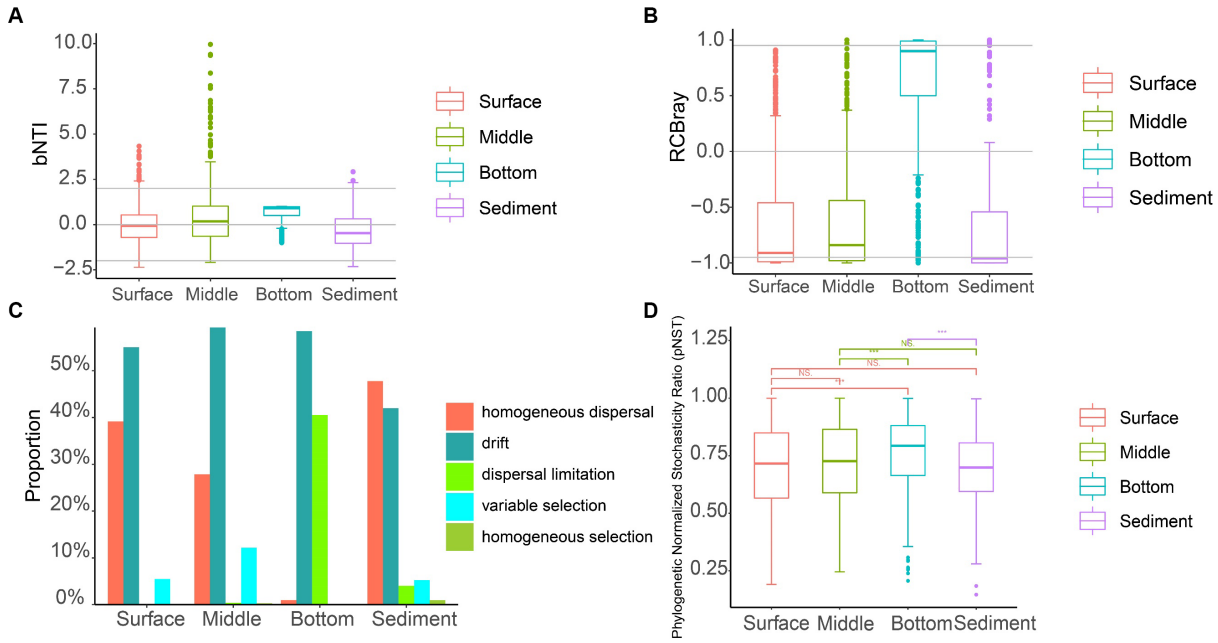

FIGURE 7
The null model analysis of fungal communities in the seawater and sediment samples of YRE. **(A)** Boxplots of the beta nearest-taxon index (βNTI) in the seawater and sediment samples. Gray lines represent βNTI values ranging from 2 to −2. **(B)** Bray–Curtis-based Raup-Crick (RCBray) values range from 0.95 to −0.95. **(C)** The contribution rate of deterministic processes (homogeneous and variable selection) and stochastic processes (homogeneous dispersal, drift, and dispersal limitation) to the fungal community assembly. **(D)** The phylogenetic normalized stochasticity ratio (pNST) distribution of fungal communities in seawater and sediment samples. "***" indicates $p < 0.001$.

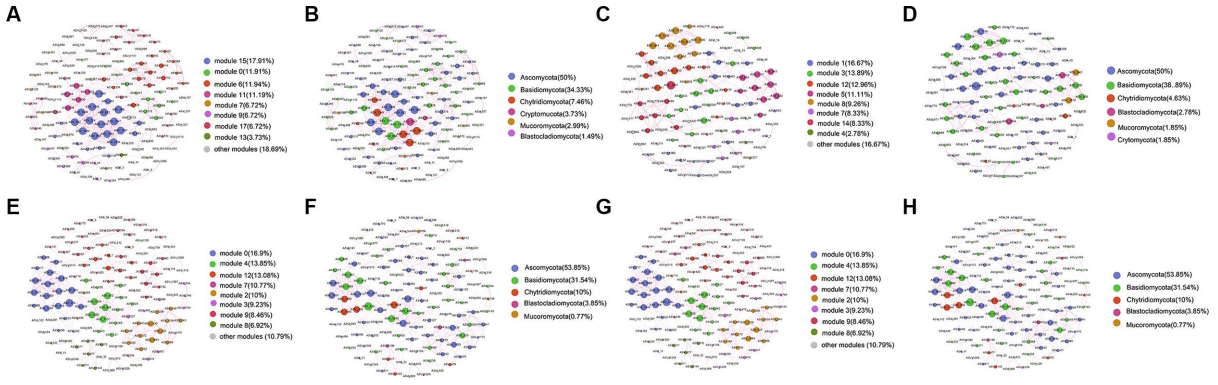

FIGURE 8
Co-occurrence network analysis of fungal communities from the surface **(A,B)**, middle **(C,D)**, bottom **(E,F)**, and sediment **(G,H)** samples in YRE. The nodes from the networks in **(A,C,E,G)** were colored based on the modularity class, and the nodes from the networks **(B,D,F,H)** were colored based on the fungal phyla. The node size was directly proportional to the degree values of the networks, and edge thickness depended on the correlation among the taxa. A positive correlation is displayed with a purple line.

Discussion

Species replacement and environmental variables served as the contributors to the fungal community variation in YRE

The current study found that there was no significant difference in the relative abundances of fungi within the collected samples, but the species diversity index (Shannon) was significantly ($p < 0.05$) higher in sediments than the seawater from different layers. This is consistent with a previous study on the Yellow River Estuary (Shi et al., 2020). However, other studies have obtained different results. For example, the diversity and abundance of fungal communities in the Western Pacific (Li et al., 2019) are obviously different in various water layers, and the fungal communities in the Bohai Sea and the Yellow Sea showed regional differences in the seawater (Gong et al., 2015; Wang Y. et al., 2017). The dispute could be probably attributed to the different sampling locations and the effect of different ocean currents on local ocean formations.

Previous studies have shown that the total β-diversity was formed by species replacement and richness difference (Baselga, 2010; Legendre, 2014; Wang et al., 2015). The species replacement, also known as turnover, reflects the species turnover along spatial or environmental gradients (Legendre, 2014), while the richness difference, known as species nestedness, represents the non-random process of species gain or loss (Baselga, 2010; Baselga, 2013). Species replacement explained the higher rate of β-diversity than richness difference in this study, implying that the β-diversity of fungal communities was mainly derived from species turnover components in the YRE. This is consistent with the previous reports on the typical dryland ecosystem of northwest China (Wang J. et al., 2017) and soil fungal communities (Liu W. et al., 2022).

Among the environmental factors collected in the current study, NH_4-N mostly shaped the fungal community and impacted the phylum relative abundances, including Ascomycota, Chytridiomycota, and Cryptomycota in the samples. Zhen et al. (2017) reported that nitrogen is essential for life activities as a direct or indirect part. In the marine environment, nitrogen is an essential nutrient element for primary production and nitrogen bioavailability, thereby shaping the plankton diversity and biological processes (Gruber and Galloway, 2008; Wannicke et al., 2018). The marine environment is typically nitrogen deficient (Zhang Y. et al., 2016). Therefore, NH_4-N could contribute to and be of value to the growth of fungal communities in the ocean. Previous studies have shown that planktonic fungal diversity and ASV abundance are largely regulated by the changes in the availability of several potential growth substrates, such as organic and inorganic nitrogen-rich substrates (Taylor and Cunliffe, 2016).

Stochastic processes dominated the fungal community assembly in YRE

Clarifying the community assembly process is ecologically crucial for understanding the adaptability of the microorganisms to the environmental variation in water-related ecosystems (Zhou and Ning, 2017). In the limited studies on the assembly process of fungal communities, the stochastic process has been demonstrated as the dominant process that drives the fungal communities in mangrove sediment (Zhang et al., 2021), smelting soils (Liu B. et al., 2022), estuarine wetlands (Huang L. et al., 2022), and coastal line (Zhao et al., 2023). Nevertheless, the detailed components, including homogenizing dispersal, dispersal limitation, and drift, in the stochastic processes are rarely assessed in the assembly of fungal communities (Zhou and Ning, 2017).

The null model analysis shows that the stochastic process plays an important role in assembling the fungal community in the YRE. More specifically, the drift in the stochastic process dominated the fungal community assembly in the seawater samples of YRE, and homogeneous dispersal in the stochastic process mainly shaped the sediment fungal communities. Ecological drift is a central concept in community ecology, which is the random change in the relative abundance of different species within a community over time to species identity due to the inherent stochastic processes of birth, death, and reproduction (Nemergut et al., 2013a; Vellend et al., 2014). A study has shown that random births and deaths are more important in shaping communities with smaller population sizes (Samad et al., 2017); therefore, the weak selection and small size community of fungi probably resulted in the increasing importance of drift for this community assembly (Chase and Myers, 2011).

The dispersal limitation also functioned for the fungal community assembly based on the distance–decay model, whose result in current study indicated that (i) the fungal communities in the YRE had spatial structure distribution patterns; (ii) fungal communities in sediment and surface seawater were more controlled by dispersal limitation due to their higher slopes; (iii) and the fungal communities in middle seawater were affected by not only dispersal limitation but also the spatial environment due to its non-significance in the model. The stronger dispersal limitation has been demonstrated in sediment fungal communities because of the microbial colonization pattern (Shurin et al., 2009; Zhao et al., 2022). Compared with other water layers, microorganisms in surface seawater dispersed more easily due to their small size and inability to counteract the flow of unidirectionality and ocean currents (Chen et al., 2019). In addition, we primarily attributed the high dispersal limitation for the fungal communities in the surface seawater to the ocean current conditions in YRE. Yangtze River diluted water, Taiwan Strait, and other currents formed a complex salt font environment between the fresh plume and salty water in YRE (Wei et al., 2007), thereby potentially limiting the diffusion of fungal communities. Similar results were obtained from other estuaries, such as the Yellow River Estuary (Wang et al., 2021) and the Pearl River Estuary (Lu et al., 2022).

In general, the endogenous (community size) and exogenous (current environment) factors were the potential reasons that increased the significance of stochastic processes for the assembly of fungal community in YRE, indicating that the changes and undulation of these factors in YRE, such as acidification and seasonal hypoxia (Lyu et al., 2022), could obviously vary the fungal communities and their ecological functions.

Keystone taxa of the fungal communities of YRE

The interactions and keystone taxa of fungal communities in YRE have scarcely been reported in former studies. The current study showed that the fungal network structure in the sediment is more complex than those in the seawater from various layers. Previous studies have found that low bacterial diversity reduces the complexity of symbiotic networks in mountain ecosystems (Li et al., 2020) and mangrove ecosystems (Chen and Wen, 2021). Therefore, the higher fungal Shannon index of sediment samples in YRE might result in more complex species interactions. In addition, studies have shown that eukaryotic plankton symbiosis networks are influenced by different environmental factors due to their various influences (i.e., pH and total nitrogen; Liu et al., 2019). Thus, the different effects of the environmental factors collected in this study on the fungal communities could be another reason for the high network complexity of the sediment samples.

The average clustering coefficients of the fungal networks in sediment samples were higher than those of seawater samples from different layers, and the average path lengths of sediment samples were lower than those of seawater samples, indicating that the fungal species in sediments were related more closely than the water samples, which could be the consequence of the sediment fungi being controlled by dispersal limitation. The higher diversity and closer

interconnection could give the fungal communities in sediments a stronger buffer against environmental disturbances. In all the networks, the proportion of positive correlation was higher than the negative correlation, which reveals that positive effects (i.e., reciprocity and/or homology, where two species exchange metabolites in favor of both) were more important than negative effects (i.e., predator–prey relationships, host–parasite relationships, and/or competition between microbes; Chen and Wen, 2021). This is similar to the result of global ocean plankton interactions conducted by the Tara Oceans Project (Lima-Mendez et al., 2015) and fungal investigation in mangroves (Zhang et al., 2021; Zuo et al., 2022), indicating that fungi tend to benefit each other in these marine environments.

Microbial co-occurrence network generally can be divided into several connected modules. These modules may reflect the habitat heterogeneity, system development close related species, ecological niche overlap, and species evolution, which is regarded as a system development, evolution, or functionally independent unit (Olesen et al., 2007). The key nodes identified in ecological network modules often represent key species that may play an important role in maintaining the stability of microbial community structure (Shi et al., 2016). However, the keystone fungal taxa remained unclear for the estuarine ecosystems. Ascomycota and Basidiomycota with high relative abundances were identified as the keystone fungal taxa in YRE, which was consistent with the former fungal study on Jinsha River (Chen et al., 2020). Mucoromycota with low relative abundances was also identified as a keystone taxon. Increasing evidence from different habitats indicates the importance of rare and less abundant species in microbial networks (Xue et al., 2018), and their removal can lead to dramatic changes in microbiome structure and function (Banerjee et al., 2018). Therefore, more attention should be paid to the detailed taxonomic information and maintenance function of these taxa in future studies on the YRE ecosystem functions.

In conclusion, the present study proved that the fungal communities in the YRE had a typical distance–decay pattern, and the stochastic process dominated the assembly of fungal communities in the YRE. This study points out the importance of drift and homogeneous dispersal for the fungal community structures in seawater and sediment samples from YRE, respectively, which enhances our understanding of fungal community aggregation and interaction and facilitates the future study of the fungal ecological functions in the YRE ecosystem.

Data availability statement

Raw sequence data are deposited at the NCBI Sequence Read Archive database (https://www.ncbi.nlm.nih.gov/sra) under the accession numbers of SRR21079128- SRR21079264.

Ethics statement

No animal studies are presented in this manuscript.

Author contributions

WQ and YZu wrote the manuscript. YZu and YZh conducted the experiments and analyzed the data. WQ and JW conceived, designed, and financially supported the research. YZu and WQ analyze the data. WQ, JW, and YZu revised the manuscript. All authors contributed to the article and approved the submitted version.

Funding

This study was funded by the Fundamental Research Fund for the Provincial Universities of Zhejiang (2021JD003) and the College Students' Innovative Entrepreneurial Training Plan Program (02110340009).

Acknowledgments

The authors want to thank the Sophisticated Ocean Front and Fisheries Investigation (SOPHI) of Zhejiang Ocean University for supporting the sampling work.

Conflict of interest

The authors declare that the research was conducted in the absence of any commercial or financial relationships that could be construed as a potential conflict of interest.

Publisher's note

Supplementary material

The Supplementary material for this article can be found online at: https://www.frontiersin.org/articles/10.3389/fmicb.2023.1220239/full#supplementary-material

References

Abadura, S. A., Lerebo, W. T., Kulkarni, U., and Mekonnen, Z. A. (2015). Individual and community level determinants of childhood full immunization in Ethiopia: a multilevel analysis. *BMC Public Health* 15, 1–10. doi: 10.1186/s12889-015-2315-z

Amend, A., Burgaud, G., Cunliffe, M., Edgcomb, V. P., Ettinger, C. L., Gutiérrez, M. H., et al. (2019). Fungi in the marine environment: open questions and unsolved problems. *mBio* 10, e01189–e01118. doi: 10.1128/mBio.01189-18

Banerjee, S., Schlaeppi, K., and van der Heijden, M. G. A. (2018). Keystone taxa as drivers of microbiome structure and functioning. *Nat. Rev. Microbiol.* 16, 567–576. doi: 10.1038/s41579-018-0024-1

Baselga, A. (2010). Partitioning the turnover and nestedness components of beta diversity. *Glob. Ecol. Biogeogr.* 19, 134–143. doi: 10.1111/j.1466-8238.2009.00490.x

Baselga, A. (2013). Separating the two components of abundance-based dissimilarity: balanced changes in abundance vs. abundance gradients. *Methods Ecol. Evol.* 4, 552–557. doi: 10.1111/2041-210X.12029

Baselga, A., and Orme, C. D. L. (2012). Betapart: an R package for the study of beta diversity. *Methods Ecol. Evol.* 3, 808–812. doi: 10.1111/j.2041-210X.2012.00224.x

Bastian, M., and Heymann, S. (2009). Jacomy M Gephi: an open source software for exploring and manipulating networks. *ScienceOpen Res* 3, 361–362. doi: 10.1609/icwsm.v3i1.13937

Beck, M. W., Heck, K. L., Able, K. W., Childers, D. L., Eggleston, D. B., Gillanders, B. M., et al. (2001). The identification, conservation, and management of estuarine and marine nurseries for fish and invertebrates: a better understanding of the habitats that serve as nurseries for marine species and the factors that create site-specific variability in nursery quality will improve conservation and management of these areas. *Bioscience* 51, 633–641. doi: 10.1641/0006-3568(2001)051[0633:TICAMO]2.0.CO;2

Brunson, J. C. (2020). Ggalluvial: layered grammar for alluvial plots. *J Open Source Softw* 5:2017. doi: 10.21105/joss.02017

Cardoso, P. M., Rigal, F., and Carvalho, J. (2014). BAT-biodiversity assessment tools an R package for the measurement and estimation of alpha and beta taxon, phylogenetic and functional diversity. *Methods Ecol Evol* 6, 232–236. doi: 10.1111/2041-210X.12310

Chase, J. M., and Myers, J. A. (2011). Disentangling the importance of ecological niches from stochastic processes across scales. *Philos. Trans. R. Soc. Lond. B Biol. Sci.* 366:2351. doi: 10.1098/rstb.2011.0063

Chave, J. (2004). Neutral theory and community ecology. *Ecol. Lett.* 7, 241–253. doi: 10.1111/j.1461-0248.2003.00566.x

Chen, W., Ren, K., Isabwe, A., Chen, H., Liu, M., and Yang, J. (2019). Stochastic processes shape microeukaryotic community assembly in a subtropical river across wet and dry seasons. *Microbiome* 7, 1–16. doi: 10.1186/s40168-019-0749-8

Chen, J., Wang, P., Wang, C., Wang, X., Miao, L., Liu, S., et al. (2020). Fungal community demonstrates stronger dispersal limitation and less network connectivity than bacterial community in sediments along a large river. *Environ. Microbiol.* 22, 832–849. doi: 10.1111/1462-2920.14795

Chen, W., and Wen, D. (2021). Archaeal and bacterial communities assembly and co-occurrence networks in subtropical mangrove sediments under *Spartina alterniflora* invasion. *Environ Microbiome* 16, 1–18. doi: 10.1186/s40793-021-00377-y

Chesson, P. (2000). Mechanisms of maintenance of species diversity. *Annu. Rev. Ecol. Syst.* 31, 343–366. doi: 10.1146/annurev.ecolsys.31.1.343

Chevillot, X., Tecchio, S., Chaalali, A., Lassalle, G., Selleslagh, J., Castelnaud, G., et al. (2019). Global changes jeopardize the trophic carrying capacity and functioning of estuarine ecosystems. *Ecosystems* 22, 473–495. doi: 10.1007/s10021-018-0282-9

Craney, T. A., and Surles, J. G. (2002). Model-dependent variance inflation factor cutoff values. *Qual. Eng.* 14, 391–403. doi: 10.1081/QEN-120001878

Csardi, G., and Nepusz, T. (2006). The igraph software package for complex network research. *Int J Complex Syst* 1695, 1–9.

del Carmen, F.-F. M., Bastida, R., Macías, A., Valencia, L., and Pérez-Lourido, P. (2006). Different nuclearities of M (II) nitrate complexes (M= co, Ni, cu and cd) with a tetrapyridyl pendant-armed hexaazamacrocyclic ligand. *Polyhedron* 25, 783–792. doi: 10.1016/j.poly.2005.07.045

Deng, Y., Jiang, Y.-H., Yang, Y., He, Z., Luo, F., and Zhou, J. (2012). Molecular ecological network analyses. *BMC Bioinformatics* 13, 1–20. doi: 10.1186/1471-2105-13-113

Edgar, R. C. (2010). Search and clustering orders of magnitude faster than BLAST. *Bioinformatics* 26, 2460–2461. doi: 10.1093/bioinformatics/btq461

Elzhov, T. V., Mullen, K. M., Spiess, A.-N., Bolker, B., Mullen, M. K. M., and Suggests, M. (2016) Package 'MINPACK. Lm'. R Interface Levenberg-Marquardt nonlinear least-Sq algorithm found MINPACK plus support bounds

Fargione, J., Brown, C. S., and Tilman, D. (2003). Community assembly and invasion: an experimental test of neutral versus niche processes. *Proc. Natl. Acad. Sci.* 100, 8916–8920. doi: 10.1073/pnas.1033107100

Fox, J., Friendly, G. G., Graves, S., Heiberger, R., Monette, G., Nilsson, H., et al. (2007) The car package. R Foundation for Statistical Computing 1109–1431

Gong, J., Shi, F., Ma, B., Dong, J., Pachiadaki, M., Zhang, X., et al. (2015). Depth shapes α-and β-diversities of microbial eukaryotes in surficial sediments of coastal ecosystems. *Environ. Microbiol.* 17, 3722–3737. doi: 10.1111/1462-2920.12763

Grömping, U. (2007). Relative importance for linear regression in R: the package relaimpo. *J. Stat. Softw.* 17, 1–27.

Gruber, N., and Galloway, J. N. (2008). An earth-system perspective of the global nitrogen cycle. *Nature* 451, 293–296. doi: 10.1038/nature06592

Harrell, F. E., and Harrell, M. F. E. (2019) Package 'hmisc'. CRAN2018 2019: 235-236

Huang, L., Bai, J., Wang, J., Zhang, G., Wang, W., Wang, X., et al. (2022). Different stochastic processes regulate bacterial and fungal community assembly in estuarine wetland soils. *Soil Biol. Biochem.* 167:108586. doi: 10.1016/j.soilbio.2022.108586

Hubbell, S. P. (2011). *The unified neutral theory of biodiversity and biogeography (MPB-32)*. Princeton University Press. doi: 10.1515/9781400837526

Huang, Y., Qu, W., Fan, Y., and Wang, J. (2022). Archaeal diversity in the seawater of Changjiang River estuary reveals its adaptability to bottom seawaters. *J Oceanol Limnol* 40, 1051–1069. doi: 10.1007/s00343-021-1035-8

Isabwe, A., Yang, J. R., Wang, Y., Wilkinson, D. M., Graham, E. B., Chen, H., et al. (2022). Riverine bacterioplankton and phytoplankton assembly along an environmental gradient induced by urbanization. *Limnol. Oceanogr.* 67, 1943–1958. doi: 10.1002/lno.12179

Jiao, S., Yang, Y., Xu, Y., Zhang, J., and Lu, Y. (2020). Balance between community assembly processes mediates species coexistence in agricultural soil microbiomes across eastern China. *ISME J.* 14, 202–216. doi: 10.1038/s41396-019-0522-9

Kembel, S. W., Cowan, P. D., Helmus, M. R., Cornwell, W. K., Morlon, H., Ackerly, D. D., et al. (2010). Picante: R tools for integrating phylogenies and ecology. *Bioinformatics* 26, 1463–1464. doi: 10.1093/bioinformatics/btq166

Legendre, P. (2014). Interpreting the replacement and richness difference components of beta diversity. *Glob. Ecol. Biogeogr.* 23, 1324–1334. doi: 10.1111/geb.12207

Li, J., Li, C., Kou, Y., Yao, M., He, Z., and Li, X. (2020). Distinct mechanisms shape soil bacterial and fungal co-occurrence networks in a mountain ecosystem. *FEMS Microbiol. Ecol.* 96:fiaa030. doi: 10.1093/femsec/fiaa030

Li, W., Wang, M., Burgaud, G., Yu, H., and Cai, L. (2019). Fungal community composition and potential depth-related driving factors impacting distribution pattern and trophic modes from epi-to abyssopelagic zones of the Western Pacific Ocean. *Microb. Ecol.* 78, 820–831. doi: 10.1007/s00248-019-01374-y

Lima-Mendez, G., Faust, K., Henry, N., Decelle, J., Colin, S., Carcillo, F., et al. (2015). Ocean plankton. Determinants of community structure in the global plankton interactome. *Science*:348:1262073. doi: 10.1126/science.1262073

Liu, L., Chen, H., Liu, M., Yang, J. R., Xiao, P., Wilkinson, D. M., et al. (2019). Response of the eukaryotic plankton community to the cyanobacterial biomass cycle over 6 years in two subtropical reservoirs. *ISME J.* 13, 2196–2208. doi: 10.1038/s41396-019-0417-9

Liu, Y.-X., Qin, Y., Chen, T., Lu, M., Qian, X., Guo, X., et al. (2021). A practical guide to amplicon and metagenomic analysis of microbiome data. *Protein Cell* 12, 315–330. doi: 10.1007/s13238-020-00724-8

Liu, W., Yang, X., Jiang, L., Guo, L., Chen, Y., Yang, S., et al. (2022). Partitioning of beta-diversity reveals distinct assembly mechanisms of plant and soil microbial communities in response to nitrogen enrichment. *Ecol. Evol.* 12:e9016. doi: 10.1002/ece3.9016

Liu, B., Yao, J., Ma, B., Li, S., and Duran, R. (2022). Disentangling biogeographic and underlying assembly patterns of fungal communities in metalliferous mining and smelting soils. *Sci. Total Environ.* 845:157151. doi: 10.1016/j.scitotenv.2022.157151

Logares, R., Lindström, E. S., Langenheder, S., Logue, J. B., Paterson, H., Laybourn-Parry, J., et al. (2013). Biogeography of bacterial communities exposed to progressive long-term environmental change. *ISME J.* 7, 937–948. doi: 10.1038/ismej.2012.168

Lu, M., Wang, X., Li, H., Jiao, J. J., Luo, X., Luo, M., et al. (2022). Microbial community assembly and co-occurrence relationship in sediments of the river-dominated estuary and the adjacent shelf in the wet season. *Environ. Pollut.* 308:119572. doi: 10.1016/j.envpol.2022.119572

Lyu, L., Liang, H., Huang, Y., Ding, H., and Yang, G.-P. (2022). Annual hypoxia causing long-term seawater acidification: evidence from low-molecular-weight organic acids in the Changjiang estuary and its adjacent sea area. *Sci. Total Environ.* 818:151819. doi: 10.1016/j.scitotenv.2021.151819

Mohamed, D. J., and Martiny, J. B. H. (2011). Patterns of fungal diversity and composition along a salinity gradient. *ISME J.* 5, 379–388. doi: 10.1038/ismej.2010.137

Nemergut, D. R., Schmidt, S. K., Fukami, T., O'Neill, S. P., Legg, T. M., Stanish, L., et al. (2013b). Microbial community assembly: patterns and processes. *Microbiol. Mol. Biol. Rev.* 77:e356.

Nemergut, D. R., Schmidt, S. K., Fukami, T., O'Neill, S. P., Bilinski, T. M., Stanish, L. F., et al. (2013a). Patterns and processes of microbial community assembly. *Microbiol. Mol. Biol. Rev.* 77, 342–356. doi: 10.1128/mmbr.00051-12

Ning, D., Deng, Y., Tiedje, J. M., and Zhou, J. (2019). A general framework for quantitatively assessing ecological stochasticity. *Proc. Natl. Acad. Sci.* 116, 16892–16898. doi: 10.1073/pnas.1904623116

Oksanen, J., Kindt, R., Legendre, P., O'Hara, B., Stevens, M. H. H., Oksanen, M. J., et al. (2007) The vegan package. Community ecology package 10: 719

Olesen, J. M., Bascompte, J., Dupont, Y. L., and Jordano, P. (2007). The modularity of pollination networks. *Proc. Natl. Acad. Sci.* 104, 19891–19896. doi: 10.1073/pnas.0706375104

Orsi, W., Biddle, J. F., and Edgcomb, V. (2013). Deep sequencing of subseafloor eukaryotic rRNA reveals active fungi across marine subsurface provinces. *PloS One* 8:e56335. doi: 10.1371/journal.pone.0056335

Pruesse, E., Peplies, J., and Glöckner, F. O. (2012). SINA: accurate high-throughput multiple sequence alignment of ribosomal RNA genes. *Bioinformatics* 28, 1823–1829. doi: 10.1093/bioinformatics/bts252

Revelle, W., and Revelle, M. W. (2015) Package 'psych'. The comprehensive R archive network 337: 338

Rognes, T., Flouri, T., Nichols, B., Quince, C., and Mahé, F. (2016). VSEARCH: a versatile open source tool for metagenomics. *Peer J* 4:e2584. doi: 10.7717/peerj.2584

Samad, T., Billings, N., Birjiniuk, A., Crouzier, T., Doyle, P. S., and Ribbeck, K. (2017). Swimming bacteria promote dispersal of non-motile staphylococcal species. *ISME J.* 11, 1933–1937. doi: 10.1038/ismej.2017.23

Shi, W., Caballero, J., Huszár, F., Totz, J., Aitken, A. P., Bishop, R., et al. Real-time single image and video super-resolution using an efficient sub-pixel convolutional neural network. arXiv [Preprint]. (2016). p 1874–1883

Shi, T., Li, M., Wei, G., Liu, J., and Gao, Z. (2020). Distribution patterns of microeukaryotic community between sediment and water of the Yellow River estuary. *Curr. Microbiol.* 77, 1496–1505. doi: 10.1007/s00284-020-01958-9

Shi, J., Zuo, Y., Qu, W., Liu, X., Fan, Y., Cao, P., et al. (2022). Stochastic processes shape the aggregation of free-living and particle-attached bacterial communities in the Yangtze River estuary, China. *J. Basic Microbiol.* 62, 1514–1525. doi: 10.1002/jobm.202100666

Shurin, J. B., Cottenie, K., and Hillebrand, H. (2009). Spatial autocorrelation and dispersal limitation in freshwater organisms. *Oecologia* 159, 151–159. doi: 10.1007/s00442-008-1174-z

Si, X., Zhao, Y., Chen, C., Ren, P., Zeng, D., Wu, L., et al. (2017). Beta-diversity partitioning: methods, applications and perspectives. *Biodivers. Sci.* 25, 464–480. doi: 10.17520/biods.2017024

Sloan, W. T., Lunn, M., Woodcock, S., Head, I. M., Nee, S., and Curtis, T. P. (2006). Quantifying the roles of immigration and chance in shaping prokaryote community structure. *Environ. Microbiol.* 8, 732–740. doi: 10.1111/j.1462-2920.2005.00956.x

Stegen, J. C., Lin, X., Fredrickson, J. K., Chen, X., Kennedy, D. W., Murray, C. J., et al. (2013). Quantifying community assembly processes and identifying features that impose them. *ISME J.* 7, 2069–2079. doi: 10.1038/ismej.2013.93

Stegen, J. C., Lin, X., Konopka, A. E., and Fredrickson, J. K. (2012). Stochastic and deterministic assembly processes in subsurface microbial communities. *ISME J.* 6, 1653–1664. doi: 10.1038/ismej.2012.22

Taylor, J. D., and Cunliffe, M. (2016). Multi-year assessment of coastal planktonic fungi reveals environmental drivers of diversity and abundance. *ISME J.* 10, 2118–2128. doi: 10.1038/ismej.2016.24

Tsui, C. K. M., and Hyde, K. D. (2004) *Biodiversity of fungi on submerged wood in a stream and its estuary in the tai Ho Bay*, Hong Kong. Fungal Diversity

Vellend, M., Srivastava, D. S., Anderson, K. M., Brown, C. D., Jankowski, J. E., Kleynhans, E. J., et al. (2014). Assessing the relative importance of neutral stochasticity in ecological communities. *Oikos* 123, 1420–1430. doi: 10.1111/oik.01493

Wang, Y., Guo, X., Zheng, P., Zou, S., Li, G., and Gong, J. (2017). Distinct seasonality of chytrid-dominated benthic fungal communities in the neritic oceans (Bohai Sea and North Yellow Sea). *Fungal Ecol.* 30, 55–66. doi: 10.1016/j.funeco.2017.08.008

Wang, X., Van Nostrand, J. D., Deng, Y., Lü, X., Wang, C., Zhou, J., et al. (2015). Scale-dependent effects of climate and geographic distance on bacterial diversity patterns across northern China's grasslands. *FEMS Microbiol. Ecol.* 91:fiv133. doi: 10.1093/femsec/fiv133

Wang, J., Wang, L., Hu, W., Pan, Z., Zhang, P., Wang, C., et al. (2021). Assembly processes and source tracking of planktonic and benthic bacterial communities in the Yellow River estuary. *Environ. Microbiol.* 23, 2578–2591. doi: 10.1111/1462-2920.15480

Wang, J., Zhang, T., Li, L., Li, J., Feng, Y., and Lu, Q. (2017). The patterns and drivers of bacterial and fungal β-diversity in a typical dryland ecosystem of Northwest China. *Front. Microbiol.* 8:2126. doi: 10.3389/fmicb.2017.02126

Wannicke, N., Frey, C., Law, C. S., and Voss, M. (2018). The response of the marine nitrogen cycle to ocean acidification. *Glob. Chang. Biol.* 24, 5031–5043. doi: 10.1111/gcb.14424

Wei, H., He, Y., Li, Q., Liu, Z., and Wang, H. (2007). Summer hypoxia adjacent to the Changjiang estuary. *J. Mar. Syst.* 67, 292–303. doi: 10.1016/j.jmarsys.2006.04.014

Wu, W., Xu, Z., Dai, M., Gan, J., and Liu, H. (2020). Homogeneous selection shapes free-living and particle-associated bacterial communities in subtropical coastal waters. *Divers. Distrib.* 27, 1904–1917. doi: 10.1111/ddi.13193

Xue, Y., Chen, H., Yang, J. R., Liu, M., Huang, B., and Yang, J. (2018). Distinct patterns and processes of abundant and rare eukaryotic plankton communities following a reservoir cyanobacterial bloom. *ISME J.* 12, 2263–2277. doi: 10.1038/s41396-018-0159-0

Yu, Y., Yang, Q., Petropoulos, E., and Zhu, T. (2022). ITS3/ITS4 outperforms other ITS region and 18S rRNA gene primer sets for amplicon sequencing of soil fungi. *Eur. J. Soil Sci.* 73:e13329. doi: 10.1111/ejss.13329

Zhang, Y., Liu, Y., Cao, X., Gao, P., Liu, X., Wang, X., et al. (2016). Free amino acids and small molecular acids profiling of marine microalga Isochrysis zhangjiangensis under nitrogen deficiency. *Algal Res.* 13, 207–217. doi: 10.1016/j.algal.2015.12.001

Zhang, Z.-F., Pan, Y.-P., Liu, Y., and Li, M. (2021). High-level diversity of basal fungal lineages and the control of fungal community assembly by stochastic processes in mangrove sediments. *Appl. Environ. Microbiol.* 87, e00928–e00921. doi: 10.1128/AEM.00928-21

Zhang, J., Xiao, T., Huang, D., Liu, S. M., and Fang, J. (2016). Eutrophication and hypoxia and their impacts on the ecosystem of the Changjiang estuary and adjacent coastal environment. *J. Mar. Syst.* 154, 1–4. doi: 10.1016/j.jmarsys.2015.10.007

Zhao, H., Brearley, F. Q., Huang, L., Tang, J., Xu, Q., Li, X., et al. (2023). Abundant and rare taxa of planktonic fungal community exhibit distinct assembly patterns along coastal eutrophication gradient. *Microb. Ecol.* 85, 495–507. doi: 10.1007/s00248-022-01976-z

Zhao, Z., Li, H., Sun, Y., Zhan, A., Lan, W., Woo, S. P., et al. (2022). Bacteria versus fungi for predicting anthropogenic pollution in subtropical coastal sediments: assembly process and environmental response. *Ecol. Indic.* 134:108484. doi: 10.1016/j.ecolind.2021.108484

Zhen, S., Deng, X., Zhang, M., Zhu, G., Lv, D., Wang, Y., et al. (2017). Comparative phosphoproteomic analysis under high-nitrogen fertilizer reveals central phosphoproteins promoting wheat grain starch and protein synthesis. *Front. Plant Sci.* 8:67. doi: 10.3389/fpls.2017.00067

Zheng, Q., Wang, Y., Lu, J., Lin, W., Chen, F., and Jiao, N. (2020). Metagenomic and metaproteomic insights into photoautotrophic and heterotrophic interactions in a Synechococcus culture. *MBio* 11, e03261–e03219. doi: 10.1128/mBio.03261-19

Zhou, J., and Ning, D. (2017). Stochastic community assembly: does it matter in microbial ecology? *Microbiol. Mol. Biol. Rev.* 81, e00002–e00017. doi: 10.1128/mmbr.00002-17

Zuo, Y., Zeng, R., Tian, C., Wang, J., and Qu, W. (2022). The importance of conditionally rare taxa for the assembly and interaction of fungal communities in mangrove sediments. *Appl. Microbiol. Biotechnol.* 106, 3787–3798. doi: 10.1007/s00253-022-11949-4

Frontiers in Marine Science

Explores ocean-based solutions for emerging global challenges

The third most-cited marine and freshwater biology journal, advancing our understanding of marine systems and addressing global challenges including overfishing, pollution, and climate change.

Discover the latest Research Topics

See more →

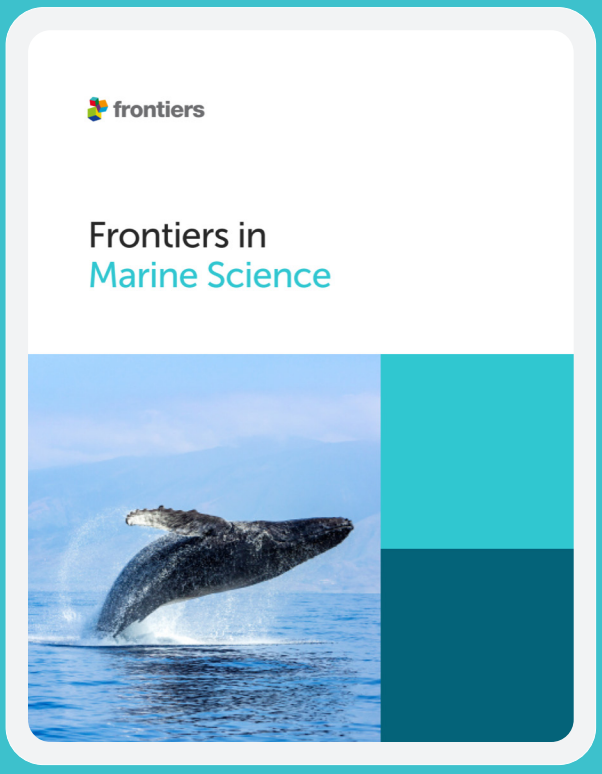

Frontiers

Avenue du Tribunal-Fédéral 34
1005 Lausanne, Switzerland
frontiersin.org

Contact us

+41 (0)21 510 17 00
frontiersin.org/about/contact